18TH INTERNATIONAL SYMPOSIUM

Water Management & Hydraulic Engineering WMHE 2024

SYMPOSIUM PROCEEDINGS

10th – 14th September 2024, Štrbské Pleso, Slovakia

SPEKTRUM STU

18TH INTERNATIONAL SYMPOSIUM

Water Management & Hydraulic Engineering

WMHE
2024

Symposium Proceedings

10th – 14th September 2024, Štrbské Pleso, Slovakia

18th International Symposium
WATER MANAGEMENT & HYDRAULIC ENGINEERING WHME 2024
10th – 14th September 2024, Štrbské Pleso, Slovakia

SYMPOSIUM PROCEEDINGS

Editors	Michaela Červeňanská, Andrej Šoltész, Dana Baroková, Lea Čubanová *Slovak University of Technology in Bratislava, Slovak Republic*
Published by	Slovak University of Technology in Bratislava in SPEKTRUM STU Publishing, Bratislava, Vazovova 5
Published in	2024
Cover Design	Michaela Červeňanská
Web site	https://wmhe2024.hydrotechnika.sk/

Note: The Proceedings contain original author's papers that have been double-blind reviewed before final submission to the Symposium. Initially, paper abstracts were read and selected by the Scientific Advisory Committee of the Symposium as possible papers for the Symposium.

ORGANIZED BY
Slovak University of Technology in Bratislava
Faculty of Civil Engineering, Bratislava, Slovak Republic

IN COLLABORATION WITH
Univeristy of Zagreb
Faculty of Civil Engineering, Zagreb, Croatia
Gdańsk University of Technology
Faculty of Civil and Environmental Engineering, Gdańsk, Poland
Ss. Cyril and Methodius University in Skopje
Faculty of Civil Engineering, Skopje, Republic of North Macedonia
Brno University of Technology
Faculty of Civil Engineering, Brno, Czech Republic

ISBN 978-80-227-5433-0
ISSN 3027-5032

SYMPOSIUM CHAIRMEN

Eva Ocvirk

University of Zagreb, Faculty of Civil Engineering, Zagreb, Croatia

Michał Szydłowski

Gdańsk University of Technology, Faculty of Civil and Environmental Engineering, Gdańsk, Poland

Andrej Šoltész

Slovak University of Technology in Bratislava, Faculty of Civil Engineering, Bratislava, Slovakia

Josif Josifovski

Ss. Cyril and Methodius University in Skopje, Faculty of Civil Engineering, Skopje, Republic of North Macedonia

Jaromír Říha

Brno University of Technology, Faculty of Civil Engineering, Brno, Czech Republic

SCIENTIFIC ADVISORY COMMITTEE

Eva Ocvirk, Dalibor Carević, Ivan Halkijević, Kristina Potočki

University of Zagreb, Faculty of Civil Engineering, Zagreb, Croatia

Michał Szydłowski

Gdańsk University of Technology, Faculty of Civil and Environmental Engineering, Gdańsk, Poland

Andrej Šoltész, Silvia Kohnová, Štefan Stanko, Jana Frankovská

Slovak University of Technology in Bratislava, Faculty of Civil Engineering, Bratislava, Slovak Republic

Josif Josifovski

Ss. Cyril and Methodius University in Skopje, Faculty of Civil Engineering, Skopje, Republic of North Macedonia

Jaromír Říha

Brno University of Technology, Faculty of Civil Engineering, Brno, Czech Republic

ORGANIZING COMMITTEE

Gordon Gilja, Domagoj Nakić, Damjan Bujak

University of Zagreb, Faculty of Civil Engineering, Zagreb, Croatia

Piotr Zima

Gdańsk University of Technology, Faculty of Civil and Environmental Engineering, Gdańsk, Poland

Michaela Červeňanská, Alexandra Vidová, Adela Rutzká, Natália Bilčíková, Réka Wittmanová, Jana Lehotová Nôtová

Slovak University of Technology in Bratislava, Faculty of Civil Engineering, Bratislava, Slovak Republic

Violeta Gjesovska

Ss. Cyril and Methodius University in Skopje, Faculty of Civil Engineering, Skopje, Republic of North Macedonia

Tomáš Julínek

Brno University of Technology, Faculty of Civil Engineering, Brno, Czech Republic

REVIEWERS

Aleksić Milica
Slovak University of Technology in Bratislava, Slovakia

Almikaeel Wael
Slovak University of Technology in Bratislava, Slovakia

Baroková Dana
Slovak University of Technology in Bratislava, Slovakia

Barloková Danka
Slovak University of Technology in Bratislava, Slovakia

Bekić Damir
University of Zagreb, Croatia

Carević Dalibor
University of Zagreb, Croatia

Ćosić-Glajsig Gorana
Zagreb University of Applied Sciences, Croatia

Červeňanská Michaela
Slovak University of Technology in Bratislava, Slovakia

Čubanová Lea
Slovak University of Technology in Bratislava, Slovakia

Danáčová Michaela
Slovak University of Technology in Bratislava, Slovakia

Donevska Katerina
Ss. Cyril and Methodius University in Skopje, Republic of North Macedonia

Đurin Bojan
University North, Croatia

Gjeshovska Violeta
Ss. Cyril and Methodius University in Skopje, Republic of North Macedonia

Halkijević Ivan
University of Zagreb, Croatia

Ilavský Ján
Slovak University of Technology in Bratislava, Slovakia

Josifovski Josif
Ss. Cyril and Methodius University in Skopje, Republic of North Macedonia

Jovanov Milorad
Ss. Cyril and Methodius University in Skopje, Republic of North Macedonia

Julínek Tomáš
Brno University of Technology, Czech Republic

Koczka Bara Márta
Slovak Academy of Sciences, Slovakia

Kohnová Silvia
Slovak University of Technology in Bratislava, Slovakia

Krvavica Nino
University of Rijeka, Croatia

Kubáň Martin
Slovak University of Technology in Bratislava, Slovakia

Leivadiotis Evangelos
Slovak University of Technology in Bratislava, Slovakia

Mitovski Stevco
Ss. Cyril and Methodius University in Skopje, Republic of North Macedonia

Nakić Domagoj
University of Zagreb, Croatia

Ocvirk Eva
University of Zagreb, Croatia

Orfánus Martin
Slovak University of Technology in Bratislava, Slovakia
Petkovski Ljupcho
Ss. Cyril and Methodius University in Skopje, Republic of North Macedonia
Posavčić Hana
University of Zagreb, Croatia
Potočki Kristina
University of Zagreb, Croatia
Rumann Ján
Slovak University of Technology in Bratislava, Slovakia
Ružić Igor
University of Rijeka, Croatia
Říha Jaromír
Brno University of Technology, Czech Republic
Sokáč Marek
Slovak Academy of Sciences, Slovakia
Stanko Štefan
Slovak University of Technology in Bratislava, Slovakia
Sušanj Čule Ivana
University of Rijeka, Croatia
Szydłowski Michał
Gdańsk University of Technology, Poland
Škrinár Andrej
Slovak University of Technology in Bratislava, Slovakia
Škultétyová Ivona
Slovak University of Technology in Bratislava, Slovakia
Škvarka Juraj
Slovak University of Technology in Bratislava, Slovakia
Šoltész Andrej
Slovak University of Technology in Bratislava, Slovakia
Šrajbek Marko
University of Zagreb, Croatia
Štefunková Zuzana
Slovak University of Technology in Bratislava, Slovakia
Šulek Peter
Slovak University of Technology in Bratislava, Slovakia
Tadić Lidija
Josip Juraj Strossmayer University of Osijek, Croatia
Velísková Yvetta
Slovak Academy of Sciences, Slovakia
Vidová Alexandra
Slovak University of Technology in Bratislava, Slovakia
Vouk Dražen
University of Zagreb, Croatia
Wittmanová Réka
Slovak University of Technology in Bratislava, Slovakia
Zeleňáková Martina
Technical University of Košice, Slovakia
Zima Piotr
Gdańsk University of Technology, Poland

TABLE OF CONTENTS

PREFACE

The 18th International Symposium on Water Management and Hydraulic Engineering (WMHE 2024) is organized by the Faculty of Civil Engineering at the Slovak University of Technology in Bratislava from 10–14 September 2024 in Štrbské Pleso – the heart of the beautiful nature of the High Tatras in Slovakia. The WMHE 2024 Symposium is the next in the series of International Symposiums in the field of Water Management and Hydraulic Engineering, organized with the participation of the University of Zagreb (Croatia), Gdańsk University of Technology (Poland), Slovak University of Technology in Bratislava (Slovak Republic), Ss. Cyril and Methodius University in Skopje (North Macedonia), University of Natural Resources and Applied Life Sciences in Vienna (Austria) as well as Brno University of Technology (Czech Republic).

The main goal of the conference is to share transboundary and interdisciplinary knowledge and experience between scientists and experts from Central Europe, from older and new EU member states as well as from South-East European candidate countries.

The first Symposium of this type was organized as a bilateral activity between the faculties of Gdańsk University of Technology and Zagreb University. Since 1998 (in Dubrovnik), the Slovak University of Technology, the Ss. Cyril and Methodius University in Skopje and BOKU University of Natural Resources and Applied Life Sciences in Vienna have joined this biannual symposium series. In 2013 Brno University of Technology, Czech Republic, joined the steering group of WMHE too.

The aim of the Symposium is to encourage and facilitate communication and exchange of experience from recent research work between scientists, engineers and professionals on different aspects of water and environmental management and hydraulic engineering, including physical and mathematical modelling. Topics of the symposium have been chosen to cover the main elements of integrated water resources management, hydraulic engineering, sanitary engineering and sustainable water use, hydrology, hydraulics, geotechnical engineering as well as environmental engineering, climate change and flood risk management. This successful series started in 1984 and is now regularly organized as a two-annual symposium meeting. During the symposium, two lectures will be given by invited internationally renowned scientists Prof. Hans – Peter Nachtnebel from BOKU University in Vienna and Prof. Jan Szolgay from STU in Bratislava.

The Symposium is co-organized by the Slovak Society of Environmental Technology under the auspices of Prof. Dušan Petráš.

We are honoured and delighted to invite you to enjoy the symposium in the beautiful nature of the High Tatras in Slovakia.

Andrej Šoltész

HYDRAULICS AND HYDRAULIC STRUCTURES

CALIBRATION OF THE XBEACH-GRAVEL MODEL

HANNA MILIČEVIĆ [1], DALIBOR CAREVIĆ [2], DAMJAN BUJAK [3]

[1] *Faculty of Civil Engineering, University of Zagreb, Croatia, hanna.milicevic@grad.unizg.hr*

[2] *Faculty of Civil Engineering, University of Zagreb, Croatia, dalibor.carevic@grad.unizg.hr*

[3] *Faculty of Civil Engineering, University of Zagreb, Croatia, damjan.bujak@grad.unizg.hr*

1 Abstract

Despite the natural and economic importance of maintaining gravel beaches in Croatia, there is a lack of knowledge about the resilience of the beach to various wave impacts and the frequency of storm events, as well as specific numerical models for predicting the morphological response of the gravel beach to storm events. This paper summarizes the calibration results of the 1D Xbeach-Gravel model to simulate the morphodynamic response of the gravel beach in Croatia during winter. The model simulation results show that XBeach-G is able to reproduce the observed change in the cross-shore profile under different wave conditions with high quantitative accuracy (BSS≥0.6).

Keywords: Xbeach-Gravel, Artificial beaches, Gravel, Modelling, Storm morphology

2 Introduction

The Croatian Eastern Adriatic Coast (CEAC, which stretches over 6000 km along the eastern Adriatic between Slovenia and Montenegro [1]) is highly valued for its biodiversity and its small, fetch limited gravel beaches, which have been intensively used by humans for centuries. All values may be affected by the current growing tourist demand for beach capacity, which has led to the construction of artificial beaches, especially pocket gravel beaches, without sufficient knowledge of the most appropriate parameters for design. However, as coasts are subject to numerous natural and man-induced stresses that affect their stability [2], coastal managers must be able to incorporate an evidence-based understanding of natural processes such as erosion and accretion [1], as well as measures to reduce the impact of storm events, in order to effectively assess and maintain coastal safety [2]. The conceptual model (Figure 1) linking the morphodynamic response of gravel barriers to the relationship between hydrodynamic forces and barrier geometry is widely accepted [3-8]. An increase in relative pressure conditions leads to morphological changes in the beach (berm formation, beach erosion), to changes in the barrier crest (crest build-up and lowering) or the entire barrier (barrier rollover) [2]. On the artificial gravel beaches in Croatia, where the maximum significant wave height does not exceed 3 m, the reactions such as berm formation, beach erosion and crest build-up occur most frequently, while the others occur very rarely or not at all. Further information on the morphological response of gravel beaches to storm events can be found in the publication by [13]. Despite the qualitative understanding of the dynamics of gravel barriers, engineers are not able to reliably predict the morphodynamic response of gravel coasts to storms [6,9]. Currently, beach management in Croatia is the responsibility of local authorities (coastal municipalities and cities) and includes issues of land and sea use, infrastructure development, cultural heritage protection, concessions, etc., as well as beach erosion [1]. However, the relevant beach management strategies and guidelines are broad and service-oriented [10] and critically ignore coastal erosion issues. To address this gap and enable the development and application of appropriate adaptation strategies by assessing future changes to beaches, an understanding of coastal processes and their impacts at local and regional scales is required. Beaches serve as energy buffers, contribute to the ecological diversity of coastal areas and provide recreational opportunities [1]. Regardless of which of these functions is the primary focus, a better understanding of the formation and evolution of beaches is crucial for effective beach protection in coastal management strategies. Such an understanding usually results from comprehensive monitoring.

Therefore, as a first step, it is essential in Croatia to identify vulnerable coastal sites and implement an appropriate monitoring plan to collect data at an appropriate spatial and temporal scale [1]. Currently, coastal managers are largely forced to rely on empirical models to make quantitative predictions about the response of gravel beach to storms [2]. Previous research has shown that applying these models outside of their scope of validity can underestimate the severity of storm impacts [2], [11-12], and because these models were developed based on data from idealized laboratory studies, this limitation also prevents the use of models to accurately predict future storm impacts under changing environmental conditions [2]. The researcher's focus is on developing a numerical model to model "cross-shore" and "long-shore" sediment transport on a gravel beach. However, mainly process-based models are used, almost all of which are geared towards sandy coasts. Numerical models developed for sandy beaches can be used to predict the morphological response of gravel beaches, but the fundamental differences between the dynamics of sand and gravel beaches preclude their application without significant modification [9]. It is therefore a necessary conclusion that no reliable numerical model is currently available for predicting the morphological response of gravel beaches to changing wave/tidal conditions on the short to medium term time scale (minutes to weeks) [9]. XBeach-Gravel is a 1D numerical model specifically designed to simulate the morphological response of gravel beaches to wave events. XBeach-G is based on the Xbeach model, a numerical model for simulating the effects of storm events on sandy coasts. It is better suited for very energetic storm events on coasts with significant wave heights of up to 10 m and peak periods of 10 s [13]. The one-dimensionality of the model is its limiting factor as it does not allow simulation of longshore processes, but the work of [14] shows how it can be coupled with a parametric longshore transport formula to achieve good results. However, the model has hardly been modeled, calibrated and validated for coarse-grained gravel beaches [15], especially not for the conditions in the Adriatic Sea [14], where gravel beaches are widespread, waves are fetch-limited, and storms are less energetic. In this study, we investigate the feasibility of the 1D model XBeach Gravel for predicting beach changes, namely the location and height of beach berms after storm events, at the artificial gravel beach Ploče in the northwestern part of the city of Rijeka in Kvarner Bay. This paper summarizes the results of a research project specifically aimed at developing the ability to predict the response of gravel beaches to wave and water level conditions in Croatia through an integrated research approach involving field surveys, comprehensive beach monitoring and innovative numerical modeling.

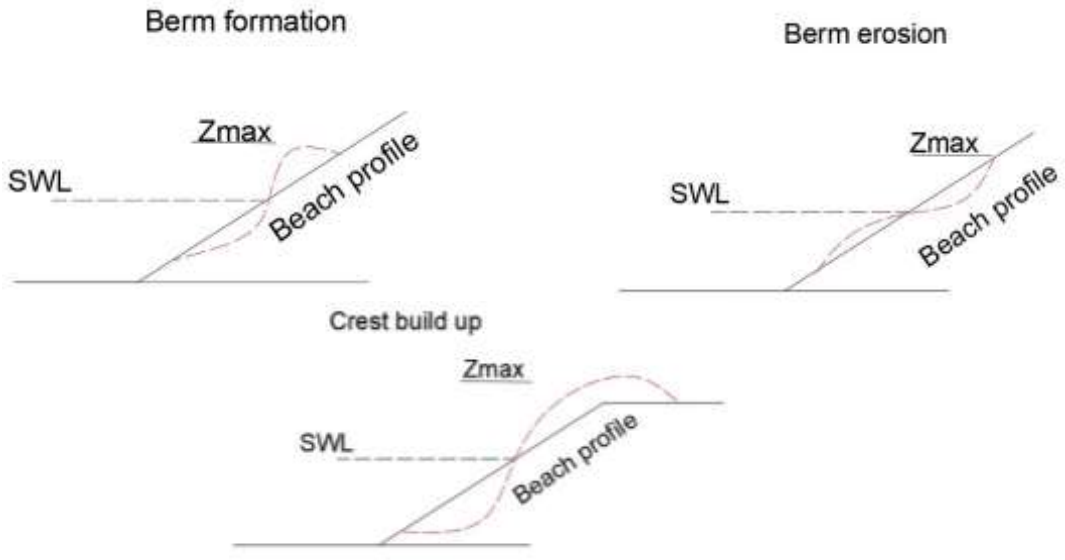

Figure 1. The most common morphological responses of a gravel beach (dashed red lines) to different wave action and water levels in Croatia. From left to right, the wave conditions become more energetic and the still water level higher, leading to higher maximum water levels on the barrier (zmax). Modified from [2]

3 Methods

3.1 XBeach-G model description

XBeach is an open-source numerical model originally developed to simulate hydrodynamic and morphodynamic processes and effects on sandy coasts with a domain size of kilometers and on the time scale of storms. The modeling of storm morphodynamics on gravel beaches is a one-dimensional (cross-shore transects) extension of the XBeach storm impact model [16] for gravel beaches through the application of (a) a non-hydrostatic pressure correction term that allows wave-by-wave modelling of surface elevation and depth-averaged flow; (b) a groundwater model that allows simulation of infiltration and exfiltration through the permeable gravel bed; and (c) sediment transport relationships that account for the transport of gravel bed loads [2]. More about the model description and the corresponding equations can be found in [2, 9].

3.1.1 Case study site and storm data

The data used in this paper to calibrate the XBeach-G model for Croatian wave conditions were collected as part of the BEACHEX project, i.e. the study of the mechanisms of morphodynamic response and restoration of gravel beaches using unmanned aerial vehicles. The artificial gravel beach Ploče, which is the subject of this study, is the largest beach complex in the city of Rijeka [17] with a total area of 14,000 m^2 and was built over two existing natural embayments. The beach is protected by three groynes extending from the existing headlands. The central groin divides the beach into two parts - the eastern and the western, both about 130 m wide (Figure 2). The beach is subject to severe erosion that occurs each fall/winter season during heavy storms. Storm events are the main cause of morphological processes, especially cross-shore gravel transport on the beaches of the eastern Adriatic [17, 18]. The prevailing winds in Kvarner Bay are Bura (NE) and Jugo (SE). Bura is a dry and cold northeasterly wind associated with the intrusion of cold air from the polar regions [18], while Jugo blows at a steady speed and generates large waves. The focus of this study is on the western beach, where the calibration of the model is performed; the eastern part of the beach will be used for model validation in future studies. All calibrations and simulations were performed on the profiles shown in Figure 2, referred to as Profile 1, Profile 4 and Profile 5. The Ploče beach was surveyed 19 times between January 17, 2020, and February 26, 2021, outside the summer season and mainly after storm events [17] by the Geodetic Institute Rijeka (GZR) and the Faculty of Civil Engineering in Rijeka (GradRi). Before the first survey, twelve ground control points (GCPs) were marked along the stable sections of the beach, namely the promenade and groynes. In April 2020, a further 16 GCPs were surveyed and the old GCPs were measured again to check whether they were still stable [17]. The GCPs are distributed over the entire surveyed beach area to avoid extrapolation in the area of interest. After marking, the aerial surveys could be carried out relatively quickly using unmanned aerial vehicles (UAVs). As a rule, it took about an hour to survey the beach. Further details about the field survey can be found in [17].

Figure 2. Map showing the location of the city of Rijeka (left) and aerial view of Ploče beach with profiles 1, 4, 5 selected for the simulation (right)

3.1.2 Model setup and calibration

The incoming waves were measured on a wave buoy (Datawell Waverider MkIII) anchored by the Hydrographic Institute of the Republic of Croatia at a depth of 57.5 m and located approximately 2.5 km southeast of Ploče at the geographical coordinates 45°19.588' N: 14°23.738' E, WGS 84 system [18]. The buoy provided 60 minutes of wave statistics (significant wave height, peak period, wave direction and spreading) for the period from December 2019 to February 2021 [13]. Figure 3 shows wave climate during the one-year observation period mentioned above and the storm events during this period. The tidal and wave boundary conditions for the model are derived from the nearest tide gage in Bakar. For this work, 5 field investigations, i.e. three storm/energetic events were selected (Table 1) as most of the visible berms formed afterwards. The first event (Table 1) due to the shortest period between topographic surveys (only one day), the second event as one of the most severe storms with large significant wave height (Table 1) during the observation period, and the third event with milder wave conditions but with a clear cross-shore sediment transport process. As we have already mentioned that one-dimensionality is a limiting factor of the Xbeach-G model and that it does not allow simulation of long-shore processes, the profiles for this study were chosen such that the long-shore sediment transport gradient should have the least impact during the storm events (Figure 2). In the first model simulation, the entire period of the storm is simulated between the pre-storm survey and the post-storm survey, which was possible due to the one-day period between topographic surveys (Table 1). In these cases, the initial cross-shore profile in the Xbeach-G model is set to the cross-shore profile measured at low tide before the simulated storm [2], and after the final beach profile is obtained using the numerical model, it is compared to the field observation after the storm event. To reduce the computational requirements and to account for the fact that XBeach-G is designed to simulate storm events and does not include processes to model medium- to long-term coastal changes (e.g., longshore transport gradients) [2], the duration of the other simulations is shortened to 2.9 h and 4.1 h around the peak due to the large time period between the cross-shore profile measurements. The equation 1 for calculating the duration.

$$t = \frac{Tp}{1.1} * n \quad (1)$$

where t is the duration in seconds, Tp is the peak wave period and n is the number of waves.
The recommended number of waves to reach dynamic equilibrium is 3000 waves [8,19]. The hydraulic conductivity and the mean grain size at Ploče beach are based on the suggestions presented in the literature by [13]. Further explanations of the chosen parameters for the hydraulic conductivity can be found in [13]. The average grain size for the Ploče beach is 0.032 m [13, 17]. The three free model parameters related to sediment transport are the inertia coefficient ci, which influences sediment transport through shear stress at the bottom, the angle of repose Φ, which controls avalanching and influences sediment transport on sloping bottoms, and the bedload transport calibration coefficient γ, which linearly scales transport rates and gradients [2]. If sufficient data are available, these model parameters can be calibrated at each gravel barrier to obtain the most accurate representation of the measured cross-shore profile changes. To evaluate the predictive power of the numerical model, three different values for the sediment transport parameters (Φ- 35°,45°,55° & γ-0.5, 1, 3) were used to find the combination best suited to describe berm formation and beach erosion, two processes that occur most frequently on Croatian artificial beaches.

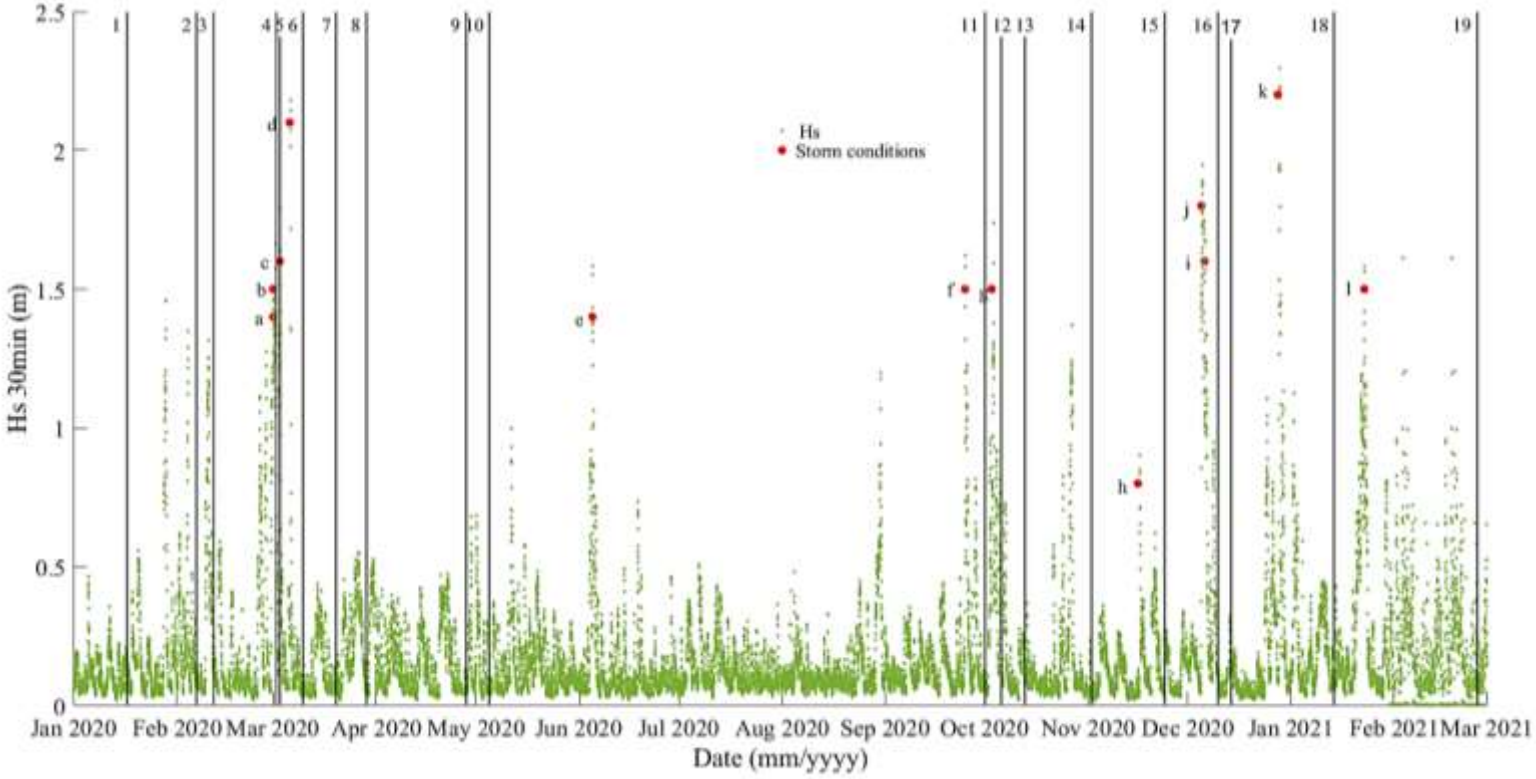
Hs
Storm conditions
Hs 30min (m)
Date (mm/yyyy)
Jan 2020
Feb 2020
Mar 2020
Apr 2020
May 2020
Jun 2020
Jul 2020
Aug 2020
Sep 2020
Oct 2020
Nov 2020
Dec 2020
Jan 2021
Feb 2021
Mar 2021

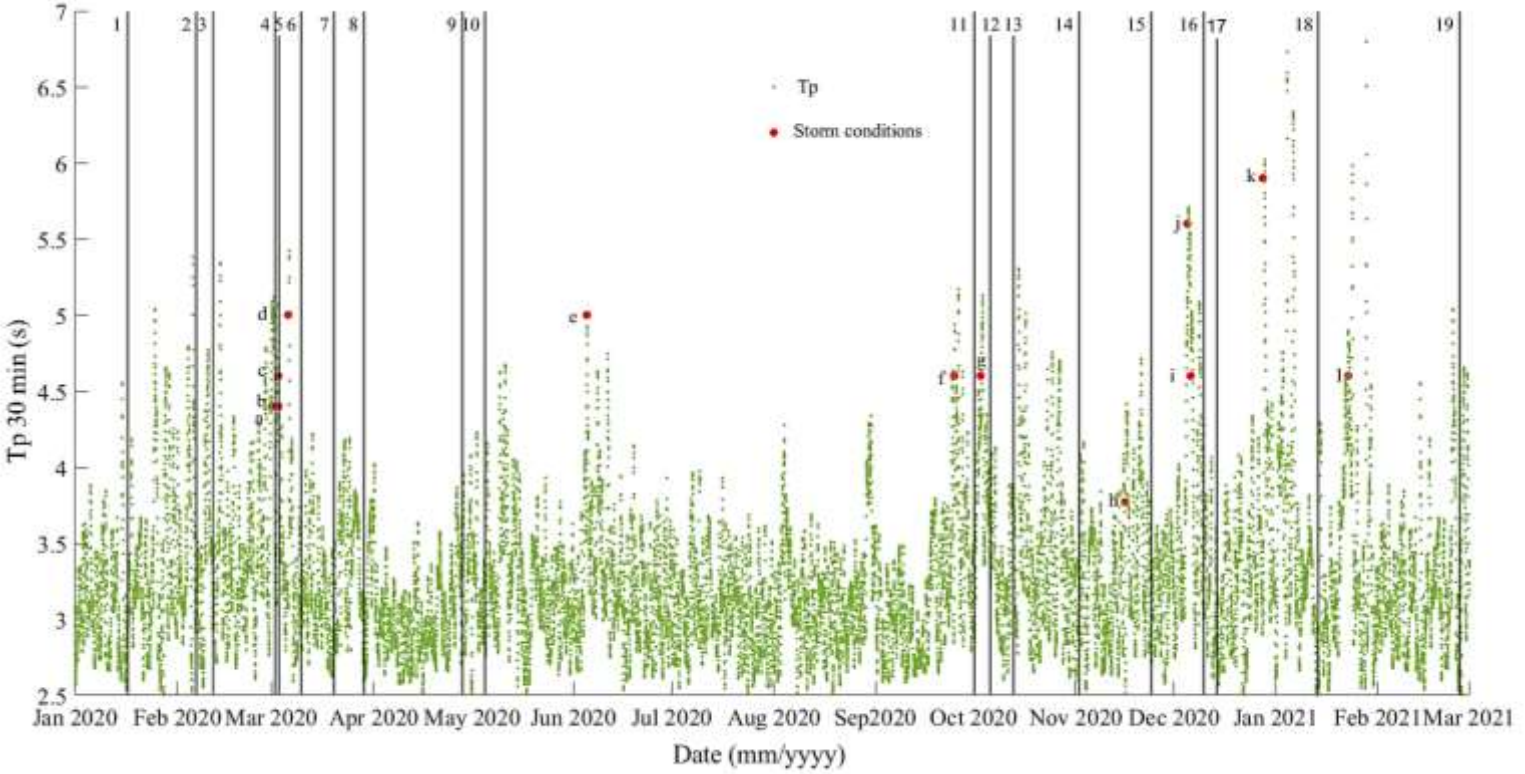
Tp
Storm conditions
Tp 30 min (s)
Date (mm/yyyy)
Jan 2020
Feb 2020
Mar 2020
Apr 2020
May 2020
Jun 2020
Jul 2020
Aug 2020
Sep2020
Oct 2020
Nov 2020
Dec 2020
Jan 2021
Feb 2021
Mar 2021

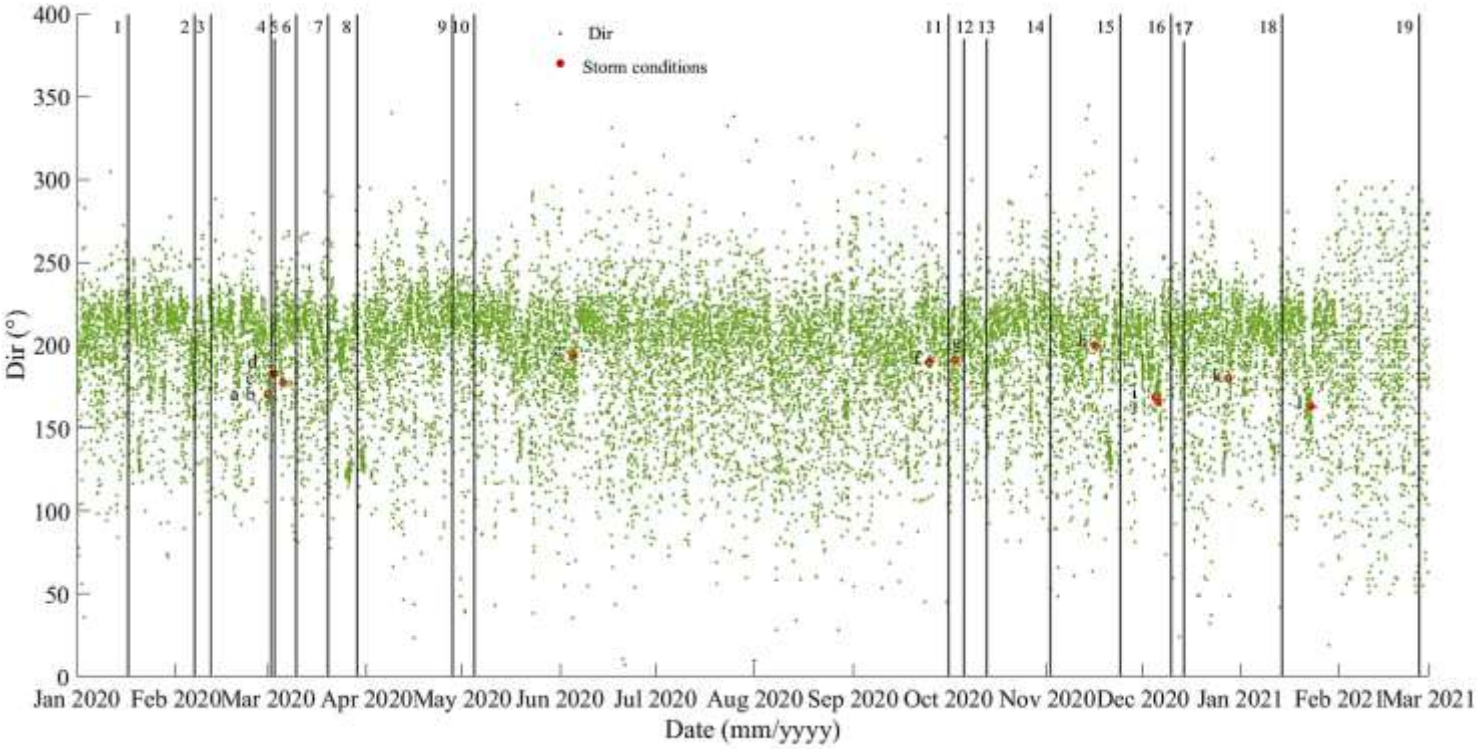

Figure 3. Wave climate during the one-year observation period (significant wave height, peak wave period and wave direction) with identified storm events (red dots) and UAV field survey data (vertical lines)

Table 1. Selected field survey data and associated storm events for the simulation

DATE	SURVEY LABEL	STORM EVENT	START OF STORM	END OF STORM	H_S [M]	T_P [S]
2 MARCH 2020	UAV4	c	3 MARCH 2020 00:15	3 MARCH 2020 02:28	1.52	4.7
3 MARCH 2020	UAV5					
2 NOVEMBER 2020	UAV14	h	16 NOVEMBER 2020 12:30	16 NOVEMBER 2020 160:0	0.80	3.77
24 NOVEMBER 2020	UAV15					
24 NOVEMBER 2020	UAV15	i	5 DECEMBER 2020 00:53	5 DECEMBER 2020 22:58	1.78	5.27
10 DECEMBER 2020	UAV16					

3.1.3 Brier Skill Score

To determine the quality of the model prediction in comparison to the measurement results, the Brier skill score is usually used in coastal modeling [2, 20]. In this work, initial geodetic survey (before the storm event) is compared with the model prediction [13]. The model prediction should approximate the measured geodetic survey (after the event). According to van Rijn, the BSS values in Table 2. show that values above 0.6 indicate a good model prediction.

Table 2. Qualification of different Brier skill score ranges according to van Rijn et.al [21]

Brier Skill Score	QUALIFICATION
0.8-1.0	Excellent
0.6-0.8	Good
0.3-0.6	Fair
0.0-0.3	Poor
<0	Bad

4 Results and discussion

All of the storm events discussed in Section 3 can be characterized by the formation of berms, where an existing berm was eroded, and a new berm was created higher on the beach profile [2]. The figures show that the model can qualitatively reproduce the observed changes for both a light and a heavy storm (Figures 4,5,6). Different conditions apply for different severity levels of storm events. However, quantitatively, Xbeach-G may underestimate the volume of the berm, and the site-specific calibration of model parameters related to sediment transport, such as angle of repose (Φ) and sediment transport coefficient (γ), may change the outcome of the model prediction. The best fit for significant wave heights (Hs) equal to or less than 1.5 m is angle of repose (Φ) 55° and transport coefficient (γ) 0.5 (Figure 4,5), for Hs greater than 1.5 m Φ is 35° and sediment transport coefficient (γ) is 3 (Figure 6). Despite the fact that site-specific calibration is required for the wave climate in Croatia, the overall skill of the model prediction is reasonable with an average BSS of 0.8 for the selected parameters (Figure 7). According to the van Rijn classification of the different Brier skill score ranges, the results are classified as good to excellent.

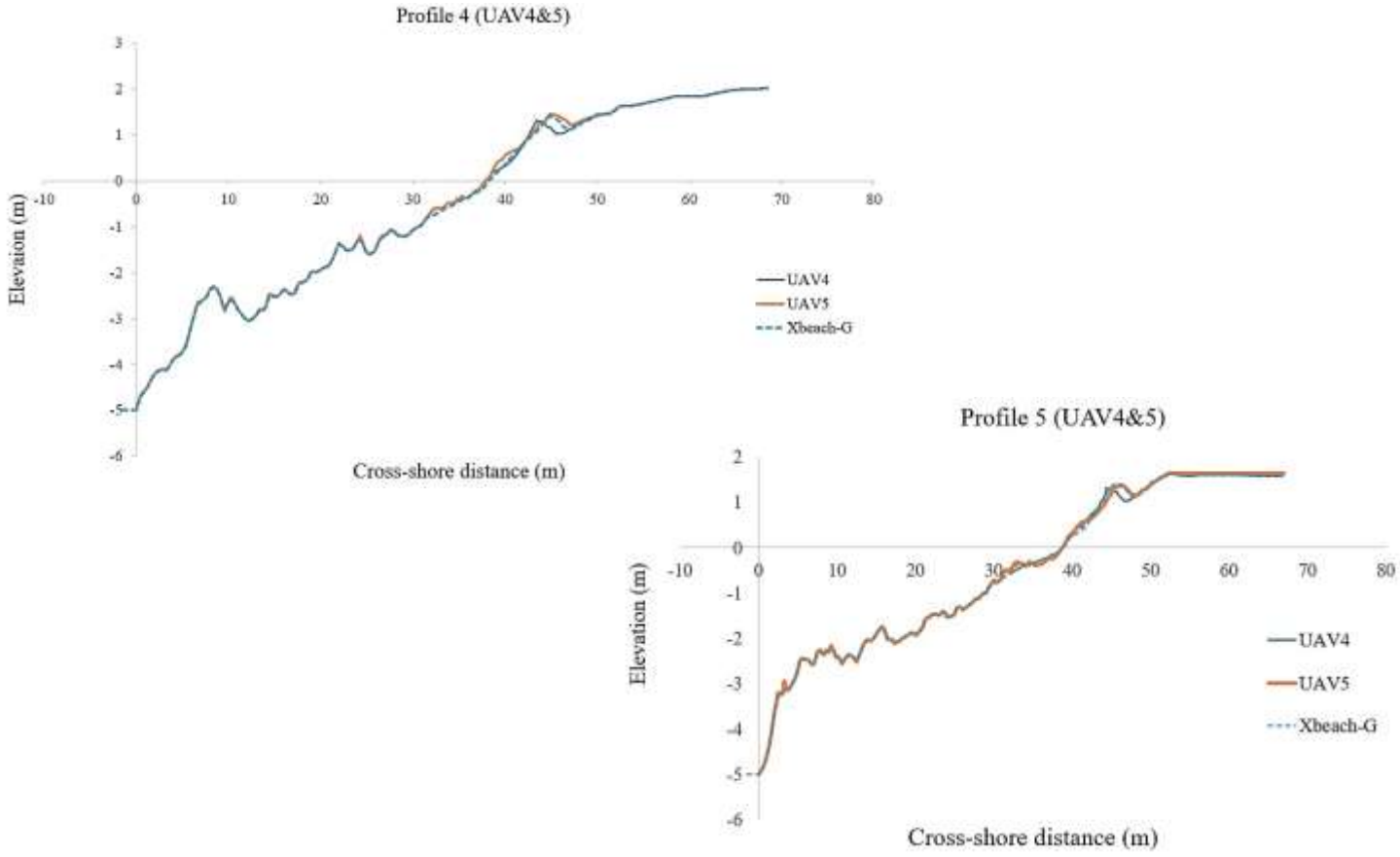

Figure 4. Modeled (dashed blue line) and measured (blue line before the storm event and orange line after the storm event) profiles using parameters resulting from the highest BSS for the UAV4&5 field survey at two profiles (Φ=55°, γ=0.5)

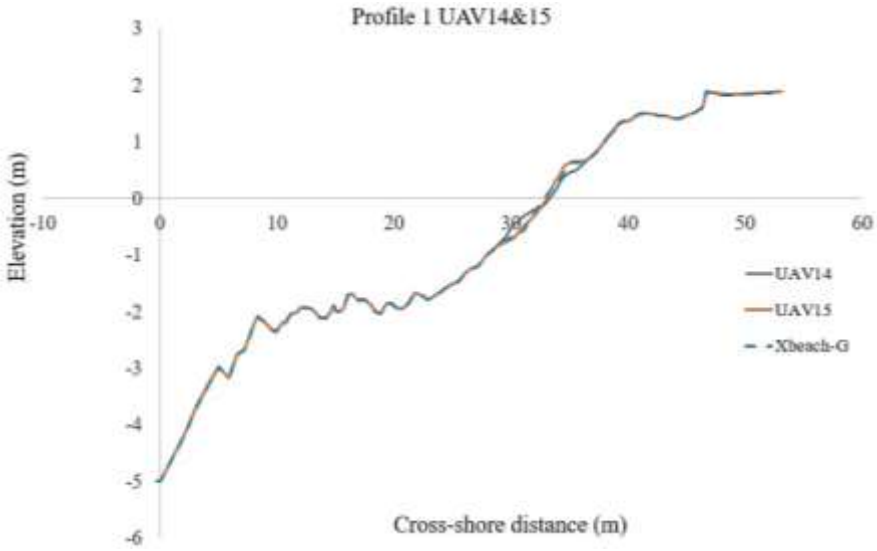

Figure 5. Modeled (dashed blue line) and measured (blue line before the storm event and orange line after the storm event) profiles using parameters resulting from the highest BSS for the UAV14&15 field survey at one profile (Φ=55°, γ=0.5)

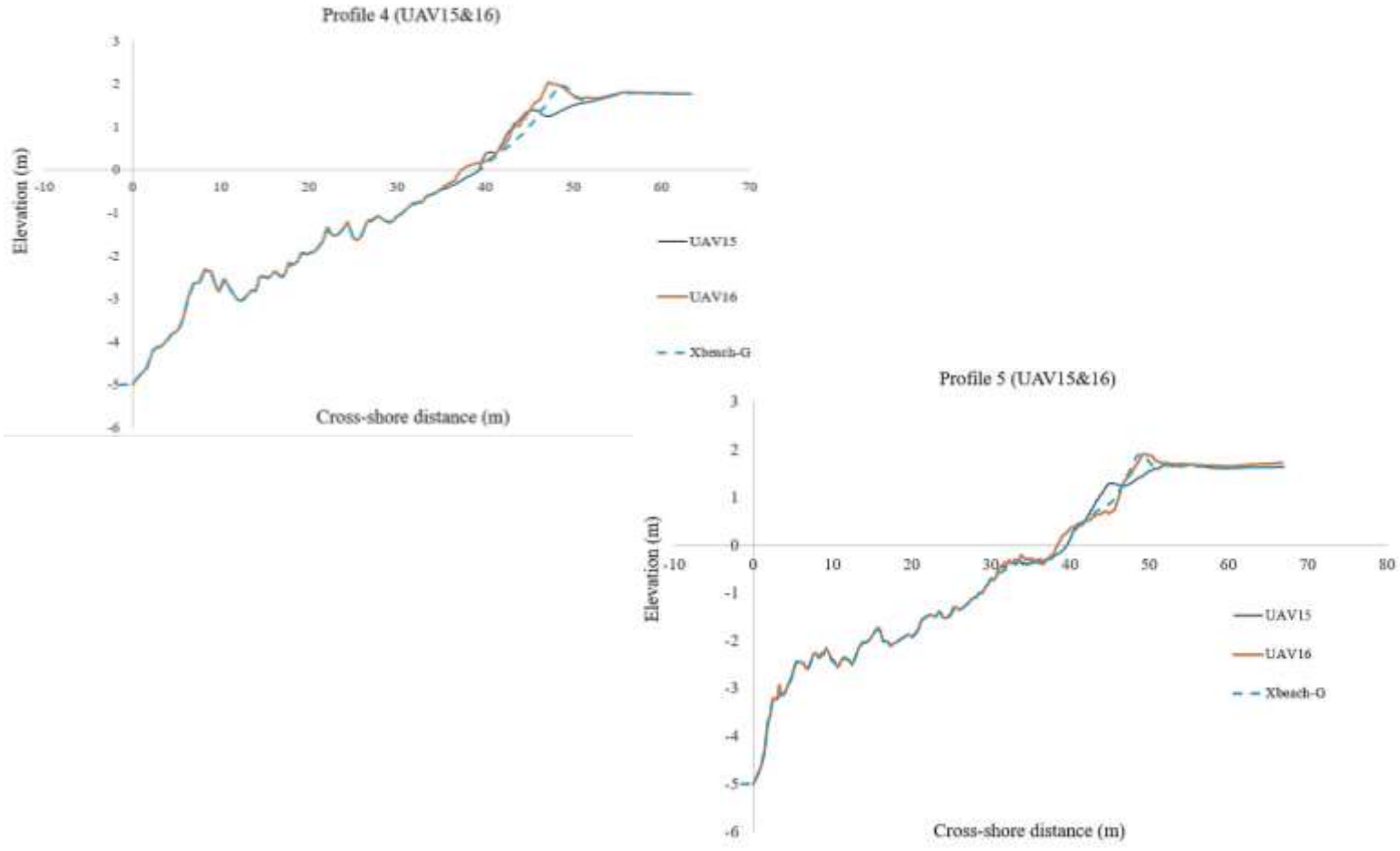

Figure 6. Modeled (dashed blue line) and measured (blue line before the storm event and orange line after the storm event) profiles using parameters resulting from the highest BSS for the UAV15&16 field survey at two profiles (Φ=35°, γ=3)

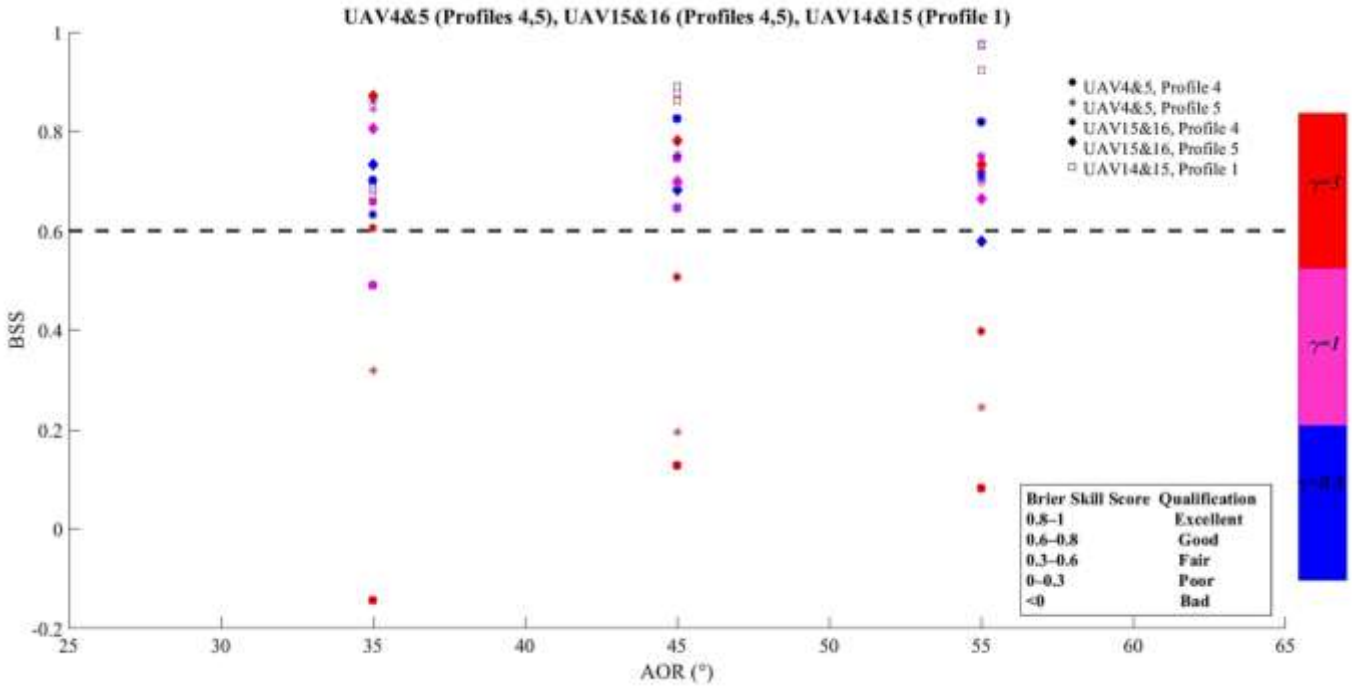

Figure 7. Relationship between angle of repose (Φ), Brier skill score, and transport coefficient (γ) for three storm events on different beach profiles

5 Conclusion

This paper presents the calibration of the numerical model Xbeach-G for low-energy wave events typical of Croatian beaches. Previous studies have shown that high-energy wave events can be simulated with a high BSS value of 0.75 without site-specific calibration, and the authors [2] have also found that the BSS value of low-energy events can be acceptable if a site-specific calibration of the model is performed [13]. The model is calibrated by simulating the morphodynamic response of the Ploče artificial gravel beach to 3 separate storm events at 3 different beach profiles. Calibrated parameters are angle of repose and sediment transport coefficient (Φ- 35°,45°,55° & γ-0.5, 1, 3). The results of the calibration show that XBeach-G can be used for the simulation of beach profile changes due to storm events on the eastern Adriatic coast. In addition, Xbeach-Gravel is relatively easy to use and faster than full 3D models. These model characteristics, together with the model's ability to simulate wave events on the Adriatic Sea as demonstrated in this paper, make the model a potential tool for beach management decisions prior to re-nourishment projects or the construction of new artificial beaches.

Acknowledgements

This work has been fully supported by the "Research Cooperability" Program of the Croatian Science Foundation funded by the European Union from the European Social Fund under the Operational Programme Efficient Human Resources 2014-2020.

References:

[1] Pikelj, K., Ružić I., Ilić S., James M.R., Kordić B.: Implementing an efficient beach erosion monitoring system for coastal management in Croatia, Ocean and Coastal Management, 156, pp. 223-238, 2017.

[2] McCall, R.T.; Masselink, G.; Poate, T.G.; Roelvink, J.A.; Almeida, L.P.: Modelling the

morphodynamics of gravel beaches during storms with XBeach-G, Coast. Eng., 103, pp. 52–66, 2015.
[3] Bradbury, A., Powell, K.A., The short-term profile response of shingle spits to storm wave action, 23th International Conference on Coastal Engineering, pp. 2694-2707, 1992.
[4] Carter, R.W.G., Orford, J.D.: Overwash processes along a gravel beach in South-East Ireland, Earth Surf. Process. Landf., 6, pp. 413-426, 1981.
[5] Orford, J.D.: A proposed mechanism for storm beach sedimentation, Eart Surf. Process. 2, pp. 381-400, 1977.
[6] Orford, J.D., Anthony, E.J.: Extreme events and the morphodynamics of gravel dominated coastal barriers: Strengthening uncertain ground, Mar. Geol. 290, pp. 41-45, 2011.
[7] Orford, J.D., Jennings, R., Pethick J.: Extreme storm effect on gravel dominated barriers, Proceedings of the International Conference on Coastal Sediments, 2003.
[8] Powell, K.A., Predicting short term profile response for shingle beaches, Tech. rep., HR Wallingford SR report 219, 1990.
[9] Masselink, G., McCall, R., Poate, T., van Geer, P.: Modelling storm response on gravel beaches using XBeach-G., Proc. ICE Marit. Eng. 167, pp. 173-191, 2014.
[10] Ministry of Tourism, 2013. Croatian Tourism Development Strategy until 2020. Official Gazzete of the Republic of Croatia 55/2013.
[11] McCall, R., Masselink, G., Poate, T., Bradbury, A., Russel, P., Davidson, M.: Predicting overwash on gravel barriers, Journal of Coastal Research Special Issue No. 65 Proceedings 12th International Coastal Symposium, pp. 1473-1478, 2013.
[12] Van Rijn, L. Sutherland, J.: Erosion of gravel beaches and barriers, Proceedings of the Coastal Sediments, World Scientific Publishing Co., Inc., Miami, 2011.
[13] Bogovac T., Carević D., Bujak D., Miličević H.,: Application of the XBeach-Gravel model for the case of east Adriatic Sea-wave conditions, J. Mar. Sci. Eng., 11, 2023.
[14] Bergillos, R.J., Masselink, G., Ortega-Sánchez, M.: Coupling Cross-Shore and Longshore Sediment Transport to Model Storm Response along a Mixed Sand-Gravel Coast under Varying Wave Directions, Coast. Eng. 129, pp. 93–104, 2017.
[15] Grottoli, E., Bertoni, D., Ciavola, P.:Short- and Medium-Term Response to Storms on Three Mediterranean Coarse-Grained Beaches. Geomorphology 295, pp.738–748, 2017.
[16] Roelvink, J.A., Reniers, A., van Dongeren, A.R., van Thiel de Vries, J.S.M., McCall, R., Lescinski, J.: Modeling storm impacts on beaches, dunes and barrier islands, Coast. Eng. 56, pp. 1133–1152, 2009.
[17] Tadić, A., Ružić, I., Krvavica, N., Ilić, S.: Post-nourishment changes of an artificial gravel pocket beach using UAV imagery, J. Mar. Sci. Eng. 10, 2022.
[18] Bujak, D., Miličević, H., Carević, D., Ilić, S.: Beach area evolution of an artificial gravel pocket beach using video monitoring system, Coastal and Offshore Science and Engineering 3, pp. 14-29, 2023.
[19] Modelling shingle beaches in bimodal seas, https://coastalmonitoring.org/ccoresources/shingleb/, 01 Dec 2016
[20] Brown, S.I., Dickson, M.E., Kench, P.S., Bergillos, R.J.: Modelling gravel barrier response to storms and sudden relative sea-level change using XBeach-G, Mar. Geol. 410, pp.164-175, 2019.
[21] van Rijn, L.C., Walstra, D.J.R., Grasmeijer, B., Sutherland, J., Pan, S., Sierra, J.P.: The predictability of cross-shore bed evolution of sandy beaches at the time scale of storms and seasons using process-based profile models, Coastal Engineering 47, pp. 295-327, 2003.

EFFECT OF DIFFERENT METHODS ON THE MANNING´S ROUGHNESS COEFFICIENT DETERMINATION FOR THE CLOSE TO NATURE FISH PASS

LEA ČUBANOVÁ [1], JÁN RUMANN [1], PETER DUŠIČKA [1]

[1] *Faculty of Civil Engineering STU in Bratislava, Radlinského 2766/11, 810 05 Bratislava, Slovak Republic, lea.cubanova@stuba.sk, jan.rumann@stuba.sk, peter.dusicka@stuba.sk*

1 Abstract

Determining Manning's roughness coefficient for a fish pass channel can be challenging. To achieve the desired depths and velocities, it may lead to serious overestimation its values. Measurements of hydraulic parameters were conducted in selected fish passes, and photographs of channel bed were taken for grain size analysis. The ImageJ analysis software was used for the determination of the grain distribution curves from the photographs. Roughness coefficients were analysed using various approaches (empirical relationships, Cowan's method, the step-by-step method). The obtained values indicate a considerable dispersion of the Manning's roughness coefficient.

Keywords: fish pass, in situ measurement, grain size distribution curve, image-processing procedure, Manning’s roughness coefficient

2 Introduction

Close-to-nature fish passes represent an ecological approach to enhance fish migration in river systems while maintaining longitudinal connectivity and passability. They imitate the natural environment of the stream, incorporating elements such as rocks, boulders, and vegetation to create conditions for migration of ichthyofauna. One of the key advantages of close-to-nature fish passes is their ability to accommodate a wide range of fish species with varying swimming capabilities. Research [1, 2] has shown that close-to-nature fish passes can significantly improve fish passage efficiency compared to conventional fish passes and demonstrated higher passage rates and reduced stress levels among fish, highlighting the effectiveness of these structures in promoting successful migration.

To design a fish pass mimicking the natural stream environment and enabling fish to move upstream and downstream more naturally, reflecting the conditions found in the watercourse is complicated. In this type of fish pass, water flow is guided by natural elements such as single stones, also known as perturbation boulders. These boulders serve to create rest areas or flow shadows (refuges), decrease velocities and enhance water depths [3]. And therefore, determination of the Manning´s roughness coefficient for such type of river bed can be difficult. Manning's roughness coefficient is a crucial parameter in hydraulic calculations for open channels and it is only parameter which is modified when using simple equations of hydraulics during the fish pass design process to achieve required depths and velocities.

Manning's roughness coefficient considers the roughness of the surface of the stream and helps to determine its resistance. The value of the coefficient is usually determined empirically based on experiences, equations or experiments. Its value depends also on the hydrology (water level position) and season (vegetation, ice) [4, 5, 6]. Roughness coefficients can be analyzed using various approaches, including empirical relationships based on the characteristic diameter of the grain of the river bed, Cowan's method, and the step-by-step method from the measured hydraulic characteristics of the profiles. The values of the Manning's roughness coefficient obtained by different approaches show a considerable dispersion.

3 Methods

For the purpose of studying the roughness coefficient, newly constructed nature-like fish passes were selected, visually resembling their natural environments. The first fish pass on the Hron River belongs to the barbel zone, while the second one on the Turiec River is located in the grayling zone (Figure 1). Both fish pass channels are constructed using river stones embedded in concrete, overlaid with gravel, and incorporating single/perturbation boulders, although they are intended to be operated at different hydraulic parameters (depths, widths, velocities, etc.), depending on the target fish species.

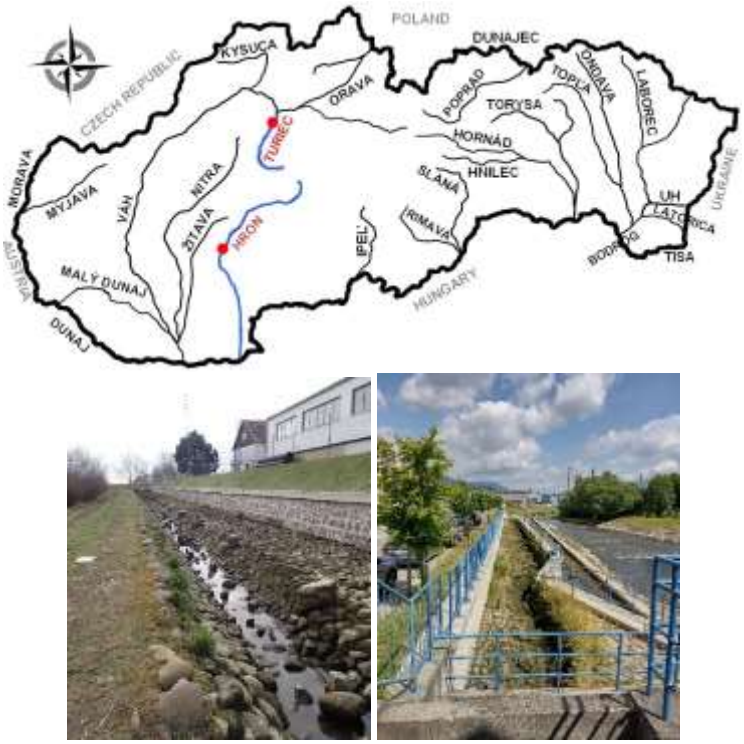

Figure 1. Location and pictures of the fish passes during maintenance on the Hron River (left) and on the Turiec River (right)

The evaluation of the roughness coefficient was done based on Cowan´s method, the optical granulometric method, in-situ measurements and values from tables. Photographs of the channel bed were taken during the maintenace period at the fish passes at selected locations, and during the operation period, the hydraulic and geometric characteristics of the channel were measured in the same locations (Figure 2).

Figure 2. Measuremets locations at the fish passes – on the Hron River (up) and on the Turiec River (down)

3.1 Cowan´s method

Cowan's method (Eq (1)) expresses the roughness determination procedure according to the subjective judgment of the verbal description of six characteristic parameters of the riverbed (Figure 3, Table 1). This method was derived from measurements of small and medium drainage channels and small natural streams with a hydraulic radius R < 4.5 m. The resulting roughness coefficient is calculated according to the equation [7]:

$$n = (n_0 + n_1 + n_2 + n_3 + n_4)m_5 \quad (1)$$

Where: n_0 – influence of the river bed material (–),
n_1 – influence of the surface irregularity (–),
n_2 – the effect of the change in the cross-sectional profile (–),
n_3 – relative influence of obstacles (–),
n_4 – influence of vegetation (–),
m_5 – degree of channel curvature (–).

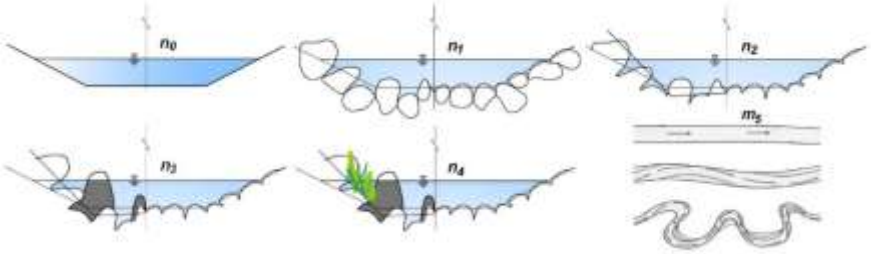

Figure 3. Illustration of individual effects of each parameter from Eq. (1) [8]

Table 1. Characteristics of the riverbed necessary for the calculation of the Eq. (1) of the Cowan´s method [9]

MATERIAL OF THE RIVER BED (GRAIN SIZE OF THE SUBSTRATE)	**n_0**
soil	0.020
bedrock	0.025
fine gravel	0.024
coarse gravel	0.028
stones	0.030 – 0.050
boulders	0.040 – 0.070
IRREGULARITY OF THE SURFACE	**n_1**
smooth trough	0.000
small (weakly eroded or deepened)	0.005
medium (weak sliding)	0.010
large (landslides, eroded banks, rocky protrusions)	0.020

VARIABILITY OF THE SHAPE OF THE FLOW PROFILE CAUSING TURBULENCE	n_2
change is happening slowly	0.000
occasional changes from large to small or the current wavering from bank to bank	0.005
frequent changes	0.010 – 0.015
EFFECTS OF OBSTACLES (TREES, ROOTS, BOULDERS)	n_3
negligible (a few scattered obstacles)	0.000
small (obstacles are isolated, occupying 15 % of the area)	0.010 – 0.015
substantial (connection of obstacles that occupy 15 – 50 % of the area)	0.020 – 0.030
large (obstacles cover > 50 % of the area or cause turbulence over most of the area)	0.040 – 0.060
VEGETATION	n_4
no or no effect	0.000
flexible seedlings or dense grass/macrophytes	0.005 – 0.010
shrub vegetation, no vegetation at the bottom of the channel, macrophytes reaching the entire depth of the flow	0.010 – 0.025
young trees with a growth of grasses and herbs, macrophytes twice the depth of the flow	0.025 – 0.050
brushy growth on the bank, dense growth in the riverbed, trees with a growth of grasses and herbs, fully leafed	0.050 – 0.100
CURVATURE	m_5
small (curvature 1.0 – 1.2)	1.00
substantial (1.2 – 1.5)	1.15
large (> 1.5)	1.30

3.2 The grain size distribution curve

The grain size distribution curve, also known as the particle size distribution curve, is a graphical representation of the range of particle sizes present in a sediment or soil sample. Using the sieve method the granulometry of the sample is determined. The curve illustrates either the amount of material that passes through or is retained on each sieve. It plots the percentage of particles by weight that are smaller than a given particle size on the vertical axis against the particle size on the horizontal axis. The curve is very practical as data set for many calculations or assessments, e.g. prediction of the soil water movement, sedimentation processes in open channels, design of filters in dams, calculation of hydraulic conductivity, seepage through dams etc.

A more efficient approach to determine the grain size distribution curve is through the photographic method, known as optical granulometry. This method relies on low water levels and is particularly suitable for gravel-like sections of streams or reservoirs, offering sufficient accuracy for practical applications. By focusing on the granulometric composition of the upper active layer of the bed material, which directly interacts with flowing water, it provides valuable insights from a hydraulic perspective. The optical granulometry operates under the assumption that the percentage distribution of mass among individual fractions mirrors the percentage distribution of surface area among those same fractions. The surface area of each fraction is extrapolated from a photograph of the intact bottom material [10]. The automated grain size analysis procedure involves digital image processing techniques to automatically identify and measure individual grains in sediment samples [11, 12].

The input data consists of an image of the sediment deposit captured by a digital camera. Samples are collected from riverbanks during low water conditions when the sediment is sufficiently exposed and by the good light conditions [13, 14]. The ImageJ software is a widely-used powerful and versatile tool for grain size analysis from images. For grain size analysis it uses segmentation of the image of the sediment sample into individual particles or grains based on user-defined criteria such as size, shape, and grayscale intensity (pre-processing steps such as thresholding to distinguish sediment particles from the background). Once the particles are segmented, various morphological parameters for each particle can be calculated (identification and measurement of the properties of individual particles within the image). The software can handle a wide range of sediment types and particle shapes, making it suitable for analyzing diverse sediment samples from various environments. The samples are computerized to obtain a grain size distribution curve from which the grain diameter needed for the empirical formulas to determine the coefficient of roughness could be subtracted.

3.3 Equations based on the characteristic grain diameter

Empirical equations based on the characteristic grain diameter play a crucial role in various fields, particularly in geology, hydrology, and sediment transport studies, but they are widely utilized in the determination of Manning's roughness coefficient in open-channel flow calculations [15]. These equations establish relationships between the size of sample grains and the roughness of channel river beds (Table 2), providing a means to estimate Manning's coefficient based on sediment properties [7]. Many of these equations for the roughness coefficient *n* are generally based on the Strickler formula and modified usign different constant *a*, grain diameter *d* and exponent *x* [16]:

$$n = \frac{1}{a} d^x \tag{2}$$

Where: a – constant (–),
d – the characteristic grain diameter of the material (m),
x – exponent (–).

Table 2. Strickler´s formula (Eq (2)) modified by various authors [15, 16]

AUTHOR	a	d	unit for d	x (exponent)
PIRKOVSKÝ	19.40	d_e	(m)	1/6 = 0.167
ANONYM	38.15	d_{50}	(m)	1/6 = 0.167
BRAY	16.86	d_{50}	(m)	1/5.6 = 0.179
GARDE, RAJU	21.30	d_{50}	(m)	1/6 = 0.167
HENDERSON	29.40	d_{50}	(ft)	1/6 = 0.167
KEULEGAN	25.30	d_{50}	(m)	1/6 = 0.167
MATTAS	10.31	d_{50}	(m)	1/5.1 = 0.196
STRICKLER	24.40	d_{50}	(m)	1/6 = 0.167
BRAY	17.83	d_{65}	(m)	1/5.6 = 0.179
IRMAY	24.00	d_{65}	(m)	1/6 = 0.167
RAUDKIVI	76.90	d_{65}	(mm)	1/6 = 0.167
HENDERSON	26.31	d_{75}	(m)	1/6 = 0.167
LANE, CARLSON	21.14	d_{75}	(m)	1/6 = 0.167
MATTAS	8.70	d_{84}	(m)	1/2.7 = 0.376
BRAY	20.20	d_{90}	(m)	1/6.3 = 0.160
IRMAY	40.20	d_{90}	(m)	1/6 = 0.167
MAYER-PETER, MÜLLER	26.00	d_{90}	(m)	1/6 = 0.167

3.4 Standard step method for non-uniform flow

The values of the roughness coefficient *n* can also be derived from the common open-channel hydraulics equation, known as the step-by-step method, using data from in-situ measurements such as cross-sectional area, wetted perimeter, hydraulic radius, discharge, and water level, as follows (in this form loss coefficient is considered as zero) [17]:

$$n = \sqrt{\frac{\Delta y - Q^2 \frac{\alpha}{2g}\left(\frac{1}{A_1^2} - \frac{1}{A_2^2}\right)}{l}} \cdot \frac{A_{average}}{Q} \cdot R_{average}^{2/3} \tag{3}$$

Where: Δy – water levels difference of neighbouring profiles (m),
Q – value of the measured discharge ($m^3 \cdot s^{-1}$),
α – coefficient expressing the uneven distribution of velocity in the profile (α = 1.1) (–),
g – gravity acceleration ($m \cdot s^{-2}$),
A_1, A_2 – flow area of the downstream and upstream profile (m^2),
l – the length of the section between the downstream and upstream profile (m),
$A_{average}$ – mean value of the flow area (m^2),

$R_{average}$ – mean value of the hydraulic radius (m).

4 Results and discussion

Based on the sample pictures of the river bed material of the fish passes (Figure 4), the grain size distribution curves were obtained (Figure 5). These curves were used to determine the required diameters of the grains of the river bed material and to calculate the Manning's roughness coefficient (Table 3, Figure 6) using the Strickler formula (Eq (2)), which has been modified by different authors (Table 2). For comparison, values obtained using Cowan's method (Eq (1)) and from commonly used tables are also provided.

Figure 4. Samples of the river bed material – left fish pass on the Hron River, right on the Turiec River

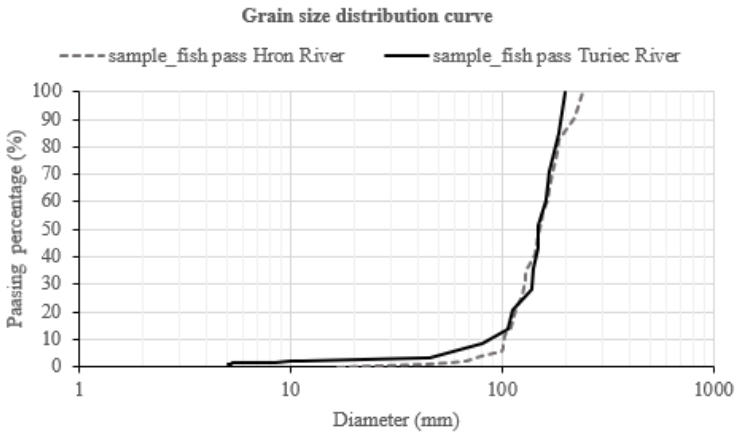

Figure 5. Grain size distribution curves for fish passes on the Hron and Turiec Rivers

Table 3. Manning´s roughness coefficient values by different authors

AUTHOR	SAMPLE – FISH PASS HRON RIVER		SAMPLE – FISH PASS TURIEC RIVER	
	d_i (mm)	n (–)	d_i (mm)	n (–)
PIRKOVSKÝ	d_e = 103	0.0353	d_e = 89	0.0344
ANONYM	d_{50} = 151	0.0191	d_{50} = 148	0.0191
BRAY	d_{50} = 151	0.0423	d_{50} = 148	0.0421
GARDE, RAJU	d_{50} = 151	0.0343	d_{50} = 148	0.0341
HENDERSON	d_{50} = 151	0.0303	d_{50} = 148	0.0302
KEULEGAN	d_{50} = 151	0.0288	d_{50} = 148	0.0287
MATTAS	d_{50} = 151	0.0670	d_{50} = 148	0.0667
STRICKLER	d_{50} = 151	0.0299	d_{50} = 148	0.0298
BRAY	d_{65} = 166	0.0407	d_{65} = 163	0.0405
IRMAY	d_{65} = 166	0.0309	d_{65} = 163	0.0308
RAUDKIVI	d_{65} = 166	0.0305	d_{65} = 163	0.0304
HENDERSON	d_{75} = 178	0.0285	d_{75} = 167	0.0282
LANE, CARLSON	d_{75} = 178	0.0355	d_{75} = 167	0.0351
MATTAS	d_{84} = 193	0.0620	d_{84} = 185	0.0610

BRAY	d_{90} = 217	0.0388	d_{90} = 190	0.0379
IRMAY	d_{90} = 217	0.0193	d_{90} = 190	0.0189
MAYER-PETER, MÜLLER	d_{90} = 217	0.0298	d_{90} = 190	0.0292

Since the grain size distribution curves of the river bed material of both fish passes are very similar (Figure 5), the calculated values of the Manning´s roughness coefficient are almost the same for both fish passes. The smallest values were obtained by the calculation according to Anonymous and Irmay (n = 0.0191 and 0.0193 for the fish pass on the Hron River, n = 0.0191 and 0.0189 for the fish pass on the Turiec River), while the maximum values are provided by the formula according to Mattas with d_{50}, namely n = 0.0670 for the fish pass on the Hron River and n = 0.0667 for the fish pass on the Turiec River. The average roughness value for the fish pass on the Hron River is n = 0.0355 and for the fish pass on the Turiec River is n = 0.0351.

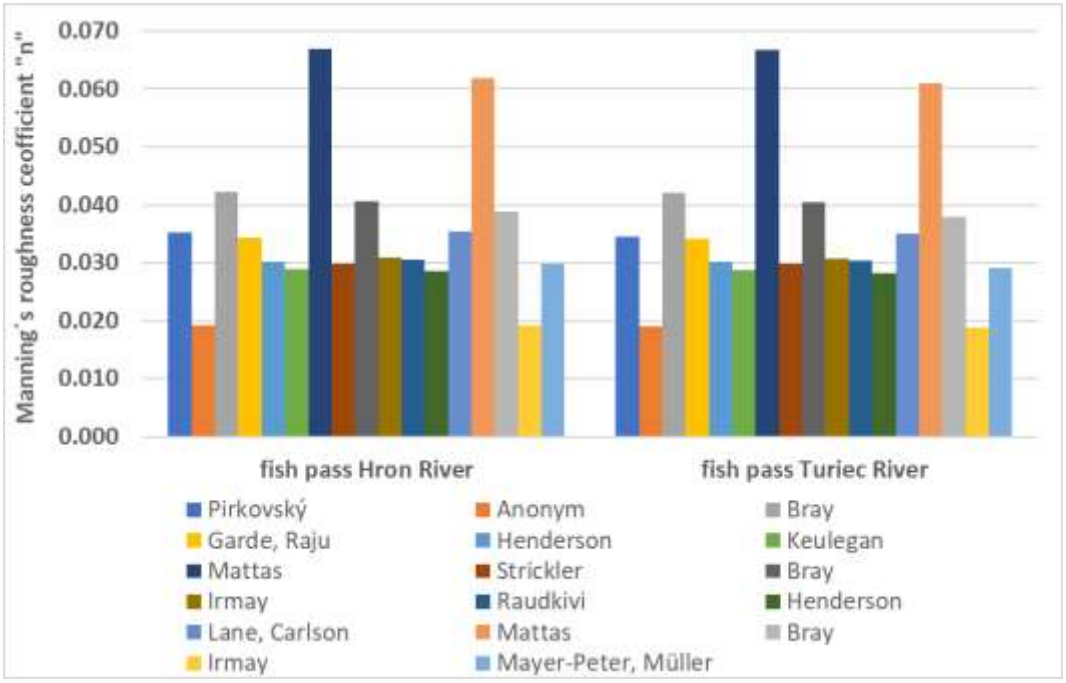

Figure 6. Graphical interpretation of the obtained results for Manning´s roughness coefficient based on Table 3.

Cowan's method is a systematic approach to estimate Manning's *n* by considering several factors contributing to roughness, while tabulated values provide empirical estimates based on typical conditions. Cowan's method involves summing up various components of roughness: base roughness, effects of surface irregularities, variations in shape and size, obstructions, and vegetation or flow conditions. Each component adds to the base roughness value, which might lead to a higher cumulative value compared to a single empirical estimate. The method is designed to ensure safety and robustness in engineering applications, often resulting in more conservative (higher) estimates of roughness to account for worst-case scenarios. Table values often represent an average condition, while Cowan's method can account for seasonal or temporary changes in channel conditions, such as increased vegetation in summer or debris during floods, which can increase the roughness coefficient. For the both fish passes the roughness coefficient was calculated using Eq (1) as follows:

$$n = (n_0 + n_1 + n_2 + n_3 + n_4)m_5 = (0.03 + 0 + 0 + 0.02 + 0) \cdot 1 = 0.050$$

Note: more variants were assessed (because there is a big range of values for parameters n_0 – n_4 and m_5), but the values are not presented here, they were noncomparable with roughness coefficients based on Strickler´s formula (Eq (2)) (they were significantly higher, in the range 0.070 – 0.695).

The best-known and most detailed tables are presented in work by Ven Te Chow in 1959 [18], where a numerical value is assigned to the verbal description of the riverbed or its material. These tables offer a comprehensive range of *n* values for various types of channels and surfaces, such as natural streams, lined channels, and floodplains, based on extensive field observations and measurements. Roughness coefficient estimation is highly subjective. For the fortified open channels with bottom covered by gravel and riprap on the banks, what correspodents to the environment of both fish passes, is value of roughness coefficient in the following range of n = 0.023 – 0.036 [15].
In situ measurements of the basic hydraulic and geometric characteristics of the cross sections in fish passes (Figure 7) (Q – discharge, WL – water level, v – velocity, A – cross sectional area, W – wetted perimeter, R – hydraulic radius, l – distance between cross sections, Δy – water level difference, i – water level slope) provided inputs for the calculation of the Manning´s roughness coefficient using step by step method modified in Eq (3) (Table 4).

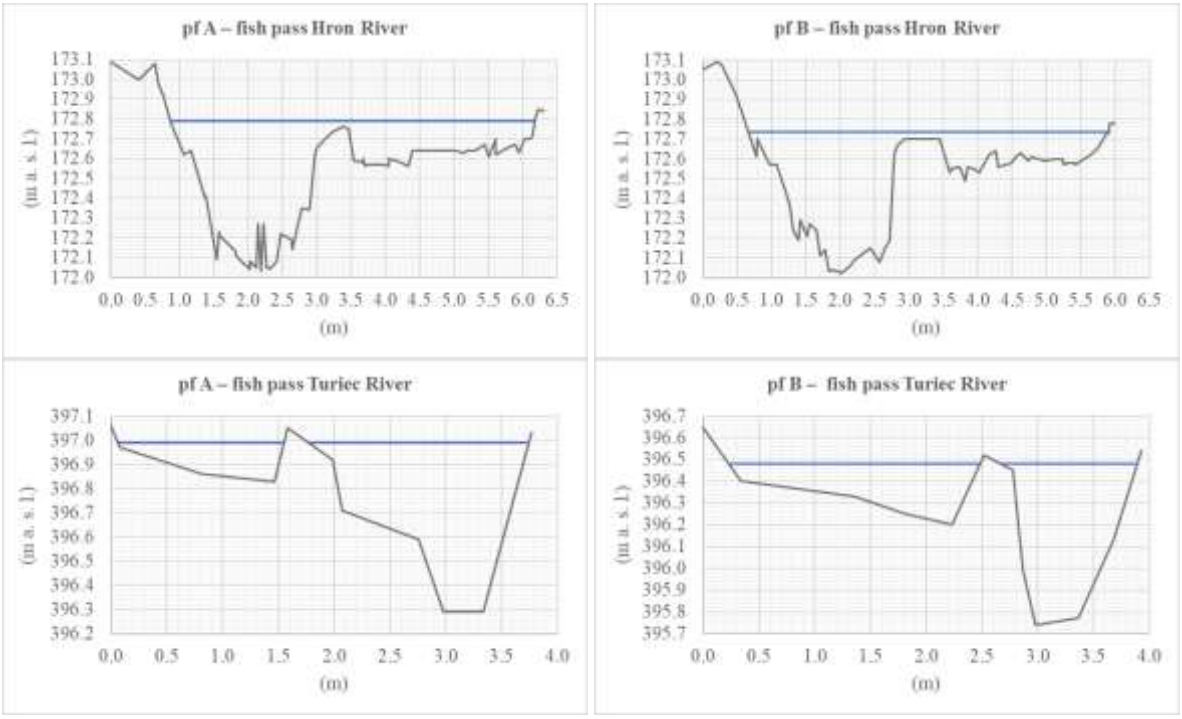

Figure 7. Measured cross sections on the fish passes – Hron and Turiec Rivers

Table 4. Measured data for cross sections on the fish passes and calculated Manning´s roughness coefficient

PARAMETER	UNIT	FISH PASS HRON RIVER		FISH PASS TURIEC RIVER	
		pf A	pf B	pf A	pf B
Q	($m^3 \cdot s^{-1}$)	1.25		0.875	
WL	(m a. s. l.)	172.79	172.74	396.99	396.48
v	($m \cdot s^{-1}$)	0.836	0.844	1.000	0.870
A	(m^2)	1.54	1.43	0.93	0.95
W	(m)	7.61	5.25	4.53	4.74
R	(m)	0.203	0.273	0.206	0.200
l	(m)	5.2		37.8	
Δy	(m)	0.053		0.51	
i	(–)	0.0102		0.0135	
$\mathbf{A_{average}}$	(m^2)	1.49		0.94	
$\mathbf{R_{average}}$	(m)	0.238		0.203	
n	(–)	**0.0435**		**0.0432**	

The value of the roughness coefficient calculated using the step-by-step method based on the measured parameters in both fish passes reached value n = 0.0435 for fish pass on the Hron River and n = 0.0432

for fish pass on the Turiec River. These values are higher than most empirical formulas and theoretical range for described environment of the fish passes based on Chow´s tables [18]. In contrast, Cowan's method yielded higher values, as did the empirical Mattas equation based on d_{50}. The best agreement was obtained with the empirical Bray formula (based on d_{50}), where n = 0.0423 and n = 0.0421, despite the fact that the equation is typically valid for gravel-bed rivers where the median grain size d_{50} ranges up to 128 mm [19]. It may not be accurate for very fine sediments (like silt or clay) or for very large boulders. However, the other conditions were met, such as uniform flow conditions (the controlled discharge Q into the fish pass is constant and we aimed to avoid highly turbulent or rapidly varied flow conditions in terms of fish pass hydraulics), additionally, there were no effects of bed forms (e.g., ripples, dunes) or vegetation.
Performing field measurements and comparing them with empirical based equations, with Cowan's method and with table values, provide a more accurate reference to adjust the estimated roughness coefficient. Using flow data from the site to calibrate the Manning's n value will ensure more accurate results, as were demonstrated on the presented results. However, since roughness also changes in relation to the longitudinal slope (with a steeper slope of the channel bottom, the roughness coefficient is also greater), and there are sections with different slopes in the fish passes, the roughness coefficient will likely vary from place to place in different parts of the fish passes.

5 Conclusion

The roughness coefficient value in natural streams is influenced by surface roughness, vegetation, bed irregularity, river bed ground plan, sedimentation and erosion, obstacles in the stream, size and shape of the river bed, water stage and flow, seasonal changes, or bed loads [14, 20, 21]. Empirical formulas assume uniform flow, which practically does not occur in natural conditions. However, in the case of a fish pass, even if close to nature, as described in this article, many influences on the roughness coefficient are excluded, or are different than in natural conditions. Whether it is the influence of vegetation, which is desirable but regulated, seasonality is also excluded, because in the fish pass is constant controlled discharge that increases only during migration periods, bed loads do not occur there, the erosion process is eliminated by the construction of the channel bed and irregularities of the river bed are negligible. The most serious is the effect of surface roughness (due to pebbles placed in the concrete) and obstacles formed by solitary/single/perturbation boulders. The flow is steady non-uniform.

Therefore, the research focused on determination of the Manning's roughness coefficient using different approaches, such as Cowan's method, commonly used tables, empirical formulas based on the diameter of the grains determined from the grain size distribution curves, and data from in situ measurements of the hydraulic characteristics of the fish pass riverbed. These methods were used for comparison. The next step in the process will be to verify the obtained values of Manning's roughness coefficient using 1D and 2D mathematical models of the investigated fish passes. This step is important to determine the reliability and applicability of the empirical equations in determining the roughness coefficient during the design phase and hydraulic calculations of new fish passes.

Acknowledgements
This contribution was developed within the framework and based on the financial support of the APVV-20-0023 and the APVV-23-0447 projects.

References:
[1] Raabe, J. K., Hightower, J. E., Ellis, T. A., Facendola, J. J.: Evaluation of Fish Passage at a Nature-Like Rock Ramp Fishway on a Large Coastal River, Trans. Am. Fish. Soc., 148, pp. 798-816, 2019.
[2] Mameri, D., Rivaes, R., Ferreira, M. T., Schmutz, S., Santos, J. M.: Climate Change Effects on Fish Passability across a Rock Weir in a Mediterranean River, Water, 13, 2758, 2021. https://doi.org/10.3390/w13192758
[3] FAO/DVWK: Fish passes – Design, dimensions and monitoring, Rome, FAO, 2002.

[4] Schügerl, R., Velísková, Y.: Change of the Manning´s coefficient in small stream influenced by vegetation, Acta Hydrologica Slovaca, vol. 24, no. 1, ISSN 2644-4690, pp. 134-140, 2023. https://doi.org/10.31577/ahs-2023-0024.01.0015
[5] Schügerl, R., Velísková, Y.: Effect of aquatic vegetation on Manning´s roughness coefficient value – case study at the Šúrsky channel, Acta Hydrologica Slovaca, vol. 21, no. 1, ISSN 2644-4690, pp. 123-129, 2020. DOI: 10.31577/ahs-2020-0021.01.0015
[6] Velísková, Y., Dulovičová, R., Schügerl, R.: Impact of vegetation on flow in a lowland stream during the growing season, Biologia, Section Botany, 72/8, pp. 840-846, 2017. DOI: 10.1515/biolog-2017-0095
[7] Smelík, L.: Návrh metodiky stanovení součinitele drsnosti otevřených koryt, Dizertačná práca, Brno,Vysoké učení technické v Brne, Fakulta stavební, Ústav vodních staveb, 2015.
[8] Laiho, D.: Session A6- Mannings "n" roughness characteristic occurring in semi-smooth turbulent flow of nature-like fishways, International Conference on Engineering and Ecohydrology for Fish Passage, Jun 28th 2011, pp. 1-27, 2011.
[9] Polák, V., Druga, V., Kubala, M., Andreji, J., Pekárik, L., Škrinár, A., Macková, M., Čiampor, F., Holubová, K., Abaffy, D., Čomaj, M. et al.: Metodika spriechodňovania priečnych bariér na vodných tokoch pre ichtyofaunu. Projekt číslo: 21501; Názov projektu: „Tvorba metodík a koncepčných materiálov, ITMS 2014+: NFP310010BAZ7“, Materiál 4: Revízia metodického usmernenia „Určenie vhodných typov rybovodov podľa typológie vodných tokov“ a jeho doplnenie o najnovšie poznatky (rok vydania 2015), Číslo revízie: 1/2023. VÚVH, Bratislava, 2023.
[10] Raplík, M., Macura, V.: Analýza granulometrie štrkopieskových korýt fotografickou metódou, Odborný seminár: Prúdenie povrchovej vody a jeho účinky na prostredie, Zborník referátov, Katedra hydrotechniky SvT SVŠT Bratislava, Odd. hydrauliky povrch. tokov ÚHH SAV, Bratislava, Tatranská Štrba – Meander, pp. 31-38, 1983.
[11] Diepenbroek, M., Bartholoma, A., Ibbeken, H.: How round is round? A new approach to the topic ‘roundness’by Fourier grain shape analysis, Sedimentology, Vol. 39, No. 3, pp. 411-422, 1992.
[12] Diepenbroek, M., De Jong, C.: Quantification of textural particle characteristics by image analysis of sediment surfaces - examples from active and paleo-surfaces in steep, coarse-grained mountain environments, Ergenzinger P., Schmidt K. H. (Eds) Dynamics and Geomorphology of Mountain Rivers, Lecture Notes in Earth Sciences, Springer, Vol. 52, pp. 301-314, 2007.
[13] Graham, D. J., Reid, I., Rice, S. P.: Automated sizing of coarse-grained sediments: Image-processing procedures, Mathematical Geosciences, Vol. 37, No. 1, pp. 1-28, 2005.
[14] Otsu, N. A.: Threshold selection method from gray-level histograms, IEEE Transactions on Systems, Man, and Cybernetics, Vol. 9, No. 1, pp. 62-66, 1979.
[15] Mattas, D.: Výpočet průtoku v otevřených korytech, Práce a studie, sešit 205, Výzkumný ústav vodohospodářský T. G. Masaryka, Praha, ISBN 978-80-87402-27-6, ISSN 1211-3727, 2014.
[16] Maňák, P.: Manningův drsnostní součinitel, Seminární práce z předmětu Morfologie a říční inženýrství, Praha, České vysoké učení technické v Praze, 2017.
[17] Dušička, P., Květon, R.: Kanálové vodné elektrárne – hydraulický výskum prevádzky derivačných kanálov, Základný hydraulický výskum, STU v Bratislave v Nakladateľstve STU, Bratislava, ISBN 978-80-227-4326-6, 2015.
[18] Chow, V. T.: Open-Channel Hydraulics, McGraw-Hill, 1959.
[19] Coon, W. F.: Estimation of Roughness Coefficients for Natural Stream Channels with Vegetated Banks, Water Supply Paper 2441, U. S. Department of the Interior, U. S. Geological Survey, Prepared in cooperation with the New York State Department of Transportation, ISBN 0-607-88701-X, 1998.
[20] Kim, Ji-Sung, Lee, Chan-Joo, Kim, Won, Kim, Yong-Jeon: Roughness coefficient and its uncertainty in gravel-bed river, Water Science and Engineering, Vol. 3, No. 2, pp. 217-232, 2010. doi: 10.3882/j.issn.1674-2370.2010.02.010
[21] Warnke, G. A.: Comparing methods for estimating Manning´s roughness coefficient on a portion of the South Fork of Chester Creek, A Project Submitted in Partial Fulfillment of the Requirements for the Degree of Master of Science in Civil Engineering, University of Alaska Anchorage, 2018.

ANALYSIS OF EXPERIMENTAL FLOW VELOCITY DATA UNDER MOBILE BED CONDITIONS NEXT TO BRIDGE PIER

GORDON GILJA [1], LUKA OPAČAK [1], ANTONIJA HARASTI [1], MANOUSOS VALYRAKIS [2]

[1] University of Zagreb Faculty of Civil Engineering, Croatia, gordon.gilja@grad.unizg.hr

[2] Department of Civil Engineering, Aristotle University of Thessaloniki, Greece, mvalyra@civil.auth.gr

1 Abstract

Bridge piers in rivers locally alter flow conditions in their vicinity, inducing scour and exposing bridge elements to increased loads that can lead to bridge failure. This research was conducted in hydraulic flume set up for bridge scour experiments, aiming to collect flow data relevant for scour development. The bridge pier was placed in the erodible bed and protected with a riprap sloping structure, focusing on flow conditions associated with mobile bed. Combinations of flow rates and flow depths were selected to include the incipient motion condition and above, targeted to collect the difference in near-bed flow that transports bed sediment downstream. Experimental data was measured using the Acoustic Doppler Velocity Profiler in the bed vicinity with 1mm resolution and 100Hz frequency over the 12 min duration. The aim of the paper is to investigate the higher order turbulence statistics (turbulent kinetic energy and Reynolds stresses) and the bed elevation change in the near-bed region.

Keywords: erosion, flume, bridge scour, turbulent kinetic energy, Reynolds shear stress

2 Introduction

Bridges built across rivers are influenced by the natural morphological development of the river channel, including erosion, deposition, and subsequent lateral migration of the channel. Bridge piers can directly influence the bed development in their vicinity, causing deposition of the scoured material in the pier shadow and subsequent morphological changes downstream. Highest rate of the morphological changes occurs during floods [1], which are considered to be most common cause of bridge failures worldwide [2]. All the aforementioned processes are intensified under climate change, exposing the existing bridges to higher loading and reducing their expected safety [3]. Since most of the large rivers in Croatia are free flowing, with regulated and consequently shortened and confined main channels, they are mostly affected by erosion [4]. Therefore, it can be considered that many bridges are vulnerable to scour, and at high risk of foundation undermining during floods [5]. Different scour countermeasures can be installed at bridge piers, tailored for the specific purpose depending on the on the flow characteristics, bridge geometry, cost, and environmental impact. Bridges can be locally protected from scour with larger stones, which in turn increases the turbulence and requires detailed flow investigation to evaluate the effect on the surrounding riverbed. In Croatia, most of the bridges over the large watercourses are protected with riprap sloping structure [6], a structure formed with a launchable stone shaped as a cone with slope approaching the angle of repose. While riprap sloping structure effectively reduces scour at the bridge pier, its effects on the downstream riverbed are unknown and scour estimation at these structures is not extensively researched. Considering the shape and size of the structure, the scour occurring at its toe will be induced by the turbulence downstream, instead of the downward flow and horseshoe vortices characteristic for the unprotected piers. Research on scour is mostly focused on the uniform pier geometry, symmetrical pier arrangement, and rarely on complex piers [7]. In the existing body of work on interaction of bridge piers with the flow, the critical areas of interest are the zones immediately downstream of the pier where the flow experiences intense turbulence [8]. It was shown that the turbulent structure patterns around piers are dominantly affected by the pier shape [9]. At the same time, the turbulent intensity in the near-bed region was found to be strongest, reducing with the

increasing distance from the bed [10]. Additional roughness elements were also found to have influence on the turbulence, resulting in higher Reynolds stress [11], which contributes to erosion and scour formation [12]. Riprap used as a scour protection next to bridge piers acts as an additional roughness element and can be designed using the near-bed turbulence intensity [13].
Understanding the flow characteristics and turbulent events at a threshold of motion is therefore crucial for understanding the scour development next to the riprap sloping structure. The aim of this study is to examine the influence of turbulence on bed deformation that would provide basis for the investigations of bed development downstream of the bridge piers protected with riprap sloping structure. The scour experiments are conducted for clear-water conditions to differentiate from other sediment transport mechanisms and provide information about local scour. However, once the bed development is initiated, flow acceleration/deceleration interacts with the bed and local turbulence governs erosion and deposition in the pier shadow. To investigate erosion/deposition on a small scale, at a single measurement point, flow rate was increased up to the incipient motion conditions which represent threshold of sediment entrainment. Turbulence was extracted from the direct velocity measurements, and compared with bed change rate to determine which events contribute to erosion and deposition.

3 Methods

A set of 5 experimental runs (Q1 ÷ Q5) combining different flow rates and flow depths was conducted using the recirculating hydraulic flume. The hydraulic conditions of the experiments correspond to the sediment transport threshold condition of the bed composition. Detailed turbulence at the incipient motion threshold conditions can be related to the critical flow conditions that lead to erosion and bed development. High frequency instantaneous velocity data can be used to extract turbulent events and bed deformation at a single point, measured using the high frequency velocimeter [14]. For this research flow velocity data was measured along the flume centerline using the acoustic Doppler velocimetry profiler Vectrino ADVP configured for the scour experiments [15,16]. The measurement setup was as follows:

- A single 30 mm high near-bed zone was selected for velocimetry measurement
- The measurement profile consisted of a series of 1 mm cells
- First measurement point is protruding below the initial bed to collect near-bed data
- Measurement duration was a total of 12 minutes
- Five combination of flow rates and flow depths was simulated

Flow profile was aligned with the position and size of the instrumented particle that will be used in subsequent experiments [17, 18]. The correlation of the Reynolds stress (RSS) and turbulent kinetic energy (TKE) with bed deformation for different flow rates close to the incipient motion threshold were analyzed to determine which events contribute to erosion and deposition. Velocity measurements are processed to obtain turbulence values with 100 Hz frequency, and calculate turbulent kinetic energy and Reynolds stress in the *uw* plane, using the following equations:

$$TKE = \frac{1}{2} \cdot (\overline{u'^2} + \overline{v'^2} + \overline{w'^2}) \quad (1)$$

$$RSS_{uw} = -\rho(\overline{u' \cdot w'}) \quad (2)$$

Where: *u*' – fluctuating component of the streamwise velocity *u* [mm/s]; *v*' – fluctuating component of the spanwise velocity *v* [mm/s]; *w*' – fluctuating component of the vertical velocity *w* [mm/s]; TKE - turbulent kinetic energy [mm^2/s^2]; RSS - Reynolds shear stress [mPa].

Results were evaluated through bed evolution and corresponding TKE and RSS_{uw} values over time. Bed evolution was calculated as absolute bed change in comparison with the in initial, undisturbed state. TKE and RSS data are calculated as semi-instantaneous values, averaged at 0.1 s intervals. Through

simultaneous analysis of this data changes in TKE and RSS as a direct result of bed deformation can be evaluated. Observing initiation of bed material transport as a series of interchanging erosion and bedload supply from the upstream allows to compare the differences between TKE and RSS for different bed conditions and identify the potential drivers of scour development.

4 Results and discussion

The initial flow rate Q1 was used as benchmark, where flow was gradually increased to threshold conditions, while the bed was immobile. Flow was gradually increased for subsequent flows until fully mobile bed conditions were achieved for Q5. When timeseries of TKE and bed development are plotted for the entire duration of the experiment (Figure 1), the following pattern can be observed. Following low TKE values for the immobile bed condition (0.001 m^2/s^2), when flow is increased to Q2 (Figure 1b) the initial bed deformation is observed where bed is perturbed, i.e. individual particles begin to move accompanied by the variability in the TKE (Figure 1a). Towards the end of the experiment, both the bed and TKE stabilize with an average value of +0.23 mm and 0.004 m^2/s^2, respectively. When flow rate increases to Q3 (Figure 1b), TKE doesn't change in comparison to the previous flow (0.003 m^2/s^2), while the bed level remains stable for the entire duration of the experiment at +0.07 mm over the immobile bed (Q1). After the bed has stabilized for the entire duration of the experiment, the flow was further increased to Q4 (Figure 1c). At this point significant bed erosion is initiated, and the bed is eroded -0.23 mm in comparison to the initial value. Bed erosion is accompanied by the increase in TKE values (0.019 m^2/s^2). Further increase of the flow rate to the Q5 (Figure 1d) results in additional bed erosion, where bed level is initially aggraded and afterwards abruptly eroded up to -12 mm. TKE trend shows continuous increase for the entire duration of the experiment, while the absolute value remains relatively high (0.007 m^2/s^2), but lower in comparison to Q4.

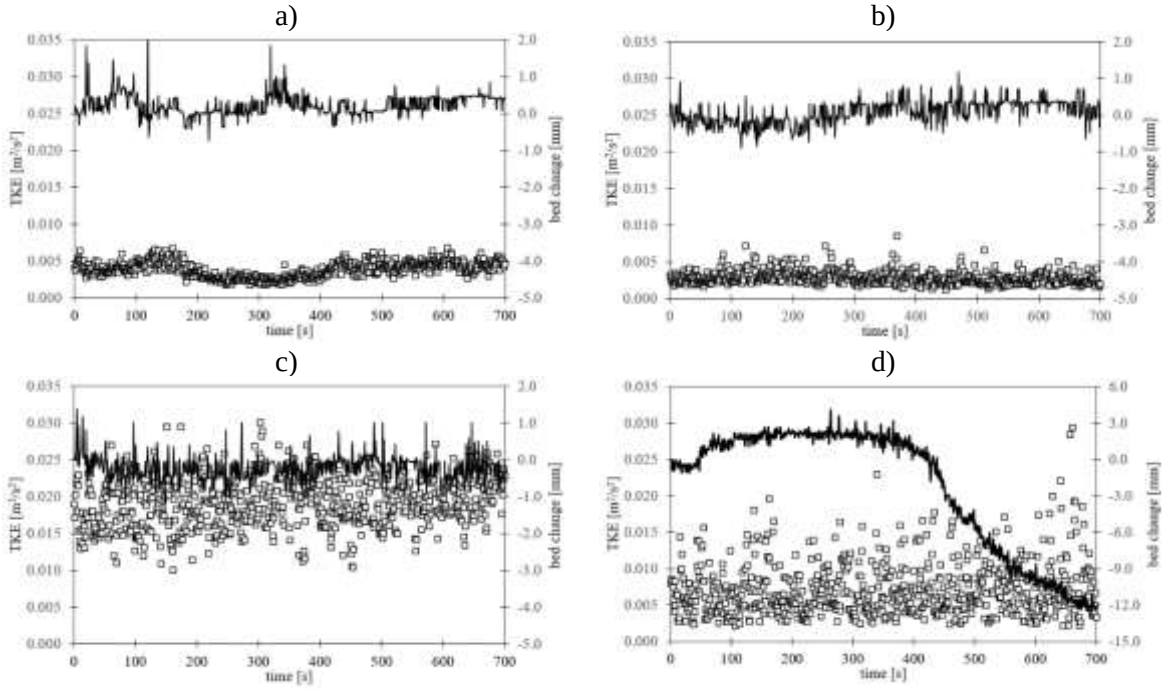

Figure 1. Bed evolution (full line) and TKE (square markers) over time for flow rates Q2 (a), Q3 (b), Q4 (c), and Q5 (d)

The analysis of the TKE and bed evolution trend was supplemented with the corresponding RSS analysis in the *uw* plane (Figure 2). For the immobile condition, the RSS_{uw} exhibits a different pattern from TKE, where RSS_{uw} values are relatively high, at 0.12 Pa on average. Flow increase to Q2 (Figure 2a) doesn't significantly change the RSS_{uw} value, and it remains unchanged on average, (0.11 Pa), but it can be seen

that significant proportion of the instantaneous values are negative. The same trend continues for Q3 (Figure 2b), where bed aggradation is accompanied by the large number of negative RSS_{uw} values, reducing an overall average to -0.02 Pa. Further increase of flow rate to Q4 (Figure 2c) and Q5 (Figure 2d) follows trend as expected –positive RSS_{uw} values are prevailing, and absolute values are increasing. The average RSS_{uw} value is 0.31 Pa and 1.32 Pa for Q4 and Q5, respectively.

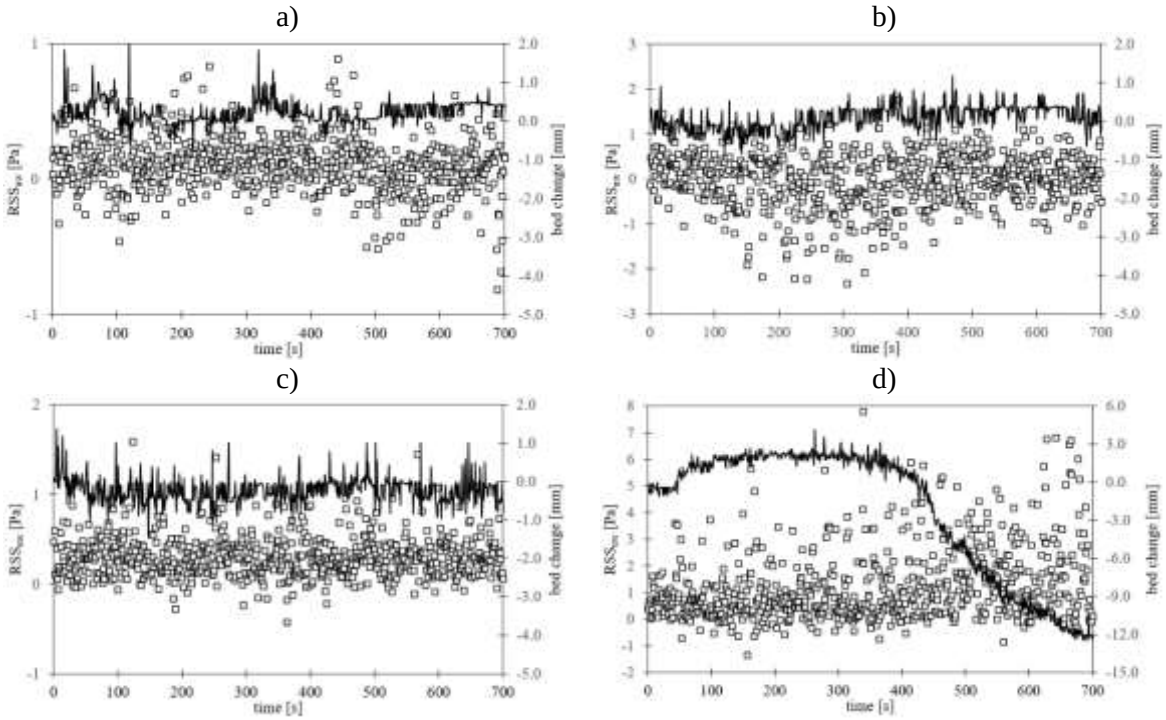

Figure 2. Bed evolution (full line) and RSS_{uw} (square markers) over time for flow rates Q2 (a), Q3 (b), Q4 (c), and Q5 (d)

5 Conclusion

This research was conducted in hydraulic flume set up for bridge scour experiments, aiming to collect flow data relevant for scour development. Combinations of flow rates and flow depths were selected to include the incipient motion condition and above, targeted to collect the difference in near-bed flow that transports bed sediment downstream. The influence of TKE and RSS on the bed material transport was evaluated through time series cumulative bed change and semi-instantaneous TKE and RSS values for different flow conditions. The results show that turbulent kinetic energy and Reynolds stresses show distinct patterns, depending on the bed development stage. As expected, positive RSS_{uw} values correspond to the bed erosion, as well as high TKE values. At the threshold conditions flow and bed conditions stabilize throughout the experiment, with bed adjusting to the change in flow conditions. Once the flow conditions are increased over the threshold, sediment entrained upstream is transported through the measurement section. From the experiments it can be observed that after the bed development is initiated, bedform moves through the system and affects the velocimetry data and turbulent characteristics. Once the sediment supply is depleted, bed development is rapidly eroded. The results show the potential link between bed development after floods, where flow can further deepen the scour hole after the sediment supply diminishes.

Acknowledgements
This work has been supported in part by Croatian Science Foundation under the project R3PEAT (UIP-2019-04-4046).

References:

[1] Tunio, I.A., Kumar, L., Memon, S.A., Mahessar, A.A, Kandhir, A.W.: Sediment transport dynamics during a super flood: A case study of the 2010 super flood at the Guddu Barrage on the Indus River, International Journal of Sediment Research, 2024

[2] Wardhana, K., Hadipriono, F.C.: Analysis of Recent Bridge Failures in the United States, Journal of Performance of Constructed Facilities, 17(3), 2003

[3] Kosič, M., Prendergast, L.J., Anžlin, A.: Analysis of the response of a roadway bridge under extreme flooding-related events: Scour and debris-loading, Engineering Structures, 279, 115607, 2023

[4] Gilja, G., Oskoruš, D., Kuspilić, N.: Erosion of the Sava riverbed in Croatia and its foreseeable consequences, BALWOIS 2010: Conference on Water observation and information system for decision support, Skopje, ffp-1826, 2010

[5] Maddison, B.: Scour failure of bridges, Proceedings of the Institution of Civil Engineers - Forensic Engineering, 165(1), 39-52, 2012.

[6] Harasti, A., Gilja, G., Potočki, K., Lacko, M.: Scour at Bridge Piers Protected by the Riprap Sloping Structure: A Review, Water, 13(24), 3606, 2021

[7] Harasti, A., Gilja, G., Adžaga, N., Žic, M.: Analysis of Variables Influencing Scour on Large Sand-Bed Rivers Conducted Using Field Data, Applied Sciences, 13(9), 5365, 2023

[8] Beheshti, A., Ataie-Ashtiani, B.: Scour hole influence on turbulent flow field around complex bridge piers, Flow, Turbulence and Combustion, 97(2), 451–474. 2016.

[9] Vijayasree, B.A., Eldho, T.I., Mazumder, B.S.: Turbulence statistics of flow causing scour around circular and oblong piers, Journal of Hydraulic Research, 58(4), 673–686, 2020

[10] Vijayasree, B.A., Eldho, T.I., Mazumder, B.S., Ahmad, N.: Influence of bridge pier shape on flow field and scour geometry, International Journal of River Basin Management, 17(1), 109–129, 2019

[11] Pu, J.H., Pandey, M., Hanmaiahgari, P.R.: Analytical modelling of sidewall turbulence effect on streamwise velocity profile using 2D approach: A comparison of rectangular and trapezoidal open channel flows, Journal of Hydro-environment Research, 32, 17-25, 2020

[12] Maity, H., Mazumder, B.S.: Prediction of plane-wise turbulent events to the Reynolds stress in a flow over scour-bed, Environmetrics, 28, e2442, 2017

[13] Amirshahi, S.M., Zarrati, A.R., Tabarestani, M.K., Tabesh, M.: Effect of Turbulence Intensity on Riprap Stability over Streambeds, Journal of Hydraulic Engineering, 148(10), 06022013, 2022

[14] Diplas, P., Dancey, C.L., Celik, A.O., Valyrakis, M., Greer, K., Akar, T.: The Role of Impulse on the Initiation of Particle Movement Under Turbulent Flow Conditions, Science, 322(5902), 717-720, 2008

[15] Gilja, G., Fliszar, R., Harasti, A., Valyrakis, M.: Calibration and Verification of Operation Parameters for an Array of Vectrino Profilers Configured for Turbulent Flow Field Measurement around Bridge Piers—Part I, Fluids, 7(10), 315, 2022

[16] Gilja, G., Fliszar, R., Harasti, A., Valyrakis, M.: Calibration and Verification of Operation Parameters for an Array of Vectrino Profilers Configured for Turbulent Flow Field Measurement around Bridge Piers—Part II, Fluids, 8(7), 199, 2023

[17] Alhusban, Z., Valyrakis, M.: Assessing sediment transport dynamics from energy perspective by using the instrumented particle, International Journal of Sediment Research, 37(6), 833-846, 022

[18] AlObaidi, K., Valyrakis, M.: Coherent Flow Structures Linked to the Impulse Criterion for Incipient Motion of Coarse Sediment, Applied Sciences, 13(19), 10656, 2023

NUMERICAL STUDY OF THE SEA WAVE LOADING ON A VERTICAL PARAPET WALL AND OVERTOPPING

DALIBOR CAREVIC [1], GORAN LONČAR [2], DAMJAN BUJAK[3], STJEPAN VIDOJEVIC[4]

[1] *Faculty of Civil Engineering, University of Zagreb, Croatia,* dalibor.carevic@grad.unizg.hr

[2] *Faculty of Civil Engineering, University of Zagreb, Croatia,* goran.loncar@grad.unizg.hr

[3] *Faculty of Civil Engineering, University of Zagreb, Croatia,* damjan.bujak@grad.unizg.hr

[4] *Faculty of Civil Engineering, University of Zagreb, Croatia,* stjepan.vidojevic@student.grad.hr

1 Abstract

The pressures along the outer contour of the parapet wall on the vertical breakwater without rubble mound were analyzed under the action of spectral and monochromatic waves, as well as the overtopping only under the action of spectral waves. The parapet wall was analyzed in two configurations, the first with the design on the outer side of the breakwater and the second with the alignment at the center of the breakwater. When the parapet wall is erected in the center of the structure, the maximum forces on the parapet increase almost fourfold compared to the forces acting on the parapet wall at the outer side of the structure. The overtopping intensities determined with the numerical model agree with the overtopping calculated on the basis of empirical equations.

Keywords: vertical breakwater, parapet wall, wave pressures, overtopping

2 Introduction

Vertical breakwaters are structures designed to protect coastlines and maritime infrastructure from the impact of sea waves. These structures are often composed of a series of vertical elements, such as columns or pillars, strategically arranged to form a protective screen. The vertical orientation allows them to effectively reduce wave height and intensity, providing a stable environment for ports and coastal developments.

Parapet walls are built on top of the vertical breakwater and provide an additional layer of protection against wave overtopping and forces [1], [2], [3]. Today, parapet walls are often used as a measure for the sea level rise adaptation measure acting as an additional protection against overtopping. The design of the parapet wall is an important factor in optimizing the overall performance of vertical breakwaters. The pressure and forces acting on the breakwater can be reduced by the proper design of the parapet wall and its placement at the top of the breakwater. Previous research has mainly focused on the design of the curved parapet walls at the outer side of the breakwater. For seas with moderate and low wave climate it is possible to use parapet walls that are positioned in the centerline of the breakwater, allowing ships to berth from the outside of the breakwater.

Overtopping is a phenomenon of interaction between wave and structure in which part of the wave passes over the top of the structure in the form of a continuous layer of water or spray. Overtopping is a complex and non-linear phenomenon that is random in time and space and depends on geometric-structural and hydrodynamic factors (sea level, height and period of the waves, structure freeboard, etc.). The importance of this phenomenon is often underestimated, as the overtopping event itself only occurs sporadically.

The complexity of overtopping assessment is precisely the reason why there are several approaches to assessing overtopping intensity itself: numerical modeling, empirical methods, neural networks, and 2D and 3D experiments on physical models [4].

Empirical methods - patterns are simplified representations of the complex physics of the process, usually presented in a dimensionless form that relates the time-averaged overtopping intensity to the main factors that characterize the phenomenon. This approach generally relies on fitting empirical expressions to the results of laboratory tests or measurements on a prototype in nature. Several authors have quantified the time-averaged overtopping intensity as a function of the main geometric and hydraulic parameters:

$$q = a \cdot e^{-b \cdot \frac{R_c}{H_s}} \cdot \sqrt{g \cdot H_s^3} \quad (1)$$

In Eq. 1 “a” and “b” are the coefficients of the empirical model (a = 0.2 and b = - 4.3 according to [5] ; a = 0.05 and b = -2.78 according to [6]; a = 0.082 and b = -3 according to [7]) , and Rc (freebord) is the vertical distance between the water surface and the top of the breakwater or parapet wall. In the work [8] nomograms are given for the calculation of overtopping intensity. For all empirical expressions and nomograms, it was assumed that the parapet wall is located on the outer side of the breakwater. The above empirical expressions were used for comparison with the values of the (numerical) model calculation of the overtopping intensity under the same geometric conditions of the structure (parapet wall on the outer side of the breakwater).
In view of the fact that there are no empirical expressions for the evaluation of the overtopping intensity in the case that the parapet wall is shifted towards the center of the breakwater, numerical simulations of overtopping for such design geometries were carried out in this work. In addition to the overtopping, it is necessary for the design to know the forces and/or pressures that occur along the contours of the parapet wall, which was also analyzed as part of this work.

3 Methodology - numerical model

The Flow 3D model was used to carry out numerical simulations. The model was developed at the Los Alamos National Laboratory in the 1970s and is still being developed and improved by the company Flow Science, Inc. ([9], [9], [11], [12]). It is based on the finite volume method and the Eulerian approach, which is used to solve the system of equations for the conservation of mass, momentum and energy. A structured computational grid in the Cartesian coordinate system is used, and the boundary conditions are defined on 6 planar surfaces of the discretization calculation block. The calculation code uses the so-called "Volume of Fluid" (VOF) formulation to include impermeable boundaries in the computational grid and the corresponding system of equations. 3D impermeable objects are treated as a set of finite volumes with associated surfaces, which supports the ability to solve systems of differential equations on an orthogonal and structured grid. The free surface is calculated using the VOF technique based on the volume fraction of each 3D cell. The mass conservation equation (continuity equation, Eq (2)) and the momentum conservation equation (Navier-Stokes equation, Eq (3-5)) in the Cartesian coordinate system are:

$$V_f \frac{\partial \rho}{\partial t} + \frac{\partial}{\partial x}(\rho u A_x) + \frac{\partial}{\partial y}(\rho v A_y) + \frac{\partial}{\partial z}(\rho w A_z) = R_{DIF} + R_{SOR} \quad (2)$$

$$\frac{\partial u}{\partial t} + \frac{1}{V_f}\left(u A_x \frac{\partial u}{\partial x} + v A_y \frac{\partial v}{\partial y} + w A_z \frac{\partial w}{\partial z}\right) = -\frac{1}{\rho}\frac{\partial p}{\partial x} + f_x \quad (3)$$

$$\frac{\partial v}{\partial t} + \frac{1}{V_f}\left(u A_x \frac{\partial u}{\partial x} + v A_y \frac{\partial v}{\partial y} + w A_z \frac{\partial w}{\partial z}\right) = -\frac{1}{\rho}\frac{\partial p}{\partial y} + f_y \quad (4)$$

$$\frac{\partial w}{\partial t} + \frac{1}{V_f}\left(u A_x \frac{\partial u}{\partial x} + v A_y \frac{\partial v}{\partial y} + w A_z \frac{\partial w}{\partial z}\right) = -\frac{1}{\rho}\frac{\partial p}{\partial z} + G_z + f_z \quad (5)$$

where: u, v, w are the components of the velocity vector in the x, y, z directions; R_{DIF} turbulent diffusion term; p pressure; R_{SOR} source or sink term; A_x , A_y , A_z flow cross-section in the calculation cell; ρ fluid density (assumed 1028 kg/m^3); Gz gravitational acceleration; f_x , f_y , f_z acceleration due to viscous effect in the x, y, z directions based on the divergence of the viscous stress tensor σ((1/ρ) ∇ .σ); V_f volume fraction of the fluid in the calculation cell calculated based on Eq. 6.

$$\frac{\partial F}{\partial t}+\frac{1}{V_f}\left[\frac{\partial(FA_x u)}{\partial x}+\frac{\partial\left(FA_y v\right)}{\partial y}+\frac{\partial(FA_z w)}{\partial z}\right]=0 \tag{6}$$

where: the value of the volume fraction F used to present the amount of fluid in each calculation cell (takes values from 0 to 1; 0 – cell filled with gas, 1 – cell completely filled with liquid).

The numerical channel (2D vertical section) has a horizontal bed with a depth of 10 m over an initial length of 200 m, after which the depth decreases continuously due to a constant bed slope (1:30). The breakwater profile is set 60 m from the start of the bottom slope (260 m from the start of the numerical channel, Figure 1) in the case of a breakwater at 8 m depth. For a breakwater at a depth of 6 m, the breakwater profile is set 120 m from the start of the bottom slope (320 m from the start of the numerical channel), while for a breakwater at a depth of 4 m, the breakwater profile is set 180 m from the start of the bottom slope (380 m from the start of the numerical channel).

The spatial discretization of the computational grid with cells of equidistant lengths in x, y and z direction (Δx = Δy = Δz = 0.2 m) is applied. The RNG k-ε turbulence model is used in the implementation of simulations ([13], [14]), and the heat transfer need not be considered for the problem under investigation. The pressure term is solved with an implicit method, the so-called GMRES (Improved Generalised Minimum residual), and viscous stresses explicitly.

The boundary conditions include JONSWAP spectral waves (γ= 3.3, σ_1 = 0.07, σ_2 = 0.09) at the input of the computational grid and a symmetric boundary condition at the sides (model domain width 0.2 m). Significant wave heights Hs and peak wave periods Tp (Hs = 3 m, Tp = 6.3 s; Hs = 3.5 m, Tp = 6.9 s) for spectral waves, i.e. wave heights H and periods T for monochromatic waves (H = 3 m, T = 6.3 s ; H = 3.5 m, T = 6.9 s ; wave steepness L/H = 21), and depths in front of the breakwater (8 m, 6 m and 4 m) were varied as part of the analysis. The boundary condition of an impermeable boundary (wall) is used for the bottom and atmospheric pressure for the top. The initial conditions are given as a resting state of water with a free surface at a constant level and a hydrostatic pressure distribution.

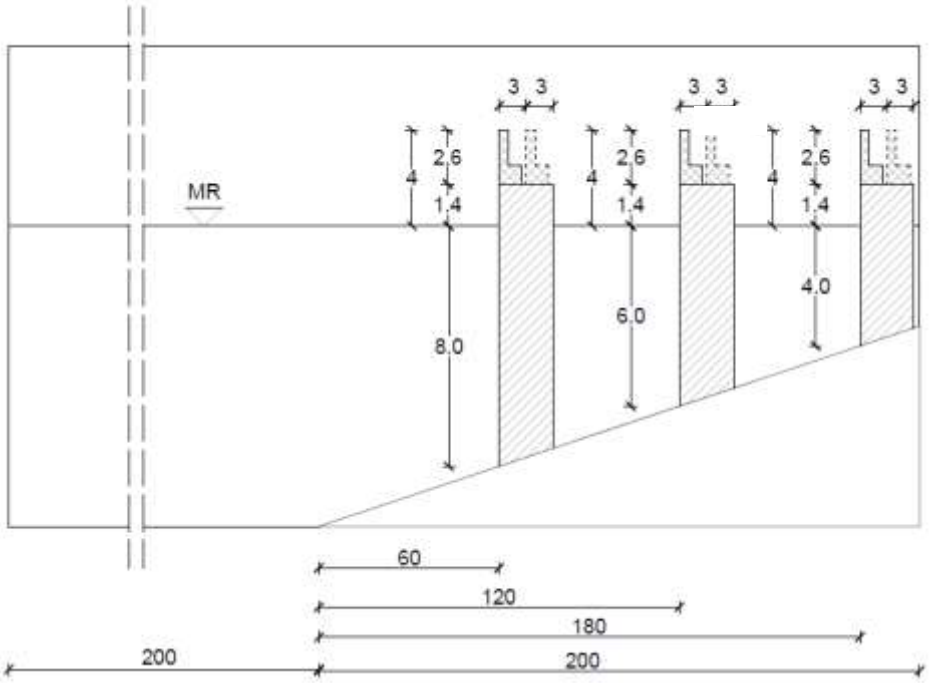

Figure 1 Schematic representation of the geometry of the numerical wave channel and the analyzed three vertical positions of breakwaters with parapet walls

Table 1 gives the list of the performed numerical simulations. As an initial condition, representative monochromatic waves and irregular waves have been chosen and those represent heavy wave conditions in front of the breakwater. Each simulation covers the period of 600s.

Table 1 List of performed numerical simulations Hs-significant wave height; H-wave height, Rc-height of the structure above sea level

Simulation	Hs (m) / H (m)	Rc/Hs, Rc/H	breakwater depth (m)	Parapet wall
1 / 13	3.5	1.14	8	outer side
2 / 14	3.0	1.33	8	outer side
3 / 15	3.5	1.14	6	outer side
4 / 16	3.0	1.33	6	outer side
5 / 17	3.5	1.14	4	outer side
6 / 18	3.0	1.33	4	outer side
7 / 19	3.5	1.14	8	center
8 / 20	3.0	1.33	8	center
9 / 21	3.5	1.14	6	center
10 / 22	3.0	1.33	6	center
11 / 23	3.5	1.14	4	center
12 / 24	3.0	1.33	4	center

4 Discussion of the results

The dynamic of the force on the parapet wall surface where the pressure gauges are located (integration with 14 numerical pressure gauges) is shown in Figure 2 - Figure 5 for spectral waves. From the presented figures it is visible that forces exerted on the parapet wall have varibale pattern due to occurrence of the irregular waves on the wall. In the cases of the parapet wall positioned on the center

of the wall crown much larger forces occurred during simulation.

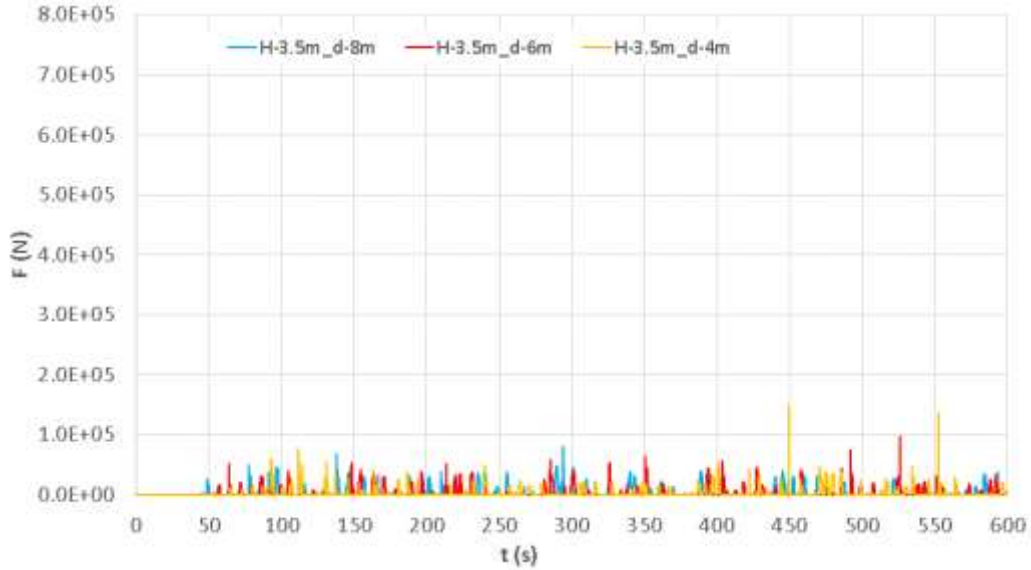

Figure 2 Dynamic of the force per m' of the parapet wall on which the numerical pressure gauges are located (analyses 1,3,5 →Hs = 3.5m; parapet wall on the outer side of the breakwater)

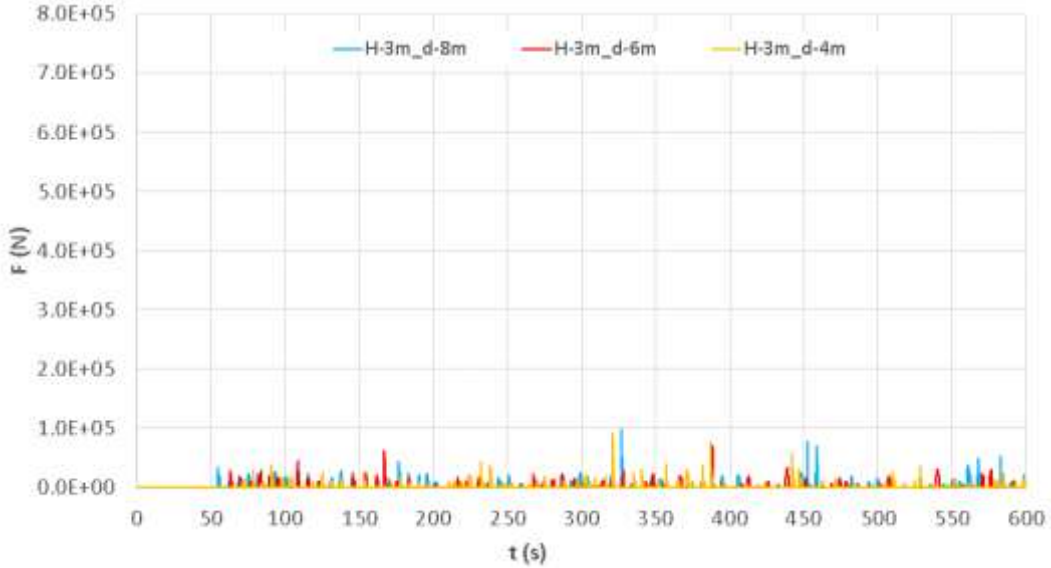

Figure 3 Dynamic of the force per m' of the parapet wall on which there are numerical pressure gauges (analyses 2,4,6 →Hs = 3.0m; parapet wall on the outer side of the breakwater)

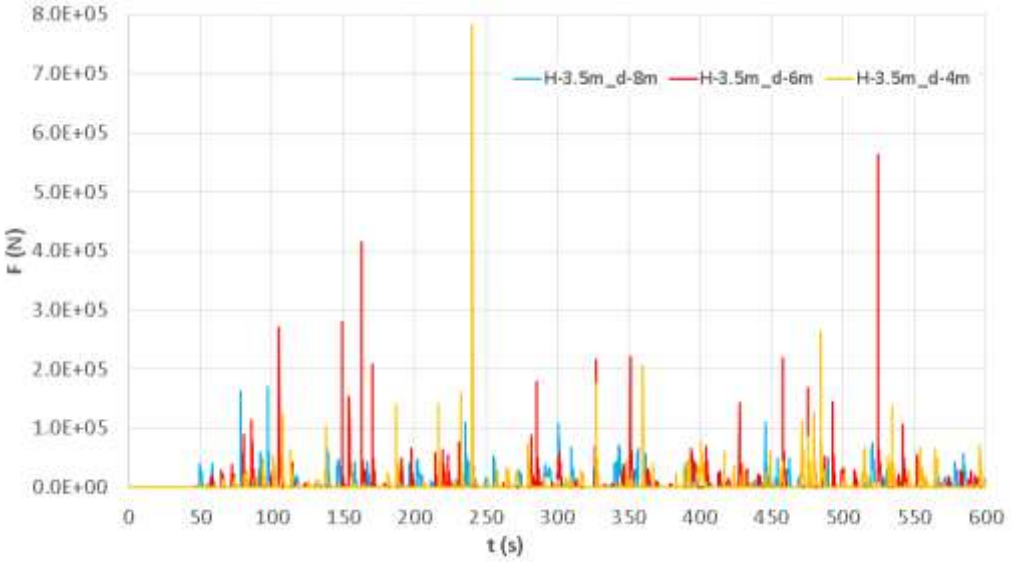

Figure 4 Dynamic of the force per m' of the parapet wall on which there are numerical pressure gauges (analyses 7,9,11 →Hs = 3.5m; parapet wall retracted in the center of the breakwater)

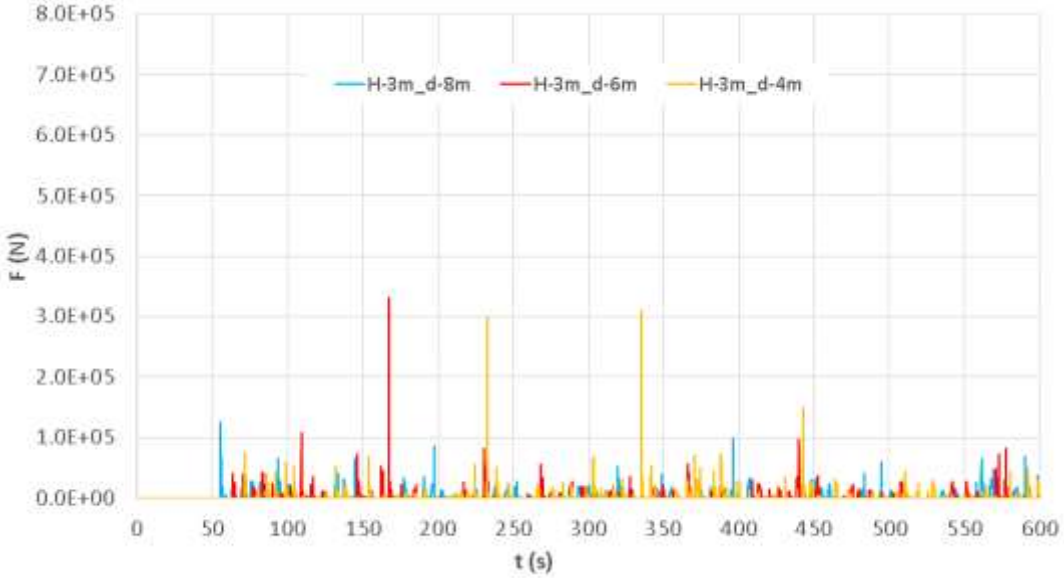

Figure 5 Dynamic of the force per m' of parapet wall on which there are numerical pressure gauges (analyses 8,10,12 →Hs = 3.0m; parapet wall retracted in the center of the breakwater)

Maximum model pressures at all gauges (from 1 at the base of the parapet wall to 14 at the top of the parapet wall) during the simulation period of 600s are shown in Figure 6. Similar in previous graphs, it is visible that pressures are larger in the cases of the parapet wall positioned in the center o the crown wall, especially in the lower part of the parapet wall around point 1. The resonable explanation for that is that volume of the water slides on the crown of the breakwater before it strikes the parapet wall. In these conditions, somethimes it happens that volume of the air is entrapped in the mass of water and explodes in the strike with the parapet wall what can be clearly observed on the

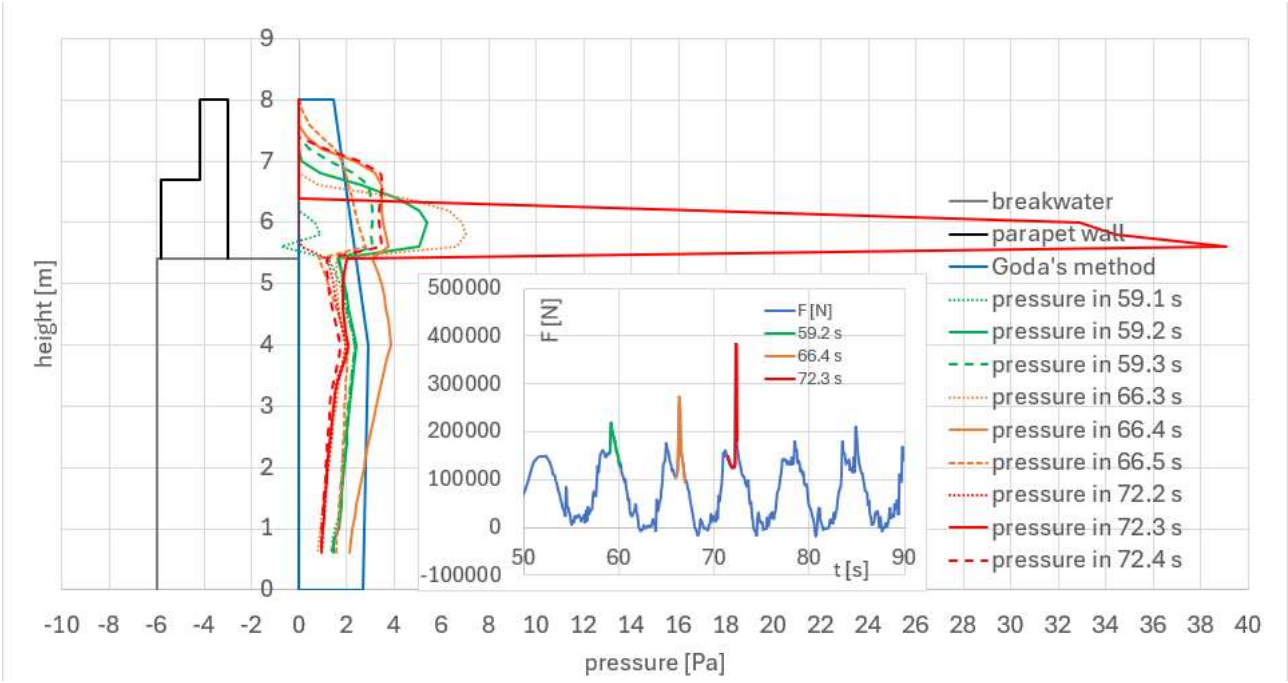

Figure 9 in the case of pressure diagram exerted at 72.3s. These conditions happen rarely but produce very large pressures as those presented in Figure 6.

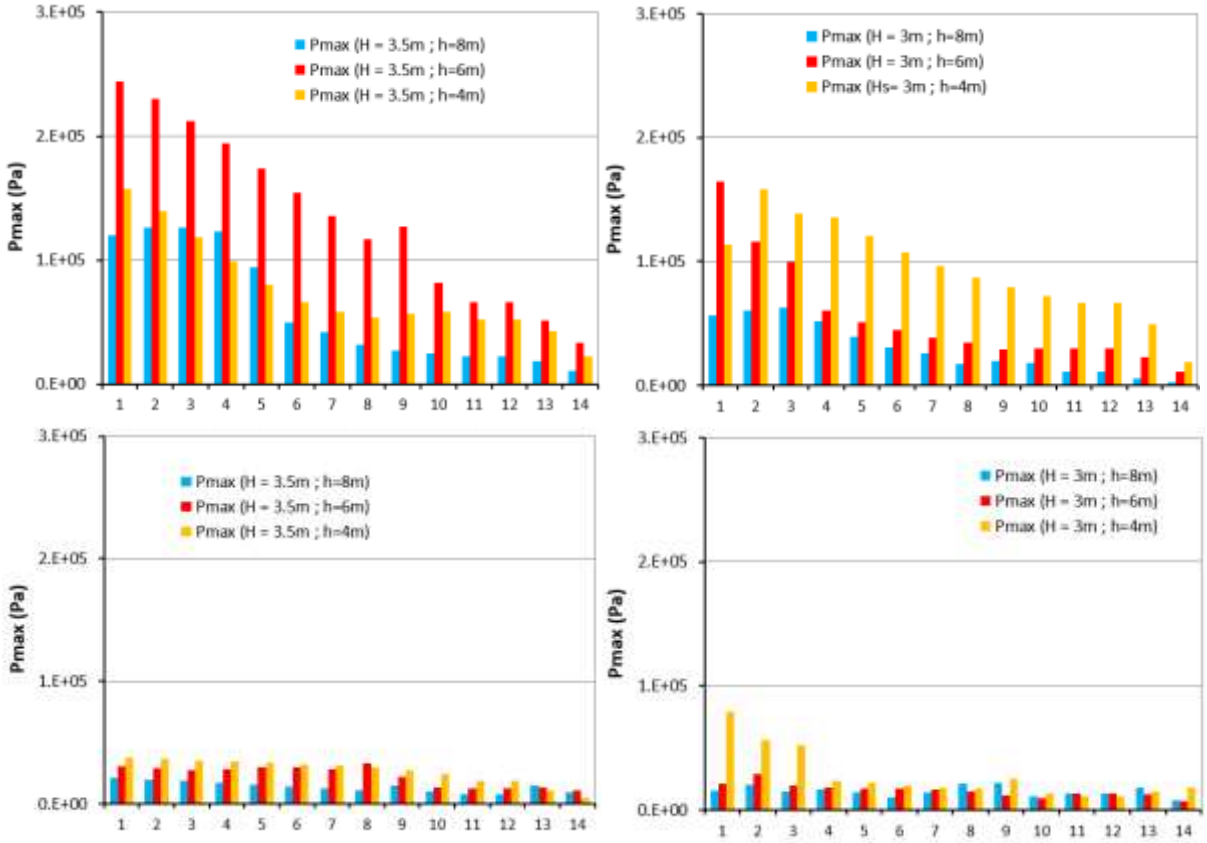

Figure 6 Maximum model pressures on all numerical pressure gauges (from 1 in the base of the parapet wall up to 14 at the top of the parapet wall) during the simulation period of 600s (left - H = 3.5m; right - H= 3.0m; upper graphs present parapet wall in the center of the breakwater and lower parapet wall on the outer side)

In the context of the previous discussion, it seems better to place the parapet walls on the outer side of the breakwater this way avoiding larger forces on the parapet wall. Considering that the parapet wall is an integral part of the entire breakwater and produces forces on it, the analysis of forces on the entire breakwater were investigated. In particular because the maximum force on the parapet wall and the maximum force on the rest of the breakwater (lower part) do not occur at the same moment. For this reason, the three largest total forces on the breakwater were calculated for each modeling period of 600s with the constant wave conditions. The results are shown in Figure 7. Like the previous conclusions, it appears that the total force is greater when the parapet wall is positioned in the center of the crown.

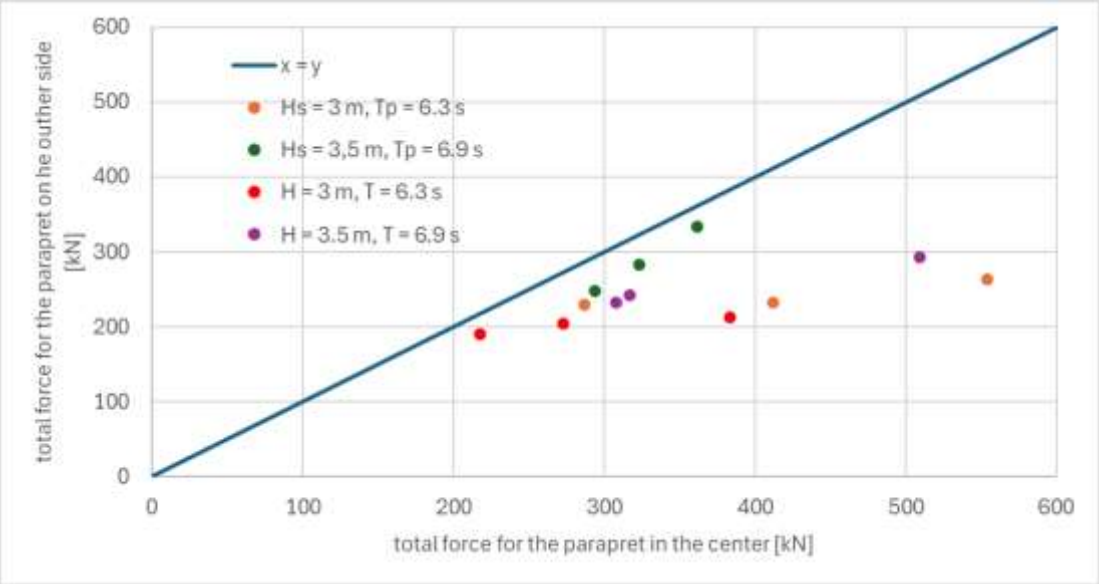

Figure 7 Total force on the breakwater resulted from numerical model for two different positions of the parapet wall on the breakwater crown (in the center and on the outer side); results are for depth d= 6 m and each color represents three largest forces in the modeling period of 600s

Figure 8 shows a comparison of the pressure diagrams that occur on the breakwater at different times during the simulation. Different colors show pressures of different monochromatic waves approaching the breakwater, and solid curves show the diagram corresponding to the maximum force exerted by that wave. The dotted curves show the pressure diagrams 0.1 second before and after this time. It can be seen from the figure that the Goda's diagram follows well modeled pressure diagrams and can be used to predict forces in the case of a parapet wall located on the outside. The case of the parapet wall in the center of the crown is shown in the

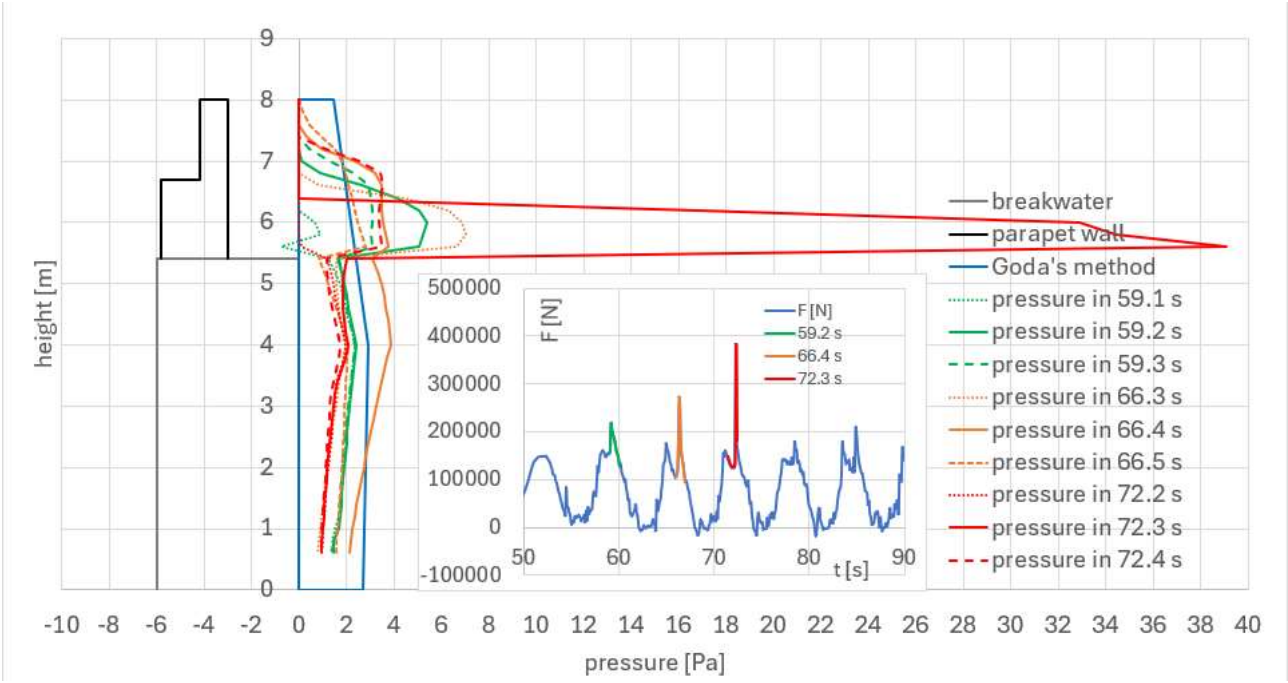

Figure 9 and there is visible situation of the trapped air explosion at the 72.3 s. The situations with air explosions are visible also in the Figure 7 where four dots are positioned extremely to the right of the graph showing much larger forces in the case of parapet wall in the center. Additional analysis should be performed to find the best method to predict this type of force, which is obviously larger.

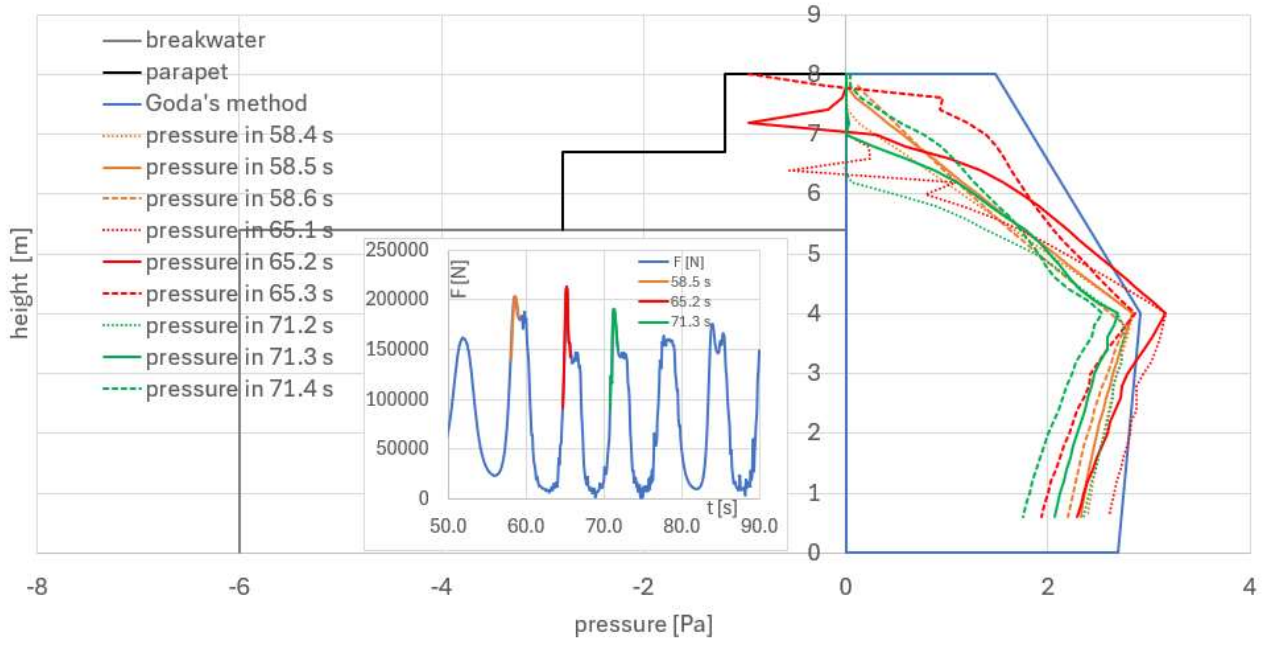

Figure 8 Pressure diagrams from numerical model test 18 (H=3m) and the position of the parapet wall on the outer side of the crown in different moments compared to the Goda's method

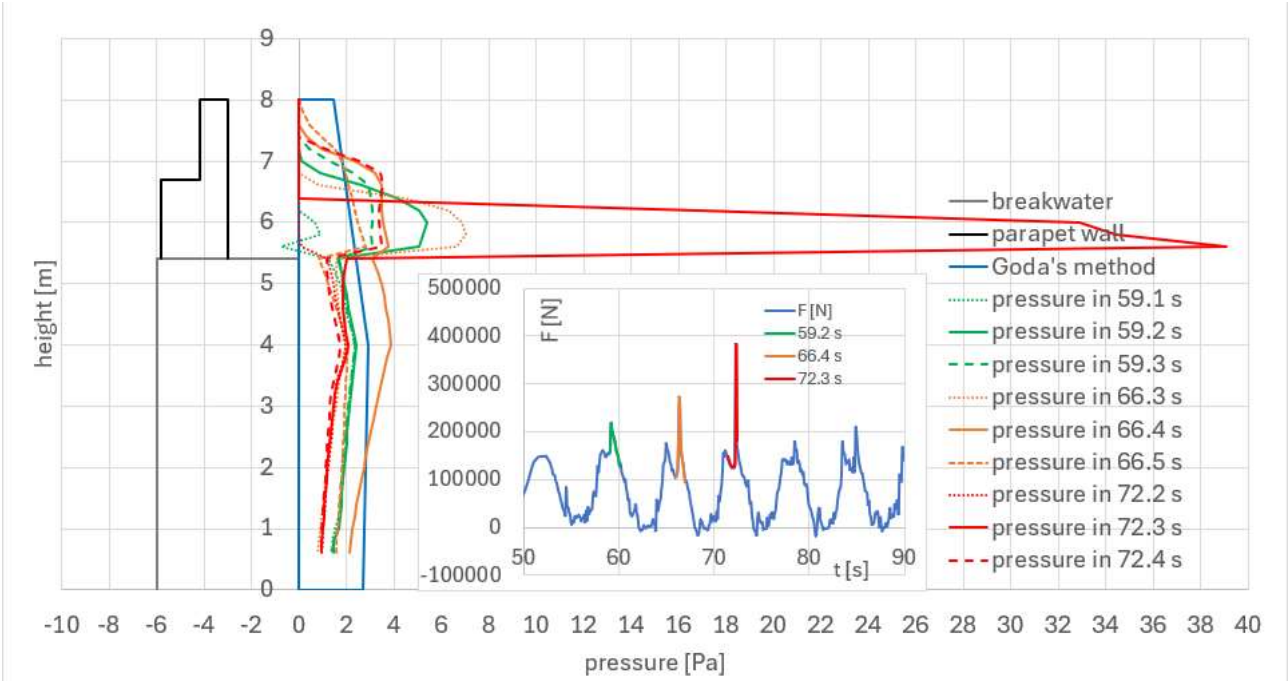

Figure 9 Pressure diagrams from numerical model test 24 (H=3m) and the position of the parapet wall in the center of the crown in different moments compared to the Goda's method

A comparison of overtopping (q - m ^{3}/s/m') obtained by numerical model and application of empirical patterns ([6], [7], [15], [5], [8]) is shown in Figure 10. The mean value of overtopping from the results of the numerical simulations is 0.016 m ^{3}/s/m' for Hs = 3m, while the mean value of overtopping based on empirical expressions is 0.017 m ^{3}/s/m'. Furthermore, the mean value of overtopping from the results of the numerical simulations is 0.063 m ^{3}/s/m' for Hs = 3.5m, while the mean value of overtopping based on empirical expressions is 0.043 m ^{3}/s/m'.

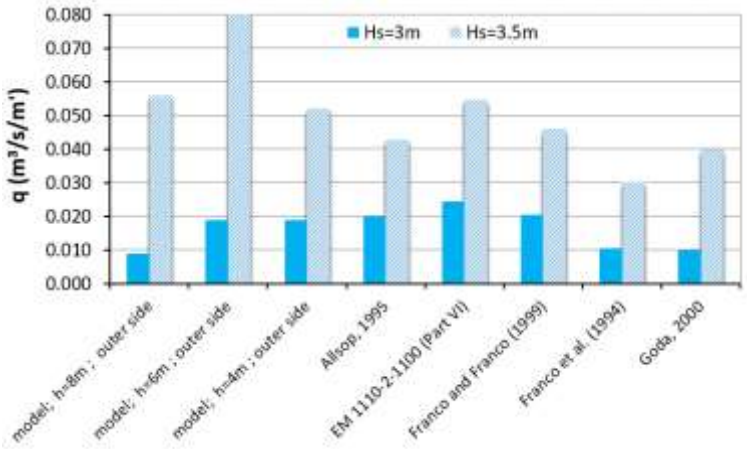

Figure 10 Comparison of overtopping obtained by the numerical model and the application of empirical relations (numerical results only for the case of the parapet wall placed on the outer side of the breakwater)

If the parapet wall is moved 3 m away from the edge, the overtopping changes, as shown in Figure 11. The average reduction of overtopping is 20% when the parapet wall is moved 3 m towards the center of the breakwater. The intensity of overtopping depends significantly on the depth at which the breakwater was built, and the maximum overtopping was achieved for a breakwater with a depth of 6 m.

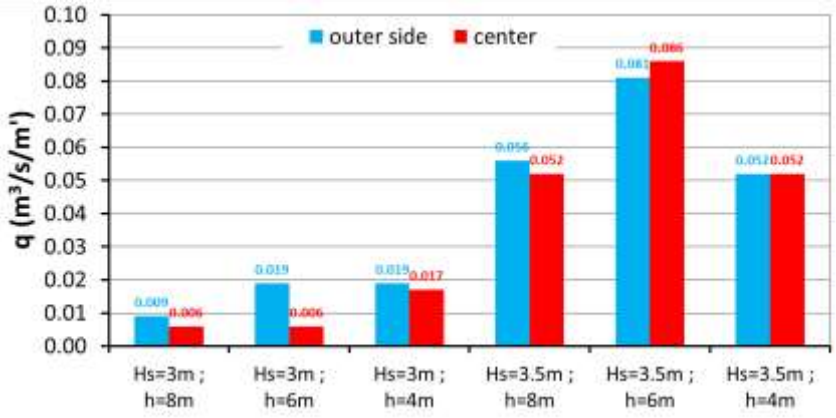

Figure 11 Comparison of overtopping intensity for the parapet wall on the outer side of the breakwater and in the center

5 Conclusion

A numerical model was created to analyze the dynamics of pressures and forces on the parapet wall placed on a vertical breakwater under the action of spectral waves. In the numerical simulations, the vertical breakwater was placed at depths of 8 m, 6 m and 4 m, with a constant bottom slope (1:30). In all simulations performed, the top of the parapet wall is at an elevation of +4.0 m (above the still water level), while the height of the breakwater is +1.4 m (the height of the parapet wall is 2.6 m). The parapet wall was studied in two configurations, the first with the position on the outside outer side of the breakwater and the second with the alignment in the center of the breakwater. The width of the breakwater is 6 m, the width of the parapet wall is 1 m. The pressure dynamics at 14 points along the outer contour of the parapet wall and the dynamics of overtopping were observed with a time resolution of 0.1 s.

The results of the simulations showed the following:

- the maximum wave force on the parapet wall is almost four times higher (on average 3.8 for spectral waves and 3.7 for monochromatic waves) when the parapet wall is built in the center of the breakwater, compared to building the parapet wall at the beginning of the structure.
- the highest registered pressure for spectral and monochromatic waves occurs at the junction between the cover plate of the breakwater and the parapet wall.
- the total forces on the entire face of the breakwater (breakwater and parapet wall) show a negative effect of the placement of the parapet wall in the center of the crown due to the increase of the forces by double or almost triple because of the explosion of the trapped air.
- overtopping intensities calculated with the numerical model (q = 0.016 m ^{3}/s/m') are very close to the values obtained with empirical equations (q = 0.017 m ^{3}/s/m') in the case of the parapet wall on the outer side of the breakwater under wave conditions Hs = 3 m and Tp = 6.3 s, while the results of numerical simulations in the case of Hs = 3.5 m and Tp = 6.9 s yield 46 % higher overtopping values.
- if the parapet wall is placed in the center of the structure, the overtopping (on average of all simulations) is 20% lower than in the case where the parapet wall is placed at the outer side of the breakwater.

- the results of the empirical models do not provide information on the difference in overtopping intensity depending on the position of the parapet wall and the influence of the depth at which the breakwater was built, which is why it is necessary to carry out numerical simulations or tests on a physical model.

Reference:

[1]. Ravindar, R., Sriram, V.: Impact Pressure and Forces on a Vertical Wall with Different Types of Parapet. Journal of Waterway, Port, Coastal, and Ocean Engineering, 147 (2021), 3, (2021), pp. 04021007. https://doi.org/10.1061/(ASCE)WW.1943-5460.0000635

[2]. Castellino, M., Romanoa, A., Larab, J., Losada, I., Girolamoa, P.: Confined-crest impact: forces dimensional analysis and extension of the Goda's formulae to recurved parapets. Coastal Engineering., 163 (2021), pp. 103814, https://doi.org/10.1016/j.coastaleng.2020.103814

[3]. Kortenhaus, J. Pearson, T. Bruce, N. Allsop, J. Van der Meer, Influence of parapets and recurves on wave overtopping and wave loading of complex vertical walls, in: Proc. Coastal Structures (ASCE), pp. 369–81, 2003.

[4]. EurOtop, 2018. Manual on wave overtopping of sea defences and related structures. Van der Meer, J.W., Allsop, N.W.H., Bruce, T., De Rouck, J., Kortenhaus, A., Pullen, T., Schüttrumpf, H., Troch, P. and Zanuttigh, B., www.overtopping-manual.com.

[5]. Franco, L., de Gerloni , M., van der Meer , JW: Wave overtopping at vertical and composite breakwaters , 24th International Conference on Coastal Engineering , Kobe, Japan, pp. 1030-1045 1994.

[6]. Allsop, N. W. H., Besley, P., & Madurini, L.: *Overtopping performance of vertical and composite breakwaters, seawalls and low reflection alternatives*, 1995, Paper presented at the final MCS Project Workshop, Alderney, UK.

[7]. *Coastal Engineering Manual Part VI: Design of Coastal Project Elements*. EM 1110-2-1100, 2012

[8]. Goda, Y.: *Random Seas and Design of Maritime Structures* , World Scientific Publishing , Singapore, 2000.

[9]. Hirt , CW and Nicholas, B.: Flow-3D User's Manual, Flow Science Inc. 1998.

[10]. Prosperetti , A., Tryggvason , G.: Computational Methods for Multiphase Flow , Cambridge University Press, (2007) pp. 488 . https://doi.org/10.1017/CBO9780511607486

[11]. Bombardelli , FA, Meireles , I., Matos , J.: Laboratory measurements and multi- block numerical simulations of the I mean flow and turbulence in the non-aerated skimming flow region of steep stepped spillways , Environ . Fluid Mech ., 11 (2011), pp . 263–288. https://doi.org/10.1007/s10652-010-9188-6

[12]. Bombardelli , F. A.: Computational multi- phase fluid dynamics to address flows past hydraulic structures , Proceedings of the 4th IAHR International Symposium on Hydraulics Structures , Porto, Portugal, pp . 9-11, 2012.

[13]. Yakhot , V., Orszag , SA.: Renormalization group analysis of turbulence . I. Basic theory , J. Sci. Comput, 1 (1986), pp. 3–51. https://doi.org/10.1007/BF01061452

[14]. Yakhot , V., Smith, LM: The renormalization group , the ε- expansion and derivation of turbulence models , J. Sci. Computer, 7 (1992), pp 35–61. https://doi.org/ 10.1007/BF01060210

[15]. Franco, C., Franco, L.: Overtopping Formulas for Caisson Breakwaters with Nonbreaking 3D Wave , Journal of Waterway, Port, Coastal, and Ocean Engineering, 125 (1999), 2, pp. 98–108. https://doi.org/10.1061/(ASCE)0733-950X(1999)125:2(98)

EFFECTIVE METHODS FOR THE HYDRAULIC ASSESSMENT OF COMBINED FUNCTIONAL STRUCTURES INVOLVING SMALL WATER AND DRY RESERVOIRS

JIŘÍ SKOKAN [1], ALEŠ DRÁB [2]

[1] *Brno University of Technology, Czech Republic, 212397@vutbr.cz*

1 Abstract

The paper explores current options for the hydraulic assessment of combined functional structures involving small water and dry reservoirs. The pursuit of cost savings often leads to the use of this type of flow control structure, which can pose significant hydraulic challenges. Economically, experimental research using physical models is typically not feasible for assessing hydraulic designs in such cases. Consequently, the paper primarily emphasizes the use of analytical and numerical calculations. For a thorough hydraulic assessment of the associated structure, a 3D numerical model was employed, encompassing all components of the structure, including the safety spillway, stilling pool, apron, and bottom outlet. Analytical calculations, coupled with a 1D numerical model, were applied for preliminary designs of the basic dimensions of the structure and comparison with the results of the 3D numerical model. The proposed computational procedures were verified through their application in the design of a dry reservoir in the locality of Kroměříž in the Czech Republic. In conclusion, the authors delve into a detailed discussion of the obtained results and provide recommendations for the practical application of these findings in engineering practice and within other research endeavours.

Keywords: dry reservoirs, small water reservoirs, hydraulic structures, flow control objects, one-dimensional model, three-dimensional model, safety, flood wave

2 Introduction

The paper focuses on the determination of the capacity of flow control objects of small water and dry retention reservoirs using analytical methods, and 1D and 3D numerical models. Small water reservoirs and corresponding dry retention reservoirs are defined according to the Czech technical standard [1] as earth-filled dams with a volume of controllable storage capacity of up to 2 million m^3 of water and their height does not exceed 9 m. The requirements for dry retention reservoirs are described in more detail in the Czech technical standard [2]. Bureau of Reclamation [3] defines small reservoirs according to their purpose, design parameters and main construction material.

The calculation of the capacity of flow control objects of small water and dry retention reservoirs directly affects its design parameters and vice versa. In practical engineering applications, simple analytical methods based mainly on one-dimensional (1D) and steady-state flow are used to determine the capacity of functional objects, as described, for example, in [4]. The advantage of these methods is fast and low-cost calculation in a commonly available spreadsheet. These methods work very well under conditions that match their simplifying assumptions, i.e., the flow can be well approximated in 1D and hydraulic phenomena such as overflow or outlet opening occur in an unsubmerged regime. Smaller dry retention reservoirs with a maximum height of 5 m are proposed on small streams in the Czech Republic [5] to capture flash floods with a repetition period of 5 to 100 years. The above-mentioned phenomena, such as unsubmerged overflow or discharge through the bottom outlet in the entire range of designed discharges, cannot be guaranteed on these objects, because the functional object of the reservoir is almost always affected by the tailwater during flood conditions due to its low height. This impact negatively affects the capacity of the designed object. The design can always be supported by experimental research on a physical model [6], but the cost of doing so usually does not reflect the significance of such small water structures. Currently, it is advisable to use a 1D numerical model or a three-dimensional (3D) CFD model to verify the parameters of the designed hydraulic structure.

Analysing the design by other independent methods can help reveal uncertainties and weaknesses in the design or, conversely, point out significantly over-dimensioned elements of the hydraulic structure. In the following chapters, we will discuss the problem of determining the capacity of flow control objects in more detail and apply the findings to a practical application of the recent proposal of a dry retention reservoir in the locality of the town of Kroměříž in the Czech Republic.

3 Methods

The chapter presents the methods used for the design and capacity assessment of the water structure's flow control objects. In principle, there are several possible approaches:

- analytical solutions,
- numerical models,
- experimental model research (not within the paper).

3.1 Analytical solution

The analytical calculations are suitable for determining the basic dimensions of the structure and its flow control objects, e.g. the apron, the bottom outlet and the safety spillway. The equations solving for steady uniform or non-uniform flow, discharge through the opening and weir overflow are considered standard practice. The disadvantage of these methods is the considerable uncertainty in the simplifying assumptions we include in the calculation, e.g. that the flow is 1D or uniform. In engineering practice, the most commonly used equation for steady, uniform, free-surface flow is the Chézy equation [7] (1):

$$v = C\sqrt{RJ_0} \tag{1}$$

where v is the mean velocity in ms^{-1}, C is Chézy's velocity coefficient in m$^{0.5}$s^{-1}, R is the hydraulic radius in m, J_0 is the grade of the energy (or ground) line.

The application of the Chézy equation is justifiable only in the case of a preliminary design of the object dimensions and the results must always be verified by more appropriate and accurate methods. The Chézy equation can be used to determine the capacity of the bottom outlet or the apron.

For the solution of the discharge through the opening or the bottom outlet without the influence of the inflow velocity, we apply the relations corresponding to the submergence rate of the outlet jet [7], [8] (the vena contracta):

A. for free surface flow unaffected by tailwater (2): $$Q = mb\sqrt{2g}h^{\frac{3}{2}} \tag{2}$$

B. for free surface flow affected by tailwater (3): $$Q = \varphi b h_\sigma \sqrt{2g(h - h_\sigma)} \tag{3}$$

C. for flooded inlet and outlet unaffected by tailwater (4): $$Q = \frac{2}{3}\mu b\sqrt{2g}\left(z_2^{\frac{3}{2}} - z_1^{\frac{3}{2}}\right) \tag{4}$$

D. for fully submerged inlet and partly submerged outlet (5):

$$Q_1 = \frac{2}{3}\mu_1 b\sqrt{2g}\left(H_\sigma^{\frac{3}{2}} - z_1^{\frac{3}{2}}\right) \tag{5}$$

$$Q_2 = \mu_2 a_2 b\sqrt{2gH_\sigma}$$

$$Q = Q_1 + Q_2$$

E. for fully submerged inlet and outlet (6): $$Q = \mu ab\sqrt{2gH} \tag{6}$$

where Q is the discharge in m^{3}s^{-1}, m is the discharge coefficient, μ, μ_1 and μ_2 are the opening's discharge coefficients, b is the width of the opening in m, φ is the velocity coefficient, g is the gravitational constant in ms^{-2} (9.81 ms^{-2}), other variables are shown in Figure 1 and have dimension m.

The above equations are valid for rectangular openings. In other technical literature, e.g. [7], corresponding relations can be found in other notations. For short bottom outlets, where the effect of friction can be neglected, values of $m = 0.36-0.16$, $\mu = 0.65-0.75$ a $\varphi = 0.96-0.79$ are generally considered [7], [8].

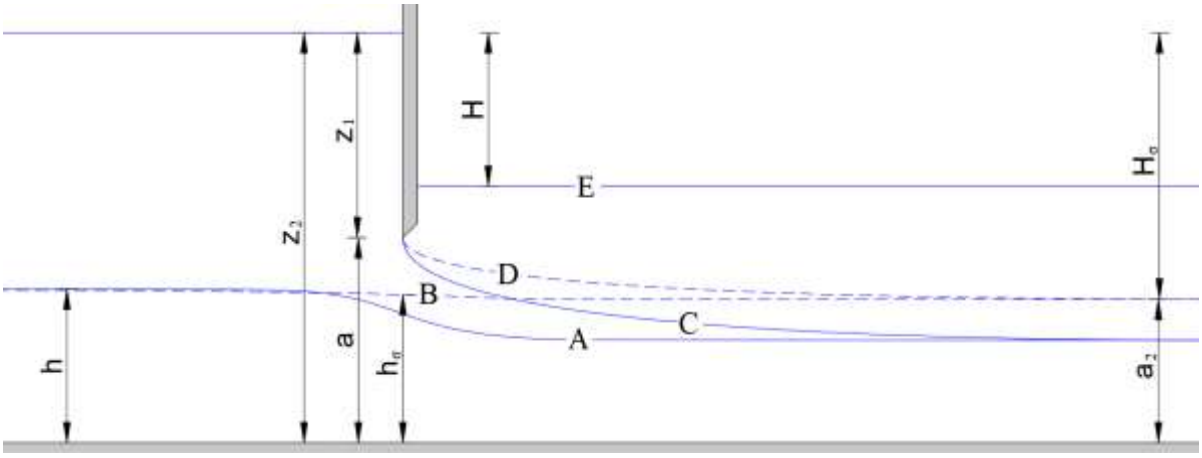

Figure 1. Schematic of the discharge through the opening

For the solution of the discharge over the safety spillway it is appropriate to use the Bazin weir equation assuming neglect of the inflow velocity [8], [9] (7):

$$Q = \sigma_z m b_0 \sqrt{2g} h^{\frac{3}{2}} \tag{7}$$

where σ_z is the submergence coefficient, b_0 is the effective width of the spillway (for the designed spillways it is practically the same as the free width of the spillway b) in m and h is the headwater elevation.

The discharge coefficient can be determined e.g. by:

A. Kramer [9] (8):
$$m = \frac{2}{3} \cdot \left[1{,}02 - \frac{1{,}015}{\frac{h}{r} + 2{,}08} + \left[0{,}04 \cdot \left(\frac{h}{r} + 0{,}19 \right)^2 + 0{,}0223 \right] \cdot \frac{r}{s_1} \right] \tag{8}$$

B. Rehbock [8] (9):
$$m = \frac{2}{3} \cdot \left[0.312 + 0.09 \frac{h}{s_1} + \sqrt{0.3 - 0.01 \cdot \left(5 - \frac{h}{r} \right)} \right] \tag{9}$$

C. Stara [10] (10):
$$m = 0.349494 + 0.307084 \frac{\frac{h}{s_1}}{\left(\frac{h}{s_1} \right)^{1.62877} + \left(\frac{s_1}{2r} \right)^{-1.45694} + 0.223402} \tag{10}$$

where r is the radius of curvature of the weir crest in m a s_1 is the height of the weir crest above the upper bottom in m.

The submergence coefficient for negative pressure spillways with a circular rounded crest has not yet been reliably determined; they are mainly used for safety spillways on higher water structures, where the nappe is not affected by tailwater [4], [11]. In the past, the submergence of negative pressure elliptically curved weirs was studied by Rozanov [12], his results can be well approximated by the empirical equation (11):

$$\sigma_z = \left[-0.78332 \cdot \left(\frac{h_z}{h} + 0.15 \right)^{1.74} + 1 \right]^{\frac{1}{1.97}} \tag{11}$$

where $\frac{h_z}{h}$ is the submergence ratio of the nappe. The equation is valid within the range of $-0.15 \leq \frac{h_z}{h} \leq 1$.

For circular rounded weirs, the submergence coefficient according to [8] is often used in engineering practice, which can be well approximated by the empirical equation (12):

$$\sigma_z = \left[-0.99128 \cdot \left(\frac{h_z}{h}\right)^{5.25} + 1\right]^{\frac{1}{1.56}} \quad (12)$$

where $\frac{h_z}{h}$ is the submergence ratio of the nappe. The equation is valid within the range of $0 \leq \frac{h_z}{h} \leq 1$.

3.2 1D model

We assume that discharge, mean velocity and flow area are only a function of position and independent of time. In such flow, we deal with frictional losses along the length and contraction/expansion losses. The problem can be solved by dividing the channel along its length into sub-sections and using Bernoulli's equation (13) related to the reference plane [13]:

$$i_{0j}\Delta L + h_i + \frac{\alpha v_i^2}{2g} = h_{i+1} + \frac{\alpha v_{i+1}^2}{2g} + h_{zj} \quad (13)$$

where i_{0j} is the grade of the ground in the sub-section, ΔL is the length of the sub-section in m, h_i, h_{i+1} is the water surface elevation in the profiles in m, α is the kinematic energy coefficient, v_i, v_{i+1} is the mean velocity in profiles in ms^{-1}, g is the gravitational constant in ms^{-2} (9.81 ms^{-2}), h_{zj} are the energy losses in the sub-section in m.

Contraction/expansion losses should be expressed as (14) [13]:

$$h_{zm} = \xi \frac{\left(v_i^2 - v_{i+1}^2\right)}{2g} \quad (14)$$

And the friction loss can be expressed by the slope of the energy line (15) [13]:

$$h_{zt} = \frac{Q^2}{S_{pj}^2 C_{pj}^2 R_{pj}} \cdot \Delta L \quad (15)$$

where h_{zm} is the contraction/expansion loss in m, ξ is the contraction/expansion loss coefficient (0−1), h_{zt} is the friction loss in m, Q is discharge in m^{3}s^{-1}, S flow area in m^2, C is Chézy's velocity coefficient in m$^{0.5}$s^{-1} a R is the hydraulic radius in m.

This method is suitable for the estimation of the water surface elevations in an apron or chute. The discharge through the bottom outlet and the safety spillway are solved by equations (2) to (12) from Chapter 3.1.

3.3 Hydraulic jump

By designing a part of the chute with a supercritical slope, theoretically a critical depth, a supercritical flow and subsequently a hydraulic jump can occur. Hydraulically, the calculation of the depth and length of the hydraulic jump and the sequent depths can be solved in several ways, see eq. (16) to (20):

A. by solving the general momentum equation [7]:

$$\frac{\beta Q^2}{gS} + zS = \theta(y) \quad (16)$$

B. by TBD [14]:

$$h_1 = \frac{q_1}{\sqrt{2g(E_v + z_v - z_1 - h_1}}$$

$$h_2 = \frac{h_1}{2}\left(\sqrt{1 + \frac{8q_1^2}{gh_1^3}} - 1\right) \quad (17)$$

C. by [15] for rectangular channels:

$$\frac{h_2}{h_1} = 0{,}5 \cdot \left[(1 + 8 \cdot Fr_1^2)^{\frac{1}{2}} - 1\right] \quad (18)$$

D. by [15] for conoidal channels:

$$L = \frac{6{,}4 \cdot h_1 \cdot (Fr_1^2 - 1)^{\frac{1}{2}}}{1 + 0{,}32 \cdot (\tan\gamma + \tan\delta_s) \cdot (Fr_1^2 - 1)^{\frac{1}{2}} \cdot \frac{h_1}{b_{s1}}} \quad (19)$$

$$\delta_s = \frac{(\tan\delta - \tan\gamma) \cdot h_1}{H} + \tan\gamma$$

$$h_2 = h_1 + \frac{0{,}114 \cdot k \cdot L}{1{,}2 - 0{,}2 \cdot \left(\frac{b_1}{h_1}\right)^{\frac{1}{3}}}$$

The length of the hydraulic jump is determined according to equation (19) or according to Novák [8] (20):

$$L = K \cdot (h_2 - h_1) \tag{20}$$

It is advisable to assess the stilling pool according to Čertousov [16] (21):

$$\sigma = \frac{H + d}{h_2} \in \langle 1{,}05\ to\ 1{,}10 \rangle \tag{21}$$

where β is the Boussinesq's coefficient, Q is the discharge in m^3s^{-1}, z is the centre of gravity of the flow area in m, S is the flow area in m^2, g is the gravitational constant in ms^{-2} (9.81 ms^{-2}), $\theta(y)$ is the hydraulic jump function, h_1 is the upstream depth in m, q_1 is the specific discharge in m^2s^{-1}, E_v is the energy head above the chute in m, z_v is the bottom elevation above the chute in m, z_1 is the elevation of the bottom of the stilling pool in m, h_2 is the downstream depth m, Fr is Froude number, L is the length of the hydraulic jump in m, γ and δ are the angles of expansion of the stilling pool in rad, H is the depth in the downstream channel m, b_{s1} is the mean channel width in m, b_1 is the bottom width in m, K is a coefficient in the range of 4 to 5.5 and d is the stilling pool depth in m. The variables are shown in Figure 2.

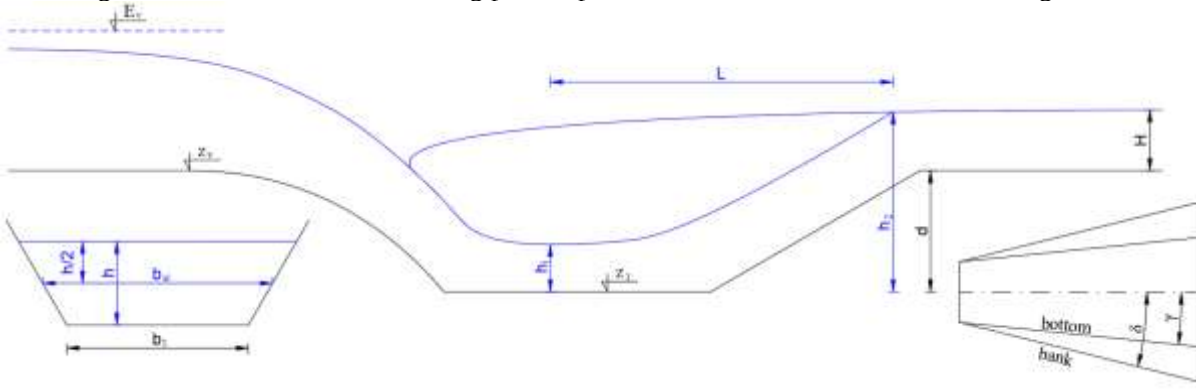

Figure 2. Schematic of the stilling pool and hydraulic jump

3.4 3D model

3.4.1 Mathematical model

The mathematical apparatus consists of continuity equation, momentum equation and turbulent model. The continuity equation is of the form (22) [17]:

$$V_F \frac{\partial \rho}{\partial t} + \frac{\partial}{\partial x}(\rho u A_x) + R\frac{\partial}{\partial y}(\rho v A_y) + \frac{\partial}{\partial z}(\rho w A_z) + \gamma \frac{\rho u A_x}{x} = R_{DIF} + R_{SOR} \tag{22}$$

where V_F is the fractional volume in m^3, ρ is the density of the medium in kgm^{-3}, u, v and w are the components of the velocity vector in ms^{-1}, A_x, A_y and A_z are the fractional flow areas in m^2, R is the coefficient for the transformation to the cylindrical coordinate system, γ is the coefficient for the transformation to the cylindrical coordinate system, R_{DIF} is the turbulent diffusion term inkgs^{-1} a R_{SOR} is the source or sink in kgs^{-1}.

The momentum equations can be written as eq. (23) to (25) [17]:

$$\frac{\partial u}{\partial t} + \frac{1}{V_F}\left\{uA_x\frac{\partial u}{\partial x} + vA_yR\frac{\partial u}{\partial y} + wA_z\frac{\partial u}{\partial z}\right\} - \gamma\frac{A_y v^2}{xV_F} = -\frac{1}{\rho}\frac{\partial p}{\partial x} + G_x + f_x - b_x - \frac{R_{SOR}}{\rho V_F}(u - u_w - \delta u_s) \tag{23}$$

$$\frac{\partial v}{\partial t} + \frac{1}{V_F}\left\{uA_x\frac{\partial v}{\partial x} + vA_yR\frac{\partial v}{\partial y} + wA_z\frac{\partial v}{\partial z}\right\} + \gamma\frac{A_y uv}{xV_F} = -\frac{1}{\rho}\left(R\frac{\partial p}{\partial y}\right) + G_y + f_y - b_y - \frac{R_{SOR}}{\rho V_F}(v - v_w - \delta v_s) \tag{24}$$

$$\frac{\partial w}{\partial t} + \frac{1}{V_F}\left\{uA_x\frac{\partial w}{\partial x} + vA_yR\frac{\partial w}{\partial y} + wA_z\frac{\partial w}{\partial z}\right\} = -\frac{1}{\rho}\frac{\partial p}{\partial z} + G_z + f_z - b_z - \frac{R_{SOR}}{\rho V_F}(w - w_w - \delta w_s) \tag{25}$$

where u, v and w are the components of the velocity vector in ms^{-1}, V_F is the fractional volume in m^3, A_x, A_y and A_z are the fractional flow areas in m^2, R is the coefficient for the transformation to the cylindrical coordinate system, γ is the coefficient for the transformation to the cylindrical coordinate

system, p is pressure in Pa, ρ is the density of the medium in kgm^{-3}, G_x, Gy and G_z are the components of the acceleration vector of the body in ms^{-2}, f_x, f_y and f_z are the components of the gravitational acceleration vector in ms^{-2}, b_x, b_y and b_z are the energy losses in the porous medium in m.

LES (large eddy simulation) was chosen as the turbulence model. In simplified terms, the LES model can be described as quantifying directly all computationally resolvable turbulent flow structures and approximating only computationally indistinguishable phenomena. The effects of turbulence that are too small to be solved by direct numerical simulation are represented by the turbulent viscosity ν_T, which is given by (26) [17]:

$$\vartheta_T = (cL)^2 \cdot \sqrt{2e_{ij}2e_{ji}} \tag{26}$$

where ν_T je kinematic turbulent viscosity in m^{2}s^{-1}, L is the length scale (in this case the size of the computational grid cells) in m, e_{ij} and e_{ji} are the components of the strain rate tensor in s^{-1} a c is the Smagorinsky coefficient.

3.4.2 Numerical model

The flow through the object was simulated by the CFD software Flow-3D, which is based on the finite volume method. Further information can be found in the documentation [17].

3.5 Flood wave transformation

Discrete point simulation was used for flood outflow modelling. The general equation of the transformation without evaporation and seepage in differential form is (25) [14]:

$$\frac{dV(t)}{dt} = Q(t) - O\big(V(t)\big) \tag{27}$$

A suitable solution to equation (25) is to use the 4th order Runge - Kutta method for 1st order differential equations [14], equations (25) to (29):

$$V_1 - V_0 = \frac{K_1 + 2K_2 + 2K_3 + K_4}{6} \tag{28}$$

$$K_1 = \Delta t \cdot \Big(Q(t) - O\big(V(t)\big)\Big) \tag{29}$$

$$K_2 = \Delta t \left(Q(t + \Delta t) - O\left(V(t) + \frac{K_1}{2}\right)\right) \tag{30}$$

$$K_3 = \Delta t \left(Q(t + \Delta t) - O\left(V(t) + \frac{K_2}{2}\right)\right) \tag{31}$$

$$K_4 = \Delta t\big(Q(t + \Delta t) - O(V(t) + K_3)\big) \tag{32}$$

where V is the volume in the reservoir in m^3, t is time in s, Q is inflow in m^3/s, O is outflow in m^3/s, Δt time-step in s, V_0 is the initial volume in the reservoir in m^3, V_1 is the volume at time $t_0 + \Delta t$ in m^3.

3.6 Practical application (case study)

The practical application of the above-described methods will be carried out on the proposed dry reservoir in the locality of the city of Kroměříž in the Czech Republic. It is a low concrete flow control object with an internal width of 7 m and a height of 4.9 m (see Figure 3).

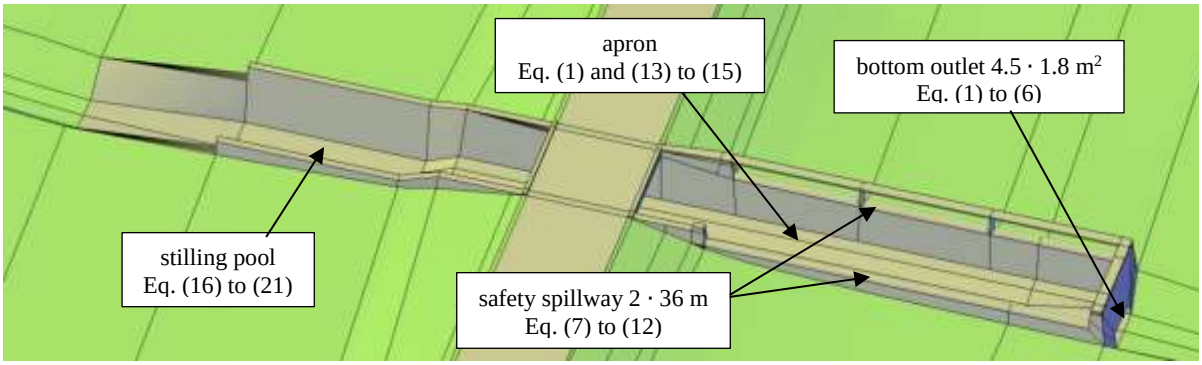

Figure 3. Visualization of the designed object

3.6.1 Analytical solution and 1D model

The calculation was performed under the assumption that water is a continuum and its properties are constant, the flow is adiabatic, single-phase and mixing with air occurs to a negligible extent. A strong assumption is that the flow is steady and, in the case of the analytical solution, uniform. The basic input data are the geometric parameters of the flow control object, in the case of the 1D model selected cross-sections of the object in which the calculation of non-uniform flow is performed.

3.6.2 3D model

The extent of the model is such as to ensure that the flow is not affected by boundary and initial conditions. The numerical simulations were performed under the assumption that water is a continuum and its properties are constant, the flow is adiabatic, single-phase and mixing with air occurs to a negligible extent, and the effect of flow turbulence can be approximated by the LES model. Gravitational acceleration has been set to $g = 9.81$ ms^{-2}. The medium used is water at temperature $T = 20$ °C, density $\rho = 1000$ kg·m^{-3} and molecular viscosity $\mu = 0.001$ Pa·s^{-1}. Flow-3D uses an orthogonal, structured computational mesh. For this computation, a 0.05 m resolution mesh with a total number of 35 million cells was used. The final configuration of the mesh was preceded by a series of test calculations with different computational cell sizes ranging from 0.025 to 0.125 m to analyze the independence of the results on the computational mesh. The basic input data is the 3D body of the designed dry retention reservoir flow control object, surface roughness and boundary conditions. The 3D model of the dry retention reservoir object was created using Autodesk Fusion 360 software. The surface roughness was determined as the Nikaraudse equivalent sand roughness, with a value of $k_s = 0.00139$ mm for concrete structures and $k_s = 0.5$ mm for the channel and other surfaces [19]. To analyze the independence of the results on the computational mesh, it is useful to monitor selected variables in the model and compare their values for each tested computational cell size. When independence on the computational mesh is achieved, the further discretization of the mesh domain is no longer significant and the result closely approximates the continuous solution. [18]

3.6.3 Flood wave transformation

For the calculations of the transformation effect of the reservoir, the hydrographs at the inflow to the reservoir developed in [20] are used. Determination of hydrographs by a non-authorised organisation, see [21], is only possible during the design study phase; for further project documentation, it is necessary to request these data from an authorised organisation in the Czech Republic. The transformation is performed according to chapter 3.5 and the pre-calculated rating curves of the flow control object according to the respective methods in chapter 3 are used to determine the outflow from the reservoir. The transformation simulation is recommended by the Czech technical standard [21].

4 Results and discussion

Figure 4 shows the rating curves of the safety spillway and the bottom outlet. In the case of a discharge through an unsubmerged bottom outlet, the analytical solution generates the greatest capacity.

Compared to the 1D or 3D model, the analytical solution neglects the influence of the tailwater in the case of an unsubmerged inlet, which results in a significant difference in capacity. The submergence of the bottom outlet opening results in a loss of capacity, where at a water surface elevation of 6 m the outlet is already so submerged that it is almost non-functional compared to the safety spillway. Interestingly, the capacity of the submerged bottom outlet, which is certainly not negligible, can be determined with relatively good accuracy by analytical methods, as well as by a 1D or 3D model. Figure 4 shows that the rating curves of the safety spillway are almost identical up to discharge Q = 80 m^{3}s^{-1}. At higher discharges, the nappe is influenced by the tailwater and the differences between the rating curves increase. In the case of analytical solutions and 1D models, the flooding of the nappe is considered from the condition when the tailwater level exceeds the crest of the spillway; this assumption is rather simplistic in the case of negative pressure spillways.

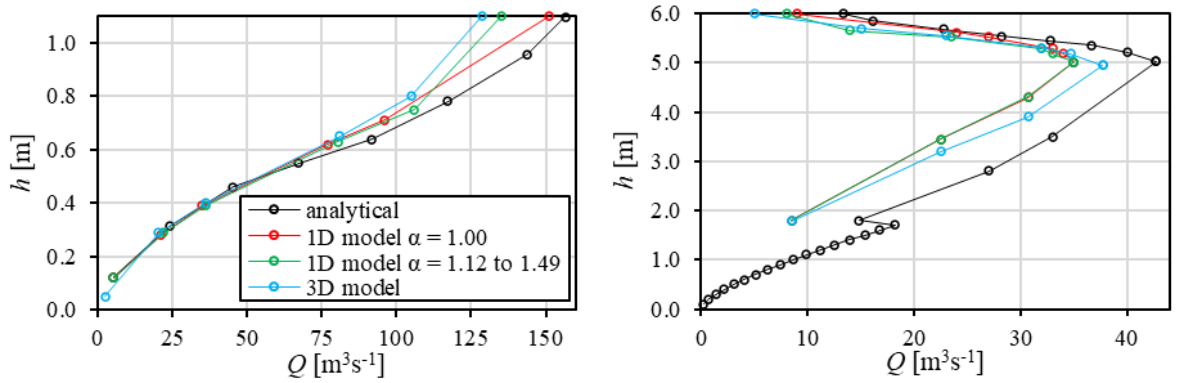

Figure 4. Rating curves of safety spillway (left) and bottom outlet (right)

The results in Figure 5 show that the calculated values of hydraulic jump depths and lengths vary considerably. It is not possible to solve the hydraulic jump in the analytical solution, we do not know its upstream depth. In the 1D models, we consider the development of critical depth and supercritical flow at all discharges. The 3D model shows the formation of a supercritical flow and hydraulic jump only at discharge $Q \geq$ 120 m^{3}s^{-1}, at lower discharges, the water surface elevation does not reach below the critical depth. From the results of the 3D model, the stilling pool seems to be over-dimensioned and it would be advisable to test a version without the stilling pool or its non-embedded variant, e.g. with fortification with a heavy rock bed.

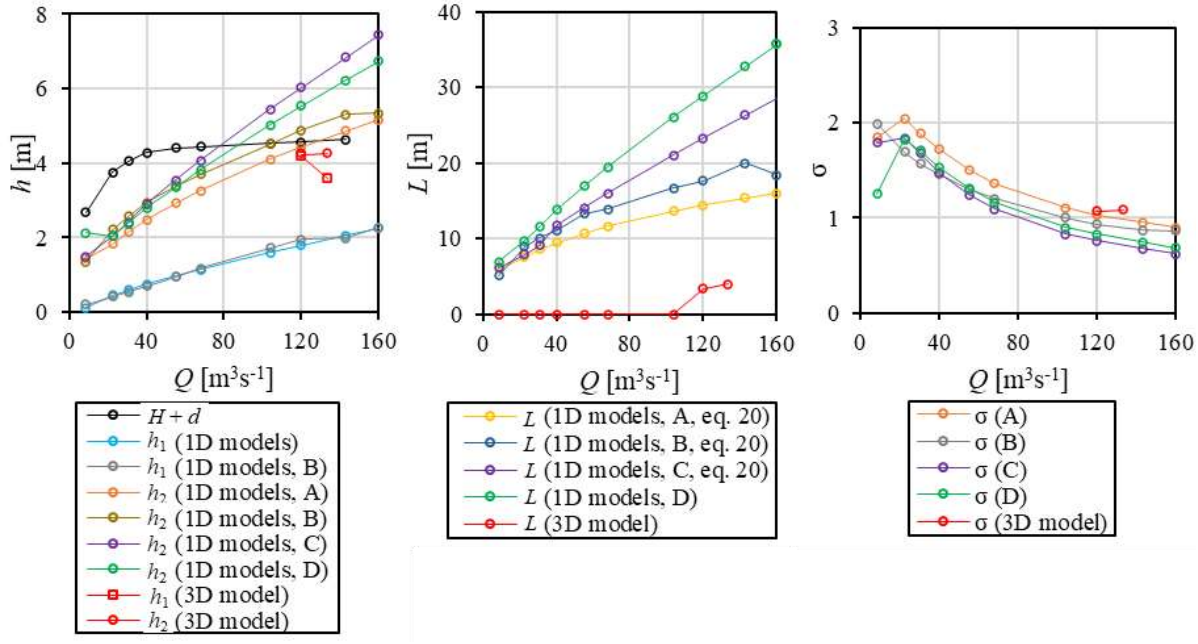

Figure 5. Sequent depths (left), and lengths (middle) of hydraulic jump and buoyancy (right)

Figure 6 shows the peak outflows and inflows in the reservoir for different methods of determining the capacity of the flow control object. Figure 7 shows the peak water surface elevations in the reservoir. The peak outflow from the reservoir during the Q_5 to Q_{100} (where Q_5 means flood with a repetition period of 5 years etc.) flood wave transformation is significantly influenced by the determined capacity of the bottom outlet. Its value varies by up to 18 % depending on the method used to determine capacity. The highest peak outflow is obtained from the analytical solution of the capacity of the object. The difference in peak-to-peak between the 1D models is minimal, and the difference between the 1D and 3D models is about 6%. These differences propagate to the length of the reservoir transformation effect, where compared to the analytical solution, the 1D and 3D model variants show up to twice the transformation length, the difference between the 1D and 3D models being about 11%. During a flood of Q_{500} or higher, a safety spillway is included in the transformation effect of the reservoir. Differences in the peak discharge are reduced by connecting the safety spillway and are in the units of percentages, because the differences in the spillway capacities are minimal in the case of an unsubmerged nappe and its influence on the discharge increases higher with the water surface elevation in the reservoir than the influence from the bottom outlet (which decreases).

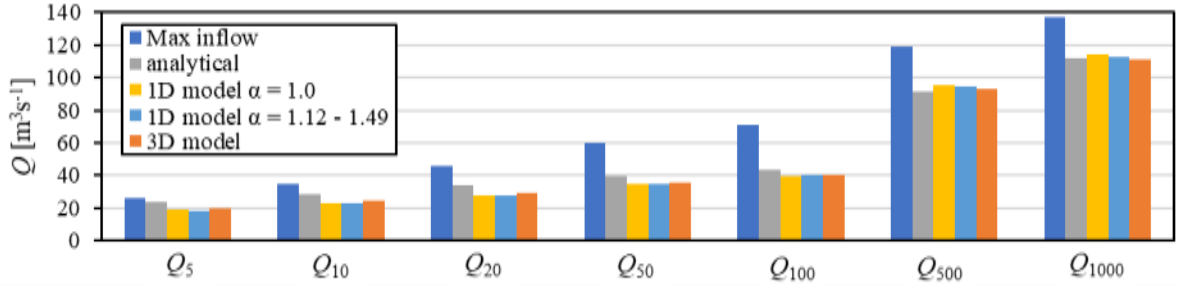

Figure 6. Peak discharges at inflow and outflow

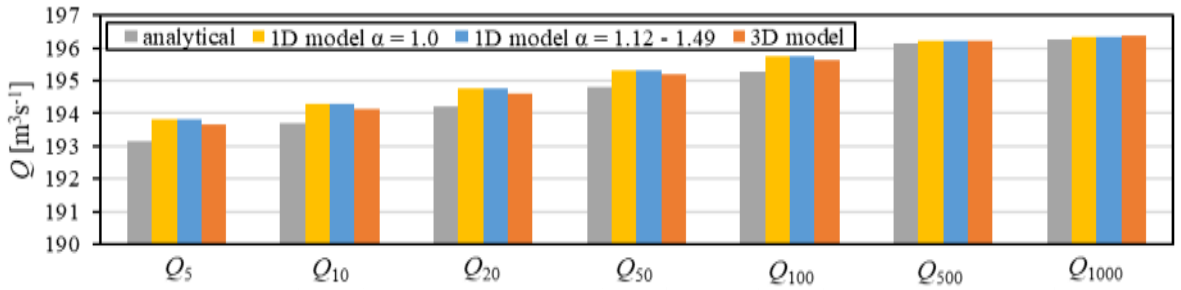

Figure 7. Max water surface elevations in the reservoir

5 Conclusion

Analytical hydraulic calculations are affected by significant uncertainties due to the simplifying assumptions they refer to. Therefore, the capacity was verified with a 1D numeric model. This solution provided basic information on the flow regime and water surface elevations in the associated dry reservoir's flow control object and highlighted other unresolved uncertainties that may compromise the safety of the reservoir, such as the occurrence and evolution of the hydraulic jump, the effect of submergence of the safety spillway and the bottom outlet, the capacity of the bottom outlet, the capacity of the spillway, and the longitudinal variability of the water surface elevation in the apron and chute. These uncertainties are common in reservoir designs where control profiles with known discharge parameters are not present (designed). These uncertainties could be resolved by experimental model research on a physical model of the flow control object. However, it can be assumed that, due to the lower significance of the proposed hydraulic structure, it will not be subjected to experimental research on the physical model. Therefore, a hydraulic analysis with 3D numerical software comes into consideration, which in this case can provide results for the hydraulic assessment or optimization of the

designed parameters of the object. 3D hydraulic calculations were performed in Flow - 3D software. The results show that the differences in the methods used are significant, especially in the range of extreme flows that can occur, i.e. Q_{500} and higher. The differences are up to 18% for the specified capacity of the safety spillway and the bottom outlet. The results show that the analytical solution of a specific flow control object is far from sufficient and it is necessary to assess the object hydraulically at least with a 1D model. The uncertainties in the hydraulic assessment of the stilling pool are mainly due to the assumption that due to the depression of the bottom of the stilling pool, we can consider the formation of a critical depth and a supercritical flow. This assumption seems to be unjustified from the results of the 3D model, at the discharge of Q_1 to Q_{500} the critical depth is not observed, it is flooded by the tailwater, in the profile of the stilling pool the supercritical flow is only observed at the discharge of Q_{1000}. The difference in the determined capacities is moderated by the transformation effect of the reservoir when solving the unsteady flood wave transformation simulation. It is worth mentioning that 3D numerical models are affected by significant uncertainties when using inappropriate methods, e.g. inappropriate resolution of the mesh domain, inappropriate turbulence model, sensitive boundary conditions or neglect of flow aeration, simplifying assumptions need to be evaluated in more detail in the conceptual model. Currently, there is no complete manual or workflow methodology for hydrotechnical research based on a 3D numerical model.

Acknowledgements
This article was elaborated with the support of the project FAST-S-24-8513 Analysis of the impact of input variables on the results of numerical models used in the safety assessment of water structures and TAČR SS07010401 Water management analysis of restoring natural floodplains and increasing the transformation effect of floodplains.

References:
[1] ČSN 75 2410 Small water reservoirs.
[2] TNV 75 2415 Suché nádrže (Dry retention reservoirs).
[3] Design of small dams. 3. Denver, USA: Bureau of Reclamation, 1987.
[4] Hager, W. H., A. J. Schleiss, R. M. Boes a M. Pfister. Hydraulic Engineering of Dams. Leiden, The Netherlands: CRC Press/Balkema, 2021. ISBN 978-0-47197289-1.
[5] Czech Act No. 254/2001 Coll. on water and on amendments to certain Acts (Water Act).
[6] Čábelka, J. a P. Gabriel. Matematické a fyzikální modelování v hydrotechnice. Praha: Academia, 1987.
[7] James, C. S., 2020. Hydraulic structures. 1. Johannesburg: Springer Nature Switzerland.
[8] Boor, B.; Kunštátský, J. A Patočka, C, 1968. Hydraulika pro vodohospodářské stavby. Praha: SNTL.
[9] Kolář, V.; Patočka, C., Bém, J., 1983. Hydraulika. Praha: SNTL.
[10] Stara, V.; Kohoutková H. Součinitel přepadu přelivu s kruhově zaoblenou korunou z fyzikálních experiment. In. 3. Vodohospodářská conference 2003 s mezinárodní účastí. Sborník příspěvků. Brno: ECON, 2003.
[11] Bos, M. G., W. Boiten, D. A. Kraijenhoff van de Leur, H. Oostinga, R. H. Pitlo, A. H. de Vries a J. Wijdieks. Discharge measurement structures. 3. Wageningen, The Netherlands: International Institute for Land Reclamation and Improvement, 1989. ISBN 9070754150.
[12] Rozanov, N. P., 1959. Voprosy projektrovanija vodopropusknych sooruženij, rabotajusčich v uslovijach vakuuma i pri bol'šich skorostjach potoka. Gosenergoizdat, Moskva.
[13] Jain, S. C., 2021. Open-channel flow. John Wiley & Sons.
[14] Říha, J.; Sedláček, M.; Smrž, P.; Veselý, R. a Žatecký, S. Návrh a realizace suchých nádrží z pohledu technickobezpečnostního dohledu. Praha: Ministerstvo životního prostředí, 2014. ISBN 978-80-7212-600-2.
[15] Šulc, J.: Příspěvek k problematice vodního skoku v divergentním korytě. Vodní hospodářství řada A, č. 9, 1983, str. 247–250
[16] Čertousov, M. D., 1957. Gidravlika - special'nyj kurs. Moskva - Leningrad.
[17] FLOW-3D® Version 2023R1 User's Manual (2023). FLOW-3D [Computer software]. Santa Fe, NM: Flow Science, Inc. https://www.flow3d.com

[18] Vreugdenhil, C. B. Numerical methods for shallow-water flow. 13. Dordrecht: Kluwer Academic Publishers, 1998. ISBN 0-7923-3164-8.
[19] Chie Yen, Ben. Channel flow resistance. 2. Colorado: Water Resources Publications, 2004. ISBN 0-918334-72-1.
[20] Černá, D. Srážko-odtokový model povodí Kotojedky. Brno, 2023. 52 s. Bakalářská práce. Vysoké učení technické v Brně, Fakulta stavební, Ústav vodního hospodářství krajiny. Vedoucí práce doc. Ing. Daniel Marton, Ph.D.
[21] ČSN 75 2935 The safety assessment of hydraulic structures during floods
[22] French, R. H. Open-channel hydraulics. USA: McGraw-Hill, 1976. ISBN 0-07-022134-0.
[23] Chow, V. T. Open-channel hydraulics. USA: McGraw-Hill, 1959. ISBN 07-010776-9.

NUMERICAL STUDY OF SCOUR HOLE DEVELOPMENT DOWNSTREAM OF RIPRAP-PROTECTED BRIDGE PIERS

ANTONIJA HARASTI [1], GORDON GILJA[2], NIKOLA ADŽAGA[3], MARK ŽIC[4]

[1] University of Zagreb Faculty of Civil Engineering, Croatia, antonija.harasti@grad.unizg.hr

[2] University of Zagreb Faculty of Civil Engineering, Croatia, gordon.gilja@grad.unizg.hr

[3] University of Zagreb Faculty of Civil Engineering, Croatia, nikola.adzaga@grad.unizg.hr

[4] Division of Materials Physics Ruder Boskovic Institute, Croatia, Mark.Zic@irb.hr

1 Abstract

This paper presents a study on local scour around a bridge riprap- protected pier. Riprap sloping structure is the most common method used to protect piers against scour on large Croatian rivers. Although the riprap sloping structure protects the pier from further scouring, a deflected scour hole appears downstream of the bridge profile. To investigate how the riprap disturbs the flow field around the pier, a numerical model is established in Flow-3D. Numerical simulation considers small-scale riprap sloping structure under submerged flood conditions. The results provide insight into the flow patterns that cause the scouring process downstream of the bridge profile.

Keywords: bridge pier, local scour, riprap protection, numerical model, Flow-3D

2 Introduction

Local scour at bridge piers is the primary mechanism of bridge failure. One of the most widely used methods to mitigate the impact of scouring on bridge piers is the riprap countermeasure. The type of riprap protection used on large Croatian rives is the riprap sloping structure [1]. This riprap structure is composed of launchable stones radially placed around the bridge pier and above the original riverbed level.

Although the riprap structure prevents further sediment erosion around the pier, it has been observed that riverbed deepening continues downstream of the bridge profile. The scour hole that is moved downstream is the opposite phenomenon that appears at single piers, where scour typically occurs at the upstream pier nose. In addition, in study on scour around different pier arrangements has been noticed that scour hole also appears downstream of the group of piers [2]. The reason could be similar as for scour around spur dikes, deflection of the main current away from the longitudinal axis induced by large flow obstruction.

Previous research has proposed a similarity between riprap sloping structure and complex piers, particularly in the widening of contours at the lower part of both structures [3]. Thus, the flow around the riprap can be described based on two processes: flow around the riprap and overflow above the top of the riprap under high water conditions.

In the literature, numerical models are frequently used for three-dimensional hydraulic simulations due to their flexibility, efficiency, and ability to provide detailed results across a wide range of scenarios. One of the most powerful CFD software in simulating scouring process is Flow-3D [4] [5] [6]. For instance, Flow-3D was used to analyze the sensitivity of bed roughness, where increasing the roughness by up to 7.5 times resulted in increase of scour depths around bridge piers up to 40% [7]. Additionally, sensitivity analyses of cell size were also carried out in Flow-3D, revealing that a 60% reduction in cell size led to a 20% increase in piers scour depth [8]. Chandara et al. [9] tested the influence of different turbulence models in Flow-3D on scour formation around bridge piers. Results showed that the LES turbulence model generates more realistic flow pattern and consequently larger scour depths, while for

spur dikes, RNG turbulence model proved to be more accurate in predicting scour depth [10].
Given that scour around riprap protection presents a global challenge in many regions, it is important to investigate processes that cause this unexplored phenomenon. The aim of this paper is to use Flow-3D to simulate flow around the riprap sloping structure installed at bridge pier and to understand how flow pattern influences downstream scour phenomenon.

3 Numerical model

3.1 Governing equations

Flow-3D is CFD software that solves RANS equations to describe the motion of turbulent flow, where governing equations are the continuity equation $\delta(vel \cdot A)/\delta x = 0$ and the momentum equation as follows:

$$\frac{\delta \bar{u}}{\delta t} + \bar{v}\frac{\delta \bar{u}}{\delta y} = -\frac{1}{\rho}\frac{\delta \bar{p}}{\delta x} + \frac{\delta}{\delta y}\left(2\nu_f \overline{s_{xy}} - \overline{\tau_{xy}}\right) , \quad (1)$$

where u is the velocity component in x direction, p is the pressure, ν_f is fluid kinetic viscosity, s_{xy} is the strain rate tensor and τ_{xy} is the Reynolds stress tensor which equations are following:

$$s_{xy} = \frac{1}{2}\left(\frac{\delta u}{\delta y} + \frac{\delta v}{\delta x}\right), \quad (2)$$

$$\overline{\tau_{xy}} = \overline{u'v'} = \nu_t\left(\frac{\delta u}{\delta y} + \frac{\delta v}{\delta x}\right) - \frac{2}{3}\rho k , \quad (3)$$

where v is the velocity component in y direction, ν_t is turbulence viscosity, and k is the turbulent kinetic energy $k = \frac{1}{2}\cdot\overline{u_x' u_y'}$. To close the Reynolds averaging process and represent the effect of turbulence, the LES turbulence model is selected to calculate turbulence viscosity parameter. LES turbulence model directly resolves large eddies in turbulent flow. Adequate selection of turbulence model is important for modeling scour due to its direct influence on local shear stress – the main indicator for bed-load erosion. Many studies recommend LES turbulence model for scour simulations because of its capability to captures the dynamics of larger turbulent structures while modelling the effects of smaller eddies [9]. However, in comparison to other turbulence models (RNG, *k-ε*, *k-ω*), LES is computationally more expensive because it requires very fine mesh [10]. Near-wall boundary conditions, represented as near bed fluid velocity, are defined using logarithmic law with the consideration of bed surface roughness:

$$u = u_\tau \cdot \left[\frac{1}{\kappa}\cdot \ln\left(\frac{y}{\frac{\nu_f}{u_\tau} + k_s}\right)\right], \quad (4)$$

where $u_\tau = \sqrt{\tau/\rho}$ is the shear velocity, y is distance from wall, κ is Von Kármán constant (0.4187), and $k_s = c_s \cdot d_{50}$ is surface roughness as a function of a median grain size. Hydraulic roughness in numerical model accounts for all imperfection on the surface and can be manually modified by user-defined coefficient c_s – roughness height multiplier. Incresing the roughness height affects the increase in shear stress and consequently increase scour and deposition magnitudes.
To model scour and deposition patterns around riprap structure in Flow-3D, a sediment transport model is fully coupled with 3D hydraulic solver. The sediment transport model simulates the changes of the geometry of the packed bed – erodible solid object that represent bed channel. Sediment transport is described through entrainment and deposition of suspended sediment, and rolling, hopping and sliding of bedload sediment. The amount of eroded packed sediment is calculated in each cell at each time step as fraction of packed sediment. The open area fraction and open volume fraction of packed bed interface is calculated with FAVOR technique [11] based on structured computational rectangular mesh. Sediments can be defined with up to 10 different non-cohesive species, specified by grain size, density of sediment, critical shear stress, and angle of repose. The amount of rolling and sliding sediment motions along the packed bed are calculated by one of the three different bedload transport equations (Nielsen 1992, Meyer-Peter Müller 1948, and Van Rijn 1984). If critical shear stress is exceeded, smaller

grains are entrained into the suspension, which velocity is calculated based on Mastbergen and Van Den Berg equation [12]. Transition from suspended sediment to packed bed sediment is defined as settling velocity of grains defined by Soulsby deposition equation [13].

3.2 Numerical setup

Riprap sloping structure around pier were set up in the small-scale model to replicate typical natural high-water conditions of submerged structure. The riprap is designed as non-erodible solid object, 8 cm above the flat bed, and with diameter at the bed channel of 30 cm. The channel is represented by the packed bed that is 2 m long, 0.8 m wide, and 0.1 cm thick. Packed bed is composed of uniform sand material sediment, containing only one sediment species with the mean diameter of 0.2 mm, mass density of 2650 kg/m^3, angle of repose of 32°, and packing fraction is 0.64. Twenty centimeters long rough packed bed is added at the inlet of the channel that is composed of larger grain size (1 cm) to induce fully developed turbulent flow and prevent erosion at the inlet. Figure 1 shows the experimental small-scale setup of characteristic riprap sloping structure around the pier in hydraulic flume.

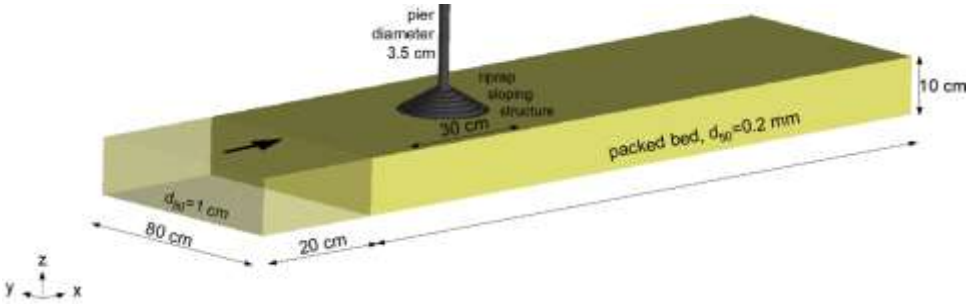

Figure 1. Configuration of numerical model represeting characteristic riprap sloping structure geometry in small scale flume

In this study the Meyer-Peter Muller equation is adopted for bedload transport equation. The selected bed load coefficient is a default value of 8, used for middle bed load transport rates. Critical Shields parameter is 0.05, while entertainment transport coefficient is 0.0018.

The inlet boundary condition is flow with longitudinal vector direction and uniform outflow specified with water surface elevation at the outlet. Numerical technique adopted to model free water surface is volume of fluid (VoF) method [14]. The initial water surface elevation is 16.5 cm, and in the beginning of the experiment discharge rate was gradually increased from 2 l/s to 28 l/s. After reaching steady flow of 28 l/s, that is in clear water scour condition, simulation was performed for 166 minutes, when equilibrium condition is achieved.

Computational mesh consists of 168,000 cells in total, with finer mesh cell sizes close to the riprap of 0.008 m which sizes gradually increase in all directions up to 0.02 m at the domain boundaries (Figure 2).

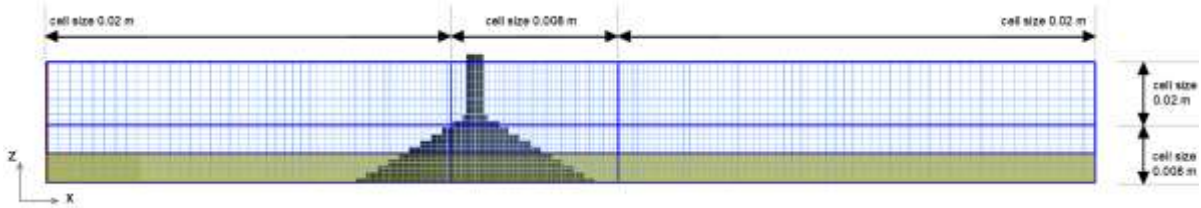

Figure 2. Computational mesh structure composed of rectangular planes

3.3 Validation setup

Since many assumptions and adopted coefficients are involved in numerical model, results were compared to the experimental data from the physical model. Validate of numerical simulation was based

on the same hydraulic boundary conditions. Experiments in physical model reached equilibrium scour depth of 3.2 cm after 30 hours. In numerical model, temporal evolution of scour depth has been observed during simulation. After 150 minutes the scour depth of 3.0 cm scour was no longer changing, it suggests that an equilibrium state has been reached. Contours of the equilibrium scour development for both the numerical and physical model are illustrated in Figure 3, where good agreement with measurements in physical model are observed.

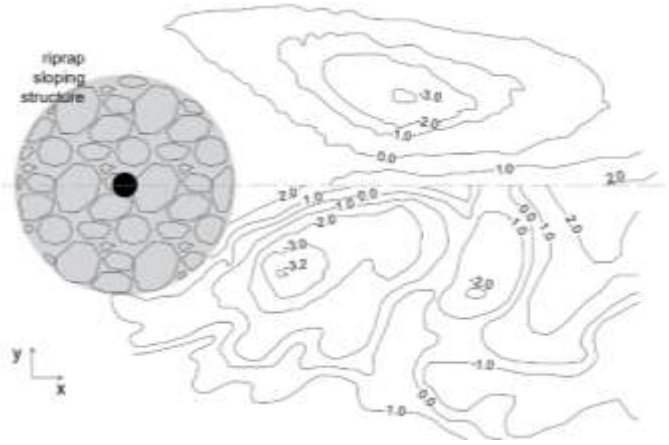

Figure 3. Scour development [in cm] around riprap sloping structure represented with contour lines for numerical model (upper part) and for physical model (down part)

Error in maximum scour depth is equal to 6.6 %, while the location of maximum scour depth in numerical model has been slightly moved downstream. Figure 4 presents temporal development of maximum scour depth comparing to experimental values scour hole evolution during time. According to the presented results, we can conclude that accuracy of numerical simulation of scour around riprap sloping structure is acceptable.

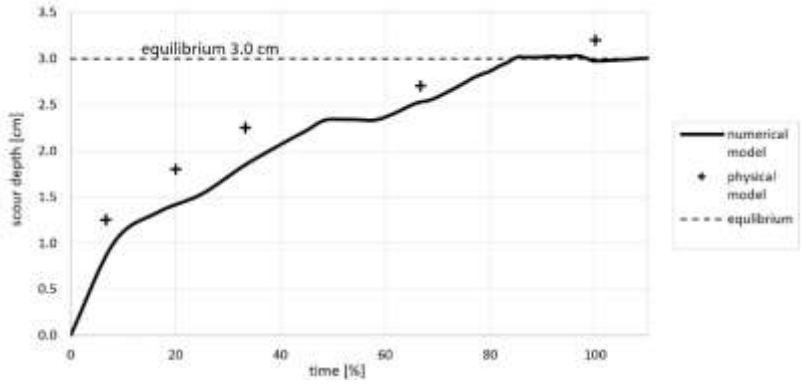

Figure 4. Temporal development od scour hole downstream of riprap sloping structure measured in physical model and simulated in numerical model

4 Results and discussion

The purpose of this study is to investigate the flow pattern that influences local scour around riprap sloping structure. Figure 5 shows bathymetry of scoured bed after reaching equilibrium stage. Results show a typical formation of two symmetrical scour holes slightly moved downstream as a consequence of disturbed flow field around the riprap sloping structure. The flow field around riprap is presented with streamlines on the right side of Figure 5 that illustrate strong vortex region behind the riprap where scouring occurs. The vertical direction of streamlines indicates that conditions for lifting sediments particles from the packed bed are achieved.

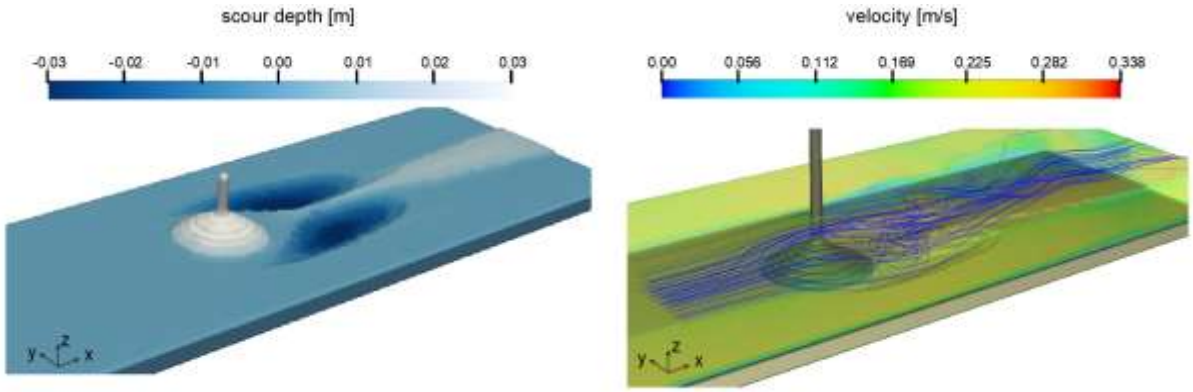

Figure 5. Surface bed bathymetry around riprap sloping structure at the equilibrium stage (left); streamlines flowing around riprap sloping structure (right)

The strong downflow, that usually appears in front of the single piers, is absent in this riprap-protected pier. The downflow usually initiates development of horseshoe vortex – primary mechanism for scour evolution in front of the single pier. Velocity vectors in front of the pier are directed up to the upstream riprap slope, which is the reason why the downflow-horseshoe system and upstream scour hole do not appear. Instead, flow approaches riprap-protected pier, separates in two strong currents that flow around and over the top of the riprap and consequently cause pair of deflected scour holes. Those two currents accelerate until the bed surface is eroded in a form of two elongated and deflected scour holes. Figure 6 presents velocity distribution at three longitudinal profiles: through the central axis of the channel, through the maximum scour hole depth and in the middle of the previous two profiles. The first longitudinal profile, through the center of the channel, shows that velocities in the wake region, behind the riprap, are small, with dominant vertical direction. The second longitudinal profile, through the inner slope of the scour hole, is characterized by the strong vortex system and flow acceleration above the riprap. The third longitudinal profile, through the maximum scour depth, shows an increase in total velocity values above the scour hole, with dominant x-direction of the vectors.

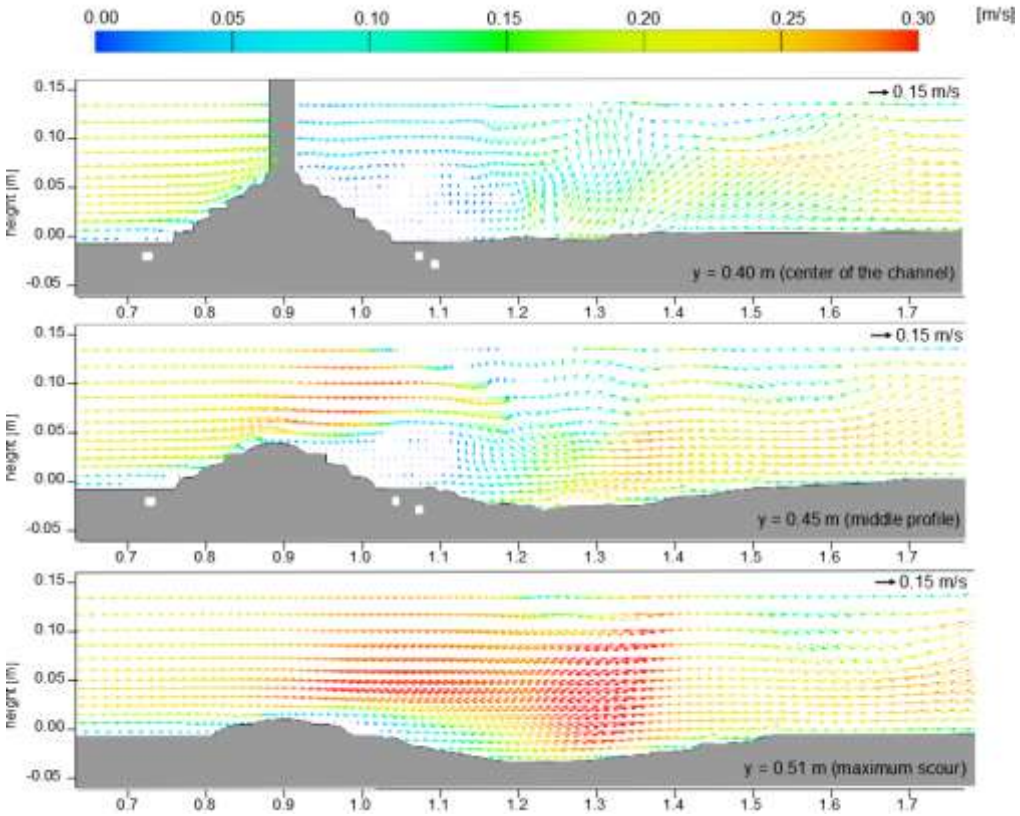

Figure 6. Longitudinal flow velocity distribution through three profiles: at the channel axis (y = 0.4m); 5 cm away from the axis; and at the maximum scour depth (0.51 m)

The scour region behind the riprap spreads approximately 2 times the riprap diameter to downstream, after which channel surface is flat. The first signs of deposition appear in the riprap wake region, between two symmetrical scour holes, while the greatest amount of deposited material can be noticed right behind the developed scour holes (Figure 5). To understand why sediment particles are deposited between the scour holes, cross-sectional profile through the maximum scour depth is plotted (Figure 7). Transverse velocities indicate two symmetrical counter-rotating vortices above each scour hole. Velocities in y-direction are large enough to move the particles towards the central axis, where they deposit because velocities in x-direction are too small to carry sediment along the channel.

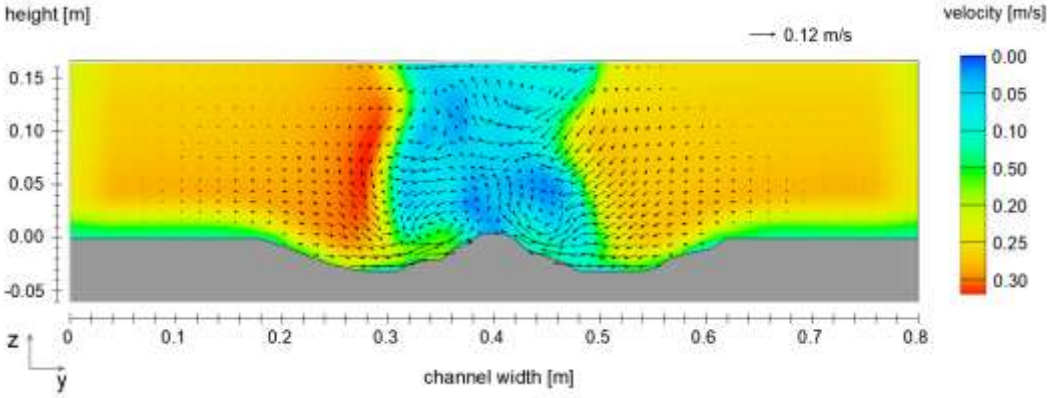

Figure 7. Transverse low velocity distribution at the cross section where the scour depth is maximum

To analyze the flow velocity more detailly, Figure 8 shows velocity distribution near the bottom at layer 1.5 cm above the initial bed level. It can be noticed that scouring is primarily influenced by main flow

acceleration in the downstream area where the wake vortex region meets the main longitudinal flow.

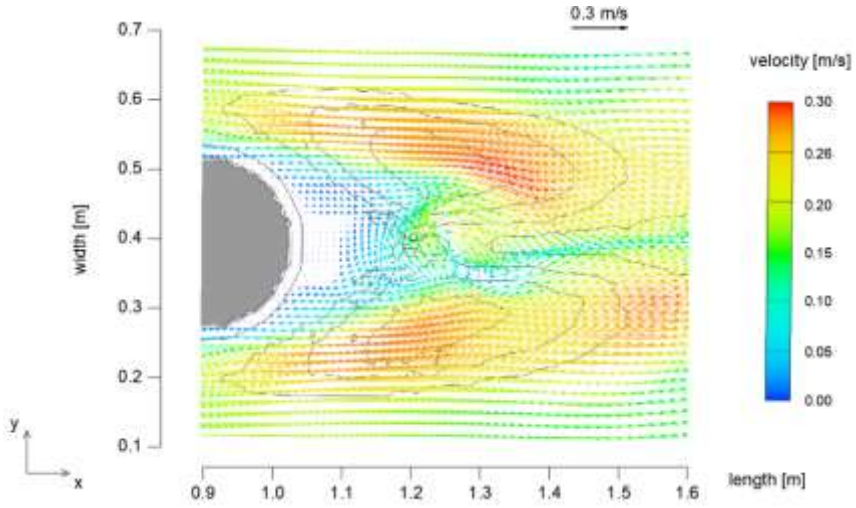

Figure 8. Flow field distribution around the riprap sloping structure at the equilibrium stage

5 Conclusion

This paper presents a numerical study on local scour around riprap sloping structure. Numerical simulation results revealed how flow structure influence scour hole development downstream of riprap-protected bridge piers. The approaching streamlines are directed up along the upstream slope of the riprap structure. Streamlines above the riprap accelerate and flow around the pier, resulting in the formation of counter-rotating vortices downstream. According to the presented results, a pair of counter-rotating vortices eject sediment from the scour holes towards the channel axis, while the main flow carries sediment downstream along the channel. At a distance of approximately two riprap diameters, the disturbed flow pattern dissipates, where the eroded sediment is deposited onto the flat packed bed. This study proved capability of sediment scour model in Flow-3D, fully coupled with hydrodynamic solver, 3D modelling of local scour around riprap sloping structure.
Riprap protection does not resolve the scouring issue; instead, it relocates the scour hole downstream within the river channel. This displacement is probably due to the elevation of the riprap structure above the riverbed level, which reduces the flow area and consequently increases the velocity of the water. In addition, the riprap surface is hydraulically very rough, which contributes to an increased turbulence intensity. To mitigate the effects of turbulence near the pier, it is suggested the riprap structure to be designed with a lower height. Future research should focus on analyzing different riprap heights to reduce the depth of the scour hole.

Acknowledgements
This work has been supported in part by Croatian Science Foundation under the project R3PEAT (UIP-2019-04-4046).

References:
[1] Gilja, G., Kuspilić, N., Bekić, D., Zubčić, K.: Pristup forenzičnog inženjerstva pri specijalističkim pregledima donjeg ustroja željezničkih mostova na rijekama, Željeznice 21, 19(1), pp. 9-19, 2020.
[2] Zhang, Q., Zhou, X.L., Wang, J.-H.: Numerical investigation of local scour around three adjacent piles with different arrangements under current, Ocean Engineering, 142, pp. 625-638, 2017
[3] Harasti, A., Gilja, G., Potočki K., Lacko M.: Scour at Bridge Piers Protected by the Riprap Sloping Structure: A Review, Water, 13(24): pp. 3606., 2021
[4] Omara, H., Tawfik, A.: Numerical study of local scour around bridge piers, IOP Conference Series: Earth and Environmental Science, 151(1), pp. 012013, 2018
[5] Jalal, H.K., Hassan, W.H.: Three-dimensional numerical simulation of local scour around circular

bridge pier using Flow-3D software, IOP Conference Series: Materials Science and Engineering, 745, pp. 012150., 2020
[6] Fox, B.: CFD Analysis of Local Scour at Bridge Piers, Engineering, Environmental Science, 00, 2019
[7] Harasti, A., Gilja G., Valyrakis M.: Scour around riprap protected piers: a numerical assessment of the effect of bed roughness. in 4th IAHR Young Professionals Congress. 2023. International Association for Hydro-Environment Engineering and Research.
[8] Harasti, A.: Influence of the relevant parameters in scour process around bridge piers protected by the riprap sloping structure (Thesis), University of Zagreb Faculty of Civil Engineering, Zagreb, 2024.
[9] Chandara, M., Zhang G., Hong V., Zhou S., Feng Y.: Assessment of Turbulence Models on Bridge-Pier Scour Using Flow-3D, World Journal of Engineering and Technology, 7, pp. 241-255, 2019
[10] Gupta, L., Pandey, M., Raj P.: Numerical modeling of scour and erosion processes around spur dike. CLEAN – Soil, Air, Water, 00, pp. 2300136, 2023.
[11] Hirt, C.W., Sicilian, J.M.: A Porosity Technique for the Definition of Obstacles in Rectangular Cell Meshes, International Conference on Numerical Ship Hydrodynamics (4th), Washington, pp. 19, 1985
[12] Mastbergen, D.R., Van Den Berg, J.H.: Breaching in fine sands and the generation of sustained turbidity currents in submarine canyons. Sedimentology, 50(4), pp. 625-637, 2003
[13] Soulsby, R.: Dynamics of marine sands, Thomas Telford Publications, 1997
[14] Hirt, C.W., Nichols, B.D.: Volume of fluid (VOF) method for the dynamics of free boundaries, Journal of Computational Physics, 39(1), pp. 201-225, 1981

ESTIMATION OF THE TRANSMISSION COEFFICIENT FOR A Π-TYPE FLOATING BREAKWATER IN THE PRESENCE OF SPECTRAL WAVES AND VARIABLE DEPTH

DAMJAN BUJAK [1], ANTONIJA TOPIĆ [2], DALIBOR CAREVIĆ [3], HANNA MILIČEVIĆ [4]

[1] *University of Zagreb, Faculty of Civil Engineering, Croatia, damjan.bujak@grad.unizg.hr*

[2] *Hidroing Osijek, Croatia, antonija.topic@hidroing-os.hr*

[3] *University of Zagreb, Faculty of Civil Engineering, Croatia, dalibor.carevic@grad.unizg.hr*

[4] *University of Zagreb, Faculty of Civil Engineering, Croatia, hanna.milicevic@grad.unizg.hr*

1 Abstract

Floating breakwaters protect ships in marinas, especially in partially sheltered areas like the eastern Adriatic coast. Consequently, thoroughly assessing wave energy transmission under the floating breakwater is essential. This paper evaluates Ruol et al.'s equation for estimating wave energy transmission through π-type floating breakwaters coefficient using lab measurements. The findings suggest that decreasing water depth causes an increase in the transmission coefficient. Furthermore, it has been observed that the empirical equation gives an underestimation of measurements by 25% when both $1.0<T_p/T_h<1.20$ and $d/h<0.2$.

Keywords: floating breakwater, waves, transmission coefficient, wave energy, marinas

2 Introduction

In the context of marina, a basin refers to a water surface that is either naturally formed or constructed to provide protection and security for the port. The marina maneuvering area and the marina mooring area are the main components of a protected basin. In order to safeguard the port and marina water areas from the impact of incoming waves, a range of coastal engineering structures have been constructed. These structures are designed to have a dual role, both facilitating safe navigation and providing shelter against the forces of nature. To ensure the safety and security of the port water area, various internal maritime structures have been implemented. These structures include the coastal wall, breakwater, pier, fortification, dolphin, buoy, and the arranged shore.

Breakwaters and similar structures are the most used coastal protection structures for safeguarding the basin. Within the protected water area, breakwaters play a crucial functional role by mitigating wave-induced agitation to an acceptable level. Typically, when we talk about acceptable wave agitation within protected water areas, we are referring to the values that are recommended by [1] or the guidelines set by the local authorities.

The most common application of a floating breakwater is seen in smaller marinas that experience a mild wave climate, characterized by wave periods of up to 4 seconds and wave heights of up to 1.5 meters [2]. In this study, we will specifically concentrate on the π floating breakwater as one of the various shapes of the cross-section of floating pontoons. The breakwater that is being considered has a cross-section in the shape of a rectangle, with two side plates that are pointed downwards. This particular shape resembles the Greek letter π, which is why this type of breakwater is referred to as such [3]. The individual prefabricated elements of the floating breakwater are securely connected to one another, and each one is individually anchored in place. The π-type breakwater has seen some research in the field of coastal engineering, with Ruol's equation giving the ability to predict the transmission coefficient of the

floating breakwater [4].

The aim of this study is to verify the validity of the Ruol et al., 2013 formula [4] for calculating the transmission coefficient under a π-type floating breakwater influenced by spectral waves. This study will focus on a region that was not tested during the equation construction, namely the low relative draft region ($d/h < 0.2$) [5]. Description is also given for the influence of water depth and overtopping over the floating breakwater.

3 Methods

3.1 Laboratory experiments

The tests, which were conducted in a wave flume, took place at the Faculty of Civil Engineering, University of Zagreb. To ensure proper fit within the wave flume, a scaling factor of 1:21 was applied to both the floating breakwater model and the generated waves. By analyzing the measured significant wave heights both in front of and behind the pontoon model, we were able to determine the corresponding transmission coefficients (K_t). Due to the limitations of the wave flume geometry, the tests that were conducted solely concentrated on the application of the orthogonal wave approach on the floating breakwater.

The wave flume is constructed with plywood side walls, while the bottom and side walls are lined with waterproof insulation for added protection. Figure1 shows that on a specific section of the wave channel, glass panels have been installed on both sides. The primary function of these panels is to provide the means to visually monitor the hydraulic phenomenology. Figure 2 provides the dimensions of the wave flume, indicating that it has a length of 18.35 m, a width of 1 m, and a height of 1.1 m. The depth in the wave flume decreases by 0.1 m when the bottom is raised at a distance of 7.6 m from the wave generator as indicated in Figure 2. The raised bottom, constructed from a durable wood material, provides the ideal surface for securely fastening the structures to the bottom of the wave channel. The implementation of this method guarantees that the waterproof membrane, which is carefully installed around the flume perimeter, remains completely intact without any damage during the installation process. Constructed from smaller stone blocks with an average diameter of 0.3 m, the dissipation section is situated at the end of the wave flume, as depicted in Figure 1. The main objective of the dissipation section is to effectively minimize wave reflection that would occur at the end wall of the wave flume. The laboratory conducted tests by utilizing a wave generator of the "piston" type, which was manufactured by the Danish Hydraulic Institute (DHI) and featured an integrated AWACS system (Active Wave Absorption Control System). By utilizing this system, it becomes possible to avoid the negative consequences associated with wave reflection from the generator plate. Consequently, this enables the collection of longer and uninterrupted measurements of the wave climate both in front of and behind the model breakwater.

The physical model of the floating breakwater is constructed according to the prototype model BRK 5320, which is manufactured by Marinetek, and has been placed at a distance of 14.9 m from the beginning of the flume. In order to convert the parameter values from prototype scale to the scale of the physical model, a physical model length scale of 1:21 was adopted. The model, which is depicted in Figure 1, was created utilizing a 3D printer. The BRK 5320 model has a width of 0.24 m and a length of 0.95 m. The floating breakwater features plates that are 0.09 m in length. The downward orientation of these plates and their resemblance to the Greek letter π are what give this type of breakwater its name. The model, as depicted in Figures 1 and 2, is securely anchored with the use of four anchor ropes. In order to anchor the pontoon model, each chain is attached to one edge of the pontoon and to anchor blocks placed on the seabed. These anchor blocks are alternatively known as "corpo morte". The length of each rope measures 1.93 meters, and there are anchor blocks weighing 1 kg placed at each end, with a distance of 0.9 meters between them. The floating breakwater is equipped with weighted plates, which serve to enhance both its weight and draft. This action was required to ensure that the floating breakwater

meets the draft requirements outlined in the Marinetek usability guidelines. The removal of these plates leads to a decrease in the breakwater's draft.

Figure 1. Photographs of a) the dissipation chamber at the end of the wave flume and b) the model of the BRK 5320 floating breakwater model with 4 mooring ropes

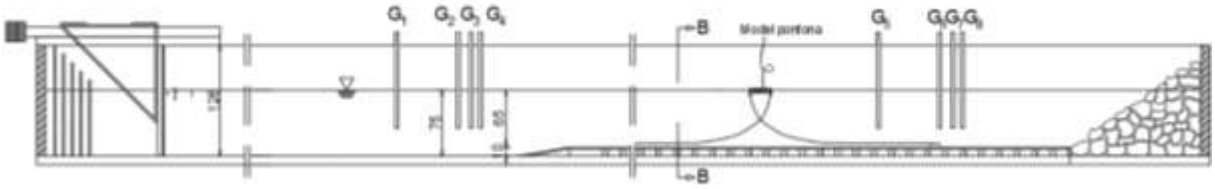

Figure 2. Drawing of the wave flume and installed equipment with indicated positions of the physical pontoon model and the positions of the measuring probes for monitoring the water surface elevation in front of and behind the tested floating breakwater

A time series of 3 minutes was used for statistical processing in order to achieve a comprehensive analysis of the spectral wave records, which provide a more detailed representation of the natural wave climate compared to simpler monochromatic waves. The selected characteristic spectral waves are typically found in seas comparable to the Adriatic in terms of fetch length, wind strength, and direction. By adjusting the significant wave height from 0.048 m to 0.057 m and the wave length from 0.952 m to 1.667 m, a range of wave steepness levels corresponding to 1/20 to 1/35 was achieved in the model scale. Furthermore, we tested the effects of three different water depths, specifically 0.55 m, 0.35 m, and 0.27 m. A grand total of 72 tests were conducted on the floating breakwater.

In order to monitor the dynamics of the water surface, a total of 8 measuring probes were set up. The probes in question were strategically placed at different distances from the starting point of the channel, as shown in Figure 2. Eight capacitive probes were strategically positioned near the floating breakwater to measure the transmission of wave energy. The first four probes (G1 - G4) were strategically placed in front of the breakwater to ensure precise measurements of the incoming wave parameters. Furthermore, to analyze the wave characteristics of the waves that transmitted through the floating breakwater, we made sure to carefully position the remaining four probes (G5 - G8) behind the breakwater. To effectively prevent undersampling, or aliasing, we can set the sampling frequency of the capacitive probes to 40 Hz. The spectral wave transmission was analyzed by separating the waves into incident and reflected waves. The ability to separate the data allowed for the determination of wave

heights, which, in turn, could be used in subsequent the coefficients of transmission, *Kt*. The reflected and transmitted wave signals have been separated using Zelt's method [6]. The placement of the wave gauges, which are labeled as G1-G8, has been carefully determined based on their respective distances from the wave generator. Specifically, G1 is positioned at 5.67 m, G2 at 6.37 m, G3 at 6.52 m, G4 at 6.63 m, G5 at 14.79 m, G6 at 15.49 m, G7 at 15.64 m, and G8 at 15.75 m.

3.2 Empirical equations for predicting the transmission coefficients

When a wave encounters a barrier, its energy can be divided into three distinct parts: the transmitted part, the reflected part, and the part that dissipates through the complex process of flowing around the structure. Although direct measurement of energy losses is not feasible, it is possible to indirectly infer them by analyzing the reflection and transmission of energy. In the two-dimensional case, the energy balance equation for a submerged structure can be expressed in a general form:

$$1 = K_R^2 + K_T^2 + K_V^2 \tag{1}$$

In this equation, we define K_r as the portion of energy that is reflected, K_t as the portion that is transmitted, and K_v as the portion that is dissipated as heat. Macagno, in his 1954 paper, proposed an equation that deals with the prediction of the transmitted wave energy passing through a fixed submerged structure [7] :

$$K_{TM} = \frac{1}{\sqrt{1+\left(kw \frac{\sinh kh}{2cosh\left(kh-kd\right)} \right)^2}} \tag{2}$$

In this equation, the wave number (*k*), breakwater width (*w*), depth (*h*), and structure draft (*d*) are all variables that need to be considered. In order to use Macagno's formula for predicting the transmission coefficient, it is important to note that it is only applicable for a specific type of pontoon and certain additional constraints must be taken into account. In the case when the draft (*d*) is equal to the water depth (*h*), transmission unexpectedly occurs, even though it is not anticipated. In the application of Macagno's formula to estimate the transmission coefficient for irregular waves, the wavelength parameter is substituted with the average wavelength value, which is determined by calculating the average wave period ($T = T_p$ / 1.1) and then using it in the formula. Due to the inaccuracy of the results obtained when applying the formula to the π-type pontoon, it has become necessary to enhance and modify Macagno's formula. In the work conducted by Ruol [4], they present the improvement and extension of Macagno's equation. The researchers provide a semi-empirical formula in their study, which can be used to calculate the transmission coefficient of π-type pontoons. The problem arises primarily due to the challenge in defining the natural heave period, T_h, for various types of breakwaters. The researchers at [4] developed a methodology to address this issue, which ultimately resulted in the formulation of the following formula for T_h:

$$T_h = \frac{2\pi}{\omega_h} \tag{3}$$

$$\omega_h = \sqrt{\frac{g}{d+0.35w}} \tag{4}$$

Where ω_h is the natural heave frequency of a particular floating π-type breakwater. After that they

defined the scaling parameter which is related to the aformentioned natural heave frequency ω_h is calculated by:

$$X = \frac{T_p}{2\pi}\sqrt{\frac{g}{d+0.35w}} \tag{5}$$

$$\beta = \frac{1}{1+\frac{X-X_0}{\sigma}e^{-(\frac{X-X_0}{\sigma})^2}} \tag{6}$$

$$K_t = \beta K_{tM} \tag{7}$$

Where σ = 0.1922 and X_0 = 0.7919. The scaling factor β is used to scale the transmission coefficient calculated using Macagano's equation. For more details about this method for prediction of transmission coefficient of a floating breakwater, the reader is referred to [4]. Some limitations of this semi-empirical equation have been detected, such as the calibrated range of the relative draft which is d/h = [0.20 – 0.45]. In this paper, we will examine the range of the relative draft d/h which is outside the calibrated range, d/h = [0.10 – 0.21].

4 Results and discussion

4.1 Influence of depth on wave energy transmission

According to the data presented in Figure 3, there is a noticeable trend indicating that the measured transmission of wave energy decreases with the reduction in water depth at the location of the floating breakwater, as shown by the filled box plots (red, yellow and green). Specifically, at a depth of 0.55 m, the transmission coefficient ranges from 0.57 to 0.92, with a mean value of 0.76 and a median of 0.78. For a depth of 0.35 m, the transmission coefficient varies from 0.57 to 0.83, with a mean value of 0.72 and a median of 0.74. At a depth of 0.27 m, the transmission coefficient ranges from 0.56 to 0.81, with a mean value of 0.68 and a median of 0.67. These data reveal that the maximum, mean, and median values of the set of measured transmission coefficient decrease as water depth decreases, whereas the minimum value remains relatively constant across all depths. In contrast, the predicted transmission coefficients, represented by the hatched box plots (green, cyan and purple) based on the Ruol's equation, exhibit a slight but opposite trend. For a depth of 0.55 m, the transmission coefficient ranges from 0.43 to 0.88, with a mean value of 0.72 and a median of 0.75. At a depth of 0.35 m, the transmission coefficient ranges from 0.43 to 0.90, with a mean value of 0.74 and a median of 0.77. For the depth of 0.27 m, the transmission coefficient ranges from 0.44 to 0.92, with a mean value of 0.71 and a median of 0.70. Interestingly, the predicted values using Ruol's equation suggest that the transmission coefficient should be highest at the shallowest depth, which contrasts with the observed data trend in this study.

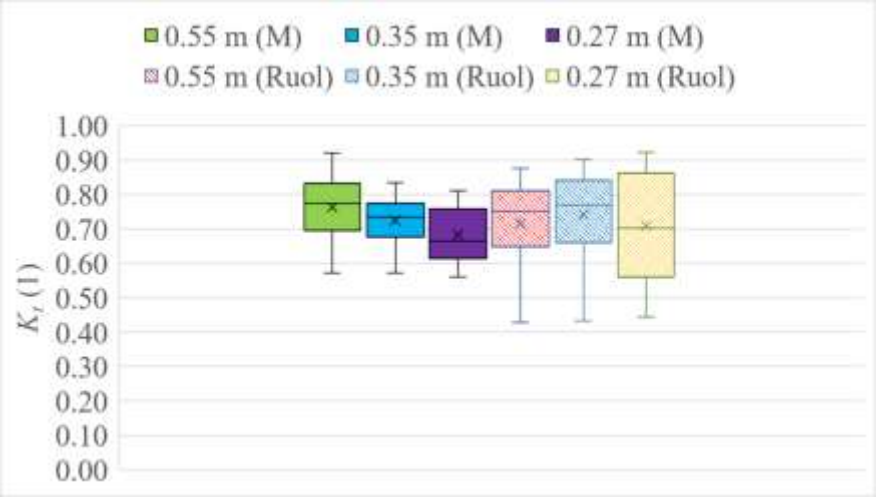

Figure 3. Results of the transmission coefficient, *Kt*, measurements by depth categories: box plots filled with color represent the measured values in this study, while hatched box plots indicate the predicted transmission coefficients according to the Ruol et al., 2013 equation **[4]**

The reason for this variation may be due to the occurrence of overtopping on the floating breakwater, which was visually observed in the majority of the tests carried out in this research (Figure 4). With shallower depths, there is a greater rise in wave height (shoaling) along the wave flume, which then results in more wave breaking and overtopping over the floating breakwater. This overtopping mechanism causes greater energy dissipation and lower wave energy transmission.

Greater energy dissipation can be seen by looking at Figure 5. Firstly, the reflection coefficient rises with the decline of the water depth, which is an expected behavior because there is a higher blockage percentage of the flow area in the water column. Furthermore, by using the relation in Equation 1, the energy dissipation can be calculated, which shows that indeed the highest energy dissipation is for the shallowest case.

It is important to note that the research conducted by Ruol et al., 2013 did not include cases with overtopping. The Ruol et al., 2013 study used plates on the front of the floating breakwater to block overtopping. Consequently, overtopping over the floating pontoon was not taken into account when developing the equation for predicting the transmission coefficient provided by Ruol et al., 2013 (description given in Section 3.2). It should be additionally noted that these tests were out of the calibration range of the Ruol et al., 2013 equation which was constructed for *d/h* in range [0.20 – 0.45], while these measurements were done in the [0.10 – 0.21] range [5].

Figure 4. Photograph of waves overtopping the floating breakwater during a test run

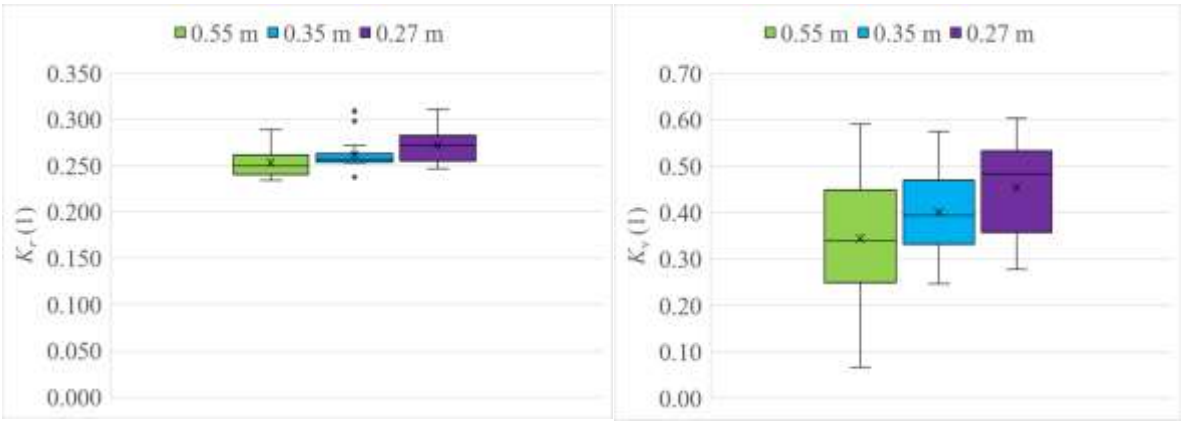

Figure 5. Results of the a) reflection coefficient, K_r, and b) dissipation coefficients, K_v, measurements by depth categories

4.2 Comparison of measured data with empirical predictions (Ruol, 2013)

In Figure 6, the relationship between the ratio of the measured transmission coefficient, K_t, and the transmission coefficient predicted by the Ruol's equation, $K_{t\text{-}Ruol}$, is shown relative to the ratio of the peak wave period to the natural oscillation period of the floating breakwater. For small values of T_p/T_h ($1.0 < T_p/T_h < 1.20$), the formula underestimates by approximately 25%. For values of $T_p/T_h > 1.20$ the Ruol's equation mostly follows the observation done in this study. Minor discrepancies are found if we observe Figure 5 in the region $T_p/T_h > 1.20$. For example, we can notice that for measurement results where the depth is 0.27 m, there is a slightly higher degree of error. In these cases, the formula overestimates by 15%, while for a depth of 0.55 m, the formula is almost entirely accurate.

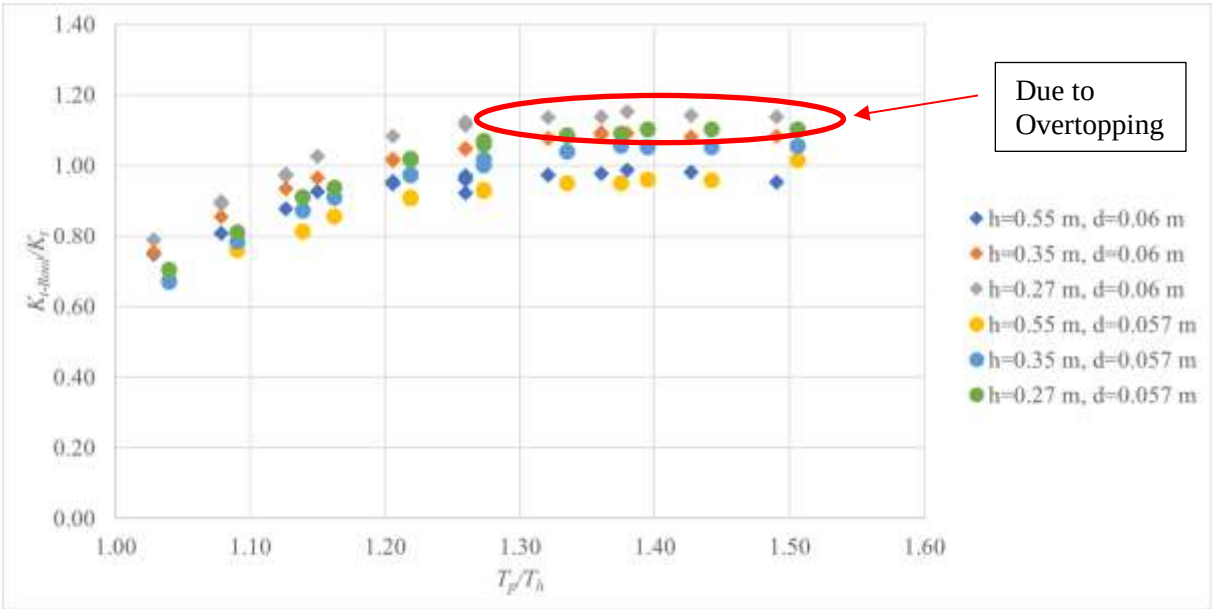

Figure 6. Ratio of the measured transmission coefficient, K_t, to the transmission coefficient predicted by Ruol et al., 2013 equation, $K_{t\text{-}Ruol}$, in relation to the ratio of the peak wave period to the natural oscillation period of the floating breakwater

The discrepancy due to water depth variation is probably due to overtopping of the floating breakwater, which is not considered when constructing the semi-empirical equation of Ruol (discussed in section 4.1). The discrepancy for low values of T_p/T_h is not readily apparent. It seems that for peak wave periods

that are near the resonant frequency of the floating breakwater, the measured transmission coefficients are 25% higher than the ones predicted using the Ruol equation. It should be noted that this is an important region, because this is the region most designer would be aiming for, in other words, the operating region of the floating breakwater (K_t of about 0.5). The authors suspect that for relatively low relative drafts, $d/h < 0.2$, which are out of the calibration range for the Ruol's equation, the semi-empirical does not hold in the $T_p/T_h < 1.2$ region. In order to remedy this issue, the author are giving a simple correction method in Section 4.3 for this case.

4.3 Simple expression for the transmission coefficient prediction for low relative draft cases

In cases where the relative draft d/h is less than 0.2 and the ratio of the peak wave period to the natural oscillation period of the floating breakwater (T_p/T_h) is less than 1.2, we can establish a relationship between the transmission coefficient and the correction of the Ruol's equation. The relationship being discussed can be better understood by referring to Figure 7.

The data presented in Figure 7 is essentially a portion of the larger dataset depicted in Figure 6. But Figure 7 focus on the $T_p/T_h < 1.2$ region, which is now seen to be problematic when using the Ruol's equation.

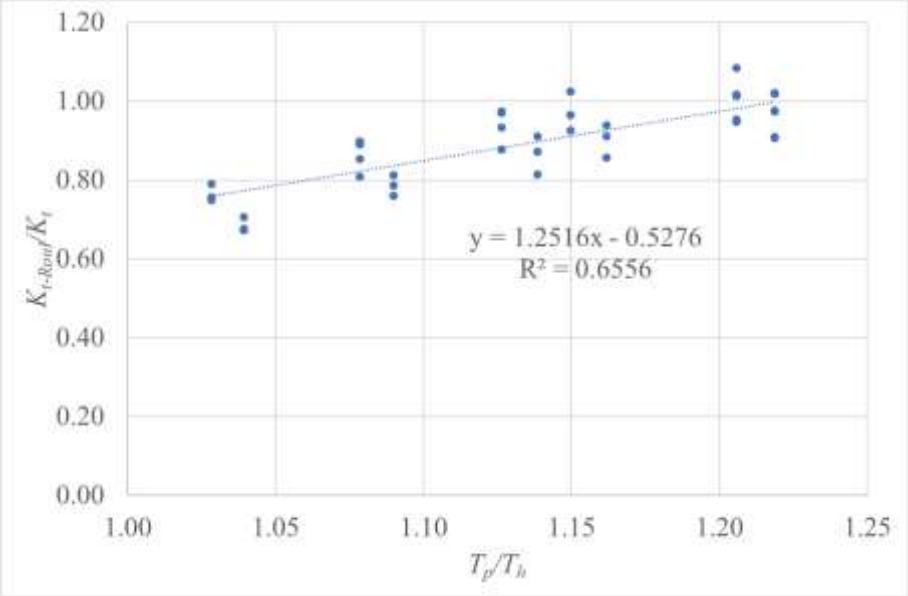

Figure 7. Ratio of the measured transmission coefficient, K_t, to the transmission coefficient predicted by Ruol et al., 2013 equation, $K_{t\text{-}Ruol}$, in relation to the ratio of the peak wave period to the natural oscillation period of the floating breakwater, with the added fitted line that approximates the relationship between the two non-dimensional parameters

Figure 7 displays a fitted line that represents the relative transmission coefficient ($K_{t\text{-}Ruol}/K_t$) and the ratio between the peak wave period and the natural oscillation period of the floating breakwater (T_p/T_h), providing an expression for determining these values. The coefficient of determination (R_2) of the fitted line is 0.66, which suggests that the fitted line provides a reasonably accurate description of the data points. It is recommended to pursue this corrective relationship only in scenarios where there is a low relative draft and the ratio of T_p to T_h falls between 1 and 1.2. If the value T_p/T_h falls outside of this range, it is possible that the formula could yield inaccurate results for the transmission coefficient. The expression is provided here in a format that is more practical and can be easily utilized:

$$K_t = \frac{K_{t-Ruol}}{1.25\frac{T_p}{T_h} - 0.53} \quad (8)$$

5 Conclusion

Breakwaters play a crucial role in protecting port water areas. A literature review shows that existing methods for assessing transmission are not always accurate for π-type floating breakwaters. The equation of Ruol, presents itself as the most capable method for predicting wave transmission for π-type floating breakwaters. In order to verify this equation in out-of-range cases of low relative draft (d/h < 0.2), laboratory tests were conducted in the Hydraulic Laboratory. The spectral waves characteristics used are conditions commonly met in the Adriatic Sea.

Analysis of the measurement results revealed a clear impact of water depth on the wave energy transmission coefficient. With decreasing water depth, a decrease in the transmission coefficient is observed. The transmission coefficient obtained by using the Ruol's equation shows a slight but opposite trend. This can be attributed to the phenomenon of overtopping over the floating breakwater that occurred in most tests, which was not considered in Ruol's research.

Comparing the ratio of the transmission coefficient calculated according to the Ruol's equation and the transmission coefficient obtained from measurements relative to the ratio of the peak wave period to the natural oscillation period of the floating breakwater, we conclude that for small values of ($1.0 < T_p/T_h < 1.20$), the formula underestimates by approximately 25%. Based on the data obtained from measurements in this study, a simple mathematical formulation was derived to give a correction for the transmission coefficient calculated using Ruol, 2013 in this region. It is important to note that this region is the one that is aimed by the coastal engineer when designing the breakwater, as it is close to $K_t = 0.5$-0.6, which makes this important in practice. While the region where $T_p/T_h < 1$ is associated with $K_t < 0.5$.

Furthermore, more laboratory and numerical modeling is required in future research to explore the low relative draft region (especially for $T_p/T_h < 1$ region) and the influence of overtopping on the transmission coefficient. The authors of this study recognize the potential for higher attenuation coefficients if the wave direction is not perpendicular to the pontoon breakwater's alignment. However, since the laboratory tests were conducted in a wave channel, such testing was not possible. Furthermore, it is characteristic of live sea waves that wave energy is dispersed directionally, which results in an increased attenuation coefficient compared to those obtained in this study. Finally, interconnecting multiple pontoon sections would also result in further increases in the attenuation coefficient. It is also noted that the tested pontoons in the observed range of wave heights and wavelengths did not exhibit floating instability, nor was there any movement of anchor blocks observed when subjected to the largest test waves.

References:

[1] PIANC. Criteria for movements of moored ships in harbours, 1995.
[2] Biesheuvel, A. C.: Effectiveness of Floating Breakwaters, 2013
[3] Gesraha, M. R.: Analysis of pi shaped floating breakwater in oblique waves: I. Impervious rigid wave boards, Appl. Ocean Res, 28:327–338, 2006
[4] Ruol, P., Martinelli, L., Pezzutto, P.: Formula to Predict Transmission for π-Type Floating Breakwaters, J. Waterw. Port Coast. Ocean Eng., 139:1–8., 2013
[5] Ruol, P., Martinelli, L., Pezzutto, P.: Limits of the new transmission formula for pi-type floating breakwaters. Coast. Eng., 2012.
[6] Zelt, J. A., Skjelbreia, J. E.: Estimating Incident and Reflected Wave Fields Using an Arbitrary

Number of Wave Gauges. In *Coastal Engineering 1992*., pp 777–789. American Society of Civil Engineers, Venice, Italy, 1993.
[7] Macagno, E.-O.: Wave action in a flume containing a submerged culvert, Houille Blanche. 40:10–37., 1954

EXPERIMENTAL AND NUMERICAL MODEL FOR ANALYSIS OF THE WATER HAMMER IN PUMP WATER SUPPLY SYSTEM

GOCE TASESKI [1], NIKOLA KRSTOVSKI [2]

[1] *Faculty of Civil Engineering Skopje, N. Macedonia,* taseski@gf.ukim.edu.mk

[2] *Faculty of Civil Engineering Skopje, N. Macedonia,* nikolatudence@gmail.com

1 Abstract

Water supply systems in such transient regimes should be hydraulically analyzed by means of basic equations for unsteady flow. For the needs of this research, by using the method of characteristics, a custom mathematical model HTM is developed for the purpose of water supply network analysis in conditions of unsteady flow, i.e. with this mathematical model, the characteristics of the water hammer in closed systems for water transport under pressure can be seen. In addition, a physical model in ratio 1:1 has been made for in-situ analyses of pressure change in occurrence of water hammer in the water supply system.

Keywords: Water supply system; water hammer; mathematical model; experimental (in-situ) model

2 Introduction

Water supply systems are complex systems which may consist of reservoirs, water treatment, water supply pipes which can be gravitational or pump-type, pressure regulators, valves, tanks and household water supply installations [1]. This complexity of water supply systems leads to water flow under pressure where flow and pressure change during time – unsteady water flow.

The phenomenon of water hammer in water supply networks is an inevitable occurrence which is most often initiated by pump stations, valves, hydro-mechanical equipment etc., and is distributed in the entire water supply network, especially noticeable in the areas of big height, pipeline sections with small hydrostatic pressure, etc. However, the water hammer parameters which can cause damage to the pipelines, hydro-mechanical equipment and to cause certain water pollution in the system are the most significant to engineers. The water hammer occurrence can have significant influence on water quality through the influence of cavitation, movement of particular microscopic particles may occur which are deposited as biofilm along the pipe volume – occurrence of "red water" in the water supply system. Also, in the occurrence of cavitation, if there are certain irregularities existing in pipe connection and small cracks in them, the possibility of underground waters infiltration in the water supply system cannot be excluded, which can amount from several liters to hundreds of liters depending on the opening size. The air captured in pipelines has also been shown to cause a lot of harm in the ductile pipes from the aspect of corrosion appearance inside the pipes, by which there is a direct influence on their quality [1].

Unsteady flow, i.e. water hammer occurrence in water supply systems represents challenge for scientific research from the aspect of making mathematical models for simulation of water hammer, which afterwards would be applied in projecting and managing water supply systems. Therefore, for the purposes of this research, by applying the method of characteristics, the HTM (Hydraulic Transient Model) mathematical model has been made for analysis of the water hammer in pumping water supply system, and the results obtained from the analytical model are calibrated and verified on a physical model – in-situ on real water supply system.

3 Numerical Model

There are many factors [1] which have influence on the flow under pressure, i.e. on the phenomenon of water hammer, such as: geometrical characteristics of the pipeline, material from which the pipeline is made, physical and pressure-deformable characteristics of water, distribution of flow speed in the cross section of the pipeline, dissipation of energy due to friction.

Starting points in the mathematical description of the water hammer are the basic equations in fluid mechanics:

The equation for maintenance of movement quantity, which, for unsteady flow in closed systems under pressure such convective acceleration is ignored, has the following form [1]:

$$\frac{\partial V}{\partial t} + V\frac{\partial V}{\partial x} + \frac{\lambda}{2D}V|V| = 0 \tag{1}$$

Continuity equation which, for unsteady flow of elastic fluid in elastic environment with assumed that pipe disposition is very small regarding the change in piezometric head, and instead of derivation the inclination of the pipe is introduced. Also, it is assumed that fluid thickness changes very little regarding piezometric head, has the following form:

$$\frac{\partial P}{\partial t} + V\frac{\partial P}{\partial x} - Vsin\alpha + V\frac{a^2}{g}\frac{\partial V}{\partial x} = 0 \tag{2}$$

In Eq. (1) and (2), P denotes the static pressure at the centerline of the pipeline at location x and time t, V is the average velocity of flow, D is the pipe diameter, λ is the friction factor in the Darcy-Weisbach formula, x is the distance along the centerline of the pipe, α is the angle between the horizontal and the centreline of the pipe, taken as positive for the pipe sloping downwards in the direction of positive x, g is the gravitational constant; and a is the celerity of the pressure surge, i.e. the velocity with which the surge is propagated relative to the liquid. The positive direction for V coincides with that for x.

3.1 Method for Solving Partial Differential Equations

The method of characteristics exceptionally solved both positive and negative pressure waves and has remained one of the widely applied methods [1,2–6]. Therefore, the method of characteristics has been proven in the research so far as a method of exceptional compatibility with numerical solutions and the same one is applied in this research.

By the method of characteristics, the basic partial differential equations which are not integrable in closed form are transformed into ordinary differential equations which have solution in closed form [1,7–11]. Basic equations, continuity equation and dynamic equation can be marked with L_1 и L_2:

$$L_1 = \frac{\partial V}{\partial t} + V\frac{\partial V}{\partial x} + g\frac{\partial P}{\partial x} + \frac{\lambda}{2D}V|V| = 0 \tag{3}$$

$$L_2 = \frac{\partial P}{\partial t} + V\frac{\partial P}{\partial x} - Vsin\alpha + V\frac{a^2}{g}\frac{\partial V}{\partial x} = 0 \tag{4}$$

From the previously stated equations, it can be concluded that it is a question of two families of curves, which are practically straight lines, where the propagation speed is constant and variously larger than the basic flow speed, and thus the system of two partial differential equations transforms into a system of four ordinary differential equations marked with C+ и C– which determine straight lines:

$$\left.\begin{aligned}\frac{dP}{dt}+\frac{a}{g}\frac{dV}{dt}+\frac{\lambda}{2D}v|v|=0\\ \frac{dx}{dt}=+a\end{aligned}\right\}C^{+} \tag{5}$$

$$\left.\begin{aligned}\frac{dP}{dt}-\frac{a}{g}\frac{dV}{dt}+\frac{\lambda}{2D}v|v|=0\\ \frac{dx}{dt}=-a\end{aligned}\right\}C^{-} \tag{6}$$

3.2 Numerical Model

Figure 1 shows discretization of physical system in numerical network with calculating steps Δx and Δt where the solutions are obtained in the section of positive and negative lines of characteristics [3,7].

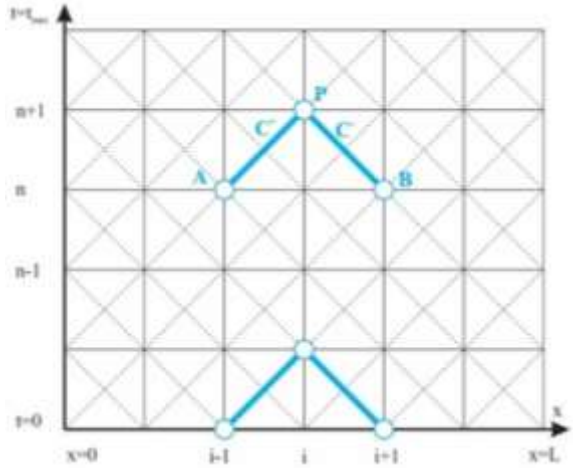

Figure 1. Numerical network for the method of characteristics

According to the given numerical method, the equations (5) and (6) may be written in the following manner:

$$\frac{d}{dt}\left(P\pm\frac{a}{g}V\right)+\lambda\frac{a}{D}\frac{V|V|}{2g}=0 \tag{7}$$

The previously stated equation can be integrated lengthwise of the positive and negative characteristic, i.e. lengthwise along the lines AP and BP, as follows and after the integration, the equations of positive and negative characteristics are written as follows:

$$\frac{P_P-P_A}{\Delta t}+\frac{a}{g}\frac{V_P-V_A}{\Delta t}+\frac{\lambda a}{2gD}V_A|V_A|=0 \tag{8}$$

$$\frac{\mathrm{P_P}-\mathrm{P_B}}{\Delta \mathrm{t}}-\frac{\mathrm{a}}{\mathrm{g}}\frac{\mathrm{V_P}-\mathrm{V_B}}{\Delta \mathrm{t}}+\frac{\lambda \mathrm{a}}{2\mathrm{gD}}\mathrm{V_B}|\mathrm{V_B}|=0 \tag{9}$$

If it is known that in the hydraulic analysis it is important to determine the flow change and height position of the hydrodynamic line in any section along the pipe, and in a certain time interval, additional approximation is introduced that the cross section of the pipe along its entire length is constant, and if it is known that median speed can be determined by the equation V=Q/A, the previously stated equations, knowing the numerical network, for the pressure, can be written in the following form:

$$P_i^{n+1}=P_{i-1}^{n}-B(Q_i^{n+1}+Q_{i-1}^{n})-MQ_{i-1}^{n}|Q_{i-1}^{n}|=0 \tag{10}$$

$$P_i^{n+1} = P_{i-1}^n + B(Q_i^{n+1} - Q_{i-1}^n) + MQ_{i+1}^n|Q_{i+1}^n| = 0 \tag{11}$$

If:

$$B = \frac{a}{gA} \qquad \text{and} \qquad M = \frac{\lambda \Delta x}{2gDA^2} = 0 \tag{12}$$

If the flow parameters in the time interval (n) are known, then the following is obtained:

$$P_i^{n+1} = CP - BQ_i^{n+1} \tag{13}$$

$$P_i^{n+1} = CM + BQ_i^{n+1} \tag{14}$$

Where:

$$CP = P_{i-1}^n + BQ_{i-1}^n - MQ_{i-1}^n|Q_{i-1}^n| \tag{15}$$

$$CM = P_{i+1}^n + BQ_{i+1}^n + MQ_{i+1}^n|Q_{i+1}^n| = 0 \tag{16}$$

From the equations (13) and (14), the basic equation of characteristics is obtained for determining the peak elevation of the hydrodynamic line:

$$P_i^{n+1} = \frac{CP + CM}{2} \tag{17}$$

3.3 Time Interval Selection for Analysis of Borderline Conditions

In real water supply systems, the problem with analysis of water hammer is always reduced to analysis of more complex systems, whereas initial and borderline conditions there are several possible ones that occur – characteristic forms of equations for borderline conditions. It is important to be mentioned here that the selection of the time calculation step has a big influence on the solution for each individual part of the complex system.

In order to determine borderline conditions in connecting one or more pipes of different geometrical and hydraulic characteristics, it is assumed that directions of positive C+ and negative C– characteristic cut in one point. This assumption in complex systems, such as water supply systems, is very rarely accurate, since the inclination of each line of characteristics depends on the propagation wave, flow speed in the pipe, horizontal position of the pipes connected in one joint and the number of sections in which the pipe is divided [1].

According to the previously stated, it can be said that in certain period, the lines of positive and negative characteristics of the connected pipes will not cut in one point. It can be said that this is a basic problem in making the mathematical model for the water hammer analysis. Due to it, in making of the mathematical model, certain assumptions about the time interval should be made in order to overcome this problem. Namely, time step should be selected in order to fulfill the Courant–Friedrichs–Lewy (CFL) "$\Delta x \geq a\Delta t$" condition of stability [7], i.e.:

$$\Delta t = \frac{\Delta x}{max|v + a|} = \frac{\Delta x}{V + a} = \frac{L}{N(V + a)} \tag{18}$$

One approach by which satisfactory results can be obtained is to reduce the time step – this procedure is used in creating the mathematical-numerical model. Namely, the time step is reduced for all pipes up to the value which enables the characteristic lines of all pipes to cut into one point. The pipe with the

smallest value of time step is called "control pipe" of the model. This approach in the model of the joint position itself where pipes are connected, will "force" the characteristic lines in some way to cut into one point. However, in the initial and final borderline conditions, cutting of characteristic lines in rectangular grid will not be provided. In order to overcome this problem, additional interpolations should be made which make the mathematical model more complex, by which the condition for the characteristic lines to cut in one point, and initial and final conditions to cut in a rectangular grid will not be disturbed. This means that pipe sections should increase in all pipes that have primarily had time step larger than the "control pipe" by which the need for interpolation becomes smaller. Finally, as presented in figure 2, in the state obtained, the characteristic lines for all pipes are cut in rectangular grid and they all have the same time step.

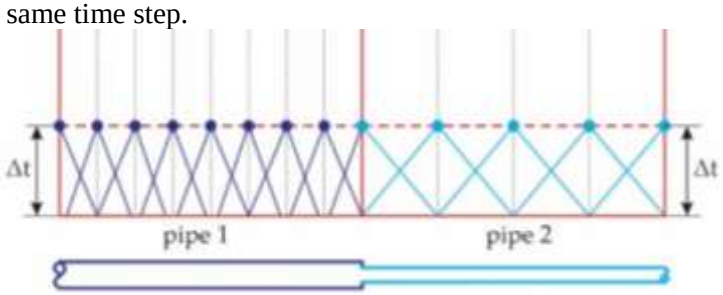

Figure 2. Connecting characteristic lines with identical time step

3.3.1 Borderline Conditions

Serial connection of two pipes in one joint:

$$Pressure: \quad P_{1,N}^{n+1} = P_{2,1}^{n+1} = P \tag{19}$$

$$Flow: \quad Q_1^{n+1} = \frac{(P_1^{n+1} - CM)}{B} \tag{20}$$

Connection of several pipes in one joint:

$$Pressure: \quad P^{n+1} = \frac{\frac{CP_1}{B_1} + \frac{CM_2}{B_2} + \frac{CM_3}{B_3} + \frac{CM_4}{B_4}}{\frac{1}{B_1} + \frac{1}{B_2} + \frac{1}{B_3} + \frac{1}{B_4}} \tag{21}$$

$$Flow: \quad -Q_{1,N}^{n+1} = \frac{P^{n+1}}{B_1} - \frac{CP_1}{B_1}; \quad -Q_{2,N}^{n+1} = \frac{P^{n+1}}{B_2} - \frac{CP_2}{B_2}; \quad -Q_{3,N}^{n+1} = \frac{P^{n+1}}{B_3} - \frac{CP_3}{B_3} \tag{22}$$

Tank at the end of pipeline:

$$Pressure: \quad P^{n+1} = P_R \tag{23}$$

$$Flow: \quad Q_1^{n+1} = \frac{(P_1^{n+1} - CM)}{B} \tag{24}$$

Pump as borderline condition:

There are several methods of presenting pumps as borderline conditions in the mathematical models for water hammer analysis in water supply networks. For preliminary analyses of the water hammer in water supply networks, as a characteristic of the pump, the parabola as a pump performance curve can be used [8]:

$$H_P = H_0 + AQ^2 + BQ \tag{25}$$

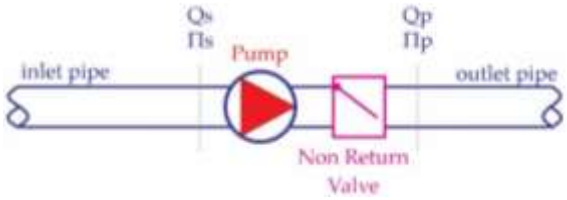

Figure 3. Pump as Borderline Condition

At the ends of the suction and pressing pipes which are connected to the pump, figure 3, the flow and height of the hydrodynamic line are unknown. From the continuity equation and the assumption that both cuts before and after the pump are at a small distance, it can be understood that Qs = Qp = Q. On the other hand, for determining the heights of the hydrodynamic line, the equations of positive and negative characteristic lines are used:

$$H_P = P_P - P_S + \frac{(V_P^2 - V_S^2)}{2g} \tag{26}$$

4 Development of HTM Mathematical Model

The mathematical model HTM is created in a way that it can analyze water supply system only in unsteady regime. The steady regime which dominates in the system before the occurrence of the unsteady state is taken from already made up-to-date software packages for analysis of systems under pressure, such as EPANET.

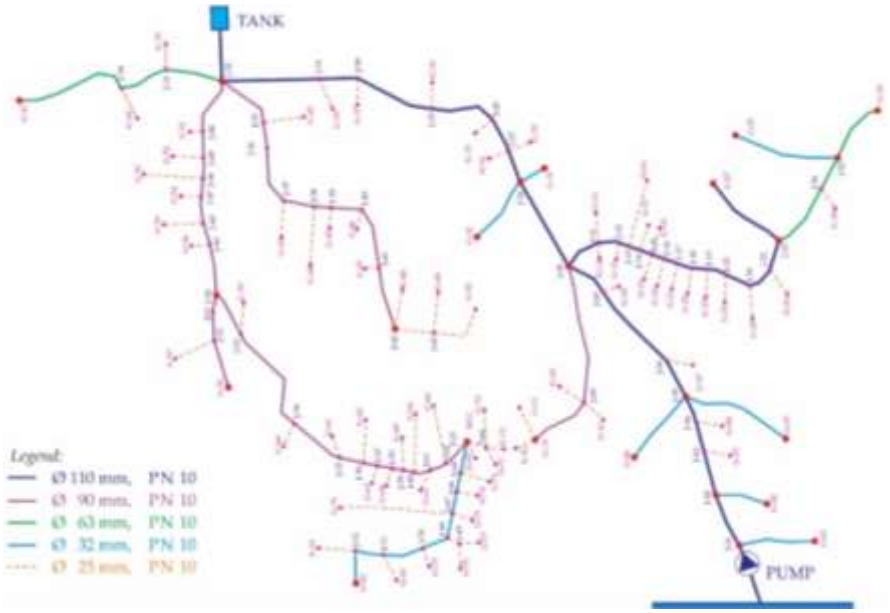

Figure 4. Schematic presentation of the real water supply system (Ø-pipe diameter, PN-Pipe's nominal pressure)

Such created mathematical model HTM is applied on real – existing water supply system, figure 4. The analyzed real water supply system is a pumping water supply system with reservoir beyond an inhabited place, while the water supply network is of branching system. Regarding the fact that it is a pumping water supply system, the initiator of the unsteady state is the pump station, i.e. in this system, the water hammer occurrence will be analyzed during pump switching on and off in the pump station.

In defining time step of the analysis, all recommendations previously stated are taken into consideration, and in this case the time step is $\Delta t = 0.02$ sec.

5 Experimental Model

For the calibration of the mathematical model HTM in this research, suitable measuring equipment has been made and built-in at certain critical places of the real water supply system, which is actually physical model in ratio 1:1. A characteristic of this water supply system is that the distribution of the consumers – households is at a large difference in height, i.e. from the minimum peak elevation of 724 m up to the maximum of 810 m, while the maximum water level in the tank is 824 m, i.e. such water supply system has a hydrostatic pressure from 14 to 100 m.

In the planning phase of this water supply system, all recommendations for dimensioning of water supply systems with assumed quasi-steady flow regime along the lines are observed. According to the calculations, it can be concluded that in none of the parts of the water supply network there are pressures larger than the maximum ones and smaller than the minimum ones - there are no negative pressures. However, in phase of certain part exploitation, frequent defects started occurring during time. Certainly, the reasons for occurrence of these defects cannot be explained by the operator/user of the system – i.e. frequent excuses refer to the quality of the material from which the pipes are made – they have no capacity to endure the pressure of 90 m although they are dimensioned by the manufacturer for such pressure. Is that the fact?

5.1 Program and Dynamics of Experimental Measurements

From the analysis of water supply network, terrain configuration, distribution of consumers and geometrical characteristics of the lines, the need for selection of a total of twenty measuring places emerged, by which entire coverage of network was provided. Figure 5 presents locations of all measuring places.

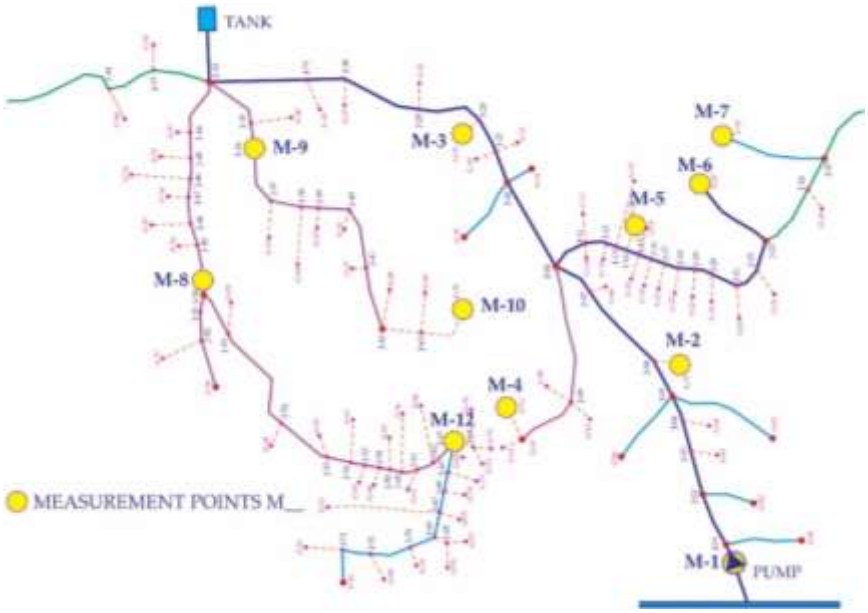

Figure 5. Arrangement of measuring places

5.2 Calibration of the Mathematical Model HTM with the Physical (in-situ) Model

For the calibration of the water supply systems in unsteady regime – in water hammer occurrence, there are certain recommendations which are used in steady regime, i.e.: calibration of pressure in joint

positions, calibration of flow along lines, calibration of hydraulic gradient.

However, in the analysis of the obtained results, it has been shown that previous calibrations in steady regime are not enough for successful calibration of the mathematical model HTM with the physical (in-situ) model to be made. This conclusion owes to the fact that the material from which the pipelines are made, and their thickness have the biggest influence on the speed of pressure wave propagation through one water supply system. At this point it can be easily said that for the calibration of mathematical models for water hammer analysis, in addition to the parameters during stationary mode, it is essential to further determine – calibrate the speed of propagation of the pressure wave. Considering that the analyzed system is a branched water supply network as well as the limitation in available equipment, the measured pressures in the analyzed points were used as parameters for calibration.

The statistical operation error variance (σ^2) was used for data analysis. The error variance is proportional to the sum of the square of the differences between the measured and modelled responses (i.e., proportional to the objective function) and represents the unbiased sample variance of the model error after calibration (i.e., the objective function divided by the number of data points minus the number of model parameters) as shown in Equation 27 [3]:

$$\sigma^2 = \frac{1}{M-N}\sum_{i=1}^{M}(H_i^m - H_i)^2 \tag{27}$$

where M is the number of measured data points, N is the number of model parameters, H_i^m is the measured pressure response and H_i is the predicted pressure response.

6 Results and Discussion

As it was previously mentioned in this paper, the need for this research was imposed by the fact to find out reasons for occurrence of defects in real water supply system which is subject to analysis. Namely, in the analyzed system from the very beginning of its exploitation of sections with small pressures, frequent occurrence of defects has been noticed, and defects of the pumping system pipeline near the pump station have started appearing later.

In addition, in the following figures there are output results of the performed analysis presented, i.e. for the characteristic states - during pump switching on and off.

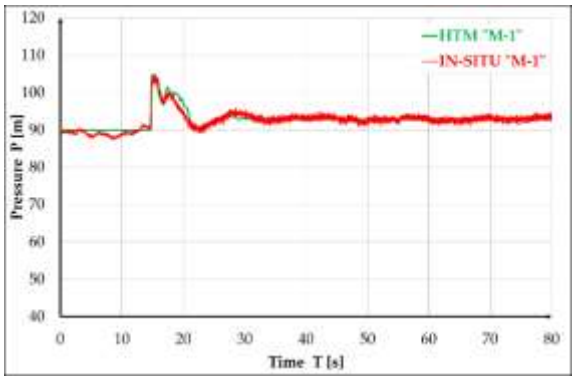

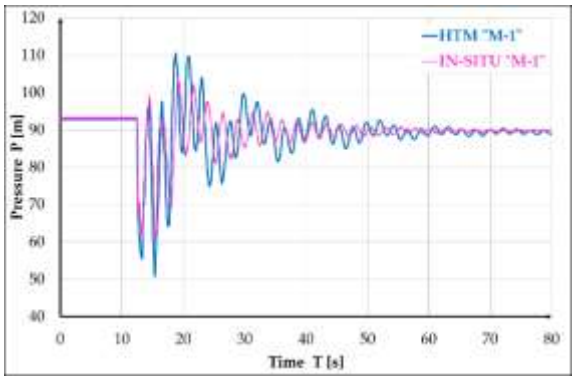

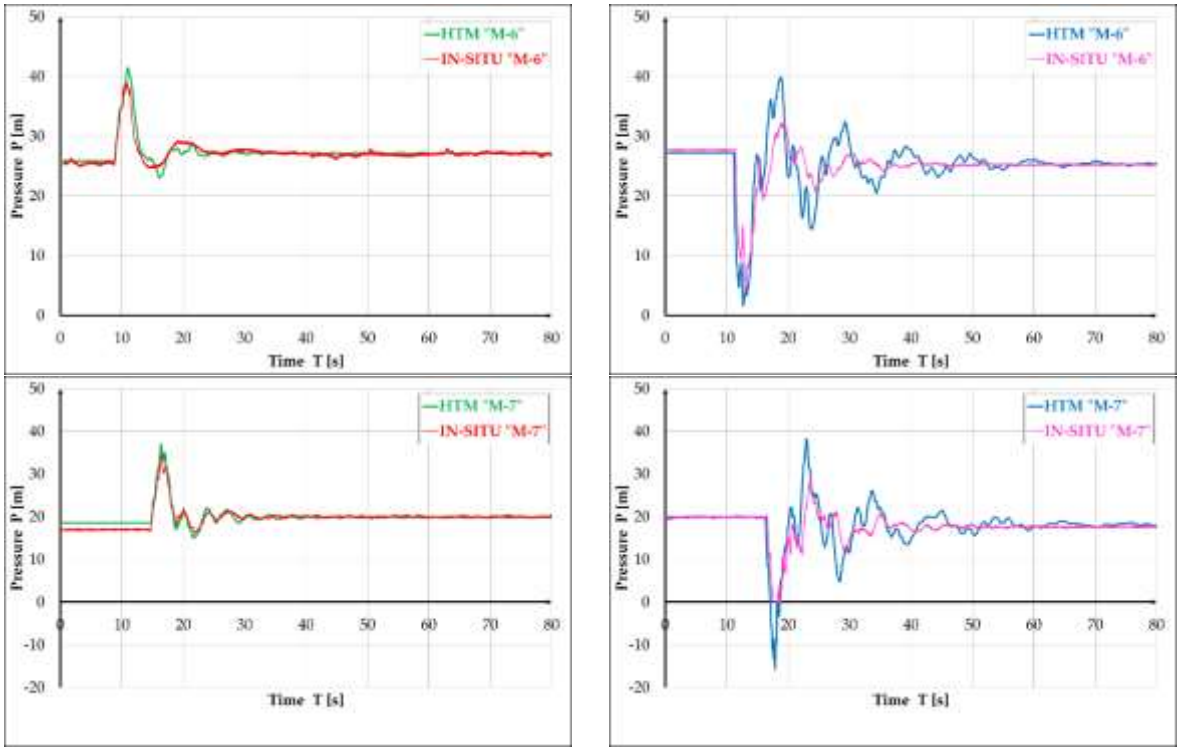

(**a**) (**b**)

Figure 10. Characteristics of water hammer, experimental from performed in-situ measurements and analytical from HTM model during pump (a) switching on and (b) switching off in the pump station

If we analyze the graphs of the pressure change in the pump station (measuring place M-1), where in the immediate vicinity frequent defects can be noticed, it can be noted that in both switching on and off of the pump, the maximum pressure in water hammer occurrence is larger than 100 m (10 bar), whereas in steady regime of operation, the same one is smaller than 100 m (10 bar), i.e. it does not exceed the value of 90 m (9 bar), and if it is known that on that line to the pump station the pipeline is from HDPE PE100 NP 10 bar, it can be immediately concluded that water hammer occurrence is the reason for occurrence of defects along that line. It is understandable that in the initial exploitation period these defects have not been noticed, which primarily owes to the age of the pipe material which, during time, due to constant exposure to pressure above the maximum permitted one has led to material wear and tear – the pipeline has lost its elasticity and defects have increased occurring.

While analyzing the graph of pressure change at the measuring position M-7, it can be noticed that in state of switching off the pump, there are negative pressures occurring which due to limitation of capability of measuring equipment, which can measure only positive values of the pressure, they are not detected on the experimental model (in-situ). However, on the graph it can be noticed that in the period of the negative pressure occurrence, the measuring device shows zero value. Precisely the occurrence of negative pressure – vacuum in the pipeline, in the very beginning of the system exploitation, and occurrence of frequent defects has been noticed in the immediate vicinity of the measuring place M-7. It is important to be mentioned here that water hammer occurrence in real water supply system takes place during each pump switching on and off, i.e. it happens several times during the day, and exactly besides the occurrence of increased/decreased pressures in the system, the main reason for occurrence of defects is the frequency – repetition of increased, i.e. decreased pressures.

7 Conclusions

From the aspect of hydraulic analysis, water supply systems where occurrence of water hammer is expected should be analyzed and dimensioned in such manner that they can be "adjusted" to both steady

and unsteady flow regime. This recommendation should especially be respected in water supply systems in which in the exploitation phase there is even slightest possibility of water hammer occurrence, such as pumping water supply systems with reservoirs beyond inhabited place, i.e. as the analyzed system in this research. Actually, as it can be seen from the results in this research of the subject, it is significant to analyze the locations with increased pressure, but also the locations with minimum pressures in order to avoid occurrence of vacuum in these sections.

References:

[1] Taseski, G.; Popovska, C. (2015). Water hammer analysis-impact of the pipe material in water supply system"; WMHE2015, 103-110
[2] Loh. Lohrasbi, A. & Attarnejad, R. (2008). Water Hammer Analysis by Characteristic Method. American Journal of Engineering and Applied Sciences, 1(4), 287- 294
[3] Stephens, M.L., Lambert, M.F., Simpson, A.R. and Vitkovsky, J. (2011). Calibrating the water hammer response of field pipe networks using a mechanical damping model. Journal of Hydraulic Engineering, Vol. 137, No. 10, Oct., 1225-1237
[4] Goldberg, D.E.; Wylie, E.B. Characteristic method using timeline interpolations. Journal of Hydraulic Engineering 1983, 670–683.
[5] Chaudhry, M.H. (2013). Applied hydraulic transients; 3rd ed.; Springer; ISBN 13: 978-1461485377.
[6] Parmakian, J. (1995). Water hammer Analysis; 1st ed.; Prentice Hall, Inc; ISBN B0000CJ5U0.
[7] Mohamed, S.; Ming, Z.; Duncan, A.M. (2005). A Review of Water Hammer Theory and Practice. Applied Mechanics Reviews, Vol. 58.
[8] Kishore, S. (2007). Transient analysis in pipe networks. Master thesis,
[9] A.R.D. Fluid Transients in Pipeline Systems, Second Edition (Pipelines and Pressure Vessels); The American Society of Mechanical Engineers; ISBN 13: 978-0791802106, 2004.
[10] Stephen L., W. (2011) Modeling of Pipeline Transients: Modified Method of Characteristics. http://digitalcommons.fiu.edu/etd.
[11] Vitkovsky, J.P.; Liggett, J.A.; Simpson, A.R.; Lambert, M.F. [2003]. Optimal Measurement Site Locations for Inverse Transient Analysis in Pipe Networks. Journal of Water Resource Planning and Management.

VEGETATION EFFECTS ON FLOW CHARACTERISTICS AND SEDIMENT STORAGE IN A LOWLAND STREAM CHANNEL OVER TIME

SAEID OKHRAVI*, VALENTÍN SOČUVKA, RADOSLAV SCHÜGERL, MAREK SOKÁČ, RENÁTA DULOVIČOVÁ, YVETTA VELÍSKOVÁ

Institute of Hydrology, Slovak Academy of Sciences, Dúbravská cesta 9, 84104, Bratislava, Slovak Republic

**Corresponding author: Saeid.okhravi@savba.sk*

1 Abstract

Aquatic vegetation significantly influences fluvial dynamics and sediment budgets. This study investigates the impact of in-channel vegetation on flow resistance and sediment storage in a lowland Slovak stream, using field data from 2018 and 2023. The findings reveal that increased vegetation between 2018 and 2023 resulted in reduced flow velocity and discharge, alongside a substantial rise in sediment storage. Sediment accumulation in 2023 ranged from 3927 to ~5800 kg/m², up to 50% higher than in 2018.

Keywords: River, Aquatic vegetation, Flow characteristics, Flow resistance, Sediment budgets

2 Introduction

Vegetation, whether located on the floodplain, along the banks, or in the channel, significantly influences fluvial system dynamics and plays a central role in river management. This study specifically examines in-channel aquatic vegetation, composed mainly of macrophytes, both submerged and emergent, which are vital components of many lowland river ecosystems. In-channel vegetation increases local and boundary flow resistance [1, 2], traditionally viewed as problematic due to increased energy losses [2]. Consequently, mean velocity decreases, limiting the river channel's capacity to convey discharge, potentially heightening flood risks by increasing depth [2]. This study emphasizes addressing the resistance aspect of aquatic vegetation in fluvial hydrodynamics, particularly in areas where vegetation reduces the river's conveyance capacity.

Studies on vegetated river flows have typically examined the impact of vegetation on flow velocity profiles and shear stress distributions, both in fully vegetated beds and around patches of vegetation [1, 3]. Vegetation patches create regions of reduced flow velocity and shear stress that promote local sedimentation [1]. Researchers have scrutinized the influence of vegetation elements, whether rigid or flexible, as sources of drag within water flow, employing laboratory experiments [4] and numerical modeling [5] to understand vegetation-flow interactions and analyze flow fields, particularly velocity profiles and turbulence [1, 3], as well as energy loss [2]. Initially, they have developed methods to predict drags of aquatic vegetation based on flow and plant characteristics such as plant form, morphology, size, height and density of vegetation patches [1, 3]. This is crucial for facilitating parameterizations of aquatic vegetation-induced flow resistance. One aspect of the interactions between vegetation, river flows, and transported sediments that remains relatively understudied pertains to their role in the within-channel storage of fine sediment, a factor of potential significance in comprehending the sediment budget within river reaches and catchment areas [6]. Research into sediment budgets has yielded significant insights into both the natural and anthropogenic sources, storages, and transfers of sediment across riverine landscapes. Accurately estimating in-channel sediment storage, particularly of fine sediment, is essential not only for the sediment budget assessments but also due to the profound impact of fine sediment on the structure and function of river ecosystems [7].

In recent decades, research has elucidated the significant role of aquatic vegetation in sediment retention and landform development within riverine environments. This change in river channel morphodynamics has underscored the potentially positive ecological effects of vegetative presence [8, 9]. Specifically, regions characterized by low flow velocities facilitate the accumulation of particulate nutrients [10]. Moreover, aquatic vegetation has been shown to exert a positive influence on water

quality by uptaking heavy metals and nutrients, as well as by fostering oxygenation in stagnant locales [11]. Additionally, vegetative coverage serves to increase soil integrity, while root systems bolster soil stability, thereby mitigating erosion risks. Consequently, aquatic plants assume the role of ecosystem engineers, creating favorable conditions conducive to the establishment and persistence of vegetative canopies [12]. These contributions may facilitate the development of stable habitats supportive of both terrestrial and aquatic wildlife. Moreover, the spatial heterogeneity engendered by vegetative presence within river flows fosters habitat complexity, thus augmenting biodiversity within aquatic ecosystems. Consequently, the processes governed by vegetation emerge as pivotal components in the dynamics of river channels, underscoring their paramount importance in numerical modeling endeavors aimed at simulating the morphological evolution of alluvial river systems.

This study assesses the influence of aquatic vegetation on flow dynamics, including velocity, flow resistance, and sediment deposition. Utilizing field data collected from four stream cross-sections in the years 2018 and 2023, the research examines the impacts of in-channel vegetation on flow patterns and sediment accumulation over time. The primary objective is to evaluate sediment storage within the active channel of a lowland stream, with a specific focus on understanding how the presence of aquatic vegetation influences flow characteristics and sedimentation dynamics across years.

3 Applied method in the study area

The selected cross-sections were located on a lowland stream named Gabčíkovo-Topoľníky in southwestern Slovakia, not far from the capital city of Bratislava. This stream exhibits all typical characteristics of lowland rivers, including a low water surface slope (low gradient rivers < 2 m/km), low flow energy and velocity, homogeneous morphology and bed forms across the selected reach (mostly dune), high relative submergence or small-scale roughness ($R/d_{84} > 10$, where R is the hydraulic radius and d_{84} is the grain size diameter at which 84% of the particles in a sediment sample are finer), and the presence of vegetation. In lowland rivers, relative submergence is usually high, and sediment motion is only initiated with low shear stress. Therefore, the effects of relative submergence on sediment transport rate can often be neglected [2, 13, 14]. One of the significant resistance components in lowland rivers is due to the presence of aquatic vegetation, which complicates flow resistance calculations. Okhravi et al. [2] stated that approaches connecting dynamic flow characteristics and velocity distribution over a river course with flow resistance values (such as Manning's roughness and Darcy-Weisbach friction factor) can incorporate the effects of vegetation into flow resistance calculations. These methods utilize flow discharge as the characteristic that shapes the channel and take into account the irregular bed topography and water elevation variations, often referred to as the hydraulic geometry approach.

The applied method is fully described in the referenced paper by the authors of this work [2]. We use the developed predictor, which connects Manning's roughness to dimensionless unit discharge ($q^* = \left(Q/w\right)/\sqrt{gR^3 S_f}$), as given in Eq. 1. The values of n_r will be compared with the traditional method of Manning's calculation ($n_m = R^{2/3} S_f^{1/2}/u$) in the following part of the paper.

$$n_r = 0.32 q^{*-0.978} \tag{1}$$

In this study, we selected a 4-kilometer reach of the Gabčíkovo-Topoľníky channel in southwestern Slovakia (Fig. 1). This reach includes four uniformly spaced cross-sections: two upstream and two downstream of a bridge prone to accumulated vegetative debris (Fig. 2) and submerged vegetation. Aquatic plants in the channel are permanently submerged species, while grass and shrubs are found on stream banks and floodplains and are not always submerged.

Field velocity measurements were performed using the SonTek RiverSurveyor-M9 during two field visits in 2018 and 2023. Analysis of bathymetric data and streamwise velocity distribution was conducted to examine sediment depth changes across the reach over time. The measured and calculated hydraulic parameters for the corresponding years are summarized in Tables 1 and 2. The relevant parameters include: flow depth (h), stream width (w), wetted area (A) and perimeter (P), longitudinal slope of the water surface (S_f), flow velocity (u), shear/friction velocity (u_*), flow discharge (Q), area of retained sediments (A_s) in the bed channel, Froude number (Fr), and roughness coefficients (n).

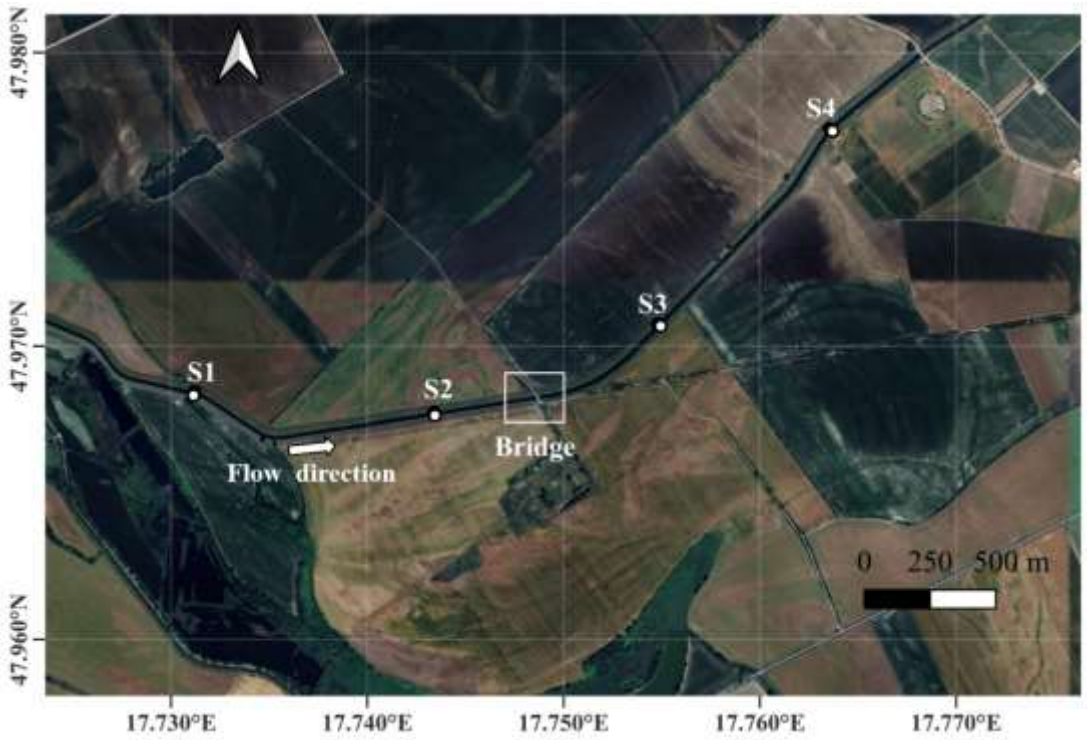

Figure 1. Location of four cross-sections at the Gabčíkovo-Topoľníky stream channel

The method used to quantify sediment retention at each cross-section of the selected reach involved measuring the depth of fine sediments from the surface to the underlying rocks using graded metal rods. As shown in Fig. 2, a handheld graded metal rod, equipped with a bubble level, was employed by a person to measure sediment depth at one-meter intervals across the stream, from bank to bank. Depth changes and associated storage areas over time (measured in 2018 and 2023) were recorded in the same vegetation type within the reach (Tables 1 and 2). The area of fine retained sediment (A_s) was calculated from the measured sediment depths, based on the differences between the base (rock level) and the surface level of fine sediment in each stream cross-profile. Similar studies on fine sediment budgets in river beds have used a unit of kg/m², and to ensure comparability, we also report the retained sediment in this weight unit. To convert the storage area (A_s in Table 1) to this typical unit, we used the average density of rocks ($\rho_m = 2650$ kg/m^3) and assumed a porosity (ϕ) of 0.4, as shown in Eq. 2, which is suitable for relatively fine sediments, similar to the study by Gurnell and Bertoldi [6]. V_s is the total volume of fine sediments calculated by A_s with a unit length of one meter. The porosity value can range from 0.25 to 0.45, with lower values corresponding to more heterogeneous and coarser sediments [15, 16].

$$m_s = \rho_m(1 - \phi)V_s \quad (2)$$

The calculated flow and sediment characteristics from the two measurement periods were compared to address changes in the stream bed and quantify sediment retention by aquatic vegetation. In this study, we focus on total sediment retention rather than just fine sediment retention within the stream channel. The relationship between sediment deposition and changes in flow characteristics will be further analyzed and compared with relevant field studies.

4 Results and discussion

The calculated and measured hydraulic parameters, along with A_s, from the same reach in the two measurement periods, 2018 and 2023, are summarized in Tables 1 and 2, respectively. The width of the cross-sections has remained almost unchanged along the stream reach from 2018 to 2023, as has the hydraulic radius for each corresponding cross-section. However, flow parameters and the water surface slope have altered between the two measurements. Since there have been no construction activities nearby and no extreme changes in flow throughout the reach, there are no external sources affecting the

cross-sectional geometric shape or sediment size distribution in the selected reach. Therefore, the changes in flow parameters can be attributed to the presence, density, and properties of the vegetation within the channel.

Figure 2. Typical view of submerged aquatic vegetation in the studied stream channel

Table 1. Hydraulic parameters of four selected cross-sections: May 2018 measurements

Sections	h (m)	w (m)	A (m^2)	P (m)	R (m)	S_f	u (m/s)	u_* (m/s)	Q (m^3/s)	A_s (m^2)	Fr	n_m	n_r
S1	1.49	16	22.41	18.73	1.20	0.000038	0.120	0.021	1.88	2.73	0.035	0.08	0.07
S2	1.41	16.5	21.36	19.10	1.12	0.000014	0.115	0.012	1.90	2.54	0.035	0.04	0.04
S3	1.57	14.5	21.77	17.85	1.22	0.000016	0.103	0.014	1.93	1.75	0.03	0.05	0.04
S4	1.76	17.0	27.03	20.13	1.34	0.000053	0.090	0.026	2.00	2.47	0.025	0.12	0.10

Table 2. Hydraulic parameters of four selected cross-sections: June 2023 measurements

Sections	h (m)	w (m)	A (m^2)	P (m)	R (m)	S_f	u (m/s)	u_* (m/s)	Q (m^3/s)	A_s (m^2)	Fr	n_m	n_r
S1	1.59	16.5	25.25	19.4	1.3	0.000092	0.062	0.034	1.39	3.62	0.017	0.21	0.17
S2	1.48	15.5	20.86	18.35	1.14	0.000057	0.061	0.025	1.31	2.62	0.018	0.13	0.11
S3	1.60	14.5	22.15	17.89	1.24	0.000066	0.064	0.028	1.69	2.62	0.018	0.12	0.10
S4	1.70	17.0	27.23	20.14	1.35	0.000043	0.044	0.023	1.47	3.27	0.012	0.15	0.12

The results showed the decrease in total discharge and section-averaged velocity in 2023 as well as Fr numbers, attributed to denser vegetation in 2023 compared to 2018. The role of aquatic vegetation has recently been assessed in lowland streams [17, 18]. According to the literature and this research, increased vegetation leads to a decrease in velocity and water conveyance power in a river channel, which results in higher Manning roughness values (n_m) and the one developed (n_r) under the previous research work of the authors [2]. It is worth noting that n_r indicated a good fit compared to n_m estimations, despite a 20% underestimation.

Patches of aquatic vegetation can impact the sedimentation process by creating areas of reduced flow velocity through the capture of flow momentum and a decrease in turbulence velocity [1], thereby promoting sedimentation [19]. A similar pattern can be observed when comparing the corresponding values of A_s in each cross-profile. The rate of increase in A_s (the area between the black star line and the blue square line in Fig. 3) could be as high as 50% (S3 in Tabels 1&2) due to the presence of vegetation and the resultant lower velocity. This points to the role of aquatic vegetation in influencing sediment storage [3], primarily through the retention and stabilization of predominantly sand and finer sediments within the channel [6]. The findings of our study indicate significant retention of fine sediment (0.001-

2 mm) by aquatic vegetation in the Gabčíkovo-Topoľníky channel, which are important insights for the prediction of sediment budgets and river functioning.

The conversion of A_s to the typical mass unit of kg/m² is presented in Fig. 4, which shows a higher range of retained sediments in 2023 at the same cross-section locations compared to the data measured in 2018. The average sediment retained across the entire cross-profiles is up to an order of magnitude higher than the average sediment retained in the active channel area of the River Blackwater in England in the spring of 2009, as reported in the study by Gurnell and Bertoldi [6]. This reflects the fact that very low flow velocities in low-gradient rivers in lowland areas provide conditions for deep fine sediment accumulations compared to higher flow energy in gravel-bed rivers [20]. Additionally, the flow depth in lowland rivers is usually greater than in gravel-bed rivers [2], facilitating sediment deposition near the bed. For example, the reported larger depth in the River Blackwater is almost 7-8 times smaller than the average flow depths measured in this study.

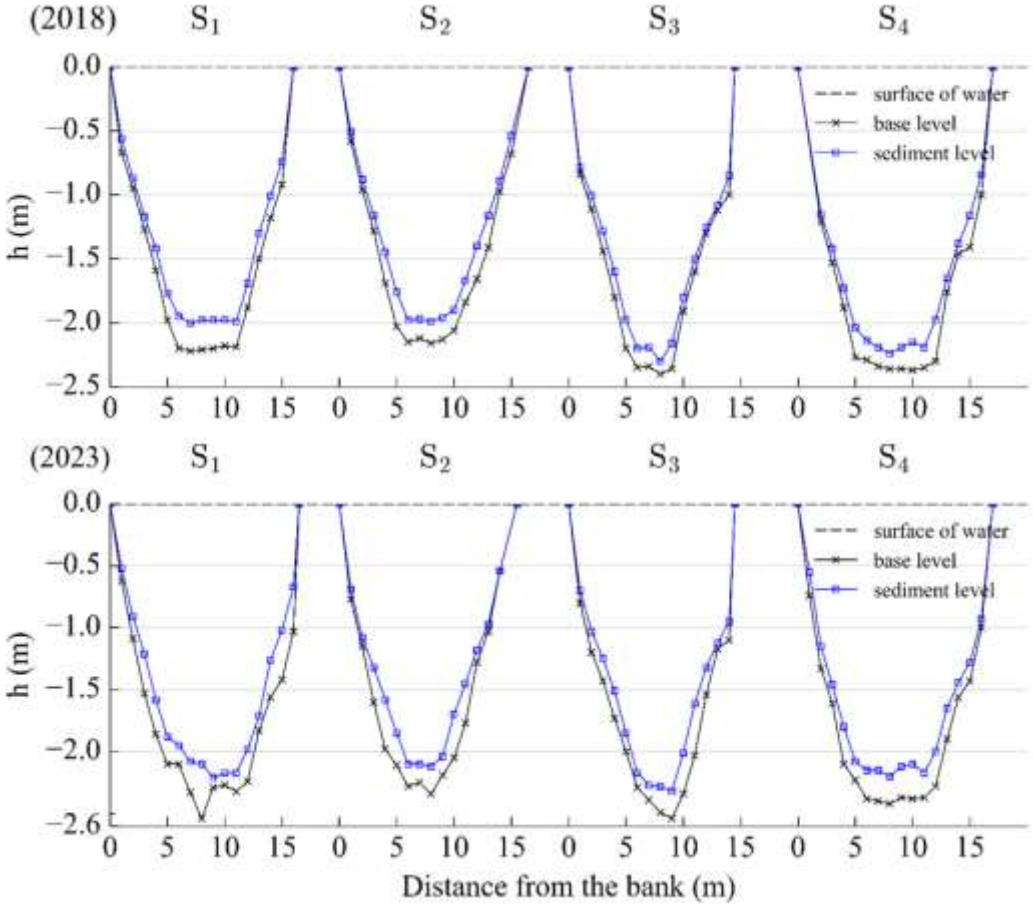

Figure 3. Variations in retained sediments within four stream cross-profiles (S1-S4) in 2018 and 2023

The measurement periods in May 2018 and June 2023 were selected to be close together to minimize the impact of temporal variation on the results. The quantities of retained sediment can fluctuate over time due to changes in river dynamics and the volume and distribution of aquatic vegetation [17]. The locations of fine sediment accumulations are also influenced by river power and the type of aquatic vegetation, whether emergent or submerged. Consequently, the spatial distribution of fine sediments will be varied over time [6]. The complexity of interactions between flow, sediment, and vegetation in river restoration and management has been addressed by O'Briain et al. [18]. Their study focused on the role of vegetation in influencing flow velocity, water depth, and substrate, which drives channel adjustments and landform development through biogeomorphic succession in a lowland river in Ireland. Their findings highlighted that vegetation regulates sediment dynamics, enhances river morphology, and creates diverse habitat patches, contributing to the river's natural renaturalization. We aim to use the preliminary results of this study, along with findings from the literature, to extend our assessment of the proportions of fine sediment retained by aquatic vegetation over larger stream reaches and longer

time frames.

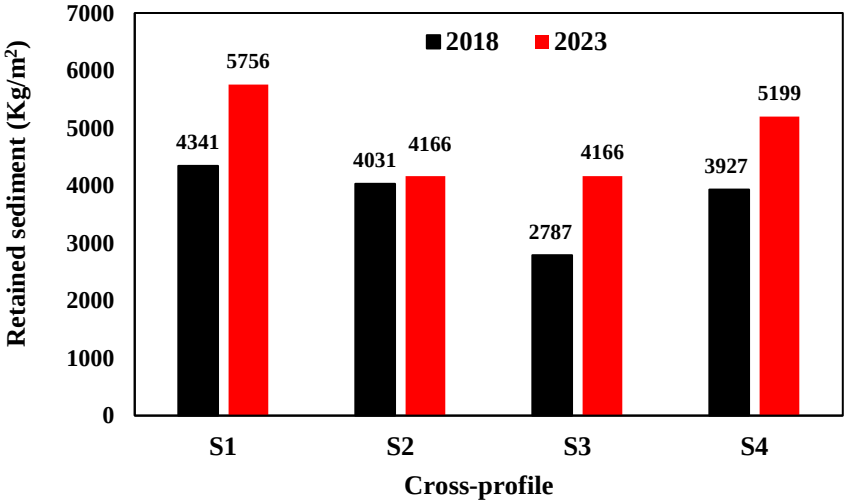

Figure 4. Quantity 2of retained sediment in each cross-profile (S1-S4) in 2018 and 2023

5 Conclusions

This study demonstrates the substantial influence of aquatic vegetation on flow characteristics and sediment retention within a lowland stream system. The comparison of hydraulic parameters between 2018 and 2023 measurements reveals that increased vegetation density significantly reduces flow velocity and discharge. This reduction is due to increased hydraulic resistance and the absorption of momentum by dense vegetation, which leads to decreased turbulence and sediment entrainment, resulting in higher sediment retention. These effects are primarily observed in fine sediment accumulation, with a calculated increase in sediment storage of up to 50%, as shown by the analysis of cross-sectional profiles (Fig. 3 and Tables 1 & 2) and the quantity of retained sediments in kg/m² (Fig. 4). These findings align with existing literature and highlight the role of aquatic vegetation in influencing stream bed morphology. This research contributes to a more comprehensive understanding of sediment budgets in lowland rivers, which is critical for river ecosystem functions. Further research is recommended to explore the long-term impacts of vegetation on sediment retention across larger river reaches. Additionally, investigating the influence of different vegetation types on flow characteristics and sediment deposition would be valuable for informing river restoration and management practices.

Acknowledgment
The authors gratefully acknowledge the financial support received from three projects, namely [VEGA 2/0028/23], [APVV-22-0610], and [VEGA 2/0140/24], in Slovakia.

References:

[1] Marjoribanks, T.I., Hardy, R.J., Lane, S.N.: The hydraulic Description of Vegetated River Channels: the Weaknesses of Existing Formulations and Emerging Alternatives. Wiley Interdisciplinary Reviews: Water, 1(6), pp. 549-560, 2014.
[2] Okhravi, S., Schügerl, R., Velísková, Y.: Flow Resistance in Lowland Rivers Impacted by Distributed Aquatic Vegetation. Water Resources Management, 36(7), pp. 2257-2273, 2022.
[3] Vargas-Luna, A., Crosato, A., Uijttewaal, W.S.: Effects of Vegetation on Flow and Sediment Transport: Comparative Analyses and Validation of Predicting Models. Earth Surface Processes and Landforms, 40(2), pp. 157-176, 2015.
[4] Zhang, J., Zhong, Y., Huai, W.: Transverse Distribution of Streamwise Velocity in Open-Channel Flow with Artificial Emergent Vegetation. Ecological Engineering, 110, pp. 78-86, 2018.
[5] Anjum, N., Tanaka, N.: Numerical Investigation of Velocity Distribution of Turbulent Flow through Vertically Double-Layered Vegetation. Water Science and Engineering, 12(4), pp. 319-329, 2019.
[6] Gurnell, A.M., Bertoldi, W.: The Impact of Plants on Fine Sediment Storage within the Active

Channels of Gravel-Bed Rivers: A Preliminary Assessment. Hydrological Processes, 36(7), e14637, 2022.
[7] Mondon, B., Sear, D.A., Collins, A.L., Shaw, P.J., Sykes, T.: The Scope for a System-Based Approach to Determine Fine Sediment Targets for Chalk Streams. Catena, 206, 105541, 2021.
[8] Corenblit, D., Steiger, J., Gurnell, A.M., Naiman, R.J.: Plants Intertwine Fluvial Landform Dynamics with Ecological Succession and Natural Selection: A Niche Construction Perspective for Riparian Systems. Global Ecology and Biogeography, 18(4), pp. 507-520, 2009.
[9] Gurnell, A.M., Grabowski, R.C.: Vegetation-Hydrogeomorphology Interactions in a Low-Energy, Human-Impacted River. River Research and Applications, 32(2), pp. 202-215, 2016.
[10] Sand-Jlnsen, K.A.J., Jeppesen, E., Nielsen, K., van der Bijl, L., Hjermind, L., Nielsen, L.W., Ivlrsln, T.M.: Growth of Macrophytes and Ecosystem Consequences in a Lowland Danish Stream. Freshwater Biology, 22(1), 15-32, 1989.
[11] Schulz, M., Kozerski, H.P., Pluntke, T., Rinke, K.: The influence of macrophytes on sedimentation and nutrient retention in the lower River Spree (Germany). Water Research, 37(3), pp. 569-578, 2003.
[12] Bertoldi, W., Drake, N., Gurnell, A.M.: Interactions Between River Flows and Colonising Vegetation on a Braided River: Exploring Concepts Using Satellite Data. Earth Surface Processes and Landforms, 36, pp. 1474-1486, 2011.
[13] Sulaiman, M.S., Sinnakaudan, S.K., Azhari, N.N., Abidin, R.Z.: Behavioral of Sediment Transport at Lowland and Mountainous Rivers: A Special Reference to Selected Malaysian Rivers. Environmental Earth Sciences, 76, pp. 1-15, 2017.
[14] Okhravi, S., Alemi, M., Afzalimehr, H., Schügerl, R., Velísková, Y.: Flow Resistance at Lowland and Mountainous Rivers. Journal of Hydrology and Hydromechanics, 71(4), pp. 464-474, 2023.
[15] Frings, R.M., Schüttrumpf, H., Vollmer, S.: Verification of Porosity Predictors for Fluvial Sand-Gravel Deposits. Water Resources Research, 47, W07525, 2011.
[16] Seitz, L., Haas, C., Noack, M., Wieprecht, S.: From Picture to Porosity of River Bed Material Using Structure-From-Motion with Multi-View-Stereo. Geomorphology, 306, pp. 80-89, 2018.
[17] Larsen, L.G.: Multiscale Flow-Vegetation-Sediment Feedbacks in Low-Gradient Landscapes. Geomorphology, 334, pp. 165-193, 2019.
[18] O'Briain, R., Shephard, S., McCollom, A., O'Leary, C., Coghlan, B.: Plants as Agents of Hydromorphological Recovery in Lowland Streams. Geomorphology, 400, 108090, 2022.
[19] Liu, C., Nepf, H.M.: Sediment Deposition Within and Around a Finite Patch of Model Vegetation over a Range of Channel Velocity. Water Resources Research, 52(1), pp. 600-612, 2016.
[20] Okhravi, S., Eslamian, S.: Form Resistance Prediction in Gravel-Bed Rivers. Flood Handbook. CRC Press, Taylor and Francis Group, pp. 125-138, 2022.

ANALYSIS OF THE 2D HYDRAULIC EQUATIONS FOR THE FISH PASS MODELLING

ALEXANDRA VIDOVÁ [1], LEA ČUBANOVÁ [1]

[1] *Faculty of Civil Engineering STU, Department of Hydraulic Engineering, Radlinského 2766/11, 810 05 Bratislava, Slovakia, alexandra.vidova@stuba.sk, lea.cubanova@stuba.sk*

1 Abstract

Numerical modelling plays a crucial role in designing and evaluating fish passes, particularly close-to-nature fish pass designs. However, these simulations pose challenges due to complex geometries requiring precise mesh resolution and adherence to time-step limitations. This study investigates a rock ramp fish pass on the Myjava stream, renaturalized by weir removal. The two-dimensional HEC-RAS model was developed to assess low-flow conditions critical for fish migration. Calibration employed in-situ data. Governing equations (diffusion wave, shallow water with/without turbulence) were compared, while shallow water equations with turbulence yielding the best agreement with measurements. The model captured flow patterns around individual boulders, highlighting the limitations of the HEC-RAS for detailed simulations of small, complex areas.

Keywords: fish pass, HEC-RAS, 2D model, shallow water equations, diffusion wave equations, Courant number.

2 Introduction

Designing fish passes is essential for overcoming barriers in streams and restoring aquatic ecosystems [1]. Fish passes mimic natural conditions to help fish navigate around obstacles like dams, supporting by the European Union's goal of preserving biodiversity. 2D hydraulic modelling has become a key tool in fish pass design [2]. Detailed water flow can be simulated in these structures using software like the HEC-RAS as one dimensional [3] or two dimensional [4]. To conduct unsteady flow analyses this software utilizes equations such as the diffusion wave and shallow water equation, with options for turbulence models. Developing a 2D fish pass model involves considering type of fish pass (in terms of very detailed geometry of internal environment), materials (considered by the Manning´s roughness coefficient) and appropriate boundary conditions, which are specified to accurately simulate the hydraulic conditions. The Courant criterion is crucial in ensuring stable model computation by determining the appropriate time step relative to the spatial resolution, preventing numerical instabilities. Numerical methods solve water flow equations, producing visualizations of velocities, water depths, and other parameters. This study compares using of different computational equations and turbulence models, enhancing the effectiveness and efficiency of fish passes design.

3 Methods

3.1 Location of the fish pass

The study was conducted on a fish pass located on the Myjava River at rkm 26.500, in the cadastral area of the Senica town in western Slovakia. The long-term annual flow rate in the profile of the fish pass is $Q_a = 2.11\ m^{3}{\cdot}s^{-1}$ [5]. A fixed weir was built on the stream to mitigate the slope and stabilize the riverbed of the Myjava River in the past (Figure 1). The weir thus constructed formed an obstacle in the stream and did not allow ichthyofauna migration [5].

Fixed weir no longer fulfilled its purpose and was therefore replaced by a full-river bed passage in form of rock-ramp fish pass (Figure 2). A depression is located in the centre of the constructed ramp, which enables the migration of ichthyofauna even at lower stages, and individual/perturbation stones are

arranged in a chessboard pattern in the bottom of the ramp.

Figure 12. Original fixed weir [6]

Figure 13 Built rock ramp fish pass [8]

3.2 Rock ramp fish pass design

The rock ramp fish pass is designed to mimic natural environment for ichthyofauna to swim both upstream and downstream, facilitating bidirectional migration. The flow is directed through natural-looking elements, such as boulders and stones, which help to reduce velocities and increase water depths. These elements are arranged to create flow shadows and pools that provide resting and refuge areas for fish during migration through the fish pass.

According to the Methodology [7] of the Water Research Institute (WRI, Bratislava, Slovakia), the modeled fish pass belongs to the barbel fish zone and recommended design parameters are as follows [9]:

- maximum cross-sectional velocity 1.2 $m \cdot s^{-1}$,
- maximum longitudinal slope 1:100 (1%),
- minimum water depth in the main streamline 0.40 m,
- minimum flooded width in water level 2.0 m.

The ramp is located across the entire width of the river bed with boulders placed on banks (black dots in Figure 5), these are important by the higher flows, and in the middle part of ramp (circles in Figure 5), these stones allows fish migration almost throughout the whole year when flows are low

and moderate (Figure 3).

Figure 14 Boulders on the river bed bottom of the fish pass

Parameters of the fish pass [5]:

- the total length of the fish pass is 19.4 m,
- overcoming a head of 0.81 m,
- slope of the fish pass is 4.17 %,
- middle part of the fish pass is shaped as triangle with the width in the base of 5.6 m,
- the boulders are arranged in a chessboard pattern in a span of 0.93 m in eight profiles, which are 2.0 m apart,
- the stones in the bottom have a size of 20 - 40 cm and the vertical resting boulders in the profiles have a transverse width of 30 - 40 cm.

3.3 Model HEC – RAS

The analysis of the existing fish pass employed the U.S. Army Corps of Engineers, Hydrologic Engineering Center's River Analysis System (HEC-RAS) software, version 6.3.1. This program enables the computation of one-dimensional and two-dimensional water flow under both steady and unsteady flow regimes.

3.3.1 Model Creation Process

The fish pass surface was generated from the project, which formed the basis for this study. The fish pass layout included points with elevations, which were connected in Autodesk Civil 3D. A digital elevation model (DEM) of the area where the fish pass is located was downloaded from the freely available ZBGIS [11] mapping portal. Both surfaces were combined into one to create the fish pass surface with the Myjava stream upstream and downstream the fish pass (Figure 4), which was exported in Tag Image File Format (.tif). Cross-section profiles identified from the situation were exported as a shapefile (.shp), which applied in the results analysis. The created fish pass surface file was imported into the RAS Mapper into the terrain layer. Boulders were designed in the fish pass and inserted into a copy of the surface according to the situation. A boulder with a width of 0.40 m was inserted, and the surface at the boulder location was raised by 0.40 m based on the technical report. Following the boulder insertion, the geometry was created and assigned the surface with boulders. The spacing of points in the computational mesh was set to 1.50 m, with a denser spacing of 0.10 m in the fish pass area for improved accuracy. The Manning's roughness coefficient was assigned according to the project as n = 0.059 [5]. This value corresponds to the roughness of small streams at lower water stages with greater profile irregularities, occasional pools, shallows, and stones [12]. Boundary conditions were set for polygons defined in the geometry. For the inflow, a flow hydrograph was set for 24 hours with a uniform flow, as hydrological records with a detailed measurement step are not available in the locality, and a constant inflow is considered for the purpose of verifying the fish pass parameters.

For the outflow, the normal depth was specified, which is determined by the longitudinal slope of the water surface.

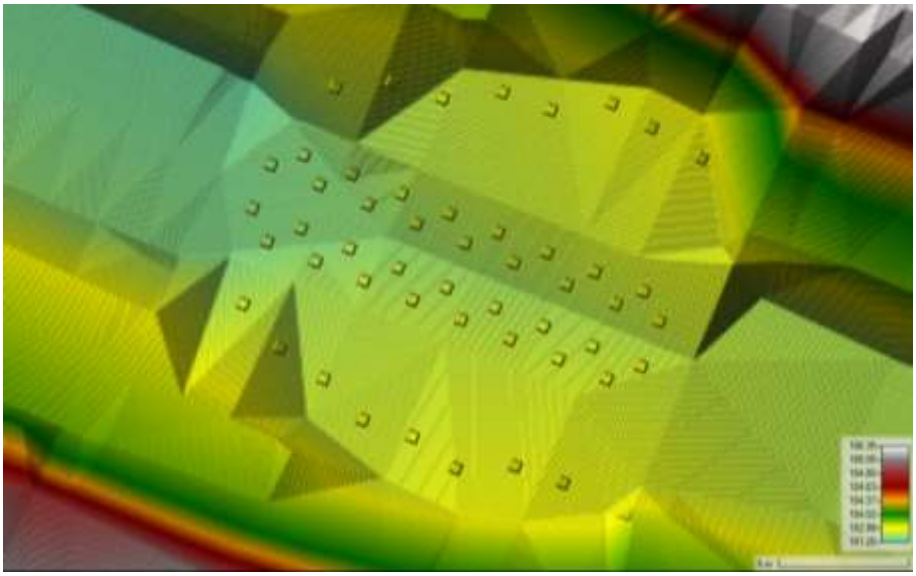

Figure 15 The surface of the fish pass with the Myjava river bed upstream and downstream

3.3.2 HEC-RAS equations

HEC-RAS (Hydrologic Engineering Center-River Analysis System) offers two primary equation sets for simulating 2D unsteady flow [10]:

1. Diffusion Wave Equation (DWE) (Eq. (1) – 2D form of momentum equations for diffusion wave):

$$g\nabla H = -c_f V \tag{1}$$

where:

g – gravitational acceleration ($m \cdot s^{-2}$),
∇H – gradient of elevation (m),
c_f – friction coefficient (s^{-1}),
V – velocity vector ($m \cdot s^{-1}$) (V = (u, v)).

DWE is a simplified form of the Saint-Venant equations, neglecting the convective acceleration term and assuming zero wave celerity. This translates to faster computations but may compromise accuracy, especially for rapidly changing flows. DWE finds application in scenarios with moderate velocities and mild channel slopes, offering a good balance between speed and accuracy.

2. Shallow Water Equations (SWEs) (Eq. (2) – 2D form of momentum equations for shallow water):

$$\begin{aligned} \frac{\partial u}{\partial t} + u\frac{\partial u}{\partial x} + v\frac{\partial u}{\partial y} &= -g\frac{\partial H}{\partial x} + \nu_t\left(\frac{\partial^2 u}{\partial x^2} + \frac{\partial^2 u}{\partial y^2}\right) - c_f \cdot u + f \cdot v \\ \frac{\partial v}{\partial t} + u\frac{\partial v}{\partial x} + v\frac{\partial v}{\partial y} &= -g\frac{\partial H}{\partial y} + \nu_t\left(\frac{\partial^2 v}{\partial x^2} + \frac{\partial^2 v}{\partial y^2}\right) - c_f \cdot v + f \cdot u \end{aligned} \tag{2}$$

where:

u, v – velocities in the Cartesian directions ($m \cdot s^{-1}$),
t – time (s),

g – gravitational acceleration ($m \cdot s^{-2}$),
H – water surface elevation (m),
ν_t – horizontal eddy viscosity coefficient ($m^2 \cdot s^{-1}$),
c_f – friction coefficient (s^{-1}),
f – Coriolis parameter (s^{-1}).

SWEs represent a more complete description of fluid motion, accounting for mass and momentum conservation. They provide detailed insights into complex flow features like eddies and vortices, particularly when turbulence effects are significant. HEC-RAS employs an implicit finite volume solver for SWEs (Euler-Lagrangian Method) enabling larger time steps compared to explicit methods.
Additionally, SWEs come with two options regarding turbulence:

- With Turbulence Model:
  This approach incorporates the influence of turbulence on flow behavior, enhancing accuracy in scenarios with high velocities or complex geometries. However, it demands more computational resources.
- Without Turbulence Model: This simplifies calculations by assuming laminar flow, making it suitable for situations with negligible turbulence or steady flows over gentle slopes.

The selection between SWEs and DWE depends on the complexity of the flow and desired level of detail. SWEs with a turbulence model are ideal for capturing intricate flow patterns in hydraulic structures or areas with high velocities. DWE is a better choice for simpler scenarios with moderate velocities and gentle slopes, where computational efficiency is a priority. Refer to the HEC-RAS user manual for further guidance on selecting the appropriate equation set for your specific modeling needs.

3.3.3 Courant Criterion

An appropriate computational time step must be selected for the modeled computational mesh. The choice of time step is a function of the cell size and the water flow velocity in that cell. In general, the time step must be chosen so that the Courant criterion is fulfilled [10]:

- Diffusion Wave Equation:

$$\mathrm{C} = \frac{V.\Delta T}{\Delta X} \leq 2{,}0 \quad (C_{max} = 5{,}0) \tag{3}$$

- Shallow Water Equation - Euler-Lagrangian Method (SWE-ELM):

$$\mathrm{C} = \frac{V.\Delta T}{\Delta X} \leq 1{,}0 \quad (C_{max} = 3{,}0) \tag{4}$$

where:

C - Courant number,
V - water flow velocity ($m \cdot s^{-1}$),
ΔT - computational time step (s),
ΔX - average cell size (m).

A computational time step of 0.10 s was selected, which is the smallest possible computational time step in the HEC-RAS model. The Courant criterion then according to Eq. (3) and Eq. (4):

$$C = \frac{V \cdot \Delta T}{\Delta X} = \frac{2 \cdot 0{,}1}{0{,}1} = 2 \tag{5}$$

where:

C = 2 (Courant number), where C_{max} = 5.0, or 3.0,
V = 2 m·s^{-1} (water flow velocity) (maximum assumed velocity in the fish pass according to measurements),
ΔT = 0.1 s (computational time step) (smallest time step and also the most suitable to meet the Courant criterion condition),
ΔX = 0.1 m (average cell size) (size of the detailed cell in the rock ramp area).

It can be concluded that the selected computational time step and cell size of the created detailed mesh in the fish pass (rock ramp) area meets the Courant number condition specified in the HEC-RAS software manual. To create a stable model 3 computational plans were created, where the computational methods/equations were changed.

4 Results and discussion

This study aimed to develop a simulation model of a recently implemented fish pass on the Myjava stream. The focus was on simulating critical low flow conditions. A specific flow rate of 0.451 m³·s^{-1} approximately equal to Q_{330}), measured in-situ during 2019, was chosen for this analysis. This low flow scenario is very important for verifying critical conditions to maintain adequate hydraulic parameters for fish migration, even during dry periods [8].

4.1 Comparison of Simulation with Measurement

The WRI measurement results were used to calibrate the constructed simulation model. As a boundary condition was entered measured flow rate of 0.451 m^3·s^{-1} for all plans. Measurements were performed in eight profiles (Figure 5) between the boulders, each in five verticals (Figure 6) [8]. For each profile, the course of the measured flow velocities was evaluated and compared with the results from the model (Figure 7, 8, 9 and 10).

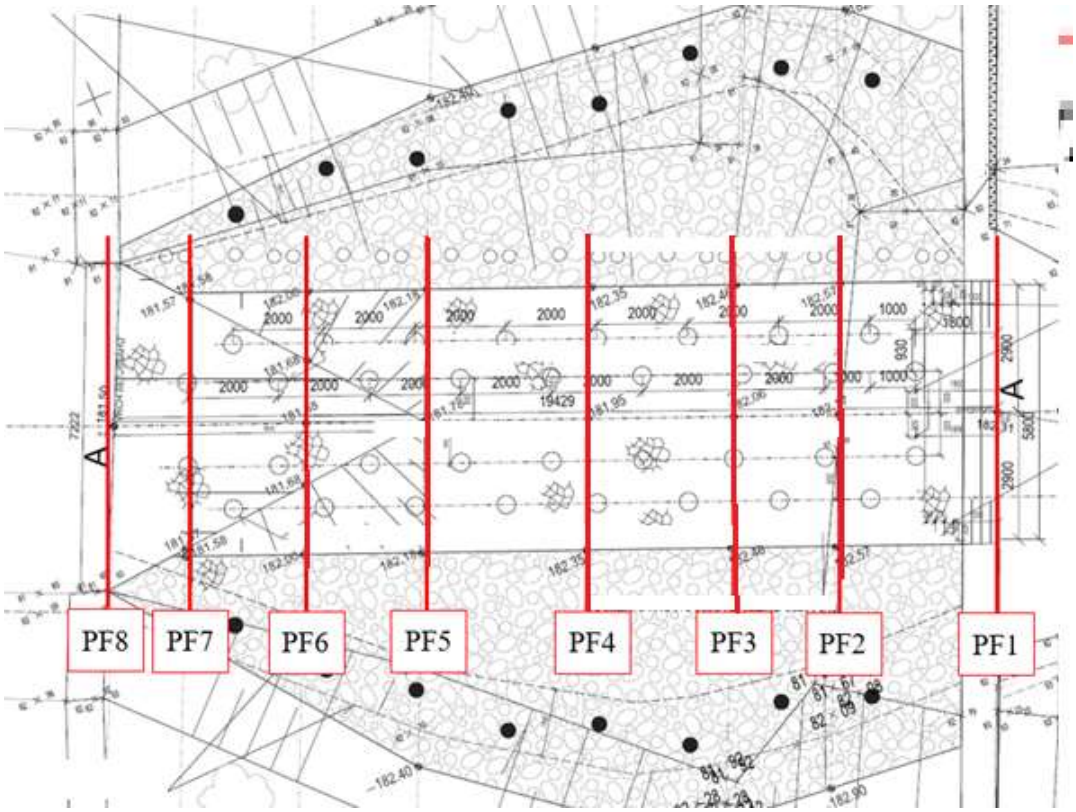

Figure 16 The situation with marked profiles from the measurement

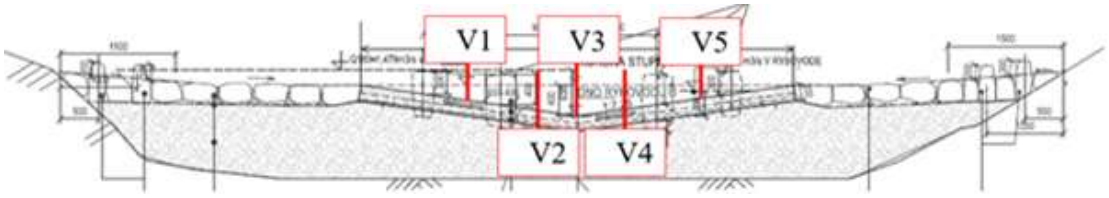

Figure 17 Cross section with marked vertical lines from the measurement

4.1.1 Plan 1

In the first plan was necessary to verify the stability of the model and the course of the calculation. In the 2D flow settings was chose the diffusion wave equation, which is more stable. After the calculation was compared the flow velocity profiles with the measurements (Figure 10). The velocities calculated in this scenario were higher than those measured (Figure 7 and 10). It can be concluded that the trend of the velocities has approximately the same shape but is not identical to the measurement (Figure 10). The inundated water level width is smaller than the measured state according to the simulation.

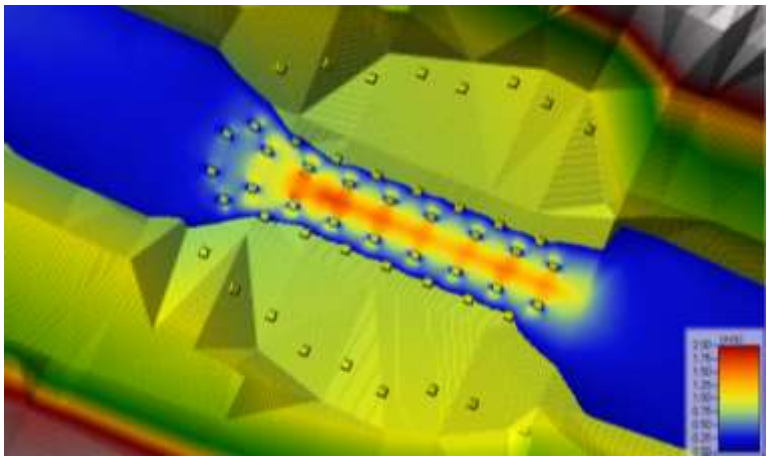

Figure 18 View of velocity field contours for plan 1

4.1.2 Plan 2

In the second plan was changed the equation to SWE-ELM without turbulence to see if the calculation is also stable for another complex equation. After the calculation, flow shadows could be seen in the results (Figure 10), which are created behind the boulders. This plan was closer to the real state, so this equation was used for the calculation of the next plan. The flow velocity profile was smaller than in plan 1, but still did not correspond to the measurements (Figure 8 and 10).

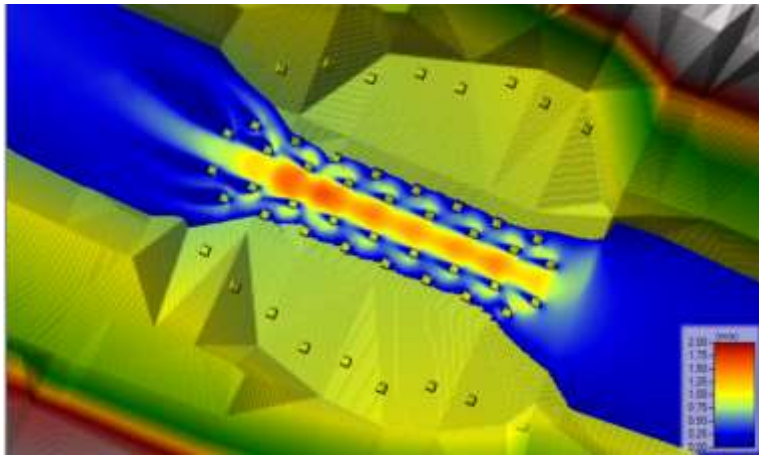

Figure 19 View of velocity field contours for plan 2

4.1.3 Plan 3

Since was assumed turbulent flow in the fish pass, turbulence was added to the calculation in the stable plan 2, so the equation SWE-ELM with turbulence was entered. The flow velocity profile was minimally affected (Figure 10), but the velocities in the center of the fish pass decreased (Figure 9 and 10).

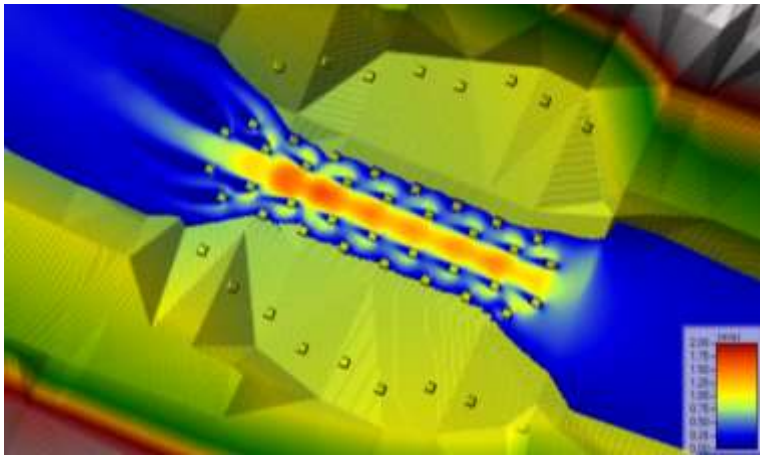

Figure 20 View of velocity field contours for plan 3

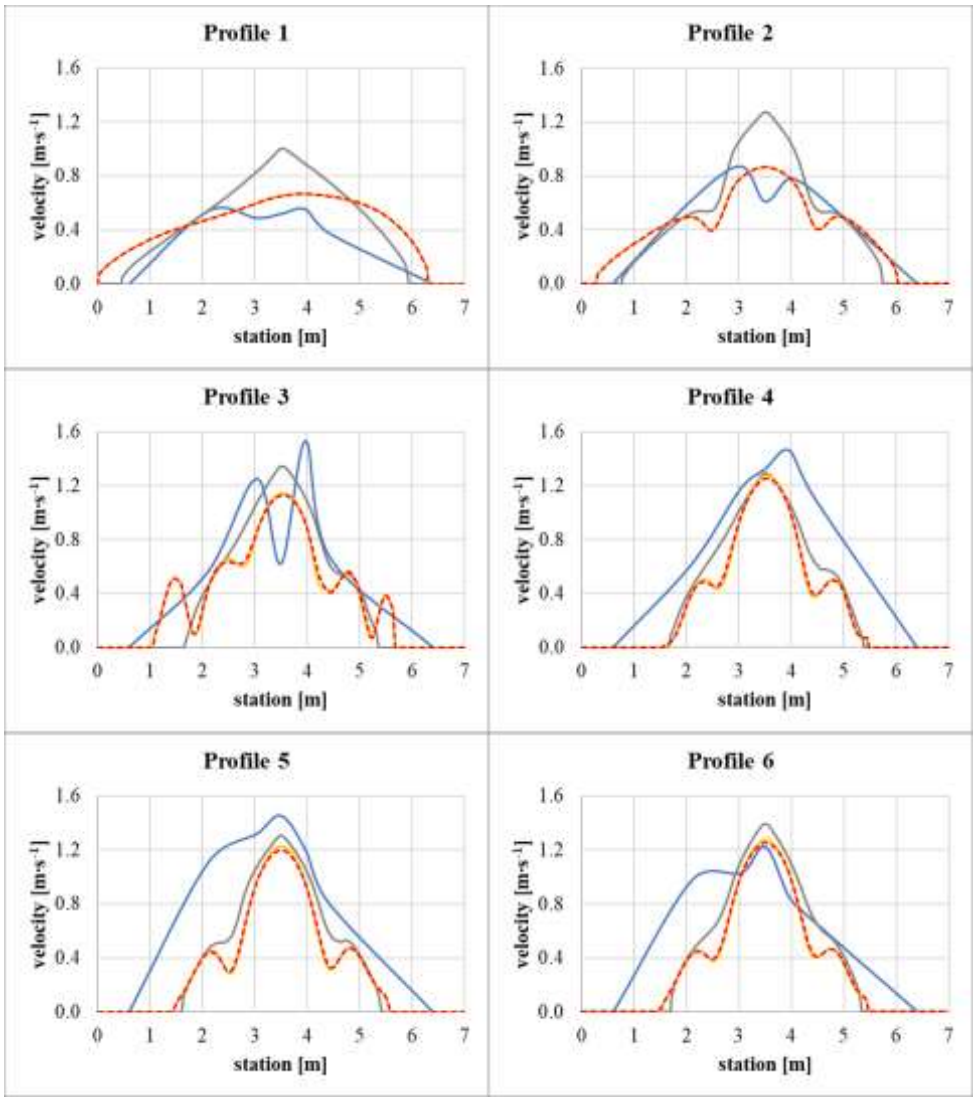

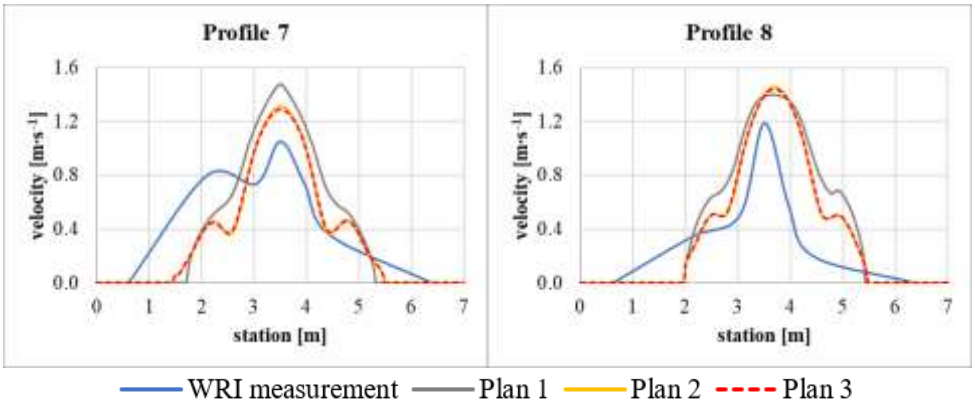

Figure 21 Results comparison of WRI measurement and study plans 1,2 and 3 for all eight profiles

5 Conclusion

2D simulation software is a valuable tool for simulating and visualizing water flow in various situations and conditions. To create a correct and most accurate model, it is necessary to obtain appropriate technical and hydrological data. Knowledge in the software utilized is essential, as it influences the precise definition of initial and boundary conditions, as well as the selection of numerical methods, to ensure the accuracy and relevance of the results. The analysis of the models carried out so far indicates the need to choose an appropriate calculation equation, to include a turbulence model, as well as to choose a time step that meets the Courant criterion, so that the model is stable. All of this affected the total simulation time (simulation of one plan took 3 hours). Due to the required detail of the model (stones with a size of 40 cm must be covered with a computational grid with a cell size of 0.1 m), the smallest simulation time step of 0.1 s must be chosen. This brings us closer to the limits of the HEC-RAS model for calculating a relatively small area, but with high detail.

The next step in the solution will be the calibration of the model. To achieve accurate results, it will be necessary to change Manning´s roughness coefficient or the computational time step. Since the program in this case no longer allows a smaller time step, only changing the roughness in the entire fish pass or individually around solitary boulders is possible. 2D software is a good tool for verifying the design of fish passes, where the most important condition is the creation of a suitable velocity field and sufficient depths for the ichthyofauna that occurs.

The simulations with different governing equations revealed that the DWE resulted in higher maximum velocity but smaller flooded width, while the SWE-ELM led to lower vertical velocities and larger flooded width. SWE-ELM accurately captured the flow shadows behind boulders, which were not captured by in-situ measurements. Further measurements at higher water levels are recommended for a more comprehensive analysis of the fish pass and verification of the calibrated model. This will allow for a better understanding of flow dynamics and model validation over a wider range of hydraulic conditions.

In conclusion, SWE-ELM with turbulence modeling stands out as the preferred approach in the HEC-RAS for designing efficient and fish-friendly passages. This method offers a superior grasp of the complexities of flow within the fish pass by incorporating both intricate flow features and the influence of turbulence. This enhanced accuracy is paramount for ensuring the functionality and success of the fish pass design. While simpler models may offer faster computation times, they come at the cost of neglecting crucial details that can significantly impact fish passage. Engineers can create fish passes that optimize flow conditions and promote successful fish migration by leveraging the strengths of SWE-ELM with turbulence modeling.

Acknowledgements
This contribution was developed within the framework and based on the financial support of the APVV-20-0023 project, "Research on hydraulic characteristics of fish passes with regard to ichthyological requirements".

References:
[1] Mao, X.: Review of fishway research in China, Ecological Engineering, 115, pp. 91-95, 2018.
[2] Baki, AB., Golpira, A., Rampinelli, GC., Patrizio, L., and Zhu, ZD.: Numerical modelling of nature-like fish passage using a 2d shallow water model, CSCE Annual Conference, Laval, Canada, p. 8, 2019.
[3] Kubrak, M., Smoliński, B., Riha, R., Kodura A., Popielski, P., Jabłoński, K.: The application of a minimum specific energy concept for a fish ladder design, Archives of civil engineering, 68, pp. 555-568, 2022.
[4] Schneider, M., Kopecki, I., Hägele, T., Quaresma, A., João Costa, M., Boavida, I., Pinheiro, A. N., Rutschmann, P., Geiger, F., Jarny, S., Schwarzwälder, K., Rüther, N., Sanz-Ronda, J.: Fishfriendly Innovative Technologies for Hydropower, D3.3 Guidelines for fish behaviour assessment at HPPs, p. 180, 2020.
[5] Sirota, E.: Opatrenia na odstraňovanie migračných bariér na vodnom toku Myjava – stupeň v rkm 26,500 - Technická správa, Bratislava: Hycoprojekt, a.s. Bratislava, 2019.
[6] Supeková, M.: Skúsenosti s prípravou a realizáciou spriechodňovania migračných bariér. Banská Bystrica: Seminár k spriechodňovaniu migračných bariér, 2019.
[7] V. Polák, V. Mužík, V. Druga, D. Abaffy, F. Rebenda, P. Matok, K. Mravcová, R. Hránková, M. Čomaj, D. Joštiaková, Určenie Vhodných Typov Rybovodov Podľa Typológie Vodných Tokov: Metodické Usmernenie Ministerstva životného prostredia SR; Výskumný ústav vodného hospodárstva Bratislava, Slovak Republic, 2015.
[8] Polák, V.: Hydraulické merania na novopostavených rybovodoch, Výsledky merania rýchlostí prúdenia vody v rybovode na rieke Myjava, v rkm. 26,500, Bratislava: Výskumný ústav vodného hospodárstva, 2019.
[9] Vyhláška č. 383/2018 Z. z. Ministerstva životného prostredia Slovenskej republiky o technických podmienkach návrhu rybovodov a monitoringu migračnej priechodnosti rybovodov
[10] HEC-RAS Documentation, [online]. Available on: https://www.hec.usace.army.mil/confluence/rasdocs [cit.11.09.2023]
[11] Mapový klient ZBGIS [online]. Available on: https://zbgis.skgeodesy.sk/mkzbgis/sk/zakladna-mapa/contact?pos=48.800000,19.530000,8 [cit. 12.09.2023]
[12] Maňák, P.: Seminární práce z předmětu Morfologie a říční inženýrství. Manningův drsnostní součinitel. Praha: České vysoké učení technické v Praze, p. 13, 2017.

MATHEMATICAL MODEL FOR THE ANALYSIS OF UNSTEADY FLOW DURING A PRESSURE PIPELINE BREAK USING THE METHOD OF CHARACTERISTICS

GOCE TASESKI [1], NIKOLA KRSTOVSKI [2]

[1] *Faculty of Civil Engineering Skopje, N. Macedonia,* taseski@gf.ukim.edu.mk

[2] *Faculty of Civil Engineering Skopje, N. Macedonia,* nikolatudence@gmail.com

1 Abstract

The goal of developing a mathematical model to analyze the occurrence of non-stationary flow is to conduct an analysis of an existing pressure pipeline - specifically, a siphon from an irrigation system in Macedonia. In this system, when a defect occurs in the pipeline, particularly in the section experiencing the highest pressure, the phenomenon of non-stationary flow arises - creating a significant vacuum within the pipeline, leading to a massive breakdown. Specifically, this concerns a steel pipeline with a diameter of D=1640 mm, operating at a maximum working pressure of 8.2 bar in the lowest part of the siphon. When non-stationarity occurs, a substantial negative pressure (vacuum) emerges, resulting in complete destruction of the pipeline over a length of 500 m.

Keywords: method of characteristics, unsteady flow, water hammer, negative pressure

2 Introduction

The appearance of unsteady flow in a pressurized pipeline is a constant occurrence and, depending on the magnitude of pressure and flow changes in the pipeline, it can cause significant damage to the pipeline. Therefore, even in pipelines where large oscillations in flow and pressure are least expected to occur within a short time interval, it is necessary to conduct hydraulic analyses for unsteady flow. These analyses are much more complex than those for steady flow and require more time, which is why they are not always performed.

However, with today's capabilities of computer technology, it is possible to perform hydraulic analyses for unsteady flow by appropriately applying the basic hydraulic equations and methods for solving them within previously defined boundary conditions that vary depending on each specific case.
In such analyses, the first step is to detect the causes of the occurrence of unsteady flow, which can be various and include:

- secondary opening or closing of a valve at the beginning, middle or end of the pipeline
- improper commissioning of the pipeline
- defect occurrence of a pipeline, etc.

According to the aforementioned, in this paper, by detecting the causes of unsteadiness and the geometric characteristics of the system – the pipeline, the procedure for creating a hydraulic model for unsteady flow will be presented. This model will be applied to a real pipeline to detect the causes of failures within it.

Additionally, with the mathematical model thus created, it will be possible to determine whether the occurrence of unsteady flow will cause damage to part or the entire pipeline. This primarily depends on the material and diameter of the pipeline, as well as the initiator of the unsteadiness, which are the basic input parameters in the model.

3 Basic equations for unsteady flow

According to Wylie [3] (1993), the water hammer is defined as the hydraulic variable occurrence of flow, which causes an increase of overpressure in a pipeline system. The unsteady flow can be generated by certain operational measures such as: opening or closing of the valve, turning the pumps on or off, abrupt cracking of the pipe etc.

Starting points in the mathematical description of the unsteady flow [4] are the basic laws in the mechanics of fluids:

- Dynamic equation – equation of motion and
- Continuity equation

The final form of the dynamic equation for unsteady flow in closed systems under pressure:

$$\frac{\partial V}{\partial t} + V\frac{\partial V}{\partial x} + \frac{\lambda}{2D}V|V| = 0 \tag{1}$$

The convective acceleration V∂V/∂x or acceleration along the pipe is significantly lower compared to the local acceleration ∂V/∂t or acceleration over time, so mostly that convective acceleration is overlooked, and the dynamic equation is written:

$$\frac{\partial V}{\partial t} + g\frac{\partial P}{\partial x} + \frac{\lambda}{2D}V|V| = 0 \tag{2}$$

Assuming that the density of the fluid changes very little in terms of piezometric height (ρ = const), the equation of continuity gets the following form:

$$V\frac{\partial P}{\partial x} + \frac{\partial P}{\partial t} - Vsin\alpha + \frac{a^2}{g}\frac{\partial V}{\partial x} = 0 \tag{3}$$

Where a is the speed of propagation of the pressure wave and it is determined by the ratio of compression of the fluid and the module of elasticity of the tube:

$$a = \sqrt{\frac{K}{\rho\left(1 + \frac{K}{E}\frac{D}{e}c_1\right)}} \tag{4}$$

The coefficient c_1 depends of the pipe anchorage and is equal to:

- $c_1=1–\mu/2$ – pipe anchorage only at the upstream
- $c_1=1–\mu^2$ – pipe anchorage throughout against axial movement
- $c_1=1$ – pipe anchorage with expansion joints throughout

In Eq. (1) to (4), P denotes the static pressure at the centerline of the pipeline at location x and time t, V is the average velocity of flow, D is the pipe diameter, λ is the friction factor in the Darcy-Weisbach formula, x is the distance along the centerline of the pipe, α is the angle between the horizontal and the centreline of the pipe, taken as positive for the pipe sloping downwards in the direction of positive x, g is the gravitational constant; and a is the celerity of the pressure surge, i.e. the velocity with which the surge is propagated relative to the liquid. The positive direction for V coincides with that for x.

3.1 Method of characteristics for solving basic equations of unsteady flow

With the method of characteristics [5] the basic partial differential equations which are not integrable in closed form, are transformed into ordinary differential equations which have a solution in a closed form.

The basic equations, the equation of continuity and the dynamic equation can be designated with L_1 и L_2:

$$L_1 = \frac{\partial V}{\partial t} + V\frac{\partial V}{\partial x} + g\frac{\partial P}{\partial x} + \frac{\lambda}{2D}V|V| = 0 \tag{5}$$

$$L_2 = \frac{\partial P}{\partial t} + V\frac{\partial P}{\partial x} - Vsin\alpha + V\frac{a^2}{g}\frac{\partial V}{\partial x} = 0 \tag{6}$$

These linear equations can be combined as follows:

$$L = L_1 + \chi L_2 = \chi\left[\left(V + \frac{g}{\chi}\right)\frac{\partial \Pi}{\partial x} + \frac{\partial \Pi}{\partial t}\right] + \left[\left(V + \chi\frac{a^2}{g}\right)\frac{\partial V}{\partial x} + \frac{\partial V}{\partial t}\right] + \frac{\lambda}{2D}V|V| - \chi V\,sin\,\alpha = 0 \tag{7}$$

The two dependent variables, the speed V and the pressure Π are in a function from the position and time, V=V(x,t) и Π=Π(x,t). The material statements of these dependent variables are total accelerations which are determined by the convective and local acceleration:

$$\frac{dP}{dt} = \frac{\partial P}{\partial x}\frac{dx}{dt} + \frac{\partial P}{\partial t} \tag{8}$$

$$\frac{dV}{dt} = \frac{\partial V}{\partial x}\frac{dx}{dt} + \frac{\partial V}{\partial t} \tag{9}$$

Comparing the expression of the convective acceleration of equation (7) to those of equations (8) and (9), follows:

$$\frac{dx}{dt} = V + \frac{g}{\chi} = V + \frac{\chi a^2}{g} \tag{10}$$

Then equation (7) is written:

$$\chi\frac{dP}{dt} + \frac{dV}{dt} + \frac{\lambda}{2D}V|V| - \chi g\,sin\,\alpha = 0 \tag{11}$$

The solution of equation (11) is:

$$\chi = \pm\frac{g}{a} \tag{12}$$

$$\frac{dx}{dt} = V \pm a \tag{13}$$

From the previous equation it can be concluded that it's about two families of curves that are practically straight lines, where the speed of propagation is constant and many times faster than the basic flow, so the system of two partial differential equations are transformed into system of ordinary four differential equations which are marked with a C+ and C– and determine straight lines:

$$\left.\begin{aligned}\frac{dP}{dt} + \frac{a}{g}\frac{dV}{dt} + \frac{\lambda}{2D}V|V| = 0\\ \frac{dx}{dt} = +a\end{aligned}\right\} C^+ \tag{14}$$

$$\left.\begin{aligned}\frac{dP}{dt} - \frac{a}{g}\frac{dV}{dt} + \frac{\lambda}{2D}V|V| = 0\\ \frac{dx}{dt} = -a\end{aligned}\right\} C^- \tag{15}$$

According the given numerical network, equations (14) and (15) can be written as follows:

$$\frac{d}{dt}\left(P \pm \frac{a}{g}V\right) + \lambda\frac{a}{D}\frac{V|V|}{2g} \mp V\sin\alpha = 0 \tag{16}$$

The previous equation can be integrated along the positive and negative characteristics, i.e. along the length of the lines AP and BP, as follows:

$$\int_{tA}^{tP}\frac{d}{dt}\left(P + \frac{a}{g}V\right)dt + \int_{tA}^{tP}\left(\lambda\frac{a}{D}\frac{V|V|}{2g} - V\sin\alpha\right)dt = 0 \tag{17}$$

$$\int_{tB}^{tP}\frac{d}{dt}\left(P - \frac{a}{g}V\right)dt + \int_{tB}^{tP}\left(\lambda\frac{a}{D}\frac{V|V|}{2g} + V\sin\alpha\right)dt = 0 \tag{18}$$

After integration, equations of positive and negative characteristic are written:

$$\frac{P_P - P_A}{\Delta t} + \frac{a}{g}\frac{V_P - V_A}{\Delta t} + \frac{\lambda a}{2gD}V_A|V_A| = 0 \tag{19}$$

$$\frac{P_P - P_B}{\Delta t} + \frac{a}{g}\frac{V_P - V_B}{\Delta t} + \frac{\lambda a}{2gD}V_B|V_B| = 0 \tag{20}$$

If it is known that in the hydraulic analysis it is important to determine the flow change and height position of the hydrodynamic line in any section along the pipe, and in a certain time interval, additional approximation is introduced that the cross section of the pipe along its entire length is constant, and if it is known that median speed can be determined by the equation *V=Q/A*, the previously stated equations, knowing the numerical network, for the pressure, can be written in the following form:

$$P_i^{n+1} = P_{i-1}^n - B(Q_i^{n+1} + Q_{i-1}^n) - MQ_{i-1}^n|Q_{i-1}^n| = 0 \tag{21}$$

$$P_i^{n+1} = P_{i-1}^n + B(Q_i^{n+1} - Q_{i-1}^n) + MQ_{i+1}^n|Q_{i+1}^n| = 0 \tag{22}$$

If:

$$B = \frac{a}{gA} \qquad \text{and} \qquad M = \frac{\lambda\Delta x}{2gDA^2} = 0 \tag{23}$$

Using the previous equations, for the pressure, i.e. for the height position of the hydrodynamic line, it can be written:

$$P_i^{n+1} = CP - BQ_i^{n+1} \tag{24}$$

$$P_i^{n+1} = CM + BQ_i^{n+1} \tag{25}$$

In the previous equations the article which include the slope of the pipes (sinα) is very small and often overlooked, so the equations (24) and (25) are written:

$$CP = P_{i-1}^n - BQ_{i-1}^n - MQ_{i-1}^n|Q_{i-1}^n| = 0 \tag{26}$$

$$CM = P_{i+1}^n - BQ_{i+1}^n + MQ_{i+1}^n|Q_{i+1}^n| = 0 \tag{27}$$

Knowing the piezometric height (Pi) in the time period (n+1), the flow (Qi) is determined by equations (26) and (27).

$$P_i^{n+1} = \frac{CP + CM}{2} \tag{28}$$

3.2 Borderline Conditions

The conditions of the flow that govern within the boundary of the system under pressure – the water supply system is defined as boundary conditions. Their definition is of crucial importance for getting the solution at the points in the system. Follow-on are the most common cases of boundary conditions encountered in the water supply systems [1, 2].

Serial connection of two pipes in a junction

$$Pressure: CP = \Pi_{1,N}^{n+1} = \Pi_{2,1}^{n+1} = \Pi^{n+1} \tag{29}$$

$$\text{Flow: } Q_{1,N}^{n+1} = Q_{2,1}^{n+1} = Q^{n+1} = \frac{CP_1 - CM_2}{B_1 + B_2} \tag{30}$$

Reservoir (open channel) at the end of pipeline

$$Pressure: \Pi_1^{n+1} = \Pi_R \tag{31}$$

$$\text{Flow: } \quad Q_1^{n+1} = \frac{(\Pi^{n+1} - CM)}{B} \tag{32}$$

Valve at the middle of the pipeline (pipe break point)

$$\begin{gathered}\text{Pressure: } \Pi_{1,N}^{n+1} = CP_1 - B_1 Q_{1,N}^{n+1}, \quad \Pi_{2,1}^{n+1} = CM_2 - B_2 Q_{2,1}^{n+1}, \\ CP_1 - B_1 Q^{n+1} - CM_2 - B_2 Q^{n+1} - C_1 Q^{n+1} |Q^{n+1}| = 0\end{gathered} \tag{33}$$

$$Flow: Q^{n+1} = \frac{-(B_1 + B_2) + \sqrt{(B_1 + B_2)^2 + 4C_1(CP_1 - CM_2)}}{2C_1} \tag{34}$$

4 Development and application of Mathematical Model

Unsteady flow in pipelines that transport pressurized water is a constant occurrence, regardless of the geometric characteristics of the pipeline, the amount of water being transported, the change in hydrostatic and hydrodynamic pressure along the length of the pipeline during steady-state conditions, as well as the boundary conditions at the entry and exit of the siphon. However, the magnitude of the changes in pressure and water flow in the siphon primarily depends on the cause of the unsteady flow, i.e., the initiator of the unsteadiness, which can be varied, including:

- Sudden release of water during siphon filling
- Opening/closing of a valve along the length or at the end of the siphon
- Defect in the pipeline – bursting of the pipe and sudden draining of the siphon

The application of the hydraulic model for unsteady flow aims to analyze the oscillations in flow and pressure in a pressurized pipeline - siphon in the event of a defect along the length of the pipeline - Case study of the siphon from the irrigation system "Makarija". Specifically, this involves analyzing a pipeline constructed in 1965 with a length of 2150 m and a maximum flow rate of 3.8 m^3/s. The pipeline is constructed from two materials:

- In the section where pressures are lower than 3.5 bars, reinforced concrete pipes lined on the inside with a steel sheet, 4 mm tgick and with a diameter of 1640 mm, have been applied.
- For the sections where the pressure in the pipeline exceeds 3.5 bars, steel pipes with a diameter of 1640 mm are used. The thickness of the pipe varies depending on the pressure: 6 mm, 8 mm and 9 mm.

On May 27, 2023, a major incident occurred in the lowest part of the pipeline - the siphon (see Fig.1),

resulting in damage to a total length of 400-450 meters of the pipeline (see Fig.2). Although it was initially considered that such a failure was likely due to multiple factors such as aging of the pipe, local deformations, or torsion in the cross-section of the pipeline, the question arises as to why the damage extended over such a length if the defect occurred only in a small part of the pipe.

Figure 1. Layout and profile of the pipeline location of the defect, and the par that is damaged

It is important to note that no issues were observed in the operation of the siphon before the incident. Practically, for the siphon operator, such a major failure is a surprise and challenge to define the exact causes of the failure, and it is crucial to prevent its recurrence in the future.

Figure 2. Condition of the pipeline after the accident

According to basic hydrotechnical observations of the pipeline's condition after the accident, it is clear that the cause of such a failure is the occurrence of a vacuum in the pipeline, or the presence of unsteady flow. Therefore, the primary goal of this study is to develop a hydraulic model to analyze unsteady flow

in a pressurized pipeline, focusing on examining changes in flow and pressure when unsteadiness occurs due to a pipeline defect. In the hydraulic modeling process, the pipeline defect is simulated as a boundary condition, acting like a valve that opens within fractions of a second. Its dimensions correspond to the size of the opening where the defect occurred.

For the analysis of unsteady flow, the characteristics of both the pipeline and the water as a fluid are also significant, as provided in the following Table 1.

Table 1. Material characteristics of pipelines and water as fluid

Characteristics	Value
STEEL PIPES	
Young modulus of elasticity	207 GPa
Poisson factor	0.30
FLUID – WATER	
Temperature	20°C
Density	998 kg/m^3
Modulus of elasticity	2.19 GPa
Kinematic viscosity	1.01×10^{-6} m^2/s

5 Results and Discussion

In hydraulic analysis, the first step involves calibration and verification of the model under steady-state operation of the system. Through the model, it was practically confirmed that the maximum capacity of the pipeline is 3.8 m^3/s. This calibrated model serves as the basis for hydraulic analysis under unsteady flow conditions.

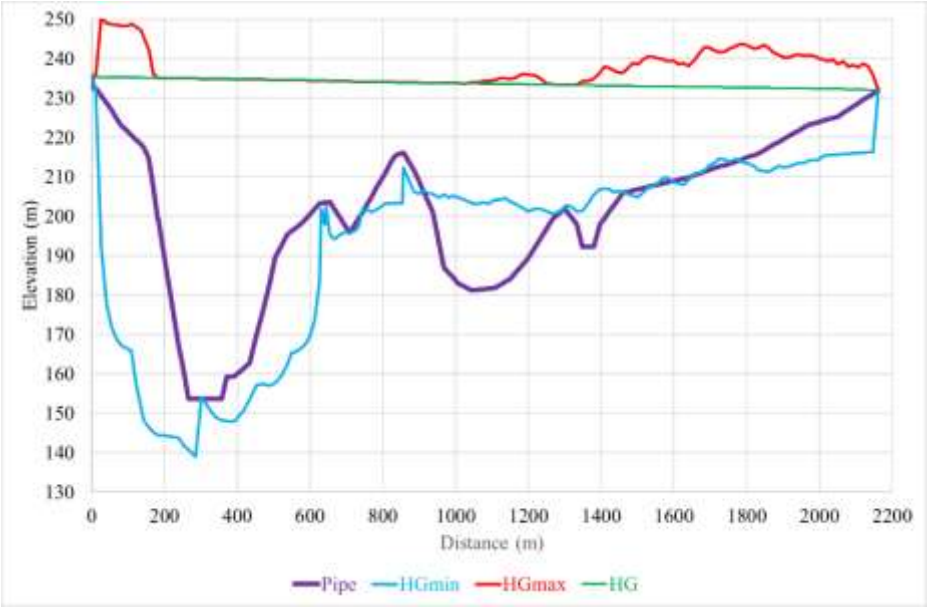

Figure 3. Maximum and minimum possible pressures in each part of the pipeline

Based on the results for the maximum and minimum possible pressures for each part of the pipeline shown in the graph (Figure 3), it can be concluded that the occurrence of the highest negative pressure – vacuum – appears from the very beginning of the pipeline and continues up to after the 600th meter.

The graph for the maximum and minimum possible pressures also shows the occurrence of negative pressure ranging from -1 to -1.5 bar in the last 200-300 meters of the final section of the pipeline. Although it was initially assumed that there was no damage in this section, after obtaining the results

from the model and conducting a follow-up field inspection, minor insignificant damages were found in this part of the pipeline. This is primarily due to the fact that the minimum pressures are not sufficiently high to cause a complete collapse of the pipeline in that section.

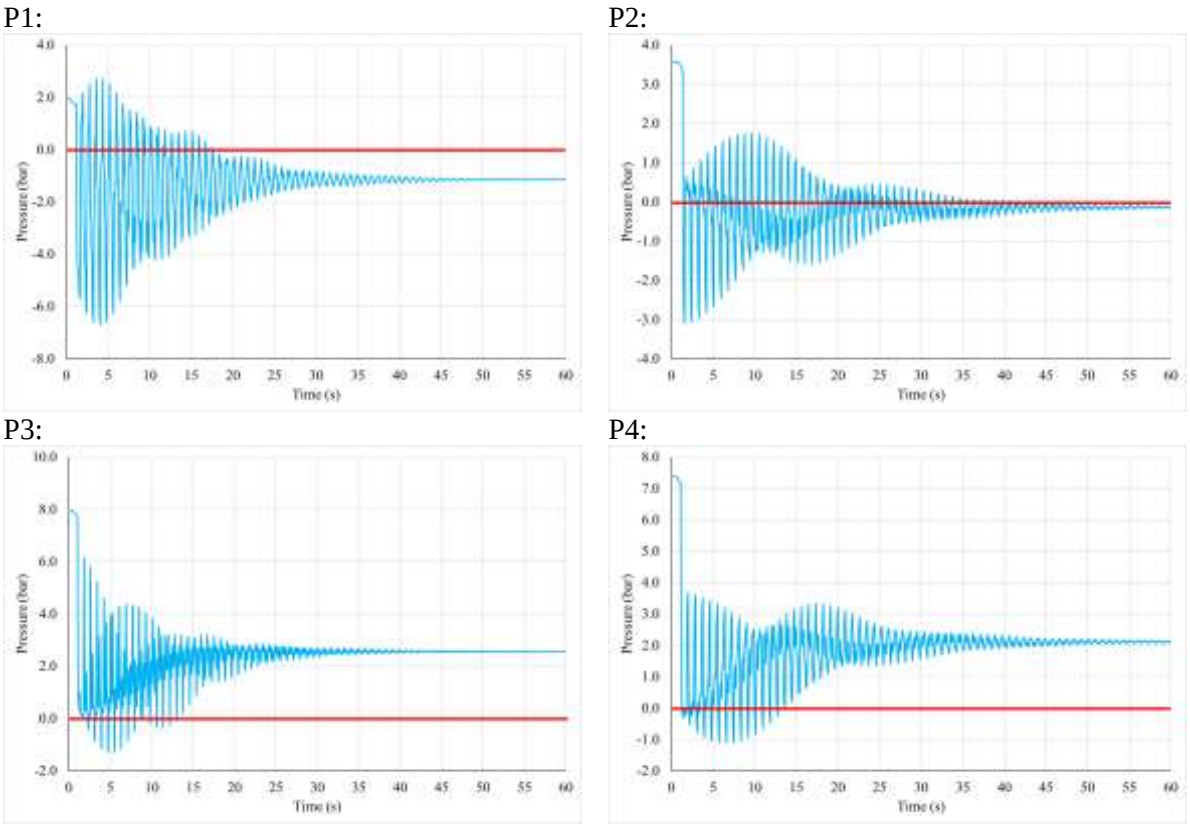

Figure 4. Results from the hydraulic model at characteristic points along the pipeline

6 Conclusions

The occurrence of unsteady flow in a pressurized pipeline, is a common phenomenon. However, the occurrence of such rapid accidental draining of the pipeline and the resulting unsteadiness with significant negative pressures is an accidental event. Such occurrences are not typically anticipated during the design phase of these systems.

The main cause of such a major accident is the occurrence of the initial defect - the bursting of the pipeline, specifically in the section where maximum pressures are present. This created conditions for the onset of significant negative pressures in a very short period - fractions of a second, where there was no opportunity to eliminate them, leading to a catastrophic failure of substantial proportions.

The occurrence of such a failure – a rupture of a large section of the pipeline – is highly unlikely and practically impossible to predict during the design phase, as well as later during the operational phase, with technical measures that would protect the pipeline while still being economically justified.

References:

[1] Goce Taseski (2015). „Characteristics of water hammers in water supply networks“. Doctorate dissertation, Skopje, Macedonia,
[2] Cvetanka Poposka (2000). „Hydraulics“. Publisher Civil Engineering Faculty, University Ss. Cyril and Methodius, ISBN 9989-43-100-0.
[3] Loh. Lohrasbi, A. & Attarnejad, R. (2008). Water Hammer Analysis by Characteristic Method.

American Journal of Engineering and Applied Sciences, 1(4), 287- 294.
[4] Josef Zaruba (1993). “Water hammer in pipe-line systems”, Publisher: Elsevier Science, ISBN-13: 978-0444987228.
[5] A.R.D. Thorley (2004). Fluid Transients in Pipeline Systems, Second Edition (Pipelines and Pressure Vessels), Publisher: The American Society of Mechanical Engineers; 2nd edition, ISBN-13: 978-0791802106.
[6] Kaveh Hariri Asli (2013). “Water Hammer Research: Advances in Nonlinear Dynamics Modeling”, Publisher: Apple Academic Press, ISBN 9781926895314 - CAT# N10708.
[7] Izquierdo, J., Inglesias, L.P. (2004), “Mathematical modelling of hydraulic transients in complex systems”. Mathematical and Computer Modelling, 39,529-540.
[8] Thomas Repp, (2011). Fluid Dynamic Water Hammer Simulations with Consideration of Fluid-Structure Interaction, https://www.hzdr.de/FWS/publikat/JB98/jb08.pdf.

WATER RESOURCES MANAGEMENT AND HYDROLOGY

PREDICTION OF MONTHLY FLOW BY SUPERVISED LEARNING ENSEMBLE CHAIN MODELS

JADRAN BERBIĆ [1], EVA OCVIRK [2]

[1] *Technical High School Šibenik, Croatia, jberbic@hotmail.com*

[2] *Faculty of Civil Engineering, University of Zagreb, ocvirk@grad.hr*

1 Abstract

The objective of the work is twofold: improve modelling procedure of mean monthly flows prediction by supervised learning and find the appropriate way to treat small hydrological dataset, with less than 800 samples. Chosen models are artificial neural networks (ANN), support vector machine (SVM), histogram gradient boosting regressor (HGBR) and elastic net (EN). All models are supervised learning models, applied in chain modelling procedure. Afterwards, models with optimised hyperparameters were combined into different ensembles in order to maximise performance on the calibration part of the data.

Keywords: ensemble learning, chain models, supervised learning, mean monthly flow, genetic algorithm

2 Introduction

Mean monthly flow is of particular importance for long-term planning in water resources management, therefore, simplified and robust procedure could be of benefit for both practitioners and researchers. The applied methodology generally consists of the following steps: 1. Dataset preparation, inspection, and split, 2. Data analysis and treatment, 3. Selection of features, 4. Choice of models, 5. Optimization of model hyperparameters and creation of final model, 6. Evaluation of model. The emphasis of the work is on the 4th and the 5th step, while the other steps are covered briefly. Dataset was split into training, calibration and verification parts in ratios 40, 15 and 45%.

The work is the continuation of previous research in which the accuracy of ANN and SVM were exhaustively analysed [1] followed by development of hyperparameter optimization procedure by GA and simulated annealing [2]. It is also the continuation of recent research in which genetic algorithm was tested for optimization of chain model's hyperparameters, by maximization of coefficient of determination and by minimization of scaled root mean squared error [3]. In this work ensemble models are created based on the single models developed in previous research.

The goal of the research is to model mean monthly flow at hydrological station Vinalić, located on river Cetina in the Republic of Croatia, by using precipitation and temperature from three near-by stations (meteorological station Knin, precipitation gauge Vinalić and climatological station Sinj). Previously developed supervised learning models [3], with hyperparameters optimized by genetic algorithm (GA) were used as base models for creation of ensemble models, in order to improve accuracy. Python environment and its libraries scikit-learn [4,5], pandas [6] and tensorflow [7] in Anaconda software [8] were used for development of all procedures.

3 Methods

3.1 Dataset preparation, data treatment and selection of features

Overall mean (1946-2015) flow at Vinalić is 11,88 m^3/s with standard deviation of 9,48 m^3/s. As independent (also called input variable) variables, monthly mean, maximum and accumulated precipitation (Knin and Vinalić), and mean, minimum and maximum temperatures (Knin and Sinj) were created from existing historical time series of data (a total of 12 input variables). A total of 675 samples were left for modelling after the preparation and inspection of data. The given dataset consisting of 65

years of data (1951-2015) for all stations [9,10] was split into training, calibration, and verification parts in ratios 40, 15 and 45 % (in order 270, 101 and 304 samples). Any further analysis of the data was done on the training and the calibration part, while the verification part was left intact to avoid any leakage of information to the model or the modeller and to preserve consistency of the model.

Based on the merged set of the flow data from the training and calibration parts (270+101 = 371 samples), fast Fourier transform is applied to obtain periodicities and produce additional features similarly as recommended in time series forecasting tutorial [7]. Yearly and half-yearly periodicity described by sine and cosine functions showed significant correlation with flow and were chosen as four additional input variables. To avoid the occupation of space, it is noted that any further information about stations and data may be found in previously published papers [1-3]. All in all, at the end of the 3rd step, 16 input variables with 18 consecutive steps (12 past steps and 6 future steps corresponding to 6 steps of mean monthly flows) for each variable were prepared, resulting in totally 288 features and 263 training, 98 calibration, and 297 verification samples. For prediction in chain modelling manner, 6 successive mean monthly flows per each sample were prepared. In the chain modelling procedure, successive mean monthly flows are predicted based on the features and already predicted preceding flows. So, the first predicted flow Q_{avm} (t) is predicted solely based on 288 features, the second Q_{avm} (t+1) is predicted based on 288 features and already predicted preceding flow Q_{avm} (t). The last one of the 6 outputs Q_{avm} (t+5) is predicted based on 288 features and already predicted preceding flows Q_{avm} (t), Q_{avm} (t+1), …, Q_{avm} (t+4).

3.2 Creation of ensemble models

Supervised learning models chosen for prediction are artificial neural network (ANN), support vector machine (SVM), histogram gradient boosting regressor (HGBR), and elastic net (EN). Previously (before creation of ensemble models), genetic algorithm (GA) has been applied to select optimal model hyperparameters of each model due to the criteria of maximization of the coefficient of determination (R^2), and also due to the criteria of minimization of scaled root mean squared error (*RMSE). The details and results related to the optimization were provided in previous research [3]. Hyperparameters optimized by GA due to the criteria of minimization of *RMSE are chosen as hyperparameters of base models (ANN, SVM, HGBR, EN).

As concluded from the previous research, in the terms of accuracy, the results of optimization by using these two different criteria are not substantially different on the calibration part of the data - *RMSE obtained slightly better results for SVM, and slightly worse results for ANN. Overall optimization for *RMSE took 1100,7 minutes (ANN-680,3; SVM-13,1; HGBR-395,2; EN-12,1 minutes), while for R^2 took 1111,2 minutes (ANN-746,1; SVM-4,3; HGBR-332,1; EN-28,7 minutes). In terms of total duration of procedures there is no significant difference. Therefore, it cannot be concluded that any of the optimization criteria achieves better or worse results. However, generally there is a wide range of hyperparameter's values to choose from, causing inefficient retrieval of optimal values when those are manually chosen. So, in terms of methodology, as one of the crucial steps in creation of supervised learning model, both criteria can be of a benefit for efficient retrieval of accurate model by developed automatised optimization procedure.

Afterwards, models with optimized hyperparameters were combined into 7 different ensembles in order to maximize performance on calibration part of the data. Results of single and ensemble models are shown in the Table 1.

Table 1. Results of single and ensemble models on training and calibration parts

	TRAINING			CALIBRATION		
	R^2 [/]	MAE [m^3/s]	RMSE [m^3/s]	R^2 [/]	MAE [m^3/s]	RMSE [m^3/s]
ANN	0.858	2.801	3.621	0.567	5.374	7.087
SVM	0.985	0.472	1.168	0.574	5.245	7.034
HGBR	0.996	0.374	0.575	0.561	5.216	7.136
HGBR* (Q.=0.95)	0.337	6.238	7.813	0.143	8.365	9.978

EN	**0.739**	**3.658**	**4.907**	**0.629**	**5.127**	**6.570**
EN-**ANN**	0.770	3.428	4.603	0.659	4.770	6.292
EN-ANN-**ANN**	**0.843**	**2.880**	**3.810**	**0.671**	**4.553**	**6.178**
EN-HGBR*-**ANN**	0.798	3.285	4.312	0.644	4.938	6.431
ANN-EN-HGBR*-**ANN**	0.845	2.875	3.781	0.650	4.765	6.377
ANN-EN-HGBR*-**SVM**	0.832	2.941	3.942	0.610	5.042	6.728
ANN-EN-HGBR*-**EN**	0.834	2.974	3.921	0.627	5.061	6.585
D-D-EN-ANN-**ANN**	**0.841**	**2.855**	**3.825**	**0.665**	**4.564**	**6.234**

As performance metrics, coefficient of determination (R^2), mean absolute error (MAE) and root mean square error (RMSE) were chosen. It was decided to use HGBR as sort of bias for high flows (HGBR*) in ensembles, that is, for prediction of upper 95 % quantile. Therefore, HBGR's hyperparameters were optimized with quantile loss function, while the single model was used with (HGBR*) and without (HGBR) quantile estimation, and both of them with optimised hyperparameters.

Among single (base) models, the highest accuracy on the calibration part of the data was obtained by EN. Neither of the single models provided significantly more accurate than the other models. Beside the results in Table 1, in order to illustrate mentioned, the comparison of observed and predicted flow for ANN and EN are shown in the Figure 1. Beside highest accuracy, EN is simple model, with low amount of duration for training. Therefore, it seemed logical to use it in the ensemble model. As the ensemble model, stacking regressor (SR) was used. SR combines the outputs of base models and use them as the input for final model (bold in the Table 1). Final model predicts final results based on the results of base models (single models) by using them as input variables (stacks results into the final result) [5]. So, to train SR it is needed to choose base models and train the final model. For a final model, it was expected that satisfying results could be obtained by ANN. The best performance considering accuracy and consistency on training and calibration parts, absence of overfitting, and bias, was achieved by ensembles EN-ANN-ANN and D-D-EN-ANN-ANN. The abbreviation D-D indicates two dummy regressors – simple regressors which were introduced to produce bias for low and high flows, in particular for this ensemble, for prediction of 10 % and 90 % quantile (Figure 2).

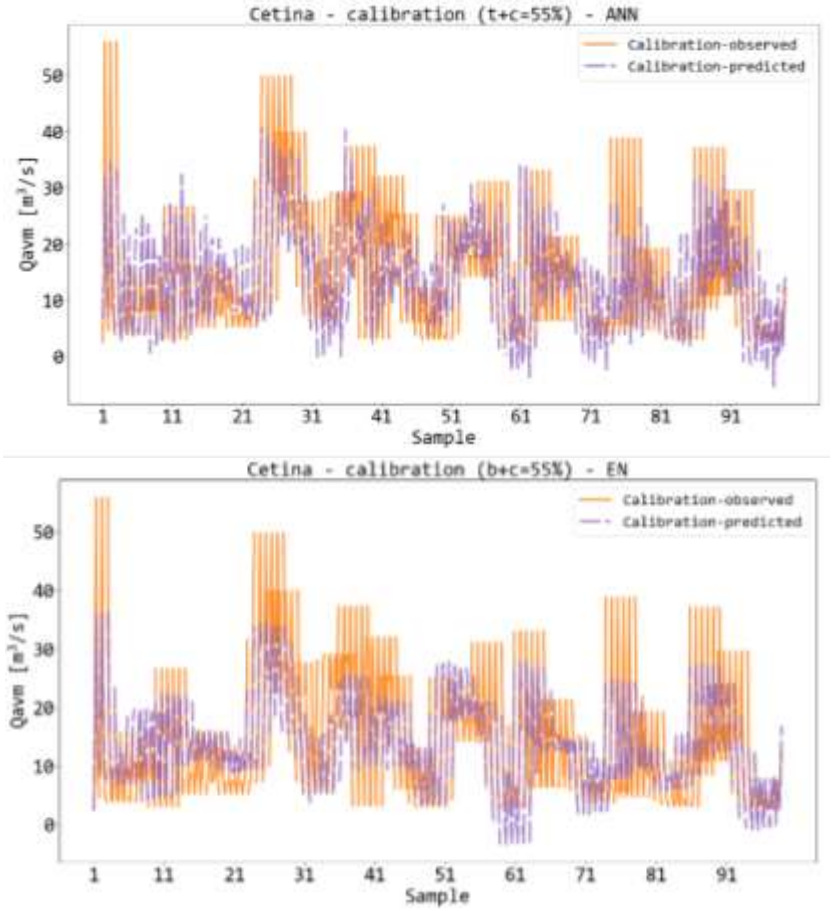

Figure 1. Comparision of observed and predicted mean monthly flow by ANN and EN on calibration part

In order to give closer insight into the model's performance on the calibration part of the data, graphs with comparison of observed and predicted mean monthly flow by EN and D-D-EN-ANN-ANN are plotted (Figure 3). It can be visually noted that by solely using the EN, the values of flows in range 10-30 m^3/s are generally well described, and that models generally follow the tendency of flows. However, models fail to accurately describe high (> 30 m3/s) and low (<10 m3/s) flows. By adding the D10 and D90 base models, the prediction of the lower and upper quantiles of flow becomes more accurate in the lower flow zone. 6 same successive observed values of flows (orange colour) represent the parts of the 6 successive samples of chains, as presented on the graphs. Another improvement of the model's performance is reflected in the fact that ensemble model does not make any, or makes less errors, like predicting negative values. On the Figure 1 it can be noted that both ANN and EN predict negative values around samples 61 and 95. Out of 2166 predicted values on both training and calibration parts (6 values in chain times 361 samples), ANN produced 58 negative values, and EN produced 63 negative values. Ensemble model D-D-EN-ANN-ANN produced 11 negative values out of 2166, while EN-ANN-ANN did not produce any negative values. Following minimum values were obtained by EN-ANN-ANN (training + calibration) for Qavm(t), …,Qavm(t+1): 0.64, 0.43, 1.21, 1.259, 0.20, 0.43.

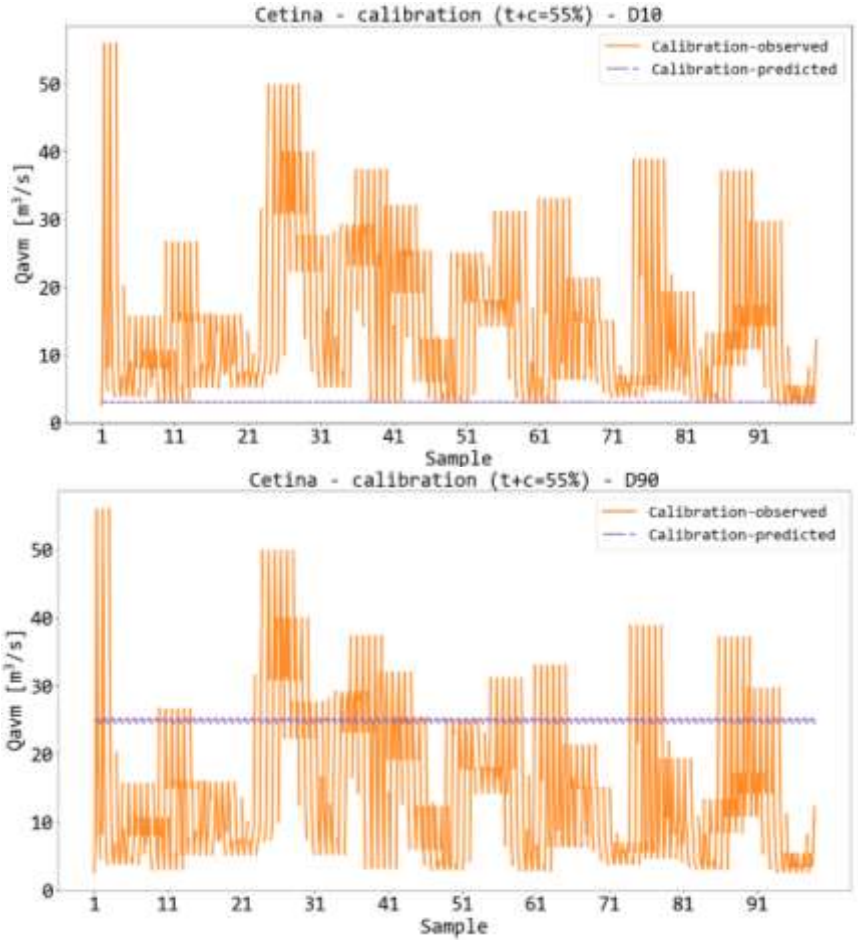

Figure 2. Performance of dummy models D10 (up) and D90 (down) used as base models for D-D-EN-ANN-ANN, calibration part

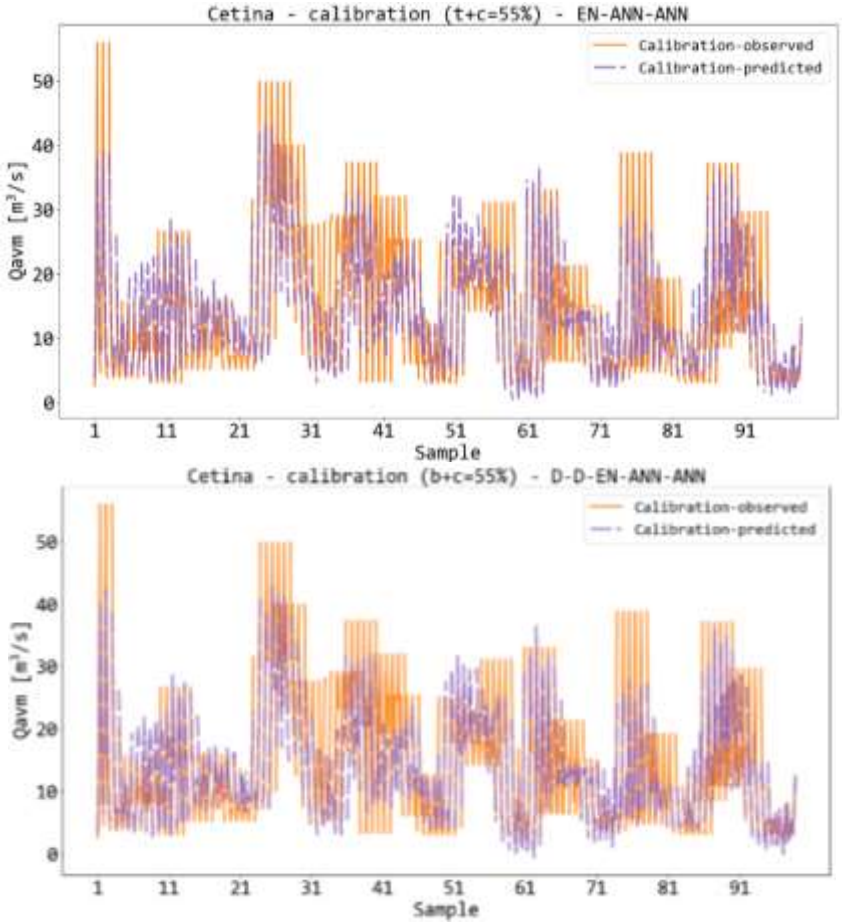

Figure 3. Comparison of observed and predicted mean monthly flow by EN and D-D-EN-ANN-ANN on calibration part

4 Results and discussion

Given below is the standard deviation of residuals obtained based on the difference of observed and predicted values on the training and calibration parts for each successive chain (Table 2). After the calibration process, training and calibration parts of the output flow were concatenated, separately for observed and for predicted values (a total of 371 samples). The process is illustrated in Figure 4. For each member of the chain ($Q_{avm}(t)$,…, $Q_{avm}(t+1)$), standard deviation of residuals is separately calculated.

Table 2. Standard deviation of residuals obtained based on difference of observed and predicted values, on training and calibration parts – for every successive chain

	STANDARD DEVIATION OF RESIDUALS [m^3/s]					
	$Q_{avm}(t)$	Q_{avm} (t+1)	Q_{avm} (t+2)	Q_{avm} (t+3)	Q_{avm} (t+4)	Q_{avm} (t+5)
EN	**5.44**	**5.45**	**5.47**	**5.36**	**5.34**	**5.49**
EN-ANN-**ANN**	**4.86**	**4.30**	**4.44**	**4.99**	**4.49**	**4.41**
D-D-EN-ANN-**ANN**	**4.54**	**4.58**	**4.56**	**4.68**	**4.58**	**4.75**

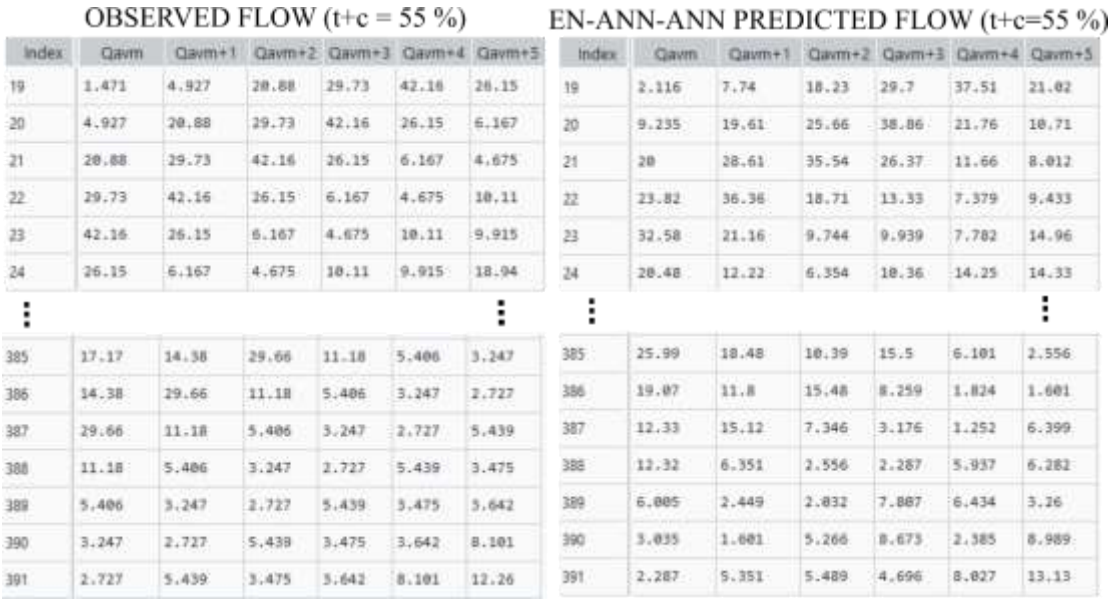

index	Qavm	Qavm+1	Qavm+2	Qavm+3	Qavm+4	Qavm+5
19	1.471	4.927	20.88	29.73	42.16	26.15
20	4.927	20.88	29.73	42.16	26.15	6.167
21	20.88	29.73	42.16	26.15	6.167	4.675
22	29.73	42.16	26.15	6.167	4.675	10.11
23	42.16	26.15	6.167	4.675	10.11	9.915
24	26.15	6.167	4.675	10.11	9.915	18.94
⋮						⋮
385	17.17	14.38	29.66	11.18	5.406	3.247
386	14.38	29.66	11.18	5.406	3.247	2.727
387	29.66	11.18	5.406	3.247	2.727	5.439
388	11.18	5.406	3.247	2.727	5.439	3.475
389	5.406	3.247	2.727	5.439	3.475	3.642
390	3.247	2.727	5.439	3.475	3.642	8.101
391	2.727	5.439	3.475	3.642	8.101	12.26

index	Qavm	Qavm+1	Qavm+2	Qavm+3	Qavm+4	Qavm+5
19	2.116	7.74	18.23	29.7	37.51	21.02
20	9.235	19.61	25.66	38.86	21.76	10.71
21	20	28.61	35.54	26.37	11.66	8.012
22	23.82	36.36	18.71	13.33	7.379	9.433
23	32.58	21.16	9.744	9.939	7.782	14.96
24	20.48	12.22	6.354	10.36	14.25	14.33
⋮						⋮
385	25.99	18.48	10.39	15.5	6.101	2.556
386	19.07	11.8	15.48	8.259	1.824	1.601
387	12.33	15.12	7.346	3.176	1.252	6.399
388	12.32	6.351	2.556	2.287	5.937	6.282
389	6.005	2.449	2.032	7.887	6.434	3.26
390	3.035	1.601	5.266	8.673	2.385	8.989
391	2.287	5.351	5.489	4.696	8.027	13.13

Figure 4. Concatenated training and calibration parts of observed values and values predicted by EN-ANN-ANN

The accuracy of models calculated on the verification part (Table 3) shows the best performance of D-D-EN-ANN-ANN. Although the used metrics reveal meaningful information of model's performance, it could be wrong to conclude that the D-D-EN-ANN-ANN is the model with the highest accuracy. D-D-EN-ANN-ANN produced 13 negative values, out of 1782 (6 values in chain times 297 samples), with minimums: 0.70, -1.26, 0.21, 0.08, -0.38 and 0.10 for members of chain, in order $Q_{avm}(t)$,…,$Q_{avm}(t+5)$. EN-ANN-ANN did not produce any negative values (minimums are 0.98, 0.55, 1.22, 1.19, 0.22, 0.37, in order). In the previous description, crossing of confidence intervals into the area of negative values is neglected.

Table 3. Results of single model EN, and ensemble models EN-ANN-ANN and D-D-EN-ANN-ANN on verification part of the data

	VERIFICATION		
	R^2 [/]	MAE [m^3/s]	RMSE [m^3/s]
EN	**0.678**	**3.716**	**4.862**
EN-ANN-**ANN**	**0.752**	**3.098**	**4.267**
D-D-EN-ANN-**ANN**	**0.773**	**2.934**	**4.08**

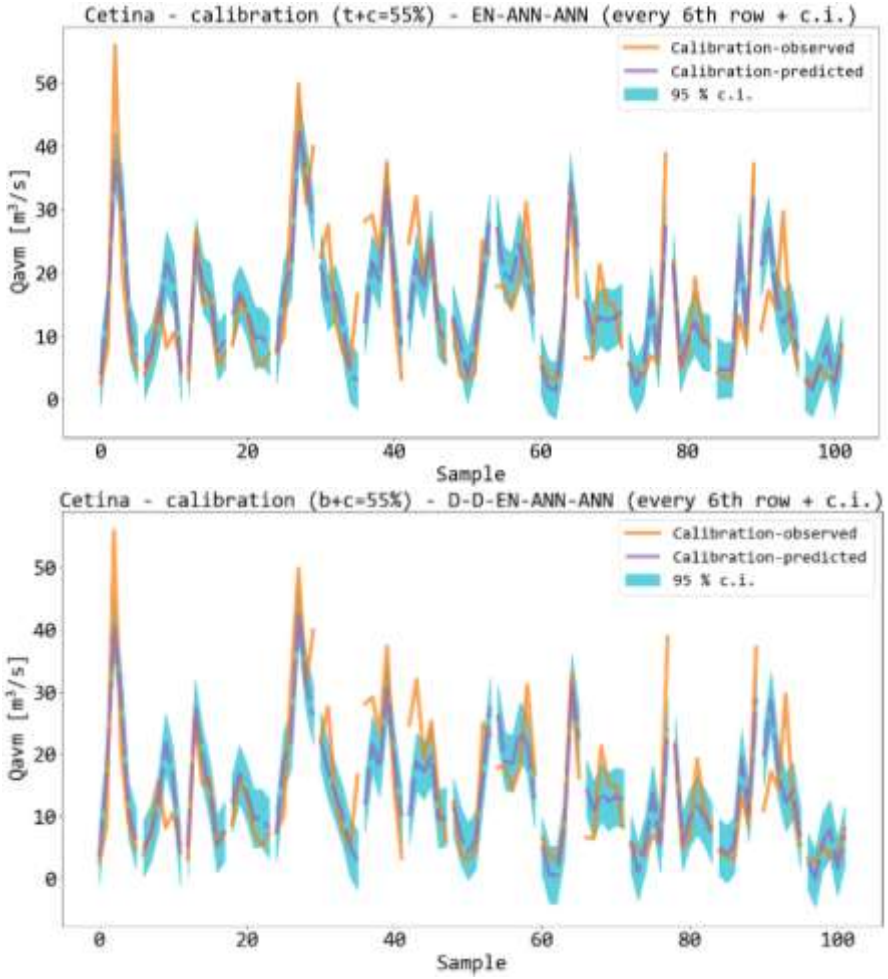

Figure 5. Comparision of observed and predicted mean monthly flow by EN-ANN-ANN and D-D-EN-ANN-ANN on calibration part**,** on every 6th step, with 95 % confidence intervals

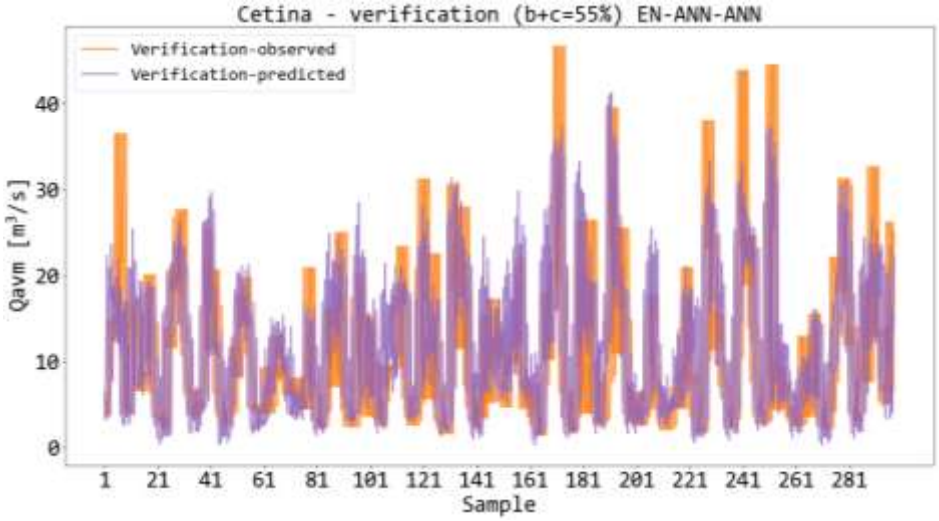

Figure 6. Comparision of observed and predicted mean monthly flow by EN-ANN-ANN on calibration part

For a better insight into the model's performance, the comparison of the observed and every 6th step of the predicted mean monthly flows by EN-ANN-ANN and D-D-EN-ANN-ANN-ANN on the calibration part is given in Figures 5 and 6. Highlighted blue are the standard deviations of residuals with 95 %

confidence (the difference between the measured and the predicted data on the training and calibration steps). On both models a relatively inaccurate prediction of the flow can be observed in the zones of higher flows (> 30 m3/s). A similar situation can be observed in the verification part as well (Figure 7), while the lower flow zones (< 10 m3/s) show a more accurate prediction.

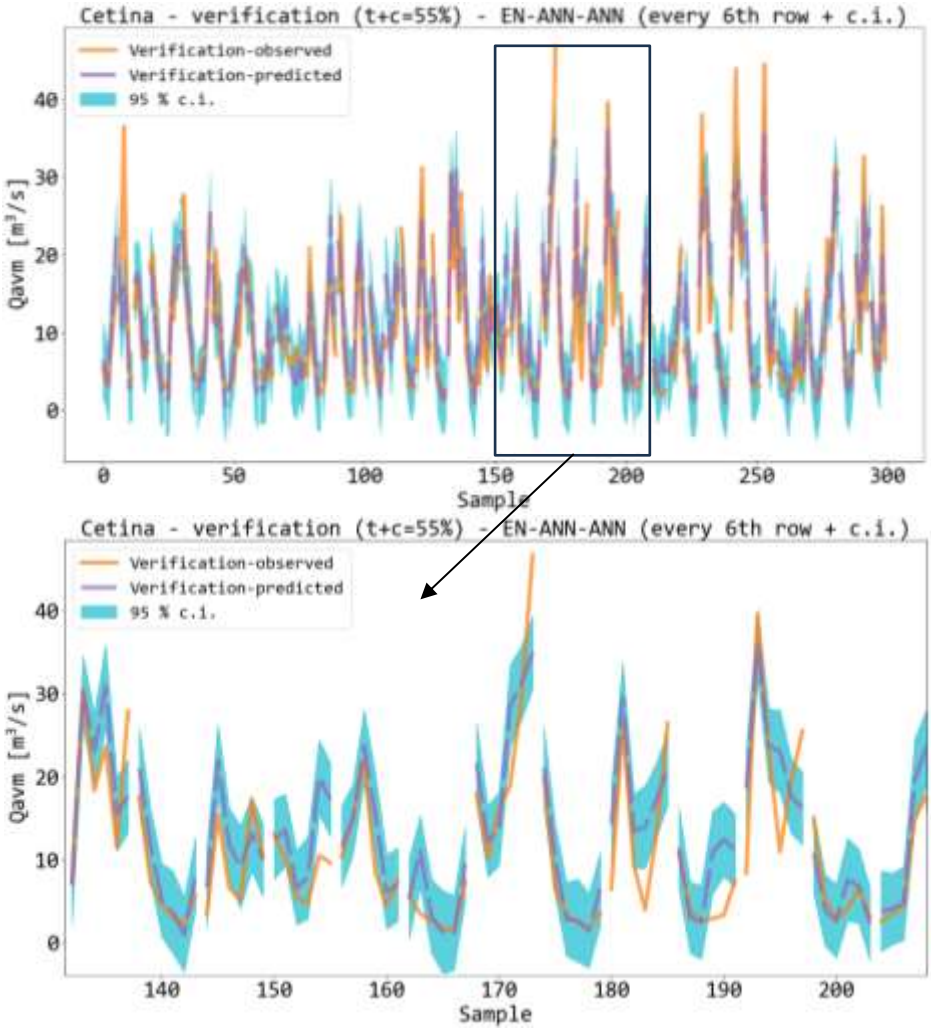

Figure 7. Comparision of observed and predicted mean monthly flow by EN-ANN-ANN on verification part**,** on every 6th step, with 95 % confidence intervals

5 Conclusion

The application of the ensemble model has shown improvement in the verification part dataset when compared to the single (base) models showcased in previous research. Specifically, this applies to the lower and higher flow zones (10 and 95% quantile), which were predicted relatively inaccurately with the single models. Additional advancement was achieved by including the base model expressly set to predict the upper 90 % and the lower 10 % of the flow. All in all, ensemble modelling presents improved and yet simple modelling technique by incorporating quality sides of several base models into one model. Moving forward with the development of the ensemble model, the goal will be to further improve prediction of flows in the high flow area. Maybe additional improvements should be sought in appropriate calculation of confidence intervals (e.g., by quantile-quantile regression or Monte Carlo simulation). As the supervised learning models "learn" based on the observed data, in circumstances where the highest flows are in fact the least frequent flows, it is irrational to expect significant

improvements in predictions of high flows area. But appropriately incorporating the confidence intervals could help to surpass shortcomings in modelling procedures and provide meaningful information about the predicted flow.

References:

[1] Berbić, J., Ocvirk, E., Gilja, G.: Comparison of Supervised Learning Methods for Prediction of Monthly Average Flow, Građevinar 70(8), pp. 643-656, 2018.
[2] Berbić, J., Ocvirk, E., Gilja, G.: Optimization of supervised learning models for modeling of mean monthly flows, Neural Comput & Applic 34, pp. 17877–17904, 2022.
[3] Berbić, J., Ocvirk, E.: Optimization of supervised learning chain models for monthly flow prediction, 8th IAHR Europe Congress, Lisbon, Portugal, 2024. (in print)
[4] Van Rossum, G., Drake, F.L.: Python 3 Reference Manual, Scotts Valley, CA: CreateSpace, 2009.
[5] Pedregosa, F., Varoquaux, G., Gramfort, A., Michel, V., Thirion, B., Grisel, O., Blondel, M., Prettenhofer, P.P., Weiss, R., Duborg, V., Vanderplas, J., Passos, A., Cournapeau, D., Brucher, M., Perrot, M., Duchesnay, É.: Scikit-learn: Machine Learning in Python, Journal of machine learning research 12(85), pp. 2825-2830, 2011.
[6] McKinney W, and others (2010) Data structures for statistical computing in python, Proceedings of the 9th Python in Science Conference, 51–56
[7] Abadi, M., Agarwal, A., Barham, P., Brevdo, E., Chen, Z., Citro, C., ... & Zheng, X.: TensorFlow: Large-scale machine learning on heterogeneous distributed systems, arXiv preprint arXiv:1603.04467, 2015.
[8] Anaconda Software Distribution (2020): Anaconda Documentation. Anaconda Inc., url https://docs.anaconda.com/
[9] DHMZ - Croatian Hydrological and Meteorological Service: Hydrological Database, HIS 2000, 2017.
[10] DHMZ - Croatian Hydrological and Meteorological Service: Relational Meteorological Database, 2017.

RELIABILITY OF STANDARD RAIN GAUGE PRECIPITATION MEASUREMENTS IN RELATION TO LYSIMETER OBSERVATIONS

ANDREJ TALL [1], BRANISLAV KANDRA [1], DANA PAVELKOVÁ [1], MILAN GOMBOŠ [1]

[1] *Institute of Hydrology, Slovak Academy of Sciences, Slovakia, tall@uh.savba.sk*

1 Abstract

This study compares two methods of measuring precipitation: standard tipping-bucket rain gauge vs. precision weighable lysimeter. Lysimeter measurements were chosen as the reference measurement method. The comparative experiment lasted 4 years (2019–2022). The comparison showed that the tipping-bucket rain gauge underestimates the rainfall compared to the lysimeter. Cumulative precipitation for the entire monitored period captured by the rain gauge was 2.8% lower compared to lysimeter measurements. A comparison based on precipitation intensity showed a decreasing trend in measurement accuracy with increasing precipitation intensity.

Keywords: precision weighable lysimeter, tipping-bucket rain gauge, precipitation measurement, rainfall intensity

2 Introduction

Measuring the amount of precipitation and its distribution in time and space is extremely important for hydrological, climatological and agricultural purposes [1], [2]. Atmospheric precipitation can be defined as water that reaches the earth's surface in a liquid or solid state through the process of condensation from the clouds. Most precipitation falls by gravity in the form of rain or snow. Other forms are drizzle, ice hail, snow grains and ice pellets. Moisture from the atmosphere can also be transferred to the earth's surface through the process of condensation in the form of dew, frost, rime, fog, or soil water vapour adsorption, but these forms are not included in the definition of precipitation according to the World Meteorological Organization (WMO) [3].

The most common conventional (or standard) instrument for measuring precipitation are rain gauges. They are devices with a precisely defined surface area. According to the method of measurement, we distinguish several types of rain gauges. Accumulation rain gauges are the simplest, where the amount of precipitation is directly read using the scale on the collection container. Another type is weighing rain gauges, where precipitation mass is measured on the scales. The last group consists of the so-called tipping-bucket rain gauges, in which water from the collection area is directed through a funnel into tipping-bucket with a precisely defined volume. The number of flips of the tipping-bucket is measured (e.g. one flip = 0.1 mm precipitation). The disadvantage of tipping-bucket rain gauges is that, unless they are heated, they can only measure liquid precipitation in the form of rain. For meteorological purposes, rain gauges are usually placed at a height of 0.5 to 1.5 m above the ground.

The shape, size and height of the rain gauge installation are sources of systematic and random measurement errors. The most common systematic error is the deformation of the pressure field above the surface area of the rain gauge caused by wind blowing [4]. This error increases with the height of the rain gauge installation [5]. Other systematic errors are losses caused by wetting the walls of the rain gauge and subsequent evaporation and loses caused by out-splashing of water during heavy rains. Random errors are most often associated with a relatively small collecting area of rain gauges, which may not be sufficiently representative. Errors caused by incorrect readings, including incorrectly read times, are also classified as random errors.

With the introduction of modern lysimeters with precise weighing systems, great progress has been made in the accuracy of precipitation measurements [6]. A large surface area located at ground level

significantly eliminates the influence of both systematic and random errors. High weighing accuracy in combination with a relatively large surface area guarantees high sensitivity of precipitation measurement (up to 0.01 mm). Another advantage of lysimeters is that they can capture precipitation in all forms (including dew, frost, condensed water vapor, etc.). Precipitation measurement using lysimeters often serves as a reference method when comparing with other precipitation measurement methods [7].
The aim of this work is to evaluate and compare the results of precipitation measurement using a tipping-bucket rain gauge and a precise weighable lysimeter in the conditions of the humid continental climate of the Eastern Slovak Lowland (ESL).

3 Methods

3.1 Experimental site

The experiment was carried out at the Petrovce lysimeter station. The station is located in the eastern part of Slovakia, in the northern part of the ESL (Figure 1). The altitude of the lowland varies from about 100 to 180 m above sea level. According to the Slovak Hydrometeorological Institute [8], it is a warm, slightly humid area with a mild winter (average annual air temperature 10°C; average annual precipitation 600–700 mm).

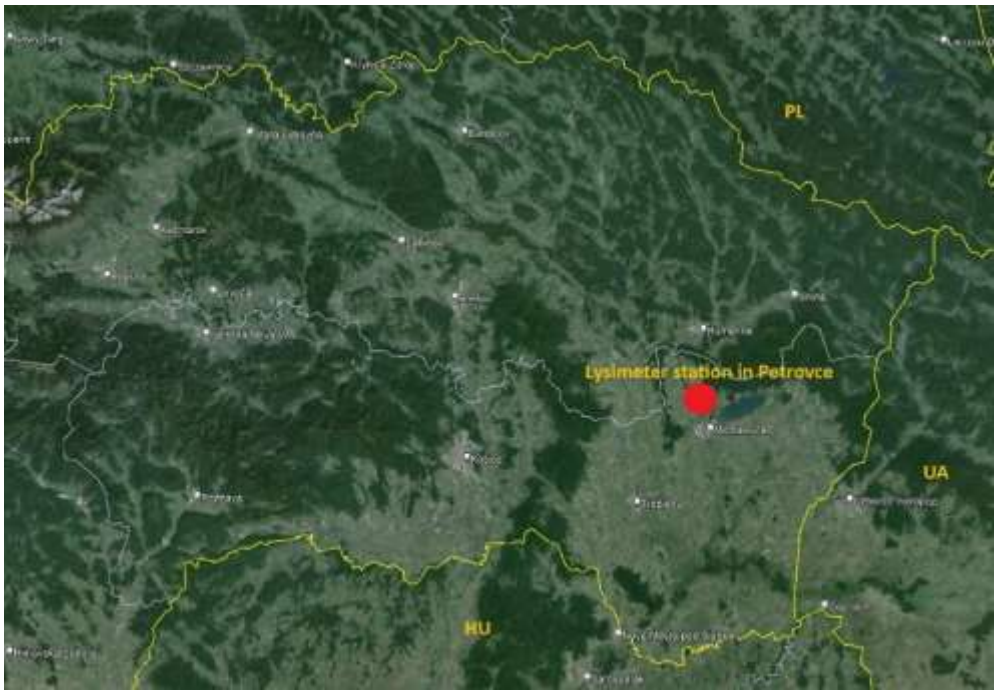

Figure 1. Location of the study area

3.2 Lysimetric station

The lysimeter station (Umwelt-Geräte-Technik (UGT), GmbH., Germany) is managed by the Institute of Hydrology of the Slovak Academy of Sciences (Figure 2). The station was built in 2014 and put into operation in 2015. It contains five weighable lysimeters (Lys 1, Lys 2, ... Lys 5), a hydrological well, a meteorological station and solar panels that provide energy for the entire station (Figure 3). A more detailed description of the lysimeter station along with technical parameters is available in the literature [9], [10]. Lysimeters are equipped with a regulation system that allows maintaining the selected height of the groundwater level. During the duration of the experiment, this height was maintained at the level of -1m below the ground. The cylinders stand on a three-point electronic weighing system that monitors the weight of the lysimeters with a resolution of 10 g, which for a lysimeter surface area of 1 m^2 corresponds to the equivalent of 0.01 mm of water column. Measured data are continuously stored in

dataloggers and from there are sent to the server once a day via a wireless connection. A Savitzky-Golay filter [11] was used to smooth out noise during weight measurement. All data from the lysimeter station are processed and stored with a time interval of one hour.

Figure 2. Lysimetric station in Petrovce

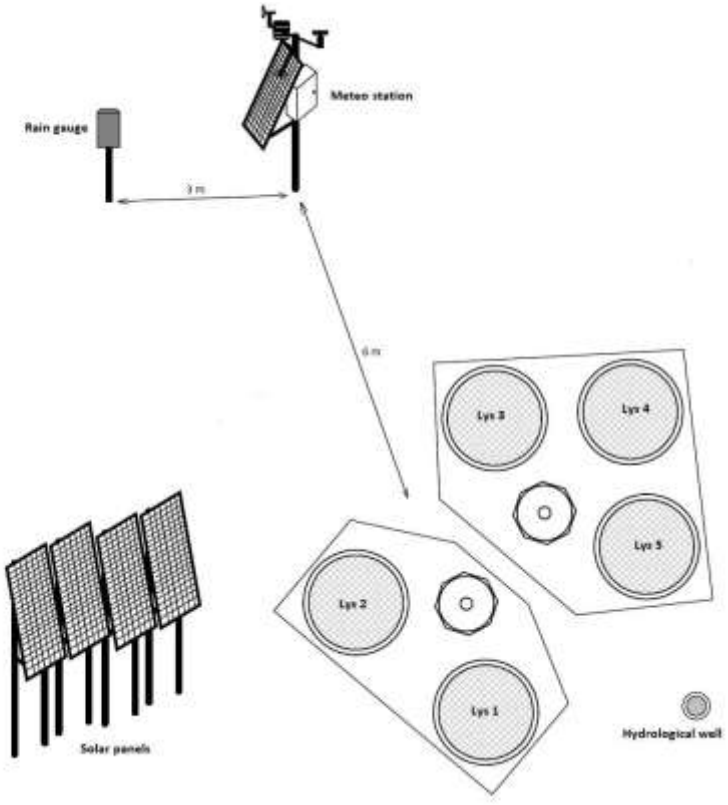

Figure 3. Scheme of the lysimeter station

3.3 Tipping-bucket rain gauge

In this comparative study, an automatic tipping-bucket (TB) rain gauge (Lambrecht, Germany) was used in an unheated version (Figure 4). It is installed at a height of 1 m. Its tipping-bucket holds 2 cm³ (2 g) of water. A surface area of 200 cm² (according to the standard of the WMO [3]) means that one flip of the bucket corresponds to a 0.1 mm of precipitation. Recorded precipitation values are stored as hourly totals. According to the manufacturer, the accuracy of the device is ±2%.

Figure 4. Location of the tipping-bucket rain gauge in the lysimeter station

3.4 Precipitation data from lysimeter

Precipitation from lysimeters is derived from mass. The total mass of the lysimeter is affected by the flows at its upper and lower limits. At the upper limit, ongoing evapotranspiration contributes to reducing the weight of the lysimeter. This includes evaporation from the surface of the soil and vegetation. Conversely, the mass increase is caused by precipitation (in all forms) and also by the condensation of water vapor on the surface in the form of dew and frost. Lysimeters are equipped with groundwater level (GWL) regulation, which also affects lysimeter mass. It is caused by water flows at the lower boundary of the lysimeters (BF – boundary flows). Water inflow (+) or outflow (-) at the lower boundary results in an increase or decrease of mass. Since GWL was held constant, positive BF values represent capillary rise and negative BF values represent gravitational flux into GWL. The procedure according to [12] was used to calculate precipitation from lysimeters (P_{Lys}):

$$\begin{aligned} &(\Delta W \pm BF) < 0 \rightarrow ET_a = \Delta W \wedge P_{Lys} + NRW = 0 \\ &(\Delta W \pm BF) \geq 0 \rightarrow ET_a = 0 \wedge P_{Lys} + NRW = \Delta W \begin{cases} P_{TB} > 0 \rightarrow P_{Lys} = \Delta W \wedge NRW = 0 \\ P_{TB} = 0 \rightarrow P_{Lys} = 0 \wedge NRW = \Delta W \end{cases} \end{aligned} \quad (1)$$

where: ΔW is change in water content of the lysimeter, BF are flows at the lower boundary of the lysimeter, P_{Lys} is the precipitation reaching the lysimeter, P_{TB} is the precipitation recorded by tipping-bucket rain gauge, NRW is the non-rainfall water (dew, fog and soil water vapour adsorption) on the surface and ET_a is the actual evapotranspiration. Since the surface area of lysimeters is 1 m^2 (1 kg of water per m^2 ≈ 1 l m^{-2} = 1 mm of water column), all the above terms are given in a unit of length [mm]. Equations (1) assume that precipitation and evaporation cannot take place during the same time interval (1 hour). The mass loss of the lysimeter ($(\Delta W \pm BF) < 0$) is due to ET_a and the weight gain ($(\Delta W \pm BF) > 0$) is due to either P_{Lys} or NRW. If a precipitation event on the rain gauge in weather station is recorded ($P_{TB}>0$) and the weight of the lysimeter is increased at the same time, then the weight gain is assigned

to the P_{Lys}. Otherwise, the weight gain is attributed to *NRW*.

3.5 Data availability and data preparation

The experiment was carried out from 2019 to 2022 (Table 1). Precipitation data from both TB and lysimeters were obtained during four consecutive periods, interrupted by three winter breaks.

Table 1. Observed periods and numbers of precipitation days, hours and precipitation events

	Months observed (period)	**Days** observed (with precipitation)	**Hours** observed (with precipitation)	**Precipitation events** count (avg. duration [hours])
2019	9 (01.03.2019–30.11.2019)	275 (106)	6 600 (567)	178 (3.2)
2020	9 (01.03.2020–30.11.2020)	275 (123)	6 600 (623)	194 (3.2)
2021	9 (01.03.2021–30.11.2021)	275 (104)	6 600 (455)	168 (2.7)
2022	9 (01.03.2022–30.11.2022)	275 (89)	6 600 (416)	152 (2.7)
Σ	36	1 100 (422)	26 400 (2 061)	692 (3.0)

As the unheated TB used cannot record non-liquid precipitation, periods with snowfall were omitted. It follows from the procedure given in equations (1) that only liquid precipitation, which is able to be captured by TB and the time-corresponding precipitation recorded by lysimeters, were included in the comparative study. The purpose was to exclude all non-liquid precipitation (snow, snow grains, snow pellets, ice pellets) and NRW (dew, fog, soil water vapour adsorption).

Precipitation was classified based on the classification of precipitation intensity (i) according to WMO criteria (Table 2). This classification was used as a basis for the evaluation of the comparison of precipitation measurements according to i (based on the reference P_{Lys}). According to this classification, the boundary between slight and moderate drizzle is 0.1 mm h^{-1}. Due to the sensitivity of the TB measurement (0.1 mm), fine drizzle and NRW cannot be clearly distinguished using the TB only. Since the total amount of precipitation classified as "slight rain" represents almost half of the total amount of precipitation in this study, this category was divided into two intervals. Precipitation in the form of drizzle was assigned to the category of "slight rain".

Table 2. Classification of precipitation into intervals according to their intensity based on the WMO [3]

Type	**Intensity** [mm h^{-1}]		**Intensity interval**
Drizzle	Slight	$i < 0.1$	I.
	Moderate	$0.1 \leq i < 0.5$	
	Heavy	$i \geq 0.5$	
Rain	Slight	$i < 1.0$	
		$1.0 \leq i < 2.5$	II.
	Moderate	$2.5 \leq i < 10.0$	III.
	Heavy	$10.0 \leq i < 50.0$	IV.
	Violent	$i \geq 50.0$	

In this study, precipitation was evaluated in the form of hourly and daily totals and also in the form of precipitation events of variable duration. The lysimeter precipitation data were considered as reference in relation to the TB data for the following reasons: an order of magnitude higher sensitivity of precipitation measurement (0.01 vs. 0.1 mm), 50 times larger collecting area (10 000 vs. 200 cm^2), measurement height above the ground (0 vs. 1 m) and five measurement repetitions (5 x Lys vs. 1 x TB).

4 Results and discussion

4.1 Data availability and data preparation

During the investigated period, precipitation was measured using five lysimeters. Therefore five sets of hourly totals (P_{Lys1}, P_{Lys2},..., P_{Lys5}) were obtained. Simple statistics is presented in Table 3.

Table 3. Parameters of the statistical probability distribution of five datasets from lysimeters

	$P_{Lys\ 1}$	$P_{Lys\ 2}$	$P_{Lys\ 3}$	$P_{Lys\ 4}$	$P_{Lys\ 5}$	P_{Lys} *(avg.)*
Count [-]	2 061	2 061	2 061	2 061	2 061	2 061
Cummulative *P* [mm]	2 078	2 103	2 074	2 048	2 077	2 076
Relative error [-]	1.00	1.01	1.00	0.99	1.00	1.00
Range [mm h^{-1}]	33.75	32.43	33.68	33.40	34.14	33.48
Mean [mm h^{-1}]	1.01	1.02	1.01	0.99	1.01	1.01
Median [mm h^{-1}]	0.40	0.41	0.40	0.40	0.40	0.40
Standard deviation [mm h^{-1}]	1.95	1.95	1.94	1.92	1.97	1.94
Standard skewness [-]	124	121	125	125	126	124
Standard kurtosis [-]	677	627	683	687	694	674

The average value from five lysimeters is 2 076 mm. Relative to their average value, the cumulative precipitation measured by Lys 2 is 1% higher than the average, and conversely, the cumulative precipitation measured by Lys 4 is 1% lower. On the remaining three lysimeters, these deviations were negligible. The statistical parameters of the probability distribution presented in Table 3 indicate a very high similarity of all five measured sets. Negligible differences in precipitation measured using five lysimeters allow us to use their average values in the next part of the study:

$$(P_{Lys}=(P_{Lys1}+P_{Lys2}+P_{Lys3}+P_{Lys4}+P_{Lys5})/5) \quad (2)$$

4.2 Comparison of cumulative precipitation data

A comparison of the cumulative rainfall recorded by the rain gauge and lysimeters during the four-year monitoring period is shown in Figure 5.

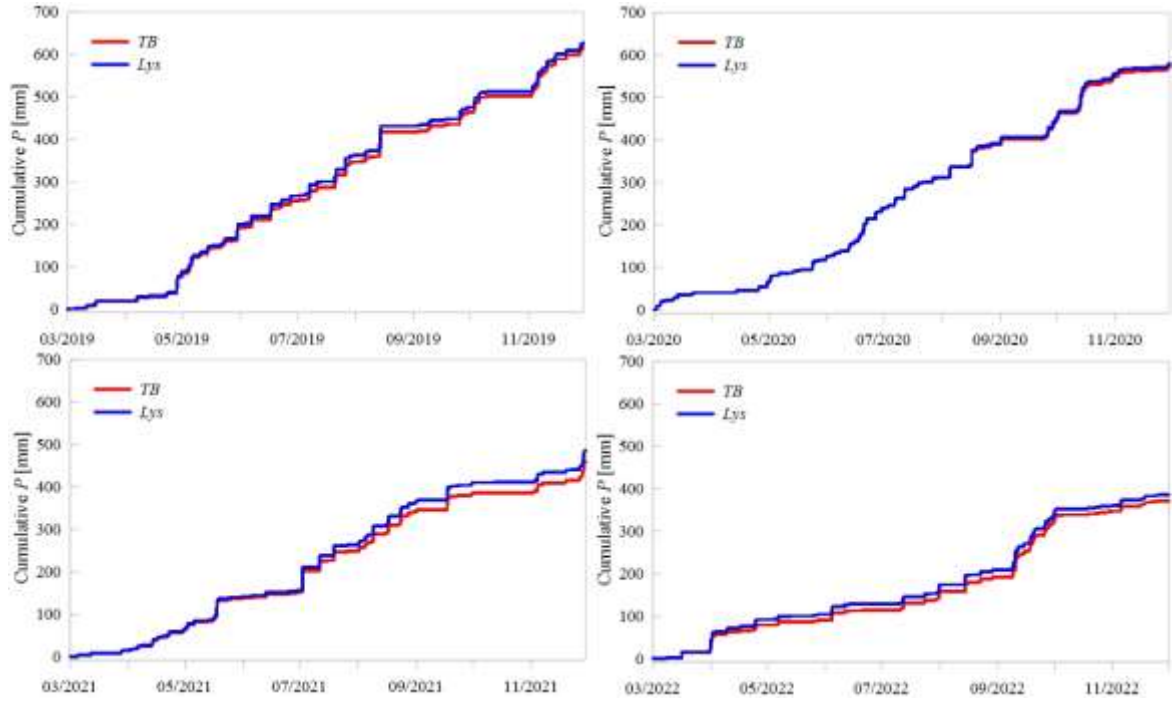

Figure 5. Cumulative precipitation measured by tipping-bucket rain gauge and lysimeters

A total of 2 076 mm of precipitation was recorded using lysimeters and 2 019 mm using a rain gauge. The difference of 57 mm means, in relative terms, a total underestimation of TB measurements compared to Lys by -2.8%. Underestimations were recorded during all four compared annual periods. The biggest difference –26 mm (-5.3%) was measured in 2021. In 2019, 2020 and 2022 it was -11 mm (-1.7%), -6 mm (-1.1%) and -15 mm (-3.8%) respectively. The reason for the interannual differences is probably due to the different distribution of precipitation during individual years.
Some results of the comparison of cumulative precipitation measured by tipping-bucket rain gauges and lysimeters published in the literature compared to this study are summarized in Table 4. In all cases, cumulative precipitation measured by TB was lower than precipitation measured by LYS. The overall underestimation of TB measurements compared to LYS ranged from -6.8 to -12.7% in published studies. In this study, an underestimation of -2.85% was measured, which is a significantly smaller value.

Table 4. Comparison of the results of published studies with the results of precipitation measurements using tipping-bucket rain gauges and lysimeters

Site	**Year**	**Observed days**	**Cum. P_{TB}** [mm]	**Cum. P_{Lys}** [mm]	**Rel. Difference** [%]
Berlin, Germany [13]	2012, 2013	389	580	664	-12.7
SW Siberia, Russia [14]	2016	114	158	170	-6.8
Vienna, Austria [15]	2011	229	365	416	-12.3
ESL, Slovakia (this study)	2019, 2020, 2021, 2022	1 100	2 019	2 076	-2.8

4.3 Comparison of precipitation measurements at hourly, daily and precipitation event scale

Comparison of hourly and daily totals and totals of precipitation events is shown in Figure 6. In all cases, a very high degree of correlation was achieved when the coefficient of determination (r^2) exceeded the value of 0.99.

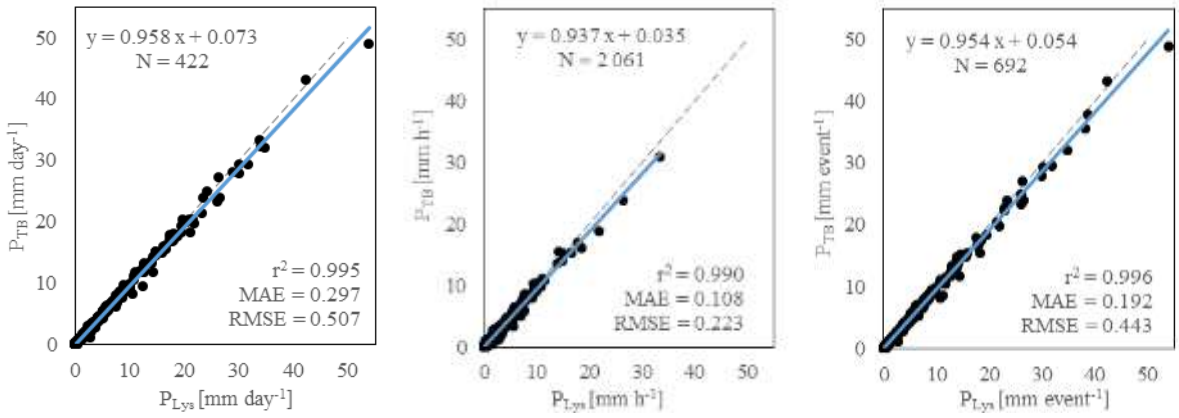

Figure 6. Relationship between precipitation data obtained by tipping-bucket rain gauge (PTB) and lysimeter (Plys) on a daily and hourly basis and on a precipitation event basis (dashed is 1:1 line)

The highest correlation was achieved when comparing precipitation events (r^2=0.996), the lowest for hourly totals (r^2=0.990). In all comparisons, there was an overall underestimation of the measured precipitation using TB compared to the reference values from the lysimeters. The mean absolute error (*MAE*) and root mean square error (*RMSE*) values indicate how similar the compared values are (zero value indicates that the compared values are identical). Both *MAE* and *RMSE* values are lowest for hourly totals and highest for daily totals. Simple statistics from precipitation measurements using TB and Lys is presented in Table 5. The table shows that the average hourly amount of precipitation is about 1 mm, the average daily amount is less than 5 mm. During a precipitation event, approximately 3 mm of precipitation falls on average.

Table 5. Basic statistical parameters of measured precipitation obtained by tipping-bucket rain gauge (TB) and lysimeters (Lys) on a daily and hourly basis and on the basis of precipitation events

		TB	Lys
Hourly totals [mm h^{-1}]	Min	0.1	0.00
	Max	30.9	33.48
	Average	0.98	1.01
	Median	0.4	0.41
Daily totals [mm d^{-1}]	Min	0.1	0.00
	Max	48.9	53.83
	Average	4.8	4.92
	Median	2.1	2.26
Precipitation events [mm $event^{-1}$]	Min	0.1	0.00
	Max	48.9	53.83
	Average	2.9	3.00
	Median	0.6	0.60
	Avg. duration [h]	3.0	3.0
	Avg. intensity [mm h^{-1}]	0.8	0.8

4.4 Comparison of precipitation measurements according to precipitation intensity

According to the values in Table 6, precipitation occurred most often from interval I. ($i < 1.0$ mm h^{-1}). With an occurrence frequency of 72%, however, they accounted for only 22% of the total amount of precipitation. As the intensity increases, the frequency of precipitation also decreases. The frequency of occurrence of precipitation in the interval IV. ($i > 10.0$ mm h^{-1}) was only 1%, but these precipitations represented 12% of the total precipitation. Precipitation with the largest share in the total amount of precipitation (39%) was from interval III. ($2.5 \leq i < 10.0$ mm h^{-1}).

Table 6. Distribution of measured precipitation according to intensity

	Intensity interval				
	I.	**II.**	**III.**	**IV.**	**(I.–IV.)**
Frequency	1 492	370	184	15	2 061
Total *P* [mm]	457	752	800	247	2 076
Frequency of occurence	72%	18%	9%	1%	100%
Contribution to total *P*	22%	28%	39%	12%	100%

The results of the comparison according to the intensity of precipitation are shown in Figure 7. The r^2 values indicate a high degree of correlation for all monitored precipitation intensity intervals, while precipitation with a higher intensity showed a slightly higher degree of correlation. The comparison of the measured precipitation using TB and the reference Lys shows that the differences between TB and Lys increase with increasing precipitation intensity. The differences between the measurements grow exponentially, which is declared by the exponentially increasing values of *RMSE* (from 0.09 to 1.53 mm h^{-1}) and *MAE* (from 0.07 to 1.17 mm h^{-1}). The values of the *bias* parameter indicate an increasing trend of underestimation of precipitation measurements using TB compared to Lys: the higher the precipitation intensity, the larger the measured deficit.

The overall underestimation of precipitation measurements using TB versus Lys is caused by the interaction of a number of random and systematic errors. Among the most important are the losses caused by the wind, the height of the TB installation, the wetting of the TB walls with subsequent water evaporation and the relatively small collecting area of the TB. With an increase in the intensity of precipitation, losses due to "out-splashing of water" also increase. During the time required to tip over the tipping bucket in the TB, small water losses occur, which increase with the increasing intensity of precipitation.

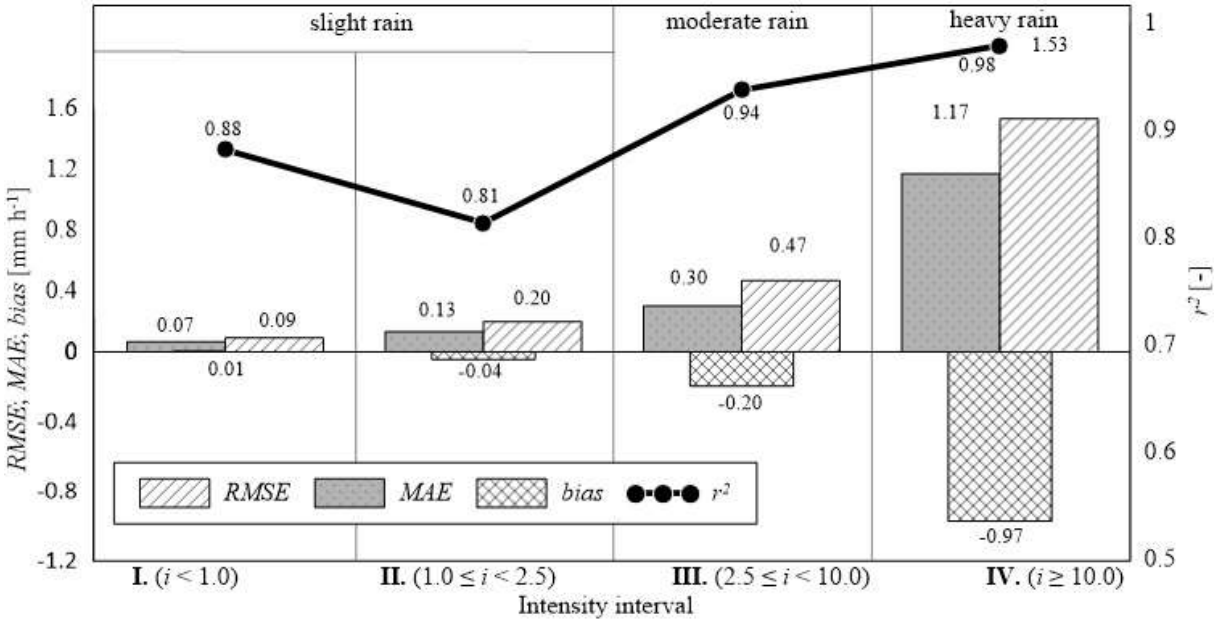

Figure 7. Values of Root Mean Square Error (*RMSE*), Mean Absolute Error (*MAE*), bias and coefficient of determination (r^2) for individual precipitation intensity intervals

5 Conclusion

The study compares two methods of measuring precipitation: measuring with a tipping-bucket rain gauge and measuring precipitation based on lysimeter measurements. The lysimeter determination of precipitation was chosen as the reference method. The comparison showed that the tipping-bucket rain gauge underestimates the precipitation compared to the lysimeter. Cumulative precipitation for the entire monitored period captured by the rain gauge was -2.8% lower compared to lysimeter measurements. The stated results indicate a relatively high reliability of precipitation measurements using standard tipping-bucket rain gauges. The advantage of lysimeter measurement of precipitation is higher accuracy and the possibility of capturing precipitation in all forms. The disadvantage is the incomparably higher costs of building and operating a lysimeter station.

Acknowledgements
This research was funded by the Scientific Grant Agency of the Ministry of Education, Research, Development and Youth of the Slovak Republic: (project VEGA No. 2/0025/24).

References:

[1] Šoltész, A., Zeleňáková, M., Čubanová, L., Šugareková, M., Abd-Elhamid, H.: Environmental Impact Assessment and Hydraulic Modelling of Different Flood Protection Measures. Water, 13, art. no. 786, 2021.
[2] Almikaeel, W., Čubanová, L., Šoltész, A.: Hydrological drought forecasting using machine learning – Gidra River case study. Water, 14, art. no. 387, 2022.
[3] WMO: Guide to Instruments and Methods of Observation (WMO-No. 8). World Meteorological Organisation, Geneva, 2021.
[4] Sevruk, B., Hertig, J.A., Spiess, R.: The effect of a precipitation gauge orifice rim on the wind field deformation as investigated in a wind tunnel. Atmospheric Environment. Part A. General Topics, 25, pp. 1173-1179, 1991.
[5] Sevruk, B.: Adjustment oftipping-bucket precipitation gauge measurements. Atmospheric Research, 42, pp. 237-246, 1996.
[6] Kohfahl, C., Saalting, M.W.: Comparising precision lysimeter rainfall measurements against rain

gauges in a coastal dune belt, Spain. Journal of Hydrology, 591, art. no. 125580, 2020.
[7] Schnepper, T., Groh, J., Gerke, H.H., Reichert, B., Pütz, T.: Evaluation of precipitation measurement methods using data from precision lysimeter network. Hydrology and Earth System Sciences, 27, pp. 3265-3292, 2023.
[8] SHMU: Klimatický atlas Slovenska [Climate atlas of Slovakia]. Slovenský hydrometeorologický ústav, 2015.
[9] Tall, A., Pavelková, D.: Results of water balance measurements in a sandy and silty-loam soil profile using lysimeters. Journal of Water and Land Development, 45, pp. 179-184, 2020.
[10] Matušek, I., Reth, S., Heerdt, Ch., Hrčková, K., Gubiš, J., Tall, A.: Review of lysimeter stations in Slovakia, 17. Gumpensteiner Lysimetertagung : Lysimeter Research - Options and Limits, Gumpenstein, pp. 209-2012, 2017.
[11] Savitzky, A., Golay, M.J.E.: Smoothing and differentiation of data by simplified least squares procedures. Analytical Chemistry, 36, pp. 1627-1639, 1964.
[12] Schrader, F., Durner, W., Fank, J., Gebler, S., Pütz, T., Hannes, M., Wollschläger, U.: Estimating Precipitation and Actual Evapotranspiration from Precision Lysimeter Measurements. Procedia Environmental Sciences, 19, pp. 543-552, 2013.
[13] Hoffmann, M., Schwartengräber, R., Wessolek, G., Peters, A.: Comparison of simple rain gauge measurements with precision lysimeter data. Atmospheric Research,174-175, pp. 120-123, 2016.
[14] Haselow, L., Meissner, R., Rupp, H., Miegel, K.: Evaluation of precipitation measurements methods under field conditions during a summer season: A comparison of the standard rain gauge with a weighable lysimeter and a piezoelectric precipitation sensor. Journal of Hydrology, 575, pp. 537-543, 2019.
[15] Nolz, R., Cepuder, P., Kammerer, G.,: Determining soil water-balance components using an irrigated grass lysimeter in NE Austria. Journal of Plant Nutrition and Soil Science, 177, pp. 237-244, 2014.

ANALYSIS OF SELECTED SOIL WATER BALANCE MEMBERS OBTAINED BY CALCULATION AND LYSIMETRIC MEASUREMENT

BRANISLAV KANDRA [1], ANDREJ TALL [1], MILAN GOMBOŠ [1], DANA PAVELKOVÁ [1],

[1] *Institute of Hydrology, Slovak Academy of Sciences, Dúbravská cesta 9, 841 04 Bratislava, Slovakia, kandra@uh.savba.sk*

1 Abstract

The presented work focused on model HYDRUS-1D verification using lysimetric measurements. Linear regression showed high agreement between measured and calculated actual evapotranspiration (ET_a) values (R^2=0.93; SE=0.05). The cumulative difference between the calculated and the measured ET_a was 42 mm (9%) for the evaluated period. In the case of reference evapotranspiration (ET_{ref}), the newer calculation approach proved more appropriate with the measured ET_a (R^2=0.94, SE=0.05), where the total difference was only 9 mm (2%). The performance of the mathematical model is assessed as satisfactory for the analysis of the soil water regime.

Keywords: weighable lysimeters, soil water regime, evapotranspiration, unsaturated soil zone, numerical simulation, water balance of soil

2 Introduction

When balancing water in the soil, evapotranspiration is an essential component on the outflow side [1], [2]. Two sub-processes are involved in evapotranspiration. The first of them is transpiration, which takes place through the stomata cells of plants and is an important production factor [3], [4]. The second is evaporation from the free surface. The evapotranspiration amount depends primarily on meteorological conditions and soil moisture. Soil moisture affects whether there is enough water for evapotranspiration and whether its potential will be reached. If this is not the case, an evapotranspiration deficit arises. The evapotranspiration can be quantified either directly by measurement or by calculation [5]. The water balance on a lysimeter is one of the evapotranspiration measuring methods [6]. The lysimeter makes it possible to quantify the flows at the upper and lower edges of the balanced soil zone. With the exact soil weight measurement, it is possible to express the evapotranspiration by water balance. Currently, lysimeter research is again coming to the attention of science society in the home and world [7].
Recently, several modern lysimeter stations have been built in Slovakia. One of them is also a station located in Petrovce nad Laborcom, which was the source of data processed in this contribution. Computational methods are based on the soil water regime numerical simulation by mathematical models. Mathematical models make it possible to calculate the individual components of the water balance and thus also the amount of evapotranspiration through water uptake by plant roots and surface flow. The model represents a cheap and fast tool for obtaining the necessary data if verified by correct measurements. The submitted contribution is focused on the HYDRUS-1D model verification by the lysimeter. Hourly totals of calculated and lysimetrically measured actual evapotranspiration were analysed for 148 days (May 27, 2017 – October 21, 2017). Model verification was performed using mathematical statistics methods. Moisture conditions in the lysimeter were maintained to achieve evapotranspiration potential. At the same time, this made it possible to verify the appropriateness of using two approaches for calculating reference evapotranspiration with measured and calculated actual evapotranspiration.

3 Methods

3.1 Research site description

The research site is near the Petrovce nad Laborcom village cca 5 km from the Michalovce district town (N 48° 47.540'; E 21° 53.175'; 117 m a.s.l.). In March 2014, the construction of a lysimeter station began in the closed area, which is currently under the administration of the Laborec basin. The station was fully commissioned in the spring of 2015 (Figure 1).

The station consists of 5 lysimeters stored in two separate plastic containers. Each lysimeter consists of a steel cylinder with an area of 1 m^2 and a height of 2.5 m. Soil monoliths in the cylinders were sampled from different sites of the East Slovak Lowland (ESL). These undisturbed samples best represented the soils of ESL. Each lysimeter has an adjustable groundwater level (GWL) system connected to a nearby well that serves as a water source. A meteorological station providing meteorological elements data is also a part of the lysimeter unit. All monoliths are weighed on scales with an accuracy of ±0.01 kg. The plant cover in the cylinders consists of grass maintained to a height of 12 cm.

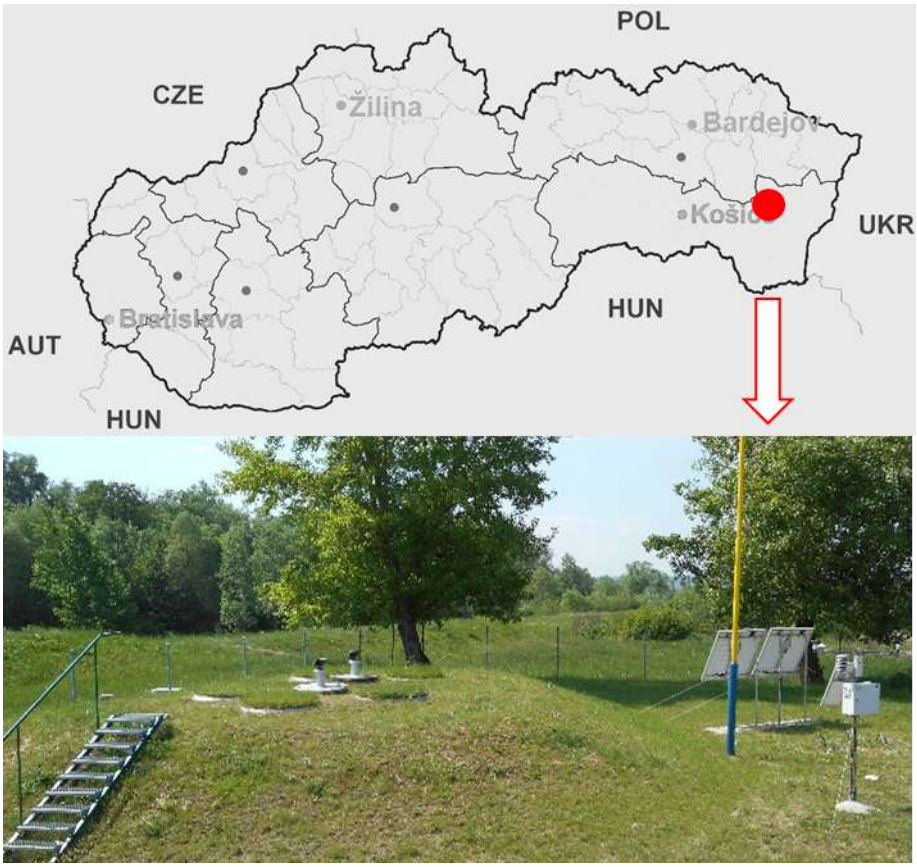

Figure 1. Lysimeter station in Petrovce nad Laborcom

The studied monolith contains soil sampled near the Poľany village in southeast ESL. The soil profile is mainly loamy-sandy to sandy, changing to sandy loam in the upper part (Figure 2).

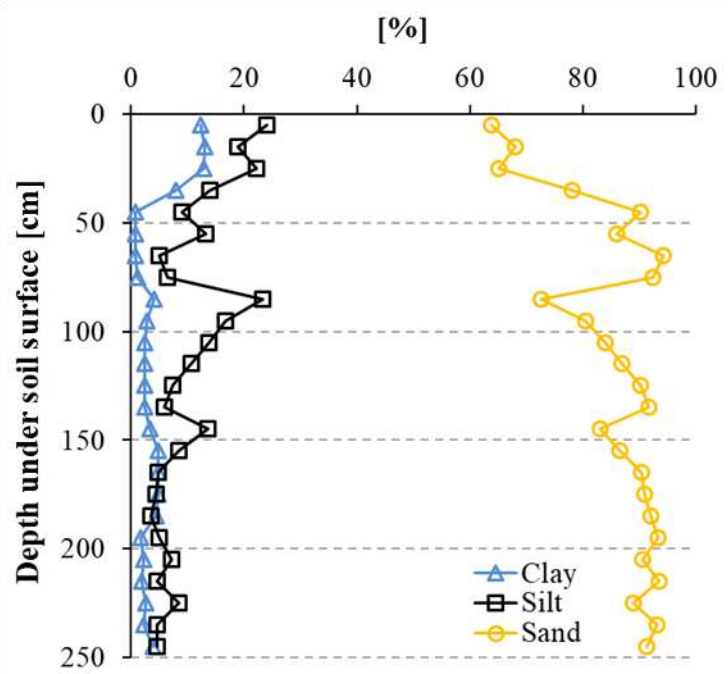

Figure 2. Soil texture of the Pol'any site

3.2 Lysimeter data processing

A lysimeter is a tool that allows quantifying the individual components of the water regime of soils through their balance in the soil – plant – atmosphere system [8]. In general, it can be expressed such a balance by a simple balance equation:

$$\Delta W=(P+I+D+CR)-(ET_a+SW) \quad (1)$$

where (ΔW) is the water content change in the lysimeter over time depending on the water inflow or outflow through the upper and lower boundaries of the balanced soil zone. The upper boundary is the area where the balanced soil zone interacts with the vegetation cover and the atmosphere. Here, water infiltrates from precipitation (P) or irrigation (I) and at the same time evaporates into the atmosphere through evapotranspiration (ET_a). Dew (D) is the amount of condensed water on the surface of the soil monolith. The lower boundary is the interaction area of the balanced soil zone with groundwater. Here the water inflow occurs from the groundwater into the balanced zone by capillary rise (CR), and the outflow from the balanced zone is by gravity flow towards the groundwater (SW – seepage water). If the values of individual balance equation members are known, it is then possible to simply express the values of ET_a. Next, it was necessary to modify the balance Eq. (1) into the form Eq. (2) [9]:

$$ET_a=P_{lys}+D-\Delta W+BF \quad (2)$$

The lysimeter body with soil monolith represents a balanced zone, and therefore the lysimeter weight is an important output parameter. Each change in weight by 1 kg represents a change in soil water content ΔW by 1 mm relative to the lysimeter area of 1 m^2. Irrigation was not applied here, and the groundwater level was set at a constant level of 1 m below the ground during the entire period. The precipitation obtained from the lysimeter (P_{lys}) was used to eliminate the inaccuracy of the rain gauge in the equation [10]. The rain gauge tended to underestimate the real precipitation, leading to faulty ET_a values. Flows at the bottom edge of the lysimeter (BF – bottom fluxes, $BF=CR-SW$) have a positive value in the case that water flows into the lysimeter, which compensates for capillary losses. Conversely, negative BF values represent the water outflow from the lysimeter i.e. gravity flow to GWL. The quantification of the water balance members in the lysimeter was based on the following conditions:

$$IF(\Delta W-BF)<0 \rightarrow ET_a=(\Delta W-BF) \wedge (P_{lys}+D)=0$$

$$IF(\Delta W\text{-}BF)>0 \rightarrow ET_a=0 \wedge (P_{lys}+D)=(\Delta W\text{-}BF)$$

The water content decrease of the lysimeter *((ΔW-BF)<0)* is due to evapotranspiration (ET_a) and the water content increase *((ΔW-BF)>0)* is due to either precipitation (P_{lys}) or dew formation (D). Suppose a precipitation event on the rain gauge in the weather station is recorded when the water content of the lysimeter is increased. In that case, the increase in water content is assigned to precipitation (P_{lys}). Otherwise, the water content gain is attributed to the dew (D).

3.3 Model used description

The mathematical model HYDRUS-1D in version 4 was used to calculate the analyzed members of the balance equation in the evaluated period. HYDRUS-1D is a one-dimensional model calculating the water flow, heat transfer and movement of soluble substances involved in subsequent first-order reactions in variably saturated soils [11]. It is based on the solution of the Richards equation for variably saturated flow and on the advection-dispersion type of equations for the heat transfer and soluble substances. The flow equation takes into account the uptake of water by plant roots.

The model setting corresponded to the real conditions in the lysimeter before and during the simulation. The simulated soil profile with a thickness of 2.5 m was divided into 20 material layers. The selected van Genuchten-Mualem hydraulic model [12] was single-pore without hysteresis. The laboratory-measured hydrophysical characteristics were defined for each layer, i.e. van Genuchten parameters of analytical expression of water retention curves and saturated hydraulic conductivity values. Next, it was necessary to set the initial and boundary conditions. The initial moisture of the individual soil layers, at the beginning of the simulation, corresponded to the real moisture in the lysimeter. The time-dependent upper boundary condition consisted of daily data of meteorological elements from the meteorological station and the rain gauge (atmospheric precipitation, solar radiation, maximum and minimum air temperature, air humidity and wind speed). The time-dependent lower boundary condition was a constant groundwater level set to 1 m below the ground. The phenological characteristics were also constant to the following values: grass height 12 cm, albedo 0.23, LAI (leaf area index) 2.88 and root depth 30 cm. The calculated actual evapotranspiration totals ET_a were obtained by summing the amount of water drawn from the soil by plant roots (transpiration) and water from the surface flux at the interface between the soil surface, plant cover and the atmosphere (evaporation). The Feddes reduction model [13] with grassland parameters was chosen for plant root water uptake. The calculation of reference evapotranspiration (ET_{ref}) was based on the Penman-Monteith combination Eq. (3) recommended by FAO [14] in the HYDRUS-1D model:

$$ET_{ref}=\frac{0.408\,\Delta\,(R_n\text{-}G)+\gamma\,\frac{C_n}{T_{hr}+273}\,u_2\,(e_s\text{-}e_a)}{\Delta+\gamma\,(1+C_d\,u_2)} \tag{3}$$

where R_n is the radiation balance of the crop surface [MJ/m^2/h]; G is the heat flux in the soil [MJ/m^2/h]; T_{hr} is the average hourly air temperature at a height from 1.5 to 2.5 m [°C]; u_2 is the average hourly wind speed at a height of 2 m [m/s]; e_s is the pressure of saturated water vapor up to 2.5 m [kPa]; and e_a is the average actual pressure of water vapor at a height of 1.5 to 2.5 m [kPa]; Δ is the derivation of saturated water vapor pressure at air temperature T_{hr} [kPa/°C]; γ is the psychrometric constant [kPa/°C]; C_n and C_d are constants that vary according to the reference type. The values of the constants in the model are C_n=900 and C_d=0.34. The newer approach of calculating ET_{ref} according to Eq. (3) with the values of constants C_n=37 and C_d=0.24 (day hours), and 0.96 (night hours) was also chosen for comparison [15].

4 Results and discussion

Figure 3 shows the hourly ET_a courses calculated by the model and obtained by balancing via lysimeter with ET_{ref} courses according to different approaches [14], [15]. For a better overview, the figure shows the first five days of June from the whole analyzed period (May 27, 2017 – October 21, 2017). Here,

the agreement between calculated and measured ET_a totals is visible clearly. The moisture conditions in the lysimeter were maintained to achieve the maximum possible evapotranspiration using a constant groundwater level of 1 m below the ground. Also, authors [16] dealt with the effect of setting the lower boundary condition on evapotranspiration and water balance in the soil. Therefore, $\Delta ET \approx 0$ applied for the evapotranspiration deficit ΔET given by the difference between ET_{ref} and ET_a. This also made it possible to verify the accuracy of various ET_{ref} calculation approaches. The figure also shows a high degree of agreement between ET_a and ET_{ref}.

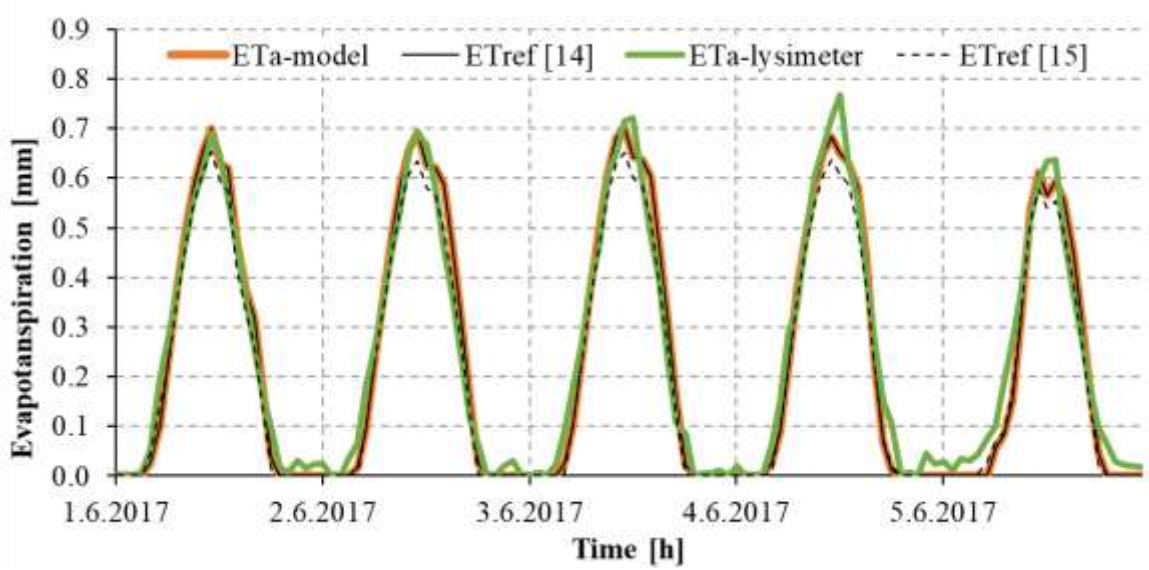

Figure 3. Comparison of the calculated and measured actual evapotranspiration (ET_a) and reference evapotranspiration (ET_{ref}) during five days at the beginning of June

The results of the linear regression show a high degree of dependence between the measured and calculated evapotranspiration values (Figure 4). The hourly ET_a totals calculated by the model correlate very well with the measured values by the lysimeter (Figure 4a). This is indicated by the high determination coefficient value R^2=0.93. Deviations range from -0.37 (MIN) to 0.25 (MAX). The standard deviation SE=0.05 means that the values differ minimally from each other. ET_{ref} values calculated by two different approaches are also correlated. The differences in total ET_{ref} calculated according to the older [14] and the newer [15] approach are minimal (Figure 4b). The deviations with the determination coefficient values are shown in Table 1. The ET_{ref} calculation according to different approaches with the measured ET_a shows some differences (Figure 4c and 4d). In the case of the older approach, the calculation overestimates the measurement and the determination coefficient is slightly lower (R^2=0.93) compared to the newer approach, where R^2=0.94. Similarly, as determination coefficients, the values of deviations show in favor of the newer approach for calculating ET_{ref} towards measured ET_a (Table 1).

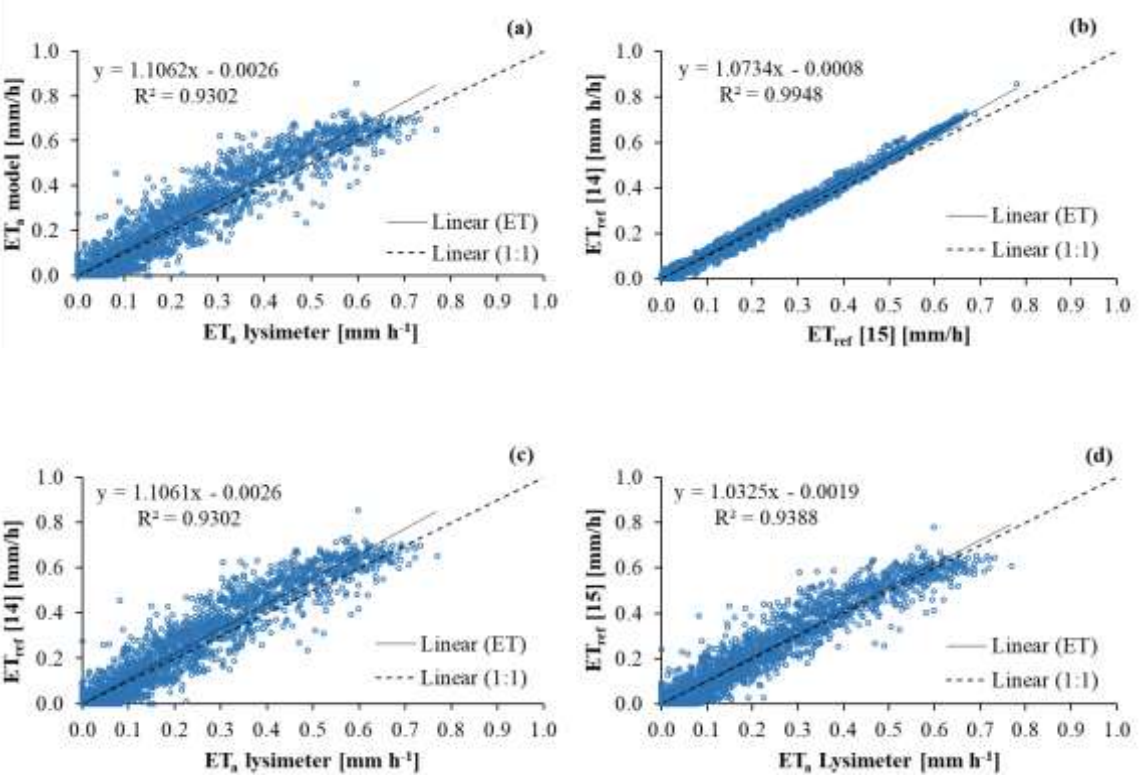

Figure 4. Linear dependencies between measured and calculated values of evapotranspiration

The differences between the measured and calculated evapotranspiration values for the entire analyzed period are in the Figure 5a. For illustration, the cumulative values of all water balance members are shown in the figure too. From the cumulative lines it follows, the total difference between calculated and measured ET_a is 42.02 mm. In the case of ET_{ref}, the difference resulting from the two calculation approaches is 33.21 mm. By comparing the measured ET_a with ET_{ref}, there is a smaller difference with the newer ET_{ref} calculation approach (8.97 mm) compared to the older one (42.18 mm). Figure 5b shows the cumulative ΔW values in the lysimeter. The ΔW courses are expressed from the measured and calculated water balance members. The results show that the model overestimated ΔW by 18 mm. This is due to the model's inaccuracy in quantifying the fluxes at the lower boundary of the balanced soil zone. The cumulative *BF* difference between calculation and measurement was 59 mm. This was reflected in higher values of ΔW and ET_a differences. The averages of the hourly evapotranspiration totals for individual months of the analyzed period gradually decreased. The highest average evapotranspiration totals were between May and August. Consequently, they significantly decreased in September and October. Average hourly totals of measured and calculated ET_a in individual months are as follows: May (0.20; 0.21 mm), June (0.19; 0.20 mm), July (0.17; 0.19 mm), August (0.16; 0.17 mm), September (0.08; 0.09 mm) and October (0.05; 0.06 mm).

Table 1. Deviations and coefficients of determination (R^2) between measured and calculated evapotranspiration

EVAPOTRANSPIRATION	ΔMAX	ΔMIN	S_E	R^2
ET_a lyzimeter – ET_a model	0.25	-0.37	0.05	0.93
$^{**}ET_{ref}$ – $^{*}ET_{ref}$	0.06	-0.09	0.01	0.99
ET_a lyzimeter – $^{*}ET_{ref}$	0.25	-0.37	0.05	0.93
ET_a lyzimeter – $^{**}ET_{ref}$	0.23	-0.31	0.05	0.94

$^{*}ET_{ref}$ [14], $^{**}ET_{ref}$ [15]

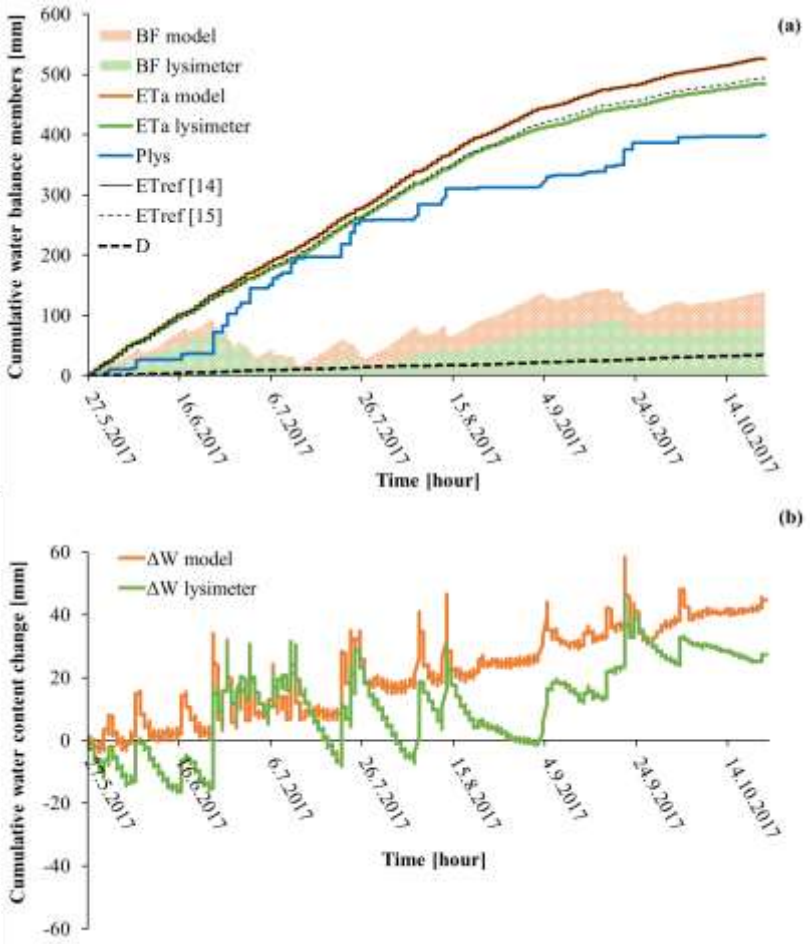

Figure 5. Cumulative values of analyzed balance members in the evaluated period (*BF* – bottom fluxes, ET_a – actual evapotranspiration, P_{lys} – precipitation, ET_{ref} – reference evapotranspiration, D – dew, ΔW – water content change in the evaluated soil profile.

5 Conclusion

The verification of the HYDRUS-1D model was performed on hourly ET_a totals for the period from May 27, 2017 to October 21. 2017. At the same time, ET_a totals were expressed using a water balance on a weighable lysimeter. The model setup corresponded to the real conditions in the lysimeter. The groundwater level was set constant at 1 m below the ground to achieve maximum evapotranspiration, while the condition $\Delta ET=(ET_{ref}-ET_a)\approx 0$ was valid. In this way, verifying the accuracy of two different ET_{ref} calculation approaches with measured and calculated ET_a was possible. Linear regression showed high agreement between measured and calculated ET_a values (R^2=0.93; SE=0.05). The cumulative difference between the calculated and the measured ET_a was 42 mm (9%) for the evaluated period. In the case of ET_{ref}, the newer calculation approach proved more appropriate with the measured ET_a (R^2=0.94; *SE*=0.05), where the total difference was only 9 mm (2%). Quantified deviations between measured and calculated values are most significant at *BF* (59 mm), which caused corresponding differences at ET_a (42 mm) and ΔW (18 mm). In general, however, it can be concluded that the model reliably simulates trends in the development of the balance members.

The verification results showed that the HYDRUS-1D model is suitable for use in conditions simulating the existing soil profile in the investigated lysimeter. Using all available data from a nearby weather station, hydrophysical characteristics of the soil profile, and phenological characteristics of the crops, it can reliably estimate the amount of evapotranspiration.

Acknowledgements
This study was supported by the Scientific Grant Agency of the Ministry of Education. Research. Development and Youth of the Slovak Republic: VEGA: 2/0025/24.

References:

[1] Wang, H., Zhang, M., Cui, L., Yu, X.: Spatial Heterogeneity in Sensitivity of Evapotranspiration to Climate Change. Pol. J. Environ. Stud., 26. pp. 2287-2293. 2017.
[2] Soltesz, A., Barokova, D., Cervenanska, M., Janik, A.: Hydrodynamic Analysis of Interaction Between River Flow and Ground Water. 16th International Multidisciplinary Scientific Geoconference (SGEM 2016). Stef92 Technology Ltd. Sofia. pp. 823-829.
[3] Novák, V.: Soil-Plant-Atmosphere System. Evapotranspiration in the Soil-Plant-Atmosphere System. Progress in Soil Science. ed. V. Novák. Springer-Dordrecht. The Netherlands. pp 15-24. 2012.
[4] Tuttobene, R., Vagliasindi, C.: Biomass accumulation and its relationship with evapotranspiration on durum wheat. Third Congress of the European Society for Agronomy. eds. M. Borin & M. Sattin. ESA-Paris. France. pp. 262-263. 1995.
[5] Abtew, W.: Evapotranspiration Measurements and Modeling for Three Wetland Systems in South Florida1. Am. Water Resour. Assoc., 32. pp. 465-473. 1996.
[6] Feltrin, R. M., de Paiva, J. B. D., de Paiva, E. M. C. D., Meissner, R., Rupp, H., Borg, H.: Use of Lysimeters to Assess Water Balance Components. Grassland and Atlantic Forest in Southern Brazil. Water Air Soil Pollut., pp. 228-247. 2017.
[7] Matušek, I., Reth, S., Heerd, CH., Hrčková, K., Gubiš, J., Tall, A.: Review of lysimeter stations in Slovakia. Lysimeter Research – Options and Limits. – Druck. Verlag. pp. 209-211. 2017.
[8] Nolz, R. A.: Review on the quantification of soil water balance components as a basis for agricultural water management with a focus on weighing lysimeters and soil water sensors/Ein Überblick über die Ermittlung von Wasserhaushaltsgrößen als Basis für die landeskulturelle Wasserwirtschaft mit Fokus auf Lysimeter und Bodenwassersensoren Die Bodenkultur. J. Land Manage., Food Environ., 67. 3. pp. 133–144. 2016.
[9] Tall, A., Kandra, B., Gomboš, M., Pavelková, D.: Kvantifikácia hydrologických procesov pomocou lyzimetra. Aktuálne problémy zóny aerácie pôdy v podmienkach prebiehajúcej klimatickej zmeny – Bratislava: Veda. pp. 285–306. 2018.
[10] Schrader, F., Durner, W., Fank, J., Gebler, S., Pütz, T., Hannes, M., Wollschläger, U.: Estimating Precipitation and Actual Evapotranspiration from Precision Lysimeter Measurements. Procedia Environ. Sci., 19. pp. 543-552. 2013.
[11] Šimůnek, J., Šejna, M., Saito, H., Sakai, M., Van Genuchten, M. TH.: The HYDRUS-1D software package for simulating the one-dimensional movement of water. heat. and multiple solutes in variably-saturated media. Version 4.0x. Hydrus Series 3. Department of Environmental Sciences. University of California Riverside. Riverside. CA. USA. 2008.
[12] Van Genuchten, M. TH.: A closed-form equation for predicting the hydraulic conductivity of unsaturated soils. Soil Sci. Soc. Am. J., 44. 892-898. 1980.
[13] Feddes, R. A., Kowalik, P. J., Zaradny, H.: Simulation of Field Water Use and Crop Yield. John Wiley & Sons. New York. NY. 1978.
[14] Food and Agriculture Organization of the United Nations: Expert consultation on revision of FAO methodologies for crop water requirements. ANNEX V. FAO Penman-Monteith Formula. Rome Italy. 1990.
[15] Allen, R. G., Walter, I. A., Elliot, R. L, Howell, T. A.: Intenfisu, D., Jensen, M. E., Snyder, R. L.: The ASCE Standardized Reference Evapotranspiration Equation. Reston. American Society of Civil Engineers. p. 216. 2005.
[16] Meissner, R., Bondarovich, A. A., Scherbinin, V. V., Ponkina, E. V., Mastyura, A. V. et al.: Calculation of water balance for the south desert area of Western Siberiaby international monitoring network data. Biological Bulletin of Bogdan Chmelnitskiy Melitopol State Pedagogical University 6. 2. pp. 223-238. 2016.

E-FLOW HOLISTIC ASSESSMENT IN DATA-LIMITED RIVER BASIN UNDER CLIMATE CHANGE IMPACT

GORANA ĆOSIĆ-FLAJSIG[1*], BARBARA KARLEUŠA[2], IVAN VUČKOVIĆ[3], MATJAŽ GLAVAN[4]

[1] *Zagreb University of Applied Sciences, Department of Civil Engineering, Croatia, E-mail: gcflajsig@tvz.hr*

[2] *University of Rijeka, Faculty of Civil Engineering, Croatia, barbara.karleusa@uniri.hr*

[3] *Elektroprojekt Consulting Engineers Section of Ecology, Croatia, ivan.vuckovic@elektroprojekt.hr*

[4] *University of Ljubljana Biotechnical Faculty, Department of Agriculture, matjaz.glavan@bf.uni-lj.si*

[*] *Corresponding author: gcflajsig@tvz.hr*

1 Abstract

Sustainable river basin water management can be achieved if appropriate flow, sediment regimes, and related river morphology quality are guaranteed. The obligation to define the environmental flow (E-flow) in the European Water Framework Directive (WFD) is not explicit and there is no official E-flow assessment methodology in the Republic of Croatia. In the previous research and paper, an innovative holistic E-flow assessment model for the present scenario was developed and presented. This paper presents the continuation of the research and the assessment of E-flow under the impact of climate change by the Soil Water Assessment Tool (SWAT).

Keywords: holistic approach, environmental objectives WFD, E-flow, climate change, SWAT, biological indicators, limited data, Sutla River Basin

2 Introduction

Related to the defined 17 United Nations (UN) Sustainable Development Goals (SDGs) for Sustainable Development until 2030, with an emphasis on SDG13 - Response to Climate Change, the need to analyse the impact of humans and climate change on water resources, and the future needs of human society regarding water resources, are crucial for defining sustainable integrated water management of the river basin. The intensive use of soil and water resources results in an imbalance between the environmental and economic objectives of the river basin management. Sustainable integrated river basin water management and environment objectives Water Framework Directive (WFD) can be achieved only if appropriate flow, sediment and nutrients (total Nitrogen (N) and total Phosphorus (P)) regimes, and related river morphology quality are guaranteed. There is no explicit obligation to define E-flow, and the implementation of the WFD is more focused on water quality. Most EU countries have developed procedures for investigating and determining the E-flow related to specific climatic, hydro-graphic, and hydrological conditions. In the Republic of Croatia, there is no official methodology to define the E-flow, and an innovative holistic model for the present scenario was developed and proposed in the paper by Ćosić-Flajsig G. et al., 2020 [1]. Despite the lack of appropriate monitoring, the holistic approach to E-flow assessment can contribute to the definition of E-flow. It includes all data analysis and available research to gain new knowledge about the river basin and its water bodies and assess the E-flow. The scientific research in this paper is based on the results of the Soil Water Assessment Tool (SWAT) model, hydrological analysis, biological investigations, and holistic approach assessment of the E-flow under the climate change impacts in data-limited river basins. This paper presents the proposed methodology of E-flow assessment under the climate change impacts based on the holistic approach to the E-flow assessment model under the climate change impact for the Sutla River basin case study. The results and discussion of the Sutla River basin case study using the developed holistic E-flow assessment model under the climate change impacts, and comparisons with existing well-known approaches and

methodologies, have been presented after that.

3 Proposed methodology

The E-flow assessment model under the climate change impact is based on the developed innovative holistic approach presented in the paper by Ćosić-Flajsig G. et al., 2020 [1]. Further research aims to determine the impact of climate change on the holistic assessed E-flow by modelling low flows, sediment, total N, and total P under eight future climate change scenarios in the data-limited river basin, using Indicators of Hydrological Alterations (IHAs) and biological indicators for the Sutla River downstream of the dam Vonarje. The model is based on the river basin pressures with climate change analysis, the occurrence of hydrological extreme impacts, and a program of basic and supplementary measures. Past (scenarios 2), present (scenario 1), and future scenarios (scenarios 3) were analysed with the SWAT model based on land use, climatic and hydrological data, climate change models, the presence or lack of the reservoir, municipal wastewater measures, and agriculture measures [2]. In addition, the holistically assessed E-flow for future scenarios for the profile on the Sutla River, as well as the holistically assessed E-flow for the present scenario, is proposed by linking hydrological, morphological, and ecological characteristics based on the research of the Sutla River, and the composition and abundance of biological quality elements. The proposed methodology is presented in Figure 1. It is prepared as the modified methodology developed by Gopal in [3].

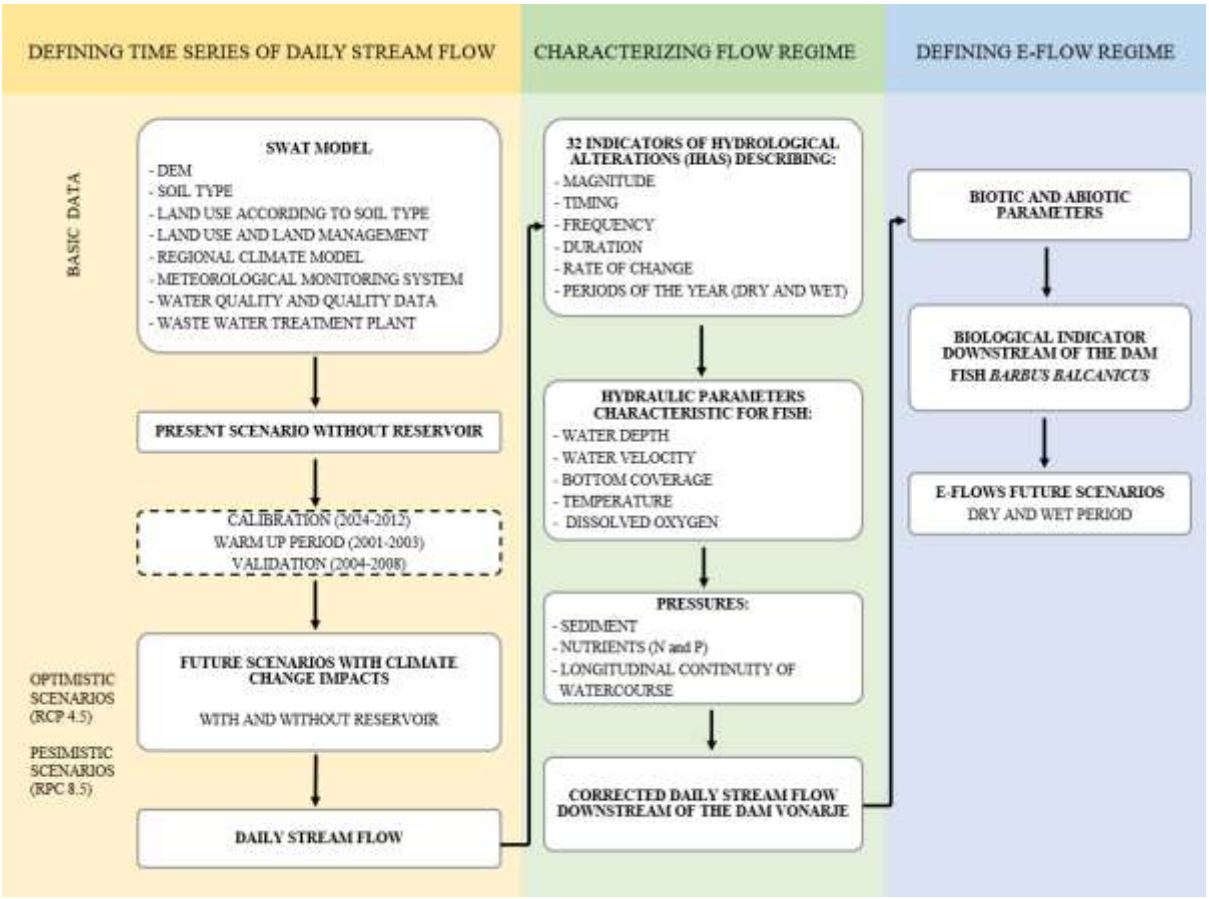

Figure 1 Methodology of a holistic approach to the assessment of E-flow for present scenario and future climate change impact scenarios (modified methodology from [3])

Biological indicators have been used to improve the methodology of a holistic approach to the assessment of E-flow for present scenarios and future climate change impact scenarios.

Biological indicators

Verification of the sufficiency of the defined value of ecologically acceptable flow by hydrological methods for the development of the necessary spatial and temporal dynamics of the basic ecological indicators (e.g. downstream of water intakes) downstream of the dam, necessity for ensuring the living conditions of characteristic fish is based on the hydraulic calculation.
The hydraulic calculation checks:

- water depth at characteristic cross-sections of watercourses or their parts provided by retained inflow defined by hydrological methods,
- water velocity at characteristic cross-sections of watercourses or their parts provided by retained inflow defined by hydrological methods,
- bottom coverage on characteristic cross-sections of watercourses or their parts that ensures retained inflow defined by hydrological methods [4],[5].

The basic ecological requirements of the selected indicator fish species, *Barbus balcanicus*, i.e. individual stages of their development, are presented in Table 1.

Table 1. Presentation of the basic ecological requirements of selected indicator species [4], [5]

		Key abiotic factors important for fish communities			
Biogeographical area	**Life stage**	**Water depth in cm**	**Water velocity in cm/s**	**Water temperature °C**	**Dissolved oxygen mg/l**
Barbus balcanicus	Spawning	Greater than body height 20 - 45	35 - 50	4 - 17 (14) *	Above 6
	<Fry	About 30	6 - 20	(15) *	Above 6
	Adults	Greater than body height 20 - 45	35 - 50	4 - 20	Above 6

*Figures in parenthesis () = optimum value

The flow values are corrected after determining the deviation of the obtained values from those that ensure the living conditions for the survival of the characteristic indicator species fish *Barbus balcanicus* (Table 1). It is defined as the flow section between water intake and restitution.
FUTURE scenarios 3 (with (3a) and without reservoir (3b)) were prepared concerning planned municipal wastewater and agricultural measures. The White Paper of the European Commission "Adapting to climate change: Towards a European framework for action" (COM/2009/147) was issued in April 2009 and sets out a framework to reduce the EU's vulnerability to the impact of climate change. On the basis of the climate change adaptation strategies for Croatia (until 2070) and Slovenia (until 2050) and the results of the regional and national models of Slovenian Environmental Agency – ARSO, future scenarios with six models, for the Representative Concentration Pathway (RCP) 4.5 (moderately optimistic scenario) and RCP 8.5 (pessimistic scenario) for the 2020–2050 and 2070–2100 periods for the Sutla River Basin (Figure 5), six dynamically downscaled regional climate models (RCMs), CCLM4 (drivModel: CNRM-CERFACS-CNRM-CM5), CCLM4 (drivModel: MPI-M-MPI-ESM-LR), HIRHAM5, INERIS, RACMO22E and RCA4), were prepared at the local river basin level using bias correction (BC) methods using empirical quantile mapping (EQM). To prevent unrealistic results at the daily level, BC was performed for precipitation, maximum air temperature, minimum air temperature, relative humidity, global solar radiation, and wind speed.
For the Sutla River Basin, eight FUTURE scenarios were developed:

- with reservoir (superscript presents the selected RCP and time period explained in following parentheses): $3a^1$ (RCP 4.5 2020–2050), $3a^2$ (RCP 4.5 2070–2100), $3a^3$ (RCP 8.5 2020–2050), $3a^4$ (RCP 8.5 2070–2100) and
- without reservoir: $3b^1$ (RCP 4.5 2020–2050), $3b^2$ (RCP 4.5 2070–2100), $3b^3$ (RCP 8.5 2020–2050) and $3b^4$ (RCP 8.5 2070– 2100) [2].

For each scenario, six characteristic climate models were used to obtain the variability in inputs and outputs described in (Figure 3).

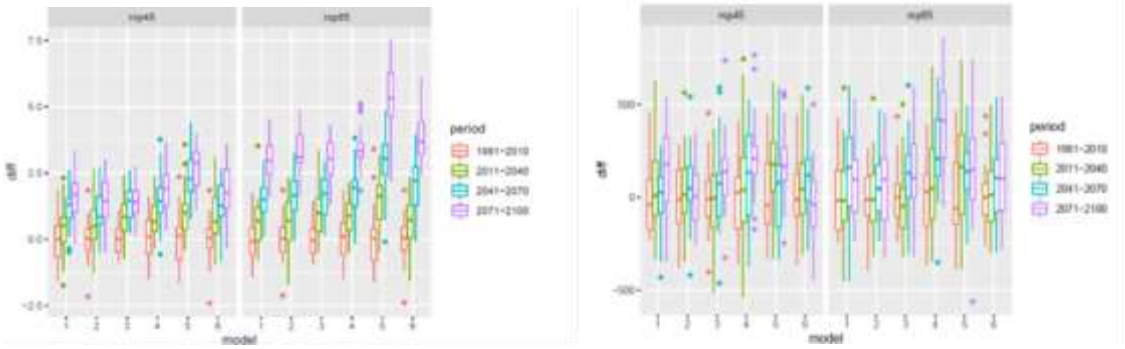

Figure 3. Average temperature (°C) - BC deviation from 1981–2010 related to RCP 4.5 and RCP 8.5, six characteristic climate models and periods (a), average precipitation (mm) - BC deviation from 1981–2010 related to RCP 4.5 and RCP 8.5, and six characteristic climate models and periods (b) [2].

3.1 Sutla Case Study

Considering the specific climatic, hydrographic and hydrological conditions and the definition of E-flow, each EU country has developed procedures for their investigation and determination. This paper presents the significant pressures that have affected the transboundary rural Sutla River basin between Croatia and Slovenia. In this paper it is continued with the E-flow assessment under the climate change impact, downstream of the dam Vonarje. The dam was built on the Sutla River in 1980 as a multipurpose hydrotechnical facility. The "biological minimum" downstream of the dam Vonarje was defined in the 1980s, as a flow of 120 l/s. To achieve the good water status and the environmental objectives of the river basin, rather than using the biological minimum flow downstream of the dam, it is necessary to define the E-flow.

Determination of E-flow means finding a balance between the water demand of the ecosystem and socio-economic setting, which necessarily leads to a holistic and comprehensive approach based on management of water resources in open channels.

The following principles need to be respected:

- E- flow is a quantity of water that provides for an ecological balance and preserves natural stability of an aquatic ecosystem,
- any abstraction of water from any watercourse asks for investigation into consequences such activity could cause upon an aquatic ecosystem,
- special attention should be paid to the protection of rare and endangered flora and fauna which is important for protection of ecological balance while taking care of flora and fauna which is the basic link in a food chain,
- to determine the E-flow, it is necessary to analyse all changes regarding both quantity and quality of water in the watercourse,
- since every watercourse is specific for its natural characteristics as well as for hydraulic engineering facilities already built or planned to be built on it, it is particularly important to have all related data.

The flow value is corrected after having determined deviations of obtained values from the values that ensure living conditions needed for survival of characteristic indicator species (Table 1). It is also necessary to take into consideration the sufficiency of the retained inflow for ensuring of necessary dynamics of living conditions throughout the year. This refers not only to indicator species, but to other species characteristic for the area under consideration as well. The defined E-flow values, as a rule, are such quantities of water which ensure ecological balance, namely preserve stability of the parent watercourse ecosystem in the reach under consideration (a reach between the intake structure and restitution).

In order to define the E-flow in the parent watercourse it is necessary to know, in addition to the hydrological data, what are the natural characteristics of the river.

Each river or its reach is specific for its natural characteristics, thus it is necessary to carry out field investigations. The field investigations are intended for collecting the information on basic biological-ecological characteristics of each potential site for determination of the environmental flow. Further, all such sites need to be photographed, the river channel, its vegetation, and the existing water inflows and intake structures. Analyzed river longitudinal profile and the Sutla Lake (reservoir) volume are prerequisites for maintaining the river ecosystem upstream and downstream from the lake ecosystem itself, and the proposal for the definition of an environmentally acceptable stream flow downstream of the dam has been prepared. The water quality management model that supports good water status is based on information from the Croatian Water monitoring program, particularly downstream of dams/reservoirs, including in the Sutla River Basin.
The holistic approach defines the E-flow for the present status, for the profile downstream of the dam, as presented in the previous research and paper [1], linking hydrological, morphological, and ecological characteristics based on the exploration of the Sutla River and its biological communities. The E-flow for the present scenario obtained by the hydrological method of vegetation with dry and wet period amounts to 0.504 m^3/s. The selection of biological indicator fish species *Barbus balcanicus* and accompanying fish species downstream of the dam was important because the entire Sutla River is protected as a NATURA 2000 site. *Barbus balcanicus* spawns between April and June, and the spawning period requires a water depth greater than 40 cm and a water velocity greater than 49 cm/s. E-flow should be increased to 0.98 m^3/s to meet the requirements of fish bioindicators (*Barbus balcanicus*) and allow the ecosystem to function normally (Figure 2).

Figure 2. Barbel (hrv.: potočna mrena) *Barbus balcanicus.*

The finally defined E-flow downstream of the dam Vonarje is 0.98 m^3/s [1].
Past, present, and future scenarios have been analysed by the SWAT model based on land use, climate and hydrological data, climate change data, presence or lack of the reservoir, and municipal wastewater and agriculture measures. The impact assessment was modelled by the SWAT to apply the basic and supplementary measures. This research aims to develop a water quality management model of rural transboundary basins to achieve environmental objectives. The model is based on river basin pressure analysis with climate changes and the occurrence of hydrological extreme impacts, as well as the program of basic and supplementary measures. Eight future climate change scenarios were obtained with optimistic RCP 4.5 and pessimistic RCP 8.5 forecasts for two periods (2020–2050, 2070 –2100), both with and without reservoir. The most significant influence of nutrients, sediment, and hot spots on river basin surface water, as shown by the surface water monitoring results and the risks of not achieving good water status and water eutrophication, have been demonstrated. This paper aims to determine the impact of current measures on future situations with the inclusion of climate change impact to create the basis for analysis and proposal of tailor-made measures [2].

4 Results and discussion

Related to the proposed Methodology of a holistic approach to assessing E-flow for present and future climate change impact scenarios (Figure 1), some characterizing flow regimes related to the 32 indicators of hydrological alternations (IHAS) describing, have been done. They are presented in Table 3. Species fish *Barbus balcanicus* – barbel is bioindicator for E-flow for the water body downstream of

the Vonarje dam, is defined for the present scenario and future scenarios. Also, longitudinal continuity of watercourses, except Vonarje dam, is assessed for the present scenario and future scenarios.
The reliability and effectiveness of this approach were illustrated by analyzing the potential impact of climate change by the SWAT model on the water availability downstream of the Vonarje dam on the Sutla River. For the flow for the past scenarios, $Q_{av,year}$, the values are like the values of the present scenario. The values of $Q_{av,year}$ for the future scenario is lowest for RCP 4.5 (2020–2050), followed by the values for RCP 8.5 (2070–2100). In Table 2 are presented average annual numerical modelling results for present, past, and future scenarios for SUBBASIN 2, for the water body downstream of the dam Vonarje.

Table 2. Average annual numerical modelling results for present, past, and future scenarios for SUBBASIN 2

Scenario	$Q_{av,year}$ (m^3/s) av.(min,max)%	Sediment (t) av.(min,max)%	Total N (t) av.(min,max)%	Total P (t) av.(min,max)%
PRESENT 1	**1,67(m^3/s)**	**2409 (t)**	**298275 (t)**	**19957 (t)**
PAST 2a	2 %	62 %	42 %	59 %
PAST 2b	0%	62 %	42 %	39 %
FUTURE $3a^1$	6% (-9;17)	7% (-15;18)	0% (-10;7)	0% (-5;4)
FUTURE $3a^2$	21% (-4;49)	14% (-18;44)	7% (-17;26)	0% (-9;7)
FUTURE $3a^3$	14% (3;33)	14% (-5;29)	4% (-8;17)	1% (-3;5)
FUTURE $3a^4$	28% (5;91)	20% (-13;105)	8% (-10;50)	0% (-8;15)
FUTURE $3b^1$	4% (-12;15)	10% (-16;23)	2% (-10;13)	0% (-5;4)
FUTURE $3b^2$	18% (-6;44)	14% (-18;44)	7% (-12;26)	0% (-9;7)
FUTURE $3b^3$	11% (1;30)	14% (-5;29)	4% (-8;17)	1% (-3;5)
FUTURE $3b^4$	25% (3;86)	20% (-13;104)	8% (-10;51)	0% (-8;15)

Note: Average percentage change values for past and future scenarios (in the brackets are the minimum and maximum % change according to the different climate models) are defined according to the absolute values of the present scenario.

The SWAT model results of the for the past (2a - with reservoir, 2b - without reservoir), present and future scenarios, for the values of the sediment, total N and total P are presented in Table 2. The values are significantly higher than the value of the present scenario given the implemented wastewater and agricultural basic measures that did not exist in the past. For the future scenarios, the higher values of sediment (average: 7 % - 20% and maximum 105% than in the present scenario) and higher values of Total N (average: 0% - 8% and maximum 51% than in the present scenario) greatly impact the ecosystem of fish bioindicator (*Barbus balcanicus*) (Table 2). In some scenarios, the range of these values shows an average flow of up to 28% with the interval of minimum and maximum values (-12; 91), 20% for sediment with the interval of minimum and maximum values (-18; 105). Minimum and maximum values for the total N (-17;51) and total P (-9;15).
For the future scenarios are presented values of the $Q_{av,year}$ (average: 4 5 – 25 % and minimum 12% than in the present scenario).
The analyses of the minimum daily flow downstream of the dam Vonarje have been prepared and presented in the Table 3. It has been prepared on the base of the average daily flow results of the 8 future scenarios with six climate models for SUBBASIN 2, for the water body downstream of the dam Vonarje.

Table 3. Specific Average daily flow modelling results of the future scenarios downstream of Vonarje dam for SUBBASIN 2

Scenario	$Q_{av, month.}$ (m^3/s) av.(min,max)	$Q_{av, month.}$ (m^3/s) dry period April –September) av. (min, max)	$Q_{av, month.}$ (m^3/s) wet period (October– -Marth av. (min, max)
FUTURE 3a[1]	1,48 (0,11;7,44)	1.58 (0,09; 7,42)	1.88 (0,05; 8,92)
FUTURE 3a[2]	1,68 (7,27; 0,14)	2,36 (0,13; 6,97)	1,94 (0,19; 6,26)
FUTURE 3a[3]	1,59 (0,12; 7,68)	1,24 (0,13; 6,23)	1,92 (0,14; 7,68)
FUTURE 3a[4]	1,80 (0,12; 7,84)	1,50 (0,13; 7,89)	2,31 (0,19; 7,30)
FUTURE 3b[1]	1,46 (0,08; 7,40)	1,31 (0,09;5,99)	1,69 (1,10;6,00
FUTURE 3b[2]	1,64 (0,11; 7,25)	1,29 (0,11;6,95)	1,98 (0,17;6,42)
FUTURE 3b[3]	1,55 (0,11; 7,62)	1,89 (0,12;6,16)	1,93 (0,13;7,62)
FUTURE 3b[4]	1,76 (0,11; 8,21)	1,26 (0,11;7,35)	2,26 (0,19;7,28)

Hydrological analyses do not significantly indicate a trend of decreasing mean monthly flows, but they indicate a trend of increasing mean minimum flows, with significant extremes of their minimum and maximum values occurring. It is especially important for dry period (average: 1,24 m^3/s – 2,36 m^3/s and minimum 0,09 m^3/s).

The presented research contributes to the knowledge and understanding of climate change impacts using long-term predictions of six different RCMs on the level of local river basin quantity (river flow) and quality (sediment load, total nitrogen load, and total phosphorus load) states of surface waters.

The application of the developed methodology has proven to be appropriate for the Sutla River Basin case study.

In the future work, the available limited data on river basins related to biological data and climate change impact modeling results by the SWAT model (hydrological data, sediment, and nutrient data), will be widely presented. On the base of the hydraulic parameters, biotic and abiotic parameters for fish species *Barbus balcanicus* - barbel (bioindicator) it will be able to correct daily stream flow downstream of the dam Vonarje and proposed E-flow for the future scenarios for dry and wet period. Using the holistic approach, linking hydrological, morphological, and ecological characteristics based on exploring the Sutla River and its biological communities, the E-flow for the present status has been defined for the profile downstream of the dam [1]. The E-flow for the profile on the Sutla River was defined by linking sediment and nutrient pressures, and hydrological, hydraulic, morphological, and ecological characteristics based on the research of the Sutla River and its biological communities.

The consequences of flow regime change are manifold. Related water quantity and water quality (ecological and chemical water status) issues can provoke socio-economic and environmental problems [5]. In particular, river ecosystem health and the provision of ecosystem services are threatened as further modifications of natural flow patterns will make species more vulnerable to extinction. Freshwater ecosystems might somehow adapt to the new conditions and probably find a new equilibrium. However, Schneider C. et al., 2013 [6] emphasized that, according to ecological impact analyses quoted, this will presumably be accompanied by a loss in biodiversity, at which especially endangered and specialized species could become extinct or be replaced by invasive species. At some point, thresholds could be crossed with unforeseeable consequences for mankind as presented in the paper by Jenkins M., 2003 [7]. In the paper, Schneider C. et al., 2013 [6] show that the need for E-flow actions is further increasing under climate change, and various effects of climate change need to be considered. To reduce further stress on river ecosystems, it is necessary to involve adaptive E-flow management.

5 Conclusion

The application of the developed methodology, presented in this paper, has proven to be appropriate for the Sutla River Basin case study. This method enables broader acquisition of basic knowledge, which includes natural processes and sources of pollution, analysis of the eutrophication process, and decreasing the risk of eutrophication by selecting the optimal set of mitigation measures. The presented research suggests the necessity of a holistic approach to E-flow assessment under the impacts of climate change as an additional measure of WFD. The holistic approach defines the E-flow for a profile on the Sutla River by linking hydrological, morphological, and ecological characteristics based on the exploration of the Sutla River and its biological communities, which makes this research unique. The full implementation of a holistic approach to the E-flow definition requires the enhancement of exploratory hydrological and biological monitoring that enables the use of habitat modeling. The environmental objectives of WFD achievement must be guaranteed by appropriate flow, sediment regime, and hydromorphology.

The presented research contributes to the knowledge and understanding of climate change impacts using long-term predictions of eight future climate change scenarios with six models and six different RCMs at the level of local river basin quantity (river flow) and quality (sediment load, total nitrogen load, and total phosphorus load) states of surface waters. The detailed research of the proposed methodology for E-flow assessment downstream of the Sutla River dam under the climate change impact, according to average monthly and annual seasonal values for flow, sediment, total N, and total P with IHAs and biological indicators, which presented in this paper gives a new E -flow holistic assessment under climate change impact.

The shortcomings/uncertainties of this research are the absence of an adequate monitoring system and limited data in the river basin. The implementation of the E-flow of the proper monitoring system is the recommendation for policymakers and stakeholders.

Acknowledgements

The research for this article and the publication of this article were partially supported by the University of Rijeka projects 23-67 and 23-74.

References:

[1] Ćosić-Flajsig, G., Vučković, I., Karleuša, B.: An Innovative Holistic Approach to an E-flow Assessment Model, Civil Engineering Journal, 6, 11, 2188-2202, doi: 10.28991/cej-2020-03091611, 2020.

[2] Ćosić-Flajsig, G., Karleuša, B., Glavan, M.: Integrated Water Quality Management Model for the Rural Transboundary River Basin - A Case Study of the Sutla/Sotla River, Water, 13, (18); 2569, 27, doi:10.3390/w13182569, 2021.

[3] Gopal B.: Methodologies for the Assessment of Environmental Flows, Environmental Science, Chapter 6, Corpus ID: 30973406, 2013.

[4] Mrakovčić, M., Kriteriji za određivanje održivog protoka na temelju ribljih zajednica, Dokumentacija Elektroprojekt d.d. Zagreb, 41 str., 2000.

[5] Cowx, I. G., Welcomme L. R.: Rehabilitation of rivers for fish. Published by arrangement with the Food and Agriculture Organization of the United Nations (FAO) by Fishing News Books, A division of Blackwell Science Ltd. Editioral Offices: Osney Mead, Oxford OX2 OEL, 25 John Street, London WC 1 N 2BL, 260 str., 1998.

[6] Schneider, C., Laize, C. L. R., Acreman, M. C., and Flörke, M.: How will climate change modify river flow regimes in Europe? Hydro.Eart.Syst. Sci. 17, 325-339., 2013.

[7] Jenkins, M.: Prospects for biodiversity, Science, 302, 1175–1177., 2003.

TESTING THE PARAMETERS OF TWO-DIMENSIONAL HORIZONTAL DISPERSION PHENOMENON IN THE COASTAL ZONE

PIOTR ZIMA [1],

[1] *Gdansk University of Technology, Faculty of Civil and Environmental Engineering, Poland, piotr.zima@pg.edu.pl*

1 Abstract

The paper analyzes the numerical solution of the two-dimensional dispersion equations in the coastal zone for the dispersion coefficients adopted for the gradient and drift velocity profiles. And then it was assessed how it affects the final result. The research was carried out in the Bay of Puck (part of the Gulf of Gdansk in the southern Baltic Sea). It is a shallow bay with an average depth of 3 m, with numerous shoals, no deeper than 1 m. The mouth of the largest stream - Gizdepka - was selected for analysis.

Keywords: coastal waters, migration of pollutants in water, two-dimensional dispersion, mass dispersion, dispersion coefficients

2 Introduction

Environmental pollution is becoming one of the pressing issue of the coming times. It occurs mainly as a result of increased human activity. Transport of pollutants with flowing waters is one of the most common processes in the natural environment. Pollutants are washed out of catchment areas into watercourses and then migrate with the flowing water to the seas and oceans. Physical processes (or rather transformations) refer to changes in physical properties associated with the state of fragmentation of a given substance.

In general, this process is described by a system of differential equations, including the continuity equation, dynamic equations (Reynolds - because it practically always concerns turbulent flow), pollutant transport equations and equations of state (e.g. [1]). They are mathematically and physically complex. For these reasons, simplified models are of great importance. For the problem of pollutant migration in the coastal zone analyzed in this paper, a two-dimensional model is particularly useful because the velocity and concentration profile is vertically averaged. The final form of the two-dimensional planar contaminant migration equations is given below.

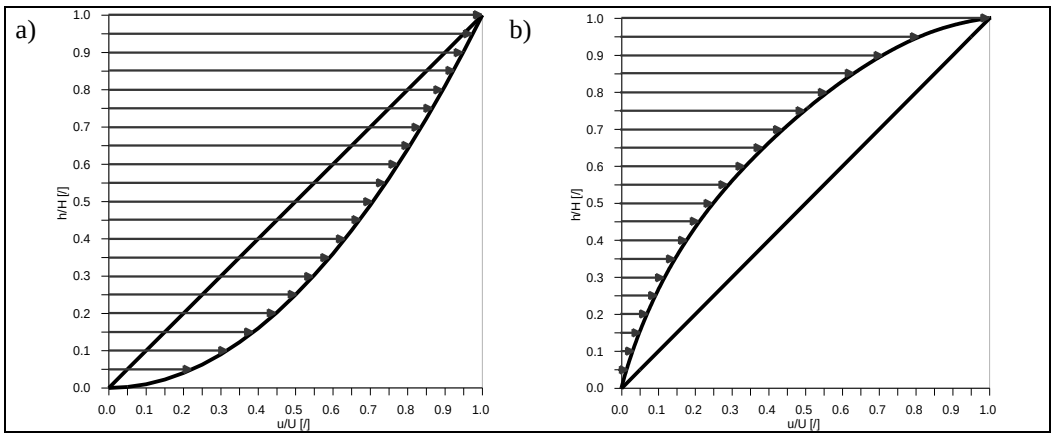

Figure 1. Vertical velocity profile: a) for gradient flow, b) for drift flow, where u [m/s] is the velocity which which varies from 0 to U, and h [m] is the depth, which varies from 0 to H.

When we discuss about flows in the coastal zone, there are two general types of profiles:
– gradient profile – when the flow is caused mainly by the component of gravity and/or by variable external pressure; the vertical distribution of horizontal velocity is exponential and the function describing it is convex (in the mathematical sense) - Fig.1a;
– drift profile – when the main driving force of the flow are shear stresses acting on the free surface; the basic case here is the movement of water caused by wind; the velocity profile in such a situation is rather diverse and similar to the concave function - Fig.1b. This also applies to cases where reverse currents are seen at the bottom, as in estuaries. The drift current in deeper water bodies disappears and changes direction with depth, so it is appropriate to think/consider before using the vertically averaged velocity model in this situation (see, for instance, the Ekman spiral). On the other hand, this might make sense for shallow coastal waters where the water layer's thickness does not surpass that of the Ekman layer ([2]), this could make sense.
The mass dispersion of the solute is a compromise between the appropriateness of using average velocity distributions and the tendency to take into account the impact of the actual differentiation of these distributions. Generally, three methods were commonly used to estimate dispersion coefficients: theoretical analysis, measurements of velocity distributions, and traditional tracer studies. A quantitative model of this process was first presented by Taylor ([3], [4]). As is known, the methods for determining mass dispersion coefficients refer to one-dimensional shear flow in a pipe. Subsequently, Aris [5] presented a theoretical analysis based on the mass concentration moment method, which was extended to generalized theoretical dispersion studies ([6], [7]).
In recent years, numerous field studies have been conducted ([8], [9], [10], [11], [12]) in which this method was used to determine the dispersion coefficients with retrieval velocity distribution data. Another method for calculating two-dimensional dispersion parameters is a method based on measuring the concentration distribution of the mass of a non-degradable solute, in which either the previously mentioned method of moments or tracer survey tracing techniques are applied to the measured concentration distribution curves ([13]). The method of moments has often been used to calculate transverse dispersion coefficients from tracer studies that were performed under steady-state conditions ([14], [15], [16], [17], [18]).

3 Methods

3.1 Analytical study

For the problem of pollutant migration in the coastal zone analyzed in this paper, a two-dimensional model is particularly useful because the velocity and concentration profile is vertically averaged. This equation can be written in the following form [13]:

$$\frac{\partial\left(h\bar{c}\right)}{\partial t}+\frac{\partial\left(h\overline{u_x}\bar{c}\right)}{\partial x}+\frac{\partial\left(h\overline{u_y}\bar{c}\right)}{\partial y}=\frac{1}{h}\frac{\partial}{\partial x}\left(hD_{xx}\frac{\partial\bar{c}}{\partial x}+hD_{xy}\frac{\partial\bar{c}}{\partial y}\right)+\frac{1}{h}\frac{\partial}{\partial y}\left(hD_{yx}\frac{\partial\bar{c}}{\partial x}+hD_{yy}\frac{\partial\bar{c}}{\partial y}\right) \tag{1}$$

where: x [m], y [m], t [s] - independent variables (spatial and time), h [m] – depth, $\bar{c}$ [kg/m^3]– depth-averaged concentration, $\overline{u_x},\overline{u_y}$ [m/s] – depth-averaged components of the velocity vector, D_{xx}, D_{xy}, D_{yx}, D_{yy} [m^2/s] – coordinates of the dispersion tensor **D**:

$$[\mathbf{D}]=\begin{bmatrix}D_{xx} & D_{xy}\\ D_{yx} & D_{yy}\end{bmatrix} \tag{2}$$

Due to the transverse isotropy of the dispersion process, the D_{ij} coefficients are expressed by local dispersion coefficients along the direction of velocity D_L [m^2/s] (longitudinal dispersion coefficient) and in the direction perpendicular to it D_T [m^2/s] (transverse dispersion coefficient):

$$\begin{aligned} D_{xx} &= D_L n_x^2 + D_T n_y^2 \\ D_{xy} &= D_{yx} = (D_L - D_T) n_x n_y \\ D_{yy} &= D_L n_y^2 + D_T n_x^2 \end{aligned} \tag{3}$$

where n_x [/] and n_y [/] are the coordinates of the **n** vector - cosines of the velocity vector **u**:

$$n_x = \frac{\overline{u_x}}{|\mathbf{u}|}, n_y = \frac{\overline{u_y}}{|\mathbf{u}|} \tag{4}$$

The velocity field is determined from the fluid dynamics equations, with several versions available.
The idea of solute mass dispersion is a compromise between the appropriateness of using average velocity distributions and the tendency to take consider the impact of the actual differentiation of these distributions. We owe a quantitative model of this process to Taylor ([3], [4]). In practice, for the free-surface flows in the coastal zone that interest us here, so the D_L and D_T coefficients are determined according to the classical proposal [19]:

$$D_L = 5{,}93hu*, \quad D_T = 0{,}23hu* \tag{5}$$

where $u*$ [m/s] – shear velocity, which can be related to the bottom stress τ_d [N/m^2] and density ρ [kg/m^3] or to the average velocity $\bar{u}$ and drag coefficient C_d [/] or using Manning's equation:

$$u* = \sqrt{\frac{\tau_d}{\rho}} = \bar{u}\sqrt{\frac{C_d}{2}} = \frac{\sqrt{g}n\bar{u}}{h^{1/6}} \tag{6}$$

where g [m/s^2] is acceleration due to gravity, n [s/m$^{1/3}$] is Manning's roughness coefficient. Dependencies (6) were derived for a regular open riverbed. In actuality, the constant multipliers in these formulas depend on the particular case and range from 30 to 3000 (for D_L) and 0.15 to 3 (for D_T) when other conditions of pollution propagation are taken into account (e.g., estuary sections of rivers or coastal zone) and the shape of the bottom system becomes more complicated ([18]). Often, these multipliers are identified based on observations of the considered system, but their values depend on the shape of the vertical velocity profile.

3.1.1 Determination of the dispersion coefficient for gradient flow

The procedure proposed by Taylor [4] and the chosen kinds of the velocity profile enable derivation of the coefficients on demand by means of some rather standard mathematical operations. For this reason in this paper only the final results are presented.
For gradient type profile:

$$u = h^{1/k} \tag{7}$$

where: u is one-dimensional velocity and $k = k_G$ is natural number. Its graph (Fig.1a) is convex up with respect to the transitional line $u = h$ (i.e. when $k_G = 1$). It seems ([20]), that as a basic version one should assume, that $k_G = 7$ (known velocity distribution, called "1/7 profile"). Coefficient of longitudinal dispersion for the gradient type flow D_{LG} can be calculated from the following equation [4]:

$$D_{LG} = \frac{\left(\frac{(k_G+1)}{4k_G^2 \cdot (4k_G+1)}\right) \cdot h^{4/3} \cdot u}{g \cdot n^2} \tag{8}$$

3.1.2 Determination of the dispersion coefficient for drift flow

For drift type profile ($k = k_D$ – natural number):

$$u = h^k \tag{9}$$

(with convex down graph – Fig.1b). When one hasn't closer information about the shape of this line, making use of the turbulent Couette flow ([21]) it is reasonable to assume, that $k_D = 5$. Coefficient of longitudinal dispersion for the drift type flow D_{LD} can be calculated from the following equation [4]:

$$D_{LG} = \frac{\left(\frac{k_G^2}{2\cdot(3k_G+2)}\right)\cdot h^{4/3}\cdot u}{g\cdot n^2} \tag{10}$$

3.2 Model of velocity distribution

For the velocity distribution was used Ekman model. This model is recommended for shallow sea waters [22]. In this model, the components of the water velocity vector field are calculated based on the wind speed:

$$|\mathbf{u}| = 0.0106\cdot|\mathbf{w}|_{10}^{1.5}\cdot h^{-0.5} \tag{11}$$

where: $\mathbf{u} = (u_x, u_y)$ [m/s] – two-dimensional vector of surface water velocity (towards the wind), $\mathbf{w} = (w_x, w_y)$ [m/s] – two-dimensional vector of wind velocity at a height of 10 m, x,y – space coordinates. By applying Eq.11, the steady water velocity distribution for given wind conditions can be calculated.

3.3 Study site

The research was carried out in the Gulf of Gdansk. Particularly convenient in terms of the conditions of the two-dimensional model is its part, namely the Bay of Puck. The Bay of Puck is the western branch of the Gulf of Gdansk in the southern Baltic Sea, separated from the open sea by the Hel Peninsula. It is a shallow bay with an average depth of 3 m, with numerous shoals, no deeper than 1 m. The waters of several agricultural or urban-agricultural streams and rivers flow into the Bay of Puck. The most important is Gizdepka. A mathematical model of coastal waters in the area of the Bay of Puck was made (Fig.3).

Figure 2. Study site.

3.4 Meteorological conditions

The hydrodynamic conditions in the Gulf of Gdansk depend largely on meteorological conditions, mainly on the direction and speed of the wind. For the purpose of this study, meteorological data from the last 15 years were analyzed from a meteorological station located in Gdansk, near the analyzed area. The average wind speed of 5 m/s was used for calculations.

3.5 Numerical study

Original programs were used for doing mathematical modelling ([23], [24]). The partial differential equation must be solved in order to solve the equations for shallow water flow and solute mass transport. In this project, will be used the Finite Volume Method (FVM) [25], and a continuous area (domain) of the solution was discretized and covered with a mesh of triangular elements (Fig.3). Applied to solve the unsteady equation, the FVM refers to physical conservation laws on the level of control volumes. This can be described by the homogeneous hyperbolic equation [25]:

$$\frac{\partial \mathbf{U}}{\partial t} + \nabla \cdot \mathbf{F} + \mathbf{S} = 0 \tag{12}$$

where: **U** – is vector of dynamic variables, **F** – is mass and momentum flux vector, **S** – is vector of source elements. As a result of the integration of Eq.12 in each finite volume *i* and the application of the Gauss-Ostrogradski theorem, we get the equation:

$$\frac{\partial \mathbf{U}_i}{\partial t}\Delta A_i + \oint_{L_i}(\mathbf{F}\cdot\mathbf{n})dL + \int_{\Delta A_i}\mathbf{S}dA = 0 \tag{13}$$

where: ΔA_i, L_i – is area [m^2] and length [m] of the edge of the cell *i*, **n** [/] – is unit vector (directional).

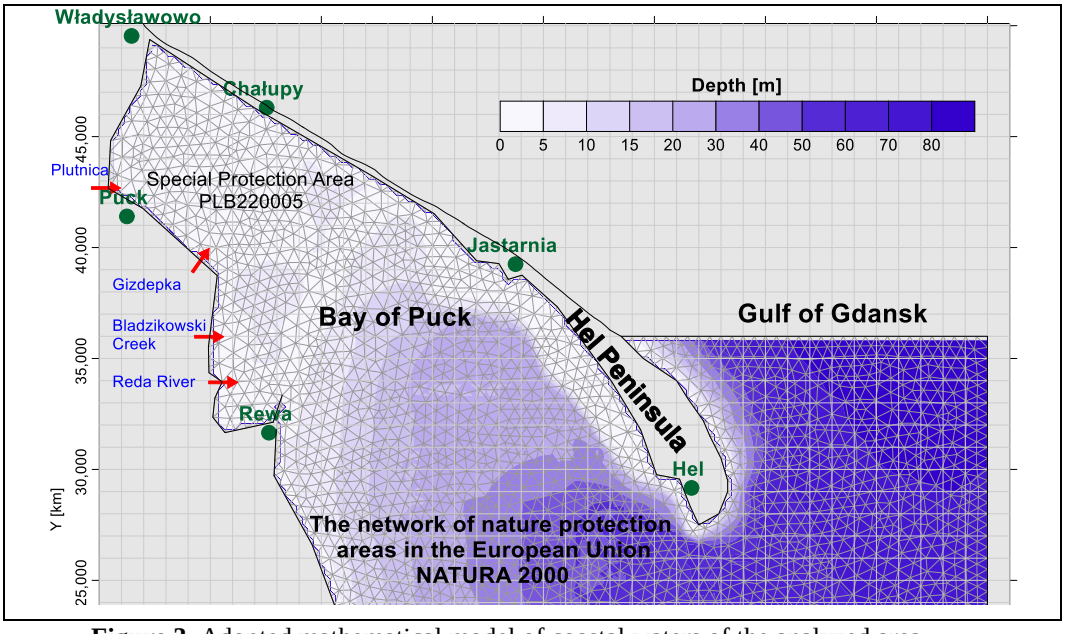

Figure 3. Adopted mathematical model of coastal waters of the analyzed area.

In the method of integrating Eq.13, it was assumed that the control area is the equivalent of a grid cell. This approach means that the values of components of the velocity vector u are given in grid points and the functions of concentration c located in the central points of cells are unknown (Fig.4). The calculation of intermediate values positioned between grid nodes (which are needed in determining the value of fluxes by individual cell edges) was determined by averaging the neighboring values. This approach was applied to the functions of concentration *c*, depth *h* and velocity vector components u_x

and u_y.

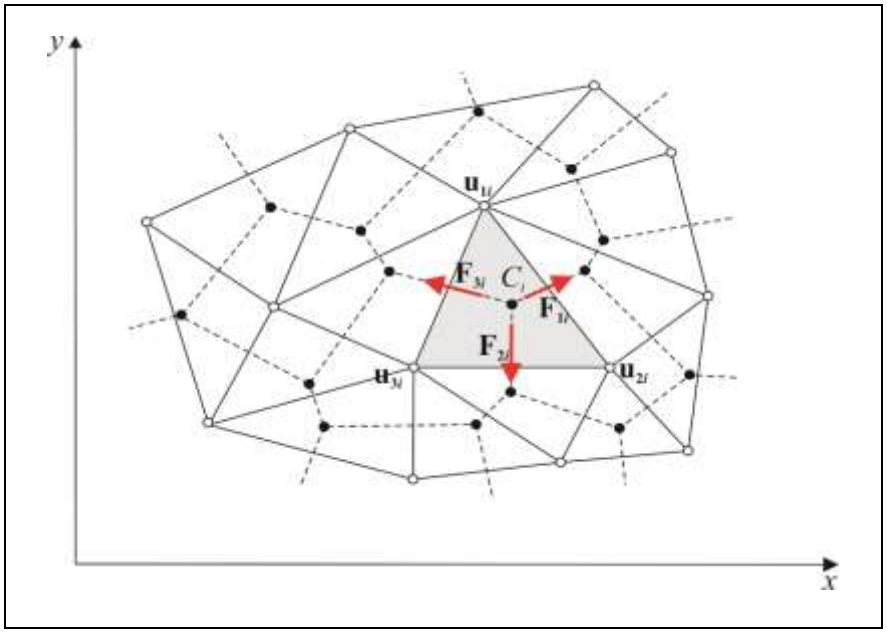

Figure 4. Discretization of the domain into two-dimensional triangular cells and adoption of the parameters of the models used in the numerical solution.

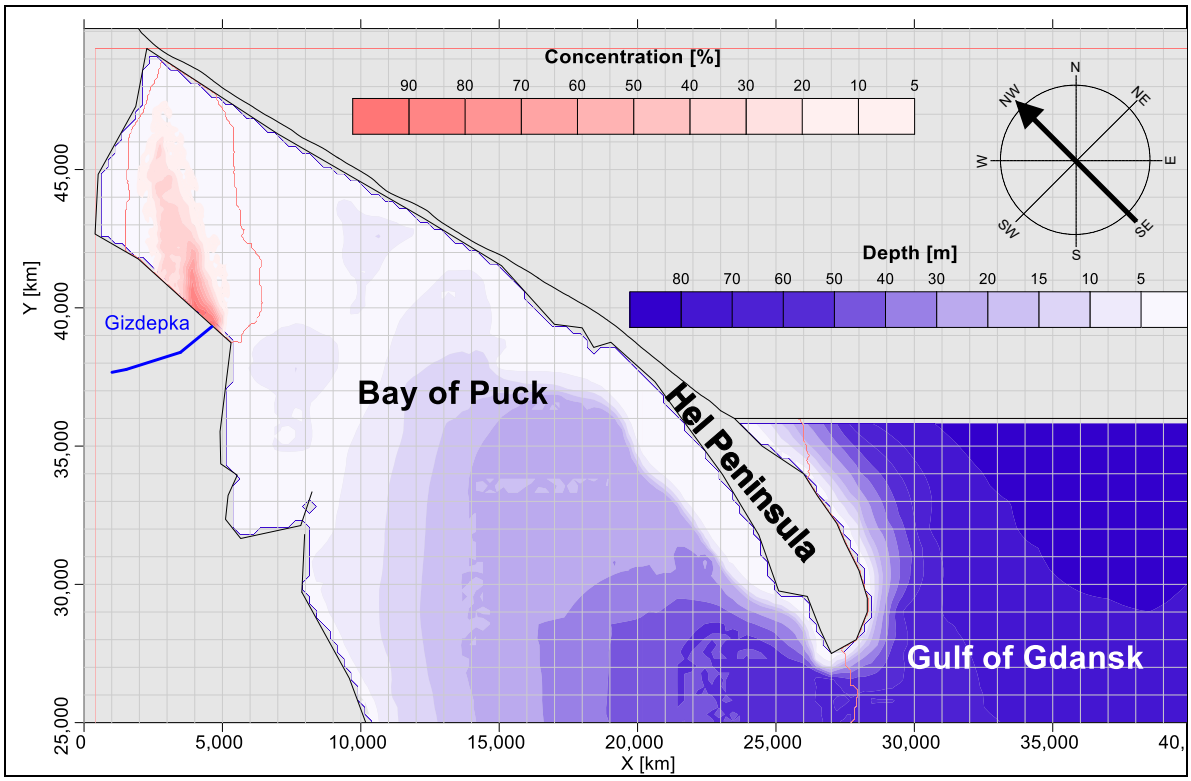

Figure 5. Numerical calculations of the spread of the pollutant flux for the D_{LG} dispersion coefficient and wind from SE direction.

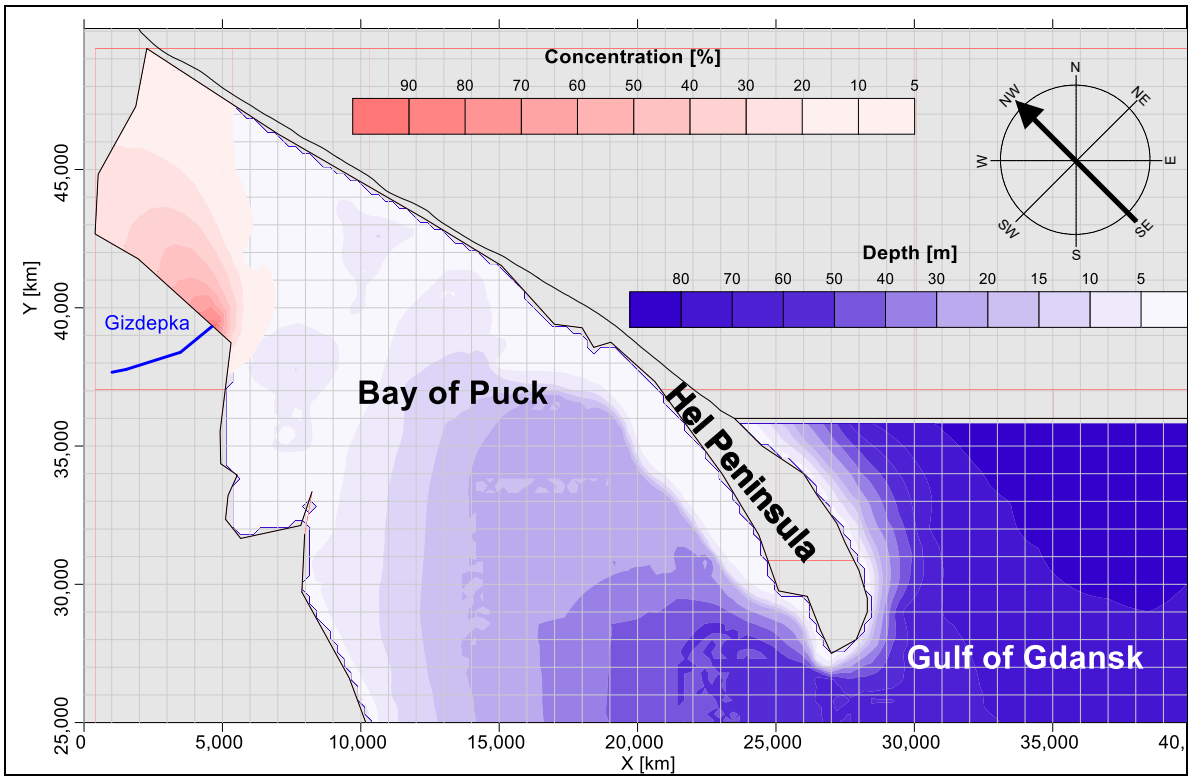

Figure 6. Numerical calculations of the spread of the pollutant flux for the D_{LD} dispersion coefficient and wind from SE direction.

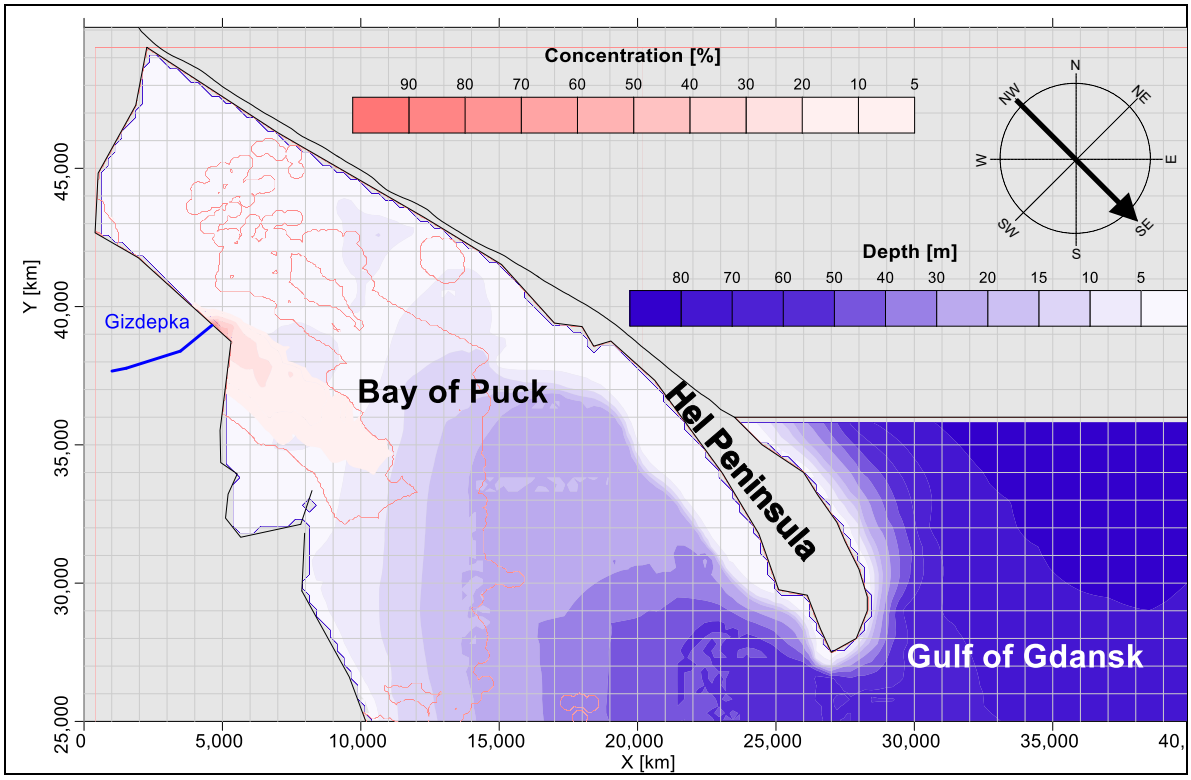

Figure 7. Numerical calculations of the spread of the pollutant flux for the D_{LG} dispersion coefficient and wind from NW direction.

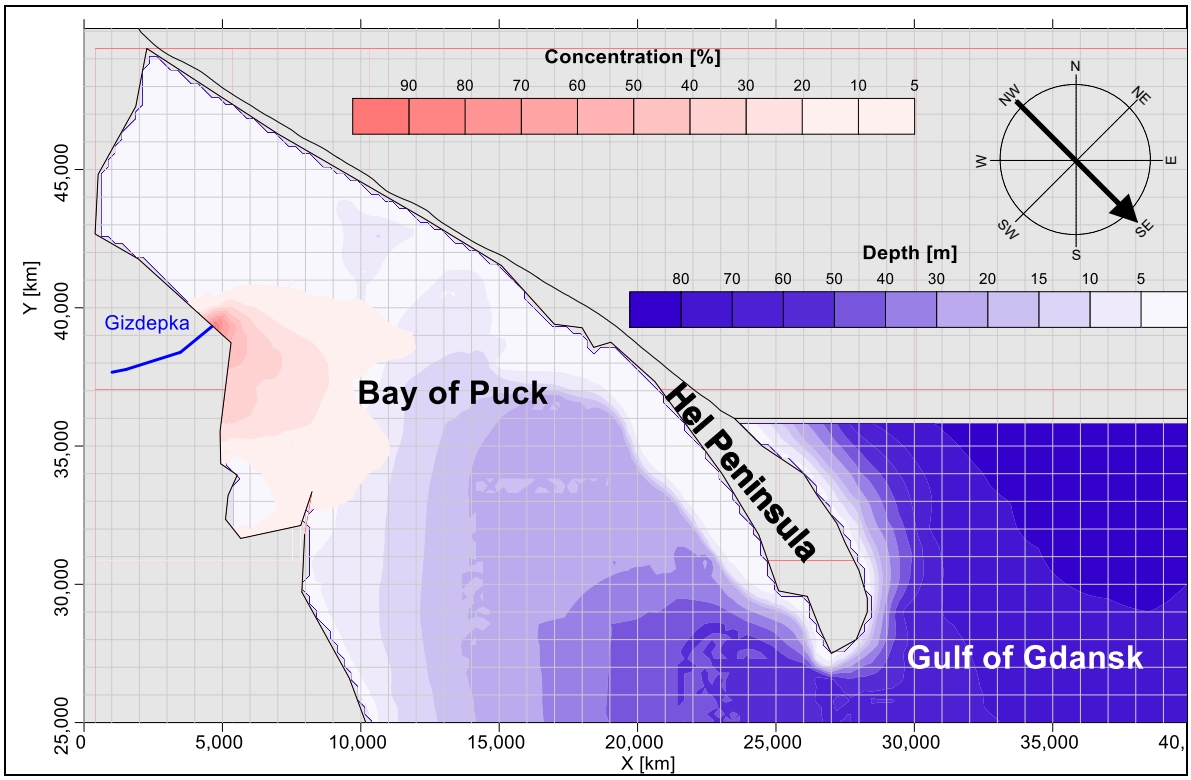

Figure 8. Numerical calculations of the spread of the pollutant flux for the D_{LD} dispersion coefficient and wind from NW direction.

4 Results and discussion

The calculations were carried out for 2 wind condition scenarios resulting from meteorological data and the shape of the Bay: wind from the northwest (NW) and southeast (SE) by 5 m/s. The selection of scenarios was made taking into account the most unfavorable conditions in terms of pollutant migration towards the nearest protected areas. The shape of the bay with respect to the wind direction (for this reason the scenario for NW and SE wind were adopted) were taken into account. The calculations were carried out until the pollution distribution was established, but no longer than 24 hours. A gradient and drift velocity distribution was assumed for each scenario. Then, the longitudinal dispersion coefficient was calculated for both profiles. For depth h = 1 m and n = 0.01, the velocity modulus values were equal to 0.12 m/s (Eq.11), D_{LG} = 0.17 (Eq.8), D_{LD} = 89.94 (Eq.9). The results are presented in Fig.5 (for the wind from NW, for D_{LG}) and in Fig.6 (for the wind from NW, for D_{LD}), in Fig.7 (for the wind from SE, for D_{LG}) and in Fig.8 (for the wind from SE, for D_{LD}). In some cases, the pollutants were "pressed" towards the shore, and their range was limited and depend very much on the dispersion coefficient and, consequently, on the assumed vertical velocity distribution. The flux of pollutants in the case of a gravity profile is compact and pollutes water in a smaller area. In the case of a pollutant flow for a drift profile, it spreads over a larger area. Analyzing the case of the Bay of Puck, pollution in the case of a drift profile covers almost the entire bay and we observe pressure onto the shore. The adoption of a gradient profile does not reveal pressure on the shore. This shows how important a problem is the proper selection of dispersion tensor parameters, especially in shallow coastal waters. Dispersion coefficient values that work in rivers (even wide ones) may not work in estuarine areas.

5 Conclusion

Analyzing the theoretical and numerical calculations should remember, that the essence of the paper is a very simplified methodology of estimation of the longitudinal dispersion coefficient. A very big differentiation of these coefficients for the gradient and drift types of flow results from the character and shape of the vertical distribution of the horizontal advection velocity. The purpose of the paper was formulation of a formally simple, but justified physically, method of determination of these coefficients. The proposed relations were derived making use of known Taylor's procedure, but are based on previous papers ([26], [27], [23], [24]). The velocity profiles were described by especially defined equations. They enable convenient fitting of the shape of this velocity distribution to the individually considered situation (expected or already stated). This is very important because, as the numerical calculations included in the work prove, it has a significant impact on the solution and, consequently, it has a significant impact on the conclusions drawn from these calculations. This is especially important in coastal areas. The adoption of a drift profile in this case may also be dictated by the influence of wind or changes in water density in the coastal zone, where river and sea waters mix.
The results for drift coefficients presented in the paper are consistent with the general shape of the solute distribution similar to that observed in the coastal zone [28, 29].

References:

[1] Slattery, J.C.: Advanced transport phenomena, University Press, Cambridge, 1999.
[2] Ekman, V.W.: On the influence of the earth's rotation on ocean currents, Arch. Math. Astron. Phys. 11, No. 2., pp. 1-51, 1905.
[3] Taylor, G.I.: Dispersion of soluble matter in solvent flowing slowly through a tube, In Proceedings of the Royal Society of London A: Mathematical, Physical and Engineering Sciences, 223, 1953.
[4] Taylor, G.: The dispersion of matter in turbulent flow through a pipe. In Proceedings of the Royal Society of London A: Mathematical, Physical and Engineering Sciences, 223, 1155, p.p. 446-468, 1954.
[5] Aris, R.:, On the dispersion of a solute in a fluid flowing through a tube. Proceedings of the Royal Society of London. Series A. Mathematical and Physical Sciences, 235(1200), 67-77, 1956.
[6] Gill, W. N.: A note on the solution of transient dispersion problems. Proceedings of the Royal Society of London. Series A. Mathematical and Physical Sciences, 298(1454), 335-339, 1967.
[7] Wang, P., Chen, G. Q.: Solute dispersion in open channel flow with bed absorption. J. Hydrol, 543, 208-217, 2016.
[8] Carr, M. L., Rehmann, C. R.: Measuring the dispersion coefficient with acoustic Doppler current profilers. Journal of Hydraulic Engineering, 133(8), 977-982, 2007.
[9] Shen, C., Niu, J., Anderson, E. J., Phanikumar, M. S. Estimating longitudinal dispersion in rivers using Acoustic Doppler Current Profilers. Advances in Water Resources, 33(6), 615-623, 2010.
[10] Kim, D.: Assessment of longitudinal dispersion coefficients using Acoustic Doppler Current Profilers in large river. Journal of Hydro-environment Research, 6(1), pp. 29-39, 2012.
[11] Erwin, S. O., Jacobson, R. B.: Influence of Channel Morphology and Flow Regime on Larval Drift of Pallid Sturgeon in the Lower Missouri River. River Research and Applications, 31(5), 538-551, 2015.
[12] Pilechi, A., Mohammadian, A., Rennie, C. D., Zhu, D. Z.: Efficient method for coupling field data and numerical modeling for the estimation of transverse mixing coefficients in meandering rivers. J Hydraul Eng, 142(6), 04016009, 2016.
[13] Fisher, H. B., List, E. J., Koh, R. C. Y., Imberger, J., & Brooks, N. H.: Mixing in inland and coastal waters. New York, NY: Academic Press, 1979.
[14] Yotsukura, N., Fischer, H. B., Sayre, W. W.: Measurement of mixing characteristics of the Missouri River between Sioux City, Iowa, and Plattsmouth, Nebraska (No. 1899-G). USGS, Washington, DC, 1970.
[15] Sayre, W. W.: Shore-attached thermal plumes in rivers. In: Modelling in Rivers., Wiley-Intersc., London, 15.1-15.44, 1979.
[16] Beltaos, S.: Transverse mixing tests in natural streams. J. Hydraul. Div, Am. Soc. Civ. Eng.,

106(10), 1607–1625, 1980.
[17] Holley Jr, F. M., Nerat, G.: Field calibration of stream-tube dispersion model. J. Hydraul. Eng. 109(11), 1455-1470, 1983.
[18] Rutherford, J. C.: River mixing. New York, NY: Wiley, 1994.
[19] Elder, J. W.: The dispersion of marked fluid in turbulent shear flow. Journal of Fluid Mechanics, 5, p.p. 544–560, 1959.
[20] Prandtl, L: Fuehrer durch die Stroemungslehre, F. Vieweg und Sohn, Braunschweig, 1949.
[21] Schlichting, H.: Boundary layer theory, McGraw-Hill Book Comp., New York, 1979.
[22] Duke, P.: Coastal and shelf sea modelling, The Kluwer International Series: Topics in Environmental Fluid Mechanics. Springer Science+Business Media, LLC, 2001.
[23] Zima, P.: Modeling of the Two-Dimensional Flow Caused by Sea Conditions and Wind Stresses on the Example of Dead Vistula. Pol Marit Res 97, p.p.166-171, 2018.
[24] Zima, P.: Simulation of the impact of pollution discharged by surface waters from agricultural areas on the water quality of Puck Bay, Baltic Sea. Euro-Mediterr. J. Environ. Integr. 4:16, 2019.
[25] LeVeque, R.J.: Finite Volume Method for Hyperbolic Problems. Cambridge University Press, New York, 2002.
[26] Sawicki, J.M., Zima, P.: The Influence of Mixed Derivatives on The Mathematical Simulation of Pollutants Transfer, 4th International Conference on Water Pollution, Bled, Slovenia, pp. 627–635, 1997.
[27] Zima, P.: Mathematical Modeling of the Impact Range of Sewage Discharge on the Vistula Water Quality in the Region of Włocławek. In: Kalinowska M, Mrokowska M, Rowiński P (eds) Free Surface Flows and Transport Processes. GeoPlanet: Earth and Planetary Sciences. Springer, Cham, p.p. 489-502, 2018.
[28] Burdziakowski P., Zima P., Wielgat P., Kalinowska D.: Tracking Fluorescent Dye Dispersion from an Unmanned Aerial Vehicle, Sensors, 21, 3905, 2021.
[29] Johansen, K., Dunne, A.F., Tu, YH. et al.: Dye tracing and concentration mapping in coastal waters using unmanned aerial vehicles. Sci Rep 12, 1141, 2022.

IMPACTS OF MAN-MADE STRUCTURES ON FLOOD WATER REGIME OF THE TOPONIČKA RIVER IN SERBIA

ALEKSANDRA ILIĆ[1], DRAGAN RADIVOJEVIĆ[2], BORKO RADIVOJEVIĆ[3], ILIJA ILIĆ[4]

1 Dr., Assistant Professor, Faculty of Civil Engineering and Architecture Niš, Serbia, aleksandra.ilic@gaf.ni.ac.rs

2 Dr., Assistant Professor, Faculty of Civil Engineering and Architecture Niš, Serbia, dragan.radivojevic@gaf.ni.ac.rs

3 MSc, PhD candidate, Faculty of Civil Engineering and Architecture Niš, Serbia, borko.radivojevic@yahoo.com

4 MSc, PhD candidate, Faculty of Civil Engineering and Architecture Niš, Serbia, ilija20ilic@gmail.com

1 Abstract

Currently in Serbia, the E-761 highway is under construction which route stretches along the West Morava valley in Western Serbia and crosses several torrential watercourses among which is the Toponička River, very specific due to its geomorphological characteristics. In this paper, the flood flows regime of the Toponička River is analysed for three approaches related to different terrain models and basin areas delineation. The analyses result in computational flow hydrographs. All hydrological models were conducted using the HEC-HMS v 4.11 software. According to presented results it showed that the designed route of the motorway E-761 could present, conditionally speaking "dam" for runoff from the Toponička river basin and changes its direction that moves laterally (left and right) to accumulate along the length of the structure within whole basin.

Keywords: heavy rainfall, flood water regime, man-made impacts, hydrograph, HEC-HMS

2 Introduction

The June 2023 witnessed extremely heavy rainfall events, a heavy stormy period in the Central and East Europe. There was also an extreme stormy period in Serbia. Short duration storms caused floods on torrential watercourses, which spilled out their minor riverbed and flooded agriculture fields and urban areas and caused enormous damage on the infrastructure, objects and land, resulting in human lives lost as well. In 52 municipalities (out of total 198 municipalities in Serbia) the state of emergency was proclaimed, while in the other 40 municipalities the state was very close to proclaim emergency. All torrential watercourses in the region had much greater flow rates than the minor riverbed capacity and they flooded surrounding area.

The Toponička River flows southerly downstream of the regional road 187 and intersects the E-761 highway, which is under construction, at km 40+500. Just before the flood event in June 2023 the Toponička riverbed was in a very bad condition. Nowadays, in addition to the low and tall vegetation, there is also a lot of debris and waste in the riverbed of the Toponička River, which is most noticeable at the downstream part of the stream. At the station about 1,200 m upstream of its confluence with the West Morava, the riverbed is completely filled with debris, waste and mud [1].

In this paper, the computational floods of Toponička River basin are estimated based on the design storms in HEC-HMS v 4.11 software. This model was applied to three basin models created on different approaches. The first approach refers to the delineation of the basin using digital terrain model (DEM) and topographic maps. The second approach takes into account all the sub-basins obtained based on consideration of the water pathways. Finally, the third access overlooks the Toponička River basin to the E-761 highway route.

3 Methods

3.1 Study area and input data

The Toponička River is the left tributary of the West Morava River (Figure 1).

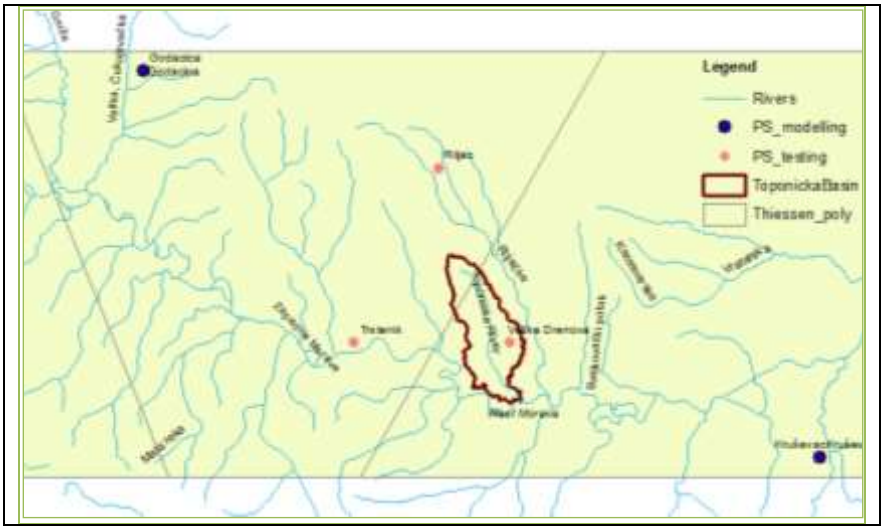

Figure 1. The Toponička River Basin with considered precipitation stations and Thiessen polygons [1]

Flood hydrograph assessment depends on whether hydrological measurements are available on a given river or not and is usually based on the event modelling, when the interception and evapotranspiration can be neglected in comparison to runoff during a relatively short time of simulation [2]. The Toponička River basin is ungauged and the hydrographs are estimated according to precipitation data from Republic Hydro Meteorological Service (RHMS) of Serbia.

The rainfall data submitted from the RHMS of Serbia for the 2 precipitation stations (PS) in the region have been used to estimate the flood peak values, observed yearly maximum of daily precipitation sum (YMDP) at the PS Kruševac and PS Godačica presented with blue dots in Figure 1.

Table 1 presents theoretical values of daily precipitation maxima.

Table 1. Theoretical values of daily precipitation maxima at selected PS

PRECIPITATION STATION	ALTITUDE (M.A.S.L)	$H_{DAY,1\%}$ (MM)	$H_{DAY,2\%}$ (MM)	$H_{DAY,5\%}$ (MM)	$H_{DAY,10\%}$ (MM)	PERIOD	DISTRIBUTION LAW
Kruševac	166	82	74.86	65.33	57.97	1961-2022	Gumbel
Godačica	295	96.7	87.62	75.51	66.15	1961-2021	Gumbel

Thiessen polygons were created. Polygons are area-based weighting scheme that assumes the precipitation measured at the gauge to be constant in the area associated with that gauge (Figure 1).

The rain duration-depth-occurrence probability curves are taken from PS Kruševac which also represents the main precipitation station (MPS) with continually records of rain depth. According to them the reduction curve was constructed (Figure 2) like it was explained in Section 3.2. This curve enables the approximation of short duration rainfall.

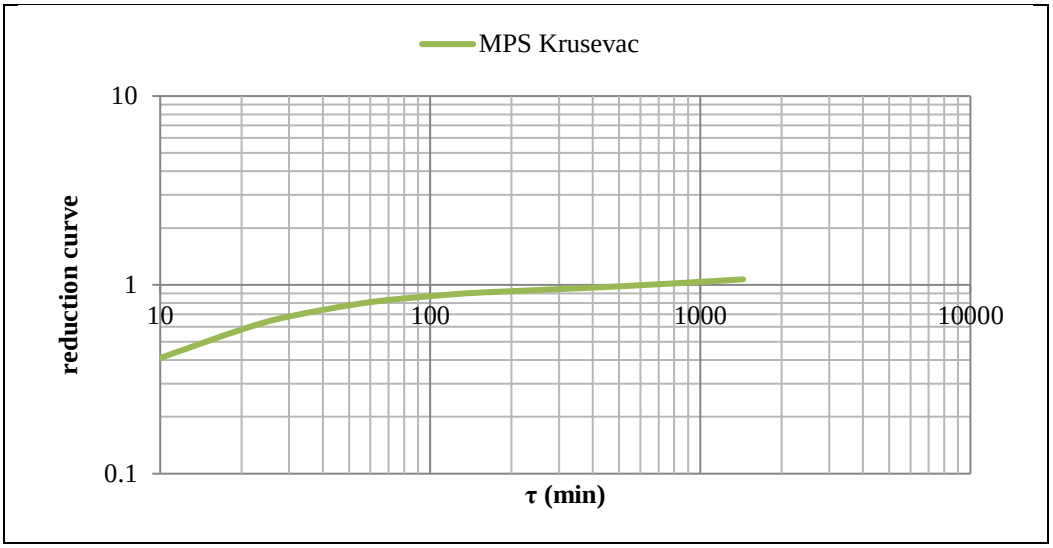

Figure 2. The reduction curve of MPS Kruševac

3.2 HEC-HMS Modelling

The way of simulating the runoff process with a mathematical model depends on the problem we need to solve. Three main components of the rainfall–runoff simulation for computational flood estimation in small river basins model should be defined first: basin model, meteorological model and control specifications. The basin model represents the basin characteristics and the methods of computing different basin processes, meteorological model describes the precipitation input and the methods for calculating snow melt and evapotranspiration, and the control specifications define the modelling time frame and time step [2].

The first step in HEC-HMS model development was terrain pre-processing which results in development of additional grid and vector datasets that describe drainage pattern of the basin and allows for stream and sub basin delineation. HEC-HMS pre-processes the digital elevation model (DEM), in this case the EU-DEM was used, which represents surface model (DSM) of EEA member and cooperating countries representing the first surface as illuminated by the sensors.

Subsequently, the following steps were applied [3]:

Reconditioning and pre-processing sinks: The Pre-processing Sinks step creates a depression less DEM. This step helps to assure that positive drainage will occur throughout the basin. The results of this step need to be scrutinized since large depressed areas may in fact exist and may influence the amount of runoff to a given location.

Preprocess Drainage: This step consists of Flow Direction Creation and Flow Accumulation Creation. The Flow Direction step (Figure 3) creates a flow direction grid by determining the direction of steepest descent for each cell. This step essentially creates the flow paths.

The Flow Accumulation step (Figure 4) determines the number of upstream grid cells flowing to a given grid cell. By knowing the size of the grid cell (which is constant for a given study) and the number of grid cells flowing to any point, the drainage area to that point is computed by multiplying the number of contributing grid cells and the cell size.

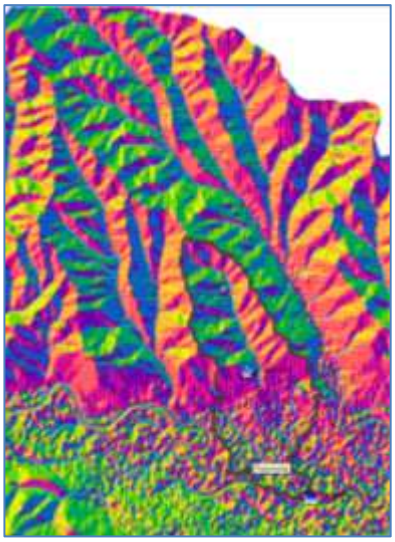

Figure 3. Flow Direction

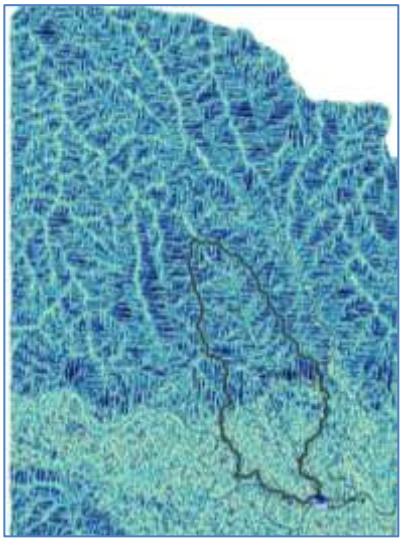

Figure 4. Flow Accumulation

Stream Identification: This step identifies the stream segments (links between tributary junctions) using the flow direction (Figure 5).

Elements delineation: In this sub-basin drainage areas are created according to user defined Break Points. Each stream can have its own drainage area (Figure 5).

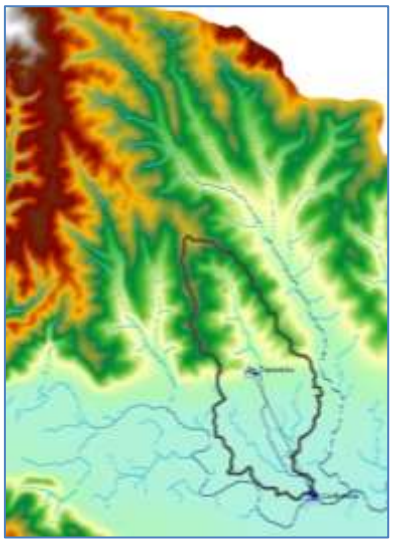

Figure 5. Stream Identification and Elements delineation in HEC-HMS model

The second step is associated with flood flow estimation which depends on data availability, size and quality.

So far, there is no standardized methodology for assessing floods on the hydrological ungagged basins in Serbia. In nowadays hydrologic practice is the most often combination of methods for assessing flood flows is synthetic unit hydrograph and SCS-CN method for separation of the effective from total precipitation. Usually attention is paid to relations between geomorphology characteristics of the basin and elements of synthetic unit hydrograph: effective rainfall duration (t_k), lag time (t_p), time of concentration (T_c), time to peak of hydrograph (T_p), recession time (T_r), time base (T_b) and peak discharge of unit hydrograph (q_{max}) [4].

Based on measured rainfall, synthetic unit hydrograph is constructed in HEC-HMS. The most commonly used hydrograph type for ungauged basins is dimensionless triangular unit hydrograph.
Starting from the basic equations of the triangular hydrograph method, the maximum hydrograph ordinate- hydrograph peak is:

$$Q_{\max} = \frac{2 \cdot P_{ef} \cdot A}{T_B} = \frac{0.56 \cdot P_{ef} \cdot A}{T_B} \tag{1}$$

or flood flow hydrograph ordinate with probability of occurrence p (%) is determined by expression:

$$Q_{\max} = P_{ef,p} \cdot q_{\max} \tag{2}$$

where:

- P_{ef} – effective rainfall;
- $q_{\max}$ – peak discharge of synthetic unit hydrograph which is determined by equation:

$$q_{\max} = \frac{0.56 \cdot A}{(1+k)(t_p + 0.5t_k)} \tag{3}$$

where:

- A – basin area (km^2);
- k – ratio of time to peak to recession time;
- t_p – lag time (h);
- t_k – applicable effective rainfall duration (h).

Time to peak (T_p) can be expressed in terms of basin lag time (t_p):

$$Tp = t_p + 0.5t_k \tag{4}$$

Time at the end of recession of triangular hydrograph is $Tr = 1.67T_p$, so that the total time base is $T_B = 2.67T_p$.

Lag time is usually defined as the time from the centroid of rainfall to the hydrograph peak. Lindsley, Kohler and Paulhus [5] proposed the following formula:

$$t_p = C_t \left(\frac{LL_c}{\sqrt{s}} \right)^n \tag{5}$$

where:

- C_t – basin storage coefficient based on regional analysis of separated unit hydrographs (1.4 to 1.7 for distances in kilometers);
- L – the main stream distance from the divide to outlet (km);
- L_c – the main stream distance from the outlet to a point opposite to the basin centroid (km);
- s – weighted channel slope (%).

According to research results in Kolubara River basin in the north-western part of Serbia for seven basins, the following formula is defined by Janković [6]:

$$t_p = 0.75 \left(\frac{LL_c}{\sqrt{s}} \right)^{0.37} \tag{6}$$

Later, based on research in the basins of rivers Vučica, Mirna and Topčiderska, Jovanović and Brajković suggested the value of C_t=0.65 [7].

Due to many factors that are present at each basin, the best way to apply such formulas is to derive coefficients from gauged streams or field studies results.

***Theoretical values of rainfall depth**:* Since unstudied area are relatively small, rainfall events that cause flood flows, especially flash floods, usually have durations ranging from few minutes to a few hours. Precipitation station (PS) network is relatively dense (in Serbia), but most rain gauges record daily accumulation of precipitation. The rain duration-depth-occurrence probability curves are available at rain gauge stations that continually record rain depth. These are main precipitation stations (MPS). The curves are usually taken from the nearest MPS to studied outlet or basin gravity centre, and rainfall depth for the storm duration less than one day is determined from [8]:

$$\psi_{\tau,p} = \frac{H_{\tau,p}}{H_{day,p}} or H_{\tau,p} = \psi_{\tau,p} \cdot H_{day,p} \tag{7}$$

where:

- $H_{day,p}$ – theoretical values of maximum daily rainfall for probability p of occurrence on the studied basin;
- $H_{\tau,p}$ – theoretical values of rain of short duration τ for the probability of occurrence p on the studied basin;
- $\psi_{\tau,p}$ – ordinate of reduction curve for high intensity storms.

Effective rainfall (P_{ef}) is obtained using well known equations [9]:

$$d = \left(\frac{1000}{CN} - 10\right)25.4$$
$$P_{ef,p} = \frac{\left(H_{\tau,p} - 0.2d\right)^2}{H_{\tau,p} + 0.8d} \tag{8}$$

where:

- d – runoff loss (mm);
- CN – curve number was estimated taking into account hydrologic, soil conditions and land use types (the CORINE land cover maps 2018) [10].

The third step is referred to model calibration. Since this is hydrological ungauged basin, the model was calibrated based on the regional distribution of specific runoff and hydrograph parameters for the probability of occurrence of 1% and 2% in the entire basin of the Western Morava [11].

4 Results and discussion

Hydrological analyses were conducted for 3 approaches:

1. The Toponička River Basin was delineated according to Digital Elevation Model (EU-DEM) 25 m and topographic maps (the 1:25,000 – scale) (Figures 6 and 7);
2. The Toponička River Basin was divided into five sub basins according to Copernicus EU-DEM 25 m and terrain survey (Figure 9);
3. The Toponička River basin was divided based to the highway E-761 route (Figure 10).

As it is presented at Figure 6, the design floods for the highway facilities design approved by RHMS of

Serbia are defined due to the Toponička River basin area delineated to its crossing with highway according to topographic maps (green line). The DEM shows the basin area was delineated to the confluence with West Morava with basin area of 20 km^2 (Figure 7). This approach was used to calibrate the model parameters as emphasized in Section 3.2.

Figure 6. The Topographic map with Toponička River Basin delineation and E-761 highway route

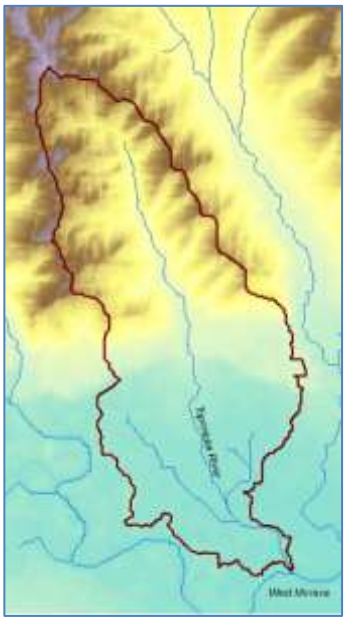

Figure 7. The Toponička River basin

The calibration of the model was preformed due to regional analysis of the specific runoff of the West Morava River basin. The numeric results of calibration are presented in Table 2. Circled in purple at Figure 8 are points representing the specific runoff values of probabilities of occurrence p=1% and p=2%, which the RHMS of Serbia issued for the purposes of designing facilities within the motorway E-761 shown also in Table 2. Circled in maroon are modelled points in HEC-HMS software. The presented graph shows good fit modelled to proposed values.

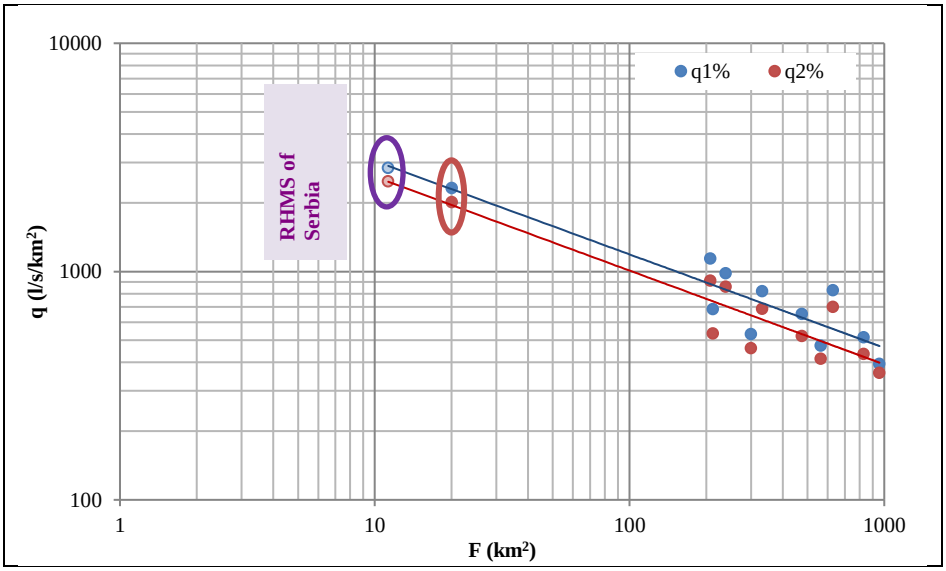

Figure 8. The specific runoff in the West Morava River basin

According to second approach (Figure 9) the Toponička river basin was divided in five subbasins. It can be seen that levees in the lower part of the basin (on the south of the regional road 187) represent in some way a barrier for the inflow of water to the Toponička River and affect the formation of two secondary streams (subbasins 2 and 3). Outflow of subbasin 2 inflows the Toponička River at the north of subbasin 4 and outflow of subbasin 3 enters the Toponička River at the north of subbasin 5.
After construction of the part of highway E-761 its route crosses subbasin 1, subbasin 2 and subbasin 3 (Figure 10). This affects the runoff from subbasins 2 and 3, while the water from subbasin 1 flows smoothly due to the designed bridge at the intersection with the highway.

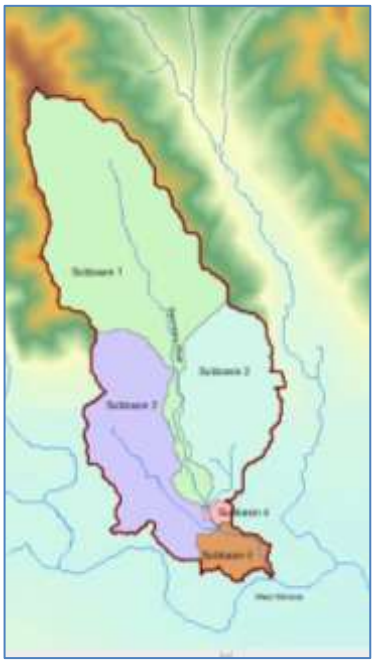

Figure 9. The Toponička River subbasins

Figure 10. The Toponička River basins with highway E-761

The results of implemented procedures for flood flow estimation for *p*=1% and *p*=2% probabilities of occurrence are shown in Table 2.

Table 2. The results of rainfall-runoff modelling in HEC-HMS

PARAMETER	A (km^2)	L (km)	L_C (km)	S (%)	HC	CN	K	t_P (h)	$Q_{1\%}$ (m^3/s)	$q_{1\%}$ ($m^3/s/km^2$)	$Q_{2\%}$ (m^3/s)	$q_{2\%}$ ($m^3/s/km^2$)
APPROACH 1												
HEC-HMS	20.1	11.67	5.53	0.78	B	86.76	1.21	3.67	46.5	2.32	40.39	2.01
RHMZ	11.3								32.1	2.84	28	2.48
APPROACH 2												
Subbasin 1	9.96	9.625	5.595	1.11	B	84.1	1.12	3.215	24.62	2.47	21.13	9.96
Subbasin 2	4.29	4.684	3.043	0.73	B	88.8	1.04	2.125	17.56	4.09	15.3	4.29
Subbasin 3	4.81	5.359	2.575	0.43	B	89.71	1.05	2.315	19.1	3.97	16.7	4.81
Subbasin 4	0.164	0.633	0.211	0.18	B	89.79	1	0.489	1.94	11.81	1.85	0.164
Subbasin 5	0.864	2.742	1.265	0.14	B	90.98	1.01	1.709	4.74	5.49	4.17	0.864
APPROACH 3												
Subbasin 1H	9.448	7.9	4.07	1.5	B	83.73	1.11	2.513	27.87	2.95	23.85	2.52
Subbasin 2H	3.763	3.237	1.678	1.29	B	88.78	1.03	1.338	22.07	5.87	19.23	5.11
Subbasin 3H	1.608	1.74	0.816	2.81	B	87.5	1.015	0.705	13.6	8.46	11.78	7.33

In order to present graphically the results of the simulation in the HEC-HMS and the impact of the E−761 highway on the runoff conditions in the Toponička river basin, Figure 10 shows theoretical hydrographs for all three approaches for 1% probability of occurrence.

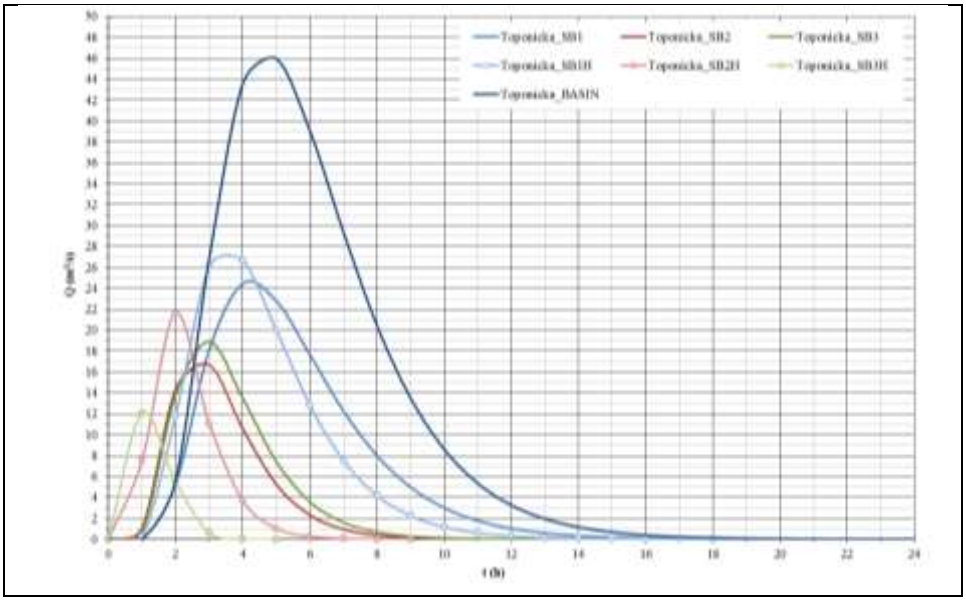

Figure 11. The Toponička River flood hydrographs for 1% probability of occurence

The data presented in Table 3 show the volume balance of the constructed hydrographs for the occurrence probabilities of 1% and 2%. It can be concluded that the data show that the presented highway impact simulation approaches are consistent and numerically give good agreement of the results. The highway is a "dam" that retains about 70% of the total runoff from the basin.

Table 3. Water balance according to flood hydrographs volumes

BASIN	**PROBABILITY**	$Q_{1\%}$	$Q_{2\%}$
		W (m^3)	W (m^3)
TOPONIČKA _BASIN (APPROACH 1)		**886342**	**769051**
SB1		434369	372795
SB2		186362	162469
SB3		218288	190859
SB4		5682	4920
SB5		41486	36497
SUM (APPROACH 2)		**886187**	**767540**
SB1H		409800	350690
SB2H		163304	142281
SB3H		65595	56859
SUM H (APPROACH 3)		**638699**	**549830**

5 Conclusion

The main goal of this paper is to show, through hydrological analysis, the influence of the highway E−761 under construction on flood flows in the Toponička river basin.
Models were created in the HEC-HMS software based on three approaches that were formed according to the method of the basin area delineation (Section 3.2), and the simulation results are explained in detail in Section 4.
It can be concluded that defined approaches to the calculation of flood flows give a good balance agreement (Table 3), so that the physical sense of the models that simulate real processes is confirmed in this way. The results show that 70% of the runoff is formed north of the highway (Table 3) and that it is necessary to pay special attention to the surface water drainage design concept in the area of the E-761 highway within the area of the Toponička river basin.

Acknowledgements
The presented research was carried out as part of the scientific research work financed by the Ministry of Education, Science and Technological Development of the Republic of Serbia according to the contract reg. No. 451-03-65/2024-03/ 200095 and the scientific project O-15-18 SANU, Branch of SANU in Niš.

References:

1. Radivojević, D., Ilić, A., Radivojević, B., Ilić, I.: Technical documentation: Flood water study and analysis of flood events during the month of June 2023 in the valley of the West Morava River on the section of the highway Pojate-Preljina, E761 from km 26+000 to km 42+000, University of Niš, Faculty of Civil Engineering and Architecture, Civil Engineering and Architecture Center, 2023.
2. Ilić, A., Plavšić, J., Radivojević, D.: Rainfall- runoff simulation for design flood estimation in small river catchments, Facta Universitatis, Series: Architecture and Civil Engineering, Vol. 16, No. 2, pp. 29-43, 2018. https://doi.org/FUACE160923003I
3. US Army Corps of Engineers, Hydrologic Engineering Center HEC – HMS User's Manual, 2022.
4. US Army Corps of Engineers, Hydrologic Engineering Center HEC – HMS Technical Reference Manual, 2000.
5. McCuen, R. H.: Hydrologic analysis and design, Pearson Education Inc., Upper Saddle River, New Jersey, 2005.
6. Janković, D.: Proračun velikih voda za neizučene tokove u slivu reke Kolubare, Vodoprivreda, No. 13-14, Beograd (796-799), Srb1971. (In Serbian)
7. Jovanović, S.: Parametarska hidrologija. Jugoslovensko društvo za hidrologiju, Beograd, 1974. (In Serbian)
8. Prohaska, S., Petkovic, T.: Methodology Used for Computing the Flood Wave Hydrograph in Small Ungauged Catchments, International Symposium on Regionalisation in Hydrology, IAHS, Ljubljana, 1990.
9. United States Department of Agriculture. Urban hydrology for small watersheds, TR-55, 1986.
10. Bossard, M., Franec, J., Otahel, J.: Corine Land Cover Techical Guide – Addendum 2000, Technical report No 40, Copenhagen (EEA), 2000.
11. Prohaska, S., Bartoš Divac, V., Ilić, A.: Velike vode Srbije na profilima hidroloških stanica, Institut za vodoprivredu „Jaroslav Černi", Beograd, 2019. (In Serbian)

CONCEPT OF THE WATER MANAGEMENT AND TECHNICAL SOLUTIONS OF SELECTED RESERVOIRS IN THE MORAVA RIVER BASIN

ELIŠKA GRMELOVÁ [1], JAROMÍR ŘÍHA [2], STANISLAV KOTAŠKA [3]

[1*] *PhD student, Brno University of Technology, Veveří 95 Brno 602 00, Czech Republic, Eliska.Grmelova@vutbr.cz*

[2] *professor, Brno University of Technology, Veveří 95 Brno 602 00, Czech Republic, jaromir.riha@vut.cz*

[3] *assistant, Brno University of Technology, Veveří 95 Brno 602 00, Czech Republic, stanislav.kotaska@vut.cz*

**corresponding author*

1 Abstract

Adaptation to climate change is vital for water management. Reservoirs play crucial role in storing water during dry spells and controlling floods. The Water Management Plan for the Czech Republic designated appropriate areas for surface water accumulation. In 2011, only a few areas from this list were selected in the Master Plan "Localities for Accumulation of Surface Waters." From this Master Plan, six reservoirs in the Morava river basin for more detailed technical solutions. These new reservoirs would provide a secured take-off of 2.5 m³/s, hydropower output of 510 kW and a good flood attenuation effect.

Keywords: climate change, protected locality for water storage, water management planning, water reservoir, dam.

2 Introduction

Current climate changes are expected to affect water resources, temperatures, and the frequency of natural extremes. To maintain a favourable water balance, measures must be implemented directly in the river catchments. One of the technical adaptation strategies is to build new water reservoirs. However, to realistically assess the effectiveness of these measures and their interrelationships, integrated tools capable to accurately quantifying the water balance in the hydrological catchment area are required.

Water management plans have been developed since the early days of water usage. With the growth of industry and increased water demands, systematic planning became more widespread. Between 1949 and 1953, the Water management plan (WMP) of the Czechoslovak Republic was created, identifying 581 potential dam sites [1]. In 1975, the update of the WMP was published, providing a more detailed assessment of the selected 581 dam sites. It also included an evaluation of the expected development of water needs and a detailed evaluation of the water management balance, which is directly related to the design of new reservoirs. The adoption of the Directive 2000/60/EC [2] of the European parliament and of the council established a framework for Community action in the field of water policy and was an impulse for new Czech legislation. This Directive emphasized sustainable water management practices and the protection of water resources. Based on the aforementioned Directive [2] was created River Basin District Management Plan (DMP) [3], where the number of locations was reduced to 186.

In 2011 the Ministry of Agriculture and the Ministry of Environment issued the General Plan for Areas Protected for Surface Water Accumulation and Basic Principles for Utilizing These Areas (LASW) [4]. However, this LASW listed only 65 selected sites. During an update in 2020 after the dry spell, the number of selected reservoirs increased to 86 [4]. Table 1 contains an overview of the number of reservoirs according to individual river basins in Czech Republic. It can be seen that the number of protected localities for the surface water accumulation fluctuated over time and after a long-term dry spell in 2018 and 2019 was increased again. This increase reflects the growing recognition of the need for enhanced reliability of water sources in response to changing climate conditions.

Table 1. The numbers of protected localities

River basin	**WMP 1975**	**WMP 2000**	**LASW 2011**	**LASW 2020**
VLTAVA	145	60	23	28
LABE	99	34	13	14
OHŘE	46	16	6	9
MORAVA	122	64	20	30
ODER	45	12	3	5
TOTAL	**457**	**186**	**65**	**86**

Both WMP and LASW contain basic information about individual protected sites, including brief description, maps with outlines of the sites and classification according to the purpose of the scheme. The localities were selected based on their geomorphological, geological, and hydrological suitability for surface water accumulation. Many locations have undergone optimization of their parameters during planning (such as extent of the reservoir area or dam location) to minimize possible potential conflicts.

This paper is focused on expanding the water management and technical concept of potential reservoirs. Six potential reservoirs in the Morava river basin was selected - Borovnice, Kuřimské Jestřabí, Vysočany, Brodce, Plaveč and Bělkovice. The localities of the reservoirs are show in **Chyba! Nenašiel s**

a žiaden zdroj odkazov..

Figure 2. Location of selected reservoirs

3 Methods

The evaluation of the suitability of the planned reservoirs is a complex process that involves numerous aspects, including technical, engineering, environmental, and social factors. Potential function of reservoirs includes water supply function, maintaining minimum discharges downstream of dams, flood attenuation and additional benefits such as hydropower generation, recreation, etc.

For each locality, the solution consisted in the following steps:

- analysis of available documents: information taken from WMP and LASW, engineering geology (geological a hydrogeological maps, database of boreholes), hydrological data, land use, environmental issues and other,
- dam site specification (location of the dam axis, dam type and height),
- basic characteristics of the scheme (reservoir volume, extent of the reservoir area, storage-area-elevation dependence, minimum residual flow),

- hydraulic calculations (bottom outlets, spillway),
- reservoir water management (storage characteristics, water balance, flood attenuation, estimate of hydropower output),
- concept of operation rules for the scheme.

In the following text methodology is always described in general and demonstrated on the example of the Bělkovice reservoir.

3.1 Analysis of available documents

The primary source of information is the WMP and the LASW. Based on these documents, a concept for the hydraulic scheme has been proposed, including its purpose, hydrological characteristics, basic parameters of the dam and the reservoir.
For potential reservoirs preliminary engineering geological survey is available including mapping of mineral deposits.
Important information is also obtained from geological map, hydrogeological map, map of landslides, mining maps, land use, maps of natural conditions, protected areas etc.
Current data on flow rates in the local streams, precipitation and temperatures in the area of interest are provided by the relevant River Basin Authority or the Czech Hydrometeorological Institute.
An essential component is also the on-site survey, which complements and refines the available data.

3.2 Dam site specification

The axis of the dam has been already proposed in the initial concept (WMP, LASW) however, it had to be adjusted to accommodate more suitable foundation conditions or spatial arrangements. Once the precise location of the dam was determined, the elevation of the dam crest, the elevation of the spillway crest and the corresponding reservoir area were established.
The type of the dam was chosen based on foundation conditions derived from preliminary geological surveys and also based on the available material nearby. For such large structures, it is advisable to choose material sources as close as possible for easy transport and coordination.
The height of the dam depends on the geomorphological conditions of the valley and on the requirements on the storage volume. The most efficient solution regarding water volume, reservoir area, dam height, and limiting factors such as built-up areas was taken into account. To determine the elevation of the dam crest, it is essential to consider the effect of wind waves as specified by the Czech Technical Standard ČSN 75 0255 [10].
In the case of Bělkovice reservoir the catchment area is about 47.3 km^2. An embankment dam with a central clayey core has been considered. The dam's axis is located at the narrowest valley profile, considering suitable foundation conditions and potential locations for appurtenant works and operational buildings, which serve as technical facilities. The proposed dam height of 106 m allows to sufficiently use of the entire area of the valley.

3.3 Basic characteristics of the scheme

After determining the axis of the dam, the type and height of the dam, basic characteristics of the reservoir, i.e., the storage-area-elevation dependence were determined. For the evaluation, the 5th Generation Digital Terrain Model (DMR 5G) [5], provided by the State Administration of Surveying and Cadastre, was utilized. The storage-area-elevation dependence was quantified using AutoCAD and Civil 3D software [6].
According to the purpose of the scheme, individual storages and their volumes were derived from the storage-elevation dependence (see section 3.5).
The minimum residual flow (MRF) was determined according to the guidelines of the Ministry of the Environment and new methodologies for regional division in the Czech Republic [7, 8]. For Trusovický stream, the MRF is 0.051 m^3/s.
A harmless flow rate was established based on the channel capacity downstream of the reservoir. The capacity of the stream was taken from the declared flood zone [9]. The capacity of Trusovický stream is about 20 m^3/s.

The division of the reservoir storage into individual storages (active, flood control, etc.) was based on the main function. Of the scheme for water supply function, attention was paid to the largest possible storage volume. In each reservoir there is a mandatory permanent storage due to consideration of ecological, hygienic and aesthetic aspects, taking into account the delay time and limitations for heating water in reservoir. In the case of the flood attenuation flood control storage was defined too.
As an example, the reservoir area and storage-area-elevation curves for Bělkovice are shown in **Chyba! N enašiel sa žiaden zdroj odkazov.**. It can be seen that the Bělkovice reservoir, with the dam height 106

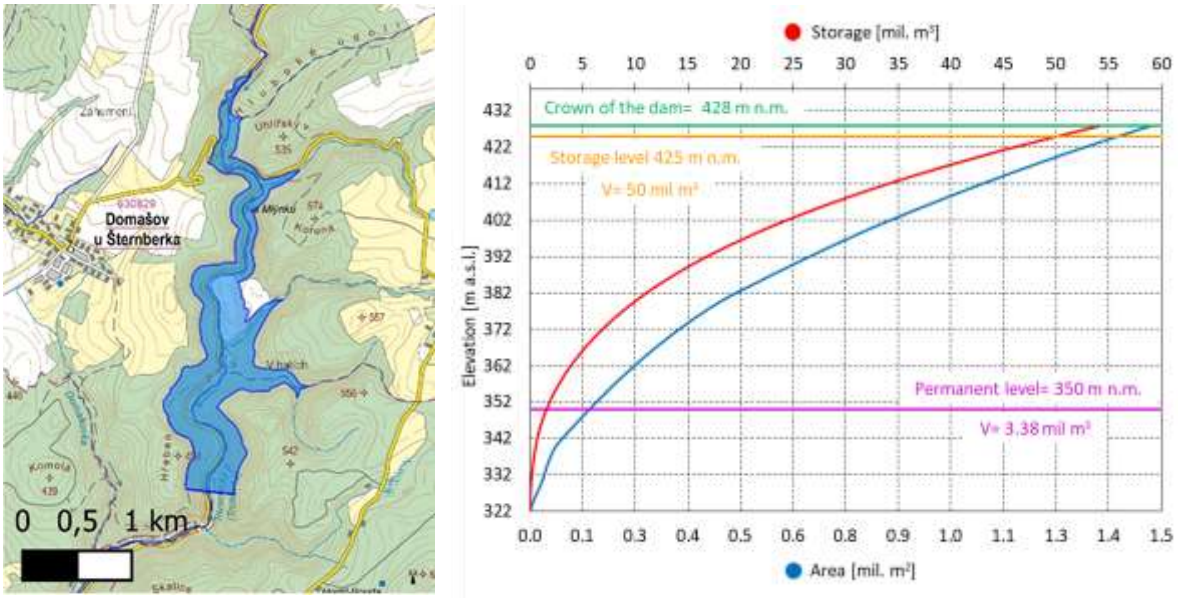

m, can provide an active storage of 50 mil. m^3. The total volume of the reservoir amounts to approximately 55 mil. m^3.

Figure 2. Bělkovice scheme – reservoir area (left) and storage-area-elevation curves (right)

3.4 Hydraulic calculations

The appurtenant works consist of spillway, bottom outlets, water supply piping and small hydropower plant (SHP).
The spillway is designed to handle the design flood Q_{1000}, with subsequent evaluation for the check flood corresponding to $Q_{10\,000}$. For the Bělkovice reservoir the spillway was considered as a lateral spillway located at the left abutment, the weir crest is 31 m long.
The capacity of the bottom outlets was designed as a harmless flow rate. The outlet pipe consists of an inlet, an inlet piece, pipe equipped with an inspection entrance, operational non-regulating and regulatory valves. Bottom outlets are used for water manipulation in standard mode. Bottom outlets consist of a pair of pipes with a diameter of 1.1 m and a total capacity of 20 m³/s. Their approximate length is 920 m.
Water supply will be provided by a combined intake facility within the reservoir area. In the lower section of the tower, there is an inlet leading to the bottom outlets. The water supply intakes will be located at the different levels, to enable take-off providing the best water quality.
The hydroelectric potential of the scheme cannot be overlooked, particularly utilizing the MRF throughout the year. The SHP can be installed on the bottom outlets or have its own inlet. In the case of the Bělkovice reservoir, potential hydropower output can be 35 kW.

3.5 Reservoir water management

Before proceeding with the actual water management solution, fundamental principles have been established. Whether an initially full or empty reservoir is considered. The priority is to secure MRF and water take-off for water supply. The water supply discharges and the values of their prescribed

reliability were derived from the classification of the reservoirs according to the criteria of the Czech Technical Standard ČSN 75 2405 [11].
The water management solution was implemented by simulating reservoir operation over a sufficiently long period using time series of average daily discharge. Based on these data, an assessment of water supply reliability was conducted regarding the duration and the volume of undelivered water. The calculation includes approximate evaporation from the reservoir derived from [11]. It was established that the minimal residual flow and water supply take-off had equal priority according to [11].
The calculation was performed using a custom-purpose application in Visual Basic (MS Excel). An example of the reservoir management using 42 years long time serie at the Bělkovice profile is in Figure 22. The period starting in 1980 is crucial for specifying the operation rules. Figure 22 shows how the water level in the reservoir changes over time depending on the inflow and take-off from the reservoir.

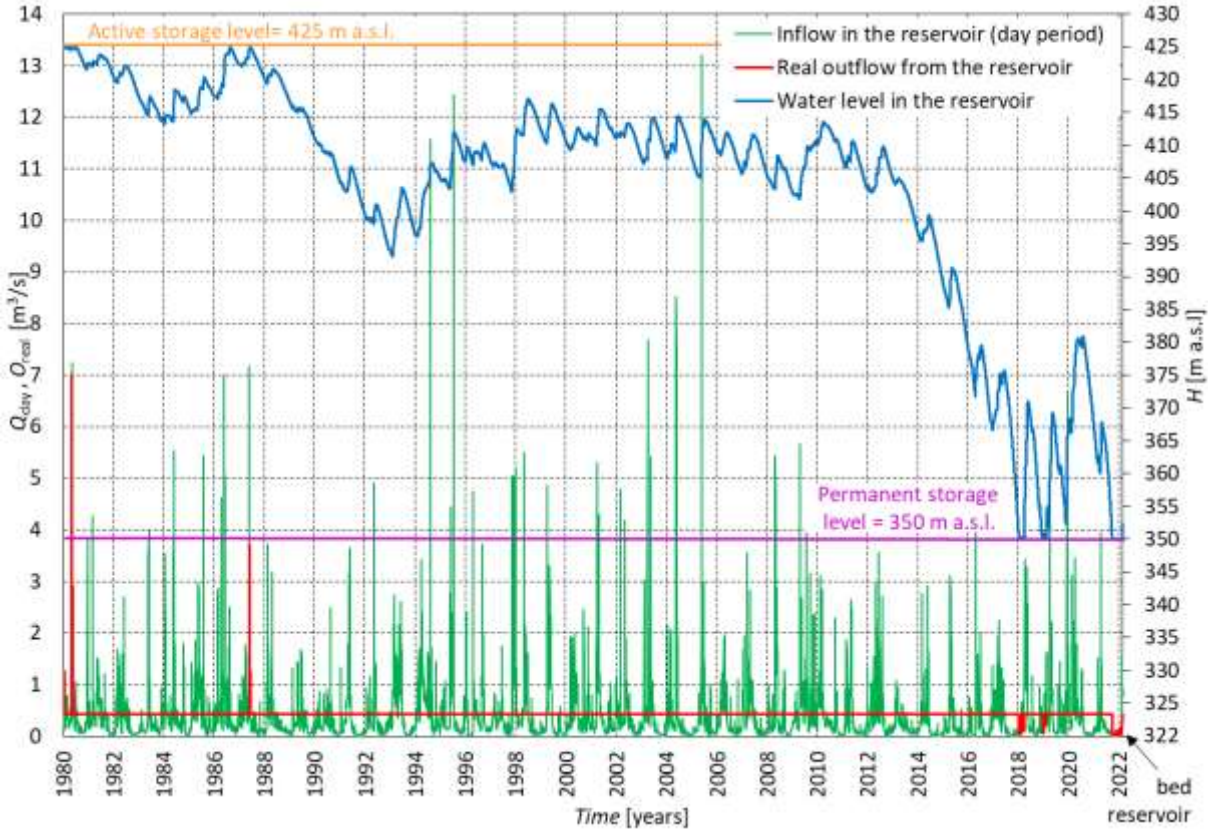

Figure 3. Water management solution for reliability level 98.5 % for Bělkovice reservoir

The reliability of the water supply is defined using [11]. The reliability p_d of the take-off discharge from reservoir with respect to the duration holds:

$$p_d = \frac{m_d - 0.3}{n_d + 0.4} \cdot 100, \quad (1)$$

where m_d represents the number of days that satisfy the required discharge, n_d is total number of days in the serie.
The reliability p_v by delivered volume holds:

$$p_v = \frac{m_v}{n_v} \cdot 100, \quad (2)$$

where m_v is delivered water volume and n_v is the total volume required discharge for water supply.

The analysis was performed for given active storage volume with the aim to determine discharge-reliability dependence. **Chyba! Nenašiel sa žiaden zdroj odkazov.** shows the dependence between the t ake-off and its reliability for the Bělkovice reservoir.

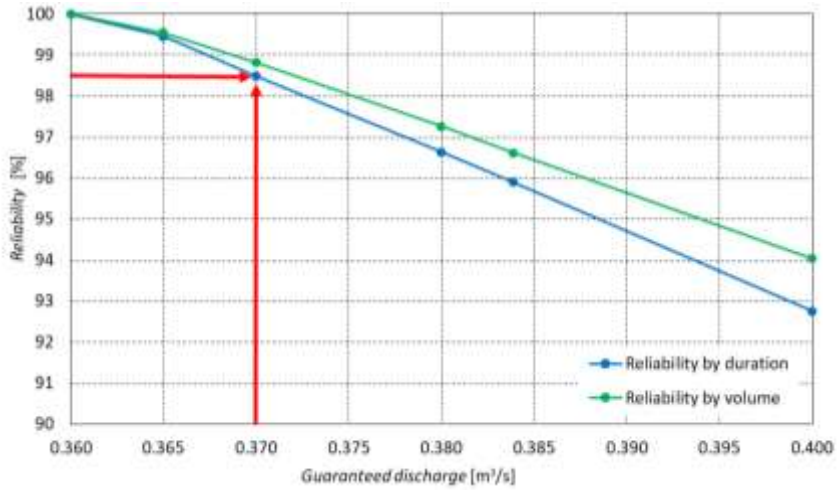

Figure 4. Reliability of the take-off discharge for Bělkovice reservoir

For the designed spillway the flood attenuation effect was determined by flood routing throught the reserovir.
The input for the calculation included the flood hydrograph, as well as the characteristics of the reservoir and the rating curves of appurtenant works (outlets, spillway). **Chyba! Nenašiel sa žiaden zdroj o dkazov.** shows flood routing for 100 and 1000-year hydrographs. An inflow to the reservoir has to be primarily discharged through bottom outlets up to their maximum capacity. After the water rises in the reservoir, the flow is diverted by the spillway accompanied by gradual closing the bottom outlet to maintain harmless discharge as long as possible.

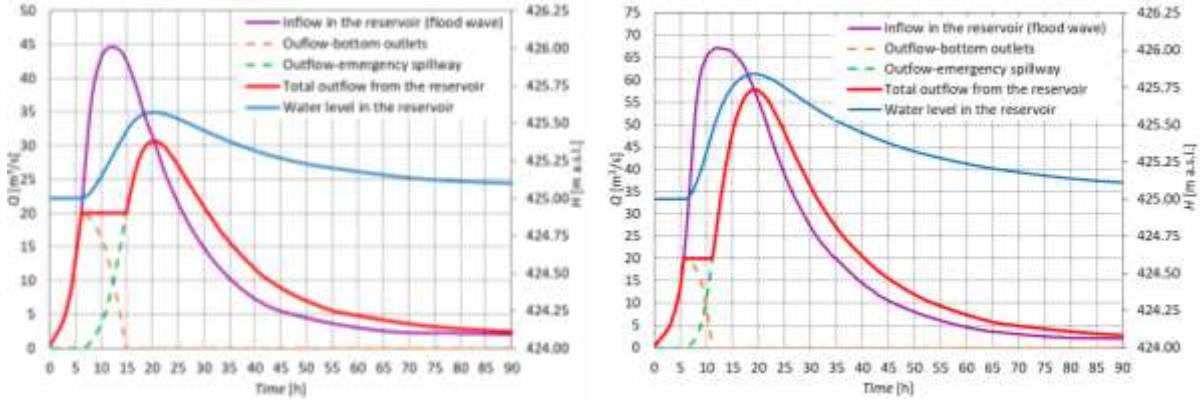

Figure 5. Flood rating for 100 and 1000-year hydrographes for Bělkovice reservoir

3.6 The concept of operation rules for the scheme

The water management and manipulation at the scheme must be carried out in a way that under normal circumstances and operational conditions, the purpose of the water structure is a priority, and the reservoir level is primarily maintained within the full storage capacity.
The permanent storage must remain permanently filled. The water level at active storage is governed by the inflow conditions and water take-off. Redundant water outflow via bottom outlets is not allowed. In the active storage the aim is to secure minimum residual flow and water supply discharges. The flood control storage is filled only during the passage of floods when the capacity of bottom outlets is

exceeded.

4 Results and discussion

In the Table 3, the summary of characteristics for 6 selected hydraulic schemes is provided. These include information about the reservoir volumes, the reliability of take-off discharges, hydropower outputs, flood attenuation effect, etc.

Table 3. Basic characteristics of the schemes

Dam	**Borovnice**	**Kuřimské Jestřabí**	**Vysočany**	**Brodce**	**Plaveč**	**Bělkovice**	**Total**
River	Svratka	Libochovka	Želetavka	Brtnice	Jevišovka	Trusovický stream	-
Catchment area [km^2]	115.70	114.41	369.40	59.71	290.02	47.28	996.52
Permanent storage volume [mil. m^3]	1.60	0.70	1.78	1.09	0.95	3.38	9.50
Active storage volume [mil. m^3]	7.30	15.53	19.28	7.18	6.45	49.99	105.73
Flood control storage volume [mil. m^3]	1.5	1.44	3.23	0.70	1.20	1.41	9.48
Total volume [mil. m^3]	10.40	17.67	24.29	8.97	8.60	54.78	124.71
Dam height [m]	23.00	46.50	44.60	23.80	25.00	106.00	-
Required water supply reliability [%]	98.50	98.50	98.50	98.50	95.00	98.50	-
Reliability take-off discharge [m^3/s]	0.650	0.400	0.567	0.265	0.200	0.370	2.452
Hydropower output [kW]	100	120	187	42	27	35	511
Transformation of peak flood discharge inflow/outflow							
Q_{100} [m^3/s]	89/78	66/50	78/48	33/23.50	54/50.22	44.70/30.73	-
Q_{1000} [m^3/s]	171/158	115/96	135/107	66.70/52.7	119/112.1	67.20/57.83	-

5 Conclusion

A comprehensive evaluation was conducted for six selected reservoirs in the Morava river basin. Overall, these schemes provide an active storage volume of more than 105 mil. m^3, primarily intended for water supply with high reliability, with total amount of almost 2.5 m^3/s.

Additionally, all identified reservoirs boast the capacity to maintain 100% MRF downstream of the dam, ensuring ecological balance. Furthermore, these reservoirs offer certain prospects for hydropower generation.

The locations of the proposed schemes are chosen in areas with minimal environmental and social conflicts. Restrictions on nature and landscape are limited to necessary extents to ensure the crucial water supply function of the reservoirs. When considering the future water supply function of reservoirs, it is prudent to specify the area to which water will be supplied and delineate the requirements for its quantity and quality more closely. This detailed specification will ensure alignment with anticipated demand and regulatory standards.

Possible conflicts were evaluated, and extended characteristics of the reservoirs were delineated to provide a clearer understanding of the potential benefits in case of the construction of dams. Reservoirs are a crucial element for the planning adaptation measures as underground water resources decline, and these strategic sites for obtaining drinking water are essential.

For a more precise determination of all dam and reservoir parameters, it is advisable to further expand the engineering geological survey and the overall site survey.

Acknowledgements

This paper was elaborated with the support of the projects SS07010401 and FAST-S-24-8513.

References

[1] Water Management Plan (WMP). Publication No.34 Water structures. MLVH, Prague, 1988.
[2] European Union. Directive 2000/60/EC of the European parliament and of the council established a framework for Community action in the field of water policy. In: EU legislation. 2000.
[3] River Basin District Management Plan. In: Water planning. 2007.
[4] General Plan for Areas Protected for Surface Water Accumulation and Basic Principles for Utilizing These Areas (LASW). The Ministry of Agriculture of the Czech Republic and a Ministry of Environment of the Czech Republic, Prague, 2020.
[5] ZABAGED - Altimetry - DMR 5G. Digital Terrain Model of the Czech Republic of the 5th generation (DMR 5G) in S-JTSK, Bpv. Geoportal ČÚZK access to map product and services: Applications.
[6] Autodesk: Autocad, Civil 3D. Autodesk 2024.
[7] Guidelines Directive No. 9/1998 of the Ministry of the Environment on the determination of minimum residual flow values in watercourses. Ministry of Environment of the Czech Republic, Prague, 2011, 5 p. [online]. [ref. 27.11.2022]. Available from: Věstník 5/98 - Metodický pokyn odboru ochrany vod MŽP ke stanovení hodnot minimálních zůstatkových průtoků ve vodních tocích (mzp.cz)
[8] Balvín, P.; Vizina, A. Determination of minimum residual flow values in the conditions of the Czech Republic. Hydrotechnical and economic information, 2018, Article 60, n.2, p.8-13, ISSN 0322-8916 [online]. [ref. 27.11.2022]. Available from: 5858-VTEI-2-18.pdf
[9] D01-ZÚ, D02-ZÚ, D03-ZÚ: D – flood areas. In: VÚV TGM Department of Geographic Information Systems and Cartography [online]. Prague: T.G. Masaryk water research institute - The Department of Water Protection. Available from: VÚV T.G.Masaryka - Oddělení GIS - Struktura DIBAVOD
[10] Czech Technical Standard 75 0255 Calculation of wave effects on waterworks.
[11] Czech Technical Standard 75 2405 Water management analysis of reservoirs.

PROBLEMS OF HYDROMETRIC APPROACH TO DETERMINE THE THERMAL MINERAL WATER FLOW TO THE BEČVA RIVER IN THE TEPLICE SPA

TOMÁŠ JULÍNEK [1*], JAROMÍR ŘÍHA [2], MIROSLAV ŠPANO [3], STANISLAV KOTAŠKA[4]

[1*] assistant professor, Brno University of Technology, Veveří 95 Brno 602 00, Czech republic, tomas.julinek@vut.cz

[2] professor, Brno University of Technology, Veveří 95 Brno 602 00, Czech republic, jaromir.riha@vut.cz

[1*] assistant professor, Brno University of Technology, Veveří 95 Brno 602 00, Czech republic, mirosla.spano@vut.cz

[1*] assistant professor, Brno University of Technology, Veveří 95 Brno 602 00, Czech republic, stanislav.kotaska@vut.cz

*corresponding author

1 Abstract

The mineral water in the Spa Teplice on Bečva springs into the Bečva river bed out of the hypogenic karst formed by Paleozoic limestones. Recently the focus on the hydrological and hydrogeological conditions of the mineral springs issues from the planning of the Skalička dam whose reservoir is believed to be interconnected with the karstic formation and may influence the regime of mineral waters. One of the related particular problems is to determine the discharge of the rising mineral water which springs into the Bečva river in the vicinity of the Spa Teplice on Bečva. For the estimate of the natural yield of the thermal water several methods were applied. One of them was hydrometric measurements by the classical current meter and measurements using the ADCP (acoustic Doppler current profiler). Several problems appeared during the evaluation of measured data.

Keywords: hydrometry, mineral water recharge, ADCP, seepage.

2 Introduction

The paper deals with assessment of mineral water springs in the area of the Teplice Spa on the Bečva River in the Czech Republic. The mineral water springs in the area origins in the karst structures formed by Paleozoic limestones [1]. One of the particular problems is to determine the discharge of the mineral water which springs into the Bečva river in the vicinity of the spa Teplice on Bečva. The objective of the work was to estimate the natural yield of mineral water within the area of the spa Teplice upon Bečva. One of the methods to estimate thermal water yield was discharge measurement along the river reach with documented thermal water discharge. To measure discharge in an open channel the standard hydrometry is used. The procedure of measurement is declared by [2] and [3]. The second regularly used hydrometric method is Acoustic Doppler Current Profiler (ADCP) [4] to [6], which is proved to be fast and efficient and applicable for measurement in shallow channel flow [5]. To verify obtained values of mineral water discharge an approach based on monitoring of the mineral water and flow in the karstic system was used [7], [8]. Three intake wells with continuous monitoring were selected as representative for the estimation of upward flow.

The area of interest is located in the area of the Teplice Spa on the Bečva River in the eastern part of the Czech Republic (Figure 1).

Figure 1. Study area location

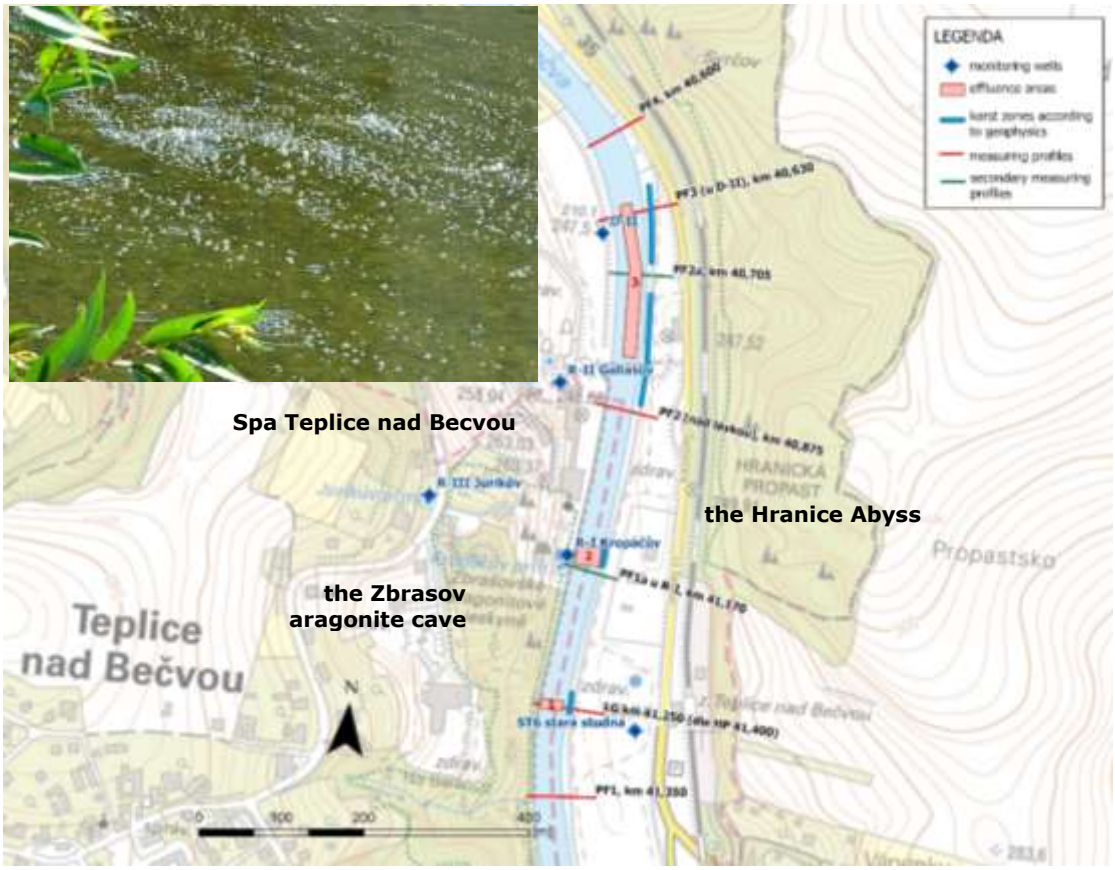

Figure 2. Location of gauging profiles and example of zone of mineral water springs into the Bečva river

The determination of the flow conditions and the assessment of the magnitude of the upward mineral water flow were carried out on the 750 m long reach of the Bečva River in the area of the Teplice Spa (TS), approximately from kilometre 40,600 to 41,350.

The karst layer is mostly overlaid by relatively impermeable paleozoic greywackes and tertiary claystones. Partly is overlaid by Quaternary layers of fluvial material of the Bečva river (sandy gravels and fluvial silts). Warm karst mineral waters spring up within the erosional base formed here by the river Bečva. Therefore, the springs are scattered and it is not possible to search for a specific spring.

Monitoring campaigns of mineral water springs in the area have been done in different locations. Long-term monitoring at the intake wells of the spa, in the Hranice Abby (HA), Zbrasov Aragonite Caves (ZAC) is supplemented with water level and discharge monitoring of the Bečva river at gauging station Teplice nad Becvou. The springs of mineral water to the Bečva River can be documented visually at number of zones in the river or by thermo monitoring of the river reach during cold seasons (see Figure 2).

3 Methods

Two methods were applied for the analysis of the yield of thermal water in the locality of the Teplice Spa. The analysis was based on discharge measurements with current meter, with acoustic Doppler current profiler and the evaluation of continuous measurements of the water level in the boreholes located in the area of interest.
In Figure 2 the profiles in which the hydrometric measurements were carried out are shown in red. In profiles PF1 to PF4, measurements were made using the ADCP method, in PF1 and PF3 were also measurements made with a hydrometric propeller (HMP). Profiles signed with "a" were used as additional control profiles. Additionally, electrical conductivity (conductometry) was measured in all hydrometric profiles and in profiles PF1a and PF2a. However, it is not further discussed in the paper.
The evaluation considered the hydraulic interaction of the Bečva River with the surrounding structures, represented on the left bank by the mineral water intakes of the TS and the ZAC complex, and on the right bank by the intakes from the Quaternary aquifer and the HA.
The methods used to analyse the yield of thermal water to the Bečva River at TS sit were based on the following approaches:

- discharge measurements in two variants:
  - with current meter - hydrometric propeller (HMP),
  - with acoustic Doppler current profiler (ADCP),
- the evaluation of continuous measurements of the mineral water level (MWL) in the boreholes located at the area of interest.

Long-term monitoring of groundwater levels in extraction and observation wells was also available. In the area of the TS, a number of wells have been drilled into the subsoil and have shown increased mineralisation of the water. The results of monitoring in wells R-I, R-II, R-III, HV-301, D-II, ST6, located in the spa area, show that the water level in the wells is practically always higher than the level in Bečva. This indicates possible the drainage effect of the Bečva River.

3.1 Current measuring by the propeller

Applied mechanical current meter is based on counting the rotations of a propeller. Depending on the instantaneous flow, the point velocities were measured in the number of verticals according to [3]. The distribution of verticals was carried out uniformly over the entire width of the channel at an equidistant span of 1 m. At the banks, the verticals were placed at a distance of about 0.5 m from the bank. Water depth measurements were made by a propeller post with a support head at the lower end. The accuracy of the depth measurements was approximately 1 cm. The number of measurement points per vertical was determined according to [3]. Due to the different flow conditions (depth, velocity), three propellers with diameters of 30 mm, 45 mm and 50 mm were used.
Four hydrometric measurements were carried from July to August 2020. In some cases, it can be noted that the flow conditions were partially variable during the measurement with variation of the water level up to 5 cm in the profile during the measurement.
When determining the value of the upward flow, the influence of the non-stationarity of the flow in the Bečva river had to be taken into account by "adjusting" the difference in the measurements in the "upper" (u) and "lower" (l) profile. The upward flow (Q_{UF}) to the Bečva River was determined as the difference of the flows determined by hydrometric measurements in the subsequent profiles (Q_{Hu} and Q_{Hl}) reduced by the difference of the flows read at the gauging station at the time of the measurements in the individual profiles (Q_{GSu} and Q_{GSl}). The value of total upward flow determined from hydrometric measurements

Q_{UFH} was calculated by the relation:

$$Q_{UFH} = (Q_{Hu} - Q_{Hl}) - (Q_{GSu} - Q_{GSl}), \quad (1)$$

where Q_{Hu} is the discharge in the upper profile, Q_{Hl} is the discharge in the lower profile, Q_{GSu} and Q_{GSl} are the discharges recorded at GS at the time of measurement in the upper and lower profiles.

3.2 Acoustic Doppler Current Profiler

ADCP contains piezoelectric transducers to transmit and receive sound signals. The traveling time of sound waves gives an estimate of the distance. The frequency shift of the echo is proportional to the water velocity along the acoustic path. Further components of an ADCP are an electronic amplifier, a receiver, a clock to measure the traveling time, a temperature sensor, positioning system and for this study purposes also conductivity sensor. The ADCP was used to measure the total water discharge.

The ADCP measurements were made using a measuring device mounted on a plastic float that was pulled across the flow on a rope. Several measurements (three or four) were always taken in one profile in immediate succession. The resulting discharge was determined by averaging obtained values of flow in a given profile and time. The observed relative deviations of velocities in the profile are used to estimate the measurement error and the reliability of the obtained discharge value.

The measurements were always started at the upstream end and then the device was pulled downstream. More detailed discharge determinations were made in each predefined profile (Figure 2).

3.3 Ground water level monitoring

It can be assumed that the upward flow is influenced by the flow conditions in the Bečva River, which is represented by water level on the gauging station Teplice nad Bečvou. Three boreholes with continuous monitoring were selected as representative for the estimation of upward flow (Figure 2). Two boreholes are 60.4 and 67.5 m deep, excavated to the limestone. One borehole is just 7.7 m deep and is excavated in valley gravels.

The characteristic periods of groundwater level monitoring were chosen with respect to the available measurements. The level in the Bečva river was taken from the gauging station in Teplice and from the calibrated stream flow model.

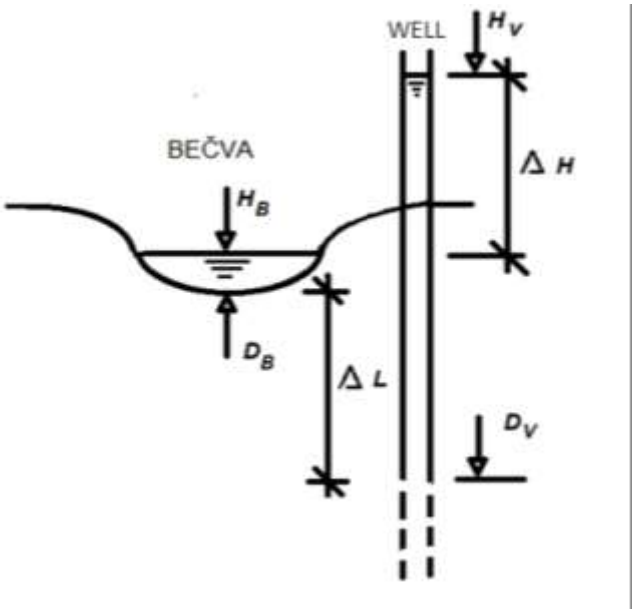

Figure 3. Scheme of upper flow (mineral water discharge) estimation

In terms of Figure 3, the hydraulic gradient of the upward flow is determined from:

$$J = \frac{U_B - U_{BR}}{B_{BR} - L_B}, \quad (2)$$

where U_B upper level in borehole, U_{BR} upper level in the Bečva river, L_B lower level in borehole, B_{BR} bottom level in the Bečva river,

$$q_{UF} = k \cdot \frac{U_B - U_{BR}}{B_{BR} - L_B}, \quad (3)$$

where k is the hydraulic conductivity.
The estimation of the total upward flow rate based on monitoring of boreholes was determined by:

$$Q_{UFB} = q_{UF} \,.\, A_{UF} \quad (4)$$

where A_{UF} is the considered discharge area.

4 Results and discussion

Hydrometric measurements were carried out in 4 campaigns. The values of the discharge were determined by both methods (HMP and ADCP) in the four profiles (see Figure 2). Figure 4 shows the values obtained in comparison with the average flow recorded at the time of measurement at the Teplice Spa gauging station. It can be seen that the hydrometric values are systematically 10 to 15% higher than those obtained at the Teplice Spa gauging station. During first campaign there were unsteady flow conditions with fluctuation +/- 3,5 m^3/s.
A certain problem is the accuracy of the GS level readings (+/- 1 cm), which corresponds to a flow increment of about 100 - 300 l/s. Therefore, when evaluating the measured flow rates to determine the magnitude of the mineral water inflow according to relation (1), the flow rates read from the GS were refined by observing the change in the water level during the measurement process using the fitted control points, to an accuracy of 1 mm. Measured values are presented in Figure 4. The values of the determined Q_{UFH} are presented in Table 1 below.

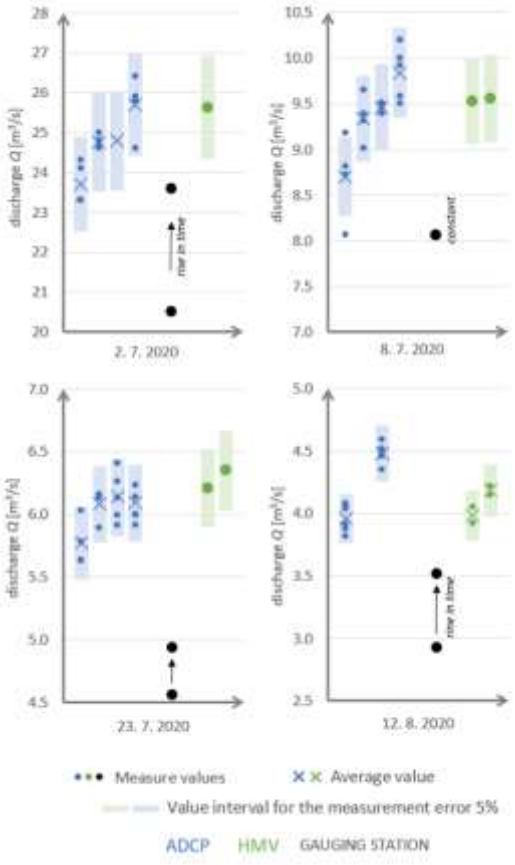

Figure 4. Results of individual flow measurements

As mentioned above, hydrometric measurements with the propeller were carried out in four campaigns. Table 1 shows only three of them with steady or slightly unsteady flow conditions The evaluated profiles were PF1 and PF3.

Tabule 1. Discharges determined by hydrometric propeller

Date	Profile	Flow Regime	Measured Discharge [m³/s]	Discharge In GS [m³/s]	Spring Discharge [m³/s]
8.7.2020	PF 1	Steady	9.18	8.07	0.270
	PF 3		9.46		
23.7.2020	PF 1	Steady	5.85	4.56	0.140
	PF 3		5.99		
12.8.2020	PF 1	Unsteady	3.99	2.92	0.090
	PF 3		4.19	3.03	

The approach based on data on the level and flow of mineral water in the karst system at the monitoring and intake wells. The upward flow was linked to measurements in wells ST6, R-I, and D-II for individual effluence areas labelled 1 to 3 (Figure 2). Corresponding zones and wells are Zone1 – ST6, Zone2 – R-I, Zone3 – D-II. The upward flow for each particular effluence area was calculated using relations (3) to (5) based on water level measured in the boreholes and in the Bečva river. All flow rates are related to the water level at the gauging station. An example of the relationship between the upward flow and the water level of the Bečva River (GS) is shown in Figure 9 for the borehole R-I. An estimate of the total upward flow consisting of single values for each effluence zone is given in Figure 10.
The upward flow was tied to measurements in wells ST6, R-I, and D-II for individual spill locations labelled 1 through 3 (Figure 2). The upward flow at the respective site (borehole) was made for the individual measured water level conditions in the boreholes and in the Bečva using relations (2) to (4). All flow rates are related to the Bečva level on the limnigraph. An example of the relationship between the upward flow and the level of the Bečva is shown in Figure 5 for the borehole R-I. An estimate of the total upward flow versus the Bečva level is given in Figure 6.

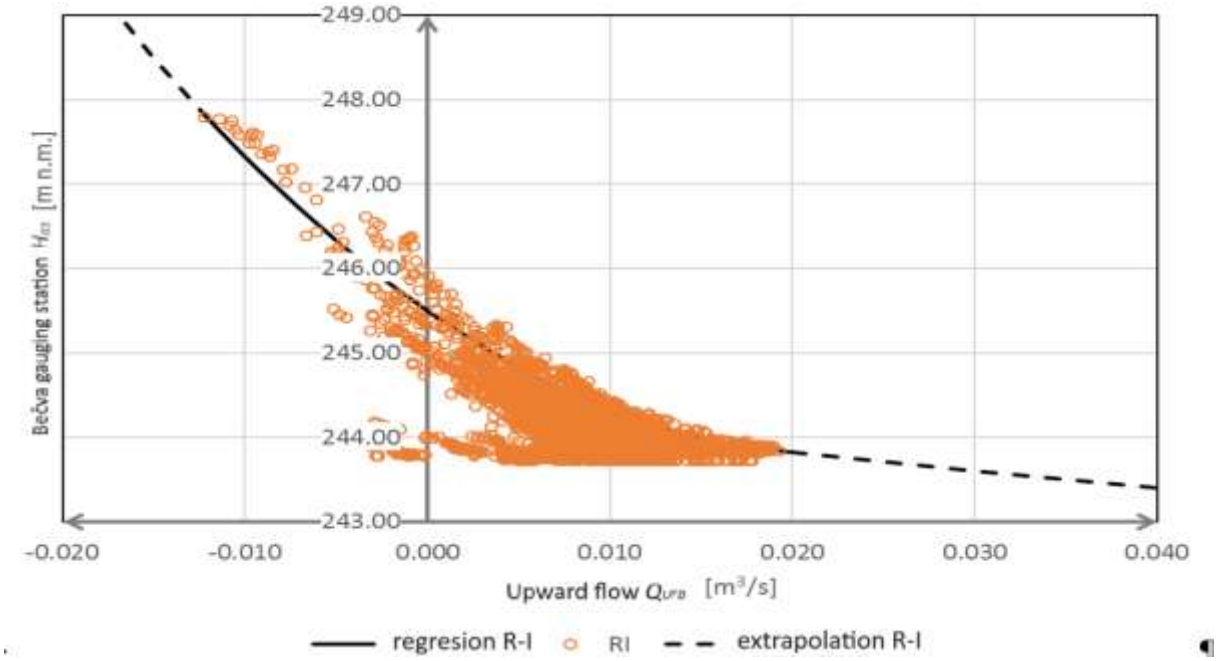

Figure 5. Relationship between upward flow rate and Bečva level for well R-I

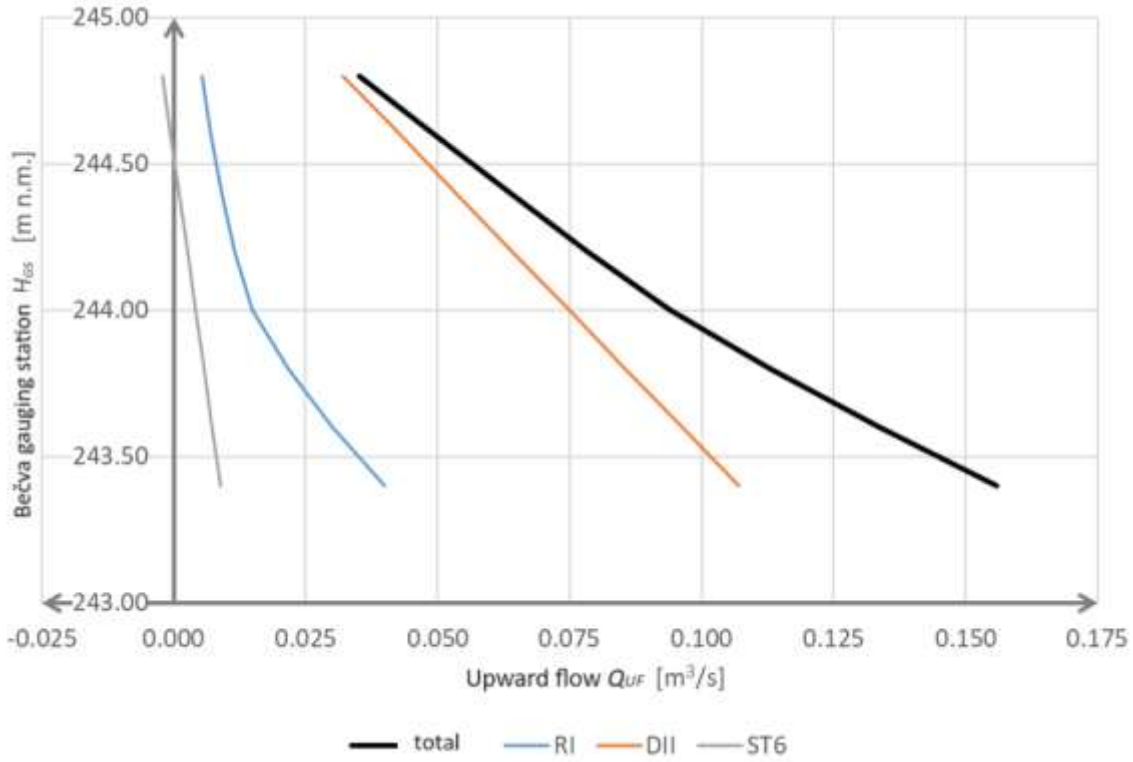

Figure 6. Estimation of the total upward flow depending on the level of the Bečva River

5 Conclusion

The results are evaluated by comparing the total upward flow rates determined by each independent method, i.e. hydrometry by propeller and ADCPand borehole measurements.
The results show reasonable agreement in the derived flow rates which ranges between 0.09 nad 0.27 m^3/s. At higher flow rates the differences in obtained values of Q_{UF} increase, which is probably due to the limited accuracy of each method. At significantly high flow rates, the results of hydrometry are baised due to measurement , which may exceed the values of the upward flows. The error rate may also increase due to changes in hydrodynamic conditions during measurement. In the case of measurements in boreholes, the estimation of flows can only be considered applicable within the range of the measured data. The results may include errors due to change in saturation rate of CO_2 which influnces density of water along the length (depth) of borehole.
Each of the methods used is subject to a degree of uncertainty. These include partial uncertainties in the hydrometric measurements and issues of the effect of pumping from individual wells. Additional uncertainties arise from the hydrology of the catchment and infiltration areas. Increased flow in the Bečva river may in some cases be caused by precipitation in a distant area, which does not affect the infiltration areas of the limestone aquifer. In other cases, the increased flow in the river may be accompanied by a significant impact on the infiltration areas. The uncertainty of the results obtained also comes from the actual measurements in the boreholes and the measurements of the flows in the Bečva river, where 1 cm difference in the level represents a change of flow up to 0.5 m^3/s for higher water levels.
It can be concluded that the upward flow rate varies approximately between 50 – 300 l/s. The absolute deviation in the values of the upward flows obtained by the various methods is around 20 l/s for low flows in the Bečva, and up to 50 l/s for higher flows and practically corresponds to the uncertainties in their determination.

Acknowledgements
This article was elaborated with the support of Czech Technological Agency projects TH04030087 and SS07010401.

References:
[1] Geršl, M., Konečný, O. Geological hazards resulting from the planned construction of a water dam "Skalička" near the Hranice Karst and the Hranice Abyss. In *Geoscience Research Reports*, Czech Geological Survey, Prague, Vol. 51, 1/2018.
[2] ISO 1088, Hydrometry-Velocity-area methods using current-meters collection and processing of data for determination of uncertainties in flow measurement. International organization for standardization, Geneva, Switzerland. 2007.
[3] ISO 748. Hydrometry – Measurement of liquid flow in open channels using current meters or floats. International organization for standardization. Geneva, Switzerland. 2008.
[4] Rehmel, M.S. Field Evaluation of shallow-water acoustic Doppler current profiler discharge measurements. In Proceedings of ASCE-EWRI Congress, May 21–25 2006, Omaha, NE.
[5] Mueller, D.S., Wagner, C.R., Rehmel, M.S., Oberg, K.A., Rainville, F. Measuring Discharge with Acoustic Doppler Current Profilers from a Moving Boat. Chapter 22 of Section A, Surface-Water Techniques. Book 3, Applications of Hydraulics. USGS. 2013.
[6] Boiten, W. Hydrometry. 2005. ISBN 0-203-97109-4. 2020.
[7] Rainville, F., Hutchinson, D., Stead, A., Moncur, D., Elliott, D. Hydrometric manual. 2016. Data Computations Stage-Discharge Model Development and Maintenance Water Survey of Canada. 40 p. 2016. Available at https://publications.gc.ca/collections/ collection_2021/eccc/en37/En37-464-2016-eng.pdf (last view 6/2024).
[8] Milanovic, P. Engineering Karstology of Dams and reservoirs. ISBN: 978-1-4987-4807-0. 2018.

MONTE CARLO APPROACH TO LOCAL SCOUR: THE SAVA RIVER BRIDGE, ZAGREB CASE STUDY

MARTINA LACKO [1], KRISTINA POTOČKI [2], NIKOLA ADŽAGA [3], GORDON GILJA [4],

[1] *Water Research Department, Faculty of Civil Engineering University of Zagreb, Croatia, martina.lacko@grad.unizg.hr*

[2] *Water Research Department, Faculty of Civil Engineering University of Zagreb, Croatia, kristina.potocki@grad.unizg.hr*

[3] *Department of Mathematics, Faculty of Civil Engineering University of Zagreb, Croatia, nikola.adzaga@grad.unizg.hr*

[4] *Water Research Department, Faculty of Civil Engineering University of Zagreb, Croatia, gordon.gilja@grad.unizg.hr*

1 Abstract

In this paper, a framework for estimating local scour around bridges was established by performing a statistical analysis of historical annual maximum discharge in combination with a Monte Carlo simulation. First, different univariate probability distributions of the historical annual maximum discharge data were tested with several goodness-of-fit tests to reduce the uncertainties associated with the different factors influencing scour behaviour. Subsequently, a Monte Carlo simulation was used to generate a larger data set of annual maxima based on the fitted distribution and its parameters, which is later used as input to a previously developed HEC-RAS model of the study area and to evaluate the uncertainties associated with the number of Monte Carlo simulations for the input data of the HEC-RAS model The research methodology was demonstrated using a case study of a bridge in Zagreb, Croatia).

Keywords: flood, bridge, local scour, Monte Carlo, HEC-RAS, R3PEAT

2 Introduction

Morphodynamic changes in the riverbed as a result of extreme flood events can lead to scouring around bridge piers [1], which impairs the stability of the bridge and is one of the main reasons for bridge failure [2]. Different types of scour like general, contraction and local scour [3] are described in literature [4, 5]. Local scour displaces sediments around a pier or abutment [6] and is driven by the downward flow at the upstream face, which generates vortices at the riverbed base [7]. At the stagnation point, where the approach flow velocity at the pier face decreases and pressure increases, the downflow rapidly intensifies resulting in sediment scour [3].

Given the significant impact of local scour on bridge stability, an accurate assessment of the hydraulic parameters and the associated uncertainties is crucial for reliable scour prediction. The local scour is presented in literature as a function of flow and bed material characteristics, fluid properties, sediment bed, pier and footing geometry [4, 5]. Considering the hydraulic characteristics of the river reach and the geometry of the bridge, the relationship between discharge and hydraulic parameters can be calculated with a hydraulic model (e.g., HEC-RAS [8]) by performing simulations for different parameters within the desired range to simulate the effects of the uncertainty of the hydraulic model parameters [9]. Parameter uncertainty can be taken into account with an analytical method by applying mathematical assumptions to simply explain a problem, approximate methods where the approximations of output random variables are used, and the Monte Carlo method [10], in which a series of samples are generated for the hydraulic parameters based on an assumed probability distribution and a hydraulic analysis is performed for each sample [11]. The Monte Carlo Method addresses parameter uncertainty in hydraulic modelling by allowing for the consideration of random variables with diverse distributions and nonlinear performance functions. However, the approach requires a large number of simulations to accurately approximate the performance functions and their probability distributions, which can be computationally demanding and impractical for complex models with many variables [12].

Incorporating Monte Carlo simulations in HEC-RAS models for scour calculation has been conducted in previous studies with tools developed for this purpose, but the tool enabled limited number of tested distributions [13]. These types of analyses, which take into account uncertainty in the hydrologic input, hydraulic parameters, and model uncertainty, serve as input for risk and reliability analyses, where an appropriate number of simulations (i.e., realizations) need to be tested [13, 14].
This paper presents a framework for estimating local scour around bridges, with a focus on dealing with the uncertainties in the input parameters of the hydraulic model by utilizing a statistical analysis on the Manning's coefficient values, historical annual maximum discharges and energy slope values coupled with Monte Carlo simulations. The aim of this study is to evaluate the uncertainties associated with the number of Monte Carlo simulations for the input data of the HEC-RAS model that is used for the calculation of the local scour around bridge located on the Sava River. The analysis is conducted to complement the ongoing research of the relationship between climate change indicators, flood wave characteristics and scour development next to the bridges crossing large rivers in Croatia with installed scour countermeasures within the R3PEAT project (Remote Real-time Riprap Protection Erosion AssessmenT on large rivers).

3 Methods

3.1 Study area and data

The Sava River is a major drainage basin and the longest right tributary of the Danube at approximately 990 km that significantly contributes to its flow. It originates from Slovenia flowing through Croatia, Bosnia and Herzegovina, and Serbia, where it joins the Danube in Belgrade. Its hydrological regime transitions from Alpine nival-pluvial upstream to Peripannonian and Pannonian pluvial-nival downstream near Jasenovac [15, 16]. Research on the Croatian section of the Sava, particularly at the Zagreb gauging station focuses on flood changes influenced by engineering works as a part of the flood protection system of Zagreb [17–21], as well as discharge regime under the influence of climate change [22]. A preliminary analysis for estimating local scour around bridges was conducted by performing a statistical analysis of historical annual maximum (AM) discharges in combination with a Monte Carlo approach on the Zagreb gauging station for the period from 1972 to 2009 (Figure 1). The input for the analysis was daily discharge data provided by the Croatian Meteorological and Hydrological Service (DHMZ) resulting in total of 38 AM discharge values. Additionally, we used a previously developed and calibrated HEC-RAS model [23] based on the geometry of control cross-section profiles from Podsused GS (rkm 717+200) to Zagreb GS (rkm 702+800). The Manning coefficient for the model was calculated (
Table 2) as a function of discharge data for each simulation, ranging from 0.016 to 0.031, and used for the calibration of the mentioned HEC-RAS model for specific boundary conditions. The corresponding energy slope values of the calibrated HEC-RAS model are used as a basis for fitting a log-normal probability distribution on which a number of Monte Carlo simulations (MCS) were applied to reconstruct full dataset.

Table 2. Selected values of the Manning's coefficient for corresponding discharge values

Q[m3/s]	2129.4	2159.1	2181.6	2201.5	2227	2237.2	2263.7	2277.3	2283.5	2296
n	0.0312	0.0292	0.0276	0.0263	0.0253	0.0246	0.024	0.0236	0.0234	0.0232
Q [m3/s]	2315	2324.7	2331.2	2350.9	2360.5	2372.9	2376.9	2384.5	2392	2403.7
n	0.023	0.0229	0.0227	0.0224	0.0219	0.0213	0.0204	0.0193	0.0178	0.016

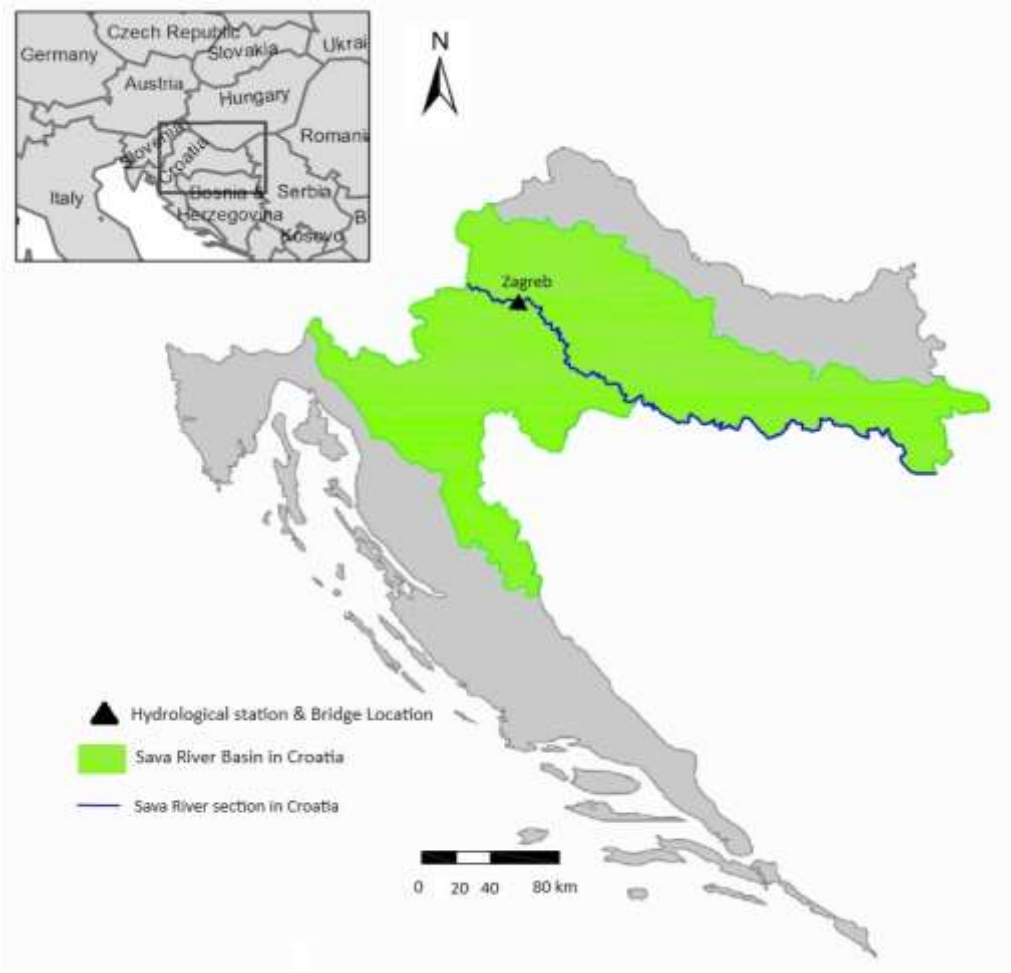

Figure 23. Map with location of bridge and gauging station Zagreb on the Sava River section in Croatia

3.2 Statistical analysis of discharge data

The statistical analysis of discharge data was conducted on the daily time step. An annual maxima method was performed to extract annual peaks, resulting in 38 values (Table 3). Six probability distributions (Gumbel, Log-Normal, Pearson Type III, Log Pearson Type III, Generalized Extreme Value, and Generalized Logistic) were then fitted to the peak discharge data using the method of L-moments [24]. Goodness-of-fit tests, including Anderson-Darling and Kolmogorov-Smirnov tests, are performed together with the Root Mean Square Error (RMSE) statistics to assess the suitability of these distributions.

Table 3. Annual peak discharge values for the AM method

Year	1972	1973	1974	1975	1976	1977	1978	1979	1980	1981	1982	1983	1984
Q [m3/s]	1941	2140	2406	1722	1422	1477	1089	2192	1941	1016	1676	1259	1372
Year	1985	1986	1987	1988	1989	1990	1991	1992	1993	1994	1995	1996	1997
Q [m3/s]	1413	1159	1443	982	1419	2070	1940	1551	1947	1025	1174	1561	1505
Year	1998	1999	2000	2001	2002	2003	2004	2005	2006	2007	2008	2009	
Q [m3/s]	2394	1258	1903	1482	1179	980	1743	1518	1824	1624	1706	1821	

3.3 Monte Carlo Simulation

Generally, the basis of the Monte Carlo simulation method relies on generating random samples that follow the distribution of the random variables relevant to the problem. For estimation of the probability of failure, the system's response is computed for each set of randomly generated variables. It was introduced [25] as a method that involves sampling across the entire space of possibilities [26] and generates random samples according to the statistical distribution functions of different random variables.

In this analysis, the MCS method was introduced to generate a large number of synthetic annual maximum discharge values based on the parameters of the best-fit probability distribution and the values for the energy slope based on the parameters of the fitted distribution. 11 different MC simulations ranging from 10 to 20000 number of simulations were conducted in order to prepare sets of input data for the HEC-RAS model.

3.4 Hydrodynamic Modelling with HEC-RAS

In order to accurately represent the hydrodynamic conditions of the part of the Sava River designated as the study area, a previously developed HEC-RAS model was calibrated using the hydrological data from the nearest gauging stations. The geometry of the model is based on the control cross-section profiles from the Podsused gauging station (rkm 717+200) to the Zagreb gauging station (rkm 702+800). The calibration process involved fine-tuning the model parameters to match the observed water surface profiles and discharge characteristics and to ensure the reliability of the model in simulating real conditions. Manning coefficient and energy slope were interpolated between observed and simulated data. Using the calibrated HEC-RAS model, 11 different simulations were performed with the set of maximum values per simulation from the synthetic annual maximum discharge data, the discharge-Manning coefficient relationship was calculated and the water level data that was generated for each simulation based on discharge, Manning and energy slope data generated by Monte Carlo simulations. The simulations were performed with input data based on the number of simulations of the MCS method - 10, 100, 300, 500, 1000, 3000, 5000, 10000, 13000, 15000 and 20000, respectively. The aim of these simulations was to calculate the parameters for the empirical equation that was later used to estimate the local scour depth.

3.5 Local Scour Prediction

The local scour depth around bridge piers was estimated using an empirical equation (Eq. (3)) calculated based on the Federal Highway Administration's (FHWA) HEC-18 [27]. The inputs for this empirical equation included the hydraulic data simulated using the HEC-RAS model, such as flow velocities, Froude number and average depth of flow directly upstream of the pier, along with specific bridge pier characteristics like pier width, shape, and orientation. These factors were estimated for the case study bridge using the historic bathymetry and flow data. The equation integrates these factors to predict the potential maximum scour depth at each pier location.

$$y_{scour} = 2 \cdot \lambda_{mf} \cdot y_0 \cdot K_1 \cdot K_2 \cdot K_3 \cdot (\frac{D}{y_0})^{0.65} \cdot Fr^{0.43}, \quad (3)$$

Where y_{scour} is scour depth, λ_{mf} is the modelling factor, y_0 is the depth of flow upstream of the pier, K1 is the pier nose shape coefficient, K2 is the angle of attack of flow coefficient, K3 is the bed condition coefficient, D is the pier width, and Fr is the Froude number defined as [28]:

$$Fr = \frac{V}{\sqrt{g \cdot y_0}}, \quad (4)$$

in which V is the mean flow velocity at the pier and g is the gravitational acceleration.

4 Results and discussion

4.1 Results

The first step of the preliminary analysis to estimate local scour around bridges by a statistical analysis of historical AM discharges in combination with a Monte Carlo approach at the Zagreb gauging station for the period from 1972 to 2009 is the fitting of 6 different univariate probability distributions to the historical annual maximum discharge data, tested with several goodness-of-fit (GOF) tests to reduce the uncertainties associated with the different factors influencing scour behaviour. The results show that the generalized extreme value (GEV) distribution for the variable peak discharge fits the data best for all tests applied (Figure 2). In addition, a log-normal distribution for the energy slope and a normal distribution for the Manning coefficient were fitted to prepare the data for the application of the Monte Carlo method (Table 4).

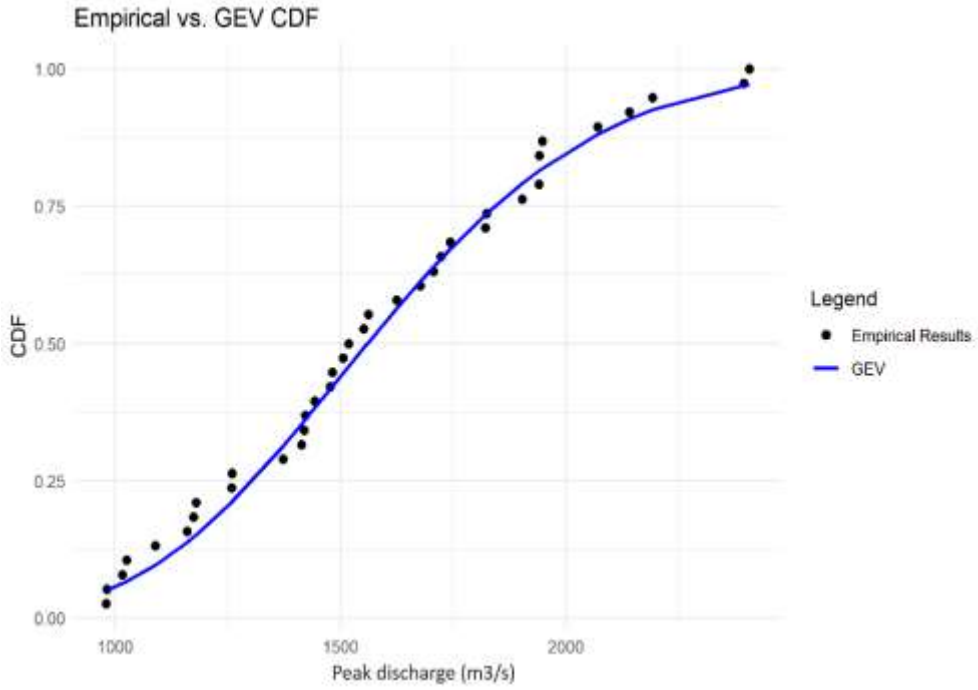

Figure 24. Example of fitting GEV distribution to the peak discharge variable

MCS method was applied to the variables peak discharge and energy slope for 10, 100, 300, 500, 1000, 3000, 5000, 10000, 13000, 15000, and 20000 simulations, respectively, based on the parameters of the best-fit probability distribution for peak discharge and the log-normal distribution for the energy slope. The results of the 11 different simulations were used as input to the HEC-RAS model as the set of maximum values per simulation from the synthetic annual maximum discharge data, the Manning coefficient data extracted from the discharge-Manning value relationship and the water level data that was generated for each simulation based on discharge, Manning and energy slope data generated by Monte Carlo simulations.

Table 4. Description of the input variables for HEC-RAS, the applied probability distributions and goodness-of-fit (GOF) tests

VARIABLE	STATISTICAL VALUES		DISTRIBUTION	GOF TEST		RMSE (m^3/s)
	MEAN	STANDARD DEVIATION		Anderson - Darling	Kolmogorov - Smirnov	
Peak discharge (m^3/s)	1586.2	387.6	Gumbel	0.4455	0.0934	62.85
			Log-Normal	0.2609	0.0788	47.81
			Pearson Type III	0.2086	0.0642	44.05
			Log Pearson Type III	0.2109	0.0640	42.73
			Generalized Extreme Value	0.2039	0.0636	42.68
			Generalized Logistic	0.2951	0.0746	57.10
Energy slope	0.0003	0.00004	Log-Normal			
Manning's coefficient	0.0233	0.0035	Normal			

The results of the HEC-RAS modelling (mean flow velocity (V), depth of the flow upstream (y_0)) were then used, along with the K1, K2, K3 coefficients (1.0, 1.0, 1.1, respectively) and the pier width (D=3.5m), to calculate local scour depth at pier using Eq (3) and Eq (4). The results show (Table 5) the statistical parameters (mean and standard deviation) of the input variables for the local scour depth equation (Eq (3)) for 11 different Monte Carlo simulations which resulted in a representation of the dependence between the number of simulations for mean/standard deviation and local scour depth**Chyba! Nenašiel sa žiaden zdroj odkazov.** (Figure 3, Figure 4).

Table 5. Statistical parameters of the input variables for the local scour equation

VARIABLE	STATISTICAL PARAMETER	NUMBER OF MONTE CARLO SIMULATIONS										
		10	100	300	500	1000	3000	5000	10000	13000	15000	20000
Flow velocity (V)	Mean (m/s)	2.808	2.812	2.801	2.797	2.796	2.795	2.795	2.795	2.797	2.796	2.797
	Standard deviation (m/s)	0.2826	0.2605	0.2616	0.2626	0.2651	0.2620	0.2631	0.2635	0.2625	0.2628	0.2647
	Minimum (m/s)	2.38	2.24	2.22	2.19	2.20	2.12	2.16	2.16	2.12	2.12	2.13
	Maximum (m/s)	3.38	3.39	3.39	3.39	3.39	3.39	3.39	3.39	3.39	3.39	3.39
Depth of the flow upstream (y_0)	Mean (m)	8.153	8.230	8.229	8.228	8.224	8.228	8.228	8.226	8.231	8.230	8.228
	Standard deviation (m)	0.3151	0.3229	0.3129	0.3122	0.2992	0.3092	0.3051	0.3037	0.3075	0.3066	0.3081
	Minimum (m)	7.47	7.46	7.46	7.47	7.47	7.46	7.47	7.46	7.46	7.46	7.46
	Maximum (m)	8.65	8.96	8.92	8.95	8.91	8.93	8.93	8.92	8.94	8.93	8.93

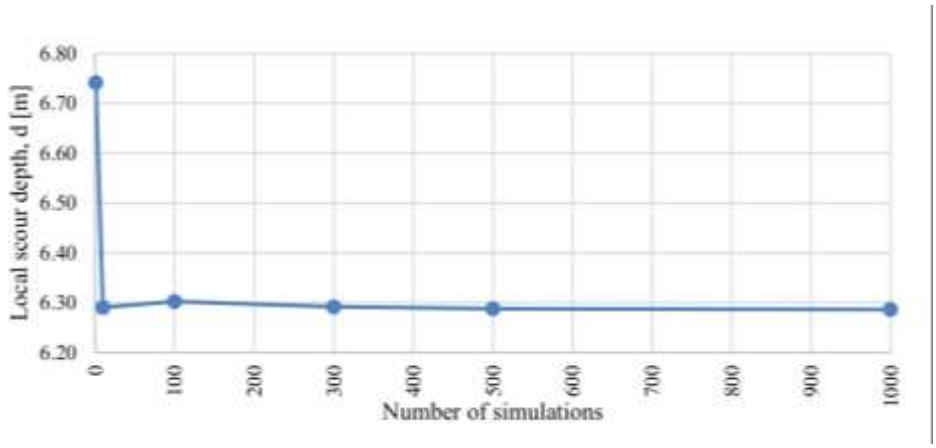

Figure 25. Number of simulations with mean value for local scour depth

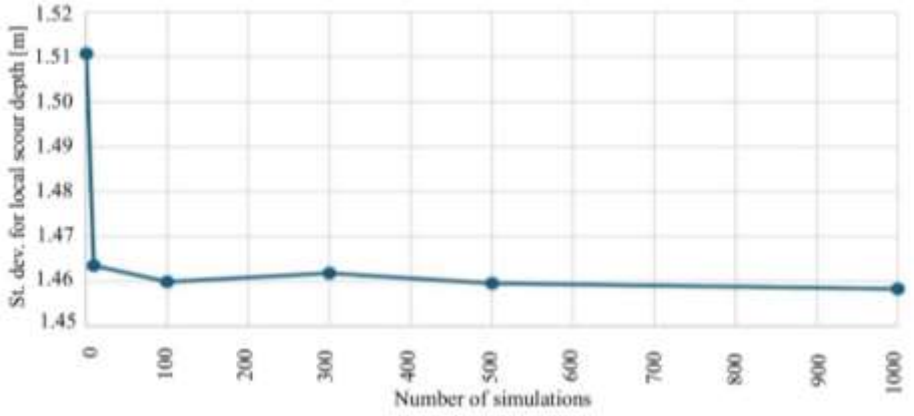

Figure 26. Number of simulations with standard deviation for local scour depth

4.2 Discussion

By performing different simulations with different numbers of simulations of the input data, the study provided a data set to be used as input to the empirical equation used to estimate the local scour depth at the pier. The analysis preformed showed that a relatively small number of simulations are required (e.g. less than 100) for the local scour depth variable at the pier to begin to converge for both the mean and standard deviation.

The integration of statistical analysis, Monte Carlo simulation, and hydrodynamic modelling in this study provides a comprehensive approach to account for the effects of uncertainty in the hydraulic model parameters when calculating the local scour depth at the bridge pier. The methodology can be adapted and applied to other rivers and bridges and provides valuable insights to engineers and researchers involved in bridge design and maintenance.

5 Conclusion

In this paper a framework for the estimation of local scour around bridges was created, taking into account the uncertainties of the hydraulic parameters through a combination of statistical analysis and Monte Carlo simulation together with a hydrodynamic model. The Generalized Extreme Value distribution was identified as the best fit for historical annual maximum discharge data, and a log-normal distribution was fitted for the energy slope. The Monte Carlo simulations generated synthetic data sets that were used in HEC-RAS modelling to predict local scour depth at the pier using the HEC-18 equation.

The results show that increasing the number of Monte Carlo simulations beyond 100 doesn't significantly improve the reliability and consistency of the estimation of local scour depth at the pier, as indicated by a stabilization of the mean value and a reduction in the standard deviation. The case study of the Sava River bridge in Zagreb, Croatia, demonstrates the practical application of the framework, contributing to the ongoing research on the relationship between climate change indicators, flood wave characteristics and scour development. The results underline the importance of considering uncertainties in hydraulic modelling and provide a basis for future studies to improve bridge safety and resilience to extreme hydrological events.

Acknowledgements

Part of this research is conducted as part of the R3PEAT project ("Remote Real-time Riprap Protection Erosion Assessment on large rivers", UIP-2019-04-4046) supported by the Croatian Science Foundation under the "Young Researchers' Career Development Project – Training New Doctoral Students" (DOK-2020-01-5354).

References:

[1] Hung, C. C., Yau, W. G.: Behavior of Scoured Bridge Piers Subjected to Flood-induced Loads. *Engineering Structures, 80,* pp. 241-250, 2014

[2] Clopper, P., Lagasse P. F., Zevenbergen, L.W.: Risk-Based Approach for Bridge Scour Prediction: Applications for Design. In: *National Hydraulic Engineering Conference 2014*. University of Iowa, 2014.

[3] Lagasse, P.F, Richardson, E. V.: ASCE compendium of stream stability and bridge scour papers. *Journal of Hydraulic Engineering*, 127, pp. 531–533, 2001.

[4] Ettema R.: Scour at Bridge Piers, PhD Thesis, University of Auckland, Auckland, New Zealand, 1980.

[5] Qadar, A.: The Vortex Scour Mechanism at Bridge Piers: *Proceedings of the Institution of Civil Engineers*, 71, pp. 739–757, 1981.

[6] Karaki, S., Haynie, R. M: Mechanics of Local Scour: Part 2, Bibliography. Report CER 59 SEK 36, Colorado State University, 51 pp, 1963.

[7] Heidarpour, M., Khodarahmi, Z., Mousavi, S. F.: Control and Reduction of Local Scour at Bridge Pier Groups using Slot. In: *Proceeding IAHIR congress. Thessaloniki, Greece.*, 2003.

[8] Brunner, G. W.: HEC-RAS, River Analysis System User's Manual, Version 4.0 Beta. *US Army Corps of Engineers*, 420, 2006.

[9] Johnson, P. A.: Uncertainty of Hydraulic Parameters. *Journal of Hydraulic Engineering,* 122, pp. 112–114, 1996.

[10] Al Rammahi, A. H. J., Khassaf, S. I.: Probabilistic Prediction of Scouring around Piers using Monte Carlo Simulation. In: *IOP Conference Series: Materials Science and Engineering*. IOP Publishing, p. 012080, 2021.

[11] Tubaldi, E., Macorini, L., Izzuddin, B. A., et al. A framework for Probabilistic Assessment of Clear-water Scour around Bridge Piers. *Structural Safety,* 69, pp. 11–22, 2017.

[12] Altarejos-García, L., Martínez-Chenoll, M. L., Escuder-Bueno, I., Serrano-Lombillo, A. Assessing the Impact of Uncertainty on Flood Risk Estimates with Reliability Analysis using 1-D and 2-D Hydraulic Models. *Hydrology and Earth System Sciences*, 16(7), pp. 1895-1914, 2012.

[13] Lagasse, P. F., Ghosn, M., Johnson, P., Zevenbergen, L., Clopper, P. Risk-Based Approach for Bridge Scour Prediction, Final Report. Transportation Research Board, 2013.

[14] Bukaçi, E., Korini, T., Periku, E., Allkja, S., & Sheperi, P. Number of Iterations Needed in Monte Carlo Simulation using Reliability Analysis for Tunnel Supports, *International Journal of Engineering Research and Applications,* 6(6), pp. 60-64, 2016.

[15] Čanjevac, I., Orešić, D.: Changes in Discharge Regimes of Rivers in Croatia, *Acta geographica Slovenica*, 58, pp. 7–18, 2018.

[16] Gilja, G., Ocvirk, E., Kuspilić, N.: Joint Probability Analysis of Flood Hazard at River Confluences using Bivariate Copulas, *Gradjevinar*, 70, pp. 267–275, 2018.

[17] Bonacci, O., Ljubenkov, I.: Assessment of Zagreb's Flood Safety from the Waters of the Sava River under New Conditions (Assessment of the Zagreb Town Protection from the Sava River Floods in New Conditions), *Hrvatska vodoprivreda,* XII (127-128), pp. 51–55, 2003.

[18] Bonacci, O., Ljubenkov, I.: Statistička analiza maksimalnih godišnjih protoka Save kod Zagreba 1926.-2000. (Statistical analysis of maximum annual discharges of the Sava River at Zagreb for the 1926–2000 period), *Hrvatske vode,12* (48), pp. 243–252, 2004.

[19] Bonacci, O., Trninic, D.: Hydrologische, durch die Aktivität des Menschen hervorgerufene Veränderungen im Flussgebiet der Save bei Zagreb (Man's Influence on Hydrological Changes on the Sava River near Zagreb), *Wasserwirtschaft,* 81, pp. 171–175, 1991.

[20] Bonacci, O., Ljubenkov, I.: Changes in Flow Conveyance and Implication for Flood Protection, Sava River, Zagreb. *Hydrological Processes,* 22, pp. 1189–1196, 2008.

[21] Kratofil, L.: Promjene Vodnog Režima Save Uzrokovane Ljudskom Djelatnošću (Changes of the Sava River Water Regime Caused by Anthropogenic Activities), *Zbornik radova okruglog stola "Hidrologija i Vodni Resursi Save u Novim Uvjetima" (Proceedings of Roundtable "The Sava River Hydrology and Water Resources in New Conditions"),* pp. 335–352, 2000.

[22] Šegota, T., Filipčić, A.: Suvremene Promjene Klime i Smanjenje Protoka Save u Zagrebu (Contemporary Climate Changes and Decrease of Sava River Flow through Zagreb), *Geoadria,* 12, pp. 47–58, 2007.
[23] Kuspilić, N., Gilja, G.: Utjecaj Vodotoka na Sigurnost Mostova (Influence of Watercourse Flow on Bridge Safety), *e-Zbornik, Elektronički Zbornik Radova Građevinskog Fakulteta,* 8, pp. 24–38, 2018.
[24] Hosking, J. R. M., Wallis, J. R.: *Regional Frequency Analysis. An Approach Based on L-Moments*, Cambridge University Press, UK, 1997.
[25] Metropolis, N., Ulam, S.: The Monte Carlo Method, *Journal of the American Statistical Association,* 44, pp. 335–341, 1949.
[26] Rashki, M.: Hybrid Control Variates-based Simulation Method for Structural Reliability Analysis of some Problems with Low Failure Probability, *Applied Mathematical Modelling,* 60, pp. 220–234, 2018.
[27] Arneson, L. A.: *Evaluating Scour at Bridges*, United States. Federal Highway Administration, 2013.
[28] Neitsch, S. L., Arnold, J. G., Kiniry, J. R., et al.: *Soil and Water Assessment Tool Theoretical Documentation Version 2009,* Texas Water Resources Institute, 2011.

POSSIBILITIES OF WATER REGIME IMPROVEMENT IN THE KLÁTOV BRANCH NATIONAL NATURE RESERVE

ANDREJ ŠOLTÉSZ [1], MARTIN ORFÁNUS [1], DANA BAROKOVÁ [1], JAKUB MYDLA [1]

[1] *Slovak University of Technology in Bratislava, Faculty of Civil Engineering, Department of Hydraulic Engineering, Slovakia, andrej.soltesz@stuba.sk, martin.orfanus@stuba.sk, dana.barokova@stuba.sk, jakub.mydla@stuba.sk*

1 Abstract

In frame of the project 'Status improvement of wetland of Klátov branch National Nature Reserve (NNR)', financed from the Norwegian financial mechanism, was the task of the Department of Hydraulic Engineering as co-researcher partner to find a solution for possible revitalisation of the water regime of the more than 30 km long Klátov branch. The Klátov branch was in the beginning of the 20th century dammed and thus cut off from the surface water source – the Little Danube. It happened after disastrous floods in 1897, and especially in 1899. Since then, the only source for the Klátov branch has become groundwater. This has resulted in the water of the Klátov branch being extremely clean with high ecological value. As the groundwater level in the area between the Danube and the Little Danube has dropped significantly in recent years, the water regime of the Klátov branch has also been affected. The paper deals with the hydraulic solution of indirect inflow of surface water from the Little Danube with possible infiltration into the Klátov branch.

Keywords: Klátov branch, surface water recharge, infiltration experiment, 2-D mathematical modelling, surface and ground water interaction, revitalisation measures

2 Introduction

The basis for the solution of our task was the analysis of hydrological, hydropedological, hydrogeological, morphological and biological characteristics of the area in Klátov branch NNR, which were complemented by own measurements of hydraulic parameters in the flow of the Klátov branch and its tributaries. Considering the proposed technical solution of the recharge of the Klátov branch from the Little Danube by filtration through the "seepage tanks" in the upper section of the Klátov branch, these documents were supplemented by infiltration experiments measuring the intensity of surface water seepage into the bedrock of the Klátov branch bed. On this basis the actual system of the seepage processing (seepage tanks, large-scale seepage experiment) from the Little Danube water into the Klátov branch was designed.

Another important base for the solution was the digital terrain model taken from the Basic Database for Geographical Information System (ZBGIS), which was supplemented within the project by data from the detailed digital surveying of the Klátov branch streambed with the related bathymetry (measurements of water depths in the Klátov branch).

These background materials served as input data for the analysis and forecast of the flow and water level regime of both surface water in the Klátov branch and groundwater in the immediate vicinity of the Klátov branch. After calibration of the 2-D mathematical model of the water level and flow regime in the Klátov branch, it was possible to develop several scenarios of water recharge to the Klátov branch and related possible morphological modifications of the channel in order to improve the flow velocity regime with the aim to set the bed sediments in the stream in motion. The proposed solutions are in line with the conclusions of the biological study, which indicated that the revitalisation measures have a high potential for improving the ecological status and that restoring the dynamics of the water regime in the affected area would mean at least approaching the environmental conditions that existed in the Klátov branch before it was cut off from the Little Danube River.

The Klátov branch is a right-side tributary of the Little Danube. It is often stated that it has no source and is not separated from any other stream, it rises from the groundwater behind the village of Orechová

Potôň - Lúky, thanks to which it is characterised by a high degree of water purity. This statement is only partly true. The original Klátov branch was directly connected to and fed by the Little Danube. The actual cutting off of the Klátov branch from the Little Danube was decided after above mentioned disastrous Danube floods at the end of the 19th century. At that time, the territory of the "Tökés Island" was threatened by the construction of dykes along the Váh, as a result of which the rising water of the Váh River caused the Little Danube to back up, spill over the inadequate dykes of the Klátov branch and flood the lower part of the territory of the "Tökés Island". The closure of the Klátov branch was implemented before the First World War, but not to a satisfactory extent. During the war, the flood protection work in the adjacent area was completely stopped and it was continued after 1918.
Figure 1 shows a map of the upper part of the Klátov branch from Orechová Potôň - Lúky to Jahodná from 1931, which shows the constructed protective dyke along the Little Danube, to which was dedicated the approval protocol from 1925 and which included the closure of the Klátov branch, as well [1].

Figure 1. Map of the Klátov branch after the approval of construction works in 1931 (Varga, 2022)

Since this period, the source of water for the Klátovský branch in its upper part has been groundwater seepage or precipitation. During the 20th century, the inflow subsidy decreased due to the gradual clogging of the Little Danube river bed, into which the former river bed-forming flows have not been discharged for a long time, only the controlled stable flow. After the construction of the Gabčíkovo hydropower plant (HPP) and its operation start in 1992, this subsidy gradually decreased, mainly as a result of the clogging of the Hrušov dam.

3 Methods

3.1 The area of interest

The actual surface water supply to the Klátov branch is provided by the right-side tributary of the Klátov channel, which is endowed by the waters of the Little Danube, partly collects seepage waters from the north-eastern territory of the upper Rye Island and flows into the Klátov branch in the Danube Klátov below the historical mill (rkm 14.020). The most important tributary to the lower part of the Klátov branch is the right-side tributary of the primary drainage channel of the SVII drainage system [2]. At the same time, it can also be described as the most reliable one, because it is still supplied with water from the Gabčíkovo HPP (GHPP) power canal and at the same time it receives the secondary drainage

channels AVII, BVII and CVII [3], which are supplied from the left-side seepage channel of the GHPP (Figure 2).

Figure 2. Illustration of the SVII channel drainage system

The climatic conditions of the Rye Island are determined primarily by geographical factors, i.e. latitude, longitude and altitude. This area is one of the warmest in Slovakia, with an average annual temperature of 9 °C - 11 °C, where the average annual temperature in January is above -2 °C and the average annual temperature in July is above 20 °C.
The average annual flow of the Danube River in Bratislava in the period from 1931 to 2000 was 2 044 $m^3.s^{-1}$. The Little Danube is the longest left-side branch of the Danube River, with a flow length of 128 km. Its average annual flow in recent years was 32.60 $m^3.s^{-1}$ at the Nová Dedinka and 35.10 $m^3.s^{-1}$ at the Trstice profile. In addition to the Danube River, the Little Danube also drains water from the south-eastern slopes of the Little Carpathians. Its largest tributary is the Čierna Voda stream. The Klátov branch, which flows into the Little Danube at Topoľníky, also forms part of the catchment area.

3.2 Conceptual design for the water supply into the Klátov branch

The pumping of water from the Little Danube and its effluent in the uppermost part of the Klátov branch was called – Large scale infiltration experiment [4]. Such an experiment should test the possibility of recharging the Klátov branch in an indirect way (by recharging groundwater with subsequent springing into the Klátov branch). The task of the large-scale seepage experiment would be not only to supplement and verify the conducted "small (point)" seepage experiments, which provide us with information about the infiltration capacity of the studied area, but also to determine the exact direction of groundwater flow in a relatively small area and also to quantify the seepage quantities. An overview of the location of the large-scale seepage is given in Figure 3.

Figure 3. Situation of the location of the large infiltration experiment

For better exploration of the uppermost part of the Klátov branch, a local simulation model of surface water flow has been developed focusing only on this partial area. The model was used to investigate the environmental risks associated with the recharge of the Klátov branch with water from the Little Danube. Figure 4 on the left shows a map of depths at a subsidy flow Q = 1 $m^3.s^{-1}$ in the actual terrain [4].

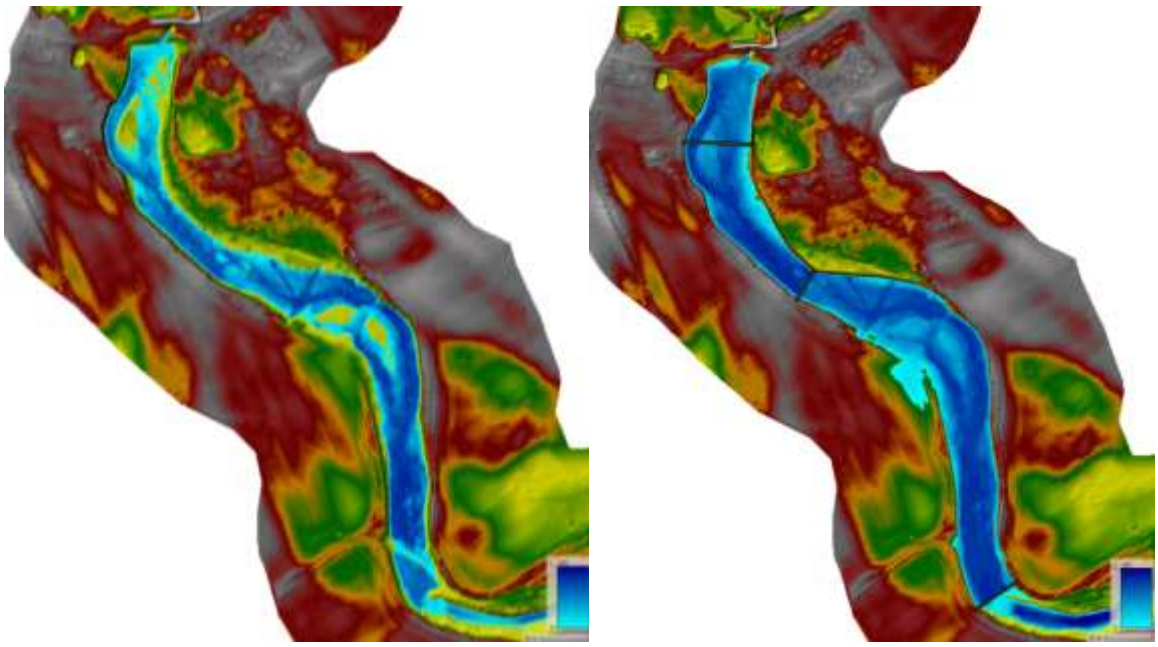

Figure 4. Depth map at flow rate Q=1.0 $m^3.s^{-1}$, actual terrain (left), with dividing barrages (right)

To support the surface water infiltration and reduce the flow velocity, which in turn will promote the sedimentation processes necessary to maximize the purification/sedimentation of the Little Danube water, 3 dividing barrages have been conceptually designed in this part of the Klátov branch (Figure 4, right).

3.3 Water level and velocity regime of the Klátov branch

The two-dimensional simulation model HEC-RAS 2-D v.6.3 was used to determine the water level regime of the Klátov branch section of interest, which was developed mainly for the purpose of use as a basic technological tool for planning and analysis of river systems. In addition to the digital terrain model and bathymetry, the necessary field measurements of flows and surface water levels in the Klátov branch and its tributaries, which were used to calibrate the model itself, are the basis for a well-constructed simualtion model. These measurements were carried out by the team of the Department of Hydraulic Engineering, Faculty of Civil Engineering, STU during the project.

Measurements of flow quantities were carried out in June 2023 in a total of 6 profiles, 4 of which were located directly at the Klátov branch. The locations and results of the measurements are shown in Figure 5. In addition to the measurement of water levels and discharges, the existing structures were also identified and measures, especially the bridges and culverts along the Klátov branch. Some structures were not accessible for our personal measurement as they were located in fenced locations. The dimensions of such structures were obtained from historical measurements. Total of 22 features (including spillways and footbridges) were identified [4].

After the calibration of the compiled simulationl model, several scenarios of the possibility of improving the water flow and level regime, as well as the scenario of a possible hydraulic sediment flushing of the Klátov branch were investigated in cooperation with the State Nature Protection organisation (SNP) due to the fact that the area is an NNR and dredging of sediments in the stream bed is not permissible.

The calibration sites were selected from a database of measurements and chosen based on compatibility with the numerical model and its computational grid. The results of the individual calibration sites with comparison to the simulation for the scenario were included more detailed in "Analysis of the current state" [4]. The largest deviation is the difference in levels at the area of the Klátov mill in the vicinity of the sluice. The more significant deviation is due to the deformation of the level at the spillway through the sluice in combination with the resolution of the computational grid for the purpose of the calculations of the whole Klátov branch.

3.4 Results of numerical modelling – proposal of possible measures to improve the velocity and water level regime

The present condition as a calibration scenario and a baseline for the analysis, as well, is characterized by low flows with very low velocities. From the practical point of view of modelling hydrodynamic conditions, the Klátov branch has been divided into 3 approximately equal length sections - lower, middle and upper. Figure 6 shows the velocity map in the lowest part of the Klátov branch for current conditions.

Due to the limited space, we only present the result of the modelling process, which was implemented in cooperation with the Slovak Water Management Enterprise (SWME) staff also within the project. This result is the representation of the velocity field change due to the design of the splitting islands in the Klátov branch flow over the road bridge in Trhová Hradská village (Figure 7), [4].

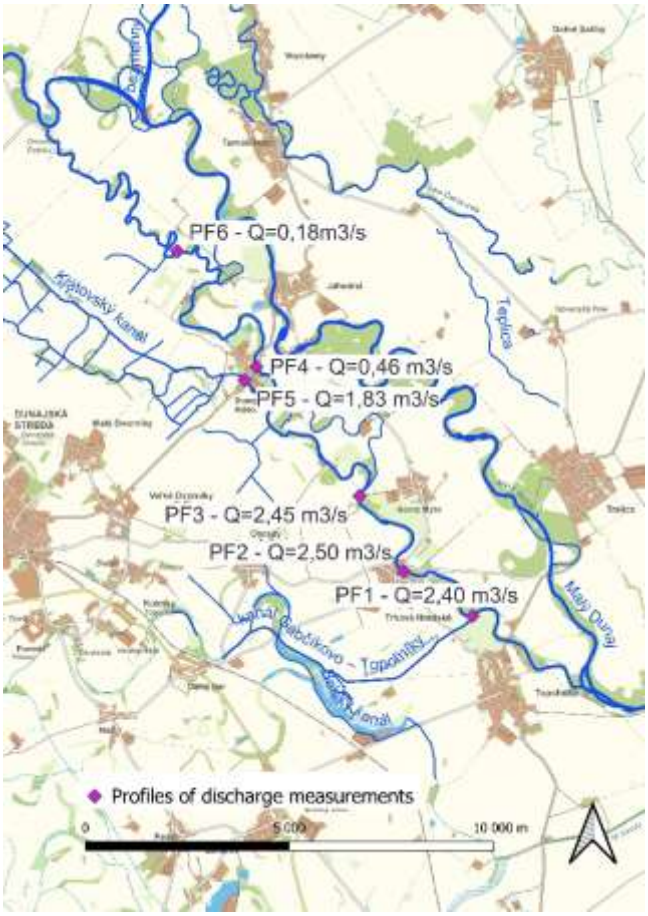

Figure 5. Presentation of flow measurement locations for model calibration

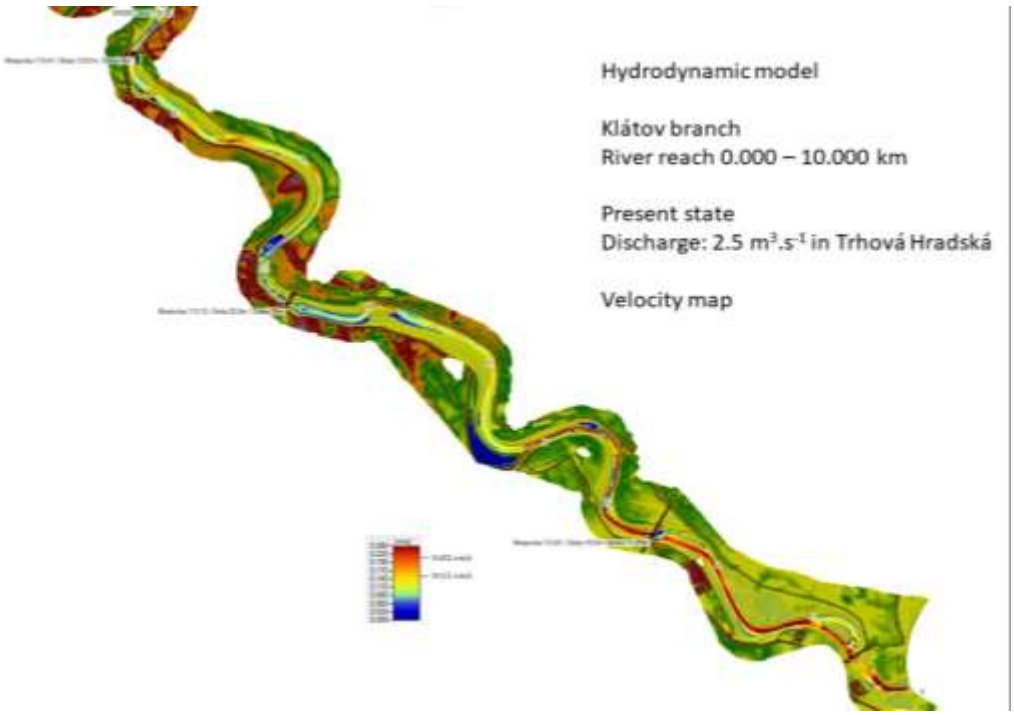

Figure 6. Map of velocities in the lower section rkm 0.000 – 10.000 of the Klátov branch

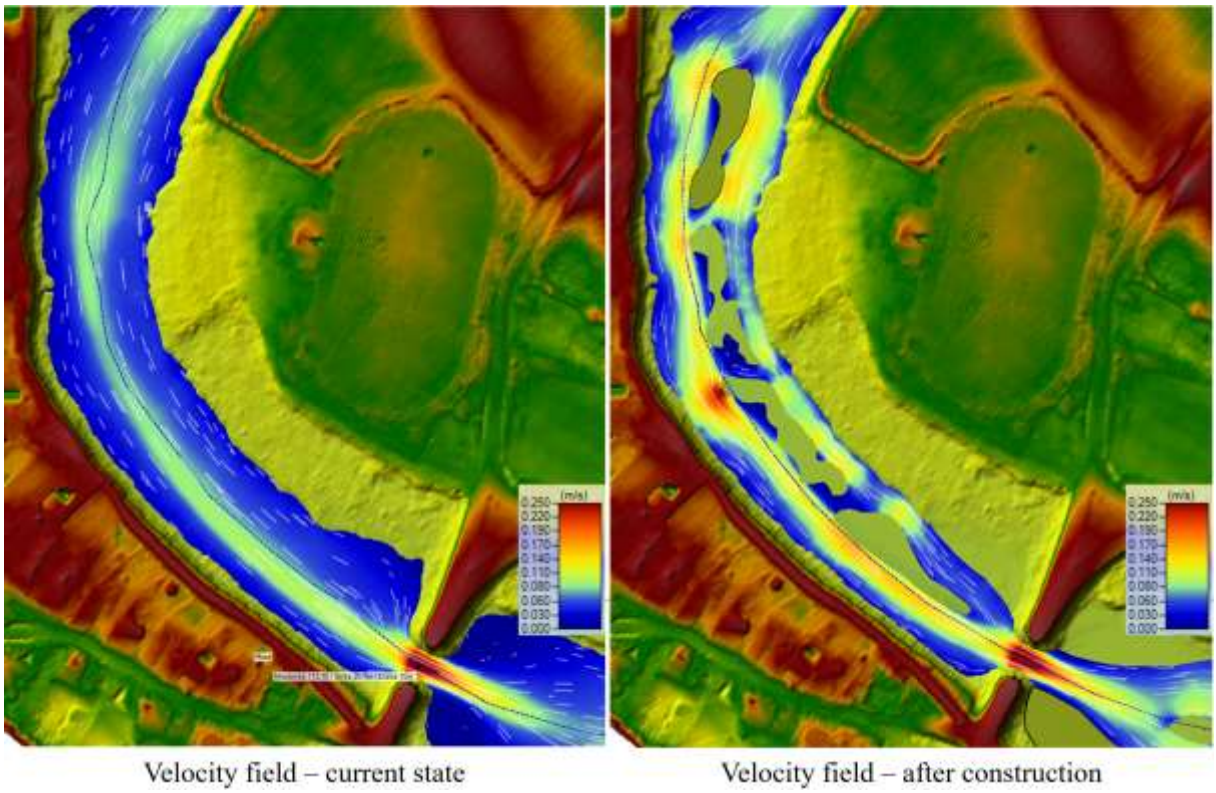

Figure 7. Comparison of the impact of island design on velocity field and flow separation before (current condition, left) and after construction of the island system design

Unfortunately, the funds in the project were only sufficient to implement one island, which is shown in Figure 8.

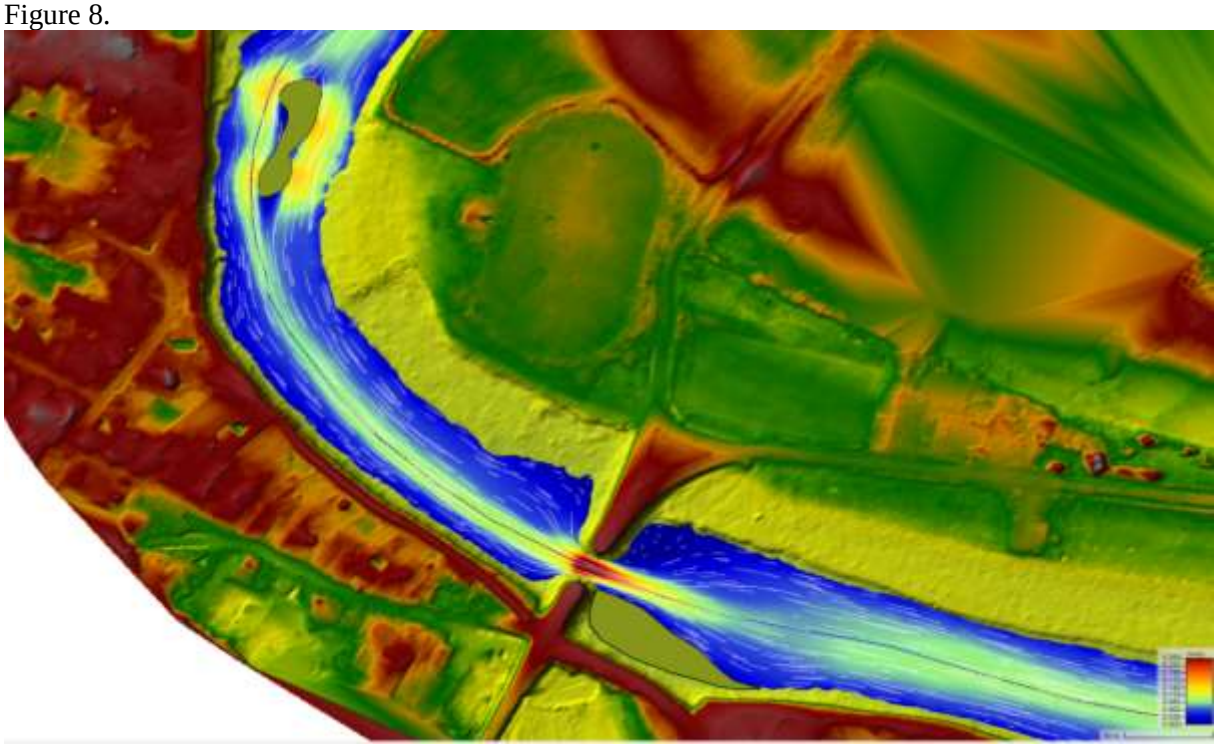

Figure 8. Presentation of the result of the 2-D modelling of the velocity field after the construction of the island in the Klátov branch in Trhová Hradská village

4 Conclusion

The main task of the research team from STU in frame of the NFP project was to create a 2-D simulation model of water flow in the Klátov branch in a GIS environment, which was gradually calibrated thanks to further field measurements focused on the discharge and water level regime in individual profiles along the Klátov branch and its tributaries. On the basis of the modelling, it was possible to develop the necessary scenarios of water supply to the Klátov branch and the related possible morphological modifications of the channel in order to improve the flow velocity regime in order to set the river bed sediments in the stream in motion. The researchers worked closely with the SNP in their preparation with respect to the water stream biota.
The results of the modelled scenarios for the improvement of the flow and water level regime were supplemented by the possibilities of determining the impact of the implementation of local directive structures or artificial islands, the task of which was to increase the water flow velocity and the associated entrainment capacity of sediments and sediment in the channel of the Klátov branch. The best proof of the research work evaluation was the implementation of the pilot island and the pilot gravel bench into the stream bed in the village of Trhová Hradská.

Acknowledgements
The paper was developed within framework and based on the financial support of the VEGA project No. 1/0728/21 Analysis and prognosis of impact of construction activities on ground water in urbanized territory and APVV project APVV-19-383 “Natural and technical measures oriented to water retention in sub-mountain watersheds of Slovakia.

References:
[1] Varga, P. (2022): Klátov branch - past, present and future. Power point presentation, SWME, Bratislava, 37 p.

[2] Gyalokay, M. (1960): Drainage of Rye Island, Works and Studies 11, Water Research Institute, Bratislava, 217 p.

[3] Schügerl, R., Velísková, Y. (2023): Change of the Manning´s coefficient in small stream influenced by vegetation, Acta Hydrologica Slovaca, vol. 24, 1, p. 134 - 140.

[4] Šoltész, A. et al. (2024): Improvement of the wetland condition of NNR Klátov branch on the territory of SKUEV0075, Water and environmental study, Faculty of Civil Engineering, STU in Bratislava, 91 p.

ANALYSIS OF ANNUAL AND SEASONAL PRECIPITATION OF THREE REPRESENTATIVE CROATIAN REEEEEGIONS

LIDIJA TADIĆ [1], JOSIP JANJIĆ [2], TAMARA BRLEKOVIĆ[3]

[1] *Faculty of Civil Engineering and Architecture Osijek, Croatia, ltadic@gfos.hr*

[2] *Faculty of Civil Engineering and Architecture Osijek, Croatia, jjanjic@gfos.hr*

[3] *Faculty of Civil Engineering and Architecture Osijek, Croatia, tamaradadic@gfos.hr*

1 Abstract

Changes in precipitation regime, besides changes in air temperatures, are one of the main climate change impacts on a global scale. This paper focuses on precipitation which is the most important and most common parameter for any hydrological analysis including drought. Time period of analysis is relatively long, between 1951 and 2022. The meteorological stations included in the research were Osijek, Zagreb, and Split, representative for the entire country. Annual and seasonal precipitations were analysed by Mann-Kendall trend test, innovative trend analysis and risk analysis.

Keywords: Mann-Kendall test, innovative trend analysis, risk analysis, precipitation, Split, Zagreb, Osijek

2 Introduction

Urbanization, population growth, economic growth and traffic are having permanent and long-lasting negative effects on the environment. A great effort of scientists of various expertise are focused on predictions, minimizations and possible solutions of climate change impacts. Precipitation is crucial component of hydrological cycle and vulnerable on climate change. During longer time periods precipitation pattern changes due to different impacts. In the recent time it is mostly due to climate change evident in the all parts of the world with stronger or milder intensity. Examining and understanding of the temporal variations and distribution in precipitation regime can have a significant impact on the amount of water available in a watershed, including extremes. Croatia also facing more frequent extreme hydrological events droughts and floods caused by changes in meteorological conditions precipitation and air temperature.

There are great number of research related to this problem on the national, regional, catchment and sub-catchment levels in Croatia [1-5]. This research of precipitation is focused on data observed on three meteorological stations: Osijek, Zagreb and Split (Figure 1). According to Köppen classification of climate zones, Osijek and Zagreb belong to the region of temperate humid climate with warm summers (Cfb) and Split belongs to region of Mediterranean climate with hot summers (Csa) [6]. Even Osijek and Zagreb belong to the same climate zone; they are in different orographic regions which well correspond with geographical positions and elevations.

Figure 1. Study area

Croatia is divided into seven spatial regions by considering annual rainfall variations and the distribution of percentiles of daily rainfall [1,2]. Osijek belongs to Region 1 (Eastern mainland). Zagreb to region 2 (Western mainland) and Split belongs to Region 7 (Central and Southern Adriatic coastal region). Period of analysis is between 1951-2022 and monthly data were used.

Table 1. Annual precipitation characteristics of analysed stations (1951-2022)

	MEAN (MM)	MAX	MIN	ST.DEVIATION	COEFF. OF VARIATION
OSIJEK	680	1042 (1955)	317 (2000)	134.1	0.197
ZAGREB	863	1318 (2014)	517(2011)	141.8	0.164
SPLIT	811	1209 (2014)	487 (1989)	158.6	0.195

Previous results reveal mostly weak changes in annual and seasonal amounts in the period 1961-2010. The only negative significant trend is detected only for precipitation in mountainous regions [1].
More specific characterization of precipitation regime is given in the Table 1. Mean annul precipitation generally decreases from west to the east. In each region maximum and minimum values occurred in different years, mostly in the 21st century. However annual data show relatively low variability, with coefficient of variations between 0.164 and 0.197.

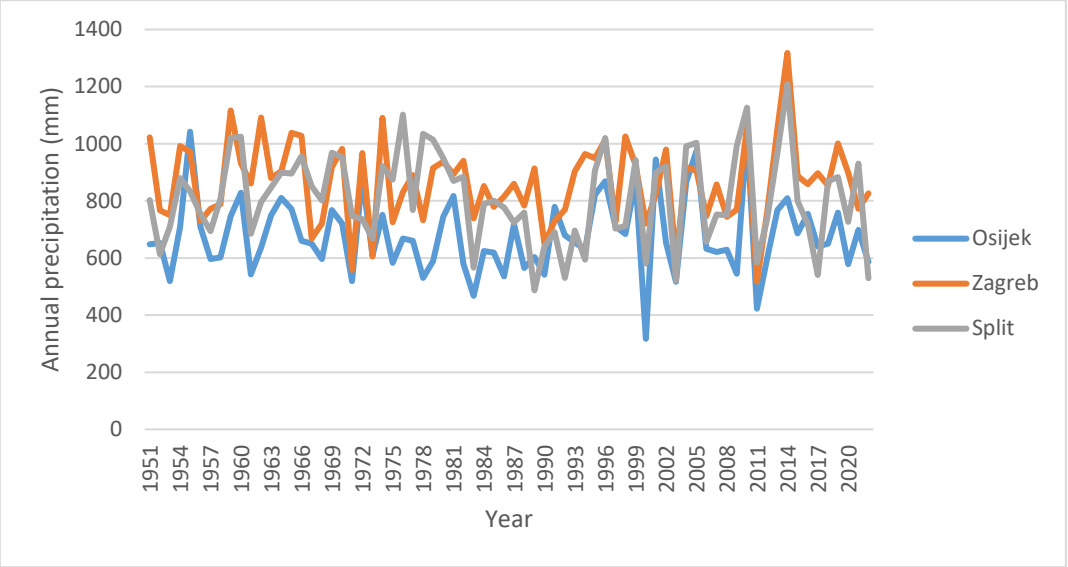

Figure 2. Annual precipitation (1951-2022) for three representative regions in Croatia

Figure 2 presents annual precipitations of the period 1951-2022 observed on three representative meteorological stations. In previous research of drought occurrence, precipitation was tested for homogeneity using the standard normal homogeneity test (SNHT) on an annual and seasonal basis. On an annual basis, there is no inhomogeneity but on the seasonal level there is inhomogeneity only in the precipitation record of the Zagreb station during autumn [5]. Further analysis of precipitation by using Mann-Kendall test (MKT), Innovative Trend Analysis (ITA) and risk analysis will be given in this paper.

3 Methods

3.1 Mann-Kendall trend test

Mann- Kendall trend test is very well known non-parametric test. It was applied in order to determine the existence of significant temporal tendencies in the annual or seasonal precipitations [7-10]. The test statistics Z_{MK} is described as Eq. (1):

$$Z_{MK} = \begin{cases} \frac{S-1}{\sigma} \text{ if } S > 0 \\ 0 \text{ if } S = 0 \\ \frac{S+1}{\sigma} \text{ if } S < 0 \end{cases} \quad (1)$$

where Zc is test statistics which follows a normal distribution, a positive Zc and a negative Zc depict an upward and downwards trend for the period respectively. Each data value is compared with all subsequent data values. If a data value from a later time period is higher than a data value from an earlier time period, the statistic S is incremented by 1. On the other hand, if the data value from a later time period is lower than a data value sampled earlier, S is decremented by 1. The net result of all such increments and decrements yields the final value of S.

Levels of significance are designated by following symbols: *** if trend at α = 0.001 level of significance; ** if trend at α = 0.01 level of significance; * if trend at α = 0.05 level of significance; $^{+}$ if trend at α = 0.1 level of significance [11].

3.2 Innovative trend analysis

Another methodology applied in this research is more recent [12,13]. Innovative trend analysis (ITA) is developed by Şen (2012) and it is based on subsections of time series plots derived from a given time

series on a Cartesian coordinate system. In this way, if there is no trend in time series subsections appear along the 45° straight line. Increasing or decreasing trends appear in upper or lower triangular areas of the square area. The rainfall intensities defined on the basis of percentiles were divided into three categories: low rainfall, bellow 40th percentile, moderate rainfall, in range between 40th and 60th percentile and high rainfall over 60th percentile [14]. The most important advance of this method is its possibility to identify and make more clearer, some no clear trends detected by the Mann–Kendall [15]. ITA method has been used all over the world (Turkey, New Zealand, China, etc). It was successfully applied on a large portion of the Italian peninsula, between ranging from the Campania and the Apulia regions in the North, to Sicily in the South [16]. Also, it was applied on monthly and seasonal rainfall during the period 1975–2015 at 38 stations on two watersheds in Coastal-Oran and Macta watersheds of Algeria (North-West of Algeria) [17].
This method allows the trend identification of the low, medium and high values of a series, while Mann-Kendall test gives general tendency of specific data series.

3.3 Risk analysis

The next subject we wanted to address is risk of occurrence under-average precipitation in two previously defined periods of 36 years (1951-1986 and 1987-2022). Measure of risk is product of severity (S) and likelihood (P) provides a measure of risk (R) which is given by the Eq. (2):

$$R = S*P \tag{2}$$

Once the potential extreme situation has been identified, the question of assigning severity and probability ratings must be addressed. In this case severity (S) is defined as difference between average annual precipitation and annul precipitation of each specific year. Eventually, the technique is consummated by the application of the risk analysis, very powerful tool for decision makers.

4 Results and discussion

The existence of significant temporal trends was tested using the non-parametric Mann–Kendall trend test. It showed negative but not significant trends in the winter and spring months in all three regions. Significant decreasing trend is observed in summer period in Zagreb and Split region. Increasing trend of precipitation is observed in autumn in the Osijek and again in the Zagreb region (Figure 3). On annual basis all three stations have decreasing, but not significant trend.

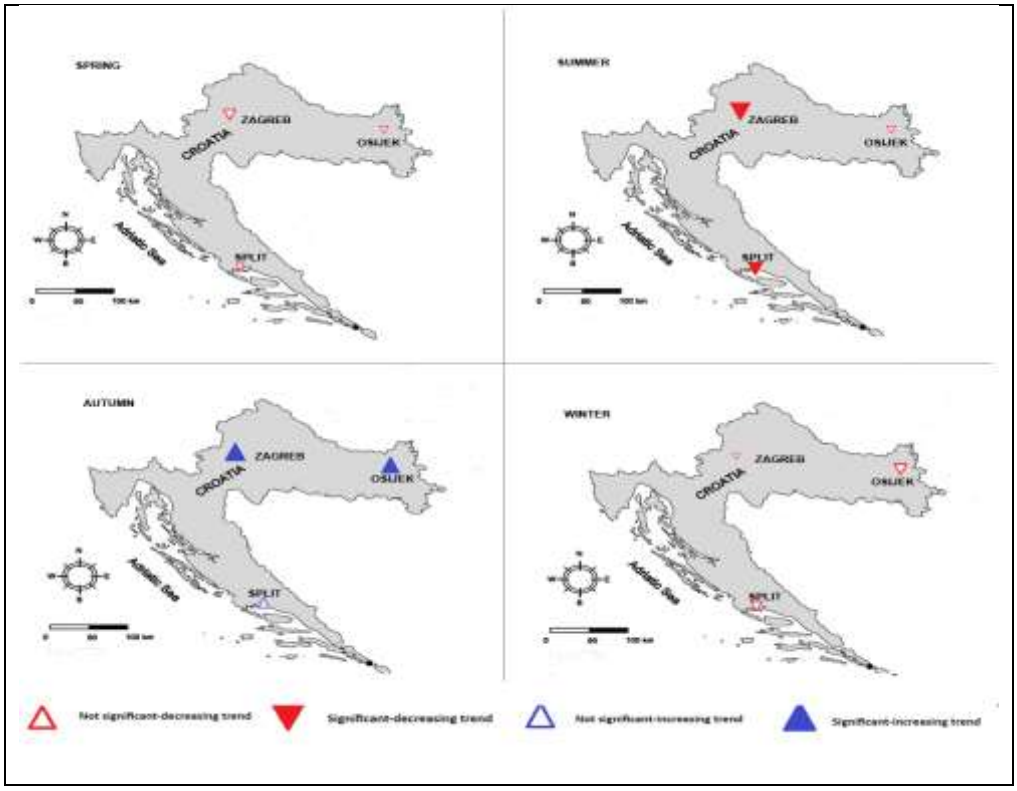

Figure 3. Mann-Kendall test applied on seasonal precipitation

Despite of differences in geographical features, there are rather similar and even unexpected precipitation regime in observed three regions. For the further analysis of annual precipitation was applied one of the most recent approach in climate change research is innovative trend analysis (ITA). It is applied on the same data set. Because there is no previously detected inhomogeneity in the data series, in this case it is divided into two equal time series (36 years long each). Comparison of these time series (1951-1986 and 1987-2022) distinguish differences in precipitation regimes of continental part of Croatia (Osijek, Zagreb) and coastal part of the country (Split) (Figure 4). In the range of low precipitation (< 40th percentile) in Osijek and Zagreb region there was no trend. In the Split region there is significant negative trend even below -10% of change (decreasing).

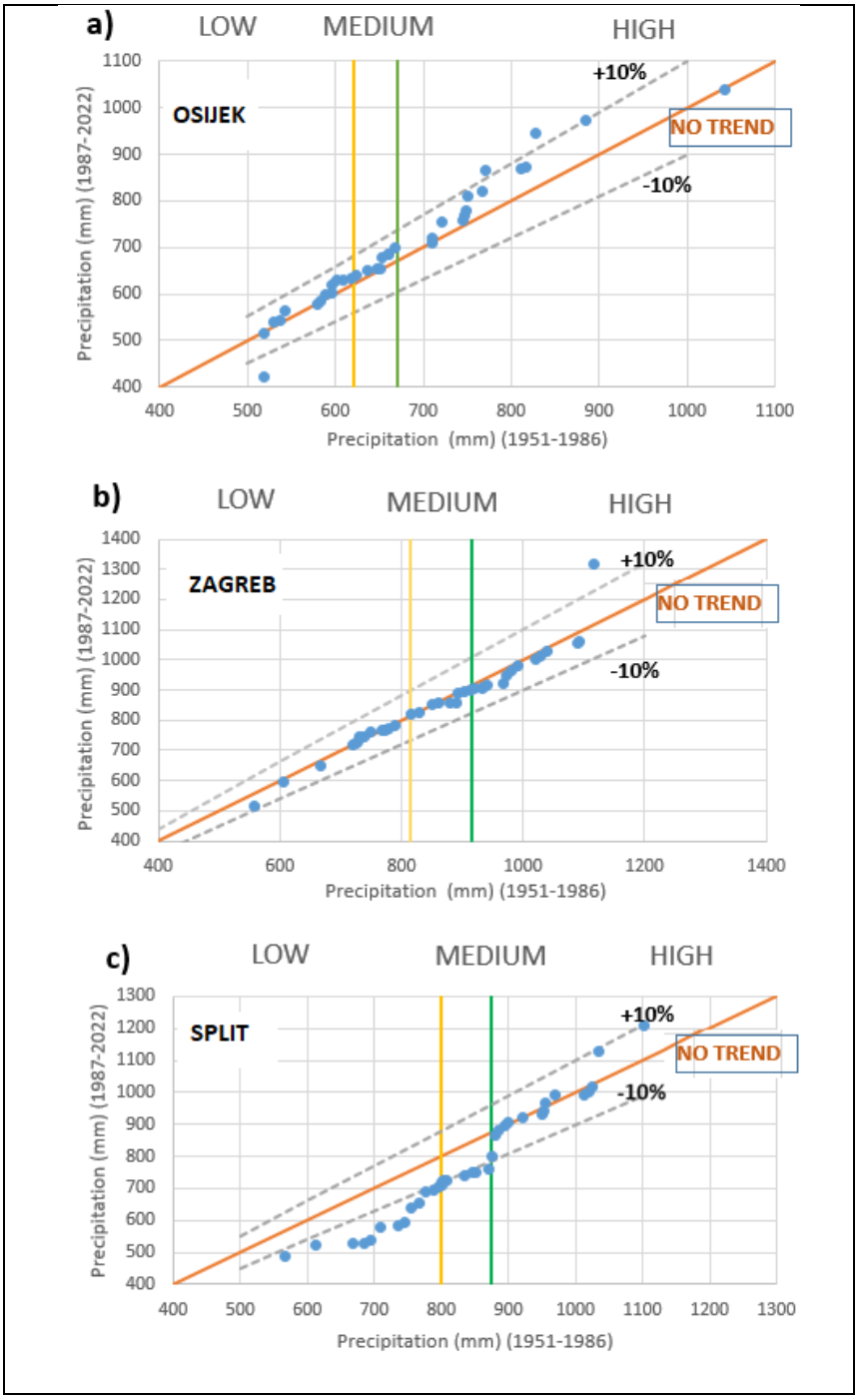

Figure 4. Innovative trend analysis applied on annual precipitations of : a) Osijek, b) Zagreb and c) Split

In the range of medium annual precipitation (40th - 60th percentile) in Osijek region start positive changes but still not significant. In Zagreb region there is no trend of medium precipitations while in Split precipitation regime decreasing trend is not so strong any more. In the range of high annual precipitation (> 60th percentile) in Osijek region there is significant increasing (more than 10%) in the second period of observation (1987-2022). The Zagreb region shows slightly negative trend but still it keeps more or less “no-trend” behavior. In Split region weakening of negative trends continues and finally disappears and turns into positive (decreasing trend). On the seasonal level, only summer precipitation was tested by ITA.

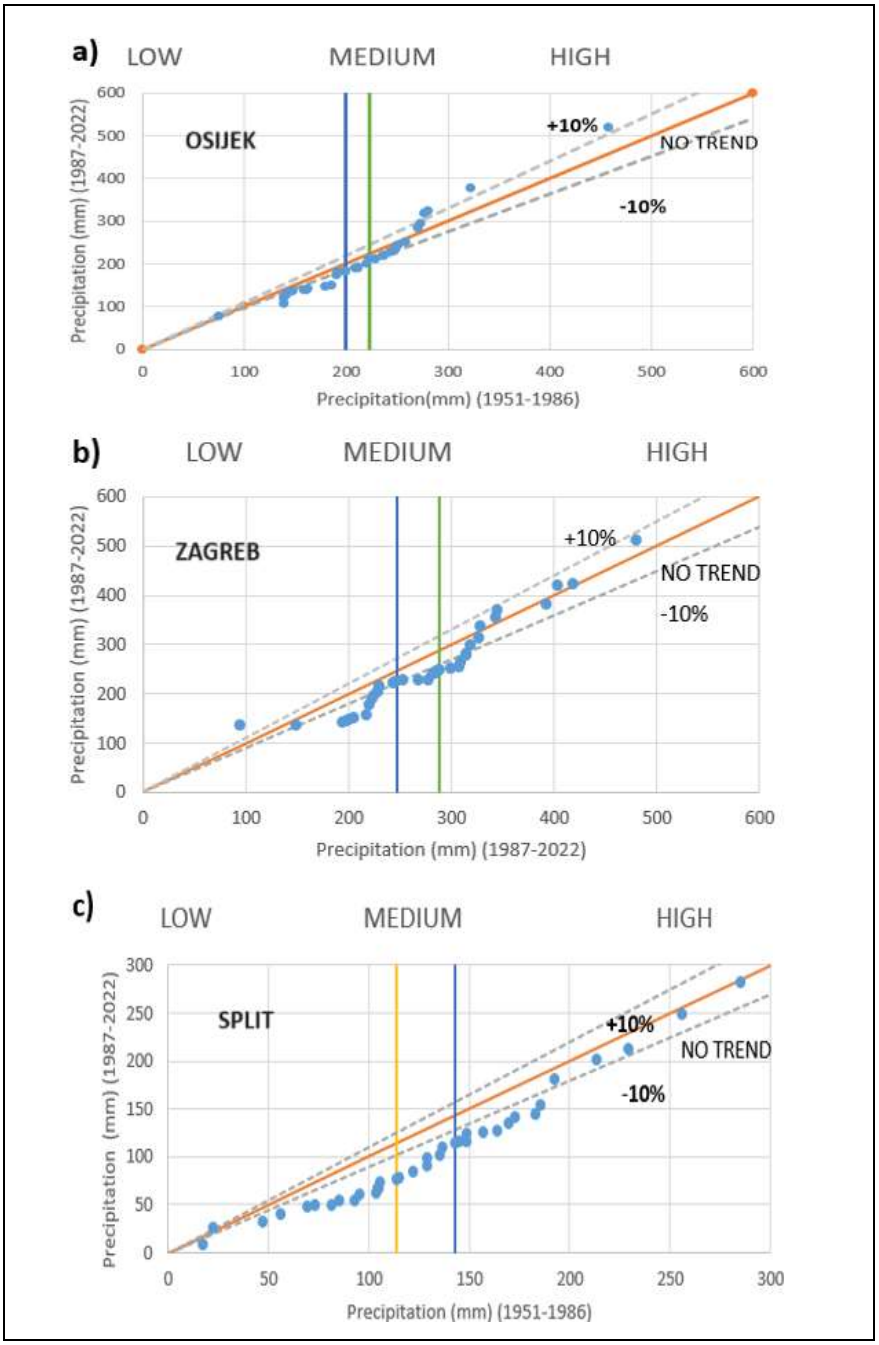

Figure 5. Innovative trend analysis applied on summer precipitations of: a) Osijek, b) Zagreb and c) Split

Comparing to the Mann Kendall test, ITA also showed significant summer precipitation decreasing. In the Zagreb region it is limited to low and medium range of precipitation, while in Split region it is evident in all ranges of precipitation (Figure 5b and 5c). There is no trend in summer precipitation changes in Osijek region. However, there is light increasing of high range of precipitation (Figure 5a). The third analysis is risk analysis of occurrence of annual precipitation lower than mean value (drought) of entire period. Again, two data series defined in the previous analysis (1951-1986 and 1987-2022) are time frame of analysis. Severity of low precipitation for Osijek region reaches much higher values in the second period and risk is higher in the range of low and severe droughts (Figure 6a). Risks of the medium precipitation deficit is stable. On contrary, the Zagreb region shows decreasing risk of mild and severe precipitation deficit (Figure 6b). In the Split region the second observed period has more expressed risk in the period 1987-2022 in all ranges of severity (Figure 6c).

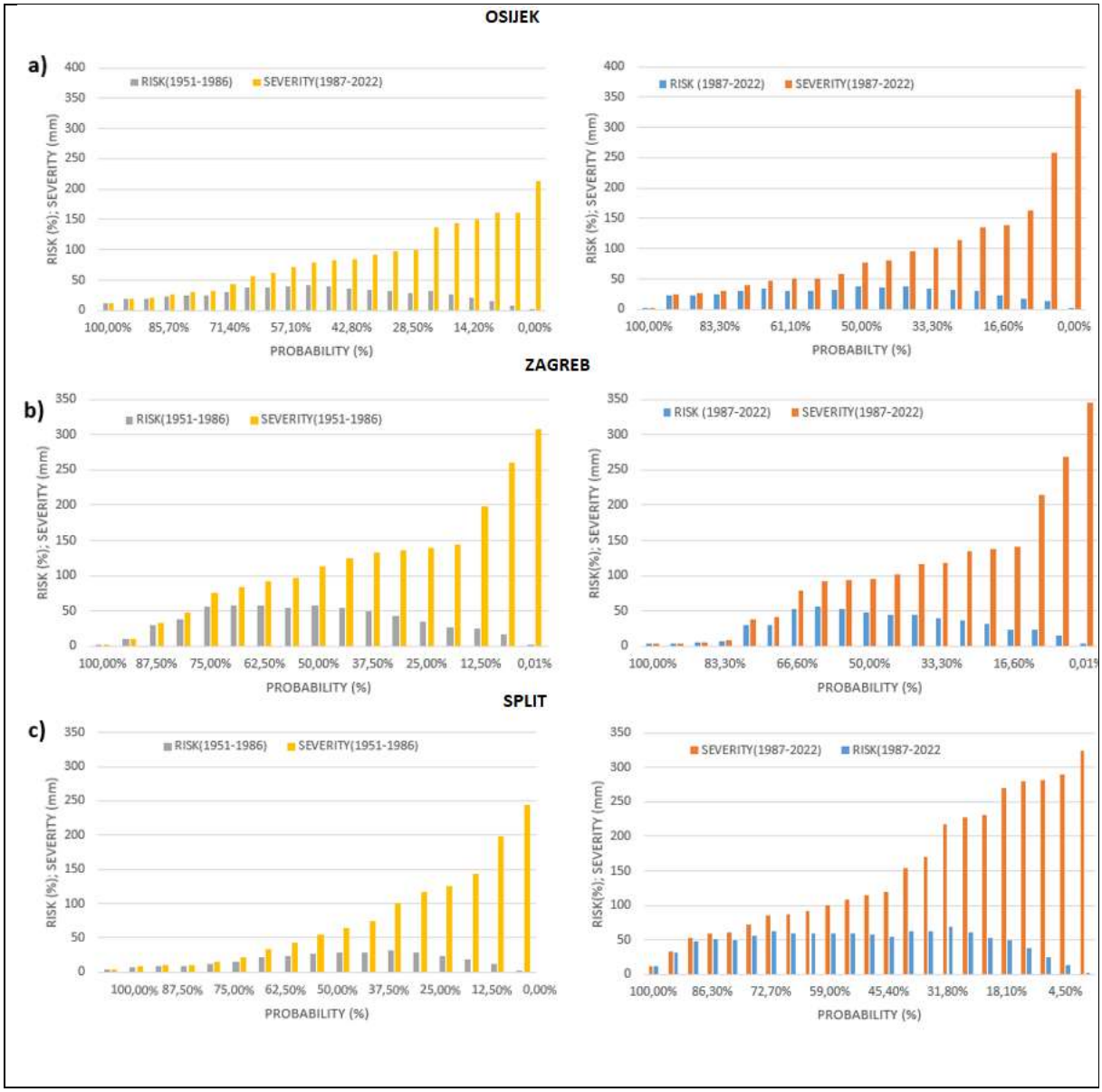

Figure 6. Risk analysis applied on annual precipitation of : a) Osijek, b) Zagreb and c) Split

While the flood risk management has very developed structure all over the world, drought risk management is dependent on methods for monitoring and prediction, what leads to quantifying the hazard, is still not well established. Besides, only quantification of extreme is not sufficient and negative consequences of a lack of precipitation has to be predicted [20].

5 Conclusion

The main objective of this research is to show and compare precipitation regimes in the different part of Croatia. We are facing climate change processes and numerous approaches and methods were developed in order to give specific and more accurate description of triggers, impacts and consequences of climate change. The most of the published papers are focused on the precipitation and air temperature changes. While the air temperature shows very strong and persistent increasing trend all over the world,

precipitation behavior is very variable and dependent on geographical features. It is well described in scientific publications. The majority of central Europe belongs to area of transitional climate type as a result of interactions between maritime and continental climates with the main characteristic of serious drying [19]. It confirms spatial complexity of the drought phenomenon particularly in an area situated in a transitional climate zone between the Continental and Mediterranean climate, where one climate often prevails [4]. This investigation also tried to gain new knowledge in drought research in Croatia on the basis of three specific regions presented by meteorological stations in Osijek, Zagreb and Split. Mean annual precipitation of observed period in Osijek region is 680mm, in Zagreb region 863 mm and in Split region 811mm. Data series used in this research are very long- period of 72 years between 1951 am 2022 should be long enough to detect any significant changes in precipitation regime on annual and seasonal temporal scale. Previously precipitation was tested for homogeneity and on annul scale all three data series were homogeneous [5]. Application of Mann-Kendall test shows that all three stations on annual basis have decreasing, but not significant trend. Next applied method, innovative trend method detected certain differences between two stablished sub-periods (1951-1986 and 1987-2022). In Zagreb region annual precipitation still shows no any trend even test divides low, medium and high precipitation quantities. Precipitation in Osijek shows increasing of high precipitations in the period 1987-2022, and no trend in medium and low precipitation quantities. The most obvious changes are in the Split regions where second period of observation have decreasing trend in low and medium precipitation and increasing in the range of high precipitation. Innovative trend analysis (ITA) gave better recognition of differences in Croatian regions. Similar conclusion can be given on the basis of risk analysis. Mediterranean region presented by Split can expect higher risks from lack of precipitation of all ranges than other parts of country.

On the seasonal time scale Mann-Kendall test results are confirmed by application of ITA. However, ITA gave more details about changes of precipitation in the range of low, medium and high precipitation. Generally high range of precipitation are decreasing, while low and medium precipitations have no trend or very small negative trends. It is proved on annual and seasonal time basis.

However, this research confirms existence of characteristics of transitional area in Europe, its great variability in meteorological responses on climate change. Also, it confirms the crucial role of air temperature on climate change severity. Drought occurrence is extremely dependent on increasing of air temperature, much more the reduction of precipitation which is not so significant, or even not present at all. According to morphoclimatic characteristics of Croatia it can be divided into three different and spatially well-defined regions with specific temporal and spatial characteristics of droughts (central northern, eastern and southern regions) [20]. It is manifested as a percentage of area affected by drought, as well as in the yearly drought occurrences rates, in both central northern and eastern regions, and an evident decrease is shown in the southern region for both 6- and 12-month standardized precipitation-evapotranspiration index (SPEI) time-scales. However, considering only precipitation such a firm conclusion cannot be adopted.

Drought, or extended period with lack of precipitation is very complex hydrological process affected by many factors. Will it yield with severe or mild drought impacts depends, among other elements, on previous precipitation episodes and air temperature or evapotranspiration.

References:

[1] Gajić-Čapka, M., Cindrić, K., Pasarić, Z.: Trends in Precipitation Indices in Croatia, 1961–2010, Theoretical and Applied Climatology, 121, pp. 167–177, 2015.

[2] Cindric Kalin, K., Patalen, L., Marinovic, I., Pasaric, Z.: Trends in temperature and precipitation indices in Croatia, 1961-2020, EMS Annual Meeting, Bonn, pp. 5–9, 2022.

[3] Marinović, I., Cindrić Kalin, K., Güttler, I., Pasarić, Z.: Dry Spells in Croatia: Observed Climate Change and Climate Projections, Atmosphere 2021, 12, 652, 2021.

[4] Tadić, L.,Brleković, T., Hajdinger, A., Španja, S. : Analysis of the Inhomogeneous Effect of Different Meteorological Trends on Drought: An Example from Continental Croatia,Water 2019, 11(12), 2625; https://doi.org/10.3390/w11122625

[5] Tadić, L., Brleković, T., Potočki, K., Leko-Kos, M.: Application of principal component analysis to drought indicators of three representative Croatian regions, Electronic Journal of the Faculty of

Civil Engineering Osijek 2021, 22, pp. 41-55, 2021.
[6] Šegota, T., Filipčić, A.: Köppenova podjela klima i hrvatsko nazivlje, Geoadria, 8, pp. 17-37, 2003.
[7] Mann, H.B.: Nonparametric tests against trend, Econometrica, 3, pp. 245–259, 1945.
[8] Kendall, M.G.: Rank Correlation Methods, Charles Griffin & Company Limited, 1955.
[9] Gilbert, R.O.: Statistical Methods for Environmental Pollution Monitoring, John Wiley & Sons, Inc., New York, 1987.
[10] Asfaw, A., Simane, B., Hassen, A., Bantider, A.: Variability and time series trend analysis of rainfall and temperature in northcentral Ethiopia: A case study in Woleka sub-basin, Weather and Climate Extremes, 19, pp. 29-41, 2017.
[11] Salmi, T., Määttä, A., Anttila, P., Ruoho-Airola, T., Amnell, T.: Detecting trends of annual values of atmospheric pollutants by the Mann-Kendall test and Sen's slope estimates – the Excel template application MAKESENS, 31, Finnish Meteorological Institute, Helsinki, 2002.
[12] Şen, Z.: Innovative trend analysis methodology, Journal of Hydrologic Engineering, 17, pp. 1042–1046, 2012.
[13] Şen, Z.: Hydrological trend analysis with innovative and over-whitening procedures, Hydrological Science Journal, 62, pp. 294–305, 2017.
[14] Brunetti, M., Maugeri, M., Monti, F., Nanni, T.: Changes in daily precipitation frequency and distribution in Italy over the last 120 years, Journal of Geophysical Research: Atmospheres, 109, 2004
[15] Kisi, O., Ay, M.: Comparison of Mann–Kendall and innovative trend method for water quality parameters of the Kizilirmak River, Turkey, Journal of Hydrology, 513, pp. 362–375, 2014.
[16] Caloiero, T., Coscarelli, R. & Ferrari, E. Application of the Innovative Trend Analysis Method for the Trend Analysis of Rainfall Anomalies in Southern Italy. Water Resour Manage 32, 4971–4983 2018 https://doi.org/10.1007/s11269-018-2117-z
[17] Oufeigh, O., Elouissi, A., Benzater, B. Trend Assessment by the Mann-Kendall Test and the Innovative Trend Analysis Method (North-West Algeria). GeoScience Engineering, 69(2), 186–233, 2023 https://doi.org/10.35180/gse-2023-0099
[16] Bachmair, S., Svensson, C., Prosdocimi, I., Hannaford, J., Stahl, K.: Developing drought impact functions for drought risk management. Nat. Hazards Earth Syst. Sci., 17, 1947–1960, 2017 https://doi.org/10.5194/nhess-17-1947-2017
[19] Cheng, S.; Huang, J. Enhanced soil moisture drying in transitional regions under a warming climate. J. Geophys. Res.Atmos.2016, 121, 2542–2555.
[20] Santos, F.J., Tadic, L., Portela, M.M., Espinosa, L.A., Brleković, T.: Drought Characterization in Croatia Using E-OBS Gridded Data, Water, 15, 2023

WATER CRISIS OF THE PONDS IN KOPAČKI RIT WETLAND

SINIŠA MARIČIĆ [1], ŽELJKO ŠRENG [2]

[1] Josip Juraj Strossmayer University of Osijek, Faculty of Civil Engineering and Architecture Osijek, smaricic@gfos.hr

[2] Josip Juraj Strossmayer University of Osijek, Faculty of Civil Engineering and Architecture Osijek, zsreng@gfos.hr

1 Abstract

Kopački rit (eastern Croatia) is a protected wetland area where the Drava and Danube rivers converge. This study examines water levels as indicators of Kopački rit's water condition. The water level in its central area, Kopačko Lake, closely correlates with nearby levels at gauges along the Drava and Danube rivers. Water level analysis (by the annual regime of the characteristic water levels and the duration curve of average daily water levels, for three consecutive periods) reveals significant changes over time, including shorter flood durations and prolonged drought periods (water crisis).

Keywords: Kopački rit, wetland, water level, water crisis

2 Introduction – Analysed area and problems of Kopački rit

Kopački Rit is the largest coastal marsh area of the entire middle Danube is understood, covering approximately 25,000 hectares of land. The Kopački Rit area is protected under the categories of Special Reserve (over 6,000 hectares) and Nature Park. The Special Zoological Reserve (SZR) represents the terrain with the lowest altitude, making it the most flooded area in the entire Park, lasting several months annually. The Hulovski Canal brings the largest amount of water from the Danube into the Special Zoological Reserve, while a much smaller amount of water flows in from the Nađhat Fok in the north and the Renovski Canal in the south. The majority of the land in the Reserve is covered by reeds and marsh vegetation, with pioneer white willow forest prevailing over woodlands. The appearance of the entire area depends on flood dynamics, with key values lying in hydro-morphological features (mosaic arrangement of land and water surfaces that change size, shape, and function depending on the water level) and significant biodiversity (with over 2,700 recorded species). Despite active use for forestry, hunting, and partially navigation, this area has retained a significant portion of its natural values. Natural flooding processes, as well as the ability to transport substances and create specific relief in floodplain valleys, along with the succession of plant communities and animal species, are to some extent jeopardized by anthropogenic impacts.

In this study, the area of the Kopački Rit Nature Park (PP Kopački Rit) and its broader scope are observed. It is a rare space in Europe that has not been significantly altered by human presence and is formally (legally) protected in a timely manner. General information about the Kopački Rit Nature Park itself and the chronology of its protection can be found in various articles (e.g., [1], [2], [3]), as well as on the official website of this Park [4]. Figure 1 shows the position of Kopački Rit and its basic functional elements.

The area of the Kopački Rit Nature Park is located in the protected and floodplain area of the largest Croatian rivers, the Danube and Drava, and as such is influenced by their waters. Apart from the main riverbeds, the hydrographic network consists of the Hulovski Canal, Čonakut, New Canal, Renovo, Nađhat, Vemeljski dunavac, Kopačko Lake, White Lake and Sakadaš Lake as its most significant parts. Most marshes and lakes are mainly remnants of the former riverbed, but there are also new ones formed by erosion during the passage of floodwaters. The well-known Kopačko Lake is connected to the Danube River via the Hulovski Canal, and to Sakadaš Lake via the Čonakut Canal. At Sakadaš Lake, there is a weir gate that regulates the inflow of the old Drava into the Kopački Rit area [5].

In floodplain areas, in addition to terrestrial and aquatic habitats, a series of transitional habitats are

formed that support the development of communities with high biological diversity. Floods stimulate the decomposition of organic matter, which is an important characteristic for such areas with high primary production. The entire complex system is driven by its hydrological characteristics, i.e., the frequency and intensity of floods [6]. It has long been emphasized and recognized that changes in the basic hydrological characteristics that shape Kopački Rit would reflect on habitat characteristics and thus on biological diversity [2], [7], [8].

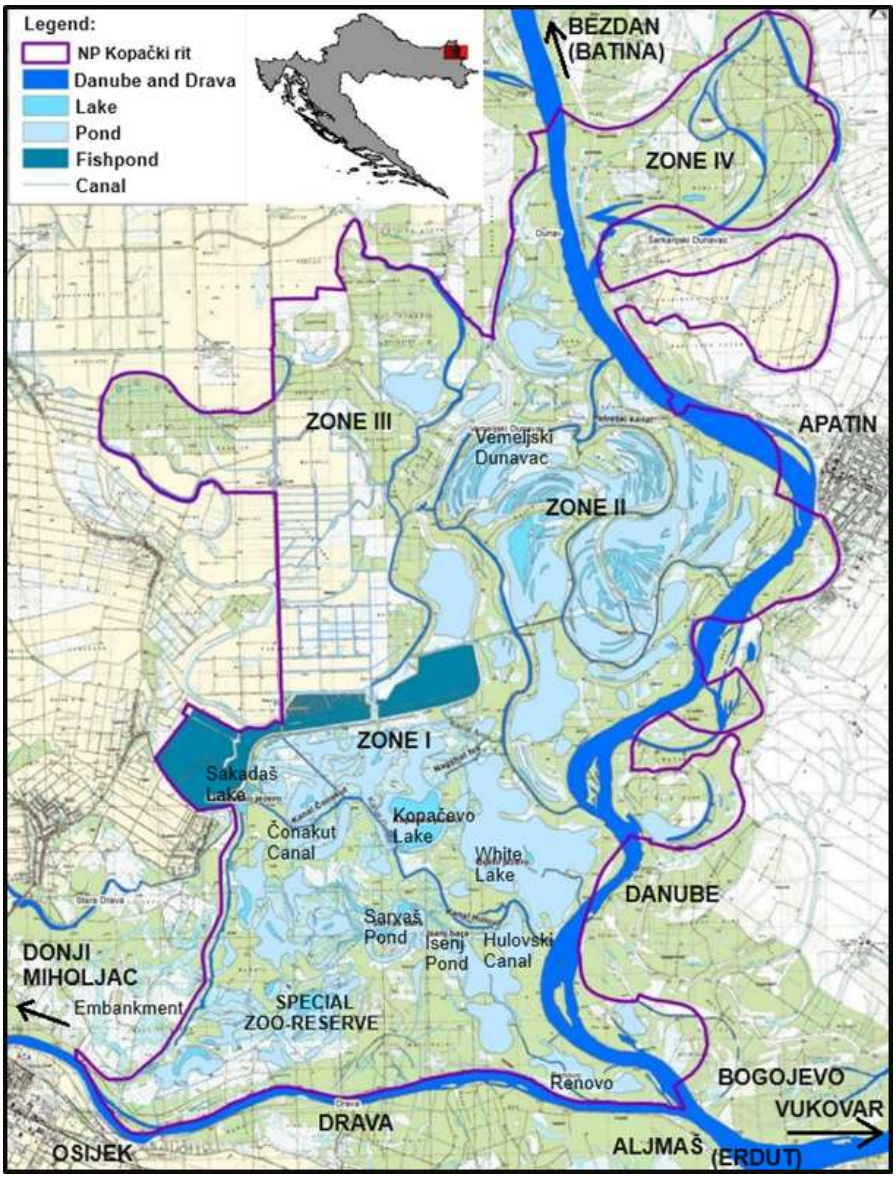

Figure 1. The position of Kopački Rit and its basic functional elements

3 Results and discussion

3.1 Introductory discussion

In ancient times, several million years ago, there existed the Sarmatian Sea, also known as the Pannonian Sea, which drained through the Danube route into the Black Sea. The remnants of this sea are present-day Lake Balaton in Hungary and the low-lying terrains visible in the eastern regions of Slavonia and Baranja. Following a tumultuous geological period and the draining of the Pannonian Sea, the river valleys of the Danube, Sava, Drava, and Vuka were formed. Due to the dynamic nature of the soil, vegetation development, and periodic significant floods, these valleys took on the appearance of a

marshy-riparian landscape, which persisted until about a thousand years ago. During this period, prior to the construction of defensive embankments, the rivers freely and widely overflowed through eastern Slavonia, Baranja, and Bačka. After major floods (water level increases > 2 m) and prolonged (> 100 days) inundations, the landscape underwent significant changes. Some meanders were cut off and disappeared, some became increasingly curved and longer, while others began to develop. Various forms of water surfaces (channels, marshes, "lakes," oxbow lakes, etc.) also took on new appearances. River confluences were spatially shifted, the mouth of the Drava river "moved" several kilometers upstream or downstream.

Thus, historical accounts of the state of the rivers in this area are encountered [3]: the Drava river flowed north towards a Pleistocene lake located near Bansko brdo and gradually filled it in (L. Loczy); the Danube river once flowed through the middle of Vojvodina (A. Bognar); around the 17th century, the mouth of the Drava river was located a gunshot away from the city of Osijek (E. Čelebija). All of this serves as evidence of the variability that has long been observed by others (Change alone is unchanging in this world! - Heraclitus, Petar Preradović). However, what has changed from those earlier times to the present day is the speed of these changes, which requires attention.

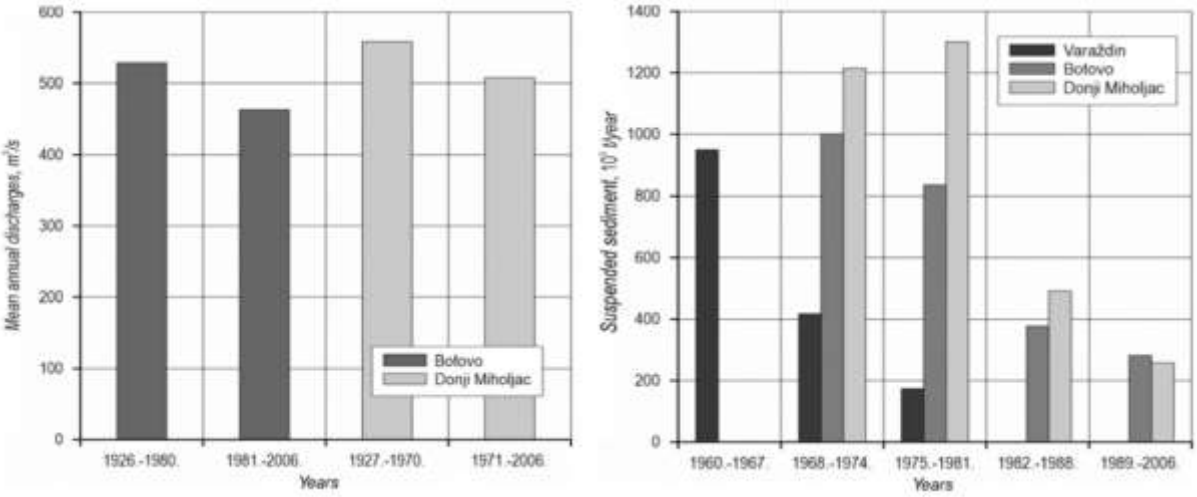

Figure 2. The reduction of annual flow and sediment transport on the Drava River upstream of the Rit [9, 10]

For the assessment of the state and changes in a particular area, it is necessary to consider various influences on it. Firstly, it can be observed that most researchers are tied to administrative boundaries (in this case, the Kopački rit Nature Park). However, natural determinants encompass a different, usually broader area. In this sense, the left bank, low-lying area of the Danube opposite Kopački rit should also be of interest here. Furthermore, influences can be viewed as direct (local), then as those of a broader environment (regional), and as global. Among the former, there are flood protection embankments present here, nearby regulatory structures on the Drava and Danube rivers, interventions in meander cutoffs and maintenance of navigational routes, excavation of various-purpose channels, and others. Excavation of navigation channels within the Rit, construction of weirs at the entrance and exit points of main channels, maintenance of navigability of waters, use of dams and pumping stations can be emphasized. The second group may include urbanization and deforestation in the Drava and Danube basins, upstream regulatory and hydroenergy interventions, water abstractions and discharges, and others. For example, 23 hydroelectric power plants have been constructed upstream on the Drava (the downstream effects of which are analyzed by Čuljak et al., [13].), and illustratively, the reduction of flow and sediment transport and the decrease in water levels of the Drava near Donji Miholjac (Figure 2) can be attributed to the construction of upstream hydroelectric power plants, [9], [10]. A special group consists of global influences (land use change, increasing water consumption, atmospheric changes, and others) whose majority is currently reflected in ongoing climate changes.

3.2 Hydrological indicators

The focus here is on the hydrological elements of Kopački rit. For the hydrology of the area, long-term measurements of meteorological elements (precipitation and temperature) are important, as well as recording surrounding water levels and determining flow functions. This has enabled various hydrological analyses and the development of basic hydrological studies that numerous researchers refer to and management plans are based on. Two studies can be highlighted: Bonacci, O. et al. (2002) - a study of hydrology and meteorology, and Vidaković Šutić, R. et al. (2021) - a study of retention capacity and the zero state of water and water-dependent ecosystems. The first study from 2002 is mainly based on data from the period 1961-1990, while the second study from 2021 mainly uses data from the new millennium and indicates newly collected data. Unfortunately, despite pointing out the need for additional observations in 2002, after 20 years, there is little new information. Using modern techniques (Lidar scanning, supplemented with bathymetric data for areas submerged underwater), a new base - the relief of Kopački rit - has been prepared. Additionally, meteorological data (from the Kopački Rit measuring station since 2004) and hydrological data (from the Zlatna Greda and Tikveš measuring stations on the Danube, with daily readings from 2004, as well as episodic data on occasional water levels of the Sakadaško Lake in Kopačevo) have been collected. It is noted that water level measurements in the Kopački rit area are quite scarce, or insufficient for more in-depth analyses, and the results obtained should be considered indicative. Data on average daily water levels measured at the limnigraph at the Kopačevo location (period 2009 and incomplete data for 2010 and 2014) were available, while water levels at the Tikveš and Zlatna Greda locations were read once daily (at 7:00 am) from a water gauge (period 2004-2019, with incomplete series).

With such data, correlation analyses of water levels were conducted in a recent study Kopački rit is represented here through two of its boundary points (locations: Tikveš and Kopačevo). This analysis was conducted for four selected high-water events with zero, one, two, three, four, and five days of delayed water levels from the first location compared to the water level of the second. According to the conducted analyses, the highest correlation coefficients, or the highest similarity of water levels, were obtained by comparing water levels for the same day (at close locations), or for 1-3 days of delay (depending on the mutual distance). Only higher individual water levels (waves) were considered, and the correlation coefficients are high (mostly 0.99-0.94). The importance of data on water levels of the Drava and Danube rivers for assessing the moisture status of Kopački rit is emphasized by all experts. Connecting these water levels with measured water levels in the central part of Kopački rit - Kopačko jezero, based on data measured during 2002-2004, was presented in the works of previous WMHE conferences ([16], [17]). The highest correlation was found between simultaneous water levels of Kopačko jezero and the Danube (h.s. Vukovar) at 0.86, slightly higher than at other stations. The reason can be interpreted by encompassing the entire range of water levels and equalizing all influences of inflow (in one direction - through channels and surface to the lake, and in the other - along a considerable stretch of the Danube riverbed to Vukovar).

Correlative analyses have consistently demonstrated the dominant influence of the Danube on the water conditions in Kopački rit. Generally, a lack of measurement points in the marsh (at significant wet positions) has been noted, and it is evident that the strength of data correlation from specific locations depends on their mutual distance and various variable circumstances along their connecting route. Previous studies ([3], [6], [11], [14], [18]) have highlighted the nature of the Danube's influence and a certain regime of filling and emptying in the Kopački rit area. They emphasize that, in the absence of other data, the water level at Apatin, as the nearest official indicator, effectively reflects the water conditions in the Kopački rit area. This was verified based on collected three-year data (2001-2003) and presented in the works of Maričić et al. ([16], [17], [19]). On this occasion, twenty water waves of the Danube were extracted from the available data set. These are individual, distinct waves, characterized by significant successive water level rises and falls. The corresponding (simultaneous) water levels of these waves are depicted in graphs a) and b) (Figure 3), where the abscissa represents the water levels at Apatin, and the ordinate represents the water levels of Kopačko Lake.

The changes in water conditions are explained and defined by the following circumstances: During the rising water wave, starting from lower values, the increase in the water level of the Danube at Apatin is not promptly and more pronouncedly reflected in the state of Kopački Lake. Roughly, only after

reaching 81.5 meters above sea level (point A on the abscissa of the graph), the increase in the water level of Kopački Lake more prominently precedes the increase in the water level at Apatin. For further values, the increase in the water level of Kopački Lake is approximately half of the increase in the water level of the Danube at Apatin. Passing the elevation of 83.5 - 84 meters (marked as B on the graph), the increase in the water level of Rita is twice as large compared to the corresponding increase in the water level of the Danube. Above 85 - 85.5 meters above sea level (point C on the graph), there is an equalization of the amount of increase in the water level at these compared locations. During the descent of the water wave, after point C towards B, it is evident that the decrease in water level at Kopački Lake is half of that at Apatin.

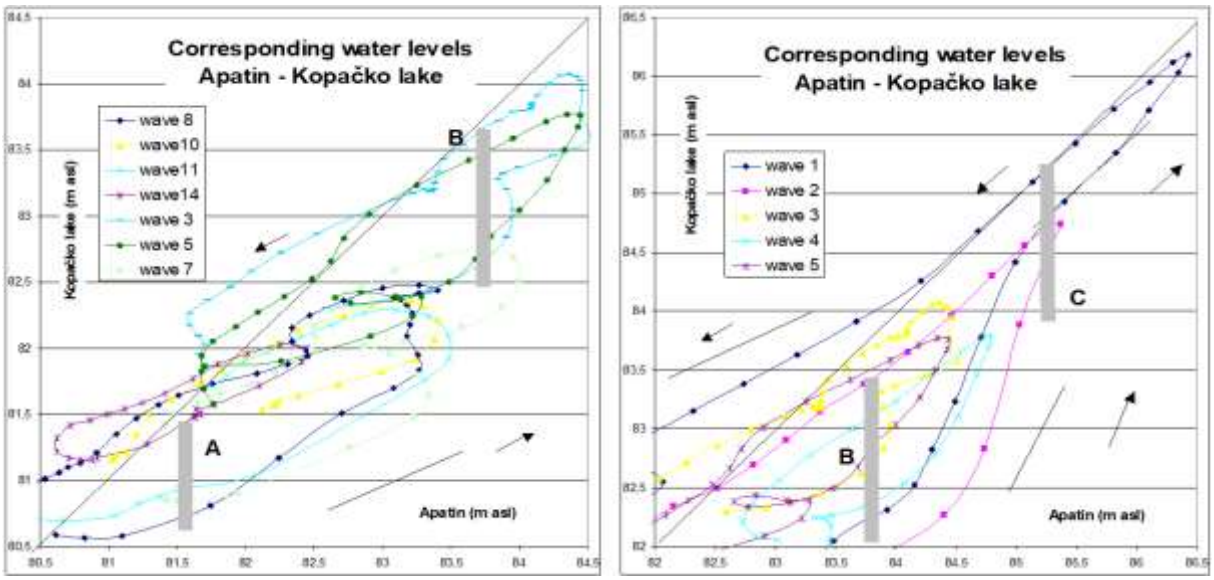

Figure 3. Corresponding (simultaneous) water levels Apatin – Kopačko lake [1]

The observations from the Figure 3 correspond to empirically known circumstances of the filling and draining of Kopački rit, arising from the existing terrain conditions. Thus, point A corresponds to the filling of the main channels and saturation of the surrounding soil with water, point B corresponds to the overflow of coastal sediments and vegetation along the channels, while point C corresponds to the complete flooding of Kopački rit. It is logical that the indicative points (A, B, C) cannot be more precisely defined because their recognition (manifestation) depends on the previous water conditions in the Rit zone. This condition depends on the influence of precipitation and groundwater inflow on the formation of groundwater, general climatic conditions affecting vegetation growth, morphological changes in riverbeds, and ultimately anthropogenic influences (e.g. tree cutting, reconstruction of riverbanks and channels, among others).

From the analysis of the duration of the water levels of the Danube at Apatin made for the measurement period (1949-1990), it is observed that the water levels between 81.5-83.0 meters lasted on average 215-90 days annually. The change in this duration was noted according to the analysis of the duration made for the new period from 1992 onwards. It was thus noted that the considered duration of the 1.5-meter range of the Danube water levels decreased by approximately 40-55 days.

Such a height range of 1-2 meters for the area of Kopački rit relates to a significant change in the surface area affected by water inundation. This is highlighted in the study [21], from which a graphical representation is transferred to the image on the right in Figure 4. It is evident that the inundation of the Rit area for 70-90 days (20-25% of the year) has decreased by approximately 50% (previously, 75% of the area was covered by inundation during that duration, but more recently, it has been reduced to around 25%).

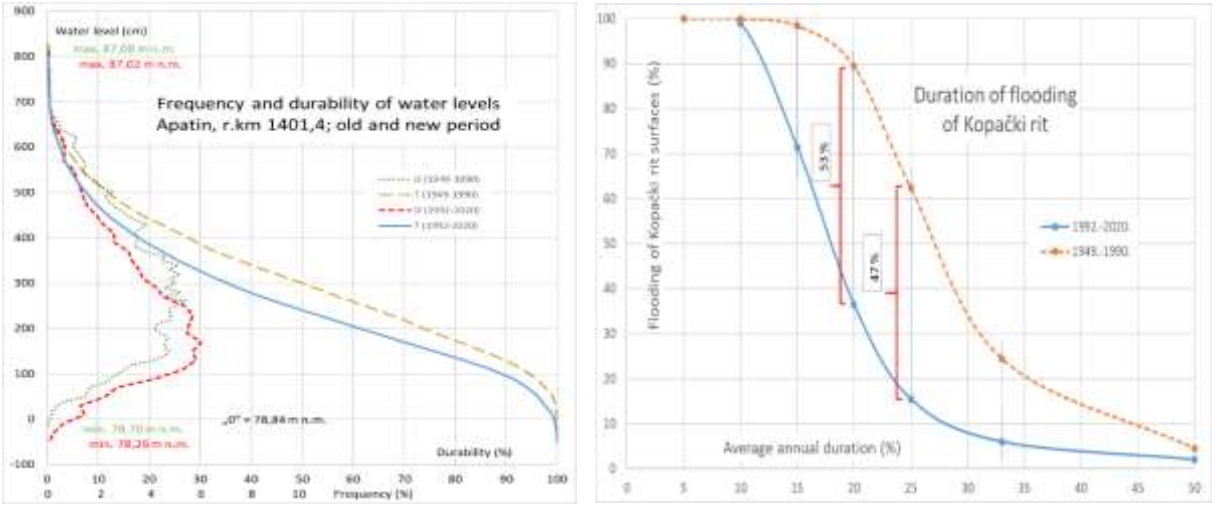

Figure 4. The characteristics of the water level of the Danube at Apatin for two periods and the resulting reduction in the flooding of the areas of Kopački Lake [3, 4]

A severe situation befell Kopački rit in the year 2022, which was dry, and the water levels of the Drava and Danube rivers reached record-low values. The duration of the Danube water levels in that year was compared to previous periods [22], as illustrated in Figure 5, where the data and analysis are for the hydrological station at Aljmaš, at the confluence of the Drava and Danube rivers. Although the water level trends indicate a concerning situation, statements from authorities during that year suggested that it is a normal occurrence in some dry years, which nature is capable of handling.

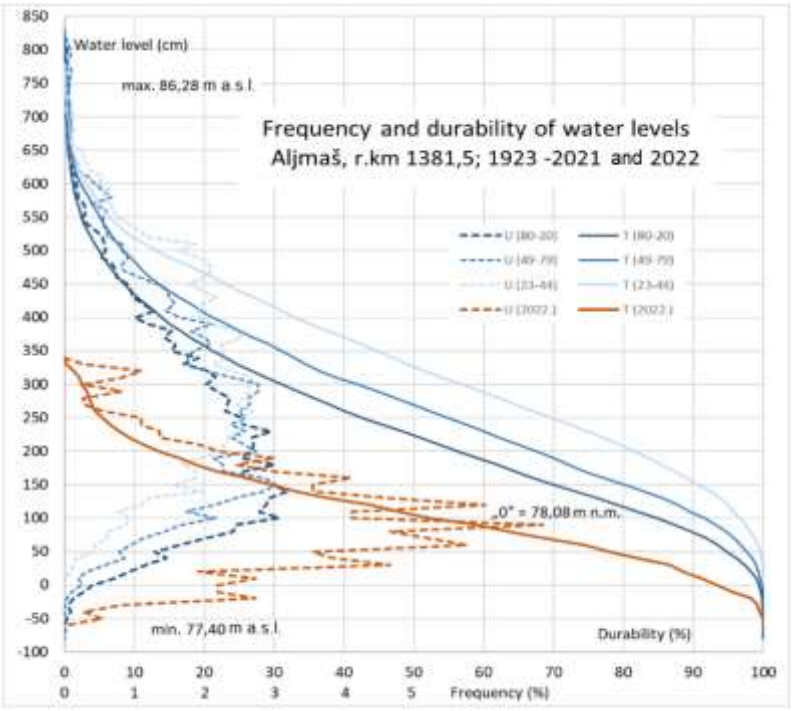

Figure 5. The frequency and duration of water levels on the Danube at Aljmaš for three successive periods and the year 2022 [4]

On this occasion, it is important to highlight that the water sustainability of the Kopački Rit ecosystem is not primarily influenced by the extreme flood waves of the Danube, as some authors suggest [23]. Instead, it is the large annual floods that significantly inundate the Rit for several tens of days, particularly during the vegetative period of the wetland ecosystems, that are crucial. Precipitation is less

significant and relatively minimal in quantity. Therefore, it is essential to observe and emphasize the changes brought about by new climatic conditions, some of which have already been noted.
The study [24] discusses "climatic" changes and issues in Slavonia, presenting Figure 6 - Walter's climate diagram for Osijek and D. Miholjac. Two meteorologically significant periods were considered (for Osijek: 1969-1995 and 1996-2022; for D. Miholjac: 1960-1991 and 1991-2022). Based on these periods, using Walter's method (climate through average monthly temperatures and monthly precipitation amounts), it is evident that the region generally does not lack moisture (with deviations in certain years, either too wet or too dry), but climate changes have occurred. A more pronounced trend of increasing air temperatures (approximately 10% on average) compared to precipitation (total increase of 5-8%) is noticeable. The smaller increase in total precipitation is irregularly distributed throughout the year, with a noticeable decrease in summer and an increase in spring and autumn. Analyzing the precipitation data for the Osijek station, it is evident that the period from 1961 to 1990 is characterized by a declining trend in annual precipitation, while the more recent period, after 1991, indicates an increasing trend in annual precipitation and increasingly pronounced annual extremes, [15]. The occurrence of increasingly extreme episodic weather events (heavy downpours and drought periods) is also highlighted.

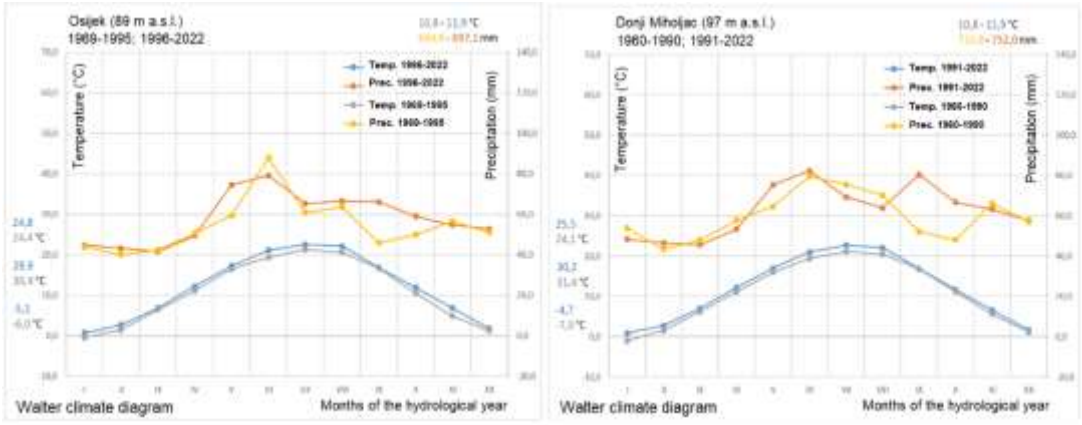

Figure 6. Climate diagrams (Walter's method) for Osijek and Donji Miholjac for two data periods [4]

Another important factor is hydrological data. It is already mentioned the "cutting" of the Drava River bed due to reduced flow and sediment transport upstream from the analysed area. The scale of this phenomenon is illustrated in figure 7., depicting the characteristic water levels of the Drava River near Donji Miholjac. Over 120 years, the levels have decreased by approximately 1.5 meters. Considering the Danube as the primary water supplier to the floodplain, it is crucial to examine water level changes on this river as well. The fluctuations in water levels (average annual and 14-year averages) over the past 100 years are presented in figure 8., showing a noticeable declining trend in these water levels.

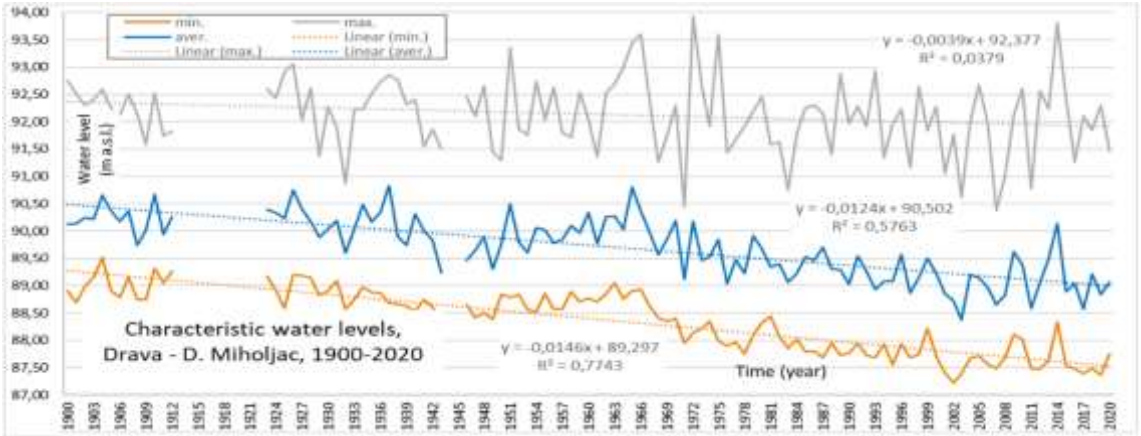

Figure 7. Changes and trends in characteristic water levels of the Drava near Donji Miholjac

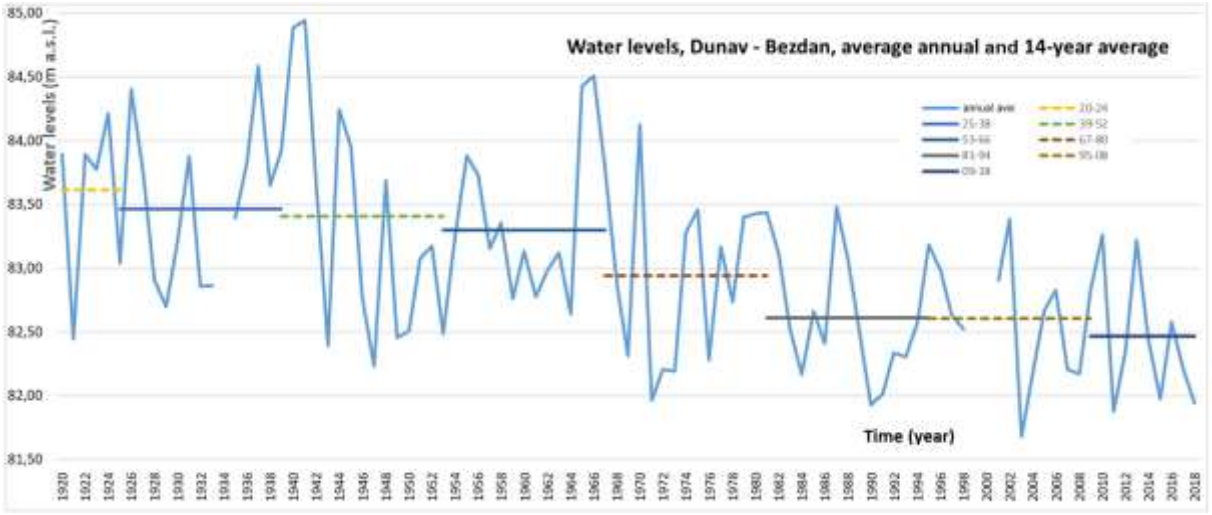

Figure 8. Water levels of the Danube near Bezdan - average annual and 14th year averages

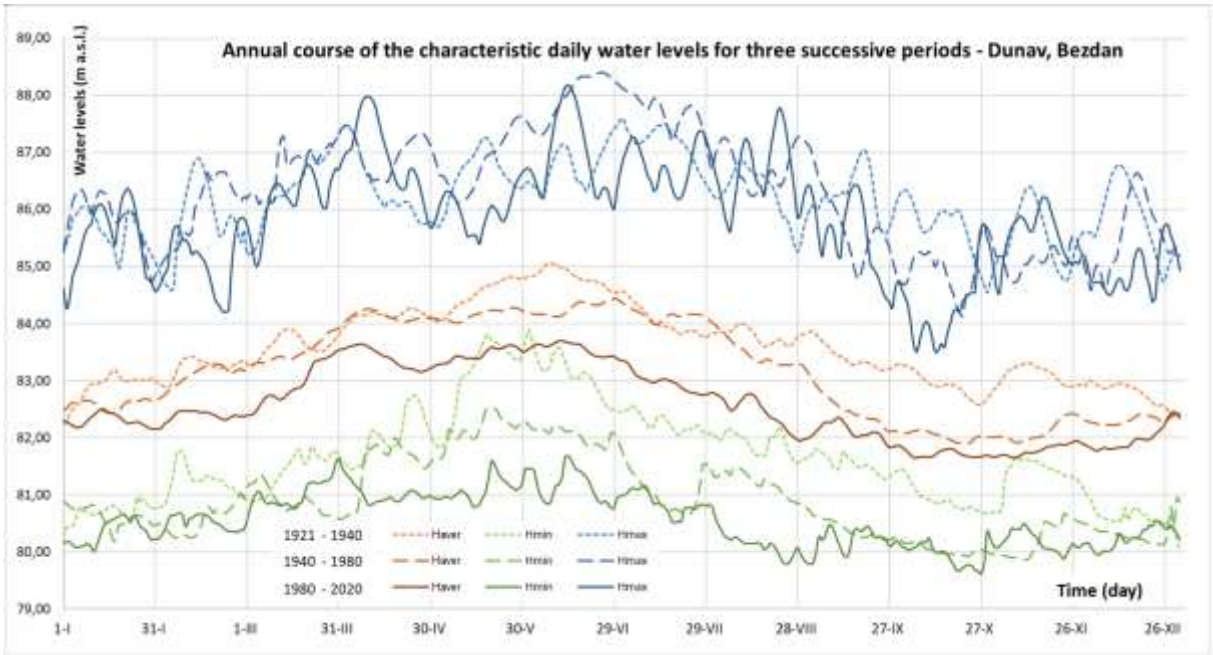

Figure 9. Annual course of the characteristic water levels (daily) of the Danube for three successive periods

Analyzing the annual water level variations of the Danube over three successive periods, as depicted in figure 9., reveals a noticeable decrease in characteristic water levels. However, maximum water levels reach higher values not only during expected periods of the year (late spring and summer) but also outside the significant vegetation period (autumn-winter). In this regard, the significance of extreme floods for the survival and prosperity of marshland ecosystems is diminished.

4 Conclusion

Numerous influences on the Danube river basins affect their drainage patterns, particularly notable for the Drava and Danube rivers, reflecting on the condition of Kopački Rit. Differentiating the contribution of each influence is challenging as the overall impact is intertwined and simultaneous in the considered area. The study examines resultant changes in meteorological and hydrological indicators. The climate in this region is warming, averaging over 1 °C in about 30 years. Rainfall is becoming slightly heavier, with more pronounced extreme events. Mean and minimum annual water levels show a decreasing trend,

indicating the incision of the lower Drava and middle Danube riverbeds. This poses a threat to Kopački Rit as its area is drained by underground water flow, jeopardizing the marshland ecosystems through desiccation. Higher and peak water levels are becoming shorter in duration, reducing the water influence through channels in the Rit, and shorter flooding periods occur throughout the year. Extreme water levels are more abrupt and occur outside the previously common timeframe, even beyond the vegetative period. Deposition and erosion processes are altered due to longer and more pronounced dry spells and sudden large water surges. In Kopački Rit itself, comprehensive monitoring in terms of hydrology is lacking, complicating the understanding of this complex issue. Currently, this poses the greatest threat to the survival of the floodplain area as we know it.

The identified changes point to a kind of water crisis in an area that needs to preserve its marshland values. Reflections are needed on what steps to take next. Towards the end of the last millennium, there were discussions about constructing water management systems and structures in the Rit, including some individual interventions. Perhaps the water indicators from 2022, starkly confirming negative trends, will prompt new risk assessments and vulnerability evaluations for Kopački Rit. The question arises whether we will merely observe natural adaptations of this area to climate and other changes or consider more substantial hydraulic engineering interventions to maintain suitable moisture levels for the marshland ecosystems. It is comforting that many natural parts have preserved their restoration potential to some extent, offering the opportunity for activities and measures to significantly improve habitat quality and processes in the Kopački Rit.

References:

[1] Bognar, A.: Najveća riječno-močvarna enklava Europe, Hrvatski Zemljopis, br. 55, Zagreb, 2001.
[2] Majstorović, V.: O opskrbljenosti vodom i opstanku Kopačkog rita, Ekološki glasnik 1-2, pp.17-22, 1991.
[3] Springer, O., Mihaljević, M., Getz, D., Božičević, S., Bognar, A., Topić, J., Merdić, E., Krčmar, S.: Hrvatska prirodna baština – Kopački rit – park prirode, ekološki turistički vodič; Barbat, Zagreb; Ministarstvo zaštite okoliša i prostornog uređenja RH, 2003.
[4] https://pp-kopacki-rit.hr/
[5] Benčina, L., Rožac, V., Bolšec, B., Mehić, B., Tot, R., Guttert, V., Šunić, Lj., Udovičić, S., Đurašević, D., Čosić, M., Malić, Z., Domazetović, H., Škrnjug, V., Kovač, Š., Tkalčević, S., Opačić, D., Eđed, A., Pašuld, D.: Plan upravljanja Parkom prirode Kopački rit 2010. – 2020., Javna ustanova „Park prirode Kopački rit", 2010.
[6] Palijan, G.: Određivanje graničnog vodostaja plavljenja Kopačkog rita na primjeru poplave u listopadu-studenom 2009. godine, Hrvatske vode 18 (74), pp.313-320, 2010.
[7] Mikuska, J.: Ekološke osobine i zaštita specijalnog zoološkog rezervata „Kopački rit" s posebnim osvrtom na ekologiju kralješnjaka, Disertacija, Prirodoslovno-matematički fakultet Sveučilišta u Zagrebu, Zagreb, 1979.
[8] Mihaljević, M., Stević, F., Horvatić, J., Hackenberger Kutuzović, B.: Dual impact of the flood pulses on the phytoplankton assemblages in a Danubian floodplain lake (Kopački Rit Nature Park, Croatia), Hydrobiologia 618, pp. 77-88; 2009.
[9] Bonacci, O., Oskoruš, D.:2010: The changes in the lower Drava River water level, discharge and suspended sediment regime, Environtal Earth Sciences 59 (8), pp. 1661–1670, 2010. https://doi.org/10.1007/s12665-009-0148-8
[10] Bonacci, O., Oskoruš, D.: Human Impacts on Water Regime. In: The Drava River Environmental Problems and Solutions, Lóczy, Dénes (ed.). Cham: Springer, pp. 125-137, 2019.
[11] Majstorović, V., Gec, D., Brna, J., Manojlović, R.: Kopački rit – hidro-ekosustav, Intergraf, Osijek, pp. 35, 1997.
[12] Đuroković, Z., Brnić-Levada, D.: Utjecaj izvedenih hidrotehničkih radova na vodne resurse u Kopačkom ritu, Zbornik radova sa 2. hrvatske konferencije o vodama (ur. D. Gereš), Hrvatske vode, Zagreb, pp. 661-666, 1999.
[13] Čuljak, A., Benković, R., Japundžić-Palenkić, B., Mirosavljević, K., Benković-Lačić, T., Antunović S.: Utjecaj izgradnje hidroelektrana na rijeku Dravu, Nova mehanizacija šumarstva 43 (1), pp. 51–65, 2022.

[14] Bonacci, O., Tadić, Z., Radeljak, I.: Plan upravljanja Parkom prirode Kopački rit – Sektorska studija Hidrologija i meteorologija, Hidroing d.o.o. Osijek, R. Hrvatska, Osijek, 2002.
[15] Vidaković Šutić, R., Šarić, I., Ričković, V., Vrcelj, B., Špoljar, M., Cvetnić, M., Buj, I., Koller, Šarić, K., Božić, H., Vuković, N., Hršak, V., Lončar, G., Vranješ, D.: Projekt Naturavita – Studija utvrđivanja retencijskog kapaciteta i nultog stanja voda i o vodama ovisnih ekosustava poplavnog područja Parka prirode Kopački rit, Institut za elektroprivredu, d.d., Zagreb, 2021.
[16] Maričić, S., Petraš, J., Brezak, S.: Water Levels as the Basic Indicator of the Kopački Rit Hydrology; VIII. International symposium on Water Management and Hydraulic engineering, Podbanske, Slovakia, October, pp. 5-9, 2003.
[17] Maričić, S.: Analyses of One of the Rare Natural Retention in the Middle Danube; Nnth International symposium on Water Management and Hydraulic Engineering, Ottenstein, Austria, 4th-7th September 2005., pp. 383-393, 2005.
[18] Tadić, Z., Bonacci, O., Radeljak, I., Tadić, L.: Vodni režim Parka prirode Kopački rit, III. Hrvatska konferencija o vodama, Hrvatske vode u 21. stoljeću, (ur. Gereš, D.); 28.-31. svibnja 2003., Osijek, pp. 941-950, 2003.
[19] Maričić, S., Petraš, J.: A few hidrological analyses of high waters of Kopački rit, XXIIInd conference of danubian countries on the hydrological forecasting and hydrological bases of water management, Beograd, Republika Srbija, 28. – 31. august 2006., pp. 52-53, 2006.
[20] Maričić, S.: Vodostaji Kopačkog rita – ugroza močvare; 7. hrvatska konferencija o vodama s međunarodnim sudjelovanjem – Hrvatske vode u zaštiti okoliša i prirode; Opatija 30. svibnja - 1. lipnja 2019.; Zbornik radova, Hrvatske vode, Opatija 2019., ur. Biondić, D., Holjević D. i dr.; pp. 153-162, 2019.
[21] Maričić, S.: Smanjenje trajanja preplavljenosti Kopačkog rita – ugroženost močvare? / Reducing the duration of the annual flooding in Kopački rit – threat to the wetland?, Zbornik sažetaka, 8. Simpozij s međunarodnim sudjelovanjem „Kopački rit: jučer, danas, sutra 2019.“; Tikveš, 26. i 27. rujna 2019., pp. 86-89, 2019.
[22] Maričić, S.: Godina 2022. prema 100 prethodnih u vodostajima rijeka Kopačkog rita / The year 2022 according to the 100 previous ones in the water levels of the Kopački rit rivers; Zbornik sažetaka, 12. Simpozij s međunarodnim sudjelovanjem „Kopački rit: jučer, danas, sutra 2023.“, Tikveš, 28. i 29. rujna 2023., pp. 142-145, 2023.
[23] Tadić L., Dadić T., Barač B.: Flood frequency modelling of the Kopački rit Nature Park, Tehnički vjesnik 20, pp.51-57, 2013.
[24] Maričić, S.: Varijacije hidroloških i meteoroloških parametara Slavonije, 8. hrvatska konferencija o vodama s međunarodnim sudjelovanjem – Hrvatske vode u proizvodnji hrane i energije, Poreč 23 - 25. svibnja 2023., Zbornik radova, Hrvatske vode, Poreč, ur. Biondić, D., Holjević, D. i Viznar, M.; pp. 149-160, 2023.
[25] Maričić, S.; Mijušković-Svetinović, T.: Water levels of the major rivers in Slavonia, 16th International Symposium on Water Management and Hydraulic Engineering; 5-7 th September 2019; (WMHE 2019) Proceedings / Pelivanovski, P.; Jovanovski, M.; Petkovski, Lj.; Don-evska, K. (ed.); Ss Cyril and Methodius University, Civil Engineering Faculty - Skopje, Skopje, pp. 181-193, 2019.

ESTIMATION OF FLASH DROUGHT EVENTS CHARACTERISTICS IN THE SOUTHWESTERN LOWLANDS OF SLOVAKIA USING REMOTE SENSING

EVANGELOS LEIVADIOTIS[1], SILVIA KOHNOVÁ[1]

[1]*Department of Land and Water Resources Management, Faculty of Civil Engineering, Slovak University of Technology in Bratislava, (Radlinskeho 11), Bratislava 81005, Slovakia, evangelos.leivadiotis@stuba.sk, silvia.kohnova@stuba.sk*

1 Abstract

Flash droughts are rapid-onset droughts with severe water deficits, posing significant threats to agriculture. This study analyzes flash droughts in Slovakia's southwestern lowlands (2007-2019) using soil moisture and evapotranspiration data from ASCAT and MODIS. Ten events were identified, primarily in spring and early summer, with varying intensification rates. The findings highlight remote sensing's importance and the need for region-specific drought management strategies using multiple indicators.

Keywords: flash drought, soil moisture, evaportranspiration, intensification rate, remote sensing, southewestern lowlands

2 Introduction

Drought phenomena, often characterized by prolonged periods of extreme conditions over months or years, have historically impacted agriculture, ecosystems, and socioeconomics [1]. Flash droughts, in contrast to traditional droughts, pose a unique concern because of their rapid onset, development, and intensity and the sudden depletion of available water, which can upset ecosystems and agricultural systems [2], [3]. Since rapid development is the primary characteristic of flash drought, early warning systems are more vulnerable than slow-evolving droughts, which result in tremendous losses [4]. The occurrence of flash droughts, exemplified by significant economic losses and environmental impacts in regions like Jiangxi Province in China (2003) [5], the central United States (2012, 2017) [6], [7], [8], [9], Southern Queensland in Australia (2018) [10] and South Africa (2016) [11] underscores the urgent need for enhanced understanding and mitigation strategies. While current estimates highlight the staggering economic toll of traditional droughts in Europe and the broader implications for climate change adaptation, the specific economic ramifications of flash droughts remain largely unexplored. As reports indicate a rise in the frequency and spatial extent of flash droughts across Europe, coupled with the likelihood of their exacerbation in regions already vulnerable to conventional droughts, there is a pressing imperative to prioritize research and policy efforts towards effective adaptation and mitigation strategies [12].

There has yet to be a consistent definition of flash droughts to distinguish them from traditional ones. Among numerous studies, a variety of definitions have been proposed, and two of them have predominated [5], [13], [14]. One is based on the duration of flash drought, and the other is based on its intensification rate. Although there are representative works about the flash drought duration proved to be too short to cause damage to agriculture systems [4], [15]. However, recent research emphasized the rapid rate of intensification [16], [17]. Given its tight association with crop development, soil moisture and evapotranspiration (ET) are acknowledged as efficient indicators of flash droughts amongst several hydrometeorological factors [18], [19], [20]. Many studies popularized the use of soil moisture percentiles to identify flash drought events and their characteristics using in situ observations or remote sensing data [3], [16], [21] [22]. Therefore, the regional Evaporative Stress Ratio (ESR), which indicates temporal anomalies in the ratio of actual to potential ET, is derived from remotely sensed canopy temperature using geostationary satellite thermal infrared (TIR) imaging like the Moderate Resolution

Imaging Spectroradiometer (MODIS) [23], [24]. This index has proven helpful for early drought detection, including the notable flash drought in 2012 [4].

The challenge of drought monitoring lies in the need for long-term, spatial, comprehensive hydrometeorological records; even if ground observations provide accurate measurements, their spatial heterogeneity due to their point-based method limits their applications. The widespread adoption of satellite observations has been supported by the continued development of remote sensing techniques, which provide broad spatial coverage and a regular overview of the dynamics of water balance variables like soil moisture and evapotranspiration [25], [26]. Many satellite soil moisture products obtained using various spaceborne microwave instruments have been available. For instance, vegetation cover and atmospheric conditions are more likely to affect observations made with instruments like WindSat, FengYun-3B, Advanced Microwave Scanning Radiometer-Earth (AMSR-E) and Advanced Scatterometer (ASCAT) at higher C- and -X band microwave frequencies [25]. Additionally, many satellite products like Landsat and MODIS offer evapotranspiration data, with MODIS being the most widely used.

Although a handful of studies focused on the US, China, Australia, or Europe, research has yet to be conducted about flash drought assessment in Central Europe, especially Slovakia, let alone studies on the Czech Republic. This study will focus on detecting flash drought events from the perspective of the rapid intensification rate in the southwestern lowlands, one of Slovakia's most vital agricultural areas. Furthermore, while many studies have explored agricultural drought using ASCAT data, this is the first instance in the literature of utilizing ASCAT data to identify flash drought events. Additionally this research proposes the use of hydrological (soil moisture) and meteorological (evapotranspiration) variables to identify the flash drought events and points out similarities and differences of their use under the veil of remote sensing techniques.

3 Methods

3.1 Definitions of flash drought

This work implemented a practical methodology to identify flash droughts considering both the rapid intensification rate and drought conditions. Specifically, a flash drought was defined when the soil moisture (SM) and ESR decreased from the 40th percentile to below the 20th percentile over a pentad period (5 days), with an average decline rate not less than the 5th percentile for each pentad. The termination of a flash drought event was indicated once the decreasing soil moisture level returned to the 20th percentile. It is noted that, from 2007-2019 (March- November), the 20th and 40th percentiles were calculated within the same pentad period, enabling a consistent comparison of changes in soil moisture and ESR. Furthermore, the 5th percentile was calculated as the difference between two percentiles at two adjacent pentads across the entire time series. Our analysis focused on understanding the rapid onset and development of flash droughts. The onset point of a flash drought is defined as the initial instance when soil moisture (SM) and ESR exceed the 40th percentile. The endpoint of the onset development phase occurs when SM and ESR drop below the 20th percentile. This phase, from the onset point (to) to the endpoint (te), defines the onset time of flash droughts, indicating a rapid drying process. The duration under drought conditions, from the to tp, is crucial for understanding the impacts, and to be considered a drought, SM and ESR should remain below the 20th percentile for at least three pentads ($tp-te \geq 3$). This criterion helps distinguish actual drought events from transient fluctuations. Therefore, the entire duration of a flash drought encompasses both the rapid onset phase (to−te) and the subsequent drought severity period (te−tp), emphasizing the importance of considering both aspects for accurate identification. Eq. (1) and Eq. (2) express the intensification rate and drought conditions.

$$\text{Intensification rate: } \begin{cases} \frac{SM_{t_{(i+1)}} - SM_{(t_i)}}{t_i - t} \geq 5th\ percentile \\ 0 < t_e - t_0 \leq 5 \end{cases} \quad (1)$$

$$\text{Drought condition: } \begin{cases} SM_{(t_0)} \geq 40th\ percentile \\ SM_{(t_e)} \leq 20th\ percentile \\ t_p - t_e \geq 3 \end{cases} \quad (2)$$

3.2 Study area and data

The Danubian Lowland, located in the southwest (SW) region of Slovakia, north of the Danube River, covers an area of 12,539.26 Km^2. It is characterized by a warm, dry environment with an average yearly air temperature of 9 to 10.5° C and 500 to 550 mm of precipitation. The average air temperature in July ranges from 19 to 21° C, while the winters are mild, with an average air temperature from -1 to -2° C in January. The area is characterized by intense agricultural activity and is mostly covered by Non-irrigated land. Figure 1 shows the land use/ land cover classes derived from CORINE (2018).

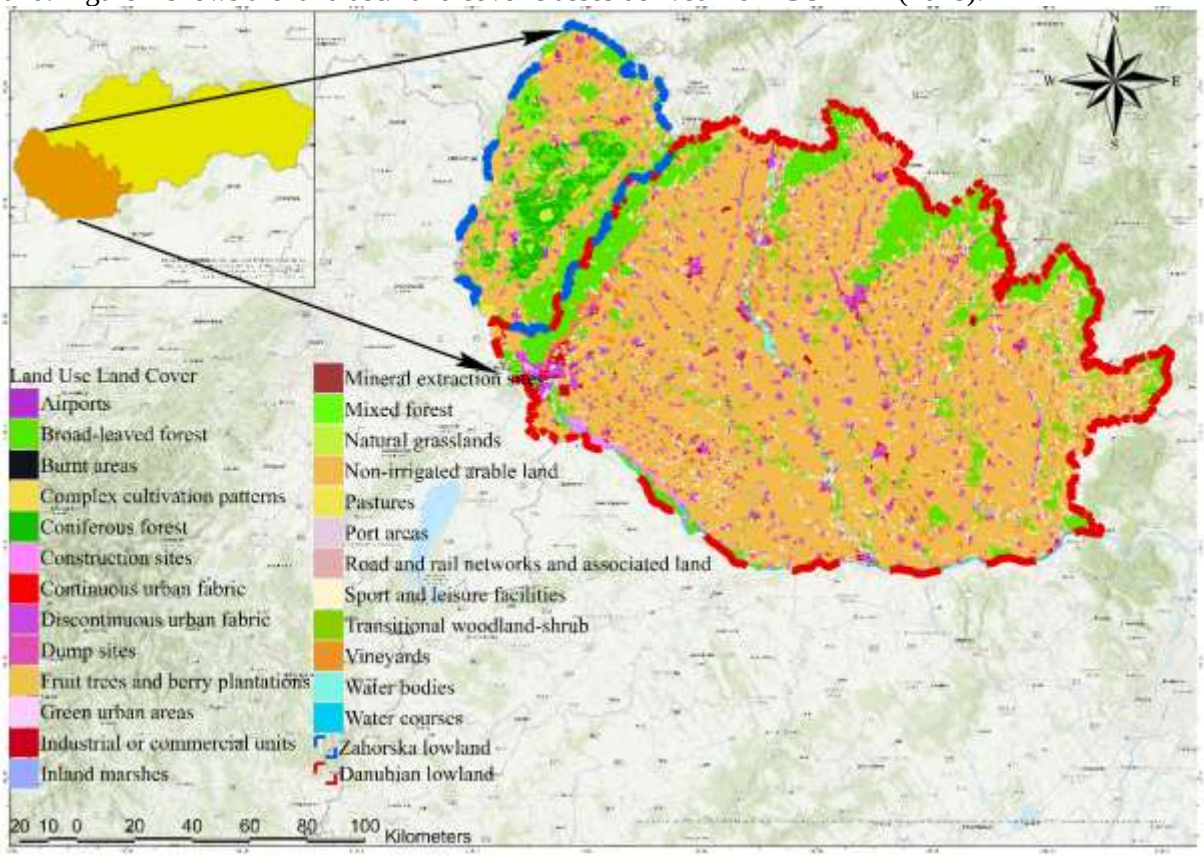

Figure 27 Land use/ Land cover of Zahorska and Danubian lowlands.

The data utilized in this study comprise the ASCAT SSM product and in situ soil moisture measurements. The ASCAT SSM product, sourced from Vienna University of Technology (TU-WIEN, http://rs.geo.tuwien.ac.at/products/), offers daily relative soil moisture data with high resolution (approximately 15-20 Km per pixel), ranging from 0 (dry) to 100% (saturated), using a change detection algorithm initially proposed by Wagner [27] and subsequently enhanced by Naeimi [28]. Specifically, data from the ASCAT SSM dataset from 2007 to 2019 were employed in this analysis. The Soil Water Index (SWI) variable assessed moisture conditions at various soil depths for each benchmark site and date. This product utilizes a two-layer infiltration model that relates surface soil moisture (SSM) retrieved from ASCAT instruments aboard METOP satellites to profile soil moisture over time [27]. The SWI formula is expressed as follows:

$$\text{SWI}(t_n) = \frac{\sum_{i=1}^{n} \text{SSM}(t_i) e^{\frac{t_n - t_i}{T}}}{\sum_{i=1}^{n} e^{\frac{t_n - t_i}{T}}} \quad (3)$$

where t_n is the observation time of the current measurement, t_i are the observation times of the previous

measurements, and T is a parameter calculated as T = L/C, with L representing the depth of the reservoir layer and C an area-representative pseudo-diffusivity constant [29]. This model, built on the importance of historic SSM time series data, assumes that the water content of the deeper layer is influenced by past moisture conditions in the surface layer and precipitation history [30]. A higher (lower) T value signifies a deeper (shallower) soil layer. Since computing SWI values necessitates historic SSM time series data, Albergel proposed a computational adaptation of this SWI algorithm [29]. Thus, the surface layer was selected to identify flash droughts as it is more connected to precipitation than the lower layers, which are affected by past conditions of soil moisture. Additionally, the Moderate Resolution Imaging Spectroradiometer (MODIS) actual (ET) and potential evapotranspiration (PET) products (MOD16A2GF.006) were downloaded from https://search.earthdata.nasa.gov/ for the period 2007-2019 (March-November). MODIS provides 500m resolution and eight (8) days. The time series of daily values of ET and PET were generated using the INDEX-MATCH functions in Microsoft EXCEL. The Evaporative Stress Ratio (ESR) was also calculated to identify the flash drought events and their intensification rate under atmospheric conditions. The Evaporative Stress Ratio is expressed from the equation below:

$$ESR = \frac{ET}{PET} \tag{4}$$

ET represents the actual evapotranspiration from the earth's surface, influenced by soil moisture availability, alongside factors such as energy availability, air temperature, wind speed, and atmospheric moisture demand conditions. On the other hand, PET signifies potential evapotranspiration, which is a significant measure of atmospheric evaporative demand and is crucial in developing droughts [28].

4 Results and discussion

The flash drought events of southwestern (SW) Slovak lowlands were assessed for the growing period (March-November) from 2007 to 2019 based on the drought condition and rapid intensification rate. The study region was divided into two separate areas: the Zahorska and Danubian lowlands. To begin with, the Zahorska lowlands experienced ten (10) flash drought events presented in Figure 2 with red stripes. The frequency duration of flash drought events accounts for 5.48% or 52 pentads (260 days). The highest duration recorded was 11 pentads and occurred from 2008-03-01 to 2008-04-25, while the lowest ones were noticed in 2010-04-15 to 2010-04-30 and 2016-04-13 to 2016-04-28, lasting only three (3) pentads. From the perspective of intensification, rate values vary from -17 to -26, the most intense rate recorded in 2018-03-10 to 2018-04-18 event accounting for -26.83 while the lowest accounted for -17.77 from 2007-06-20 to 2007-07-05, the rest of characteristics are presented in Table 1. The flash drought events of Danubian lowlands present a similar status. Figure 3 shows the ten (10) detected flash drought events marked with red stripes. The frequency duration of flash drought events accounts for 6.32% or 60 pentads (300 days). It has been noticed that the Danubian lowlands experience 40 more days of flash droughts than the Zahorska lowlands. Moreover, according to Table 2, the event with the longest duration was recorded on 2008-03-01 to 2008-04-25, lasting eleven (11) pentads (55 days). The shorted ones occurred between 2012-04-04 to 2012-04-19 and 2017-05-03 to 2017-05-18, lasting the minimum required of three (3) pentads (15 days). Furthermore, analyzing the intensification rate results, the highest value of -24.72 was recorded from 2015-03-30 to 2015-04-19, while the lowest one (-17.89) from 2012-04-04 to 2012-04-19. Both regions experience flash droughts predominantly in the spring and early summer months, indicating a seasonal pattern that similar climatic factors might influence. The duration of the flash drought events in both areas typically ranges between 3 to 11 pentads (15 to 55 days), suggesting that the regions experience similar lengths of flash drought events. Additionally, the intensification rates for flash droughts in both areas show significant drops in soil moisture content, with values often falling below -20 units, which suggests that both regions experience rapid and severe declines in soil moisture during flash drought events. A major difference between the two areas is that from 2011 to 2015 the Danubian lowland experiences two flash drought events compared to zero ones to Zahorska. Particularly, in 2012 and 2013 the Danubian lowlands experienced flash drought events with duration of three (3) and seven (7) pentads, respectively and similar intensification rates (Table 2).

One of the areas may experience a higher frequency of flash drought events than the other, indicating differences in regional climate variability or the impacts of climatic drivers such as temperature and precipitation anomalies. The specific onset and end times of flash droughts vary between the two regions, possibly due to microclimatic conditions, differences in soil properties, or varying agricultural practices that influence the timing of drought conditions. Although both areas experience rapid declines in soil moisture, the magnitude of these declines might differ, with one region potentially experiencing more severe flash droughts characterized by lower minimum soil moisture values and higher absolute intensification rates. Additionally, the persistence of drought conditions, or how long soil moisture remains below critical thresholds, could differ between the two regions, with one area experiencing quicker recovery from flash droughts. At the same time, the other endures prolonged periods of low soil moisture. It is important also to examine the nature of flash drought events and their characteristics from the perspective of atmospheric indices. In this research, the Evaporative Stress Index (ESR) was used as it is strongly connected with traditional droughts and widely implemented in flash drought studies across the globe. Compared to soil moisture, ESR results identified thirteen (13) flash drought events, as shown with red stripes in Figure 3. Table 2 presents the characteristics of flash drought events based on ESR values; the event with the highest duration lasted seven pentads (2007-05-30 to 2007-06-24). The shortest duration was noticed from 2012-03-04 to 2012-03-14, and the period from 2009-03-05 to 2009-03-30 presented the highest intensification rate (-0.08), while the lowest intensification rate (-0.027) was noticed from 2011-08-12 to 2011-09-06. Considering the fluctuations of ESR intensification rate values, it is noticed that they decrease as time passes by compared to SM intensification rate values, which increase (Figs. 4 & 5). The frequency duration of flash drought events based on ESR values accounts for 9.25%, almost two times bigger than soil moisture events. It is challenging to compare the present study's findings directly with those of other research due to the various definitions of flash drought and regions examined. Based on the literature review, this study utilized the soil moisture and Evapotranspiration Stress Ratio (ESR) as indicators to identify flash drought events due to its use on a global or basin scale. Driven by human-induced global warming, there is an increasing trend of drought-affected areas and annual spatial mean severity in Central European regions [31]. The high intensification rate values can be noticed in this study in the last few years (Fig. 4). A comprehensive case study conducted in Central Europe presented the spatiotemporal variability of flash drought events resulting in the summer months playing a significant role in triggering the onset time [31]. Finally, due to the complex nature of flash droughts, further investigation should be conducted, comparing more indices and examining the driving factors.

Table 1. Characteristics of flash drought events at Zahorska lowlands.

Year	Onset time	End time	Duration (pentads)	Intensification rate
2007	2007-03-07	2007-04-06	6	-20.46
2007	2007-06-20	2007-07-05	3	-17.77
2008	2008-03-01	2008-04-25	11	-24.23
2009	2009-03-11	2009-04-15	7	-18.92
2010	2010-04-15	2010-04-30	3	-26.70
2015	2015-03-30	2015-04-19	4	-23.87
2016	2016-04-13	2016-04-28	3	-18.26
2017	2017-03-19	2017-04-08	4	-21.79
2018	2018-03-19	2018-04-18	6	-26.83
2019	2019-03-14	2019-04-08	5	-23.26

Table 2. Characteristics of flash drought events at Danubian lowlands

Year	Onset time	End time	Duration (pentads)	Intensification rate
2007	2007-03-07	2007-04-16	8	-17.89
2008	2008-03-01	2008-04-25	11	-18.13
2009	2009-03-11	2009-04-20	8	-16.34
2012	2012-04-04	2012-04-19	3	-16.28
2013	2013-08-27	2013-10-01	7	-16.58
2015	2015-03-30	2015-04-19	4	-24.72

2017	2017-03-19	2017-04-08	4	-22.14
2017	2017-05-03	2017-05-18	3	-20.14
2018	2018-03-14	2018-04-18	7	-20.46
2019	2019-03-14	2019-04-08	5	-19.05

Table 3. Characteristics of flash drought events based on ESR.

Year	Onset time	End time	Duration (pentads)	Intensification rate
2007	2007-05-30	2007-06-24	5	-0.048
2009	2009-03-05	2009-03-30	5	-0.08
2011	2011-03-05	2011-03-25	4	-0.033
2011	2011-08-12	2011-09-06	5	-0.027
2012	2012-03-04	2012-03-14	2	-0.059
2012	2012-07-22	2012-08-16	5	-0.020
2013	2013-07-02	2013-07-27	5	-0.035
2015	2015-03-19	2015-04-23	7	-0.036
2015	2015-06-12	2015-07-07	5	-0.045
2017	2017-03-03	2017-03-23	4	-0.044
2017	2017-06-01	2017-06-26	5	-0.041
2018	2018-07-21	2018-08-05	3	-0.033
2019	2019-06-21	2019-07-16	5	-0.034

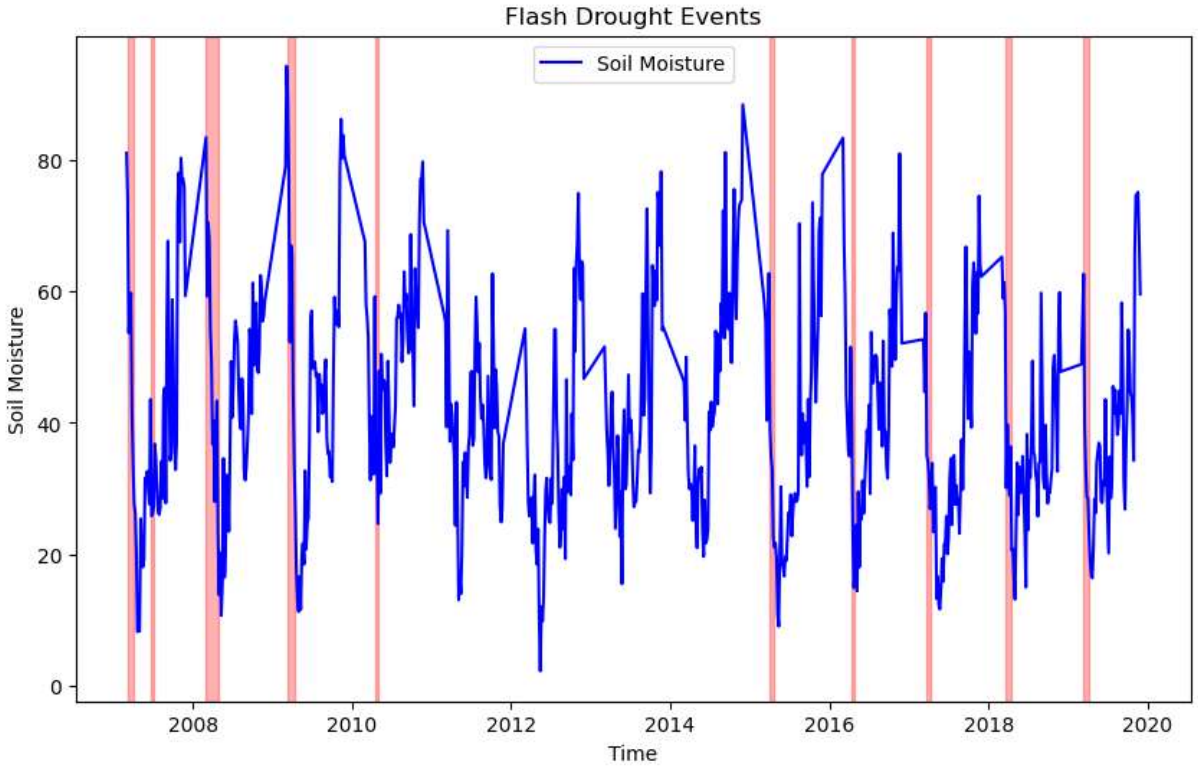

Figure 2. Flash drought events of Zahorska lowlands based on SM for 2007-2019.

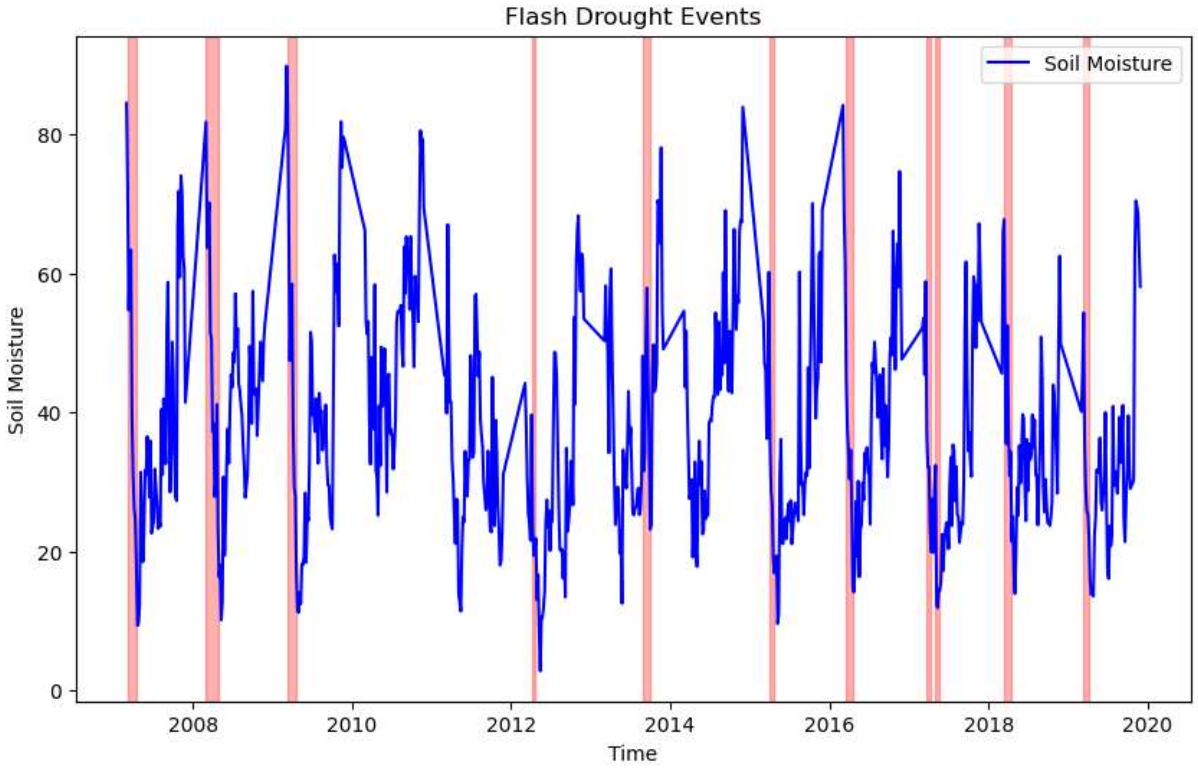

Figure 3. Flash drought events of Danubian lowlands based on SM for 2007-2019.

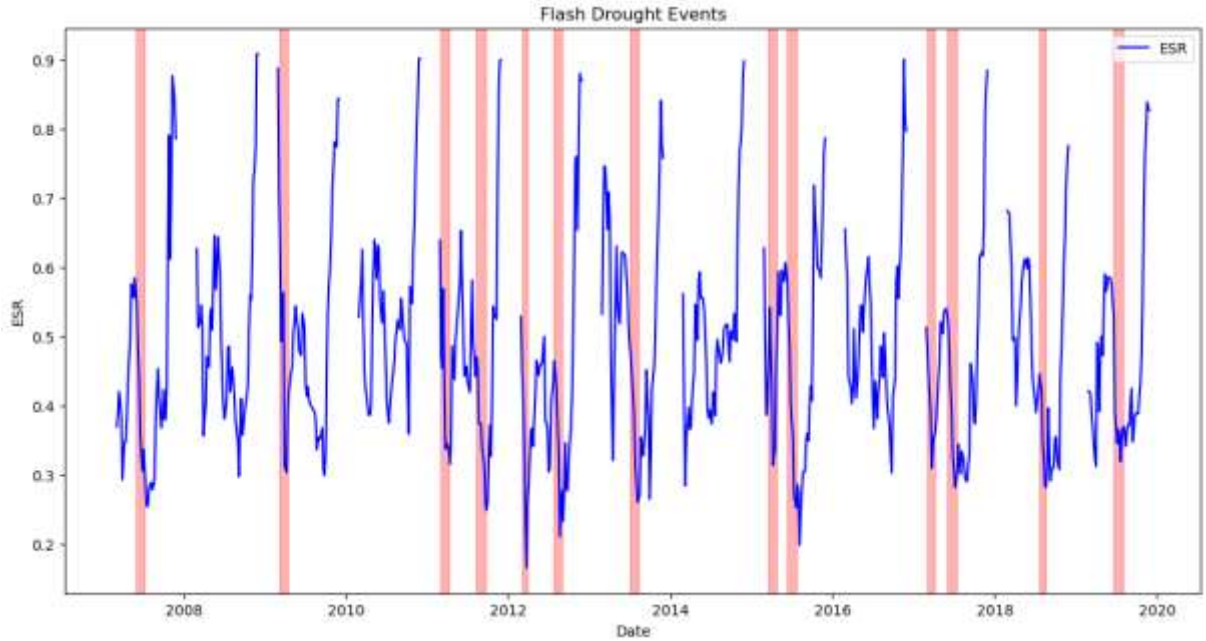

Figure 4. Flash drought events of southwestern (SW) Slovakia's lowlands based on ESR for 2007-2019.

5 Conclusion

The increasing frequency of flash droughts, characterized by their rapid onset and intensification, poses a significant threat to agriculture systems. Due to the inconsistent definition of flash drought, this study has emphasized the rapid intensification rate, underscoring the importance of utilizing remote sensing soil moisture and evapotranspiration products as a critical indicator for identifying and understanding

these events. The assessment of flash drought events in the southwestern Slovak lowlands for the growing period (March-November) from 2007 to 2019 reveals notable variability in duration and intensity, with early spring months predominantly experiencing these events. Both the Zahorska and Danubian Lowlands share common features regarding the seasonal timing, duration, and rapid intensification of flash drought events. However, they differ in the frequency of events, specific onset and end times, droughts' intensity and severity, and drought conditions' persistence. These differences highlight the need for region-specific drought management and mitigation strategies to address the unique characteristics of flash droughts in each area. While the study's findings provide insights into the characteristics of flash droughts in these regions, comparisons with other research are challenging due to differing definitions and regions studied. However, using soil moisture and Evapotranspiration Stress Ratio (ESR) as indicators highlights their relevance for understanding flash droughts, particularly amid increasing trends in drought-affected areas driven by human-induced global warming. Moreover, the analysis highlights the correlation between severe drought events and crop yields, suggesting their suitability for drought impact assessment in the Danubian Lowlands. Nonetheless, due to the complex nature of flash droughts, further investigations are needed with more hydrometeorological factors.

Acknowledgements
This research was supported by the Slovak Research and Development Agency under Contract No. APVV 19-0340 and the VEGA Grant Agency No. VEGA 1/0782/21 and VEGA1/0577/23. The authors are grateful for the support of their research.

References:
[1] Mishra, A. K., Singh, V. P. (2010). A review of drought concepts. *Journal of hydrology*, *391*(1-2), 202-216.
[2] Otkin, J. A., Anderson, M. C., Hain, C., & Svoboda, M. (2015). Using temporal changes in drought indices to generate probabilistic drought intensification forecasts. *Journal of Hydrometeorology*, *16*(1), 88-105.
[3] Ford, T. W., McRoberts, D. B., Quiring, S. M., & Hall, R. E. (2015). On the utility of in situ soil moisture observations for flash drought early warning in Oklahoma, USA. *Geophysical Research Letters*, *42*(22), 9790-9798.
[4] Otkin, J. A., Svoboda, M., Hunt, E. D., Ford, T. W., Anderson, M. C., Hain, C., & Basara, J. B. (2018). Flash droughts: A review and assessment of the challenges imposed by rapid-onset droughts in the United States. *Bulletin of the American Meteorological Society*, *99*(5), 911-919.
[5] Zhang, Y., You, Q., Chen, C., & Li, X. (2017). Flash droughts in a typical humid and subtropical basin: A case study in the Gan River Basin, China. *Journal of Hydrology*, *551*, 162-176.
[6] Christian, Jordan I., Jeffrey B. Basara, Jason A. Otkin, Eric D. Hunt, Ryann A. Wakefield, Paul X. Flanagan, and Xiangming Xiao. "A methodology for flash drought identification: Application of flash drought frequency across the United States." *Journal of Hydrometeorology* 20, no. 5 (2019): 833-846.
[7] NOAA National Centers for Environmental Information (NCEI) *US Billion-Dollar Weather and Climate Disasters*. 2017 (NOAA National Centers for Environmental Information (NCEI), accessed 1 June 2021); https://www.ncdc.noaa.gov/billions/.
[8] Gerken, T., Bromley, G. T., Ruddell, B. L., Williams, S., Stoy, P. C. (2018). Convective suppression before and during the United States Northern Great Plains flash drought of 2017. *Hydrology and Earth System Sciences*, *22*(8), 4155-4163.
[9] Hoerling, M., Eischeid, J., Kumar, A., Leung, R., Mariotti, A., Mo, K., Seager, R. (2014). Causes and predictability of the 2012 Great Plains drought. *Bulletin of the American Meteorological Society*, *95*(2), 269-282.
[10] Nguyen, H., Wheeler, M. C., Otkin, J. A., Cowan, T., Frost, A., Stone, R. (2019). Using the evaporative stress index to monitor flash drought in Australia. *Environmental Research Letters*, *14*(6), 064016.
[11] Yuan, X., Wang, L., Wood, E. F. (2018). Anthropogenic intensification of southern African flash droughts as exemplified by the 2015/16 season. *Bulletin of the American Meteorological Society*, *99*(1), S86-S90.

[12] Shah, J., Hari, V., Rakovec, O., Markonis, Y., Samaniego, L., Mishra, V., Kumar, R. (2022). Increasing footprint of climate warming on flash droughts occurrence in Europe. *Environmental Research Letters*, *17*(6), 064017.
[13] Mo, Kingtse C., and Dennis P. Lettenmaier. "Heat wave flash droughts in decline." *Geophysical Research Letters* 42, no. 8 (2015): 2823-2829.
[14] Pendergrass, A. G., Meehl, G. A., Pulwarty, R., Hobbins, M., Hoell, A., AghaKouchak, A., Woodhouse, C. A. (2020). Flash droughts present a new challenge for subseasonal-to-seasonal prediction. *Nature Climate Change*, *10*(3), 191-199.
[15] Yuan, X., Wang, L., Wu, P., Ji, P., Sheffield, J., Zhang, M. (2019). Anthropogenic shift towards higher risk of flash drought over China. *Nature communications*, *10*(1), 4661.
[16] Liu, Y., Zhu, Y., Zhang, L., Ren, L., Yuan, F., Yang, X., Jiang, S. (2020). Flash droughts characterization over China: From a perspective of the rapid intensification rate. *Science of the Total Environment*, *704*, 135373.
[17] Han, J., Zhang, J., Yang, S., Seka, A. M. (2023). Improved understanding of flash drought from a comparative analysis of drought with different intensification rates. *Remote Sensing*, *15*(8), 2049.
[18] Hunt, E. D., Svoboda, M., Wardlow, B., Hubbard, K., Hayes, M., Arkebauer, T. (2014). Monitoring the effects of rapid onset of drought on non-irrigated maize with agronomic data and climate-based drought indices. *Agricultural and Forest Meteorology*, *191*, 1-11.
[19] Zhu, Y., Liu, Y., Wang, W., Singh, V. P., Ma, X., Yu, Z. (2019). Three dimensional characterization of meteorological and hydrological droughts and their probabilistic links. *Journal of hydrology*, *578*, 124016.
[20] Liu, Y., Zhu, Y., Ren, L., Singh, V. P., Yang, X., Yuan, F. (2017). A multiscalar Palmer drought severity index. *Geophysical Research Letters*, *44*(13), 6850-6858.
[21] Qing, Y., Wang, S., Ancell, B. C., Yang, Z. L. (2022). Accelerating flash droughts induced by the joint influence of soil moisture depletion and atmospheric aridity. *Nature communications*, *13*(1), 1139.
[22] Li, P., Jia, L., Lu, J., Jiang, M., Zheng, C. (2024). A New Evapotranspiration-Based Drought Index for Flash Drought Identification and Monitoring. *Remote Sensing*, *16*(5), 780.
[23] Running, S. W., Mu, Q., Zhao, M., Moreno, A. (2017). MODIS global terrestrial evapotranspiration (ET) product (NASA MOD16A2/A3) NASA earth observing system MODIS land algorithm. *NASA: Washington, DC, USA*.
[24] Anderson, M. C., Zolin, C. A., Sentelhas, P. C., Hain, C. R., Semmens, K., Yilmaz, M. T., Tetrault, R. (2016). The Evaporative Stress Index as an indicator of agricultural drought in Brazil: An assessment based on crop yield impacts. *Remote Sensing of Environment*, *174*, 82-99.
[25] Albergel, C., De Rosnay, P., Gruhier, C., Muñoz-Sabater, J., Hasenauer, S., Isaksen, L., Wagner, W. (2012). Evaluation of remotely sensed and modelled soil moisture products using global ground-based in situ observations. *Remote Sensing of Environment*, *118*, 215-226.
[26] Wagner, W., Lemoine, G., Rott, H. (1999). A method for estimating soil moisture from ERS scatterometer and soil data. *Remote sensing of environment*, *70*(2), 191-207.
[27] Naeimi, V., Scipal, K., Bartalis, Z., Hasenauer, S., Wagner, W. (2009). An improved soil moisture retrieval algorithm for ERS and METOP scatterometer observations. *IEEE Transactions on Geoscience and Remote Sensing*, *47*(7), 1999-2013.
[28] McEvoy, D. J., Huntington, J. L., Hobbins, M. T., Wood, A., Morton, C., Anderson, M., Hain, C. (2016). The evaporative demand drought index. Part II: CONUS-wide assessment against common drought indicators. *Journal of Hydrometeorology*, *17*(6), 1763-1779.
[29] Albergel, C., Rüdiger, C., Pellarin, T., Calvet, J-C., Fritz, N., Froissard, F., Suquia, D., Petitpa, A., Piguet, B., Martin, E., 2008. From near-surface to root-zone soil moisture using an exponential filter: an assessment of the method based on in-situ observations and model simulations. Hydrology and Earth System Sciences Discussions 12, 1323-1337.
[30] Ceballos, A., Scipal, K., Wagner, W., MartinezFernández, J., 2005. Validation of ERS scatterometer-derived soil moisture data in the central part of the Duero Basin, Spain. Hydrological Processes 19, 1549–1566.
[31] Řehoř, J., Brázdil, R., Trnka, M., Balek, J. (2024). Flash droughts in Central Europe and their circulation drivers. *Climate Dynamics*, *62*(2), 1107-1121.

TREND AND CORRELATION ANALYSIS OF GROUNDWATER QUALITY AT THE BARTOLOVEC WELLFIELD IN CROATIA

MARKO ŠRAJBEK [1], IVAN KOVAČ [2], BOJAN ĐURIN [3], GORDON GILJA [1],

[1] *University of Zagreb, Faculty of Civil Engineering, Department of Water Science, Croatia, marko.srajbek@grad.unizg.hr; gordon.gilja@grad.unizg.hr*

[2] *University of Zagreb, Faculty of Geotechnical Engineering, Department of Water Management, Croatia, ivan.kovac@gfv.unizg.hr*

[3] *University North, Department of Civil Engineering, Croatia, bdjurin@unin.hr*

1 Abstract

As the quality of life has been improved and the number of people increases on a global scale, the demand for high-quality drinking water is also growing. On the other hand, more intensive economic development, and the associated emission of pollutants into the environment are placing increasing pressure on all components of the environment, including aquifers. With this in mind, it is very important to establish a functioning groundwater quality control system that carries out daily analyses so that a timely response can be made in the event of sudden pollution. However, it is equally important to monitor the quality of groundwater over the long term, as such analyses are very effective in revealing changes in trends over specific time intervals. With the aim of preserving groundwater resources, a statistical analysis of the quality of groundwater at the Bartolovec wellfield in Varaždin County in Croatia was carried out in this paper for the period 1993-2023. The values for five parameters of water quality were analysed: pH value, electrical conductivity, $KMnO_4$, chloride and nitrate concentration. The time series of the annual averages were formed, and the associated trends were analysed. A correlation analysis was carried out and the relationship between same quality parameters at different wells was analysed. The correlation between different quality parameters at the same wells was also analysed. For all quality parameters for both periods the arithmetic means were calculated and mutually compared, and the statistical significance of difference were calculated. Although new methods have been developed and used in water resources management in recent years, the results obtained in this paper show the importance of conventional statistical methods, the results of which still provide important conclusions.

Keywords: groundwater quality, time series, trend analysis, correlation

2 Introduction

Water is one of the most abundant substances on Earth and is necessary for all living beings. Even in the atmosphere, where water droplets form, it dissolves gas particles and changes its natural properties to a greater or lesser extent. When it reaches the surface of the ground in the form of precipitation, it dissolves many of the substances found there and reaches the subsoil. This water is known as groundwater and is the most important source of water for various human needs. It is estimated that in the countries of the European Union about 80% of all water consumed for human use comes from groundwater [1]. Nowadays, the interest and need for high quality water is increasing [2], but at the same time, the deterioration of groundwater quality is almost inevitable due to the increasingly intensive industrial and agricultural development and the impact of the urban areas on the environment [3, 4, 5]. As a result, new wellfields are being developed or the pumping rate of existing wells is being increased [6]. In the past, it was believed that the upper deposits of the aquifer would sufficiently protect the groundwater, but scientific studies and monitoring have shown that pollutants can easily penetrate the unsaturated zone and enter the groundwater [7, 8]. For this reason, groundwater quality and its changes

in space and time are the subject of numerous scientific studies [9, 10, 11]. In this sense, agricultural production is recognized worldwide as one of the main sources of groundwater pollution [12, 13], and the groundwater of the northern part of Croatia is no exception [14, 15]. Considering the population density and the intensity of development of the area under consideration, the protection of groundwater should be one of prerequisites for further development and improvement of the quality of life. For this purpose, a statistical analysis of certain parameters of groundwater quality in the period from 1993 to 2023 was carried out in the Bartolovec wellfield in Varaždin County in northern Croatia. For many years, there was a problem with the quality of groundwater in the observed area, and the chemical composition changed so much that in certain periods the water did not meet the legally prescribed criteria [16]. For this reason, the Varaždin wellfield, which was once the largest, is now closed. Considering its size, importance and the funds invested in the Varaždin wellfield, it can be concluded that this is an invaluable loss of large groundwater resources. In order to meet the demand for drinking water, the pumping capacity of the Bartolovec wellfield was systematically increased and today it represents the largest source of water for the local needs. Given the high vulnerability of the aquifer in which the Bartolovec wellfield [17] is located, it is very important to protect groundwater resources. In this sense, it is necessary to protect the recharge area of the wellfield [18] and to monitor the quality of the groundwater in order to be able to react in time in the event of sudden pollution. In this paper, five quality parameters for which there is a sufficiently long sampling period for reliable statistical analysis in the period 1993-20323 are analyzed. In the paper, the annual average values of each observed parameter were calculated, and a statistically significant difference was found. A trend analysis and a statistical analysis of the same parameters in different aquifers and of different parameters in the same aquifer were also carried out.

3 Methods

3.1 The Study Area

The study area is located in the north of the Republic of Croatia and includes the Bartolovec wellfield (Figure 1), which is located near the town of Varaždin. The Varaždin region is one of the most densely populated and economically developed areas in the country. Organized water supply in the area in the modern sense began in the sixties of the 20th century, when the Varaždin Regional Water Supply was established, which today consists of three wellfields: Bartolovec, Varaždin and Vinokovščak. 216 settlements with a total of about 46,000 connections are connected to the regional water supply system, which supplies water to about 151,000 inhabitants, which corresponds to 82% of the total population of Varaždin County [19]. The Bartolovec wellfield was put into operation in 1972. After the pumping capacity of the Varaždin wellfield was reduced due to the high nitrate concentration, the Bartolovec wellfield was designated as the new main wellfield for the county. As a result, pumping rate has been systematically increased over the years and today there are a total of nine wells with a total capacity of over 500 L/s.

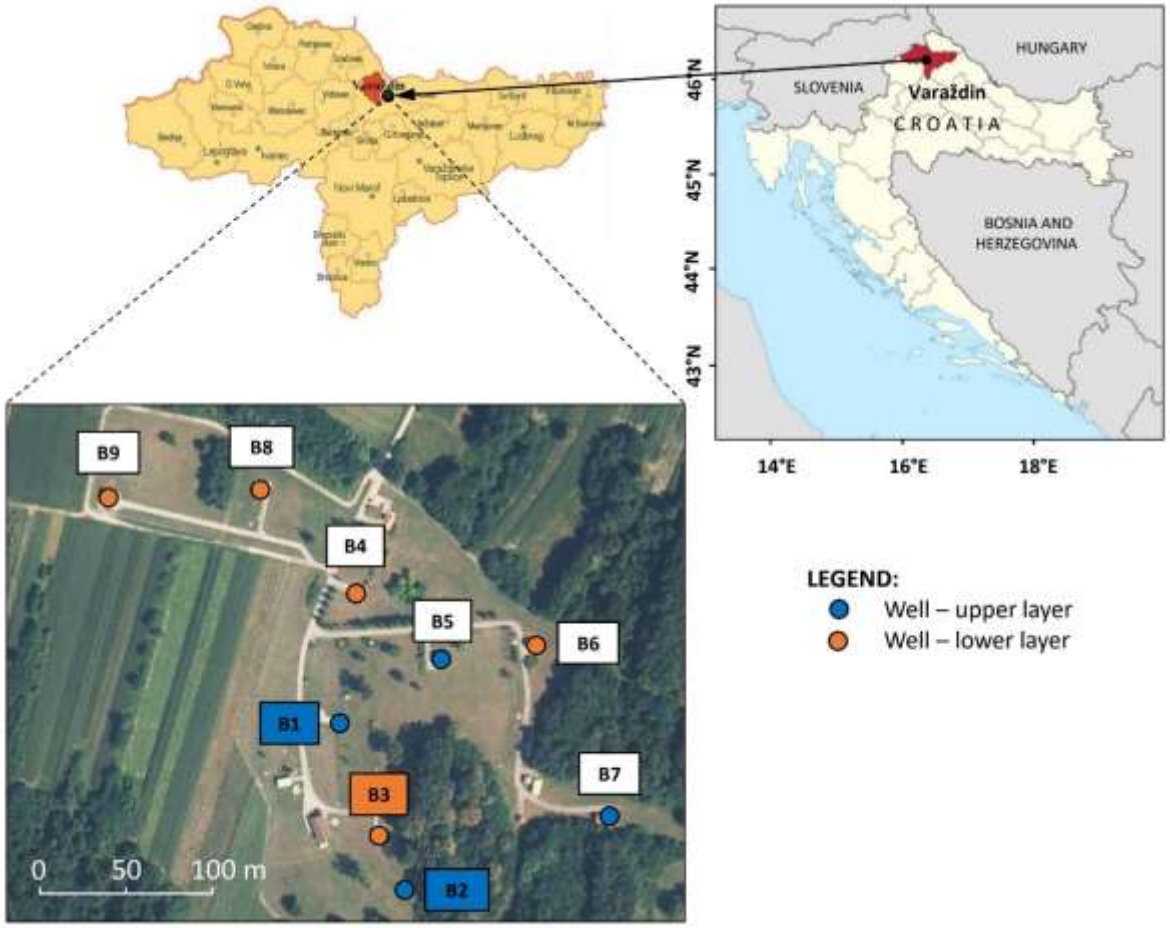

Figure 1. Location of the Bartolovec wellfield and spatial distribution of wells

3.2 Geological and Hydrogeological Conditions

The geological structures consist of coarse-grained sediments of gravel and sand, while the underlying sediments consist of silt and clay [20]. The aquifer runs parallel to the Drava River and its thickness increases from west to east. In the far west, the thickness is 5 m, while in the area of the Bartolovec wellfield it is about 100 m. In the eastern part, the thickness of the aquifer increases to a maximum of 148 m and then gradually decreases. The aquifer consists of two permeable layers of gravel and sand, most of which are separated by a semi-permeable silty and clayey aquitard [20]. The upper layer of the aquifer consists of coarse-grained gravel and sand, while the lower part consists mainly of fine-grained gravel with sand (Figure 2 and Figure 3).

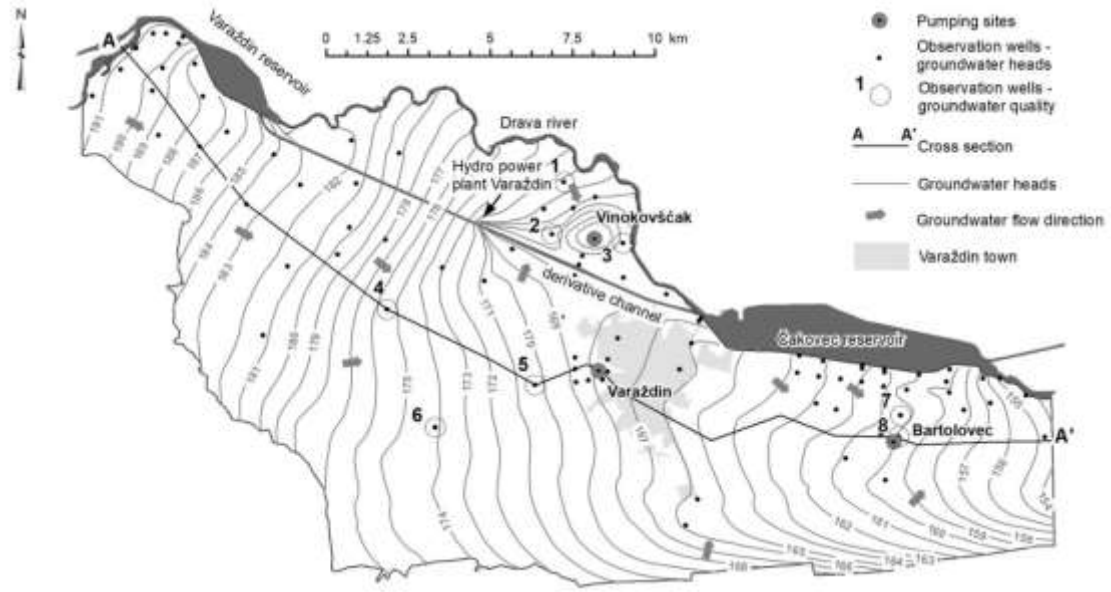

Figure 2. Plan view of the Varaždin aquifer with groundwater flow direction [17]

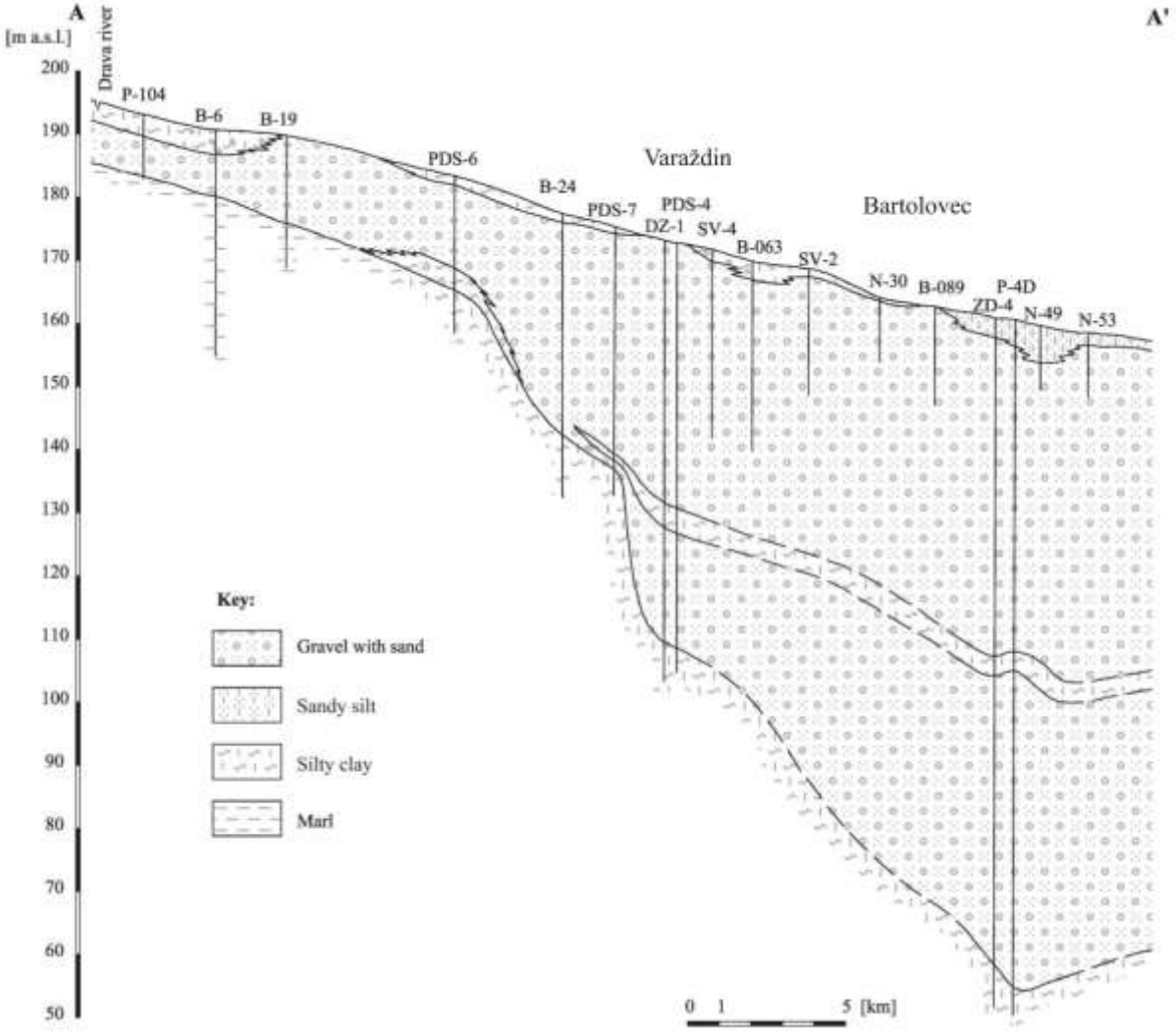

Figure 3. Longitudinal lithological profile of the Varaždin aquifer [17]

3.3 Previous research

The quality of the groundwater in the observed area has been systematically monitored since the early 1970s, and as recent studies show, it has changed considerably over time and space [19]. Nevertheless, the quality of the groundwater was generally satisfactory, with the exception of nitrate concentration. The values of this parameter were often higher than the maximum allowed concentration [MAC]. As previous studies have shown, the high nitrate concentration was initially caused by a change in the groundwater flow regime in the capture areas of the Bartolovec and Varaždin wellfields due to the commissioning of two hydropower plants [21]. More recent studies show that this influence no longer exists and that the high nitrate concentration in the Varaždin wellfield is now a consequence of point and surface sources of pollution located in the immediate vicinity of the wellfield [18, 22]. Until the mid-1990s, the Varaždin wellfield was the largest source of water for human consumption in the observed area, and in order to meet the quality parameters, pumping capacity from the Bartolovec and Vinokovščak wellfield was increased [16]. Due to the constantly high nitrate concentration, the Varaždin wellfield was put out of service in 2004 and is now generally not integrated into the water supply system. Thus, a large groundwater source was lost, and it was necessary to invest large financial resources in increasing the pumping capacity of other wellfields to meet the local population needs. The water is drawn from two aquifer layers, and studies show that the water from the lower layer is of significantly better quality [23], which is why the lower aquifer is becoming increasingly important today. The vulnerability of the aquifer is high [17], so it is extremely important to protect the entire aquifer from anthropogenic pollution, because water from the upper layer is still used in the public water supply, but it is also used extensively in many private households and farms. Table 1 shows the arithmetic mean values of certain groundwater quality parameters in the period 1993-2017 at the Bartolovec, Varaždin and Vinokovščak wellfields. As can be seen, the values of the parameters are uniform at all locations, except for the nitrate concentration at the wellfield Varaždin, emphasizing the additional importance of monitoring this parameter.

Table 1. Arithmetic means of certain groundwater quality parameters in the period 1993-2017 [19]

Parameter	Varaždin 1*	Varaždin 2**	Bartolovec 1*	Bartolovec 2**	Vinokovščak
pH	7.40	7.43	7.40	7.48	7.36
$KMnO_4$ (mg/L O_2)	0.75	0.62	0.61	0.61	0.60
Ammonia (NH_4^+ mg/L)	0.008	0.000	0.007	0.007	0.011
Nitrates (NO_3 mg/L)	79.74	54.68	20.55	11.04	24.45
Chlorides (Cl mg/L)	19.21	13.96	22.94	8.56	13.83

* upper aquifer layer
** lower aquifer layer

3.4 Experimental Data

The groundwater in the Bartolovec wellfield is systematically monitored at four wells that draw water from the upper and five wells that draw water from the lower aquifer layer. Chemical analyzes are carried out by an authorized laboratory of the Varkom d.d. utility company. The analyzes carried out as part of this work refer to the period 1993-2023, and since two wells of the upper (B1 and B2 – marked in blue in Figure 1) and one well of the lower aquifer layer (B3 – marked in orange in Figure 1) were active during this period, a database of these locations was created. Sampling was carried out at least once a week when each well was in operation. In this way, more than 1000 data were collected for each well for each water quality parameter analyzed. The parameters pH, electrical conductivity, $KMnO_4$, chloride concentration and nitrate concentration were analyzed in the paper.

3.5 Methodology

Based on the experimental data collected during the period 1993-2023, databases were created for the following groundwater quality parameters: pH, electrical conductivity, $KMnO_4$, chloride concentration and nitrate concentration. The arithmetic mean values were calculated for each parameter in both

aquifers and the statistical significance of the differences was analysed using the t-test:

$$t = \frac{\bar{x}_1 - \bar{x}_2}{\sqrt{\frac{S_1^2}{n_1} + \frac{S_2^2}{n_2}}} \quad (1)$$

$\bar{x}_1$- mean of the first sample
$\bar{x}_2$- mean of the second sample
n_1 - first sample size
n_2 - second sample size
S_1^2 - sample 1 standard deviation
S_1^2 - sample 2 standard deviation

The null hypothesis H_0 (the difference is not statistically significant) and the alternative hypothesis H_1 (the difference is statistically significant) were set. The critical t value (t_α) was determined for a significance level of 5% and the number of degrees of freedom $df = n1 + n2 - 2$.

$$\begin{gathered} H_0: \bar{x}_1 = \bar{x}_2 \\ H_1: \bar{x}_1 \neq \bar{x}_2 \\ t < t_\alpha \Rightarrow H_0 \\ t > t_\alpha \Rightarrow H_1 \end{gathered} \quad (2)$$

In addition, a trend analysis was carried out and a correlation analysis was performed between the same parameters in different aquifer layers and between different parameters in the same aquifer layer. In this way, it was determined whether there is a correlation between the two aquifer layers and a correlation between the observed groundwater quality parameters also using a t test with the number of degrees of freedom: $df = n - 2$ and a significance level of 5%.

$$t = r\sqrt{\frac{df}{1 - r^2}}$$

$$\begin{gathered} H_0: \rho = 0 \\ H_1: \rho \neq 0 \\ t < t_\alpha \Rightarrow H_0 \\ t > t_\alpha \Rightarrow H_1 \end{gathered} \quad (3)$$

r – sample correlation coefficient
ρ – population correlation coefficient
n – sample size
df – degrees of freedom

4 Results and discussion

4.1 pH value

The permissible values according to the national regulation [24] for the pH value are within the interval 6.5-9.5. These values represent negative logarithms of the molar concentration of H+ ions. In both aquifers, the annual average values lie within the interval 7.15-7.71, and the correlation in both sets of data is very small, as shown by the values of the coefficients of determination R^2 (Figure 4a). The results of the individual measurements vary from 7 to 8 and practically do not go beyond this interval. For this reason, the standard deviation values are low. A statistically significant difference was found between the average pH values in the upper and lower layers (Table 2). Nevertheless, there is a correlation between the layers (Figure 5a), and the trend analysis shows that the trend is not present in the upper

layer, while there is a downward trend in the lower layer.

Table 2. pH trend and correlation analysis

Difference	**n**	**arithmetic mean**	**standard deviation**	**tα**	**t**	**H**
upper layer	30	7.37	0.096358	1.960	-4.2981	H1
lower layer	31	7.47	0.084772			
Trend	**n**	**df**	**t_α**	**r**	**t**	**H**
upper layer	30	28	2.045	0.200	1.080	H0
lower layer	31	29	2.042	0.401	2.357	H1
Correlation	**n**	**df**	**t_α**	**r**	**t**	**H**
	30	28	2.045	0.635	4.347	H1

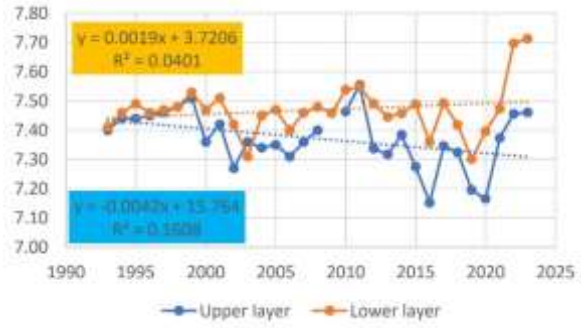

(a) pH

(b) electrical conductivity

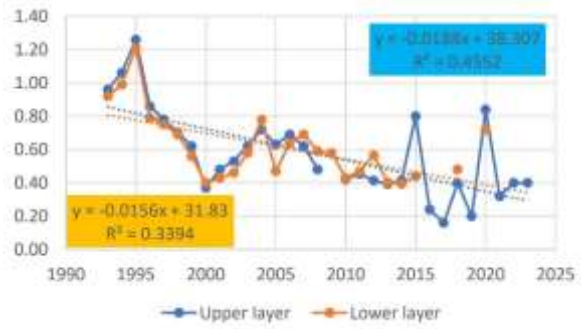

(c) $KMnO_4$

(d) chlorides

(e) nitrates

Figure 4. Time series and trend analysis of the observed parameters

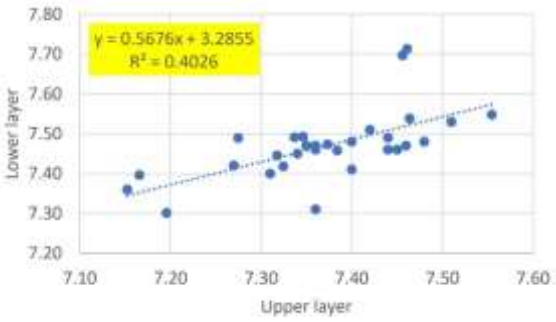

(a) pH

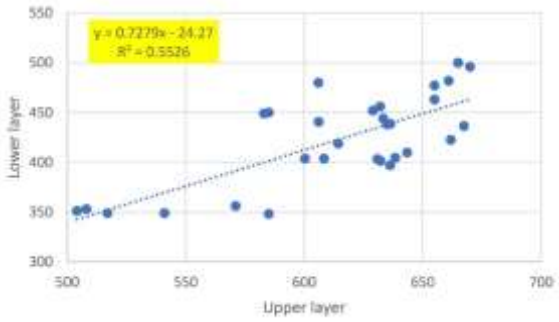

(b) electrical conductivity

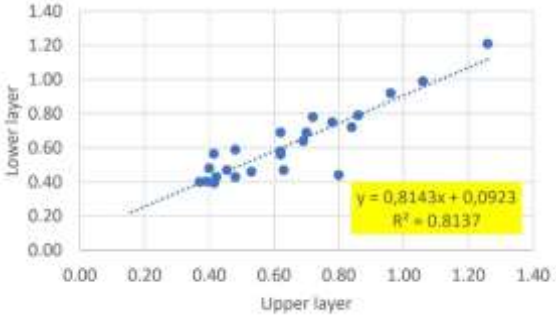

(c) $KMnO_4$

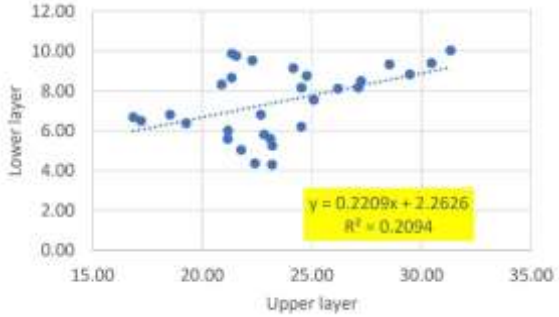

(d) chlorides

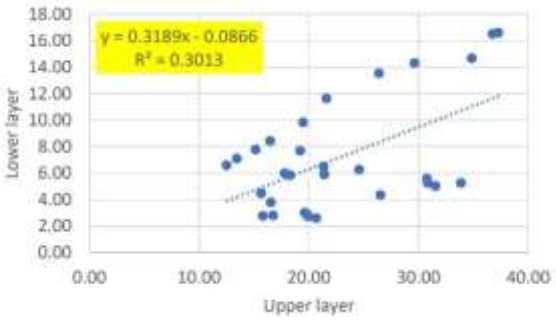

(e) nitrates

Figure 5. Correlation analysis of the observed parameters

4.2 Electrical conductivity

Electrical conductivity is the ability of water to conduct electricity. This ability depends on the presence of ions, their total concentration, the mobility and valence of the ions and the measurement temperature. The water temperature at which samples are taken to analyse water quality is specified as 25 °C. The annual average values of electrical conductivity in the upper aquifer are in the interval 504-670 µS/cm and in the lower aquifer in the interval 348-500 µS/cm and are below the MAC which is 2500 µS/cm [24] (Figure 4b). The results of the analysis show the statistical significance of the differences between the layers (Table 3). There is an upward trend in the upper aquifer layer, while there is no trend in the lower layer. Furthermore, correlations between the aquifer layers were found with the correlation coefficient of 0.7434 (Figure 5b).

Table 3. Electrical conductivity trend and correlation analysis

Difference	n	arithmetic mean (µS/cm)	standard deviation (µS/cm)	tα	t	H
upper layer	30	614	46.912	1.960	16.150	H1
lower layer	31	423	45.409			
Trend	**n**	**df**	**tα**	**r**	**t**	**H**
upper layer	30	28	2.045	0.512	3.153	H1
lower layer	31	29	2.042	0.148	0.806	H0
Correlation	**n**	**df**	**tα**	**r**	**t**	**H**
	30	28	2.045	0.743	5.879	H1

4.3 KMnO4

The annual average values of $KMnO_4$ in both aquifers are in the interval of 0.16-1.21 mgO_2/L and thus below the MAC of 3 mgO_2/L [24] (Figure 4c). Also, the values of the coefficients of determination indicate a moderate correlation in both sets of data. The statistical significance of the differences between the layers was not found, and the trend analysis shows a downward trend in both aquifers (Table 4). The correlation analysis shows a good connection between the layers, which is confirmed by the correlation coefficient value of 0.9020 (Figure 5c).

Table 4. $KMnO_4$ trend and correlation analysis

Difference	n	arithmetic mean (mgO2/L)	standard deviation (mgO2/L)	tα	t	H
upper layer	30	0.57	0.258	1.960	-0.800	H0
lower layer	25	0.62	0.206			
Trend	**n**	**df**	**tα**	**r**	**t**	**H**
upper layer	30	28	2.045	0.675	5.009	H1
lower layer	25	23	2.069	0.583	3.440	H1
Correlation	**n**	**df**	**tα**	**r**	**t**	**H**
	25	23	2.069	0.902	10.022	H1

4.4 Chlorides

The chloride concentration in the groundwater of the Bartolovec wellfield is far below the MAC value of MAC=250 mg Cl^-/L [24]. The influence of the semi-permeable layer dividing the aquifer (Figure 2) is most pronounced in this groundwater quality parameter. As can be seen from the time series of annual averages, the chloride concentration in the lower aquifer layer is lower during the entire observed period (Figure 4d). The values in the lower layer are between 4.30-10.03 mg Cl^-/L, while the values are higher in the upper layer and lie between 16.86-31.33 Cl^-/L. A statistically significant difference in the arithmetic means between the layers was confirmed (Table 5). There is no trend in the upper aquifer layer, while a downward trend was detected in the lower layer. The correlation analysis shows that there is no connection between the aquifer layers (Figure 5d).

Table 5. Chlorides trend and correlation analysis

Difference	n	arithmetic mean ($mgCl^-/L$)	standard deviation ($mgCl^-/L$)	tα	t	H
upper layer	30	23.47	3.600	1.960	21.879	H1
lower layer	31	7.52	1.756			
Trend	**n**	**df**	**tα**	**r**	**t**	**H**
upper layer	30	28	2.045	0.327	1.831	H0
lower layer	31	29	2.042	0.545	3.502	H1
Correlation	**n**	**df**	**tα**	**r**	**t**	**H**
	30	28	2.045	0.458	2.726	H1

4.5 Nitrates

The nitrate concentration at the Bartolovec wellfield fluctuates considerably over time but remains below the MAC of 50 mg/L $NO3^-$ throughout the entire period. The coefficient of determination R2 in

the lower layer shows a high correlation in the mentioned data set, while such correlation was absent in the upper layer, due to large oscillations of the values of the arithmetic means in that layer (Figure 4e). As with pH, electrical conductivity and chloride concentration, a statistically significant difference of arithmetic means between layers was determined (Table 6). As mentioned before, the difference is most likely due to the presence of the semi-permeable clay layer that divides the aquifer into two layers. The trend analysis shows that there is no trend in the upper aquifer layer, while there is a downward trend in the lower layer. The correlation analysis shows that there is no significant connection between the layers (Figure 5e).

Table 6. Nitrates trend and correlation analysis

Difference	**n**	**arithmetic mean mg/L ($NO3^-$)**	**standard deviation (mg/L NO_3^-)**	**tα**	**t**	**H**
upper layer	30	22.82	7.260	1.960	10.328	H1
lower layer	31	7.06	4.210			
Trend	**n**	**df**	**tα**	**r**	**t**	**H**
upper layer	30	28	2.045	0.052	0.276	H0
lower layer	31	29	2.042	0.805	7.308	H1
Correlation	**n**	**df**	**tα**	**r**	**t**	**H**
	30	28	2.045	0.549	3.475	H1

When analysing the time series of this parameter, it was found that the values in both aquifers change significantly over time, so that the values increase in one period and decrease in the other, indicating that the influences of sources affecting the concentration of this parameter are changing. It was also observed that the annual average curves coincide until 2003, i.e. when concentrations fall in one layer, they also fall in the other. After this year, this compliance ceases, which leads to the conclusion that in the period after this year, external sources of pollution no longer affect the upper and lower aquifer to the same extent. For this reason, the total period was divided into two sub-periods: the first up to 2003 and the second after this year. In the first sub-period, the nitrate concentrations decrease over time and the value of the arithmetic means between the layers are aligned. For this reason, a correlation analysis was carried out for the first sub-period where a correlation coefficient of 0.9853 was calculated (Figure 6a). In the second sub-period, the correlation between the two layers is significantly lower, which is confirmed by the correlation coefficient value of 0.2967 (Figure 6b). The results of this analysis confirm the above assumptions about the change in the influence of pollution sources contributing to the nitrate concentration in this wellfield.

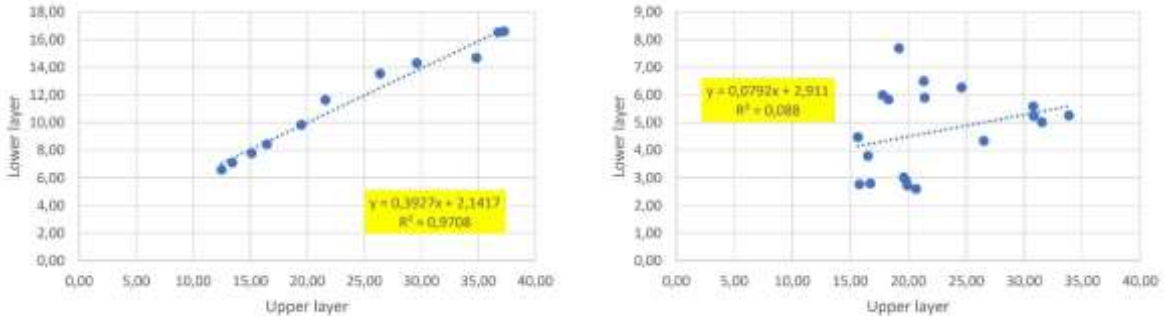

(a) Nitrates – first sub-period (1993-2003) (b) Nitrates – second sub-period (2004-2023)

Figure 6. Correlation analysis of the nitrates in sub-periods

4.6 Correlation analysis of different parameters in the same layer

The relationship between the values of different parameters from the same aquifer was analyzed to determine whether the same external factors simultaneously influence different groundwater quality parameters. First, the parameters from the upper layer were analyzed. The values of the correlation coefficients between the parameters in the upper aquifer layer are shown in Table 7. As can be seen,

certain parameters are more strongly correlated, while others are less strongly or not correlated at all. The highest correlation was observed between the chloride-nitrate concentrations, which has a high correlation coefficient value of 0.7741. There is also a certain correlation between the parameters $KMnO_4$-chloride, where the correlation coefficient is 0.5809. For other pairs, the absolute values of the correlation coefficients are below 0.5000 so it can be concluded that the correlation is insignificant.

Table 7. Correlation coefficient values in the upper aquifer layer

93 - 23	pH	Electrical conductivity	$KMnO_4$	Chlorides	Nitrates
pH	1				
Electrical conductivity	-0.4295	1			
$KMnO_4$	0.2295	-0.4956	1		
Chlorides	0.2488	-0.4517	0.5809	1	
Nitrates	-0.1422	-0.2544	0.3514	0.7741	1

The values of the correlation coefficient between the individual parameters in the lower aquifer layer are listed in Table 8. In this layer, a correlation was observed between the parameters $KMnO_4$-nitrates and between the parameters electrical conductivity-$KMnO_4$, where the correlation coefficients are 0.7233 and -0.6583, respectively. There was also a weak correlation between the parameters electrical conductivity-nitrates, while for other pairs values of the correlation coefficients were less than 0.5000.

Table 8. Correlation coefficient values in the lower aquifer layer

93 - 23	pH	Electrical conductivity	$KMnO_4$	Chlorides	Nitrates
pH	1				
Electrical conductivity	-0.0087	1			
$KMnO_4$	-0.1399	-0.6583	1		
Chlorides	-0.1334	-0.0978	0.3271	1	
Nitrates	-0.2162	-0.5641	0.7233	0.3965	1

5 Conclusion

The chemical composition of the groundwater of the Bartolovec wellfield complies with the criteria prescribed by the applicable national regulation [24] for all observed quality parameters during the entire observation period. The statistical analysis of the annual mean values showed that the values for almost all observed parameters (except for pH) are lower in the lower aquifer layer than in the upper layer. This difference is due to the influence of the clay layer, which divides the aquifer into two aquifer layers. This is particularly noticeable in the parameters of electrical conductivity, chloride and nitrate concentration. As a result, the quality of the water from the lower layer is higher than from the upper layer. The correlation analysis of the same parameters in the different layers revealed fluctuations in the relationship between the parameters, and relationships were observed for the parameters electrical conductivity, $KMnO_4$ and chlorides in the observed period. A correlation was also observed for the parameter nitrates in the first sub-period, while it was absent in the second sub-period. These results show that the aquifer layers, although separated by a semi-permeable clay layer, are hydraulically connected. The correlation analysis of different parameters in the same layer showed that some parameters are dependent, which could mean that they have the same sources. However, this assertion should be proven in further analyses. The trend analysis revealed trends in some parameters, highlighting a negative trend in nitrate concentration in the lower aquifer. However, no such trend was found in the upper aquifer layer. Given the long-standing problem of high nitrate concentration in the area of the town of Varaždin, changes in groundwater quality over time should definitely be monitored in the future. In conclusion, the analysis provides an insight into the changes in the chemical composition of the

groundwater of the Bartolovec wellfield in time. The results can serve as a basis for the search for solutions to maintain and improve the quality of the groundwater of the wellfield.

References:

[1] COUNCIL DIRECTIVE 98/83/EC of 3 November 1998 on the quality of water intended for human consumption.

[2] Plessis, A.D.: Water Resources from a Global Perspective. In South Africa's Water Predicament; Springer: Cham, Switzerland, 2023; pp. 1–25

[3] Dyvak, M.; Rot, A.; Pasichnyk, R.; Tymchyshyn, V.; Huliiev, N.; Maslyiak, Y.: Monitoring and Mathematical Modeling of Soil and Groundwater Contamination by Harmful Emissions of Nitrogen Dioxide from Motor Vehicles. Sustainability 2021, 13, 2768

[4] Kurwadkar, S.; Kanel, S.R.; Nakarmi, A.: Groundwater pollution: Occurrence, detection, and remediation of organic and inorganic pollutants. Water Environment Research, 2020, 92, 1659–1668.

[5] Zhao, X.; Wang, D.; Xu, H.; Ding, Z.; Shi, Y.; Lu, Z.; Cheng, Z.: Groundwater pollution risk assessment based on groundwater vulnerability and pollution load on an isolated island. Chemosphere 2022, 289, 133134.

[6] Kovač, I., Šrajbek, M., Kranjčević, L., Novotni-Horčička, N.: Nonlinear models of the dependence of nitrate concentrations on the pumping rate of a water supply system. Geosciences Journal, 24, 585–595 (2020). https://doi.org/10.1007/s12303-019-0045-4

[7] Das, B.; Pal, S.C.: Assessment of groundwater vulnerability to over-exploitation using MCDA, AHP, fuzzy logic and novel ensemble models: A case study of Goghat-I and II blocks of West Bengal, India. Environmental Earth Sciences, 2020, 79, 104.

[8] Umar, M.; Khan, S.N.; Arshad, A.; Aslam, R.A.; Khan, H.M.S.; Rashid, H.; Pham, Q.B.; Nasir, A.; Noor, R.; Khedher, K.M., Anh, D.T.: A modified approach to quantify aquifer vulnerability to pollution towards sustainable groundwater management in Irrigated Indus Basin. Environmental Science and Pollution Research, 2022, 29, 27257–27278.

[9] Barbieri, M., Barberio, M.D., Banzato, F., Billi, A., Boschetti, T., Franchini, S., Gori, F., Petitta, M.: Climate change and its effect on groundwater quality. Environmental Geochemistry and Health 45, 1133–1144 (2023). https://doi.org/10.1007/s10653-021-01140-5

[10] Li, J., Shi, Z., Wang, G., Liu, F.: Evaluating Spatiotemporal Variations of Groundwater Quality in Northeast Beijing by Self-Organizing Map. Water 2020, 12, 1382. https://doi.org/10.3390/w12051382

[11] Kovač, Z., Nakić, Z., Barešić, J., Parlov, J.: Nitrate origin in the Zagreb aquifer system, Geofluids, Volume 2018, Article ID 2789691, 15 p, 2018.

[12] Masoud, M., El Osta, M., Alqarawy, A., Elsayed, S., Gad, M.: Evaluation of groundwater quality for agricultural under different conditions using water quality indices, partial least squares regression models, and GIS approaches. Applied Water Science, 12, 244 (2022). https://doi.org/10.1007/s13201-022-01770-9

[13] Wendland, F., Bergmann, S., Eisele, M., Gömann, H., Herrmann, F., Kreins, P., Kunkel, R.: Model-Based Analysis of Nitrate Concentration in the Leachate-The North Rhine-Westfalia Case Study, Germany. Water 2019, 12, 550.

[14] Šrajbek, M., Kovač, I., Novotni-Horčička, N., Kranjčević, L.: Assessment of average contributions of point and diffuse pollution sources to nitrate concentration in groundwater by nonlinear regression, Environmental Engineering and Management Journal, 19 (1), 95-104, 2020.

[15] Nemčić-Jurec, J., Mesić, M., Bašić, F., Kisić, I., Zgorelec, Ž.: Nitrate concentration in drinking water from wells at three different locations in northwest Croatia, Cereal Research Communications 35, 845-848, 2007.

[16] Novotni-Horčička, N., Šrajbek, M., Kovač, I.: Nitrates in the Varaždin Regional Waterworks (Croatian title: Nitrati u Regionalnom vodovodu Varaždin). Voda i javna vodoopskrba Baška, Hrvatski zavod za javno zdravstvo, 123–131, 2010.

[17] Larva, O.; Brkić, Ž.; Marković, T. Vulnerability and Risk of Contamination of the Varaždin Aquifer System, NW Croatia. Sustainability 2023, 15, 16502.

https://doi.org/10.3390/su152316502
[18] Šrajbek, M.; Kranjčević, L.; Kovač, I.; Biondić, R. Groundwater Nitrate Pollution Sources Assessment for Contaminated Wellfield. Water 2022, 14, 255. https://doi.org/10.3390/w14020255
[19] Šrajbek, M. Nitrate pollution propagation in groundwater and wellfield impact assessment: doctoral dissertation, PhD thesis, University of Rijeka, Faculty of Engineering, 188 p, 2021.
[20] Urumović, K.; Prelogović, E.; Hlevnjak, B.; Mayer, D. Hydrogeological relations of the Varaždin aquifer (Croatian title: Hidrogeološki odnosi varaždinskog vodonosnika). Geološki Vjesnik 1990, 43, 149–158
[21] Grđan, D., Durman, P. and Kovačev-Marinčić, B.: The relationship between regime changes and groundwater quality at the Varaždin and Bartolovec pumping stations (Croatian title: Odnos promjene režima i kvalitete podzemnih voda na crpilištima Varaždin i Bartolovec), Geološki vjesnik 44, 301–308, 1991.
[22] Kovač, I.; Šrajbek, M.; Klišanin, N.; Gilja, G.: Analysis of the Distance between the Measured and Assumed Location of a Point Source of Pollution in Groundwater as a Function of the Variance of the Estimation Error. Hydrology 2023, 10, 199. https://doi.org/10.3390/hydrology10100199
[23] Kovač, I., Kovačev-Marinčić, B., Novotni-Horčička, N., Mesec, J., Vugrinec, J.: Comparative analysis of nitrate concentration in the upper and lower layers of the Varaždin aquifer (Croatian title: Komparativna analiza koncentracije nitrata u gornjem i donjem sloju Varaždinskog vodonosnika), Radovi Zavoda za znanstveni rad Varaždin, 28, 41-57, 2013.
[24] Official Gazette: Rulebook on compliance parameters, methods of analysis, monitoring and water safety plans for human consumption and the way of keeping the register of legal entities that perform the activity of public water supply, Official Gazette NN 125/2017, 20 15.12.2017., Zagreb, 2017.

BALANCING WATER FLOWS IN THE RYE ISLAND FOR THE PURPOSE OF SUPPLYING WATER TO IRRIGATION PUMPING STATIONS

MICHAELA ČERVEŇANSKÁ [1], JAKUB MYDLA [1], ANDREJ ŠOLTÉSZ [1], DANA BAROKOVÁ [1],

[1] *Slovak University of Technology in Bratislava, Faculty of Civil Engineering, Department of Hydraulic Engineering, Slovakia, michaela.cervenanska@stuba.sk, andrej.soltesz@stuba.sk, dana.barokova@stuba.sk*

1 Abstract

The paper documents the identification, quantification and optimal use of potential water sources for irrigation purposes on the Rye Island, Slovakia. The proposal of the division (balancing) of water flows by means of the existing damming and dividing structures was drawn up, ensuring sufficient distribution of water to the pumping stations located in the immediate vicinity of the main skeleton of the drainage channel system. To achieve this goal, several field measurements were conducted simultaneously with the study of the project documentation and archive studies conducted in the past.

Keywords: Rye Island, channel system, drainage channels, balancing of water flows, pumping stations, irrigation, WEF nexus

2 Introduction

The world is currently facing a challenge of securing water, energy, and food for all. The demand for freshwater, agricultural products and energy is rising. Inequalities in the distribution and access to water, energy and food are exacerbated by the impacts of climate change. Agriculture is the largest consumer of the world's freshwater resources, and more than one-quarter of the energy used globally is expended on food production and supply [1]. The water security is, according to the Food and Agriculture Organisation of the United Nations (FAO), linked to the energy and food security, meaning that the actions in any one particular area often can have effects in one or both of the other areas. The interaction between water, energy, and food as the water-energy-food (WEF) nexus has drawn much attention recently to solve upcoming uncertainty in food security. The largest nexus studies among 27 European countries have been conducted in Spain, Italy and Portugal. Most of the nexus studies were focused on the water sector. There is a large number of nexus studies in water-stressed countries (because the WEF nexus is identified as a solution to manage water supply and water demand spanning water, energy, and agricultural sectors) while there are few studies on water-abundant countries (e.g. Slovakia and Luxembourg) [2].

The Rye Island, Slovakia is an important agricultural area and an important source of quality drinking water in Slovakia. Considering the WEF nexus and consequences of climate change, by implementing appropriately chosen measures, optimal and sustainable conditions for water management can be created, thereby strengthening the competitiveness of agriculture, ensuring food security and reducing the risks resulting from ongoing climate change.

The Rye Island channel system, with its damming and dividing structures and pumping stations, can now be considered as multi-purpose. While in the past it was built for the purpose of draining waterlogged soils, especially in the wet spring season and during floods, nowadays an equally important purpose is related to irrigation, which is directly imposed in the warmest region of Slovakia with the longest growing season and the richest water resources, both surface and underground; and to regulating the water level regime, such as the necessary distribution of water between drainage areas. It is self-evident that the channel system, with its capacity, represents an important source of irrigation water, which can be regulated in time and space on the entire territory of the Rye Island.

There are numerous studies, which are taking place in the Rye Island, for example [3], [4], [5] and [6]. Some studies take place in the East Slovak Lowland, for example [7] and [8], which channel system is similar to the one in the Rye Island. However, these days, there aren't many studies dealing with the water level regime or possibilities for their improvement in these channel systems.

3 Methods

3.1 The area of interest

The Rye Island is located in the Podunajska lowland, in the southwestern part of Slovakia. The channel network of the Rye Island consists of seven main partially interconnected channels (Figure 1): the Gabčíkovo-Topoľníky channel, the Chotárny channel, the Čalovo-Holiare-Kosihy channel, the Aszód-Čergov channel, the Čergov-Komárno channel, the Dudváh channel and the Komárňanský channel. The area drained using the constructed channel network has 1252 km^2. The total length of the channel network is almost 1000 km; thus, its density is approximately 1 km/1,25 km^2.

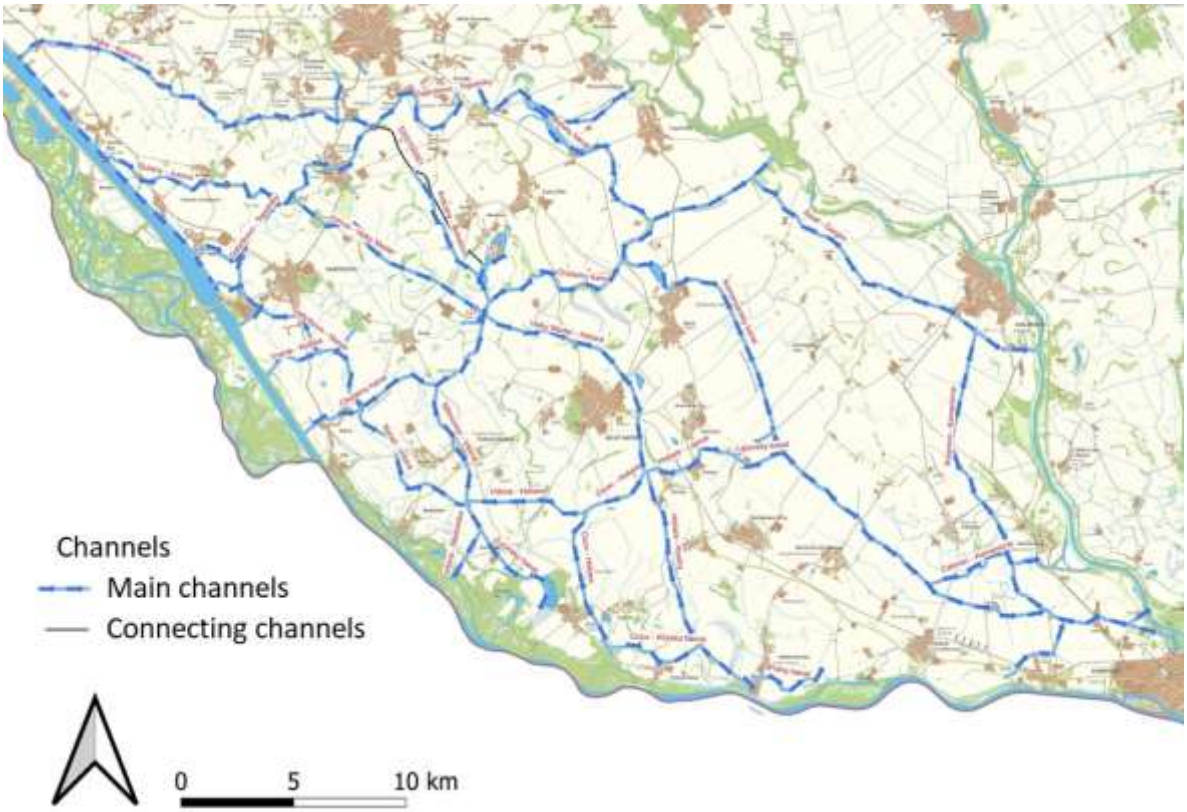

Figure 1. The main skeleton of the drainage channel system on the Rye Island, Slovakia, with the directions of surface water flow from the source (the seepage channel and the supply channel of the WS Gabčíkovo) to the southernmost area (Komárno)

3.2 Sources of water for the Rye Island channel system

The hydrological regime of the Rye Island is strongly affected by the construction of the Gabčíkovo water structure and the seepage channel of the Hrušovská reservoir. The left-side seepage channel was designed for the steady state of seepage waters from the Hrušovská reservoir for a capacity of 20 m^3. s^{-1}. Currently, it is the most important source of filtered surface water through the dams of the Hrušovská reservoir (with groundwater quality), which is available for water distribution in the channel system of the Rye Island. After construction of the Gabčíkovo water structure (WS), the decrease of the groundwater level in the adjacent area of the River Danube was observed. The groundwater regime, as well as the water level regime in drainage channels, changed. To improve and to control the groundwater

regime in the floodplain area, a water supply structure situated on the left side of the seepage channel was constructed. This structure allows an artificial water supply into the channel system and consequently into the groundwater.
Based on the previous statements, there are 3 main water sources for the Rye Island channel system:

- **inflow from the supply channel** of the Gabčíkovo water structure **to the Gabčíkovo-Topoľníky channel (S VII)** through a small hydropower plant with two turbines with a capacity of 4.0 $m^3.s^{-1}$ of each turbine. This represents the value of 8.0 $m.s^{-1}$ according to the most recent valid 'Temporary handling order of the set of water works Gabčíkovo – Nagymaros' [9];
- **inflow from the left-side seepage channel** of the Gabčíkovo water structure **to the channels Vojka-Kračany (A VII), Šuľany-Jurová (B VII) and Baka-Gabčíkovo (C VII)**, and subsequently to the Gabčíkovo-Topoľníky channel (S VII);
- **by draining the groundwater**.

The inflow into the A VII channel is through a culvert with two openings with a maximum capacity of 6.0 $m^3.s^{-1}$. The inflow into the B VII channel is through an inlet object with a sluice gate with a maximum capacity of 6.0 $m^3.s^{-1}$ as well. The third in order, the C VII channel is subsidized through an inlet object with a maximum capacity of 1.9 $m^3.s^{-1}$.
When we look at the amount of water that can be supplied into the channel system on the Rye Island along the supply channel of the WS Gabčíkovo, it can be concluded that it is potentially a value of over 20 $m^3.s^{-1}$. However, there are certain limitations that prevent water managers (or farmers) from working towards this value.
The first limiting condition for withdrawals from the left-side seepage channel is the water level and flow regime in it. Since the start of operation of the Gabčíkovo hydropower plant, this has been determined by the amount of water that seeps through the protective dam of the Hrušovská reservoir. This seepage is dependent on the colmatation of the bottom of the Hrušovská reservoir, which can cause a decrease in the value of the seepage quantity, which will cause a decrease in the water level in the seepage channel and thus also a decrease in the amount of water actually taken into the drainage channels connected to the left-side seepage channel.

3.3 Study of the project documentation and field measurements

Another very important characteristic is the capacity of each channel. This was determined from the available project documentation [10]. The goal was not to determine the exact value of this characteristic, what was important at this stage of the solution was the fact whether the given channel is able to transfer the designed quantity. It should be noted that project documentation was not available for all channels of the main skeleton of the drainage system. That is why an additional reconnaissance of the individual objects of the channel system of the lower Rye Island was carried out.
According to the project documentation, the capacity of the S VII channel is approximately between 10.8 and 17.5 $m^3.s^{-1}$, which allows it to easily transfer the inflow from the supply channel of the WS Gabčíkovo.
The most significant limitation is the capacity of the channels AVII, BVII and CVII, which, due to their dimensions and longitudinal slope, are not able to transfer the aforementioned amounts of water. This was proven both by our measurements [11] and also by [12].
Considering what was written up to now, the most reliable source of water for supplying the drainage system of the Rye Island is the inflow of water from the supply channel to the main channel S VII. The limitation that can occur (and already occurred in the year 2023) is a technological limitation, i.e. reconstruction (or repair) of a turbine in the small hydropower plant. Because of this, the inflow to the S VII channel was reduced to 4.0 $m^3.s^{-1}$.
The field measurements, using the GNSS receiver Leica VIVA GS15 and controller Leica VIVA CS15, were carried out in order to determine the water level and flow regime, cross sections and the longitudinal profiles of the drainage channels and the flow velocities (used to determine the discharge) in the upper part of the area of interest that provides water supply to the Rye Island, i.e. the secondary drainage channels A VII, B VII and C VII; as well as the main drainage channel S VII. The locations of field measurements (small red dots) are shown in Figure 2.

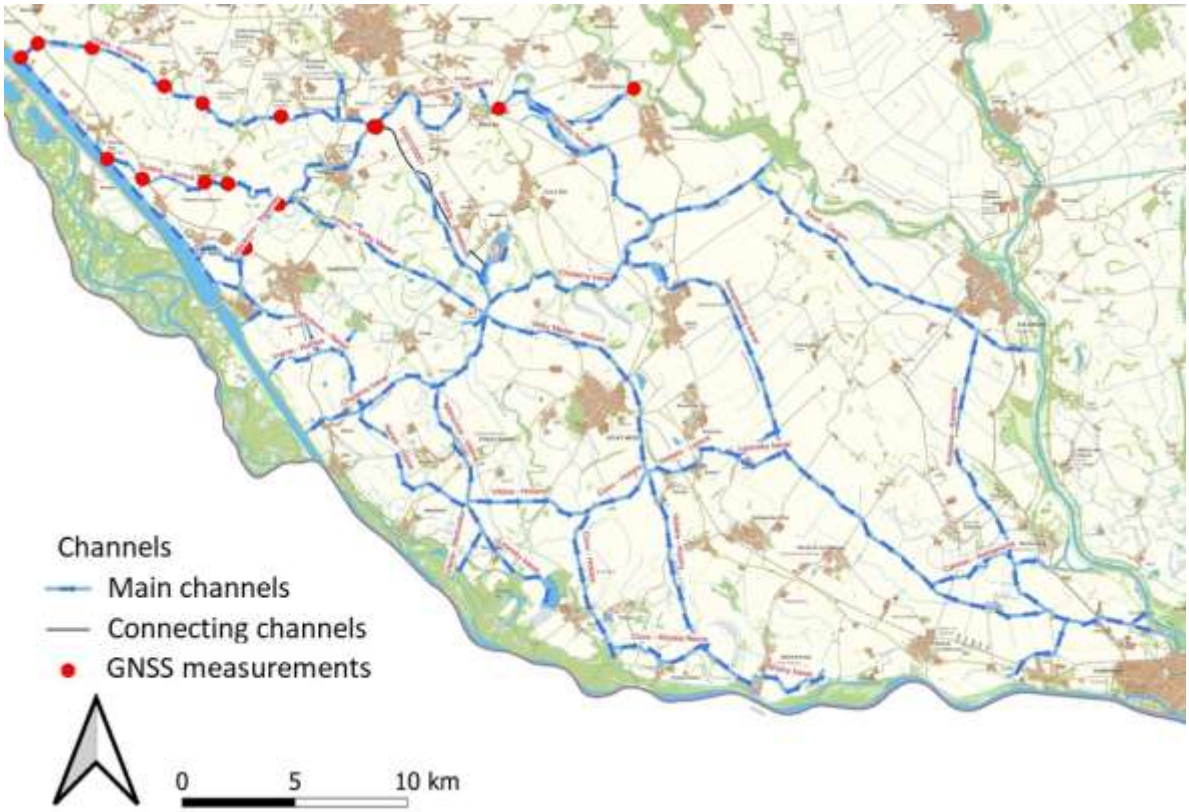

Figure 2. The location of field measurements

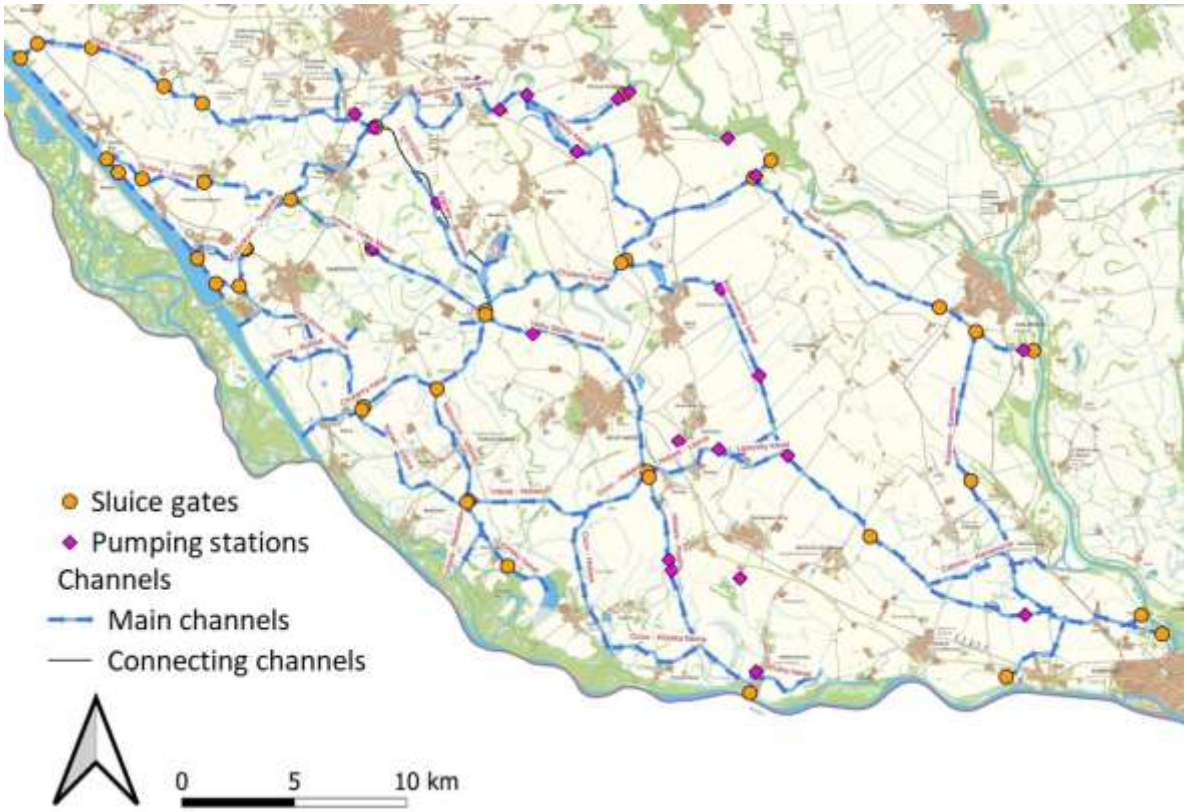

Figure 3. The main skeleton of the drainage channel system on the Rye Island, Slovakia, with the damming and dividing structures and irrigation pumping stations

3.4 Damming and dividing structures on the Rye Island channel system and irrigation pumping stations

The next part of the research was the localization and parameterization of individual objects on the drainage system of the Rye Island. This task carried out in a close cooperation with the Slovak Water Management Enterprise, state enterprise (SWME). Our effort paid off and we were able to create a catalogue of every damming and dividing structure with its parameters (width, height of structures, height of the concrete threshold of the structure above sea level, or barrier height). This is an integral part for the future model of the operation and manipulation with the structures of the drainage system. The location of each structure is shown in Figure 3 (red dots).

Figure 3 also shows the location of existing functional irrigation pumping stations with their maximum capacity, represented by green marks. Data has been provided from the GIS database of the Hydromelioration, state enterprise. The total capacity of all functional pumping stations is 7.07 $m^3.s^{-1}$. However, the total capacity of the irrigation pumping stations that can be supplied with water from the drainage channel system is approximately 5.63 $m^3.s^{-1}$.

4 Results and discussion

Considering everything that was written above, we drawn up our first proposal (in a graphic form) for the redistribution of water flows in the individual branches of the drainage system in order to achieve a sufficient amount of water (flow rate, level) for the irrigation pumping stations, which are located in the immediate vicinity of the main framework of the drainage system of Rye Island.

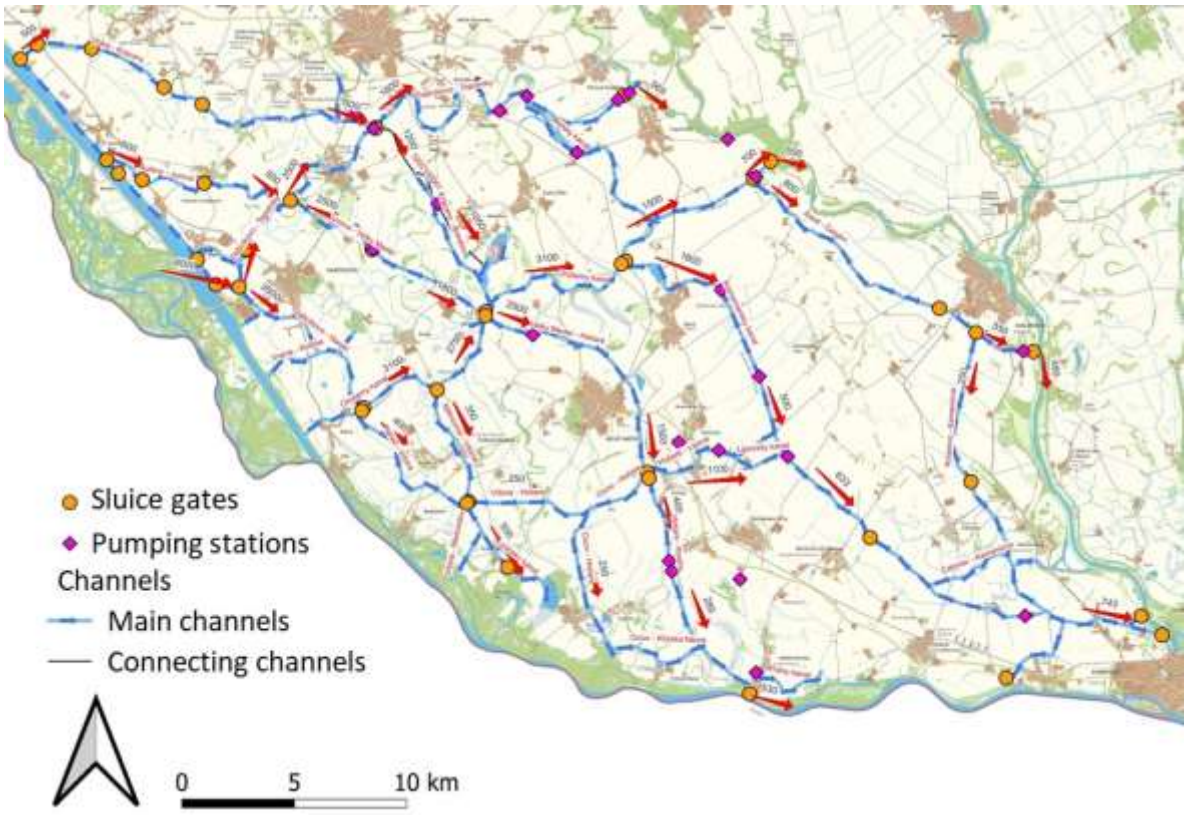

Figure 4. Distribution of water flows in the main skeleton of the Rye Island drainage channel system assuming the total inflow of 9.0 $m^3.s^{-1}$

The first proposal assumes a total inflow to the drainage system of 9.0 $m^3.s^{-1}$, consisting of an inflow of 8.0 $m^3.s^{-1}$ into the main channel SVII through two turbines of the small hydropower plant from the supply channel of the WS Gabčíkovo; an inflow of 500 $l.s^{-1}$ from the seepage channel into the AVII channel, and the same inflow into the BVII channel. These values are based on our actual measured

flows in these channels during the vegetation period (the inflow into channel CVII is so small that we did not consider it). We redistributed this subsidy flow through the damming and dividing structures to the entire drainage system of the Rye Island, taking the required amount of water for irrigation pumping stations into account. This proposal, which we call balance, is shown on Figure 4.
It is obvious from the Figure 4, that the drainage channel system is able to ensure the drainage of any area and at the same time transfer water for irrigation purposes to any place of the system. This fact was already claimed by experts in the past.
Due to the undergoing reconstruction of one of the turbines, the second scenario (Figure 5) was created with significantly reduced amounts of inflow from the seepage and supply channel to the drainage system of the Rye Island. We assumed a water inflow into the channels AVII and BVII with a value of 200 $l.s^{-1}$ for each and an inflow of 4.0 $m^3.s^{-1}$ into the main channel SVII. This scenario is all the more relevant because the operator of the small hydropower plant assumes the shutdown of the turbine for a period of 15 to 18 months and then prepares for the reconstruction of the second turbine, which means a scenario that will last approximately 2.5 to 3 years.

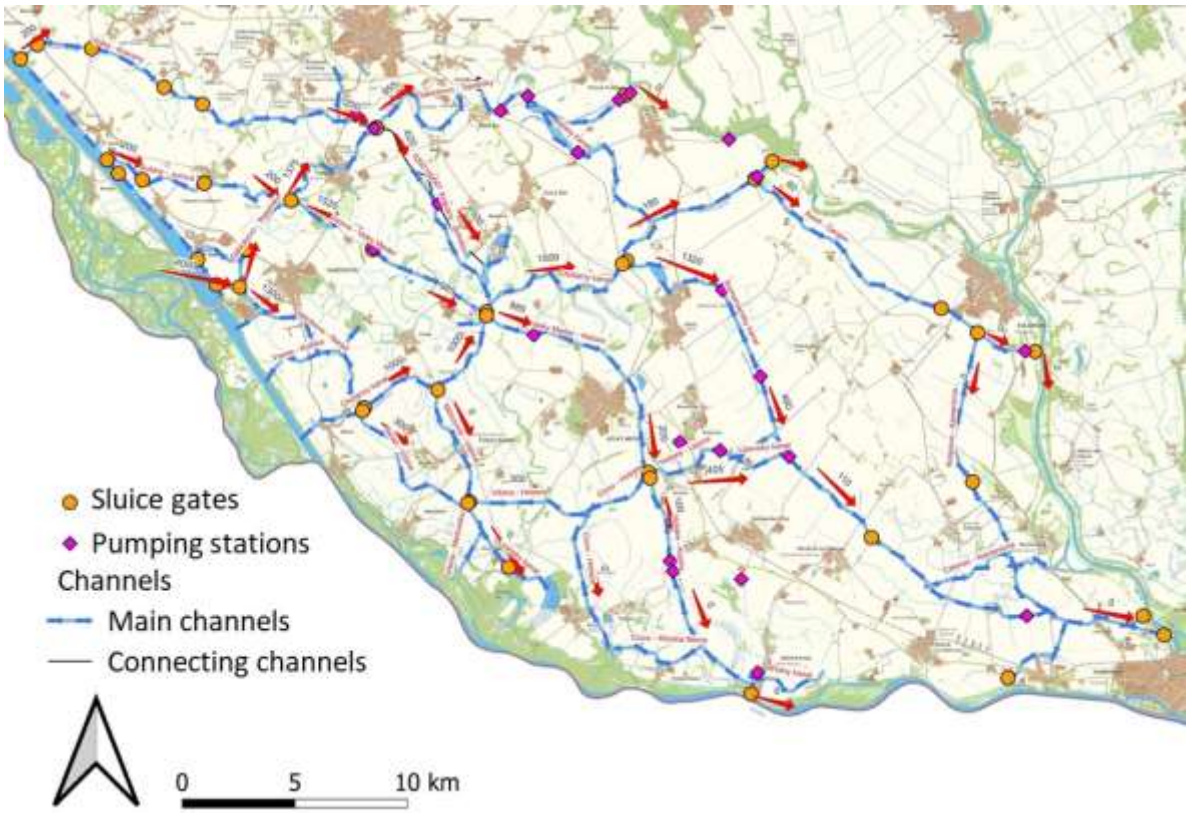

Figure 5. Distribution of water flows in the main skeleton of the Rye Island drainage channel system assuming the total inflow of 4.4 $m^3.s^{-1}$

The second scenario covers approximately 75% of the water need for irrigation from the drainage system on the Rye Island. The basic assumption we used when creating the scenarios is to cover the water requirements of all irrigation stations at once, which will definitely not happen. This gives us hope that despite the reduced inflow into the channel system, it is still possible to transfer the water in required quantity to all irrigation pumping stations.
However, the fact is that in the GIS database contains only irrigation pumping stations that are firmly built and are registered. From field inspections and from our cooperation with the SWME, we found out that several agricultural cooperatives (farms) have permission for irrigation water by pumping it directly from the channel system. This is a form of water extraction that was not taken into account in our study at all. It is possible that such withdrawals will not affect the level and flow regime in the channel system (their capacity ranges from 8.0 – 15.0 $l.s^{-1}$). Moreover, they cannot be used anywhere, because they need

a sufficient depth of water in the channel for the correct function of the pumping system.

5 Conclusion

The Rye Island, Slovakia, is an important agricultural area and an important source of quality drinking water in Slovakia. Considering the WEF nexus and consequences of climate change, by implementing appropriately chosen measures, optimal and sustainable conditions for water management can be created, thereby strengthening the competitiveness of agriculture, ensuring food security and reducing the risks resulting from ongoing climate change.

The Rye Island channel system was built for the purpose of draining waterlogged soils, especially in the wet spring season and during floods. Nowadays an equally important purpose is related to irrigation in the dry growing season and to regulating the water level regime, such as the necessary distribution of water between drainage areas, making it a multi-purpose system.

The paper documents the identification, quantification and optimal use of potential water sources for irrigation purposes, along with their distribution in the necessary quantity through the existing drainage channel system to the irrigation pumping stations. The main result of our work is a proposal for the division (balancing) of water flows by means of the existing damming and dividing structures on the main skeleton of the drainage system of the Rye Island, ensuring sufficient distribution of water to the pumping stations located in the immediate vicinity of the main skeleton of the drainage channel system. The proposals were drawn up for two scenarios – for the inflow of 9.0 m^3-s^{-1} (Figure 4) and 4.4 $m^3.s^{-1}$ (Figure 5) into the channel system through the main channel Gabčíkovo-Topoľníky (S VII) and two secondary channels Vojka-Kračany (A VII) and Šuľany-Jurová (B VII).

The first proposal (Figure 4) assumes an inflow of 8.0 $m^3.s^{-1}$ into the main channel SVII through two turbines of the small hydropower plant from the supply channel of the WS Gabčíkovo and an inflow of 500 $l.s^{-1}$ from the seepage channel into the AVII channel and the BVII channel.

The second scenario assumes a reduced inflow of 4.0 $m^3.s^{-1}$ into the main channel SVII due to the undergoing reconstruction of one of two turbines of the small hydropower plant, and an inflow into the channels AVII and BVII with a value of 200 $l.s^{-1}$ for each and. This is the scenario for the next approximately 2.5 to 3 years.

The results show that with suitable measures, the drainage channel system is able to ensure the drainage of any area and at the same time transfer water in required quantity for irrigation purposes to any place of the system. The second scenario covers approximately 75% of the water need for irrigation from the drainage system on the Rye Island with the assumption of all irrigation stations pumping at once, which is not likely to happen.

It is self-evident that this balance distribution needs to be verified by hydraulic calculation of the entire drainage system using a modern numerical model, where it is possible to determine the necessary amounts of water based on the actual morphological conditions of the channel system (sediment contamination, overgrowth and the associated roughness of the riverbeds, longitudinal profiles of channels) and manipulation on the damming and dividing structures.

Acknowledgements

Funded by the EU NextGenerationEU through the Recovery and Resilience Plan for Slovakia under the project No. 09I03-03-V04-00274.

The paper was developed within framework and based on the financial support of the VEGA project No. 1/0161/24 Research utilization an artificial intelligence methods in the management of multipurpose water-management systems.

References:

[1] FAO: The Water-Energy-Food Nexus. A new approach in support of food security and sustainable agriculture, Rome: Food and Agriculture Organization of the United Nations, 28 p., 2014.

[2] Rezaei Kalvani, S., Celico, F.: The Water–Energy–Food Nexus in European Countries: A Review

and Future Perspectives, Sustainability, 15, 4960, https://doi.org/10.3390/su15064960, 2023.
[3] Schügerl, R., Velísková, Y., Dulovičová, R., Sočuvka, V.: Influence of submerged vegetation on the Manning's roughness coefficient for the Gabčíkovo-Topoľníky channel, Acta Hydrologica Slovaka, 22, 1, pp. 61-69, https://doi.org/10.31577/ahs-2021-0022.01.0007, 2021.
[4] Dulovičová, R., Schügerl, R., Velísková, Y.: Hydraulic conductivity of saturated bed silts in Chotárny channel, ŽO area, Slovakia, Acta Hydrologica Slovaka, 23, 2, pp. 180-1189, https://doi.org/10.31577/ahs-2022-0023.02.0020, 2022.
[5] Schügerl, R., Velísková, Y., Dulovičová, R, Sočuvka, V.: Determination and comparison of hydraulic conductivity values of bed silts along Chotárny channel using grain size analysis, Acta Hydrologica Slovaka, 21, 2, pp. 139-144, https://doi.org/10.31577/ahs-2020-0021.02.0017, 2020.
[6] Dulovičová, R., Schügerl, R., Velísková, Y.: Actual values of saturated hydraulic conductivity of channel bed silts and its distribution along Komárňanský channel, Acta Hydrologica Slovaka, 21, 1, pp. 61-69, https://doi.org/10.31577/ahs-2020-0021.01.0012, 2021.
[7] Pavelková, D., Kandra, B., Tall, A., Hlavatá, H., Gomboš, M.: Comparison of meteorological drought over two normal periods, Acta Hydrologica Slovaka, 24, 2, pp. 221-231, https://doi.org/10.31577/ahs-2023-0024.02.0025, 2023.
[8] Kandra, B., Tall, A., Gomboš, M., Pavelková, D.: Quantification of Evapotranspiration by Calculations and Measurements Using a Lysimeter, Water, 15, 2, pp, https://doi.org/10.31577/ahs-2023-0024.02.0025, 2023.
[9] Water Management Construction, state enterprise: Temporary handling order of the set of water structures Gabčíkovo – Nagymaros on the territory of the Slovak Republic (Update XII, January 2023) (in Slovak), 131 p., 2023.
[10] Vongrej, J.: The use of drainage systems for irrigation in connection with the construction of water structures on the Danube (in Slovak), Administration of Water Management Development in Bratislava, 98 p., 1966.
[11] Šoltész, A., Červeňanská, M., Mydla, J.: INTERREG CENTRAL EUROPE: DEEPWATER-CE. Final report on cooperation on activities implementation of the project, Faculty of Civil Engineering, Slovak University of Technology in Bratislava, 29 p., 2021.
[12] Sikora, A., Slota, R.: Research of discharge and water level regime in left-hand side branch system of the Danube by method of physical modelling, Bratislava: Water Research Institute, 42 p., 1992.

WATER SCARCITY MANAGEMENT IN SLOVAKIA – CURRENT STATE

IVANA BAJKOVIĆOVÁ [1], STANISLAV KELČÍK [2]
[1] Water Research Institute, Slovakia, ivana.bajkovicova@vuvh.sk
[2] Water Research Institute, Slovakia, stanislav.kelcik@vuvh.sk

1 Abstract

As a result of climate change and less even distribution of precipitation over time, water scarcity management is becoming increasingly important, even in countries that did not encounter such issues in the past.
The poster gives an overview of water scarcity management in Slovakia - current legislation and strategic documents, available databases, methodological approaches, as well as the identified gaps, challenges and possibilities.

Keywords: water scarcity, water resources management, climate change, water allocation, prevention

2 Introduction

Increased frequency and severity of droughts is being discussed more frequently, both globally and in national contexts. This is one of the key adverse impacts of climate change on water availability - uneven distribution of rainfall and changes in the hydrological regime of rivers (manifested in particular by more extreme flows and changes in seasonality), and decline in groundwater reserves.
From the water management point of view, the objectives of which are sustainable use and protection of water resources, arises the issue of satisfying human water needs - or water scarcity management. Water scarcity is a situation in period of drought, in which not all human water demands are met.

Drought and water scarcity management related activities, in terms of response timing, can be divided into "before - during - after" the drought. In this sense we are talking about monitoring, risk analysis, mitigation, preparedness, early warning, operational responses, post analysis and lessons learned.
Remaining aware of the above-mentioned context, in the following work we will focus less on monitoring, early warning and operational response processes, and more on strategic drought policy, water scarcity prevention, planning, long-term goals of reducing exposure and vulnerability, and acquiring water resilience of the country.

3 Methods

3.1 Identifying key elements of drought policy planning and drought management

3.1.1 Bodies, institutions

In Slovakia, the Ministry of Environment is competent for water. However, if we also take into account water use, the issue of drought and water scarcity is multisectoral (Ministry of Agriculture and Rural Development, Ministry of Economy, Ministry of Interior). Moreover, water scarcity involves not only economic issues, but also social issues, in period of drinking water scarcity (Ministry of Health).

Among the sectoral institutions, we can name in particular those listed in

Table 4.

Table 4. Institutions in the field of water scarcity management

	Name	Mission	Ref.
1	Slovak Hydrometeorological Institute (HMI)	hydrological and meteorological services at the national and international level, data collection and processing	[1]
2	Slovak Water Management Enterprise, s.e.	management of watercourses and material investment assets built on it	[2]
3	Water Research Institute (WRI)	research base for water sector, advisory services for water management and water planning	[3]
4	State Geological Institute of Dionýz Štúr (SGI DS)	geological research and exploration, information system on geological works results, including hydrogeology	[4]
5	Vodohospodárska výstavba, s. e.	construction and operation of water structures	[5]
6	Slovak Environmental Agency (SEA)	information and communication on climate change adaptation at local and regional levels	[6]

Within the academic sector, the Slovak Academy of Sciences and universities in Slovakia also contribute to water scarcity management - mostly through specialized research, contribution to methodological documents and education of experts.

3.1.2 Legislation

Drought policy in European Union (EU) - water legislation:

- The Water Framework Directive (WFD), Directive 2000/60/EC of the European Parliament and of the Council of 23 October 2000 establishing a framework for Community action in the field of water policy) [7]
- The EU Green Deal (Climate change policy, Climate law) [8]

European legislation is fully transposed into Slovak legislation, also in the field of drought and water scarcity.

Drought policy in Slovak - water legislation:

- The Water Act, Act No. 364/2004 Coll. on water and on amendments to the Act of the National Council of the Slovak Republic No. 372/1990 Coll. on offences, as amended [9]
- Act No 305/2018 Coll. on protected areas of natural water accumulation and on amending and supplementing other acts,
- and other subordinate legislation.

3.1.3 Strategic documents

Drought policy and strategic documents in EU:

- EU Strategy on adaptation to climate change – action plans
- Integrated Drought Management Programme (IDMP), National Drought Management Policy Guidelines in Central and Eastern Europe (CEE) [10]
- Common Implementation Strategy (CIS) Guidance 24 on river basin management in a changing climate (update finalization in 2024) [11]

Drought and water scarcity policy in Slovakia:

- Master Plan of Protection and Rational Use of Water, 2002 [12]
- Action plan to address the consequences of drought and water scarcity – H_2Odnota je voda (The

Value is Water), 2018 [13]

- Adaptation Strategy of the Slovak Republic to Climate Change, 2018 [14], plus Action Plan for Adaptation
- Water Policy Concept until 2030 with a prospective to 2050 (2022) [15]

  The Water Policy Concept sets objectives and actions, among others, in areas:
  - 3. Sustainable water use: Sustainable and efficient use of surface and underground waters without endangering their quantity and quality (Goal 3.1.), Functional crisis management in times of drought and water shortages (Goal 3.2.)
  - 4. Water for all residents: Ensuring the supply of health-safe drinking water for all residents (Goal 4.1.)

  Related milestone in the Concept: 1.7. Legislative proposal to establish prioritization of individual users' demands for water abstraction and use (regulation of water abstraction and use in case of water scarcity and/or drought) (objectives 3.1., 3.2.)
- The Water Plan of the Slovak Republic (Danube River Basin Management Plan, Vistula River Basin Management Plan, Plan for the development of public water supply systems for the territory of the Slovak Republic) – Update 2021 [16]

  The plan ensures the goal consistency with the Water Policy Concept. The measures are linked to the documents Action plan to address the consequences of drought and water scarcity and Adaptation Strategy of the Slovak Republic to Climate Change.

  In the river basin management planes 2021 the "Negative impacts of climate change (drought, water scarcity and other impacts)" are recognized as a significant water management issue.

In Slovakia, the issues of available water resources and the coverage of human water needs were treated as a comprehensive water management issue most recently in the document • Master Plan of Protection and Rational Use of Water, 2002 [12]. In the following years, river basin management plans were developed in the spirit of the WFD, which places greater emphasis on maintaining or restoring good water status.

The needs and trends in water use appeared in the strategic documents partially, among other sectors, or on a too general level. While water protection belongs to the environmental sector, the water use has mainly an economic and water supply also a social character, which makes this issue cross-cutting.

Since 2020, in the scope of river basin management plans, Slovakia has ranked drought and water scarcity among the Significant Water Management Issues related to climate change. The most typical consequence of climate change is a less even distribution of precipitation over time, i.e. greater extremes and shifts of seasons during the year. This encourages not only to better understanding of the trends related to drought, but also to develop a proper water scarcity management.

3.1.4 Information base

The national drought monitoring in Slovakia collects historical, real-time and periodic data on meteorological, hydrological and agricultural drought. Data analyses using indicators for meteorological drought (Standardized Precipitation Evapotranspiration Index – SPEI), hydrological drought (Relative monthly discharge, M-day discharge, Groundwater level) and agricultural drought (Soil drought intensity) enable HMI to provide timely information for use in operational drought management and respond to drought events effectively. Agricultural drought information system "Intersucho" (with Czech Republic and Central Europe) gives an information on current state of drought, 10 days soil saturation prediction and long-term predictions (2 months, 6 months). [1]

For long-term drought and water scarcity management (planning, preparedness and resilience), an understanding of water quantity and regime, and also the impact of climate change, is needed.

As a result of the data analyses on natural water regime plus human water use, for each past year, the following documents are prepared in HMI [1]:

- Water balance of surface water quantity,

- Water balance of ground water quantity.

In addition, the Prospective surface water quantity balance is updated annually (in WRI), also using prospective water use data, to determine the rate of water security for the needs of particular types of users. [3]

Numerous methodologies, reports, research and other documents have been developed in professional institutions to address specific topics in the areas of drought, water security and water resources protection.

3.2 Gaps and issues, potentials

Although the drought issue belongs to the Ministry of Environment sector, the issue is strongly multi-sectoral. There is a need for a central authority to coordinate the drought and water scarcity management, in an effort to increase the resilience of the country. No drought committee (or other competent authority responsible for drought management) is established in Slovakia in present.

A framework on drought in natural disaster, water, agriculture, climate change, biodiversity and forestry strategic documents is set at a general level, and it is not properly linked.
There is potential to align some approaches in drought management with the EU settings (structured to: 1 - Monitoring and early warning, 2 - Risk and impact assessment, 3 - Risk mitigation, preparedness and response). Moreover, a regular planning needs to be introduced as part of long-term development towards water resilience.

There is no drought management plan developed in Slovakia, to set up the drought emergency response measures across the country.
The water resource management in the river basin management plans is oriented mostly on the measures to achieve good ecological status of water bodies, but not to the water use possibilities and water scarcity resilience.
There is no updated Master plan of sites protected for surface water retention and storage. There is no dedicated structured register of structures with water retention capacities in Slovakia.

The issue of water allocation is not addressed at any level. There is no prioritisation in the water use established in legislation. The existing register of water permits is not properly structured and is not accessible to all the relevant parties. The permitting process, which is done at the local level (municipalities), is methodologically inconsistent and data on its results are not properly managed.
A progress was made on the e-flow issue by developing a methodology for determining ecological flows. However, the use is yet to be implemented. A relevant regulation (decree) is awaited, and it is also necessary to legislate the position of e-flow in the water use prioritization.

The information base is not consolidated. There is no sectoral water information system.

4 Results and discussion

The given facts show the need and importance of inter-sectoral cooperation. There is a need for a central authority to address drought and water scarcity, which links and coordinates responsibility and cooperation across the vulnerable sectors.

Operational management of drought and water scarcity needs to be regulated through a drought management plan, which will include development of monitoring and early warning, assessment of drought risk and impact, as well as measures for risk mitigation, preparedness and response.

In the scope of the water resilience planning and long-term development, preventative measures can be

a part of river basin management plans. In addition to understanding natural hydrological conditions and trends related to climate change, it is necessary to have comprehensive data on water use and also its prediction, related to the development of particular sectors. After quantifying the water demands, the best solutions to provide the water can be designed. In geographical areas identified as deficient or vulnerable, it is necessary to plan specific solutions and allocate funds for it. A space (land) must be reserved for future surface water retention and storage.

The topic of water scarcity and water allocation is to be completely developed. For the proper decision-making, it is necessary to establish water use priorities in legislation. In water permits issuing, a systematic methodologically uniform approach is essential. There is a need to develop a water balance based methodology for permitting abstractions, emissions, and other interventions in the quantity and regime of surface water and groundwater. The data on permits, issued at district level, should be included into a structured register accessible to all involved parties, and use for further water management analyses.

The information base should be systematically upgraded and supplemented with more information on natural conditions, trends in climate change, water use, water demand, development projections, risk assessment, etc. A sectoral water information system is also essential for the proper flow of data, assessments, activity instructions and communication.

5 Conclusion

Although extreme alerting events of drought and water scarcity have not been identified in Slovakia in recent years, trends resulting from climate change point to the need for preparedness. It is essential to avoid a crisis-oriented drought policy with reactive measures of restrictions and drought impacts treatment.
The above analyzes show the need and importance of inter-sectoral cooperation (with a central authority established) to address drought and water scarcity. Paralell to regulation of operational crisis management through a drought management plan, the water resilience planning and long-term development preventative measures are to be included to river basin management plans. It is necessary to quantify water needs and possibilities of their coverage in the best possible way, to establish priorities in water use. A systematic, methodologically uniform approach and a good information system are essential in water allocation. In geographical areas identified as deficient or vulnerable, it is necessary to plan specific solutions and allocate funds for it.
In Slovakia, there is still time to learn and build a systematic drought policy, based on knowledge, prevention and strengthening the long-term water resilience - also in accordance with the principles elaborated in this paper.

References:
[1] Slovak Hydrometeorological Institute, https://www.shmu.sk/en/?page=1
[2] Slovak Watermanagement enterprise, s.e., https://www.svp.sk/sk/uvodna-stranka/
[3] Water Research Institute , https://www.vuvh.sk/en/about-us/basic-information/
[4] State Geological Institute of Dionýz Štúr, https://www.geology.sk/about-us/?lang=en
[5] Vodohospodárska výstavba, https://www.vvb.sk/en/o-nas/
[6] Slovak Environmental Agency, https://www.sazp.sk/zivotne-prostredie/environmentalna-informatika
[7] Directive 2000/60/EC of the European Parliament and of the Council of 23 October 2000 establishing a framework for Community action in the field of water policy, https://eur-lex.europa.eu/legal-content/EN/TXT/?uri=celex%3A32000L0060
[8] EU Green Deal – Climate change policy, https://commission.europa.eu/strategy-and-policy/priorities-2019-2024/european-green-deal/climate-action-and-green-deal_en#documents
[9] Water Act, Act No. 364/2004 Coll. on water and on amendments to the Act of the National

Council of the Slovak Republic No. 372/1990 Coll. on offences, as amended, https://www.slov-lex.sk/pravne-predpisy/SK/ZZ/2004/364/vyhlasene_znenie.html
[10] Global Water Partnership Central and Eastern Europe (2015): Guidelines for the preparation of Drought Management Plans. Development and implementation in the context of the EU Water Framework Directive, Global Water Partnership Central and Eastern Europe, 48pp, https://www.droughtmanagement.info/literature/GWPCEE_Guidelines_Preparation_Drought_Management_Plans_2015.pdf
[11] CIS Guidance 24 on river basin management in a changing climate, https://circabc.europa.eu/sd/a/a88369ef-df4d-43b1-8c8c-306ac7c2d6e1/Guidance%20document%20n%2024%20-%20River%20Basin%20Management%20in%20a%20Changing%20Climate_FINAL.pdf, 1.6.2024
[12] Ministry of Environment of Slovak Republic: Master Plan of Protection and Rational Use of Water, Bratislava, 2002. https://hsr.rokovania.sk/3250/14-/?pg=2
[13] Ministry of Environment of Slovak Republic: Action plan to address the consequences of drought and water scarcity – H_2Odnota je voda (The Value is Water), Bratislava, 2018. https://www.minzp.sk/files/sekcia-vod/hodnota-je-voda/h2odnota-je-voda-akcny-plan-riesenie-dosledkov-sucha-nedostatku-vody.pdf
[14] Ministry of Environment of Slovak Republic: Adaptation Strategy of the Slovak Republic to Climate Change, Bratislava, 2018. https://www.enviroportal.sk/dokument/strategia-adaptacie-sr-na-zmenu-klimy
[15] Ministry of Environment of Slovak Republic: Water Policy Concept until 2030 with a prospective to 2050, SAŽP, 2022. https://www.minzp.sk/voda/koncepcne-dokumenty/koncepcia-vodnej-politiky-roky-2021-2030-vyhladom-do-roku-2050.html , 2022
[16] Ministry of Environment of Slovak Republic: The Water Plan of the Slovak Republic– update 2021, Bratislava, 2022. https://www.minzp.sk/voda/vodny-plan-slovenska/

A PRECIPITATION TREND INVESTIGATION RESEARCH OF HUMENNE, SLOVAKIA

YUNUS ZİYA KAYA [1], MARTİNA ZELENAKOVA [2]

[1] *Civil Engineering Department, Hydraulics Division, Osmaniye Korkut Ata University, Turkey, yzkoku@outlook.com*

[2] *Department of Environmental Engineering, Faculty of Civil Engineering, Technical University of Kosice, Slovakia, martina.zelenakova@tuke.sk*

1 Abstract

Precipitation is one of the main parameters of the hydrological cycle, and fluctuations in the precipitation amount of the regions directly affect the water management plans of the related catchments. Due to global climate change, these fluctuations and extreme weather conditions are increasing. The negative impacts of the changes on the precipitation amounts must be eliminated. To do this, It is essential to analyze the variations of the precipitation over past years for a specific region. In this study, the authors investigated the trend dependences of Humenne, Slovakia, using a relatively new method, namely the Innovative Şen Trend test. Precipitation trends of the mentioned region were investigated on a monthly, seasonal, and annual basis by applying the Innovative Şen Trend test, Mann-Kendall test, and Linear Regression Line approaches. When the traditional trend investigation methods are generally based on the acceptance or rejection of the null hypothesis, the Innovative Şen Trend method is based on the distribution of the time series. The innovative Şen Trend Test approach is a graphical trend investigation method that gives users the opportunity to evaluate the trends based on their own experiences. The nonparametric Mann-Kendall test was applied to the data set within the 95 percent confidence interval. While any trends were not detected by using the traditional Mann-Kendall method within the given confidence interval, various monthly, seasonal, and annual trends were determined by using the Innovative Şen Trend test. The Innovative Şen Trend test was evaluated based on the three classifications. Those classifications were selected as low, medium, and high classes. This identification helps researchers to understand the extreme conditions for the calculated time scale.

Keywords: Precipitation, Trend, Mann-Kendall, Innovative Şen Test, Climatological Fluctuations

2 Introduction

Precipitation pattern changes in regions have great impacts on the area's water supply. Due to global climate change, precipitation frequencies are changing. Some parts of the world are facing a serious shortage of water because of the changes in precipitation, and some parts are facing extreme rainfalls. Changing conditions force the authorities to better understand the fluctuations of the weather parameters. Recently, in terms of climatological parameters, many studies have been done using trend investigation approaches. Mann-Kendall's (MK) approach is one of the most popular approaches for trend detection of time series. [1], performed a trend investigation study for the Hilly region of Bangladesh. They applied the Mann-Kendall test to the historical data set. They found a decreasing trend for annual evaluation, but they indicated that the trend was not significant. [2], conducted rainfall and temperature trend research for a highly vulnerable area to climate change. They selected the MK test for trend investigation, and they used Sen's slope estimator for the significance level of the trends. [3], performed a study for a research area that is vulnerable to floods. They investigated the rainfall characteristics of the region by utilizing MK and modified MK tests. They did the analysis for 40 years period from 1971 to 2010. They found some increasing and decreasing trends in monthly evaluations.

In the literature, trend investigations of the climatological parameters are not limited to the application of traditional methods. The Innovative Şen Trend investigation method was also tested for various regions. [4], used the modified MK test and Innovative Şen Trend method to analyze the monthly

maximum temperature of a station located in Oxford. He selected a long-term data set that started in 1854. He detected significantly increasing trends for January, March, May, July, August, September, October, November, and December. [5], took attention to the increasing drought risk for some parts of the world based on climate change, and they performed a trend research study by using the most popular MK test and newly developed Innovative Şen Trend method for a river basin located in Turkey. They did their research for nine-gauge stations. They concluded that when, in some cases, the MK test can not detect any trends, the Innovative Şen trend test was able to detect some rising or decreasing trends. [6], preferred to use the MK test and the Innovative Şen Trend test for analyzing streamflow trends of the Tigris River. As a result of their study, they underlined that the MK test and the Innovative approach generally have similar trend directions. More studies about the application of the Innovative approach for trend detection can be found in [7-11].

In this study, the precipitation trends of the Humenne, Slovakia was investigated based on the traditional MK test and the Innovative Şen Trend approach. The objective of this study is examining the precipitation fluctuations of the mentioned region on a monthly, seasonal and annual basis.

3 Methodology

The Innovative Şen Trend, MK, and Linear regression slope methods were used to detect the precipitation trends of the Humenne station. The Innovative Şen trend test is a graphical-based trend investigation approach developed by [12]. This approach is basically about the distribution of the time series on the x and y axis of a two-dimensional graph. A developed version of the approach, which is preferred in this paper, can be found in Dabanlı, 2017 PhD thesis [13]. This developed version of the Innovative Şen Trend test aims to add negative and positive lines to the distribution of data. These reference lines help users to identify trends with percentages. The users should make a decision about the distribution of the data within the reference lines. Mann-Kendall test is one of the most popular trend investigation approaches. It is a non-parametric test that allows users to work in a chosen confidence interval. The decision for the trend generally is given based on the probability values. According to the probability value, the null hypothesis can be accepted or rejected. The null hypothesis typically defines the cases that have no trends. Further information about the theory of the MK test can be found in [14]. The Linear Regression approach was used by evaluating each time step's regression line slope. These values were considered for the determination of the magnitude of the slope and the general directions of the distribution of the data.

Table 1. Statistics belonging to the precipitation data set (1972-2021)

Precipitation (mm)	**Min**	**Max**	**Mean**	**Standard Deviation**	**Skewness**
January	4.3	110	36.49	21.94	1.34
February	1.6	104	35.134	19.56	0.94
March	1.6	98.8	36.91	21.22	0.75
April	12.2	122.8	52.38	25.14	0.47
May	24.4	254.5	79.598	39.70	1.84
June	9.4	206.1	89.536	38.92	0.67
July	5.2	210.3	102.348	56.07	0.41
August	7.5	195.4	78.494	39.49	0.50
September	6.8	214.9	69.114	38.62	1.46
October	3.1	296.5	58.248	49.07	2.44
November	0.4	105.9	48.572	24.42	0.38
December	3.8	121.4	45	26.64	0.79
Winter	17.2	78.1	38.9	13.22	0.71

Spring	29.20	117.77	56.30	16.84	1.11
Summer	40.8	143.5	90.1	23.36	-0.09
Fall	21.5	129.0	58.6	20.55	0.85
Annual (avg)	46.48	93.67	60.99	8.36	1.15

The annual average value given in Table 1 is the average of 12 months' records. The minimum and maximum values of the annual averages of annual (avg) are the minimum values of yearly averages. December, January, and February were considered as winter, March, April, and May as Spring, June, July, August as Summer, and September, October, and November as Fall season. The monthly, seasonal, annual minimum, maximum, mean, standard deviation, and skewness coefficient stats of the precipitation data are shared in Table 1. The location of the study area is marked in Figure 1. Figure 1 was created by using Google Earth.

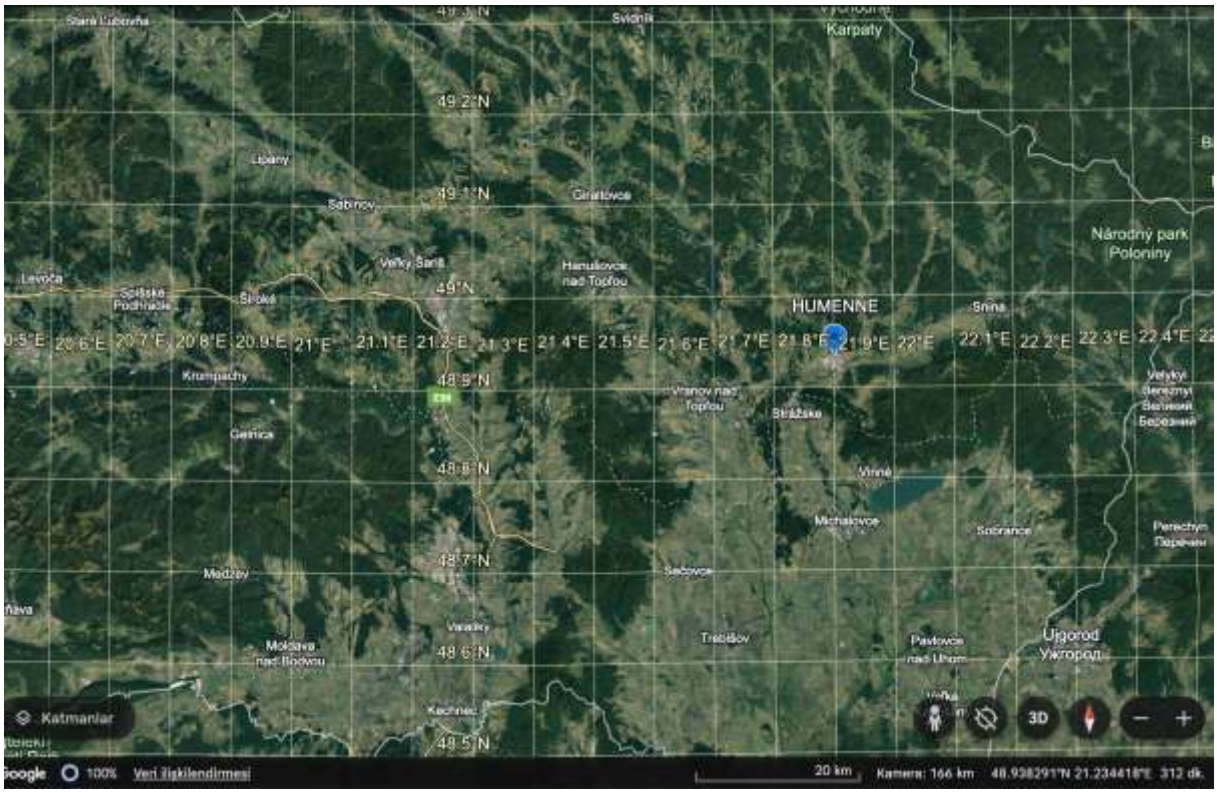

Figure 1. The location of the study area

The Humenne town is a part of the Presov region of eastern Slovakia. Its total area is 28.63 $km^{2,}$ with an average elevation of 155 m. The population of the town in 2021 was 30,925. From a hydrological standpoint, the region of Humenne falls within the basin of the Badrog River. The Laborec River flows through the settled area of the town, which is equipped with a safety barrage that serves to safeguard the area from floods. Water accumulation is typical during the months of December through February, with the highest levels of discharge occurring in March and the lowest in September. The average annual discharge of the Laborec River in Humenne is approximately 10 m^3 per second [15]. The data set is provided by the Slovak Hydro-Meteorological Institute. The data set originally contained monthly records, and it is based on the hydrological years (October to September). The data set started in the 1971-1972 hydrological year and ended in the 2022-2023 hydrological year.

4 Results

The MK test was applied to the data set within the 95 percent confidence interval, and the alpha value was chosen as 0.05. For the given confidence interval, no significant trends were detected for the MK approach. The calculations of the MK tests are shared in Table 2.

Table 2. Mann-Kendall test results

Hydrologic Time Scale	Alpha	MK Stat.	Critical Z Value	Z Stat.	Trend
January	0.05	165.00	+1.96 -1.96	1.37	-
February		196.00		1.63	-
March		-43.00		-0.35	-
April		-86.00		-0.71	-
May		43.00		0.35	-
June		-192.00		-1.60	-
July		-3.00		-0.02	-
August		100.00		0.83	-
September		-83.00		-0.69	-
October		155.00		1.29	-
November		20.00		0.16	-
December		25.00		0.20	-
Annual		-23.00		-0.18	-

When Table 2 is examined, it will be seen that any Z stats calculated based on the MK stat are not higher or lower than critical Z values. This is why any significant trends can not be mentioned for the confidence interval. Even if it is not statistically significant, numerically, the highest value was calculated for February, which tends to be the rising direction. The numerically lowest Z stat was calculated for June.

Table 3. The Innovative Şen Trend Results

Time Scale	Classification	Trend	Approximate Percentage	Linear Regression Line's Slope
January	Low	Increase	7,00%	0,27
	Medium	Decrease	4,00%	
	High	Increase	>10	
February	Low	Increase	6,00%	0,32
	Medium	-	-	
	High	Increase	>10%	
March	Low	Decrease	1,00%	-0,09
	Medium	Decrease	4,00%	
	High	Increase	1,00%	
April	Low	Decrease	4,00%	-0,15
	Medium	Decrease	8,00%	
	High	Decrease	>10%	
May	Low	-	-	0,34
	Medium	Increase	7,00%	
	High	Increase	>10%	

June	Low	Decrease	9,00%	-0,86
	Medium	Decrease	9,00%	
	High	Decrease	>10%	
July	Low	Decrease	6,00%	0,06
	Medium	Increase	>10%	
	High	Increase	>10%	
August	Low	Decrease	5,00%	0,44
	Medium	Increase	7,00%	
	High	Increase	>10%	
September	Low	-	-	-0,23
	Medium	Decrease	9,00%	
	High	Increase	>10%	
October	Low	Increase	4,00%	0,14
	Medium	Decrease	3,00%	
	High	Decrease	>10%	
November	Low	Decrease	4,00%	-0,03
	Medium	Increase	8,00%	
	High	Decrease	9,00%	
December	Low	-	-	-0,01
	Medium	Decrease	1,00%	
	High	Decrease	>10%	
Winter	Low	Increase	7,00%	0,19
	Medium	Decrease	5,00%	
	High	Decrease	10,00%	
Spring	Low	Decrease	4,00%	0,03
	Medium	Increase	5,00%	
	High	Increase	>10%	
Summer	Low	Increase	1,00%	-0,12
	Medium	Increase	4,00%	
	High	Increase	7,00%	
Fall	Low	-	-	-0,04
	Medium	Decrease	3,00%	
	High	Decrease	>10%	
Annual	Low	Decrease	1,00%	0,02
	Medium	Increase	3,00%	
	High	Increase	>10%	

Table 3 is created based on the outputs of the each time step graphical evaluation. As can be seen from Table 3, the Innovative Şen Trend test detected both increasing and decreasing trends for almost every class and time step. Using this type of classification is advantageous for seeing the extremme values on the graph. However, It is not possible to share every graph of the Innovative Şen Trend analysis created for this study. Table 3 was created to summarize the results. It should be kept in mind that the Innovative Şen Trend analysis lets users include their experiences in the evaluation. In this study, the minimum and maximum values of each graph were selected based on the min. and max. records of the related time steps. So, the initial conditions of each graph are not exactly the same as it is expected. An additional

Linear Regression Slope Line was added to the table to make it easier to analyze outputs.

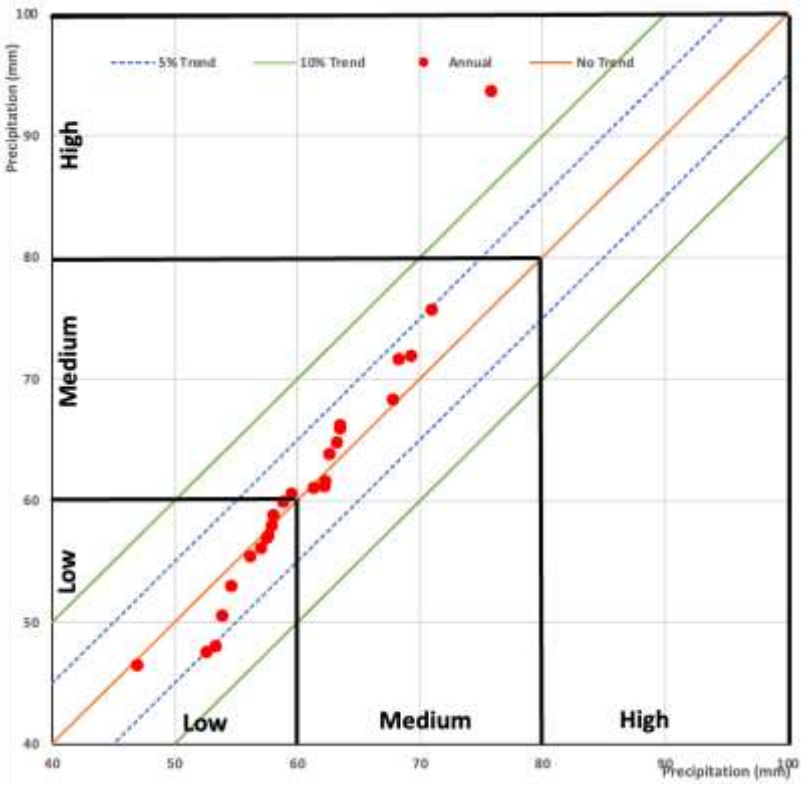

Figure 2. Innovative Şen Trend Test Annual Evaluation

The annual graph belonging to the Innovative Şen Trend approach is given in Figure 2. Figure 2 was created based on the inclusion of minimum and maximum parameters, as it was done for all the other months and seasons. Figure 2 is shared to give an example of the Innovative Şen Tend test. As given in Figure 2, statistically significant trends were not detected on an annual scale in the low-class and medium-class for annual averages. However, an increasing trend higher than 10 percent was detected in the high class. When checking the slope of the regression line of the annual scale, It is going to be seen that there is not a significant slope value when in the Innovative Şen trend test in high class, there is a statistically significant trend. The reason for this has two stages; first of all, in the Innovative Şen trend test, each class was evaluated separately. Secondly, in the high class, there are probably just a few extreme data that cause the highly increasing trends. The monthly, and seasonal graphs of the Innovative Şen Trend test were drawn and evaluated separately. The results of each time scale are given in Table 3.

5 Conclusion

In this study, precipitation fluctuations of the Humenne, Slovakia, were investigated by using conventional and unconventional methods. As conventional methods, Mann-Kendall and Linear Regression line slope was selected. As an unconventional and relatively new approach, the Innovative Şen Trend test was applied to the data set. All three mentioned methods were applied to 50 years of historical data. The Mann-Kendall test did not detect statistically significant trends in any of the monthly, seasonal, or annual time steps for precipitation.

The Innovative Şen Trend test detected some significant increasing and decreasing trends for given time periods. In the high class of Annual, Spring, and Summer steps, increasing trends of more than 10

percent were seen. These outputs are important because they may call attention to extreme records that occurred recently. This can also be researched in terms of floods because there may be some extreme records, and they tend to be increasing. Similarly, decreasing trends in low classes of June, July, and August can be explicated as a sign of precipitation shortage in the summer times.

Acknowledgment
The Mann-Kendall test analysis for this paper was generated using the Real Statistics Resource Pack software (Release 8.9.1). Copyright (2013 – 2023) Charles Zaiontz. www.real-statistics.com.

References
[1] Mondal, K. K., Akhter, M. A., & Mallik, M. A. K. (2020). Temporal trend analysis of historical climatic data at northeastern hilly region of Bangladesh using Mann-Kendall test. *Journal of Engineering Science*, *11*(2), 19-25.
[2] Asgher, S., Ahmad, M., Kumar, N., & Kumari, M. (2021). Trend analysis of temperature and rainfall using Mann Kendall test and Sen's slope estimator in Bhaderwah Tehsil of Doda District. Res. J. Agric. Sci, 12, 1021-1026.
[3] Mondal, A., Kundu, S., & Mukhopadhyay, A. (2012). Rainfall trend analysis by Mann-Kendall test: A case study of north-eastern part of Cuttack district, Orissa. International Journal of Geology, Earth and Environmental Sciences, 2(1), 70-78.
[4] Alashan, S. (2020). Combination of modified Mann-Kendall method and Şen innovative trend analysis. Engineering Reports, 2(3), e12131.
[5] Tosunoglu, F., & Kisi, O. (2017). Trend analysis of maximum hydrologic drought variables using Mann–Kendall and Şen's innovative trend method. River Research and Applications, 33(4), 597-610.
[6] Gumus, V., Avsaroglu, Y., & Simsek, O. (2022). Streamflow trends in the Tigris river basin using Mann− Kendall and innovative trend analysis methods. Journal of Earth System Science, 131(1), 34.
[7] Ali, R., Kuriqi, A., Abubaker, S., & Kisi, O. (2019). Long-term trends and seasonality detection of the observed flow in Yangtze River using Mann-Kendall and Sen's innovative trend method. Water, 11(9), 1855.
[8] Wang, Y., Xu, Y., Tabari, H., Wang, J., Wang, Q., Song, S., & Hu, Z. (2020). Innovative trend analysis of annual and seasonal rainfall in the Yangtze River Delta, eastern China. Atmospheric Research, 231, 104673.
[9] Şen, Z. (2017). Innovative trend significance test and applications. Theoretical and applied climatology, 127, 939-947.
[10] Kisi, O., & Ay, M. (2014). Comparison of Mann–Kendall and innovative trend method for water quality parameters of the Kizilirmak River, Turkey. Journal of Hydrology, 513, 362-375.
[11] Dabanlı, İ., Şen, Z., Yeleğen, M. Ö., Şişman, E., Selek, B., & Güçlü, Y. S. (2016). Trend assessment by the innovative-Şen method. Water resources management, 30, 5193-5203.
[12] Şen Z (2012) Innovative Trend Analysis Methodology. J Hydrol Eng 17:1042–1046. https://doi.org/10.1061/(asce)he.1943-5584.0000556
[13] Dabanlı İ (2017) Türkiye'de İklim Değişikliğinin Yağış-Sıcaklığa Etkisi ve Kuraklık Analizi: Akarçay Örneği. İstanbul Teknik Üniversitesi, PhD Thesis.
[14] Mann HB (1945) Nonparametric Tests Against Trend. Econometrica 13:245. https://doi.org/10.2307/1907187
[15] Url: https://www.humenne.sk/English-version/, Access date: 08/03/2024

WATER ECONOMY PLANNING ON THE RIVER TRESKA BASIN BY SIMULATION MODEL

STEVCHO MITOVSKI[1] , FROSINA PANOVSKA GEORGIEVSKA[2] , LJUPCHO PETKOVSKI[3] SONJA GEORGIEVA[4]

[1] *Associate professor, Ss. Cyril and Methodius University in Skopje, Faculty of Civil Engineering, RN Macedonia,* smitovski@gf.ukim.edu.mk

[2] *Teaching assistant, Ss. Cyril and Methodius University in Skopje, Faculty of Civil Engineering, RN Macedonia,*

fpanovska@gf.ukim.edu.mk

[3] *Professor, Ss. Cyril and Methodius University in Skopje, Faculty of Civil Engineering, RN Macedonia,* petkovski@gf.ukim.edu.mk

[4] *Civ. Eng, Spatial Planning Agency, RN Macedonia,* sonja.depinova@gmail.com

1 Abstract

Water management planning is crucial for long-term economic, social and environmental stability in civilized societies. One can only make plans with stored water, i.e. water impounded in reservoirs, formed with construction of dams. The process of long-term water planning and management includes creation of new reservoirs, adding new water users to existing reservoirs, as well as improved management of the existing reservoirs. Such analyses are done for the river Treska basin, located in the western part of R.N. Macedonia. With total basin area of 2068 km^2 and average flow of Q=24,2 m^3/s, currently there are three existing dams with reservoirs – Kozjak, St. Petka and Matka – supplying water for power production, as well providing flood protection of the city of Skopje. During the water economy planning process, four new reservoirs are planned – Greshnica, Podvis, Makedonski brod and Kalugjerica - in order to suffice the lack of fresh drinking water for the analysed basin, as well as water for irrigation of agricultural land for the upcoming 20 years. In order to oversee the new planned scheme for the river Treska basin, simulation model is prepared with application of HEC ResSim software. The simulation modelling is carried out on river scale extent, by inclusion of the existing and planned dams with reservoirs. The output results of the simulation model point out that the basin has enough capacity to suffice the water demands for water supply and irrigation, and in addition, it provides increased power production from renewable energy sources, for the next 20 years.

Keywords: water economy planning, river scale, water demand, simulation model

2 Introduction

Planning the development of water economy systems at country level is a complex issue that implies a long-term planning, with optimal utilization of the available water resources, by taking into account the sustainability (providing possibility for future generations to also use the water resources) and integrality (complex systems solution that during the planning is optimized throughout compliance of the water economy interests and other parts of the spatial planning). In English, the closest term for the preparation of such a long-term plan is the so-called Water Master Plan. Within a document of this caliber, in the chosen scheme for the water management systems, the interests of the water economy sector and other users of the space - who usually have conflicting interests - should be harmonized.

Water economy planning precedes the implementation of water economy projects in the direction of achieving the most expedient development of human society and the use of water resources. In general, the goal of water economy planning is to enable the most effective use of water resources by meeting the anticipated short-term and long-term water needs [1].

From the water economy point of view, the only structures that ensure the temporal and spatial redistribution of water resources are water reservoirs, which are created by the construction of large dams. Storage of water is increasingly proving to be a necessary and key active measure to mitigate

spatial and temporal hydrological unevenness, to overcome asynchrony between available water and water demands, as well as to effectively reduce damage caused by extreme hydrological phenomena (droughts and floods).
In the paper, the water economy planning of the Treska River basin, in the Republic of North Macedonia, is outlined and described. The planning was done by applying a mathematical simulation model, with which the system's response to various hydrological and operational tasks is perceived.

3 Study area and input data

3.1 Treska River basin

The Treska River is a right tributary of the Vardar River, with a total catchment area up to the confluence in river Vardar of F = 1880 km^2. The mean annual measured flow before merging with river Vardar is Q = 23.34 m^3/s . Three dams with reservoirs were built in the Treska River basin - the Kozjak dam, St. Petka and Matka. According to water economy planning in the next 20 years, the Kalugjerica, Makedonski brod, Podvis and Greshnica reservoirs should be built in the Treska River basin. The reservoirs St. Petka and Matka represent single-purpose systems with a single purpose - power production. The Kozjak reservoir has two purposes - power production, and retention of flood wave of the Treska river. The Greshnica reservoir is planned for the power production and the provision of water for irrigation. The reservoirs Podvis, Kalugjerica and Makedonski Brod are planned for the production of electricity, provision of water for irrigation and water supply. In all reservoirs, in addition to the mentioned users, the mandatory environmental discharge is planned downstream of the dam, which is estimated at 17.5% of the average annual flow in the reservoir.
The location of all reservoirs in the Treska River basin is shown in Figure 1.
The Kozjak reservoir has the largest active storage of all reservoirs in the basin - planned and existing - with a total volume of V = 550·10^{6}m^3, of which 100·10^{6}m^3 are planned for retention space for mitigating the flood wave of the Treska river for the mean of protection of the city of Skopje in case of flood. Reservoir elevations, active storage volume and mean annual inflow for each reservoir in the basin are given in Table 1.

Table 1. Characteristic elevations of the reservoirs (Z_{nwl} – normal water elevation, Z_{max} – maximal water elevation, Z_{crest} – crest elevation), active volume (V) and average annual inflow (Q_{inflow}).

Status	Reservoir	Znwl	Zcrest	V	Q_{inflow}	Status	Reservoir	Znwl	Zmax	V	Q_{inflow}
		[masl]	[masl]	[10^6 m^3]	[m^3/s]			[masl]	[masl]	[10^6 m^3]	[m^3/s]
Existing	Kozjak	459	471.1	550	19.65	Planned	Greshnica	790	795	31.2	1.32
	St. Petka	357.3	366	1.10	20.65		Podvis	770	775	50.43	2.13
	Matka	315.5	318.4	3.55	20.85		Makedonski brod	560	565	3	10.11
							Kalugjerica	527	532	250	18.86

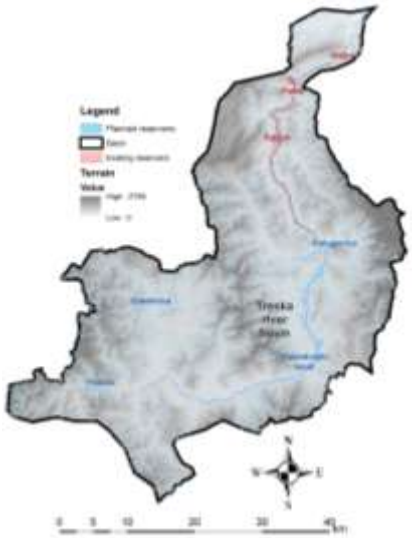

Figure 1. Overview of the catchment area of the Treska River basin with the planned and existing reservoirs. Map created with data from www.land.copernicus.eu.

For the water needs distribution in the basin, according to the water economy planning, the following reservoirs are planned for water supply: Podvis, Makedonski brod and Kalugjerica. The average demand for water supply in the basin is V = 0.39 m^3/s. Since this is a water economy planning on long-term scale, the water needs are distributed throughout the planned reservoirs with percentage share, according to the size of their active volume, varying every month throughout the year, for 20 years ahead. The percentage share for each reservoir in the total water supply needs is given in Table 2. It can be noted that the largest amount for water supply is assigned on Kalugjerica reservoir since it is the largest planned reservoir in the basin, whereas reservoir Makedonski brod will be accounted for fulfilling a very small percentage of water supply demand.

Table 2. Percentage distribution of water supply needs by reservoirs, for the Treska River basin.

Reservoir	$V \cdot 10^6\ m^3$	P=V/V_sum
Podvis	50,430	0.166
Makedonski brod	3,000	0.010
Kalugjerica	250,000	0.824
V_sum=	303,430	

For fulfilling the demand of water for irrigation, the following reservoirs are planned: Greshnica, Makedonski Brod, Kalugjerica and Podvis. The total demand of water for irrigation per year is estimated at $7.88 \cdot 10^6$ m^3/year, varying monthly from April through September each year. Since this is a water economy planning on long-term scale, the water needs are distributed throughout the planned reservoirs with percentage share, according to the size of their active volume, and the percentage share in the total irrigation needs is given in Table 3.

Table 3. Percentage distribution of irrigation needs by reservoirs, for the Treska River basin.

Reservoir	$V \cdot 10^6\ m^3$	P=V/V_sum
Greshnica	31.20	0.09
Podvis	50.43	0.15
Makedonski brod	3.00	0.01
Kalugjerica	250.00	0.75
V_sum=	334.63	

3.2 Reservoir Greshnica

The Greshnica reservoir is located near the village of Kjafa, on the border between the municipalities of Gostivar and Kichevo. The reservoir is planned, with active storage of V = $31.20 \cdot 10^6 m^3$. The topographic properties of the reservoir (surface and volume curves) are shown in Figure 2. The total basin to the dam site is F = 64.55 km^2. The estimated mean inflow in the reservoir is Q = 1.32 m^3/s, and inflow hydrograph is shown in Figure 2.

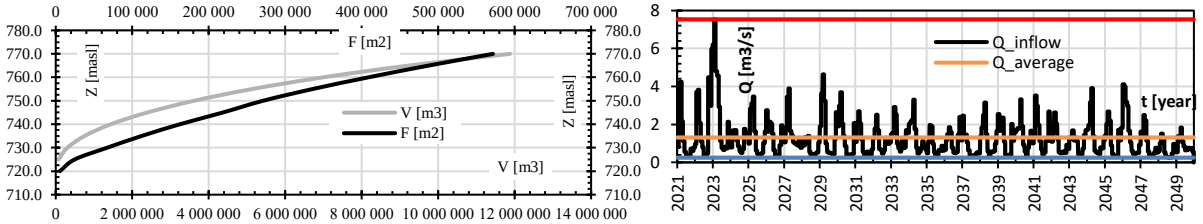

Figure 2. Topographic curves of Greshnica reservoir (graph on the left) and inflow hydrograph in the reservoir (graph on the right).

3.3 Reservoir Podvis

The reservoir Podvis is located near the village of Podvis, west of the town of Kichevo. The reservoir is planned, with a live storage of V = 50.43 · 10^6m^3. The topographic properties of the reservoir are shown in Figure 3. The total basin to the dam site is F = 117.23 km^2. The estimated mean inflow in the reservoir is Q = 2.13 m^3/s, and inflow hydrograph is shown in Figure 3.

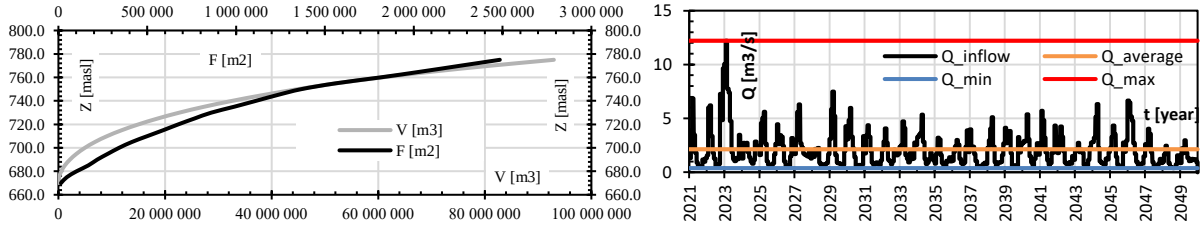

Figure 3. Topographic curves of Podvis reservoir (graph on the left) and inflow hydrograph in the reservoir (graph on the right).

3.4 Reservoir Makedonski brod

The Makedonski Brod reservoir is located near the town of the same name. The reservoir is planned, with an active storage of V = 3·10^6 m^3. The topographic properties of the reservoir are shown in Figure 4. The total basin to the dam site is F = 886 km^2. The estimated average inflow in the reservoir is Q = 10.17 m^3/s, and inflow hydrograph is shown in Figure 4.

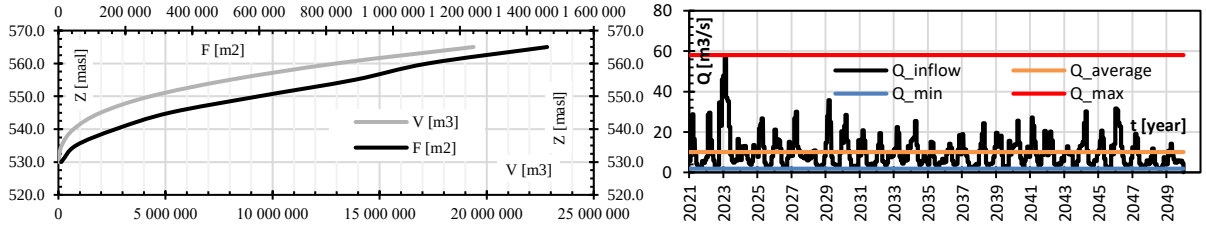

Figure 4. Topographic curves of reservoir Makedonski brod (graph on the left) and inflow hydrograph in the reservoir (graph on the right).

3.5 Kalugjerica Reservoir

The Kalugjerica reservoir is located upstream of the existing Kozjak reservoir. The reservoir is planned, with an active storage of V = 250·10^6m^3. The topographic properties of the reservoir are shown in Figure 5. Total basin to the dam site is F = 1605 km^2. The estimated mean inflow in the reservoir is Q = 18.86 m^3/s, and inflow hydrograph is shown in Figure 5.

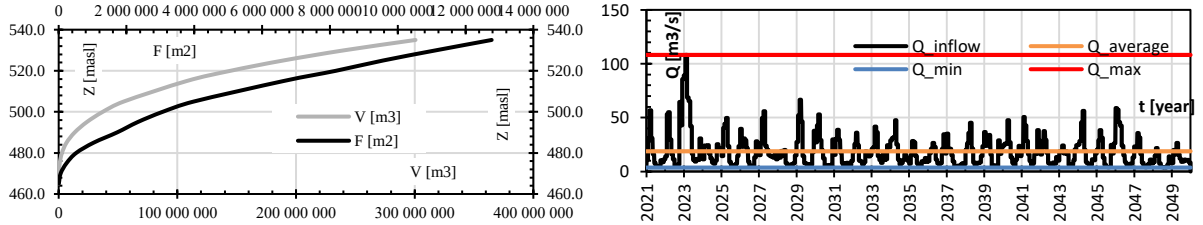

Figure 5. Topographic curves of Kalugjerica reservoir (graph on the left) and inflow hydrograph in the reservoir (graph on the right).

3.6 Kozjak reservoir

The Kozjak reservoir is an existing reservoir on Treska river, formed with the construction of Kozjak dam in 2004. The primary purpose of Kozjak reservoir is retention of flood wave of Treska river in the retention space of the reservoir of $V = 100 \cdot 10^6$ m^3. In addition to retention of the flood wave, the reservoir is also planned for the production of electricity. For this purpose, the Kozjak HPP was constructed downstream of the dam with an installed capacity of Q = 100 m^3/s and an installed power of P = 82 MW. The active storage of the reservoir is $V = 550 \cdot 10^6$m^3. The topographic properties of the reservoir are shown in Figure 6. The estimated mean inflow in the reservoir is Q_{av} = 19.65 m^3/s, and inflow hydrograph is shown in Figure 6.

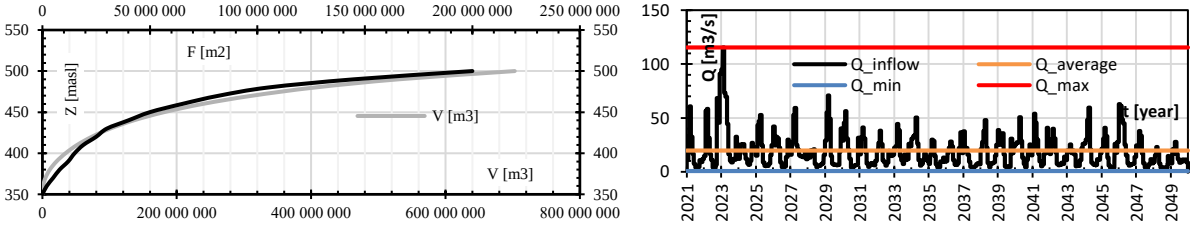

Figure 6. Topographic curves of Kozjak reservoir (graph on the left) and inflow hydrograph in the reservoir (graph on the right).

3.7 Reservoir St. Petka

The reservoir St. Petka is an existing reservoir located downstream of the Kozjak reservoir, formed with the construction of the dam St. Petka in 2012. The primary purpose of the reservoir is the production of electricity. The installed capacity of the hydropower plant is Q = 100 m^3/s and P = 36.4 MW. The active volume of the reservoir is $V = 1.1 \cdot 10^6$m^3. The topographic properties of the reservoir are shown in Figure 7. The estimated mean inflow in the reservoir is Q = 20.65 m^3/s, and inflow hydrograph is shown in Figure 7.

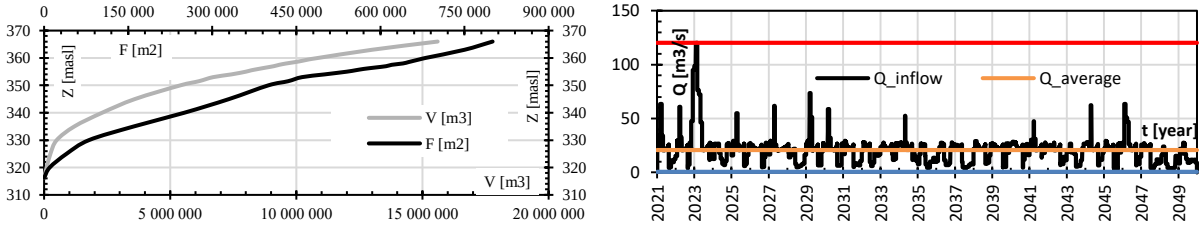

Figure 7. Topographic curves of reservoir St. Petka (graph on the left) and inflow hydrograph in the reservoir (graph on the right).

3.8 Matka reservoir

The Matka reservoir is an existing reservoir that was created with the construction of the Matka dam, built back in 1938. It is the first dam built in R. Macedonia. The primary purpose of the reservoir is the production of electricity. The installed capacity of the hydropower plant, after the construction of the new machine building, is Q = 42 m^3/s and P = 9.6 MW. The active volume of the reservoir is $V = 3.55 \cdot 10^6$m^3. The topographic properties of the reservoir are shown in Figure 8. The estimated mean inflow in the reservoir is Q = 20.85 m^3/s, and inflow hydrograph is shown in Figure 8.

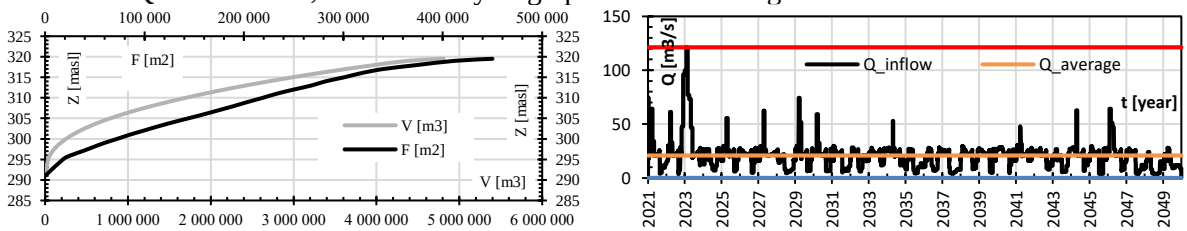

Figure 8. Topographic curves of Matka reservoir (graph on the left) and inflow hydrograph in the reservoir (graph on the right).

4 Simulation model

For the study of the water economy planning in the Treska River basin, a mathematical simulation model was developed in the HEC ResSim software.
HEC-ResSim is a software used to model complex water resources planning and management for multidimensional and multipurpose systems, in order to meet the demands of the water users. With the help of the software, it is possible to model reservoirs for flood defense, water supply for population and industry, power production, as well as combinations of operational policies and prioritizing multiple water users according to the demands [2].
Before developing the watershed model, it is necessary to define: (1) inflow hydrograph in each reservoir, (2) physical properties of the reservoir, (3) water demands, and (4) operational rules for system operation. In addition to the mentioned steps, in the models it is important to define the placement of the reservoirs and their mathematical connection in order to carry out successful analyses. Namely, the discharge from the upstream reservoir should appear as inflow in the downstream reservoir. Such interactions are defined based on Figure 9, where the calculation scheme for the complex water resources system for Treska River basin is displayed.
The hydrographs of inflows in each reservoir are formed according to the measured inflows in gauging stations Kicevo, Makedonski Brod, Zdunje and St. Bogorodica. Each inflow hydrograph for the modeled reservoirs are shown in Figures 2 through 8.
Water demand for water supply and irrigation are defined according to the percentage distribution, given in Table 2 and Table 3. In all reservoirs, in addition to the mentioned water needs, the mandatory environmental discharge is planned downstream of the dam, which is estimated at 17.5% of the average annual inflow in the reservoir.

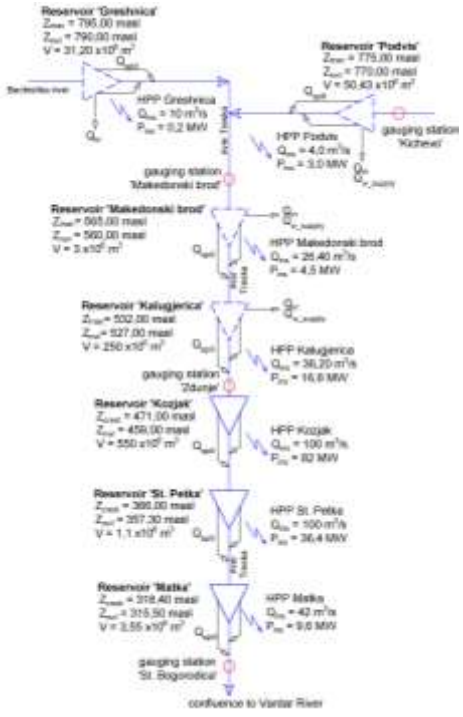

Figure 9. Calculation scheme of the complex water economy system of the Treska River basin.

5 Output results and discussion

As follows, results are shown obtained with the simulation model of Treska River basin.

5.1 Output results for the planned reservoirs

In case of Greshnica reservoir, it can be seen that throughout the entire simulation period the reservoir is full

(Figure 10), and irrigation demand and required environmental flow are almost completely meet (Figure 11-12). The average annual power production through the hydropower plant is E=1.03 GWh /year (Figure 13).

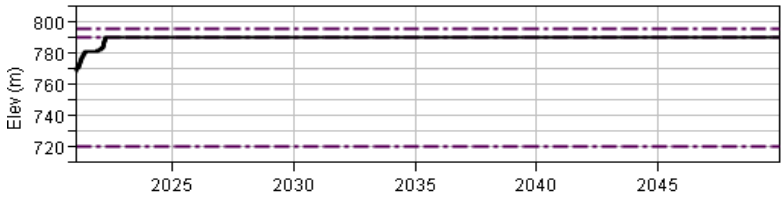

Figure 10. Fluctuation of water level in Greshnica reservoir.

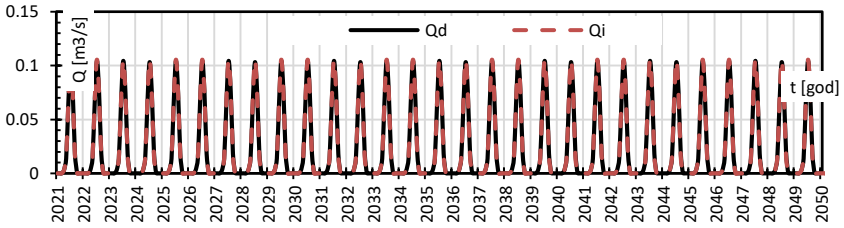

Figure 11. Comparative display of irrigation demand (Q_i) and delivered water (Q_d) from Greshnica reservoir.

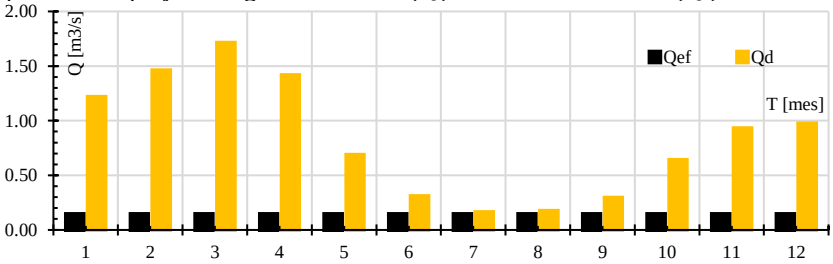

Figure 12. Comparative display of required environmental flow (Q_{ef}) and delivered water (Q_d) from Greshnica reservoir.

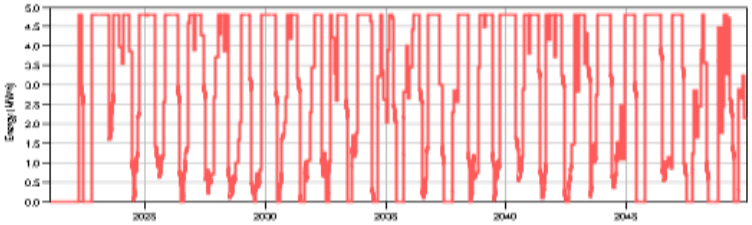

Figure 13. Power production from HPP Greshnica, average annual production E= 1.03 GWh/year.

In case of Podvis reservoir, it can be seen that throughout the entire simulation period, the reservoir is full (Figure 14), the water supply and irrigation demands are fully met (Figure 15 and 16) as well as the required environmental flow (Figure 17). The average annual power production is E = 13.55 GWh /year (Figure 18).

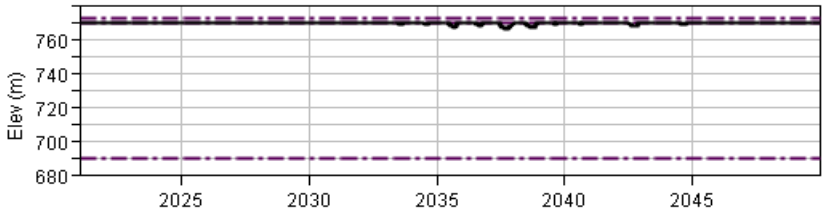

Figure 14. Fluctuation of water level in reservoir Podvis.

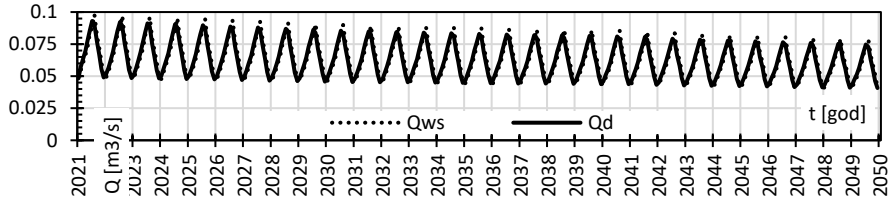

Figure 15. Comparative display of water supply demand (Q_{ws}) and delivered water (Q_d) from Podvis reservoir.

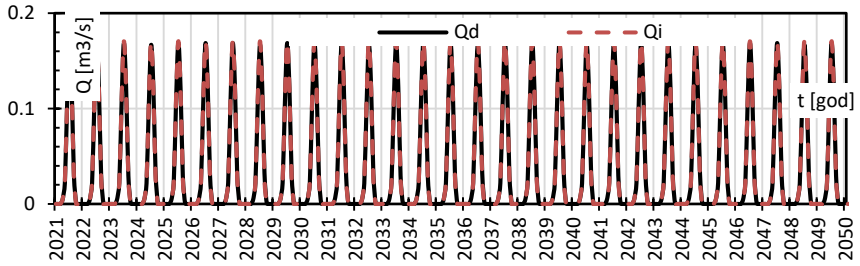

Figure 16. Comparative display of irrigation demand (Q_i) and delivered water (Q_d) from Podvis reservoir.

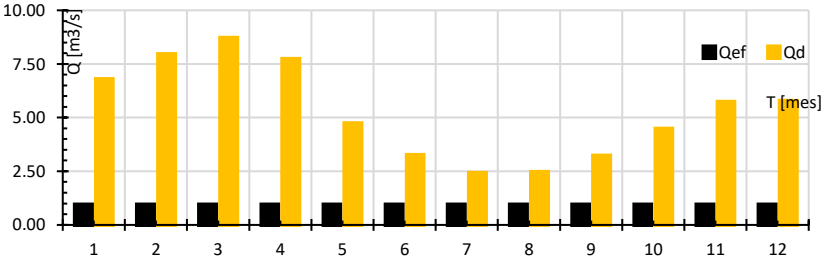

Figure 17. Comparative display of required environmental flow (Q_{ef}) and delivered water (Q_d) from Podvis reservoir.

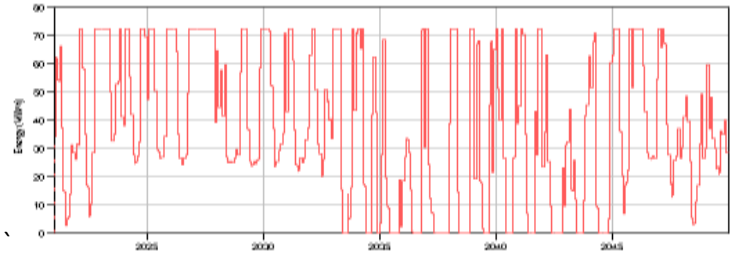

Figure 18. Power production from HPP Podvis, average annual production E = 13.55 GWh/year.

For Makedonski Brod reservoir, it can be seen that throughout the entire simulation period the level in the reservoir periodically varies (Figure 19), and the water supply and irrigation demands are met (Figure 20 and 21) as well and the required environmental flow (Figure 22). The average annual power production is E = 8.59 GWh /year (Figure 23).

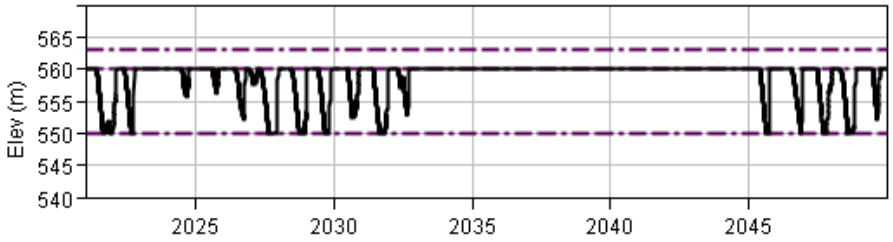

Figure 19. Water level fluctuation in the Makedonski Brod reservoir.

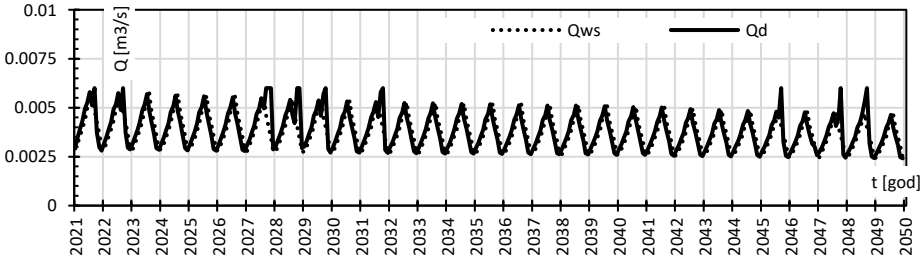

Figure 20. Comparative display of water supply demand (Q_{ws}) and delivered water (Q_d) from Makedonski Brod reservoir.

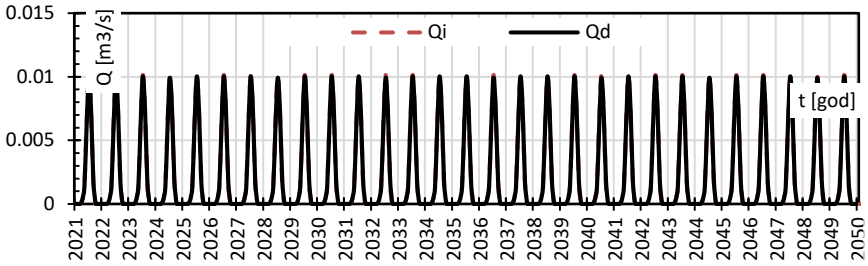

Figure 21. Comparative display of irrigation demand (Q_i) and delivered water (Q_d) from Makedonski Brod reservoir.

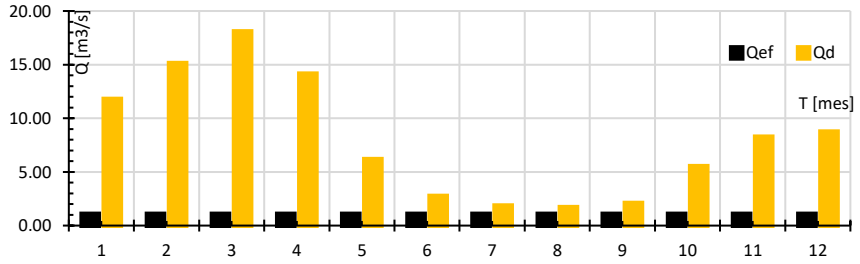

Figure 22. Comparative display of required environmental flow (Q_{ef}) and delivered water (Q_d) from Makedonski Brod reservoir.

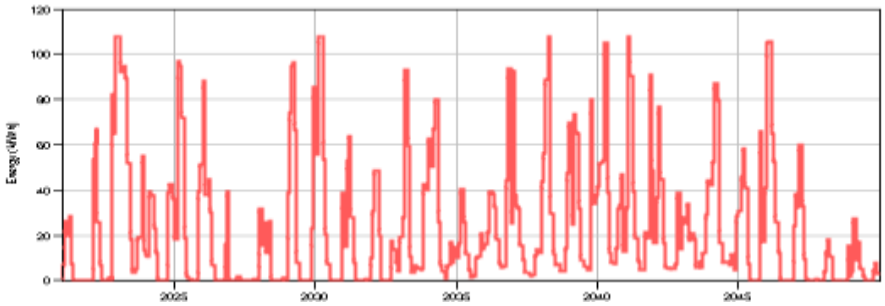

Figure 23. Power production from HPP Makedonski Brod , average annual production E= 8.59 GWh/year.

At Kalugjerica reservoir, it can be seen that throughout the simulation period the level in the reservoir is completely at normal water level (Figure 24) and the water supply and irrigation demands are fully met (Figure 25-26) as well and the required environmental flow (Figure 27). The average annual power production is E= 44.46 GWh /year (Figure 28).

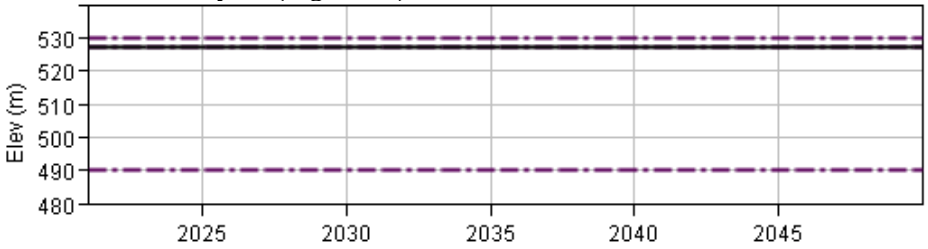

Figure 24. Water level fluctuation in Kalugjerica reservoir.

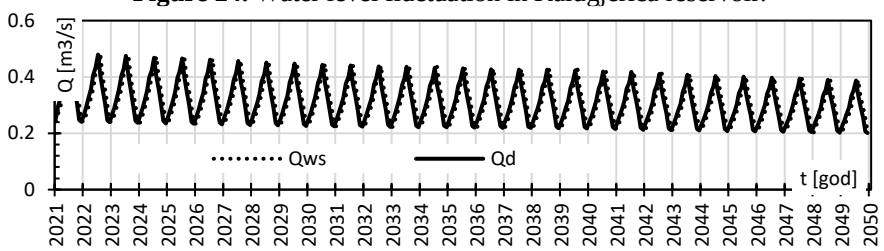

Figure 25. Comparative display of water supply demand (Q_{ws}) and delivered water (Q_d) from Kalugjerica reservoir.

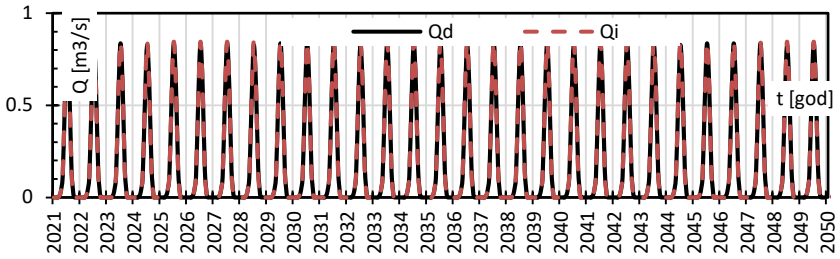

Figure 26. Comparative display of irrigation demand (Q_i) and delivered water (Q_d) from Makedonski Brod reservoir.

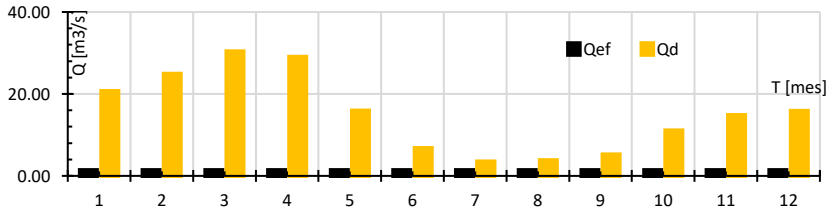

Attachment 27. Comparative display of required environmental flow (Q_{ef}) and delivered water (Q_d) from Kalugjerica reservoir.

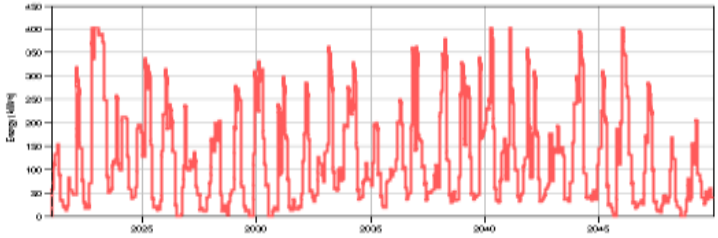

Figure 28. Power production from HPP Kalugjerica, average annual production E= 44.46 GWh/year.

5.2 Results for the existing reservoirs

The modeled existing reservoirs – Kozjak, St. Petka and Matka have been analyzed from the aspect of power production.

At Kozjak reservoir, during the simulation period the reservoir level is varying (Figure 29) in accordance with the set operational policy for power production. Namely, in the time period of analysis of 20 years in the simulation model, the average annual power production in HPP Kozjak is 80.21 GWh/year (Figure 30). According to the Reports on the work of ESM - the company that manages this hydropower plant, the average power production in the past 18 years, for the period from 2004 to 2021, is 123.62 GWh, with 44.3 GWh/year as minimal production in 2004, and 250.9 GWh/year as maximal production in 2010 [3].

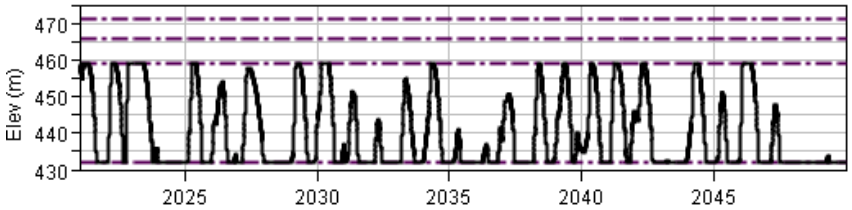

Figure 29. Water level fluctuation in Kozjak reservoir.

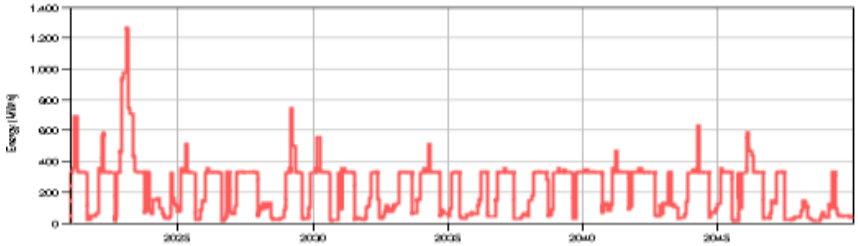

Figure 30. Power production from HPP Kozjak, average annual production E = 80.21 GWh/year.

At St. Petka reservoir, during the simulation period the reservoir level is varying (Figure 31) in accordance with the set operational policy for power production. The average annual power production in HPP St. Petka, according to the simulation model, is 45.85 GWh/year (Figure 32). According to the Reports on the work of ESM, the average power production in the past 10 years, for the period from 2012 to 2021, is 45.4 GWh, with 12.2 GWh /year as minimal production in 2012, and 75.8 GWh /year as maximal in 2015.
At Matka reservoir, during the simulation period the reservoir level is varying (Figure 33) in accordance with the set operational policy for power production. The average annual power production in HPP Matka, according to the simulation model, amounts to 24.21 GWh /year (Figure 34). According to data from EVN - the company that manages this hydropower plant, the average annual power production is 30 GWh /year.

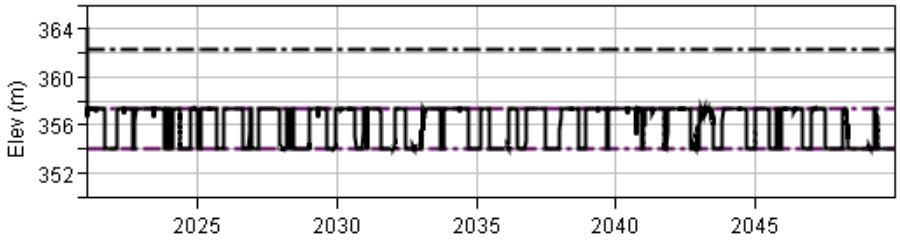

Figure 31. Fluctuation of water level in reservoir St. Petka.

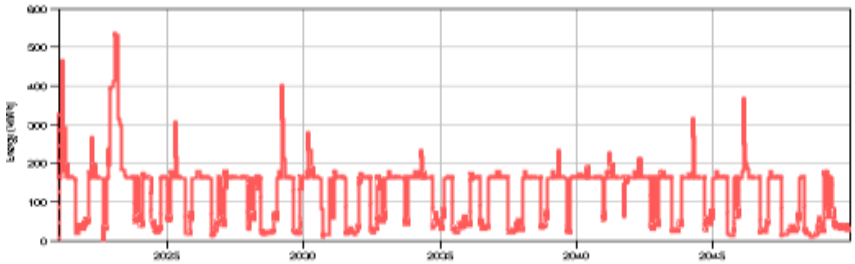

Figure 32. Power production from HPP St. Petka, average annual production E= 45.85 GWh/year.

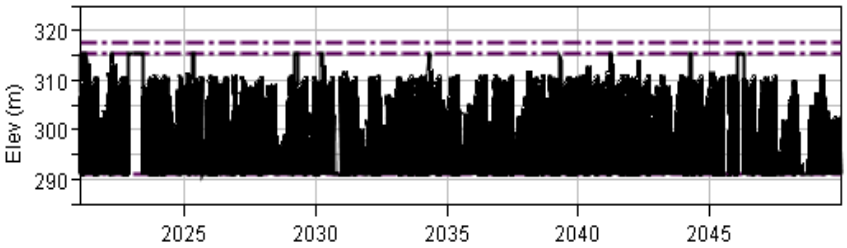

Figure 33. Water level fluctuation in Matka reservoir.

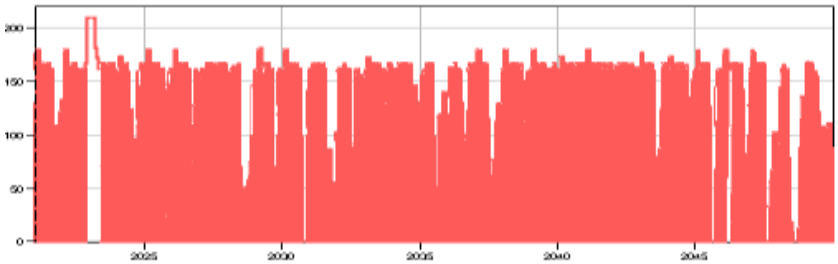

Figure 34. Power production from HPP Matka, average annual production E=24.21 GWh/year.

6 Conclusions

In order to analyze the adopted scheme for development of the Treska River basin with construction of new dams with reservoirs, a simulation analysis is conducted in HEC ResSim software. Three existing reservoirs are included in the model – Kozjak, St. Petka and Matka, and four newly planned reservoirs are included – Greshnica, Podvis, Makedonski Brod and Kalugjerica. All reservoirs are modeled for

fulfilling a certain demand – water supply, irrigation needs and/or power generation. The goal of the analyses is to oversee the response of the reservoirs in the basin while maximal demands are required, with gauged hydrographs assigned as inflow for each reservoir, for a simulation period of 20 years and time step of the analyses of 1 day.

Based on the conducted simulation analysis of the complex water economy system for the Treska basin with the given hydrological parameters, operational management policy and the comparative analysis of the output results with the water needs, we single out the following conclusions:

1) The water level in the reservoirs is kept partially constant, with small variations in the active storage zone, with the exception of the reservoirs Kozjak, St. Petka and Matka, where a significant variation of the water level is observed in the active storage zone in correlation with applied operational policy based on the criterion for maximizing of the power production.
2) The ecological criterion (providing environmentally guaranteed flow) is met (or exceeded) in all reservoirs.
3) The water supply demands are met in all reservoirs, where the abovementioned purpose is foreseen.
4) The irrigation demands are met in all reservoirs, where the abovementioned purpose is foreseen.
5) The power production is correlated with the available amount of water (water level in reservoir and hydraulic head), according to the specified operational policy which gives priority of meeting the other water demands (water supply and irrigation). The average annual power production at basin level (as the sum of the average annual production of the individual planned HPPs within the basin, obtained by the simulation analysis) is estimated at 67.63 GWh /year. The cumulative average annual power production at the basin level (as the sum of the average annual production of the planned and existing HPPs within the basin) is estimated at 217.90 GWh/year. Basically, with construction of the new four reservoirs – Greshnica, Podvis, Makedonski Brod and Kalugjerica, additional 67,63 GWh will be generated for the electricity grid as a renewable energy.

References:

[1] Kuiper, E.: Water resources development – Planning, Engineering and Economics, New York, Springer Science Business Media, 1965
[2] US Army Corps of Engineers: HEC ResSim User's Manual, version 3.3, 2021
[3] ESM – Power production of RN Macedonia: Annual report for 2021, web: https://www.esm.com.mk/wp-content/uploads/2023/04/AD-ESM-GODISEN-IZVESTAJ- 2021.pdf
[4] Zavod za vodostopanstvo: Vodostopanska osnova na R. Makedonija (Water master plan of R. Macedonia), 1977
[5] Goodman, A.S.: Principles of Water Resources Planning, Englewood Cliffs: Prentice – Hall, 1984
[6] Opricovic, S.: Optimizacija Sistema, Belgrade, 1992
[7] Savenije, H.H.G.: Water Resources Management Concepts and Tools, IHE Delft, 1996
[8] Votruba, L.: Analysis of water resources, Prague, Technical University of Prague, 1988
[9] Spatial planning agency in R. Macedonia: Spatial planning of R Macedonia for the period of 2002 – 2021, Skopje, 2002
[10] Panovska, F., Mitovski, S., Petkovski, L.: Simulation model for analysis of hydropower system on Crna Reka for alternative with two pump-storage hydropower plants, Proceedings of the 5th Congress on Dams, Macedonian Committee on Large Dams, Struga , R. Macedonia, 2021
[11] Mitovski, S., Panovska, F., Petkovski, L.: Application of simulation models for management of complex water resources system, 17th International Symposium of Water Management and Hydraulic Engineering - WMHE, September, Sopot, Poland, 2022

SANITARY AND ENVIRONMENTAL ENGINEERING, SUSTAINABLE WATER USE

HYDRAULIC ANALYSIS AND OPTIMIZATION OF A PART OF THE WATER SUPPLY SYSTEM OF THE BUZET CITY

ELVIS ŽIC [1], PETRA ČERNEKA [2], GORAN VOLF [1]

[1] *Faculty of Civil Engineering Rijeka, Radmile Matejčić 3, 51000 Rijeka, Croatia, elvis.zic@uniri.hr; goran.volf@uniri.hr*

[2] *ZIP KONTIĆ D.O.O., Krizmani 91B, 52424 Novaki Motovunski, Croatia, cerneka.petra@gmail.com*

1 Abstract

This paper deals with the optimization of the water supply network (WSN) of the Buzet City and describes the characteristics of the area and the required water quantities. Dimensioning calculations were carried out for water reservoirs and pumping stations. The hydraulic analysis using the WaterCAD V8i computer program examined three variants of gravitational inflow, taking into account changes in flow velocity, flow rate, pressure and water level with different pipe materials and fire loads. To maintain the system pressure, two reservoirs were defined that offer optimization scenarios.

Keywords: Buzet City, water supply system, hydraulic analysis, water reservoir, pump, WaterCAD V8i.

2 Introduction

The Buzet City is located in the heart of the Istrian Peninsula. It is among the first cities in Istria County where a water supply system (WSS) was built in 1930. A part of the Buzet City was chosen for the design and analysis of the WSS. The WSS is planned for a final number of 7,082 inhabitants at the end of the project period of 30 years. The Buzet City is located in a valley that is surrounded by the valleys of the upper course of the Mirna River, the flysch hills better known as Siva Istra, and the limestone Ćićarija as White Istra. It is located in a hilly area between altitudes of 30 and 160 m a.s.l. and extends over an area of approximately 165 km^2. According to the 2011 population census, the Buzet City has 70 settlements with a total of about 6,100 inhabitants [1]. In the eastern area of the city above 500 m a.s.l. (Ćićarija) the mountain climate prevails, while in the lower areas of the Mirna river valley a moderately warm climate is present. Precipitation has a relatively regular schedule and is mostly present in the winter (October and November) and spring months. Dry periods were recorded in early spring (March) and summer months (August). The average annual air temperature is between 12 and 13 °C [2], while the average annual precipitation is between 1,100 and 1,200 mm. The mean amount of precipitation for winter varies between 300 and 500 mm, and between 300 and 400 mm in summer. In the given area, the air humidity ranges between 70 and 80 % [2].

Most of the Buzet area is composed of flysch, which is why this area is rich in a river network of surface streams that are mostly torrential in nature. Flysch and Quaternary impervious deposits condition the surface flow of mostly sudden and large flow oscillations [1]. Occasional surface springs, such as Pivka and the karst spring of Tombasin near the spring of Sv. Ivan. Quaternary formations cover a small area of the Buzet City, and are covered by alluvial deposits and, to a lesser extent, by sipar. In the area of carbonate rocks, there is an underground movement of water that springs to the surface in the form of springs, like the permanent springs of St. Ivan and Bulaž.

The existing water reservoirs in the town of Buzet are the Industrija reservoir with a capacity of 1300 m^3, which serves to meet the needs of industry and the settlements of Most and Juričići. The water that supplies the population of Buzet is pumped by pumps with a capacity of 5 l/s to a height of 33 m to the Baštion reservoir and the Fontana reservoir. With a capacity of 66 m^3, the Baštion reservoir is the smallest reservoir in the system and supplies the population of the old town centre of Buzet [1]. Most of the town of Buzet (63%) is supplied with water from the Fontana reservoir, which has a capacity of 150 m^3. A hydrophoretic station is located next to the Baštion reservoir to ensure the working pressure in the water supply network. The water comes from the St. Ivan spring and is pumped via the Štrped

pumping station into the Štrped reservoir with a capacity of 600 m^3, which then supplies the settlements of Štrped, Sv. Duh, Podrečak, Abrami, Škuljari, Opatija, Žonti, Trkusi, Požane, Mlini and Ugrini. In the Krbavčići reservoir with a capacity of 600 m^3, water is pumped via the Sv. Martin pumping station to the settlements of Krbavčići, Rumeni, Stupari, Majcani, Mandaši and part of the settlement of Sv. Martin [1]. The water from the spring of Sv. Ivan, from where it branches into two main pipelines. This paper considers variants with two new main reservoirs that would replace the function of the existing reservoirs and their impact on the optimization of the water supply system.

3 Relevant quantities of water

In order to determine the relevant quantities of water required for the dimensioning of the WSS, it is important to define the categories of consumers, therefore the needs of the local population, industries and tourists staying in private accommodation, the Fontana Hotel***, the future planned hotel**** and the Camp are taken into account (B category). It is necessary to consider the necessary quantities of water needed for extinguishing fires and the quantities spent on maintaining the WSS. The water supply system of part of the Buzet City (Figure 1.) is designed for a period of 30 years on the basis of geometric growth ($N_k = N_0(\frac{p}{100} + 1)^{Rp}$), where N_o are the current number of inhabitants, p [%] defines the percentage of annual population growth, and R_p [year] represents the project period [3].

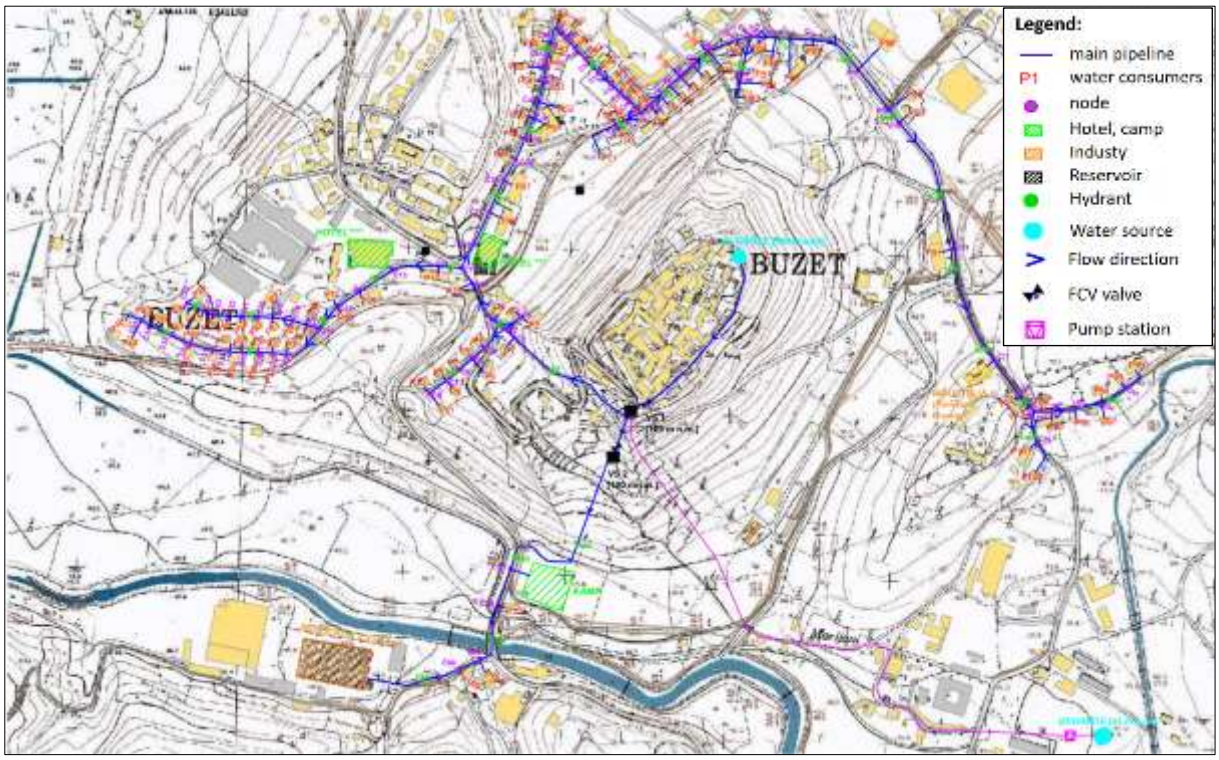

Figure 1. Distribution of consumers on the water supply system of the Buzet City

Annual population growth in the last ten years is 0.21%. The number of inhabitants in 2021 was 6,650 [1], and it is assumed that after 2021 the annual growth rate will be 0.21%. The final number of inhabitants in 2051 will be 7,082. The number of tourists staying in the Buzet City is 2,000, of which 200 tourists can be accommodated in the existing Hotel Fontana***, 400 tourists in hotel****, 500 tourists in Camp of B category and 900 tourists staying in private accommodation, Table 1.

Table 1. Distribution of specific consumption of q_{sp} water for certain categories of consumers [1]

Consumer category		Specific water consumption q_{sp} [l/tourist/day]
Hotel	****	400
	≤ ***	300
Camp	Category B	120
Private accomodation		300

Based on the knowledge of the final number of inhabitants N_k, i.e. tourists and specific water consumption q_{sp}, it is possible to calculate the average daily water consumption $\bar{Q}_{av.d.}$ [l/day], the maximum daily water consumption $Q_{max.d}$ [l/day] and the maximum hourly water consumption $Q_{max.h}$ [l/h] for individual consumers (Table 2).

Table 2. Average daily, maximum daily and maximum hourly water consumption for individual consumers on the water supply system (unevenness coefficients are given in parentheses)

	$\bar{Q}_{av.d.}$ [m^3/day]	$Q_{max.d}$ [m^3/day]	$Q_{max.h}$ [m^3/h]
Population	1,770.5	2,655.75 (1.5)	199.18 (1.8)
Hotel***	60	96.0 (1.4)	8.80 (2.5)
Hotel****	160	224.0 (1.6)	23.33 (2.2)
Camp	60	120.0 (1.8)	11.50 (2.2)
Private accomodation	270	486.0 (2.0)	44.55 (2.3)

The total maximum hourly water consumption for the entire WSN is 79.8 l/s. There are two different industries in the designed area, the CIMOS Buzet Ltd. factory is engaged in the production of automotive parts and castings and Pivovara Bruman Ltd. According to the Request for determination of the unified environmental protection conditions of the factory P.P.C. BUZET Ltd. (CIMOS) in accordance with the *Regulation on the procedure for establishing unified environmental protection conditions* (Narodne novine 114/08) - Rev 1, industrial plant CIMOS Ltd. consumes 35,254 m^3/year [4]. Pivovara Bruman is a small brewery opened in 2018, where the current daily production of beer is equal to 125 l [5]. Assuming further growth and development of the brewery, the forecast is that in 5-10 years the daily production of beer will be 3,000 l. One liter of beer requires 50 liters of water, which would mean that the daily consumption of water in the brewery is equal to 150,000 liters. By summing the water consumption of both industries, the required amount of water is obtained of 246,586.30 l/day. Both industries work from 6 a.m. to 10 p.m., which is 16 hours of work, during which the amount of water required is equal to 5 l/s.

Requirements for fire hydrant networks and other examples in which fire hydrant networks are used for fire protection are prescribed by the *Ordinance on fire hydrant networks* (Narodne novine 8/2006). Based on the total number of residents and tourists, the required amount of water for extinguishing fires in the settlement was determined with a total of 108 m^3/s, while for extinguishing fires in industry, 144 m^3/s of water was determined. 10% of the average daily amount of water (232.05 m^3/s) was taken for the purpose of own maintenance of the WSS.

4 Hydraulic calculation of the water supply system

For the WSS of part of the Buzet City the hydraulic calculation of the branch network was carried out. Two cases were observed. In the first case, three variants of the system were performed with different dispositions of the water reservoir, and in the second case, one variant with a different position of the branch network compared to the previous three variants. The hydraulic calculation was made for all four variants in which the water from the reservoir flows by gravity towards the consumers. The purpose is to see how the position of the water reservoir affects the dimensioning of the system in the form of changes in pipeline dimensions, velocities and working pressures in order to obtain the most optimal and economically profitable WSS. The minimum working pressure of 2.61 bar is determined for the first case of the WSN where Reservoir 1 is located at 124 m a.s.l., while the maximum working pressure of 6.56 bar is determined for the network where Reservoir 1 is positioned at 126 m a.s.l.. For the second

case (where an additional branch of the system leaves from Reservoir 1 supplying the right part of the WSS), the working pressures were obtained as for the first variant (with the position of the reservoir at 125 m a.s.l.).
The hydraulic calculation is carried out using a tabular representation, for which it is necessary to determine the relevant flows, i.e. the total maximum hourly water consumption. After defining the sections and their lengths, the specific water consumption per meter was determined as $q_{spec.} =$ $=0.014024$ l/s/m'. All pipes of the WSN were dimensioned through calculations of pipe diameter *D* [mm], flow velocity *v* [m/s], longitudinal drops *I* [‰], major losses Δh [m] and velocity heights $v^2/2g$ [m]. The relevant diameters of pipelines in the designed WSS range from 200 to 350 mm. Working pressures in the WSS satisfy values between 2.5 and 6 bars. After calculations for both cases, the highest major losses in the network occur in the first case, given that the total length of the supply network is longer. Therefore, the use of larger pipe profiles is also required. Ultimately, greater losses in the supply system and installation of pipes with larger diameters result in more expensive investment construction and a greater need for system maintenance. Therefore, the second case is more profitable, considering that on the changed route of the section there are lower major losses compared to the first case, and due to the shorter length of the newly formed section, the requirement for the installation of a pipe diameter of 250 mm is reduced from 13.93 % (first case) to 0.50% (second case), with the fact that there is no need in the second case to use pipes with the largest obtained profile of 350 mm.

5 Calculation of the water reservoir

Water storage in the water reservoir implies the provision of an operational reserve, V_{RO}, provision of a fire protection reserve, V_{PR}, and provision of a safe reserve, V_{RS} of water in cases of disruption of the WSS. The calculation of the total volume of the water reservoir for the gravity inflow of water to consumers from the water reservoir from the source is carried out for two water reservoirs, one of which is the main water reservoir (Reservoir 1, 125 m a.s.l.) and the other serves to ensure water for a smaller part of the city (Reservoir 2, 100 m a.s.l.). Based on the hydraulic calculation of the water reservoir the total volume of the water reservoir for the WSN was determined (Figure 1, Table 3). It should be noted that after dimensioning the reservoir for the case of water inflow into the reservoir by gravity (V_{RU} = $V_{RU,Res1}$ + $V_{RU,Res2}$ = 1,509.8 + 480.68 = 1,990.48 m^3) and water inflow into the reservoir by pumping (with the same hourly water consumption and 10-hour water pumping from the water source), the final total volume of the water chamber of the main reservoir was assumed to be 3000 m^3. For the hydraulic calculation of the WSN in the WaterCad V8i computer program, the cylindrical shape of the water chamber of the water reservoir was modified in the amount of 3,019.07 m^3, which was used for the hydraulic analysis in Variants 1-3.

Table 3. Calculation of the total volume of the reservoir for gravity inflow into the reservoir

	$\%Q_{max.d}$	Operational reserve V_{RO} [m^3]	Fire protect. res. V_{PR} [m^3]	Security reserve V_{RS} [m^3]	The total volume of reservoir V_{RU} [m^3]
Reservoir 1	24.7	955.8	252 / 378	302.0 /133.4	1,509.8 **(2,000 m^3)**
Reservoir 2	40.0	34.0	252 / 378	140.24 / 68.78	480.68 **(500 m^3)**

The operational reserve is carried out under the assumption of daily leveling, where the daily inflow is equal to the daily water consumption of the settlements downstream from the water reservoir, which is expressed as a percentage of the maximum daily consumption in certain hours $\%Q_{max.d}$. The budget was made for a small town with industry. The fire protection reserve is required for extinguishing fires in accordance with the valid *Rulebook on technical standards for the hydrant network for fire extinguishing*. The fire reserve is calculated without or with neutralization of fire, separately for population and industry. The safety reserve is used for interruption of water supply, pressure tests, testing of pipelines and the like. Two methods of calculating the safety reserve of the water reservoir are applied. According to the first method, the safety reserve of the water reservoir is 25% of the sum of the operational reserve and the fire reserve without neutralization, and according to the second

method, the safety reserve is 10% of the sum of the operational reserve and the fire reserve of the water reservoir with neutralization. In the designed area, there is a smaller Reservoir 2 that supplies the southern part of the city to Industry 2. The design of an additional water reservoir is necessary in order to meet the working pressures on that part of the WSN.

6 Hydraulic analysis of the submodel

The WaterCAD V8i computer program is used worldwide by various utility and engineering companies to design, analyze and optimize water supply infrastructure [6]. The import of topography and marking of node heights is possible based on geospatial data downloaded from files of certain formats (GIS, AutoCAD, etc.). The program enables the comparison of an unlimited number of different cases of water needs, terrain topography and physical and design scenarios [7]. Hydraulic modeling enables the design of the pumping system, including complex combinations of pumps to obtain an optimal solution with minimal costs of operation and maintenance of the pumps and maximum system efficiency achieved.
The WSN is drawn directly into the WaterCAD program from the AutoCAD program. Within the WSN it is necessary to define all water supply objects (consumers, nodes, pipes, water reservoirs, shut-off chambers, pumps, reducer valves, etc.), and their characteristics (lengths, diameters, altitudes, reduced pressures, characteristics of *Q-H* curves when choosing a type pumps, etc.). In order to ensure the design quantities of water for firefighting, it is necessary to install a hydrant network on the WSN in accordance with the *Ordinance on hydrant network for firefighting*. The maximum mutual distance between the hydrant and the protected building is 80 m and the minimum is 5 m. The external hydrant network must ensure minimum flow from 600 l/min (10 l/s) to 2,100 l/min (35 l/s) for extinguishing fires in populated areas. It is necessary to assign its fixed water consumption to each node and consumer. Water consumption in the supply system varies from hour to hour within a day. Such variations are especially visible for small towns with industry. In this paper, three samples were created, one for the population, the second for firefighting purposes and the third for ensuring the necessary amounts of water for industries in the project area, all in accordance with the defined coefficients of unevenness of water consumption during the day (Figure 2).
There are two reservoirs in the designed area, Reservoir 1 (VS-1) and Reservoir 2 (VS-2). The reservoirs set up in this way do not contain real characteristics and it is necessary to define their total volumes and the inflow into the reservoir itself. The total volume of the water tank is determined in Chapter 4 and accordingly the cylindrical shape of Reservoir 1 and Reservoir 2 is defined.

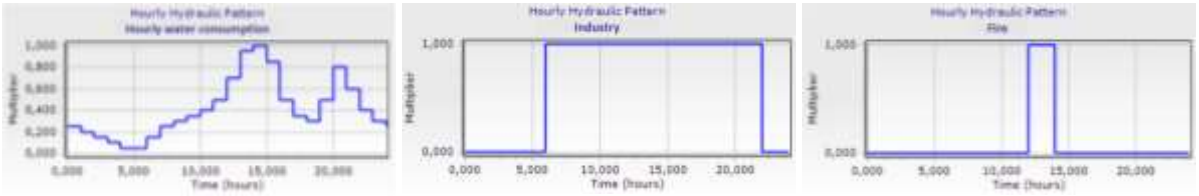

a) b) c)

Figure 2. Defining the hydraulic pattern of water consumption for a) population, b) industry and c) firefighting within the WaterCad V8i computer program

We install pumps in the WSS to connect the water source (43 m a.s.l.) and the main Reservoir 1 (125 m a.s.l.). They are defined according to the total calculated pressure gauge heights and the required flow to ensure the water reservoir. The calculation defined three main and three reserve pumps, where one pump raises a flow of 107 l/s to a height of 44.5 m. After defining the water supply elements within the system in the WaterCad V8i computer program, a hydraulic analysis is performed to obtain feedback on the correct functioning of the WSS and all its elements. The first analysis observes the stationary flow, giving calculation results for one time step, while the second type of analysis refers to the simulation of an extended period (*Expanded Period Simulation, EPS*), in which the model is observed during a certain time. The duration of the EPS and the time steps are set depending on the desired observation time of the model, within which its changes in individual physical quantities will be seen. For the selected EPS

budget, the observation time is 24 hours with a time step of 0.1h. According to such an analysis, it is possible to observe the filling and emptying of the water reservoir in a certain time, on the basis of which the operation of the pumps inside the pumping station can be corrected.

6.1 Hydraulic analysis of the gravity inflow of water in Water Reservoir 1

The hydraulic analysis will be carried out for three versions of the gravity inflow of water in Reservoir 1 depending on its disposition and altitude. For each of the variants, the results obtained according to the use of different types of pipe materials will be presented below.

6.1.1 Variant 1 – Water Reservoir 1

Water Reservoir 1 is located at an altitude of 125 m a.s.l. (Figure 1). The volume of 3,019.07 m^3 was calculated as the relevant volume of Reservoir 1. In order to protect the supply system from taking too much water a flow control valve (FCV) can be installed. The valve limits the flow to a certain value. The calculation of the gravity flow of water in Reservoir 1 is carried out for the maximum hourly consumption of water that occurs during the time of the highest demand for water. The maximum hourly consumption according to the given multiplier occurs from 12:00 to 14:00 and takes into account the needs of the population, tourists and industrial plants. During the maximum hourly consumption, the highest flow in the system is the flow of 84.82 l/s, which occurs in the section from the source to Reservoir 1. The highest flow velocities in the system were recorded in the section IZVOR-VS-1 and VS-1-J-1 (v=0.88 m/s) and between nodes J-36 – J-37 and J-41–J-40 (v=0.76 m/s). The highest working pressure of 6.39 bar is found in the network at the node/consumer C-44 (a reducer valve is placed in front of it with a reduction of the working pressure of 3 bar) and the lowest working pressure is 2.74 bar at the node/consumer C-2 for the application of cast iron pipes with a roughness coefficient C=130 according to the Hazen-Williams criterion. Cast iron pipes, steel pipes and pipes made of synthetic material (PVC-polyvinyl chloride) were analyzed in the hydraulic calculations. Based on the hydraulic calculation the working pressures when using PVC pipes range from 2.75 to 6.45 bar. When calculating with PVC pipes, the roughness coefficient C=150 according to the Hazen-Williams criterion was used. When calculating with steel pipes (C=140) the maximum working pressure has a value of 6.40 bar and the minimum is 2.74 bar.

A sample of water consumption for fire fighting was created. To display such a scenario, it is necessary to define an alternative that represents a group of data and requirements for a certain part of the model (Figure 3).

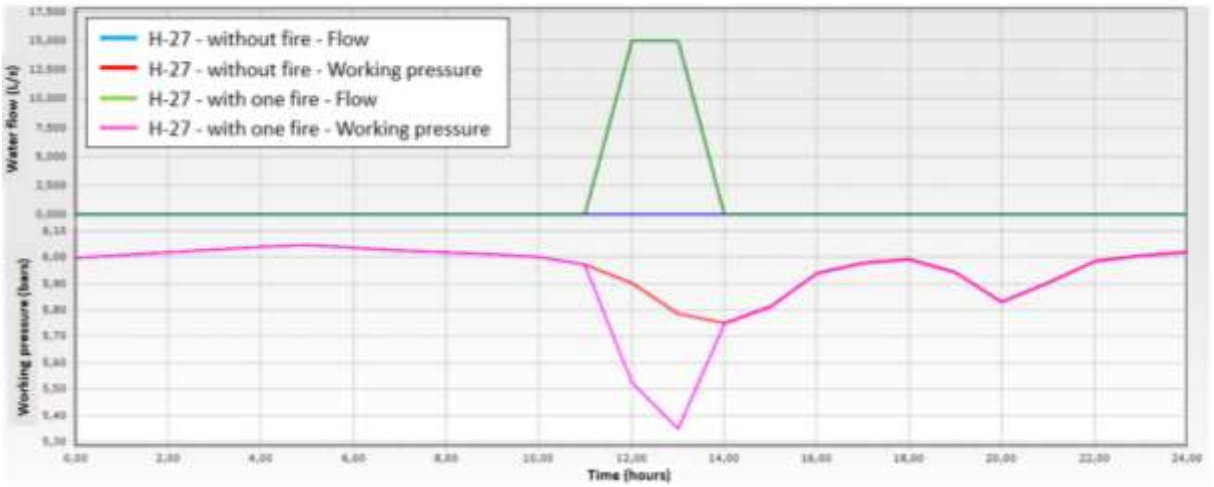

Figure 3. Water flow and working pressure diagram for hydrant H-27, Variant 1

Each created alternative can contain different requirements and data and thus enables the comparison of models in different situations and for differently defined features. Water consumption for fire extinguishing is determined with a value of 15 l/s for the population and 20 l/s for industry for

extinguishing a single fire. For such a scenario, it is necessary to define the water consumption for the farthest hydrant H-27 (a fire extinguishing sample was set at the time of maximum hourly water consumption), Figure 3 and 4.

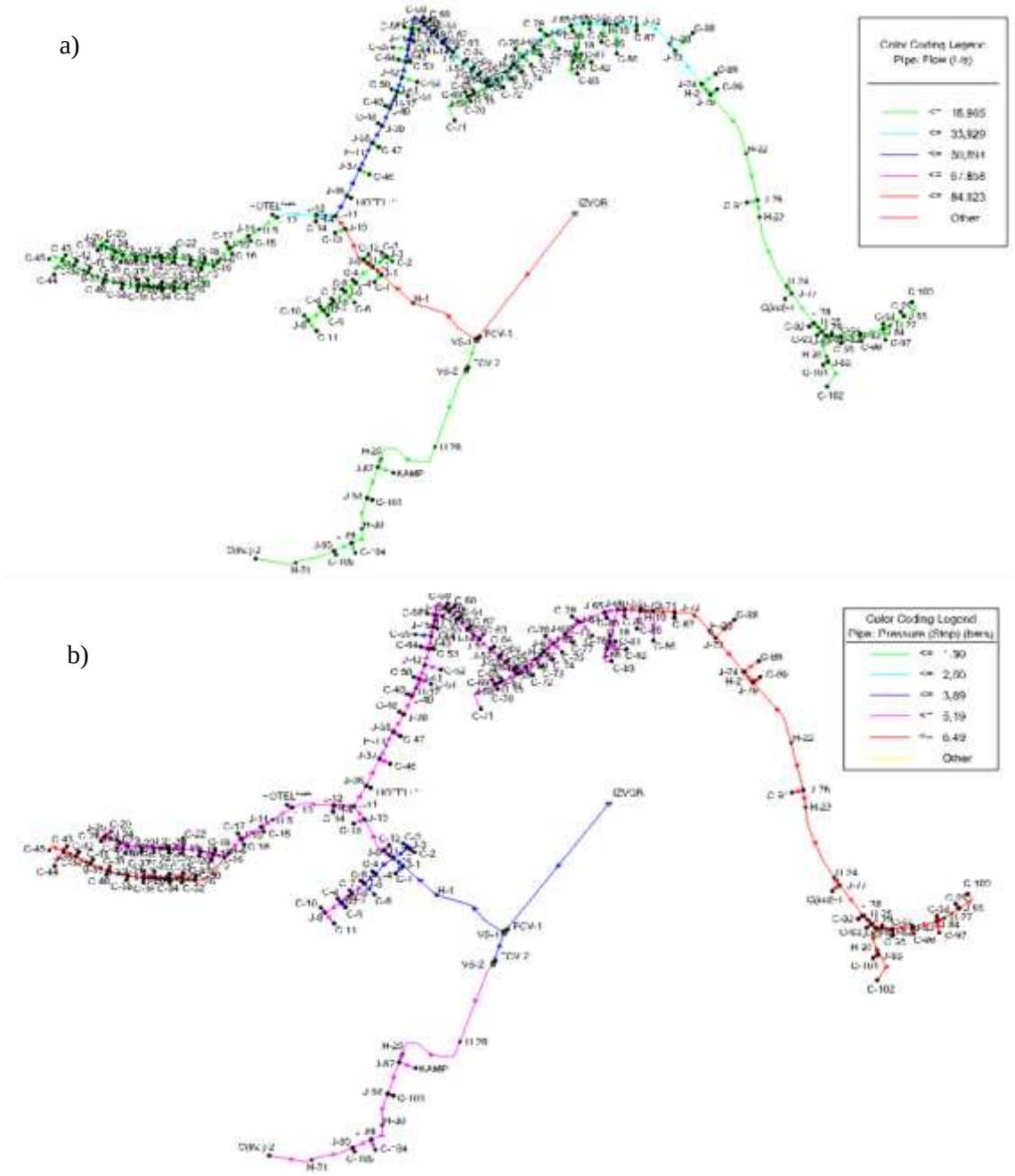

Figure 4. Display of changes in water flow (a) and working pressure (b) within the water supply system using the "Color Coding" option during the maximum hourly consumption (14h), Variant 1

After the analysis for the situation with one fire, the changes in speed and flow in the WSS can be observed which occur at the time of maximum hourly water consumption according to the defined fire pattern. Figure 3 shows the change in flow and working pressure at the H-27 hydrant due to the use of 15 l/s for extinguishing residential fires. On the diagram of flow and working pressure it can be seen that the working pressure decreases due to the increase in water flow. The WaterCad V8i computer program enables the display of the results of the analysis of individual physical quantities with colors, thus enabling a graphic and clear display of changes in flow, water velocity, working pressure and other

physical quantities within the entire modeled WSS, Figure 4. Through hydraulic analysis it is necessary to compare certain physical quantities in different periods of the day when water consumption is variable. The use of such displays provides a clear picture of the behavior of the WSS.

6.1.2 Variant 2 – Water Reservoir 1

Reservoir 1 in this variant is placed at an altitude of 126 m a.s.l. (Figure 1). The volume of Reservoir 1 is 3,019.07 m^3. Unlike the first variant, where a situation without a fire and with one fire was observed, in the second variant a situation with two simultaneous fires was included. The changes in the working pressures in the pipes due to the use of different pipe materials are observed. The calculation of the gravity flow of water in Reservoir 1 is carried out in the same way as in Variant 1. The maximum hourly water consumption occurs from 12:00 to 14:00 and takes into account the needs of the population, tourists and industrial plants. The highest water flow in the system has a value of 84.82 l/s.
The lowest velocities in the system occur for a pipe with a diameter of 200 mm and they occur on short sections where connections to consumers are made. The highest working pressure in the system is 6.41 bar (consumer C-44), and the lowest working pressure of 2.76 bar is present in the network at consumer C-2. Working pressures were obtained on the basis of cast iron pipes (*C*=130). Working pressures when using PVC pipes range from 2.77 to 6.43 bar (*C*=150). When calculating with steel pipes (*C*=140) the highest working pressure is 6.42 bar and the lowest is 2.76 bar.
In the second variant a new alternative was created where the scenario was observed during two simultaneous fires at the time of maximum hourly water consumption. The duration of the fire is defined according to the fire pattern, and it takes place between 12:00 and 14:00 when the need for water is the greatest. A water consumption of 15 l/s was defined for hydrant H-27 and a water consumption of 20 l/s for hydrant H-31 located immediately before the industry. Based on the created alternative „With two fires“, the water consumption is set for the furthest hydrant H-27 from Reservoir 1 and the hydrant H-31, which is the furthest from Reservoir 2. On hydrant H-31 it can be noted that the drop in operating pressure was recorded and after the maximum hourly water consumption due to the lowering of the water level in Reservoir 2, which has a smaller volume than Reservoir 1 (Figures 5 and 6). In Figure 6, one can see the increased output flow at the time of the occurrence of two simultaneous fires, when the maximum hourly water consumption also occurs.

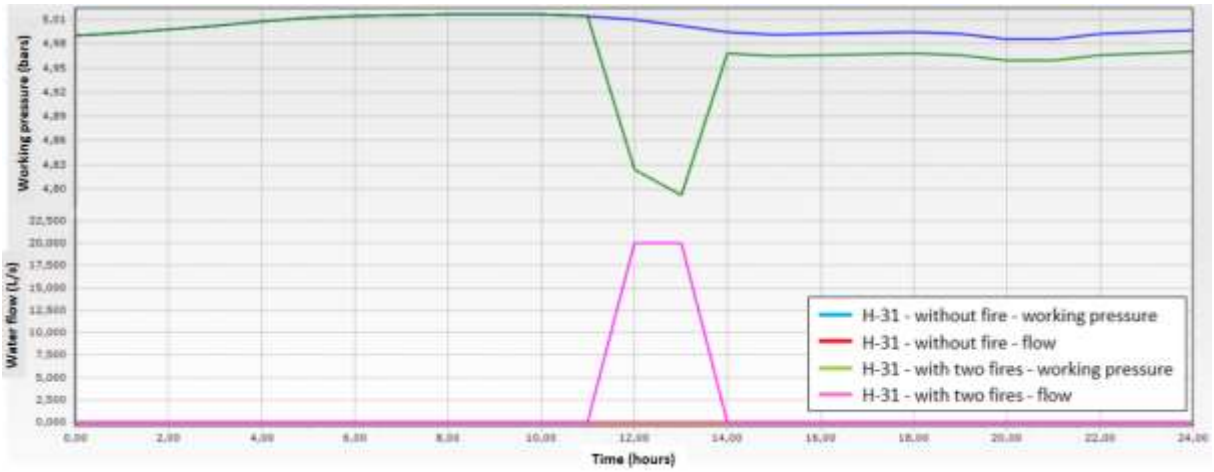

Figure 5. Display of water flow and working pressure change for hydrant H-31, Variant 2

At the same time, the percentage of water filling of the water chamber of Reservoir 2 just before the occurrence of the maximum hourly water consumption without the occurrence of a fire is approximately 77.5%. After the maximum hourly consumption of water without the occurrence of a fire, the water chamber is filled with water approximately 74.5%, while in the event of two simultaneous fires the percentage of filling the water chamber drops to approximately 65%.

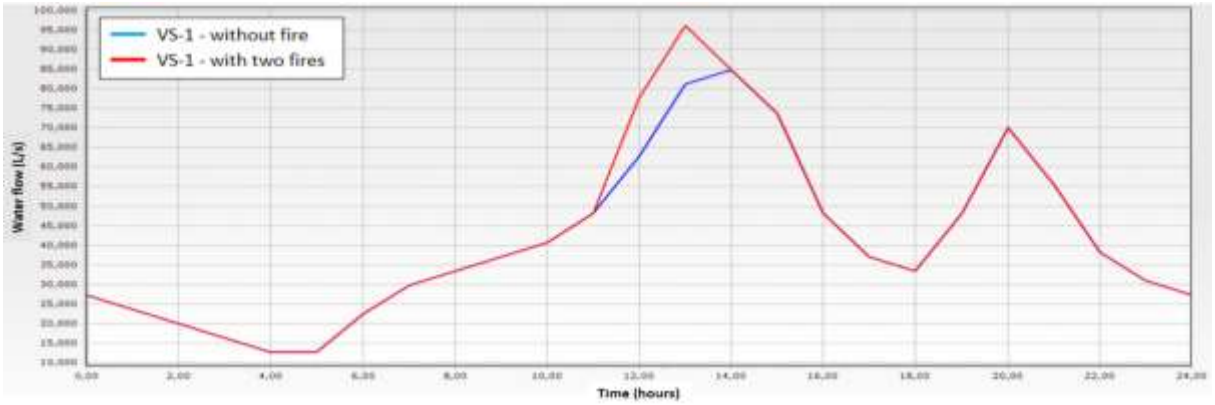

Figure 6. Diagram of output flow at the time of two simultaneous fires, Variant 2

6.1.3 Variant 3 – Water Reservoir 1

Water Reservoir 1 (124 m a.s.l., Figure 1) has a volume of 3,019.07 m^3. Variant 3 examines the case during three simultaneous fires and the behavior of the reservoir due to different water levels in it. Calculations were made for three different pipe materials (cast iron, PVC and steel pipes) and their influence on the change in operating pressures within the WSS was considered. The calculation of the gravity flow of water in Reservoir 1 is carried out for the maximum hourly consumption of water that occurs during the time of the highest demand for water. The maximum hourly water consumption occurs from 12:00 to 14:00 and takes into account the needs of the population, tourists and industrial plants. The highest flow in the system during the maximum hourly consumption is 84.9 l/s, which occurs on the section from the source to Reservoir 1. The highest flow velocities in the system for cast iron pipes (C=130) were recorded at 0.88 m/s. The highest working pressure is 6.24 bar, while the lowest is 2.59 bar. Working pressures when using PVC pipes (C=150) range from 2.61 to 6.28 bar. For PVC pipes the working pressures are slightly higher than when using cast iron and steel pipes. When calculating with steel pipes (C=140), working pressures range from 2.60 to 6.26 bar. Although the working pressures in the system are the lowest for cast iron pipes (2.59 bar), for Variant 3 it would be better to use steel or PVC pipes that have a higher coefficient of roughness (Figure 7).

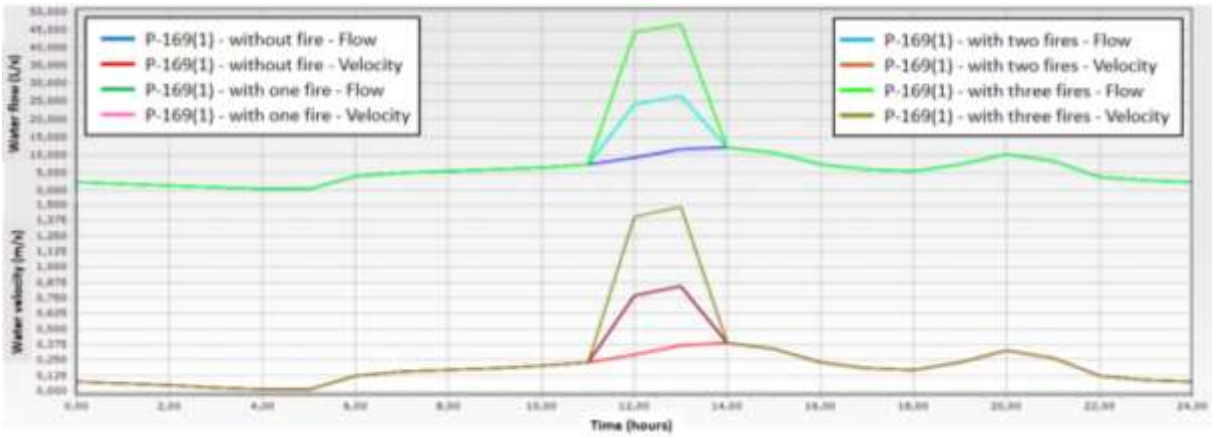

Figure 7. Diagram of water flow and velocity for section P-169(1), Variant 3

In the third variant a new alternative was created where the scenario for extinguishing three simultaneous fires at the time of maximum hourly water consumption is observed (between 12:00 and 14:00). After the analysis for the situation with three simultaneous fires, the sudden changes that occur at the time of the maximum hourly water consumption according to the defined pattern for the fire can be seen on the diagram of flow and flow rates (Figure 7).

7 Conclusion

The WaterCAD V8i computer program was used for the purposes of creating this paper, which proved to be an excellent tool for modeling and analyzing the WSS, but also effective in optimizing the WSS/WSN. In the work, three variants of the gravity WSN were implemented, depending on the disposition of the main water reservoir. Greater losses in the system and the installation of pipes with larger diameters result in more expensive investment construction and a greater need for system maintenance. Therefore, the second variant is more profitable, considering that there are smaller major losses on the route formed in this way compared to the first variant, and due to the shorter length of the newly formed section, the requirement for the installation of a pipe diameter of 250 mm is reduced from 13.93% (Variant 1) to 0.50% (Variant 2).
In all implemented sub-models of gravity water inflow in Reservoir 1, the highest output flow at the time of maximum hourly water consumption (12:00-2:00 pm) is equal to 84.82 l/s and the highest water flow velocities occur at the water outlet from Reservoir 1, while they appear least on derived connections for consumers. For each sub-model, alternatives are defined regarding the use of water for fire extinguishing and without the presence of fire. In the first sub-model, the situation without and with one fire was analyzed, in the second sub-model the situation without fire, with one and two fires, and in the third the situation without, with one, two and three simultaneous fires. During a fire, in accordance with the increased required flow on the hydrants, the working pressure decreases. For PVC pipe material, the working pressures are the highest in the system and when using cast iron pipes, the working pressures are the lowest. The differences in the minimum and maximum working pressures for different types of pipes are so insignificant that the choice of material would be of crucial importance when designing the system. The most optimal working pressures in the system were obtained in the variant where Reservoir 1 was placed at 124 m a.s.l. Through this paper, it is possible to further develop and study the behavior of the WSS through different scenarios and alternatives, as well as implement additional variants of simultaneous fires or find a more optimal period of time for the pumps to operate. A part of the branched network can be connected into a ring network, and in this way, a hydraulic analysis can be carried out on how the flow and working pressure are distributed in the water supply system.

References:

[1] Spatial plan of the Buzet City, Book I., Buzet, 2005. (https://www.buzet.hr/fileadmin/prostorni_plan/prostorni_plan_knjiga_I.pdf), downloaded on 5/22/2021.
[2] Zaninović, K.: Climate Atlas of Croatia 1961-1990, 1971-2000, http://klima.hr/razno/publikacije/klimatski_atlas_hrvatske.pdf , downloaded on 5/22/2021.
[3] Žic, E.: Calculation of relevant quantities of water, work materials for solving the program for Course „Water supply and water conditioning“, Faculty of Civil Engineering, University of Rijeka, 2020.
[4] Request for determination of the unified environmental protection conditions of the factory P.P.C. Buzet Ltd. (CIMOS) in accordance with the Regulation on the procedure for establishing unified environmental protection conditions (Narodne novine 114/08), Rev 1, Rijeka, August 2014.
[5] Lončarić, L.: In addition to making great beer, these Istrian brewers also send hidden messages with their imaginative labels, newspaper article, Jutarnji list, June 30, 2021.
[6] Water Distribution Modeling and Analysis Software, Bentley promotional materials, https://www.bentley.com/en/products/product-line/hydraulics-and-hydrology-software/watercad, downloaded on 13.8.2021.
[7] Water Distribution Modeling and Management, Bentley promotional materials, https://prod-bentleycdn.azureedge.net/-/media/files/documents/product-data-sheet/pds_watercad_ltr_en_hr.pdf?la=en&modified=20181030141022 , downloaded on 13.8.2021.

COMPARISON OF OPERATION ON THE WASTEWATER TREATMENT PLANT USING SBR AND MBR TECHNOLOGY

ELVIS ŽIC [1], JOHAN KLARIĆ [2], GORAN VOLF [1]

[1] *Faculty of Civil Engineering Rijeka, Radmile Matejčić 3, 51000 Rijeka, Croatia, elvis.zic@uniri.hr; goran.volf@uniri.hr*

[2] *Komunalac Delnice Ltd., 51300 Delnice, Croatia, jklaric11@gmail.com*

1 Abstract

The paper compares two technologies for wastewater treatment (WWT): Sequencing Batch Reactor (SBR) and Membrane Bioreactor (MBR). The SBR, which is used in Delnice (Croatia), is flexible and efficient and uses the activated sludge process. The MBR, which is used in Siffiano (Italy), combines activated sludge with membrane filtration and offers high treatment performance, especially for municipal and industrial wastewater. The study concludes that MBR has higher costs but better effluent quality when considering investment and operating costs, space requirements, complexity and performance.

Keywords: WWTP, Sequencing Batch Reactor (SBR), Membrane Bioreactor (MBR), Delnice City, Siffiano village, mechanical pretreatment, biological treatment, treatment of excess sludge, comparison.

2 Introduction

A realistic comparison of two WWT technologies, in this case SBR and MBR technologies, is presented on the example of built and functional wastewater treatment plants (WWTPs). In order for the comparison to be possible and realistic, it was necessary to find WWTPs of nearly capacity and input load that have been operating for many years, but of course with different technologies. Delnice WWTP has a capacity of 6,600 PE with SBR technology and Siffiano WWTP in Italy, autonomous province of Bolzano, has a capacity of 6,000 PE with MBR technology. It is necessary to establish certain criteria that will be used to evaluate the technologies. For them were used the criteria that are used when creating variant solutions, from investment and operational costs, through the spatial component, the complexity of control and processes to the final effect of treatment. The percentage of their share in the overall assessment was determined for each of the provided criteria. The WWT system with SBR and MBR technology is divided into mechanical pretreatment, biological treatment and treatment of excess biological sludge. Their work is described with reference to the requirements and specifics related to the applied technology and specific data on the costs required for the operation of the plant in the form of energy sources, process management and maintenance. WWTPs operate at different levels of treatment, which makes them incomparable in terms of operating costs, but for this paper this can be accepted.

3 Description of SBR and MBR wastewater treatment technologies

SBR technology (*eng. Sequencing Batch Reactor*) is one of the most commonly used technologies in the WWT system. This sequential batch reactor is a biological treatment process that works on the principle of activated sludge and dates back to the beginning of the 1900s. The biological processes of nitrification and denitrification take place in the same basin, which requires its larger volume, but that is precisely why it results in high efficiency and represents a flexible solution for large fluctuations in organic and hydraulic load. The biological process is designed in such a way that microorganisms such as bacteria, yeast and algae, and organisms such as protozoa and metazoa, which are associated with suspended substances with which they form flocs of activated sludge, break down organic and nutrient

substances in wastewater [1].
Membrane Bioreactor (MBR) represents technological progress in WWT and appeared in the 1960s. Despite the many shortcomings of the time, the development of membrane technology that uses activated sludge for treatment in combination with membrane filtration experienced its development in the 1980s in Japan [2]. The MBR system is essentially a suspended biomass reactor with a porous membrane on which the final result of WWT depends. Today, the application of the MBR process is present both in the treatment of municipal wastewater and industrial wastewater with a high degree of treatment. In order for the permeate or filtrate to pass through the pores on the membrane and for the concentrated dissolved substance (concentrate or retentate) to remain in the reactor, a force called transmembrane pressure is required [3].
SBR and MBR differ mainly in the way they work and the quality of production. With SBR, a single tank is used for all treatment phases in batch operation, which offers flexibility and user-friendliness for smaller systems. In MBR, biological treatment is combined with membrane filtration, allowing for continuous processing and excellent effluent quality with low suspended solids and pathogens, suitable for stringent standards and reuse. MBRs require more complex systems and higher costs, while SBRs are simpler and less expensive but have lower effluent quality.

4 Characteristics of the considered WWTPs

In order to get a better insight into the way SBR and MBR WWT technologies work, the operation of two plants that use the mentioned technologies will be presented. SBR technology is used for treatment at Delnice WWTP and MBR technology at Siffiano WWTP. These two plants were chosen for comparison due to similar characteristics such as size, geographical location and climate.
The city of Delnice is located in the central part of Gorski Kotar in the Primorje-Gorski Kotar County. At 698 m a.s.l. it is the highest city in Croatia with 3,861 inhabitants. The area of the city is 230 km^2 and the total number of inhabitants in all 55 settlements is 5,135. In its northeastern part is the Delnice WWTP (Figure 1). Due to the influence of climate change, there are increasing deviations from average temperatures, so in the last few years, summer temperatures can reach 30 °C. The area is characterized by a large number of rainy days with a high annual precipitation average of more than 2,000 mm. Delnice WWTP (Figure 1) is located on the very edge of Delnice city, only 50 m away from the nearest residential buildings on a separate plot of 7,496 m^2. WWTP load of 6,600 PE as it exists today was put into operation in 2017 as plant of II. degree of WWT with aerobic sludge stabilization [4].

Figure 1. Location of Delnice WWTP marked with a yellow arrow (Photo: Johan Klarić)

The village of Siffiano is located in the Republic of Italy, the region of Trentino-Alto Adige, the province of Bolzano and belongs to the municipality of Renon-Ritten from which the city center of Klobenstein is about 1.4 km away (Figure 2). Located at 936 m a.s.l. on a plateau with a beautiful view of the Dolomites, this small, lively village with a rich history has only 48 inhabitants. The area is characterized

by a moderate continental climate from the class of snow-forest climates characterized by harsh winters, short spring and warm and humid summer with maximum temperatures over 30 °C, a small number of rainy days per year and more than 300 sunny days per year.

Figure 2. Location of Siffiano WWTP marked with a yellow arrow (Photo: Johan Klarić)

The Siffiano WWTP (Figure 2) is located 250 m south of the Siffiano village in a depression of land that has been drained and developed for these purposes on a total area of 6,850 m^2. In addition to municipal water from the Siffiano village, the plant also treats wastewater from the capital of the municipality of Klobenstein and the small town of Lengmoos and the surrounding area. The original Siffiano WWTP with a capacity of 5,000 PE was built and put into operation in 1984 which decomposed wastewater in open aerated basins. In order to improve the functionality of the system, the technological equipment was renewed and upgraded over the years, so a new fine sieve was installed in 2000 and in 2001 new compressors for the WWTP with activated sludge. To improve the work and satisfy the legal regulations, the construction and commissioning of the WWTP with MBR technology (2009) with a capacity of 6,000 PE with a central sludge treatment plant proved to be the optimal.

5 Comparison of technologies through the work of the considered WWTPs

The comparison of the work of the described WWTPs will be considered through functional parts, that is segments of the technological process. The comparison of work is carried out according to the following units: mechanical pretreatment of wastewater, biological treatment of wastewater, and processing of excess biological sludge. In order to be able to compare technologies, it is necessary to set certain criteria that are evaluated to reach the final conclusion and assessment. The qualitative analysis includes the following parameters: investment costs (10% of the final assessment), operational costs (10%), spatial component (5%), complexity of control and processes (60%) and effects of WWT (15%). The analysis of investment costs and operating costs includes the financial aspect, whereby the final value and operating costs are taken for each WWTPs in a period of one year (2022), Table 1. The emphasis is on the comparison of two technologies that differ in the essential part, namely the technology of the process, so that this was given the greatest importance, which is clearly emphasized in the work. The evaluation was made according to experience and the general evaluation practice that is usually carried out when selecting the technology in the preparation and design phase. The aim of the comparison is to obtain a realistic representation of the differences between the technologies and the effects achieved on the basis of specific data and costs of the operator, which cannot be adequately represented in the selection of the optimal technology by variant solutions. Scoring of investment costs is determined according to the Eq. (1):

$$C_I = \frac{C_n}{C_v} \cdot 50 \tag{1}$$

which is used when scoring the most economically advantageous offer in the public procurement process. The C_I number represents the number of points for the considered technology, C_n is the lower

investment cost of the two technologies, C_v is the investment cost of the technology for which the calculation is made, and 50 is the maximum number of points that can be achieved for this parameter.

Table 1. Scoring method for the investment cost parameter

Technology	Investment cost (€)	Number of points (0 – 50)
SBR (Delnice WWTP)	2,073,627.31	0 – 50
MBR (Siffiano WWTP)	2,428,623.38	0 – 50

Scoring of operating costs is determined according to the same principle as for investment costs according to the Eq. (2):

$$C_O = \frac{C_n}{C_v} \cdot 50 \tag{2}$$

where C_O is the number of points for the considered technology, C_n is the lower operating cost of the two technologies, C_v is the operating cost of the technology for which is calculated, and 50 is the maximum number of points (Table 2).

Table 2. Scoring method for the operating cost parameter

Technology	Operating cost (€/year)	Number of points (0 – 50)
SBR (Delnice WWTP)	79,868.00	0 – 50
MBR (Siffiano WWTP)	129,992.00	0 – 50

For the comparison, inflation was taken into account due to the time lag in construction, which according to statistical data corresponds to the difference in standard, and the real investment costs were treated. For the comparison of values, it should be noted that WWTP was built and put into operation within 8 years, Siffiano in 2009 and Delnice in 2017. If we take into account the difference in the contract period from 2006 to 2014, the inflation rate in Italy was about 13%, but there is also a real difference in the standard and thus in the value of goods and services between Italy and Croatia. It can be said that the investment values are realistically comparable. The spatial component for WWTP is partly related to construction costs, because the need for larger land and facilities implies higher investment costs. Therefore, this parameter includes the spatial aspect in the form of the area occupied by the objects, the terrain configuration and other relevant spatial components and possible limiting factors (Table 3).

Table 3. Scoring method for the spatial component parameter

Criterion	SBR (Delnice)	MBR (Siffiano)
Built-up area (0 – 10)	0 – 10	0 – 10
Required volume/area of objects (0 – 20)	0 – 20	0 – 20
Communications and layout of facilities (0 – 20)	0 – 20	0 – 20
Total (0 – 50)	0 – 50	0 – 50

A very important parameter that is considered is the complexity of the control and process, given that it requires many other prerequisites and requirements, such as the professional training of the staff, the degree of possible automation, technological specifics etc. (Table 4 and 5).

Table 4. Scoring method for the control and process complexity parameter

Criterion	SBR (Delnice)	MBR (Siffiano)
Mechanical pretreatment (0 – 5)	0 – 5	0 – 5
Sensitivity to variations in the input hydraulic load (0 – 5)	0 – 5	0 – 5
Sensitivity to variations in input organic load (0 – 5)	0 – 5	0 – 5
Simplicity of managing the process (0 – 5)	0 – 5	0 – 5
Automation of work (0 – 5)	0 – 5	0 – 5
Impact of floating sludge (0 – 5)	0 – 5	0 – 5
Production of excess sludge (0 – 5)	0 – 5	0 – 5
Sludge dehydration (0 – 5)	0 – 5	0 – 5
Appearance of unpleasant odors (0 – 5)	0 – 5	0 – 5
Scope of maintenance work (0 – 5)	0 – 5	0 – 5
Total (0 – 50)	0 – 50	0 – 50

Table 5. Scoring method for the WWT effect parameter

Criterion	SBR (Delnice)	MBR (Siffiano)
Effluent quality (0 – 35)	0 – 35	0 – 35
Percentage of removal of suspended matter (0 – 5)	0 – 5	0 – 5
Percentage of COD removal (0 – 5)	0 – 5	0 – 5
Treatment percentage of BOD_5 (0 – 5)	0 – 5	0 – 5
Total (0 – 50)	0 – 50	0 – 50

5.1 Mechanical pretreatment

The wastewater at Delnice WWTP is brought to the automatic coarse screen through a DN 400 mm supply pipeline. The clear opening between the bars of the coarse screen with a clear opening between the bars of the grating with s = 20 mm is intended to retain and separate a larger part of the larger waste found in the wastewater and thus prevent possible blockages in the further stages of treatment. The capacity of the automatic coarse screen is Q_{max}=80 l/s due to larger amounts of wastewater and larger waste due to the inflow of rainwater during the rainy season [5]. Next to the automatic clear opening between the bars of the coarse screen is a compact unit for receiving the contents of septic tanks and black pits. On the fine automatic coarse screen of the clear opening between the bars of the coarse screen of the input drum with s=6 mm, larger content as well as some sand and grease are retained. The pumping station is equipped with a mixer with a propeller to prevent the accumulation of organic substances on the walls of the pumping station [5]. The complete wastewater and the medium left after treatment on the automatic clear opening between the bars of the coarse screen goes by gravity to the inlet pumping station. There, pumping aggregates with individual capacity Q=60 l/s in alternating operation take it to a compact plant for mechanical pretreatment. The compact unit consists of a fine sieve with a press, a clear opening between the bars of the coarse screen of the input drum with s=3 mm, an extended aerated grit chamber and grease trap, and an inclined spiral conveyor that transports the separated sand from the medium. A large number of moving and rotating elements, as well as pumping units, require constant control, management and cleaning which affects operating costs (Table 6).

Table 6. Operating costs of mechanical pretreatment of Delnice WWTP and Siffiano WWTP

Charge	Delnice WWTP [€/year]	Siffiano WWTP [€/year]
Energetics	7,685.00	3,253.00
Process management	3,410.00	2,184.00
Maintenance and other	11,881.00	7,877.00
Total	22,976.00	13,314.00

The price of electricity in Italy and Croatia is of course not the same, and the comparison is made in kWh. When analyzing the operating costs of Siffiano WWTP, the costs of III. the degree of treatment and the costs of processing sludge from other WWTPs were taken into account. In order to present the costs realistically, a price per kilowatt hour (kWh) was used for electricity costs (which is by far the largest operating cost), i.e. the price applicable in the Croatia. In the calculation of personnel costs at Siffiano WWTP, they were also reduced due to the real difference in the level of personal income in the two countries. For the other costs considered, there are no major price differences between the two countries, so any difference in the calculation is considered negligible.

It should be noted that the mechanical WWT at the Siffiano WWTP is not fundamentally different from that at the Delnice WWTP, but the water pipeline is laid differently and is entirely by gravity, so the entire volume of wastewater does not have to be pumped. The grit and grease separation technology used is also classic with an open basin, which primarily saves on electricity consumption compared to the compact mechanical pre-treatment system installed in Delnice.

With regard to Siffiano WWTP wastewater from settlements included in the local public drainage system is brought to the location of WWTPs through a supply pipeline of DN 315 mm profile. The mechanical treatment process begins on a fine sieve dimensioned for maximum rain inflow Q=60 l/s. A fine sieve with a basket profile press of 800 mm was installed, which serves to separate organic and inorganic waste larger than 2 mm, which performs four work processes simultaneously in that integrated unit (sieving, transfer, washing and drainage and disposal). The waste collected on the fine sieve is

deposited in bags, and the wastewater is sent by gravity for further treatment to the building of sand pits and grease trap designed for a maximum flow of *Q*=25 l/s. The separation of sand and inert material is provided by an aerated longitudinal sand catcher, which is constructed as a rectangular longitudinal tank with a conical bottom 12.00 m long, 2.30 m wide, 2.05 m water deep. In the aerated basin, the sand is deposited, while in the still one, the floating fat is collected and separated by a self-propelled scraper with two blades. The maximum hydraulic load is *Q*=13.3 l/s in normal operation and *Q*=18 l/s short-term. To compensate for the maximum daily amount of precipitation, a rain basin with a capacity of 750 m^3 was built, which collects all the daily amount of wastewater that cannot be processed in normal operation. When it rains, the plant together with the buffer can absorb a daily amount of wastewater of 2,021.32 m^3 [6]. At WWTP there is also a station for receiving faeces from septic tanks and collection pits of households which are brought by special vehicles and emptied into an underground tank (capacity 13.8 m^3).

5.2 Biological treatment

After mechanical pretreatment, wastewater from Delnice WWTP is collected together with the filtrate of the spiral press from mechanical sludge dehydration, water from the "wet" scrubber for gas treatment during sludge dehydration with lime and water from the filtering drum of the press in the pumping station in front of the SBR reactor. The pumping station is equipped with two pumping units *Q*=45 l/s that work alternately filling the reactors in automated operation depending on the processing process [5]. The dimensions of the SBR reactor were obtained by dimensioning for the process with activated sludge with simultaneous aerobic stabilization of the sludge and occasional denitrification in accordance with the German norms ATV-DVWK-A 131-Dimensioning of Single-Stage Activated Sludge Plants (05/2000) and DWA-M210-Aeration plants with dam operation (SBR) (07/2009). The length of the SBR reactor is 20.55 m, the width is 14.00 m, the maximum water level is 6.00 m and the volume of one basin is 1,726.00 m^3. Due to the higher organic load of the incoming wastewater (BOD_5=566.81 mg/l) and the necessary treatment of the contents of septic tanks and black pits where the decomposition of organic matter is slower (BOD_5=1,000-20,000 mg/l), in two SBR reactor, a water treatment cycle lasting 8 hours was selected (application of SCADA program). Three blowers were installed to supply air to the SBR reactors. Biological treatment of wastewater is the most demanding and complex stage of treatment within SBR technology (Table 7).

Table 7. Operating costs of biological treatment of Delnice WWTP and Siffiano WWTP

Charge	Delnice WWTP [€/year]	Siffiano WWTP [€/year]
Energetics	20,260.00	50,746.00
Process management	11,083.00	16,378.00
Maintenance and other	8,923.00	20,155.00
Total	40,266.00	87,279.00

The biological treatment unit of the Siffiano WWTP consists of an underground open denitrification basin (DEN zone) and a biological basin with activated sludge and closed basins for membrane units (MBR basin), a basin for temporary storage and return from sludge dewatering, a floating sludge shaft and engine rooms. The optimal dimensions of the biological treatment unit (length 21.70 m, width 13.00 m, basin depth 5.50 m, water depth 4.07-4.55 m) were obtained by calculating the maximum hydraulic load *Q*=13.3 l/s in normal operation and *Q*=18 l/s in short-term. The process of biological treatment begins in the denitrification basin, where wastewater after mechanical treatment, recirculation from the MBR basin, supersludge water from the sludge tank and excess water after dehydration of the sludge are fed. The DEN zone is an anoxic zone, and it consists of one basin with a volume of 150.12 m^3 in which a mixer with a built-in drive motor is installed to maintain complete suspension and mix the contents of the basin [6]. The wastewater is drained by gravity into the nitrification zone, which consists of two lines of aerated basins with a volume of 2*177.05 m^3. The optimal concentration of activated sludge in the treatment process with MBR technology is 10 g/l, based on which the volume of the complete biological unit is dimensioned. Part III. of the WWT stage is the chemical removal of phosphate, which is also carried out in the aeration basin by direct addition of a solution of iron chloride

($FeCl_3$). By calculating for an average daily wastewater inflow of 540 m^3/day, the total required filter area (membrane) of 1,920 m^2 was obtained [6].

5.3 Processing of excess biological sludge

At Delnice WWTP the excess sludge after the process in the SBR reactors is pumped out into the excess sludge tank with a capacity of 65.10 m^3, which is dimensioned based on the daily excess sludge, its daily inflow and volume per cycle, and the concentration of dry matter in the separated sludge [5]. The sludge separated into the tank from the biological treatment process is aerobically stable, before further processing it does not need to be additionally thickened, but only homogenized, which is done with an immersed mixer-aerator. The capacity of the spiral press is Q=7.50 m^3/day, which turned out to be much more than necessary, because on average about 3.00 m^3/day (max. 5.00 m^3/day) is processed at Delnice WWTP, Table 8. The final treatment of mechanically dehydrated sludge is stabilization with micronized quicklime (CaO) in a contact reactor, which completely destroys any pathogenic organisms remaining in excess sludge. The concentration of dry matter in the produced sludge is from 25% to 30%.

Table 8. Operating costs of treatment of surplus biological sludge of Delnice WWTP and Siffiano WWTP

Charge	Delnice WWTP [€/year]	Siffiano WWTP [€/year]
Energetics	6,986.00	11,060.00
Process management	2,558.00	3,276.00
Maintenance and other	7,082.00	14,993.00
In total	16,626.00	29,329.00

At Siffiano WWTP the excess sludge is drained through a pressure pipeline towards the central sludge treatment system into a 350 m^3 excess sludge tank. Digested and settled sludge from all surrounding settlements is brought to Siffiano WWTP via tanks in liquid form, where it is emptied into an underground collection tank with a volume of 25 m^3. During the construction of the Siffiano WWTP, it is planned that the plant will annually process about 1,300 m^3 of sludge from the surrounding WWTPs and 1,500 m^3 of sludge from the Siffiano WWTP, which makes a total of 2,800 m^3/year, resulting in about 450 m^3 of dehydrated sludge per year [6]. Sludge is pumped from the sludge tank to dehydration, which is done with a centrifuge along with polyelectrolyte dosing, and the sludge piping system is designed to process 100 m^3/day of sludge with 2-5% dry matter. After processing with a centrifuge the concentration of dry matter in the dewatered sludge is 25-30% (Table 8).

5.4 Results of the work of the considered WWTPs

Regardless of the fact that Siffiano WWTP has III. degree of treatment, for an optimal comparison were considered the parameters of II. degree of treatment. Permitted WWT parameters in the Croatia are defined by the *Ordinance on limit values for wastewater emissions* [7], where, in accordance with the *Decision on Designation of Sensitive Areas* [8], the Delnice City is within the water area of the Danube River (Table 9).

Table 9. Required output parameters of II. degree of treatment of Delnice WWTP [5,7]

Parameter	Maximum allowed concentration	Minimal input load reduction
Total suspended solids (SS)	35 mg/l	75%
Biochemical oxygen consumption (BOD_5)	25 mg/l	70%
Chemical consumption of oxygen (COD)	125 mg/l	90%

Analyzes have proven that during the summer months, when the delivery of content is more intensive, the input organic load increases several times. Despite this, all the parameters of the outgoing wastewater are lower than the maximum allowed concentration for the reference year 2022 (Table 10).
With regard to the Siffiano WWTP *Provincial Law* of June 18, 2002, No. 8 "Regulation on water" stipulates that all WWTPs with a capacity greater than 2,000 PE must be subject to II. degree of treatment that enables compliance with the limit values of emissions from the same law (Table 11).
Siffiano WWTP was put into operation in 2009, since then influent and effluent analyzes have been carried out and parameters for sensitive areas have been monitored in accordance with regulations. Due

to the established III. degree of treatment by MBR technology, there is no obligation to monitor the total suspended matter, so the amount less than 1 mg/l is taken as the output parameter. All parameters of the effluent (2022 year) are lower than the maximum allowed concentration (Table 12).

Table 10. The results of the analyzes for Delnice WWTP in 2022

Parameter [mg/l]	03/2022		06/2022		09/2022		12/2022		%
	input	output	input	output	input	output	input	output	
SS	281	9.2	1,086	2	399	4.1	81	7.9	96.44
BOD_5	460	7.0	4,800	5	750	4.0	150	5.0	98.63
COD	746	36.0	7,424	30	1,195	30.0	336	30.0	95.83

Table 11. Required output parameters for Siffiano WWTP [6]

Parameter	Maximum allowed concentration	Minimal input load reduction
Total suspended matter, SS	35 mg/l	90%; input > 350 mg/l
Biochemical consumption of oxygen, BOD_5	25 mg/l	90%; input > 300 mg/l
Chemical consumption of oxygen, COD	100 mg/l	80%; input > 500 mg/l
Total phosphorus, P	2 mg/l	80%; input > 10 mg/l
Total nitrogen, N	15 mg/l	70%; input > 50 mg/l
Ammonium nitrogen, NH_4-N	8 mg/l for T 12 °C, 12 mg/l for T 10 °C	-

Table 12. Results of analyzes for Siffiano WWTP in 2022

Parameter	Input	Output	Reduction [%]
Total suspended matter, SS	30 – 170	< 1.0	99.80
Biochemical consumption of oxygen, BOD_5	386	2.7	99.30
Chemical consumption of oxygen, COD	687	19.8	97.12
Total phosphorus, P	7.14	0.66	90.76
Total nitrogen, N	62.8	15.4	75.48
Ammonium nitrogen, NH_4-N	49.6	3.46	93.02

5.5 Evaluation of treatment technologies and comparison

For the reconstruction of the Delnice WWTP and the establishment of SBR WWT technology the investment cost for all the necessary works in order to achieve full functionality was 2,073,627.31 € without VAT, while for the construction of the Siffiano WWTP with MBR technology it was necessary invest 2,428,623.38 € without VAT. The number of points for the investment value in the process of this analysis for Delnice WWTP is

$$C_I = 2{,}073{,}627.31/2{,}073{,}627.31 \cdot 50 = 50.00 \quad (3)$$

while for Siffiano WWTP it is

$$C_I = 2{,}073{,}627.31/2{,}428{,}623.38 \cdot 50 = 42.69 \quad (4)$$

According to the values of each individual investment as well as the number of achieved points in the parameter of investment costs, it can be concluded that the establishment of MBR technology (Siffiano WWTP) and without taking into account elements III. degree of treatment is expectedly more expensive than the establishment of SBR technology.

According to data for the 2022 obtained from the operator, operating costs for Delnice WWTP amount to 79,868.00 €, while 129,992.00 € was spent on the operation and maintenance of Siffiano WWTP. The cost of electricity is the biggest operating cost. For Delnice WWTP the value of C_o amounts to

$$C_o = 79{,}868.00/79{,}868.00 \cdot 50 = 50.00 \quad (5)$$

was calculated, that is, for Siffiano WWTP the value of C_o amounts to

$$C_o = 79{,}868.00/129{,}992.00 \cdot 50 = 30.72 \quad (6)$$

It can be seen that the operating costs of Siffiano WWTP are significantly higher than the operating costs of Delnice WWTP and therefore a solar power plant (30% of own production) was built at the location of Siffiano WWTP.

When considering the surfaces of the buildings, the difference in the biological process between the applied SBR and MBR technology comes to the fore, while there are no significant differences in the mechanical part and sludge treatment (Table 13).

Table 13. Display of scoring for the spatial component parameter

Criterion	SBR (Delnice)	MBR (Siffiano)
Built-up area (0 – 10)	10	10
Required volume/area of objects (0 – 20)	10	20
Communications and layout of facilities (0 – 20)	18	20
Total (0 – 50)	38	50

With SBR technology, the total required volume of SBR reactors in which the entire process takes place is 3,452 m^3 compared to 807.74 m^3 in Siffiano (including all units and stages of biological treatment). Therefore, the MBR technology requires a smaller space and volume of the WWT basin (Table 13).
Analyzing the description of the work of the two WWTPs it can be said that each has almost the same processing elements, fully fulfilling its assigned function, but for the most part through different technical solutions. The difference is in the phase of separation of sand and grease, where at Delnice WWTP the fine sieve is placed in the unit of mechanical pretreatment, while in Siffiano it is separated, with the aerated grit chamber and grease trap being a separate building. The result of the chosen technology is increased energy consumption and more demanding maintenance in the Delnice WWTP. The increased hydraulic load at the Delnice WWTP has a negative effect on the biological processes in the basins. On the example of MBR technology, this problem is solved with a buffer (rain basin) which is able to temporarily receive a larger amount of inflow while regulating the pressure on the membranes and thus increase the capacity (while increasing the costs). SBR technology in its biological process is not so flexible to increase the organic load, because it has a younger sludge and a lower concentration (about 4 g/l). Looking at the process at both WWTPs it can be seen that the production of sludge is approximately the same. Dehydration of sludge at both WWTPs gives good results and after technological treatment the concentration of dry matter is on average 25-30%. Both technologies are highly efficient and the final result (Table 14.) favors the MBR technology.

Table 14. Display of scoring for the control and process complexity parameter

Criterion	SBR (Delnice)	MBR (Siffiano)
Mechanical pretreatment (0 – 5)	4	5
Sensitivity to variations in the input hydraulic load (0 – 5)	3	4
Sensitivity to variations in input organic load (0 – 5)	4	5
Simplicity of managing the process (0 – 5)	4	3
Automation of work (0 – 5)	5	5
Impact of floating sludge (0 – 5)	4	5
Production of excess sludge (0 – 5)	5	5
Sludge dehydration (0 – 5)	5	5
Appearance of unpleasant odors (0 – 5)	5	5
Scope of maintenance work (0 – 5)	5	4
Total (0 – 50)	44	46

On the example of both WWTPs it is evident that with proper management of the process, both SBR and MBR technology can meet the parameters of WWT prescribed by law. From the analysis of the work of Siffiano WWTP it is evident that the results of all required parameters for shade are better than those in Delnice WWTP, which is attributed to the installed MBR technology (Table 15).

Table 15. Scoring display for the refinement effect parameter

Criterion	SBR (Delnice)	MBR (Siffiano)
Effluent quality (0 – 35)	35	35
Percentage of removal of suspended matter (0 – 5)	4	5
Percentage of COD removal (0 – 5)	4	5
Treatment percentage of BOD_5 (0 – 5)	4	5
Total (0 – 50)	47	50

Regarding the technological process of WWT (Table 16), MBR technology ultimately has a kind of advantage, but it is conditioned by higher investment costs, higher consumption of electricity and more demanding maintenance.

Table 16. Calculation of the final evaluation of the technology comparison

Parameter	Parameter coefficient	SBR points (Delnice)	MBR points (Siffiano)	Rating SBR (Delnice)	Rating MBR (Siffiano)
Investment cost	0.10	50.00	42.69	5.00	4.27
Operating cost	0.10	50.00	30.72	5.00	3.07
Spatial component	0.05	38.00	50.00	1.90	2.50
Control and process complexity	0.60	44.00	46.00	26.40	27.60
Purifying effect	0.15	47.00	50.00	7.05	7.50
Total	**1.00**	**229.00**	**216.58**	**45.35**	**44.94**

6 Conclusion

The analyzes of the effluent of Siffiano WWTP related to II. degree of treatment show slightly higher percentages of treatment, although both technologies show treatment values lower than the minimum allowed concentrations. The reasons for such results of the work of Siffiano WWTP are certainly to be found in the MBR technology, where with regular maintenance of the membranes in the effluent, it is practically impossible to find a concentration of suspended matter higher than 1 mg/l. Perhaps this is the key difference in process management compared to SBR technology, where the responsibility rests on the knowledge and ability of the WWT operator to keep the organic load and suspended matter in the effluent within the permitted concentrations.

In accordance with the applicable legal regulations for II. degree of treatment in Italy, which is almost equal to the one in Croatia, SBR technology would provide the required results with a significant reduction in operational labor costs. On the other hand, MBR technology would be applicable at the Delnice WWTP, where probably the biggest intervention would be in terms of construction due to the necessary construction of an equalization basin. In terms of environmental protection, only negligible amounts of chemicals are used, more precisely as much as is necessary for the process to achieve a high-quality and desired result. The situation is similar at Siffiano WWTP, where more chemicals are used due to the third degree of WWT, although these costs and this process are excluded from the comparison. Chemicals are part of the process and unavoidable, and anyone can determine from experience which chemicals are optimal and in what quantities. Due to the high electricity consumption at the Siffiano WWTP, a solar power plant was built to cover 30% of the total annual electricity consumption, i.e. around 400,000 kWh. SBR and MBR systems are used worldwide, from cold regions (where low temperatures can affect biological activity) to warm, humid climates (which can increase the risk of odor and operational problems). These systems are generally adaptable, but their design and operating parameters often need to be tailored to the specific environmental conditions to maintain efficiency.

References:

[1] Felber, H., Fischer, M.: Handbook for technical managers of wastewater treatment plants, 17th edition, edited by F. Hirthammer, Zagreb, 2014.
[2] Stephenson, T., Judd, S., Jefferson, B., Brindle, K.: Membrane Bioreactors for Wastewater Treatment, IWA Publishing, London, 2000.
[3] Mijatović, I., Matošić, M.: Water technology (internal script), Faculty of Food and Biotechnology, University of Zagreb, updated edition, Zagreb, 2020.
[4] ECOINA Ltd.: Conceptual project for choosing the optimal variant of the reconstruction of Delnice WWTP, Zagreb, 2009.
[5] PRONGRAD BIRO Ltd.: Amendment and addition to the main project "Reconstruction of Delnice WWTP", Folder 1-14, Zagreb, 2015.
[6] H&T PlanungsBüro: Neubau Kläranlage Siffian, Anlagenbemessung zur Abwasserreinigung A1.1, H&T PlanungsBüro, Bozen, 2006.
[7] Ordinance on limit values for wastewater emissions (Narodne novine 26/2020), Ministry of Environmental Protection and Energy, Narodne novine, Zagreb, 2020.
[8] Decision on Designation of Sensitive Areas (Narodne novine 79/2022), Government of the Republic of Croatia, Narodne novine, Zagreb, 2022.

PREDICTION OF E. COLI BACTERIA ON DRINKING WATER TREATMENT FACILITY BUTONIGA

GORAN VOLF [1], IVANA SUŠANJ ČULE [1], ELVIS ŽIC [1], SONJA ZORKO [2]

[1] *Faculty of Civil Engineering, Department of Hydraulic engineering, University of Rijeka, Croatia, goran.volf@uniri.hr, isusanj@uniri.hr, elvis.zic@uniri.hr*

[2] *Istarski Vodovod d.o.o. Buzet, Croatia, sonja.zorko@ivb.hr*

1 Abstract

The microbiological quality of the water is a critical factor influencing the convergence of human, animal, and environmental health. In this research, the machine learning algorithm M5P for induction of model trees integrated into the WEKA modelling software is used to predicted E. coli bacteria concentrations with a seven-day time step. Obtained model for prediction of the E. coli bacteria seven days in advance, in the form of a model tree, has ten equations from which the abovementioned concentrations of E. coli bacteria seven days in advance can be calculated. The model does not have so high correlation coefficient with a value of 0.48 and has also low prediction of peak values. Model has good prediction of concentrations up to 100 CFU/100 ml, while higher values are under forecast. The reason for this is that high values have a high probability expectation. Regardless of, obtained model through the prediction of E. coli bacteria can help to manage certain drinking water treatment processes depending on the biological quality of raw water in the Butoniga reservoir.

Keywords: E. coli bacteria, prediction models, machine learning, drinking water treatment facility Butoniga, microbiological water quality.

2 Introduction

Drinking water treatment facilities (DWTFs) are essential facilities designed to generate clean, high-quality water for human consumption at an affordable cost, adhering to established standards and public health regulations. Consequently, DWTFs play a crucial role in ensuring the reliable provision of ample and safe drinking water to the community [1].

The microbiological quality of the water is a critical factor influencing the convergence of human, animal, and environmental health. Collaborative endeavours persist in exploring methodologies for the monitoring, prediction, and management of microbiological water quality. However, the escalating pace of human activities, exemplified by urbanization and industrialization, has significantly disrupted environmental equilibrium. Aquatic systems endure most of this disturbance, thereby imperilling the microbiological integrity of water bodies through the influx of untreated domestic wastewater and other anthropogenic discharges [2].

Among the array of indicators employed to evaluate water quality, Escherichia coli (E. coli) emerges as a pivotal bacterium, acting as a marker for faecal contamination in water systems. The detection of E. coli bacteria signals the potential presence of pathogenic microorganisms, posing health hazards to individuals who consume the water [3].

Machine learning (ML) methods possess the capability to track the progression of water quality, analyse and forecast its condition, and uncover the migration and alteration of pollutants. This capability enables a transition from addressing present issues to proactively identifying risks and dynamically enhancing facilities [1].

Some applications of ML can be seen in research made by Khan et al. [4] which used superposition learning-based model (artificial neural network-ANN) for prediction of E.coli in groundwater using physiochemical water quality parameters. Their results show that the model having Turbidity, pH, Total Dissolved Solids (TDS), and Electric Conductivity (EC) as inputs displayed the best performance R. values of 0.90 and lowest MSE values of 0.0892. Sokolova et al. [5] for predicting microbial water quality in the drinking water source using E. coli monitoring and hydrometeorological data with data-driven models. Their study showed that models which included multiple predictors, i.e. VAR, LASSO Regression, Random Forest, TPOT, performed better than univariate models, i.e. Naive baseline, Exponential Smoothing and ARIMA. Also, external predictors increased the model performance, indicating that some of these models are informative for forecasting E. coli concentration at the water intake.

This study is an extension of the research done by Volf et al. [6, 7, 8] and deals with the development of prediction models for concentrations of E. coli bacteria in Butoniga reservoir. In study made by Volf et al. [6] ML method in form of rule-based models was applied on data measured at intake of raw water from Butoniga reservoir to predict Water Quality Index (WQI) one, five, ten and fifteen days in advance. Predictions of WQI are done according to current values of measured parameters at intake of raw water. Obtained models have high correlation coefficients and gives accurate predictions of WQI correctly predicting the peak values when compared to calculated data of WQI. As expected, the highest correlation coefficient has one day prediction, followed by five, ten and with the lowest correlation coefficient fifteen days prediction. In research made by Volf et al. [7] prediction models for Mn, Fe and NH_4 concentrations in raw water for seven days in advance were built with use of ML method in form of the model trees, which was applied on measured data for the DWTF Butoniga. Models were built to cope with problem of high concentrations of Mn, Fe and NH_4, which occurs during summer months, when higher chemical consumption is required for treatment processes and when water is captured from the lowest water intake, i.e. the lowest water layer in the Butoniga reservoir. Predictions of the Mn, Fe and NH_4 are done according to current values of measured parameters at the intake of the raw water. Obtained models have high correlation coefficients and thus provide accurate predictions of the Mn, Fe and NH_4, including the predictions of the peak values when compared to measured data. In a study conducted by Volf and Zorko [8], analysis revealed that turbidity exhibited the highest correlation coefficient and was identified as a potential indicator for E. coli bacteria. This suggests that elevated turbidity levels generally correspond to higher concentrations of E. coli bacteria. Additionally, parameters such as Mn, Fe, and UV254 were found to be closely associated with E. coli bacteria, alongside turbidity. Furthermore, the relationship between E. coli bacteria and various water intakes was examined. It was observed that higher concentrations of E. coli bacteria were present when water was sourced from lower water intakes (mainly in summer months), characterized by increased water turbidity [8].

Specific objective of this study is to develop prediction model for E. coli bacteria for seven days in advance that can be used for optimizing of the treatment processes of the DWTF Butoniga. According to the agreement with the chief technologist at the facility, a time period of seven days was initially taken in order to be able to respond in a timely manner to the increased concentration of E. coli bacteria in the water.

Through this research and by the synergy of knowledge and expertise of the research team members, innovative methods, techniques and tools for modeling and managing microbiological water quality have been used and implemented into strategic, but also operational management of water resources in order to achieve the sustainable development goals (SDGs), with an emphasis on: SDG6 Clean water and sanitation.

3 Methods

3.1 Study area and data description

To acquire drinking water at the DWTF Butoniga, the process begins by drawing raw water from the Butoniga reservoir (depicted in Figure 1). Situated roughly 600 m downstream from the Butoniga reservoir's dam, the DWTF Butoniga occupies an area of 80,000 m^2 (as shown in Figure 1). Its initial phase is engineered to process 1,000 l/s or 3,600 m^3/h, with provisions made for certain components to accommodate a final capacity of 2,000 l/s, slated for the second phase. All processing units are designed for 24-hour full capacity with a hydraulic reserve of 25 %. The plant offers operational flexibility, capable of adjusting its capacity from 20 to 100 % of the nominal capacity [9].

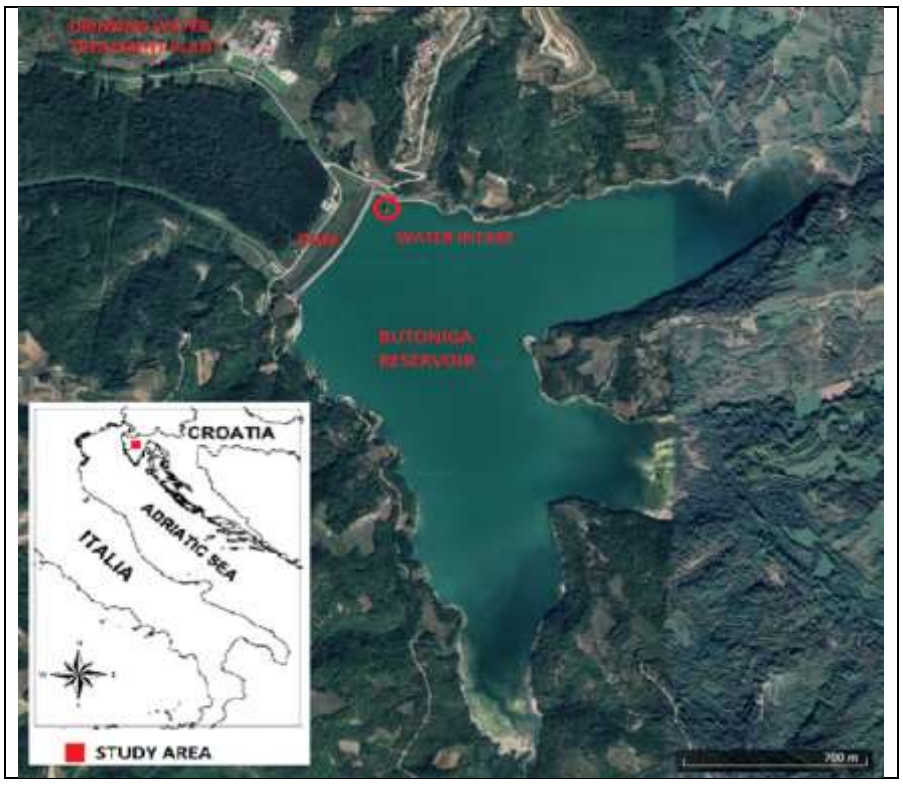

Figure 1. Location of the Butoniga reservoir and DWTF.

The primary drinking water treatment process (illustrated in Figure 2) encompasses several key units: raw water intake, pre-ozonation, coagulation-flocculation, flotation, rapid filtration, main ozonation, slow sand filtration, disinfection, final pH adjustment, pressure pumping, and chlorination. Complementing this main process, the auxiliary treatment (depicted in Figure 2) involves additional units such as sand cleaning stations for slow sand filters, treatment of filter washing water, sludge management, and neutralization of chemical wastewater [10].

The plant's construction finished in June 2002, with operations commencing in the spring of 2004, and has since remained operational. Notably, the DWTF's operational patterns are closely tied to the tourist season. Among the 5,000,000 m^3 of water produced and distributed annually, a substantial portion, 3,000,000 m^3, is generated and supplied during the period from June 15 to September 15, coinciding with the period of lowest water quality in the Butoniga reservoir [10].

The dataset used for constructing the E. coli bacteria prediction model (refer to Table 1) encompasses various physical, chemical, and microbiological parameters. These parameters were measured daily at the raw water inflow point of the DWTF from 2011 to 2020. Physiochemical factors include variables such as water temperature (Temp), pH level, turbidity (Tur), oxygen concentration (O_2), total organic

carbon (TOC), potassium permanganate ($KMnO_4$) levels, ammonia (NH_4) concentration, manganese (Mn) content, aluminium (Al) concentration, iron (Fe) levels, and the quantity of organic substances (UV254). These concentrations were determined within the internal laboratory of the DWTF Butoniga using standardized analytical methods compliant with ISO standards, specifically following the norm HRN EN ISO 5667-3. Microbiological parameters consist primarily of E. coli bacteria, which play a pivotal role as an indicator of faecal contamination within water systems. The detection and enumeration of E. coli bacteria were conducted using the Colilert method, in accordance with the norm HRN EN ISO 9308-2:2014.

All data underwent pre-processing tailored to modelling and research objectives. The entire temporal range of the measured data from 2011 to 2020 was utilized for developing prediction models. Instances of missing data were addressed through cubic spline interpolation to achieve the best possible fit.

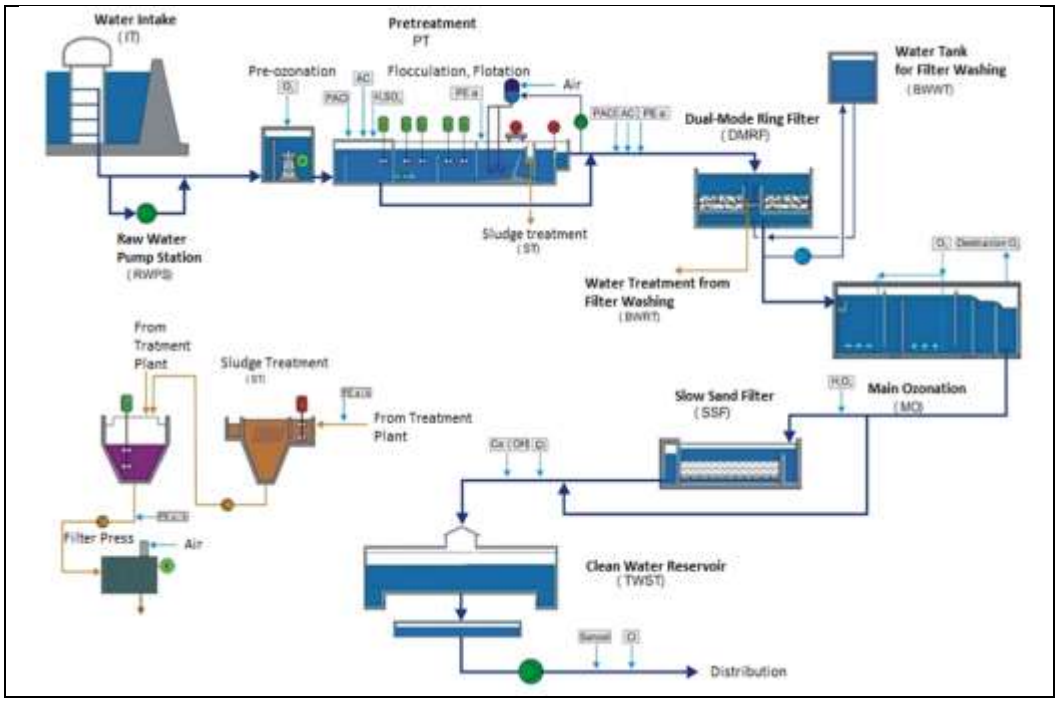

Figure 2. Treatment processes scheme for DWTF Butoniga.

Table 1. Data used for modelling.

SYMBOL	DESCRIPTION	UNIT
TEMP	Water temperature	°C
PH	pH	-
TUR	Turbidity	NTU
O_2	Oxygen concentration	mg/L
TOC	Total organic carbon	mg/L
$KMnO_4$	Potassium permanganate	mg/L
NH_4	Ammonium	mg/L
MN	Manganese	mg/L
AL	Aluminum	mg/L
FE	Iron	mg/L
UV254	Organic matter in water	1/cm
E. COLI	E. coli bacteria	CFU/100 mL
E. COLI_PRED	E. coli bacteria prediction for 7 days	CFU/100 mL

3.2 Modelling methods-model trees

Model trees are hierarchical structures comprised of nodes and branches. Within these structures, internal nodes conduct tests on input attributes, with each branch representing an outcome of the test. Predictions for the values of the target variable, such as class predictions, are stored in the leaves, which serve as terminal nodes in the tree. If a leaf contains a single value for class prediction, it is referred to as a simple regression tree. However, if a linear equation is utilized for prediction within the leaf, it is named a model tree [11].

One widely used algorithm for inducing model trees is the M5 algorithm, which builds upon the top-down induction of decision trees (TDIDT) algorithm. In this research, a variation of the M5 algorithm called M5P was employed, implemented within the Weka software package. The M5P algorithm integrates a decision tree as the base model, augmented with linear regression models at the leaf nodes. This augmentation allows for the creation of more intricate models capable of handling continuous target variables effectively. The M5P algorithm operates by initially growing a decision tree based on input data and subsequently fitting a linear regression model to the data at each leaf node. The resulting model combines these decision tree and linear regression components, facilitating predictions on new data [11].

Following the construction of the tree from the training dataset, it becomes essential to evaluate the model quality, specifically the accuracy of predictions. This evaluation can be accomplished by simulating the model on a testing dataset and comparing predicted target values with actual values. Alternatively, cross-validation can be employed, whereby the training dataset is partitioned into a chosen number of folds, typically 10. Each fold is sequentially utilized for testing, while the remaining folds are used for training. The final error is determined as the average error across all models throughout the procedure [11].

To assess model accuracy, various measures can be employed to calculate the disparity between actual and predicted values, including root mean-squared error (RMSE), mean absolute error (MAE), root relative squared error (RRSE), relative absolute error (RAE), and correlation coefficient (R) [11]. In the conducted experiment, model accuracy was evaluated using all these measures.

4 Results and discussion

As previously mentioned, all data underwent pre-processing tailored to the specific modelling and research objectives, guided by the expertise of modelling professionals familiar with the analysed DWTF. The model was developed to predict E. coli bacteria concentrations seven days in advance, aiming to enhance treatment processes at the DWTF in response to variations in raw water quality from the Butoniga reservoir. Consequently, the model aids in managing treatment processes that hinge on the quality of raw water from the Butoniga reservoir. For this experiment, the M5P machine learning algorithm, integrated within the Weka modelling software, was utilized. Predicted concentrations of E. coli bacteria seven days ahead served as the target variable for each model constructed, while water temperature, pH, turbidity, $KMnO_4$, NH_4, Mn, Al, Fe, O_2, TOC, UV254, and concentrations of E. coli bacteria (refer to Table 1) were designated as independent variables from which the predicted values of E. coli bacteria were derived. These parameters were primarily chosen as they most accurately represent the components of the system (DWTF and Butoniga reservoir) upon which the target variable relies [8].

The objective of the resulting prediction model is to be highly applicable and valid for forecasting E. coli bacteria, striving for maximum accuracy. To achieve this, standard procedures for model building and testing were employed: the entire dataset was utilized for training while validation was conducted using 10-fold cross-validation (as outlined in Section 3.2). To optimize the correlation coefficient (R) and determine the optimal number of rules, default parameter values for model construction were utilized within the Weka modelling software [11].

The model demonstrating the highest accuracy based on the validation method was chosen as the representative model for prediction purposes. The accuracy of the models is assessed through measures including RMSE, MAE, RRSE, RAE, and R [11].

Using the Weka modelling software and employing the M5P algorithm, a prediction model for E. coli bacteria concentrations seven days in advance was developed [11]. As outlined in section 3.1, the entire dataset spanning from 2011 to 2020, with daily sampling frequency, was utilized for constructing prediction models. Missing data were handled through cubic spline interpolation, and the selection of the best model followed the procedure outlined in section 3.1.

The prediction model for E. coli bacteria concentrations is depicted in Figure 3, with corresponding model equations provided in Table 2. This model comprises ten leaves, each representing an equation used to forecast E. coli bacteria concentrations seven days ahead, utilizing parameters specified in the model tree nodes (Figure 3). Analysis of the model tree nodes reveals that the most influential parameters include the current concentration of E. coli bacteria (as expected), pH values, and oxygen concentrations, followed by NH_4, Fe, and $KMnO_4$ concentrations, as well as turbidity levels.

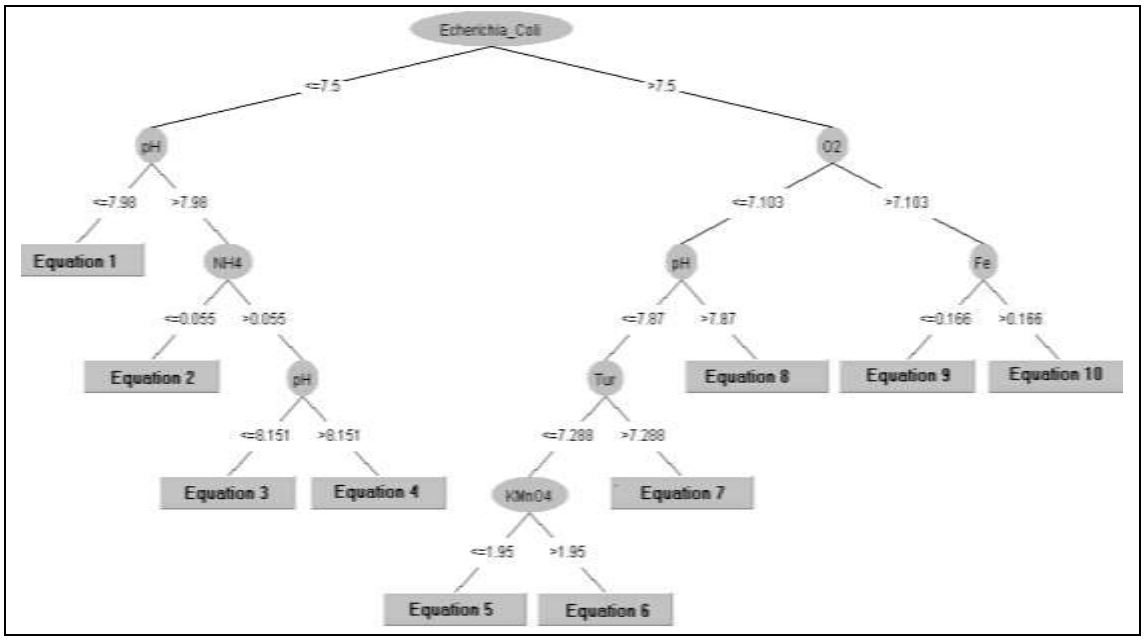

Figure 3. Model tree for E. coli bacteria prediction seven days in advance.

Table 2 presents the equations associated with the model tree leaves, incorporating parameters such as oxygen concentration, pH value, $KMnO_4$ and Fe concentrations, and current E. coli bacteria concentrations. The selection of equations within the model tree leaves depends on the values of variables in the tree nodes. Once the selection is made based on these variable values, the corresponding equation is applied to forecast E. coli bacteria levels seven days ahead.

The obtained model does not have so high correlation coefficient with a value of 0.48 (moderate correlation). Other parameter of model are, MAE of 26.5, RMSE of 57.7, RAE of 69.3 % and RRSE of 73.8 %. The performance of the prediction model is presented in Figure 4. From Figure 4 can be noticed why correlation coefficient is not so high, and that is low prediction of peak values. Model has good prediction of concentrations to 100 CFU/100 ml, while higher values are under forecast. The reason for this is that high values have a high probability expectation.

Table 2. Equations for model tree presented on Figure 3; E. coli bacteria prediction.

No. of Equation	EQUATION
1.	E. coli_pred=-0.0094*O_2-1.0048*pH+0.0719*$KMnO_4$-0.302*NH_4+0.6454*Fe+0.0017*E. coli+27.4774
2.	E. coli_pred=-0.0094*O_2-1.7702*pH+0.0719*$KMnO_4$-0.6939*NH_4+0.6454*Fe+0.0017*E. coli+23.4384
3.	E. coli_pred=-0.0094*O_2-1.4932*pH+0.0719*$KMnO_4$-0.3272*NH_4+0.6454*Fe+0.0017*E. coli+19.8177
4.	E. coli_pred=-0.0094*O_2-1.5966*pH+0.0719*$KMnO_4$-0.3272*NH_4+0.6454*Fe+0.0017*E. col+17.6368
5.	E. coli_pred=-0.0445*O_2-0.4569*pH+0.2575*Tur-0.1558*$KMnO_4$+1.4384*Fe+0.0014*E. coli+47.3177
6.	E. coli_pred=-0.0445*O_2-0.4569*pH+0.2575*Tur-0.1558*$KMnO_4$+1.4384*Fe+0.0014*E. coli+35.5702
7.	E. coli_pred=−0.0445*O_2-0.4569*pH+0.6061*Tur-0.744*$KMnO_4$+1.4384*Fe+0.0014*E. coli+90.2576
8.	E. coli_pred=-0.0445*O_2-0.4569*pH+0.3106*Tur+0.0609*$KMnO_4$+1.4384*Fe+0.0014*E. coli+69.5288
9.	E. coli_pred=-0.0525*O_2-0.5132*pH+0.0291*Tur+0.0609*$KMnO_4$+3.8009*Fe+0.0014*E. coli+20.6872
10.	E. coli_pred=-0.0525*O_2-0.5132*pH+0.0291*Tur+0.0609*KMnO+3.3453*Fe+0.0014*E. coli+39.9425

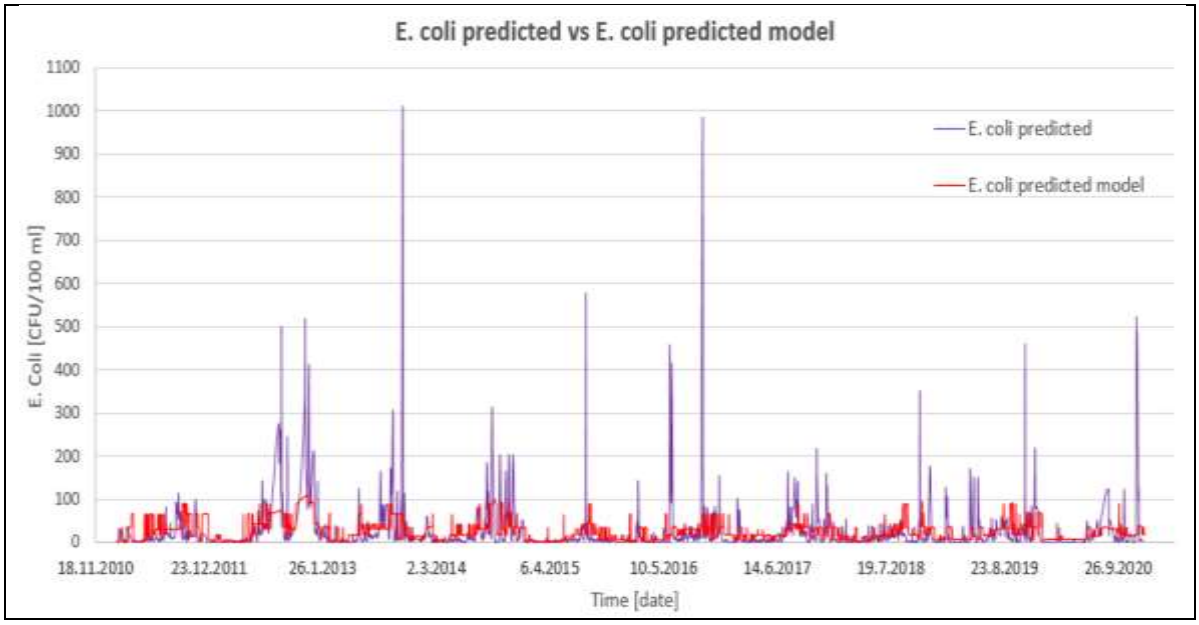

Figure 4. Performace of the prediction model-measured "shifted" data for seven days in advance (purple) vs. modeled predicted E. coli concentrations seven days in advance (red).

Regardless of, obtained model through the prediction of E. coli bacteria can help to manage certain drinking water treatment processes depending on the biological quality of raw water in the Butoniga reservoir.

Currently, the adoption of ML techniques is progressively expanding across multiple facets of DWTF modeling, encompassing prediction, optimization, and facility management. Presented below are instances illustrating the utilization of ML methods.

Khan et al. [4] in their research used superposition learning-based model for prediction of E.coli in

groundwater using physiochemical water quality parameters. Their results show that the model having Turbidity, pH, Total Dissolved Solids (TDS), and Electric Conductivity (EC) as inputs displayed the best performance R· values of 0.90 and lowest MSE values of 0.0892. Sokolova et al. [5] for predicting microbial water quality in the drinking water source using E. coli monitoring and hydrometeorological data with data-driven models. Their study showed that models which included multiple predictors, i.e. VAR, LASSO Regression, Random Forest, TPOT, performed better than univariate models, i.e. Naive baseline, Exponential Smoothing and ARIMA. Also, external predictors increased the model performance, indicating that some of these models are informative for forecasting E. coli concentration at the water intake.

As mentionoed, nowadays, when there is increasing thread of pollution of water sources, and also with regard to the new Europian Union Drinking Water Directive (EU DWD) [12], which came into force at the begining of the 2021, predicting the quality of a water resources is of great importance for water treatment technologies. In the new EU DWD some of the drinking water parameters are tightened, new limit values for water quality parameters have been added, and also the requirements for monitoring the quality of drinking water and the water sources are tightened [12].

The main objective of these prediction model is to enable swift and efficient management of the DWTF Butoniga. Particularly during critical periods marked by elevated levels of E. coli bacteria there is a heightened necessity for providential and ongoing process monitoring. This entails increased chemical usage to uphold stability in the treatment process and to guarantee that all effluent water samples remain below the Maximum Acceptable Concentration (MAC) [13]. Also, to prevent pollutions in the future, it would be advisable to more tighten the protective zones around Butoniga reservoir.

5 Conclusion

The significance of DWTFs in providing safe drinking water for human consumption is now more pronounced than ever. Consequently, a model that accurately captures the operations and dynamics of a DWTF emerges as a crucial and valuable tool. Such a model aids in devising strategies and management approaches that enhance its efficiency and resource utilization through optimized treatment processes, while simultaneously mitigating the risks associated with inadequate actions.

This research involved the construction of a prediction model for E. coli bacteria concentrations in raw water, forecasting seven days in advance using a ML approach in the form of model trees. The model was applied to measured data from the DWTF Butoniga to address the challenge of elevated E. coli bacteria concentrations, primarily occurring during summer months when water is extracted from the lowest layer of the Butoniga reservoir. Predictions of E. coli bacteria levels are based on current measurements taken at the raw water intake.

The resulting model exhibits a moderate correlation coefficient (0.48), indicating its capability to predict concentrations up to 100 CFU/100 ml reasonably well. However, it tends to underestimate peak values, particularly for higher concentrations. Nevertheless, despite these limitations, the model's predictions of E. coli bacteria levels can aid in managing specific drinking water treatment processes contingent upon the biological quality of raw water in the Butoniga reservoir.

Also, through conducting this research, innovative methods, techniques and tools for modeling and managing microbiological water quality have been used and implemented into strategic, but also operational management of water resources in order to achieve the SDGs, with an emphasis on: SDG6 Clean water and sanitation.

Future work is focused to obtain more accurate prediction models which can be used for management purposes. This also implies additional models verification through a direct measuring of E. coli bacteria

concentrations in the Butoniga reservoir, alongside parallel modeling, i.e. testing and subsequent comparison of the obtained results.

Acknowledgements
This study received support from several projects. The first project, titled "Implementing innovative methodologies, technologies and tools to ensure sustainable water management" (23-67), and the second project, titled "Hydrology of water resources and identification of flood and mudflow risk in karst" (uniri-tehnic-18-54), were funded by the University of Rijeka. Additionally, the research also falls under the ZIP UNIRI project line of the University of Rijeka, specifically for the projects ZIP-UNIRI-1500-3-22 and ZIP-UNIRI-1500-2-22.

References:

[1] Godo-Pla, L., Emiliano, P., Valero, F., Sin, G., Monclus, H.: Predicting the oxidant demand in full-scale drinking water treatment using an artificial neural network: Uncertainty and sensitivity analysis, Process Saf. Environ. Prot., vol. 125, pp. 317-327, 2019.
[2] Shahid Iqbal, M., Nauman Ahmad, M., Hofstra, N.: The Relationship between Hydro-Climatic Variables and E. coli Concentrations in Surface and Drinking Water of the Kabul River Basin in Pakistan, AIMS Environ. Sci., 4 (5), pp 690-708, 2017.
[3] Odonkor, S.T., Ampofo, J.K.: Escherichia coli as an indicator of bacteriological quality of water: an overview. Microbiol. Res., 4 (2), 2013.
[4] Khan, M., Gupta, R., Sekhri, S. et al.: Superposition learning-based model for prediction of E. coli in groundwater using physico-chemical water quality parameters, Groundwater for Sustainable Development, 13, 2021.
[5] Sokolova, E., Ivasson, O., Liliestrom, A., Speicher, N.K., Rydberg, H., Bondelind, M.: Data-driven models for predictingmicrobial water quality in the drinking water source using E. coli monitoring and hydrometeorological data, Science of the Total Environment, 802, 2022.
[6] Volf, G., Sušanj Čule, I., Žic, E., Zorko, S.: Water Quality Index Prediction for Improvement of Treatment Processes on Drinking Water Treatment Plant, Sustainability, vol. 14, 2022.
[7] Volf, G., Krbavčić, M., Sušanj Čule, I., Zorko, S.: Prediction models for manganese, iron and ammonium in raw water for a drinking water treatment plant Butoniga (Croatia). Eng. Rev. 43 (3), 2023.
[8] Volf, G. and Zorko, S: Relationship between E. coli and physiochemical parameters in Butoniga reservoir, 4th International Conference WATERS IN SENSITIVE AND PROTECTED AREAS, Pula, 2024.
[9] Hajduk Černeha, B.: Akumulacija Butoniga u Istri-Prva iskustva u korištenju za vodoopskrbu, Proceedings of Vodni dnevi, Rimske Toplice, 2021.
[10] Zorko, S.: Akumulacija Butoniga-pritisci u slijevu i zaštita voda,Zbornik radova-Upravljanje jezerima i akumulacijama u Hrvatskoj i Okrugli stol o aktualnoj problematici Vranskog jezera kod Biograda na Moru, Biograd na Moru, 2017.
[11] Witten I.H. and Frank, E.: Data Mining: Practical Machine Learning Tools and Techniques, 2nd ed., Elsevier, 2005.
[12] EU Drinking Water Directive Directive (EU) 2020/2184 of the European Parliament and of the Council of 16 December 2020 on the quality of water intended for human consumption.
[13] Croatian regulations for drinking water: *Pravilnik o parametrima sukladnosti, metodama analize, monitoringu i planovima sigurnosti vode za ljudsku potrošnju te načinu vođenja registra pravnih osoba koje obavljaju djelatnost javne vodoopskrbe*, available online https://narodne-novine.nn.hr/clanci/sluzbeni/2017_12_125_2848.html. [Accessed: 21 March 2024].

ENERGY CONSUMPTION AND IDLE ENERGY COMPENSATION ON DRINKING WATER TREATMENT FACILITY BUTONIGA

GORAN VOLF [1], DAVID KRAJCAR [2], SONJA ZORKO [2]

[1] *Faculty of Civil Engineering, Department of Hydraulic engineering, University of Rijeka, Croatia, goran.volf@uniri.hr*

[2] *Istarski Vodovod d.o.o. Buzet, Croatia, david.krajcar@ivb.hr, sonja.zorko@ivb.hr*

1 Abstract

A prominent challenge confronting the water industry is the integration of sustainability considerations into design methodologies and the mitigation of carbon emissions associated with energy-intensive procedures. Water treatment, an imperative stage for upholding public health standards, constitutes a particularly energy-intensive process. Drinking water treatment facility Butoniga is one of the main drinking water supply facilities for potable water in Istria, Croatia. Water for treatment process is captured from the Butoniga reservoir, which is a small and relatively shallow reservoir. Water pumping to the water tank and then to the water supply network is carried out through six big pumps with power of 1000 kW, and one small pump with power of 315 kW. The largest consumption of energy on the facility is associated with the pumping operations and the energy consumption is mainly related to delivered water, i.e., water pumped to the water tank and then to the water supply network. Idle energy in pumping water systems refers to the energy consumed by a pump when it is operational but not actively pumping water or when it's running at a capacity higher than necessary to meet the current demand. This can be a source of inefficiency in water supply systems. By adjusting pump operations to match demand, idle energy compensation improves overall energy efficiency. On drinking water treatment facility Butoniga, regarding compensation of idle energy, power factor ($\cos \varphi$) moves within 0.90 and 0.99.

Keywords: Drinking water treatment facility, Butoniga reservoir, energy consumption, idle energy compensation.

2 Introduction

Drinking water treatment facilities (DWTFs) are essential facilities engineered to produce safe, top-grade water for human use, meeting stringent standards and health regulations while remaining cost-effective. As a result, DWTFs play a crucial role in guaranteeing consistent and secure access to plentiful, safe drinking water for the community [1].

Water treatment is a process that demands a significant amount of energy and it is one of the pressing issues being faced by the water industry today [2]. The energy consumption associated with drinking water treatment encompasses several aspects, including energy for water conveyance, unit operations within the DWTF, facility-related equipment (such as lighting, heating, and ventilation), and energy for water distribution [3].

The energy required for water treatment varies depending on factors such as the quality of the raw water, its source, the age of the water supply system, conveyance distance, water storage capacities, and elevation differences. Approximately 80 % of the energy usage is attributed to conveying or pumping water, with the remainder allocated to water treatment [3].

Various studies have extensively examined this energy consumption aspect involved in treating drinking water [2, 3, 4]. Bukhary et al. in first study [3] gives an analysis of energy consumption and the use of renewables for a small DWTF, while in second [4] are presented design aspects, energy consumption

evaluation, and offset for DWTF operation. First study results showed that the dependency of a DWTF on the traditional electric grid could be greatly reduced by the use of photovoltaics (PVs). The largest consumption of energy was associated with the pumping operations, corresponding to 150.6 Wh/m^3 for the booster pumps to covey water to the storage tanks, while the energy intensity of the water treatment units was found to be 3.1 Wh/m^3 [3]. Second study results showed that the largest consumers of energy, after the water distribution pumps were the processes of coagulation and flocculation. Also 500 kW PV system was found to be sufficient to offset the energy consumption of the water treatment only operations, for a net present value of 0.24 million dollars [4]. Tow et al. [2] presents modelling the energy consumption of potable water reuse schemes. Presented model was used to identify the most promising avenues for further reducing the energy consumption of potable reuse, including encouraging direct potable reuse without additional drinking water treatment, avoiding reverse osmosis in indirect potable reuse when effluent quality allows it, updating pipe networks, or using more permeable membranes [2].

It's anticipated that future energy demands for water treatment will rise due to various factors, mainly due to population growth and aging infrastructure [3]. These factors can motivate DWTFs to explore and implement various methods to decrease their overall energy consumption, so employing alternative energy generation methods such as renewables or implementing energy conservation measures can aid in reducing overall costs [4].

Idle energy in pumping water systems refers to the energy consumed by a pump when it is operational but not actively pumping water or when it's running at a capacity higher than necessary i.e., designed to meet the current demand. This can be a source of inefficiency in water supply systems. By adjusting pump operations to match demand, idle energy compensation improves overall energy efficiency [5].

In this research will be presented energy consumption and idle energy compensation on DWTF Butoniga.

Through this research and by the synergy of knowledge and expertise of the research team members, innovative methods, techniques and tools for modeling and managing energy consumption and idle energy compensation on DWTF have been used and implemented into strategic, but also operational management of water resources in order to achieve the sustainable development goals (SDGs), with an emphasis on: SDG6 Clean water and sanitation.

3 Methods

3.1 Study area description

At the DWTF Butoniga, the process of obtaining drinking water begins with the extraction of raw water from the Butoniga reservoir (Figure 1). Located approximately 600 meters downstream from the dam of the Butoniga reservoir, the DWTF Butoniga spans an area of 80,000 m^2.

Its initial phase is designed to treat 1,000 l/s or 3,600 m^3/h, with provisions in place to accommodate a final capacity of 2,000 l/s in the second/final phase. All processing units are configured to operate at full capacity for 24 hours, with a hydraulic reserve of 25 %. The plant is flexible in operation, capable of adjusting its capacity from 20 % to 100 % of the nominal capacity [6]. Figure 1 shows the location of the Butoniga reservoir and DWTF Butoniga.

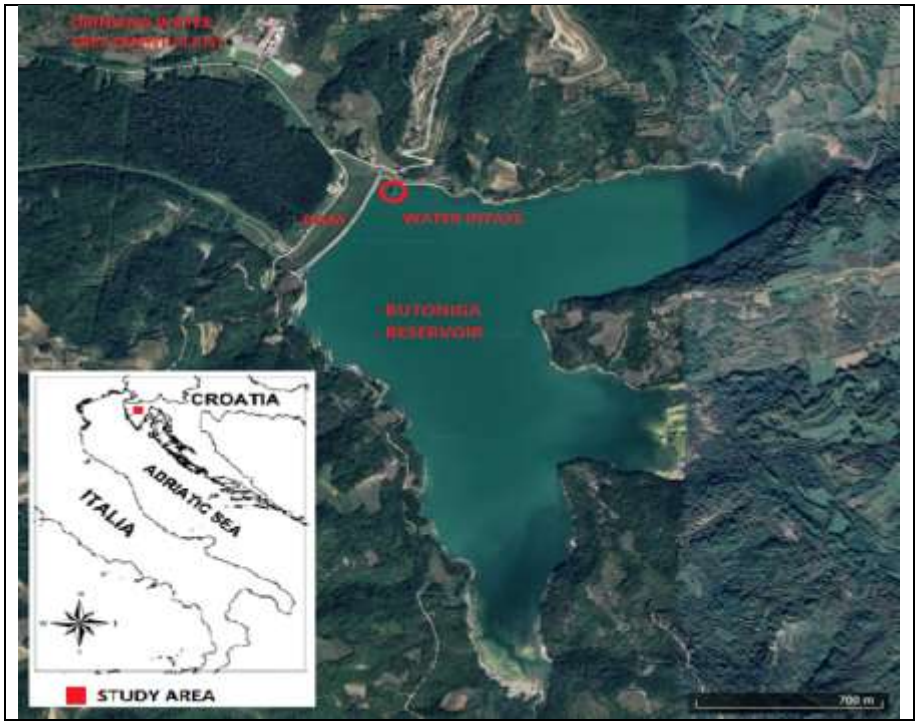

Figure 1. Location of the Butoniga reservoir and DWTF.

3.2 Treatment process on DWTF Butoniga

The primary drinking water treatment process (outlined in Figure 2) consists of several essential units: raw water intake, pre-ozonation, coagulation-flocculation, flotation, rapid filtration, main ozonation, slow sand filtration, disinfection, final pH adjustment, pressure pumping, and chlorination. Additionally, the auxiliary treatment process (shown in Figure 2) includes supplementary units such as sand cleaning stations for slow sand filters, treatment of filter washing water, sludge management, and neutralization of chemical wastewater [7].

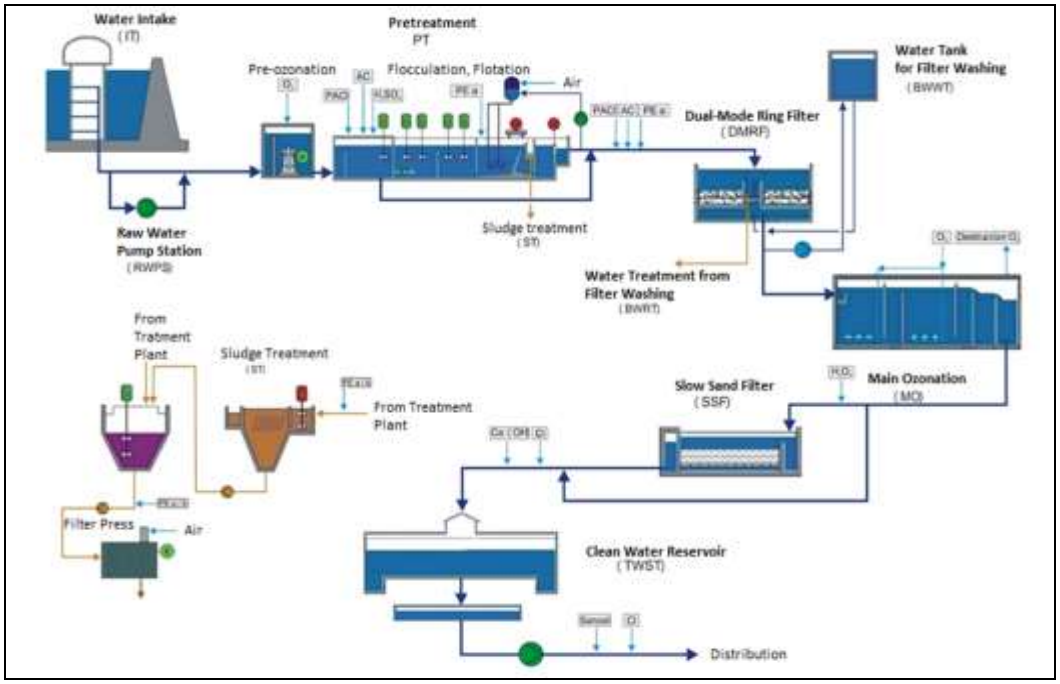

Figure 2. Treatment processes scheme for DWTF Butoniga.

Construction of the facility was completed in June 2002, with operations commencing in the spring of 2004, and has since been continuously operational. Notably, the operational schedule of the DWTF is closely linked to the tourist season. Out of the 5,000,000 m^3 of water produced and distributed annually, a significant portion, amounting to 3,000,000 m^3, is generated and supplied between June 15 and September 15, corresponding to the period of lowest water quality in the Butoniga reservoir [7].

3.3 Water pumping and energy consumption

Water pumping on the DWTF Butoniga to the water tank and then to the water distribution network is carried out through six big pumps with power of 1,000 kW, and one small pump with power of 315 kW (showed on Figure 3). The largest consumption of energy on DWTF is associated with the pumping operations. Over 70 % of energy consumption on the DWTF Butoniga is related to the pumping operations.

Figure 3. Pumps location on DWTF Butoniga.

3.4 Idle energy compensation

Changing of electro-magnetic fields in electric motors which move water pumps generate idle power. So, the higher is the ratio of idle to real power, the smaller is their power factor (cos φ). Idle energy in pumping water systems refers to the energy consumed by a pump when it's operational but not actively pumping water or when it's running at a capacity higher than necessary to meet the current demand. This can be a source of inefficiency in water distribution systems. By adjusting pump operations to match demand, idle energy compensation improves overall energy efficiency [8].

Solutions for idle energy compensation can be divided into four main groups [9]:

1) Power capacitors, which can be used to compensate idle power demand. The capacitor battery provides the required idle power, so the transmission facilities are relived as no idle power is drown from the utility,
2) Synchronous electric motors, which can be used to supply a certain amount of idle power required by the industrial load,
3) Active filters are devices that eliminate or cancel out harmonics within the current and they also provide dynamic idle power compensation and power factor correction in harmonic polluted lines,

and

4) Passive filters, which are composed of reactors, inductors and capacitors in a series circuit. They offer power factor correction capacity and generate some amounts of idle power which reduces the idle power drawn from the grid [9].

On DWTF Butoniga, idle energy is compensated using capacitors. Each pump, respectively its electric motor, has its own capacitor. Regarding compensation of idle energy, power factor (cos φ) varies between 0.90 and 0.99. According to this, more than 90 % of apparent power is real power. On DWTF Butoniga are used Roederstein capacitors units of 3x10kV and 241kVAr for each pump. Capacitors units are showed on Figure 4.

In brief, for compensation of idle energy, a capacitor battery is used which usually consist of a regulator and various accessories. The regulator automatically switches on the appropriate number of devices, depending on the idle power needs, to maintain a power factor cos φ at the required level. There are few kinds of capacitors, these are most often common batteries, amplified batteries, batteries with thriystor linkages, protective shell batteries, etc. [10].

Figure 4. Capacitors units on DWTF Butoniga.

4 Results and discussion

On Figure 5 are presented captured and delivered amounts of water in cubic meters from DWTF Butoniga with total energy consumption in kWh for the period from 2011-2020. It can be seen that the energy consumption on DWTF Butoniga is manly related to delivered water, i.e., water pumped to the water tank and then to water supply system i.e., network.

Also, from Figure 5 can be observed that the operation of the DWTF is primarily related to the tourist season. Out of the total annual production and distribution of average 5,000,000 m^3 of water, 3,000,000 m^3 is generated and distributed between June 15 and September 15 (summer month) [7].

As for energy consumption, the minimum value is 1,502 kWh, the maximum value is 81,906 kWh, while the average energy consumption in observed period on the DWTF Butoniga is 19,970 kWh.

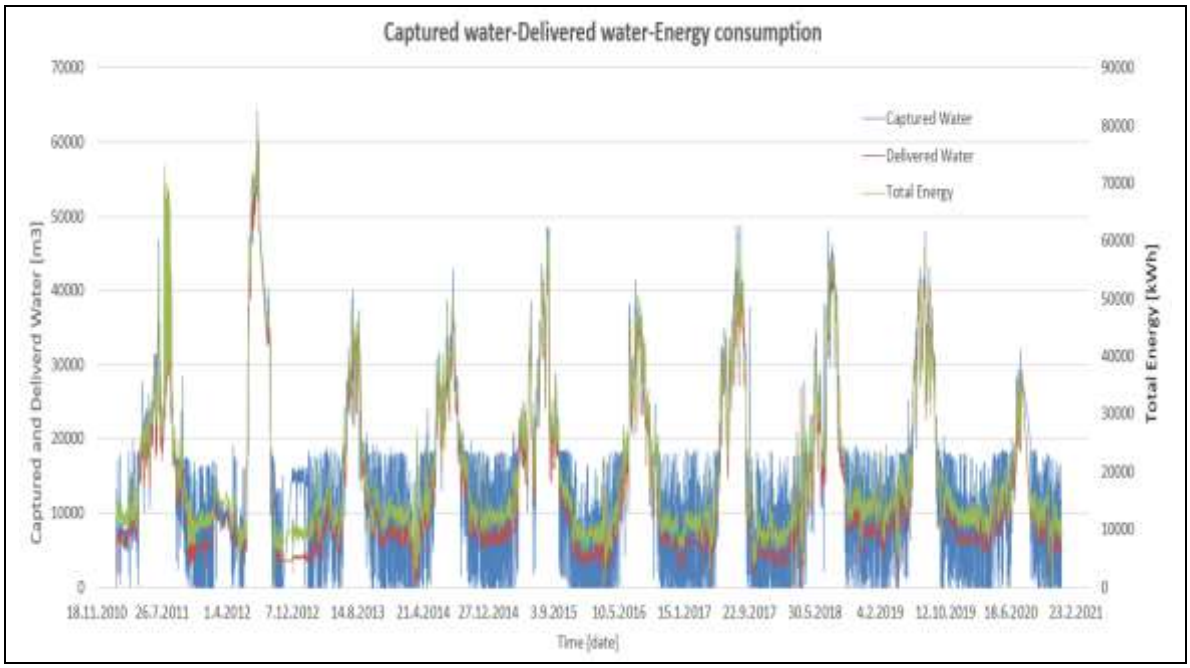

Figure 5. Representation of amounts of captured and delivered water with total energy consumption on a DWTF Butoniga in observed period from 2011 to 2020.

On Figure 6 is given representation of delivered water to water tank and then to the water supply system i.e., network and idle energy on DWTF Butoniga in period 2011-2020. The idle energy follows amounts of delivered water, i.e., according to Figure 5, follows energy consumption on DWTF Butoniga. From Figure 6 can be seen that idle energy consumption, the minimum value is 100 kVArh, the maximum value is 20,972 kVArh while the average idle energy consumption in observed period on the DWTF Butoniga is 4,917 kVArh

It must be noticed that energy consumption is given in kWh (kilowatt hour), while idle energy is presented in kVArh (kilovolt ampere reactive hour), which measures the reactive power in an electrical system. As mentioned, reactive power is required to establish and maintain the electric and magnetic fields of electrical equipment.

As mentioned in Section 3.4 idle energy on DWTF Butoniga is compesated using Roederstein capacitors units of 3x10kV and 241kVAr for each pump where power factor (cos φ) varies between 0.90 and 0.99. According to this, more than 90 % of apparent power is real power. From solutions which can be used for idle energy compesation [9], the designers of the DWTF Butoniga chose capacitors as the best solution at that time which was also economical and the most profitable. Power capacitors have battery which provides the required idle power, so the transmission facilities are relived as no idle power is drown from the utility. Power factor correction which is based on capacitors are common in the industry as they are more economic. So with the reduction in power losses and low idle power demand from the facility this type of solution can also save more on electricity bills [9].

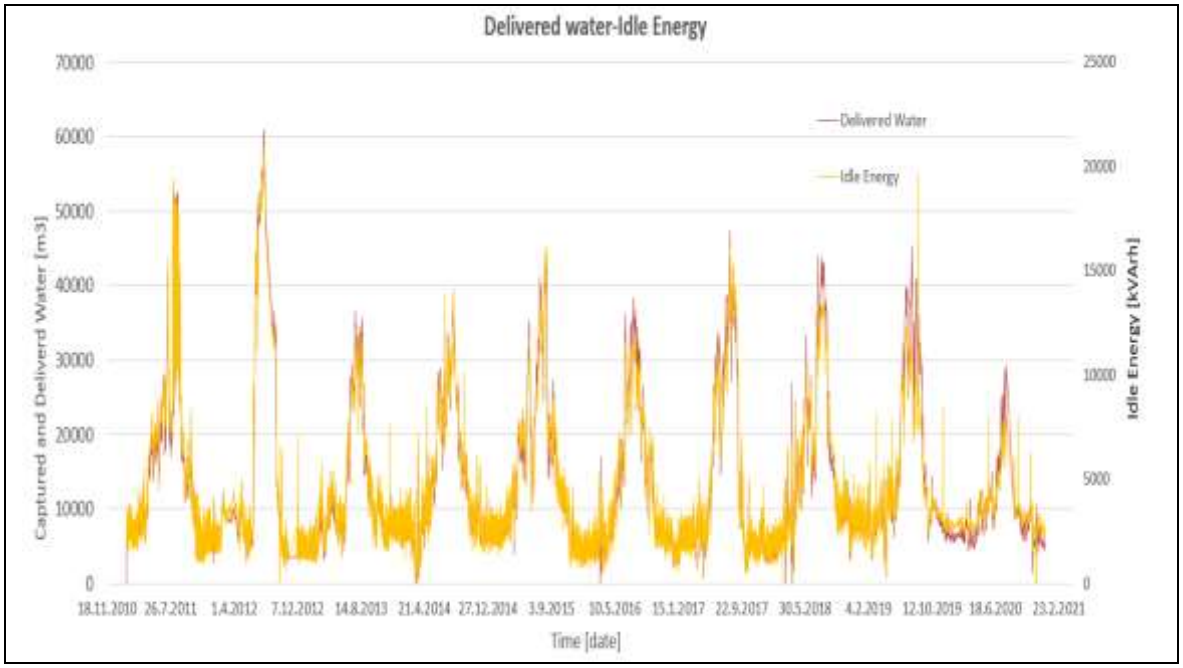

Figure 6. Representation of amounts of delivered water with idle energy on DWTF Butoniga in observed period from 2011 to 2020.

The largest consumption of energy on DWTFs is associated with the pumping operations. As can be seen from Figure 7, more than 70 % of energy consumption on the DWTF Butoniga is related to the pumping operations (pumps and compressors). For many DWTFs, pumping operations consume most of the energy, so special attention must be paid to them [4], [5].

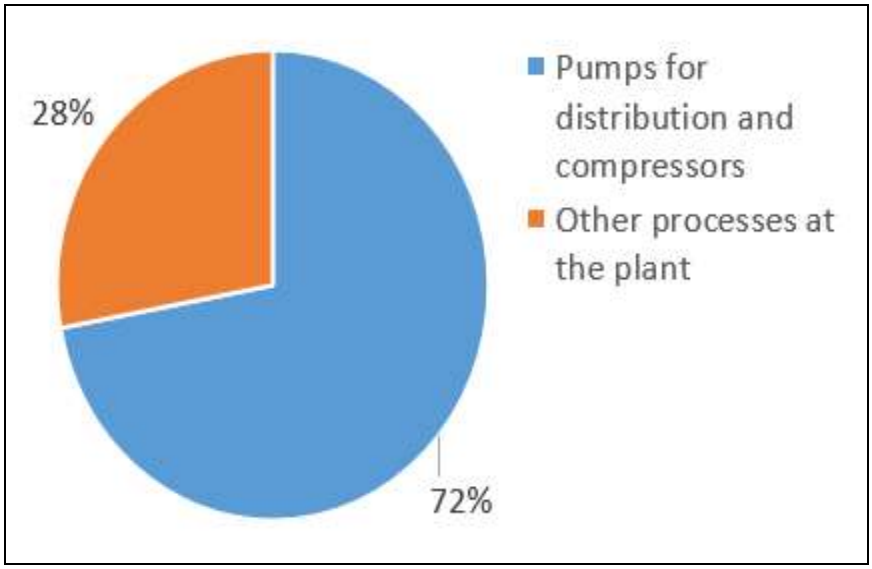

Figure 7. Distribution of energy consumption on DWTF Butoniga in observed period from 2011 to 2020.

In summary, managing energy consumption and incorporating idle energy compensation strategies are essential components of sustainable and efficient water pumping systems. These approaches help align energy use with actual demand, optimizing the operation of pumping systems. For other parts of the DWTF, i.e., water treatment operations, for energy savings can be used some other systems, like PVs system [4].

5 Conclusion

This paper presents energy consumption and idle energy compensation on DWTF Butoniga, which is one of the main drinking water supply facilities for potable water in Istria, Croatia. After treatment process water is pumping to the water tank and/or water supply network which is carried out through six big pumps with power of 1,000 kW, and one small pump with power of 315 kW. The primary energy consumption at the facility is attributed to these pumping activities (more than 70 %), with energy usage primarily linked to the volume of water delivered, specifically the water pumped into the distribution system.

On DWTF Butoniga, idle energy is compensated using capacitors, where each pump, respectively its electric motor, has its own capacitor. Regarding compensation of idle energy, power factor (cos φ) is moving between 0.90 to 0.99. According to this, more than 90 % of apparent power is real power. The idle energy follows amounts of delivered water, i.e., follows energy consumption (pumping operations) on DWTF Butoniga.

In essence, effectively managing energy usage and integrating strategies to compensate for idle energy are crucial elements of sustainable and efficient water pumping systems. These methods ensure that energy consumption is in sync with real-time demand, thereby maximizing the performance of pumping systems.

Also, it is very important to choose the right idle energy compensation solutions for each observed system i.e., facility so that chosen solution would be efficient, and ultimately at the end reduce the electricity bills.

Acknowledgements
This study received support from several projects. The first project, titled "Implementing innovative methodologies, technologies and tools to ensure sustainable water management" (23-67), and the second project, titled "Hydrology of water resources and identification of flood and mudflow risk in karst" (uniri-tehnic-18-54), were funded by the University of Rijeka. Additionally, the research also falls under the ZIP UNIRI project line of the University of Rijeka, specifically for the projects ZIP-UNIRI-1500-3-22 and ZIP-UNIRI-1500-2-22.

References:

[1] Godo-Pla, L., Emiliano, P., Valero, F., Sin, G., Monclus, H.: Predicting the oxidant demand in full-scale drinking water treatment using an artificial neural network: Uncertainty and sensitivity analysis, Process Saf. Environ. Prot., vol. 125, pp. 317-327, 2019.
[2] Tow, E.W., Hartman, A.L., Jaworowski, A., et al.: Modeling the energy consumption of potable water reuse schemes, Water research X, 13, 2021.
[3] Bukhary, S., Batista, J., Ahmad, S.: Design Aspects, Energy Consumption Evaluation, and Offset for DrinkingWater Treatment Operation, Water, 12, 1772, 2020.
[4] Bukhary, S., Batista, J., Ahmad, S.: An Analysis of Energy Consumption and the Use of Renewables for a Small Drinking Water Treatment Plant, Water, 12, 28, 2020.
[5] Figura, R., Szychta, L: Pumping energy consumption in water transportation systems, Archives of Transport System Telematics, 3, 2, 2010.
[6] Hajduk Černeha, B.: Akumulacija Butoniga u Istri-Prva iskustva u korištenju za vodoopskrbu, Proceedings of Vodni dnevi, Rimske Toplice, 2021.
[7] Zorko, S.: Akumulacija Butoniga-pritisci u slijevu i zaštita voda,Zbornik radova-Upravljanje jezerima i akumulacijama u Hrvatskoj i Okrugli stol o aktualnoj problematici Vranskog jezera kod Biograda na Moru, Biograd na Moru, 2017.
[8] Web address: https://www.huber-technology.com.br/br/solucoes/eficiencia-da-energia/infrastructure/power-supply.html (accessed 3. March, 2024).
[9] Web address: https://www.powermatrix.in/what-are-the-reactive-power-compensation-solutions/

(accessed 27. July, 2024).
[10] Zebala, K.: Reactive power compensation and energy saving, Technical Transactions, Civil Engineering, 3-B, 2014.

THE EFFECTS OF ULTRASOUND IN OILY WASTEWATER TREATMENT

HANA POSAVCIC [1], IVAN HALKIJEVIC [2], DRAZEN VOUK [3], DOMAGOJ NAKIC [4]

[1] *Faculty of Civil Engineering, University of Zagreb, Croatia, hana.posavcic@grad.unizg.hr*

[2] *Faculty of Civil Engineering, University of Zagreb, Croatia, ivan.halkijevic@grad.unizg.hr*

[3] *Faculty of Civil Engineering, University of Zagreb, Croatia, drazen.vouk@grad.unizg.hr*

[4] *Faculty of Civil Engineering, University of Zagreb, Croatia, domagoj.nakic@grad.unizg.hr*

1 Abstract

Ultrasonic technology can be used in various branches of industry, but its use in water and wastewater treatment has not yet been sufficiently researched. The aim of this paper is to investigate the application of ultrasound in wastewater treatment, with a focus on oily wastewater. In the experimental study, ultrasound was combined with electrocoagulation to remove mineral oil and it was shown that this treatment increased mineral oil removal from 15% to 50% compared to electrocoagulation alone.

Keywords: electrochemistry, cavitation, intensity, oil, ultrasound, wastewater treatment

2 Introduction

Ultrasound (US) is an acoustic wave generated at frequencies above 20 kHz [1]. It is classified as an advanced oxidation process and has been considered and developed as a potential technology for wastewater treatment in recent decades [2-5].

Ultrasonic technology can be used in various industries, but its application in water and wastewater treatment has not yet been sufficiently explored. The aim of this paper is therefore to explain the basics of ultrasound, its advantages and disadvantages and its application in water and wastewater treatment.

This paper is divided into two main parts. The first part gives a general overview of ultrasonic technology, including the advantages and disadvantages of this technology and a description of the parameters that influence the process, such as operational and geometric characteristics. The second part contains an experimental investigation carried out on a laboratory-scale device, using a combination of electrochemical and ultrasonic technology to remove mineral oil from oily wastewater. In this part, various operating parameters (number of cycles, flow rate, current density and electrode material) were tested to determine the effects of electrochemistry on mineral oil removal and then to determine the contribution of ultrasound to this technology.

3 The theory of ultrasound

The source of the vibrations that generate acoustic waves are ultrasonic transducers, devices that can convert mechanical and electrical energy into high-frequency waves (sounds) [6]. However, the acoustic wave itself is not efficient enough to remove the pollutants from the wastewater, so the removal process relies on ultrasonic cavitation [3], figure 1. Cavitation is a process in which microbubbles release a large amount of energy in less than a microsecond [7, 8].

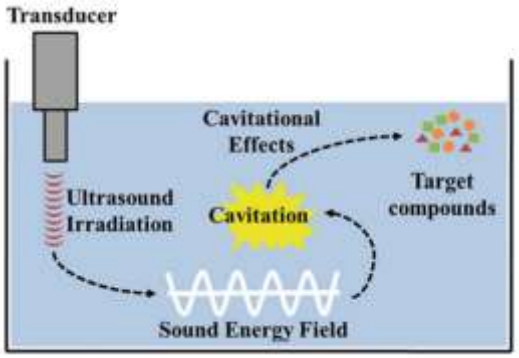

Figure 1. Cavitational reaction mechanisms by ultrasonic irradiation [3]

When ultrasound is used in water and wastewater treatment, acoustic waves are generated by the vibration of ultrasonic probes or transducers. Zones of higher and lower pressure are created in which microbubbles form and implode [1, 9].

When the bubbles implode, a large amount of energy is released and zones of extreme pressure (≈1,000 bar) and extreme temperature (≈4,725 °C) are created in which the bubbles are decomposed into hydrogen and hydroxyl radicals (·OH) [3, 9]. Hydroxyl radicals oxidize or reduce organic and inorganic compounds in wastewater. If the pollutants are hydrophobic, for example, they can penetrate the cavitation bubble and be exposed to the extreme conditions that occur during implosion [7, 10, 11].

The advantages and disadvantages of ultrasound are listed in Table 1 [1, 9, 10, 12-18].

Table 1. Advantages and disadvantages of ultrasound

ADVANTAGES	DISADVANTAGES
Can be used when solids are present in the water.	It is used successfully in laboratory and pilot plants (on a small scale), but there are only few studies for large quantities.
The pollutants are degraded to water, carbon dioxide and inorganic ions.	Dead zones occur because intense cavitation takes place near the probe or transducer.
The equipment is simple, affordable and can be retrofitted to conventional treatment reactors.	The service life of the equipment is short due to erosion.
It has proven to be effective in combination with aerobic and anaerobic treatments.	High operating costs compared to conventional treatments.
Degradation is faster than with conventional aerobic oxidation.	

Ultrasound has already been shown to be effective in the removal of various pollutants (aromatic compounds, herbicides, pesticides, dyes, alcohol, pharmaceuticals, bacteria, etc.), but is still the subject of intensive research [8, 14, 19]. For oil in wastewater, low-frequency ultrasound has been used for emulsification and high-frequency ultrasound for de-emulsification [20]. On the other hand, some researchers have shown that ultrasound alone is not sufficient for the complete mineralization of organic matter. Therefore, it is recommended to combine ultrasound with other advanced oxidation processes, or other conventional treatments [1, 2, 9, 21, 22].

3.1 Parameters that influence ultrasound

The parameters that influence ultrasound can be differentiated as follows: operative parameters, medium and geometric characteristics [12].

Power, frequency, intensity, duration, mode (continuous or pulsed) and the shape of the waves are considered as operational parameters. They all have in common that they influence the formation of cavitation [3, 12, 14]. For example, if the power is kept constant, higher frequencies lead to increased production of low energy bubbles as the phases of compression and expansion are more frequent. If

other frequencies are used, the implosion of the bubbles can be more intense. However, most ultrasonic devices only operate at one frequency [8, 14]. Frequencies from 20 kHz to 50 kHz are usually used in water and wastewater treatment [7].

Media properties that influence ultrasound are the type of pollutant, temperature, viscosity, pressure and dissolved gases [12, 23]. These parameters are important because they increase cavitation. For example, when the temperature rises up to 60 °C, cavitation occurs more easily, but the implosion is less violent [24, 25].

Geometric characteristics are the least researched parameters, but interest in them arose from the need to design and optimise ultrasonic devices at an industrial level [3]. Ultrasound can be used in two ways. The first is direct sonication, where ultrasonic transducers or probes are directly immersed in water. The ultrasonic probe (sonde, horn) is a representative example of this case, as it is directly immersed in the water, the ultrasonic radiation is of high intensity and acts locally, close to the probe. The probe is therefore only suitable for small volumes [1, 18, 26]. The other variant is indirect sonication, in which the ultrasonic transducers are mounted outside the reactor and are not in direct contact with the water. The ultrasonic waves propagate over a larger area, but the intensity is lower compared to a probe [1, 18].

The most common ultrasonic systems are shown in Figure 2.

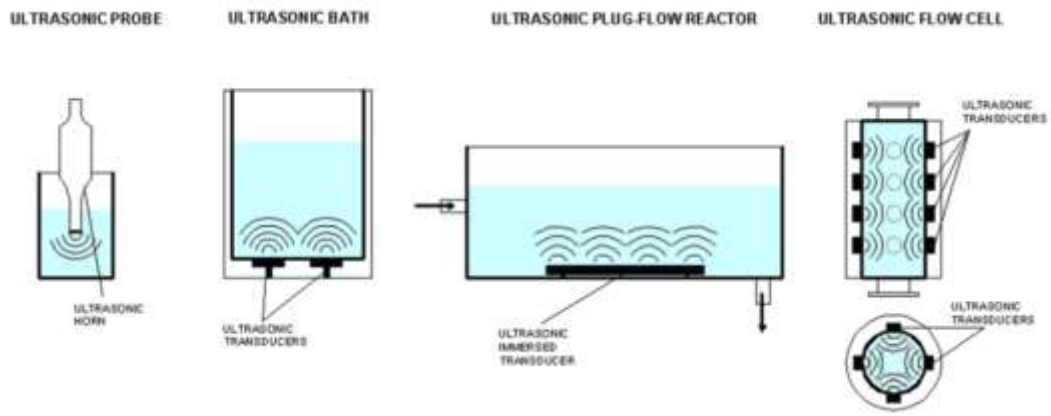

Figure 2. Typical ultrasonic systems [1]

3.2 Application of ultrasound in water and wastewater treatment – previous research

Considering previous research in water and wastewater treatment, ultrasound has been used in membrane filtration as it increases membrane fouling [27, 28], disinfection [1, 7, 27, 29, 30], removal of organic pollutants [5, 18, 27, 31], oil [10, 32-36], pharmaceuticals [37-38], trihalomethanes [39, 40], algae [7], turbidity and total suspended solids [7, 27].

Previous studies have also shown that ultrasound has a positive effect on electrocoagulation. For example, ultrasonic waves inhibit anode passivation and thus increase the production of metal hydroxides, which in turn increases treatment efficiency [41, 42]. This increased production of hydroxides also shortens the required treatment time. In addition, free radicals and cavitation increase electrical conductivity, and hydrogen production has a positive effect on flotation [41]. On the other hand, the separation of metal ions from the electrodes increases electrode consumption [42, 43], and high-frequency ultrasonic waves can lead to the decomposition of the flocs [41, 44].

In the combination of ultrasound and electrocoagulation in the treatment of oily wastewater, ultrasound was usually used as a substitute for a magnetic stirrer [43, 45, 46].

In experimental research, the effect of ultrasound alone on mineral oil removal has not been investigated, as other studies [1, 2, 9, 21, 22, 43, 45, 46] and preliminary results [47] showed that the removal effect is not sufficient for contaminant removal.

4 Experimental research

4.1 Materials and methods

In each experiment, 8 liters of oily wastewater circulated (flowed) through a sono-EC device. Initial mineral oil concentrations varied from 541 mg/l to 847 mg/l. The device consisted of four electrodes (iron or aluminium) and eight ultrasonic transducers. The electrodes were completely immersed in the wastewater and were placed at a distance of 10 mm and connected to a power supply (LBN-1990, MC Power, Germany) (Fig. 3). The ultrasonic transducers with a total power of 480 W and a frequency of 40 kHz were fixed to an insulated steel plate and attached to the bottom of the reactor (Fig. 4). The flow was ensured by a pump (Kennet K7, Stuart Turner Ltd, UK). The experimental part consisted of different variations of flow rate (0.1 to 0.75 l/s), current density (20 to 120 A/m^2), number of cycles (how many times the water circulated through the device – from 3 to 20), electrodes (iron or aluminium) and methods used (EC or sono-EC). A total of 68 experiments were performed by combining these parameters.

Figure 3. Electrodes immeresed in oily wastewater [47]

Figure 4. Ultrasonic transducers attached on the underside of the reactor [47]

5 Results and discussion

The result, considering the optimal flow rate, current density and number of cycles, have already been presented in the papers [35] and [36]. For sono-EC with iron electrodes, the optimal conditions were 10.948 cycles, a current density of 107.12 A/m^2 and a flow rate of 0.468 l/s. In this case, 93.3 % of the mineral oil was removed [35]. For aluminum electrodes, the experimental results showed that this hybrid system can effectively reduce the mineral oil by 94.3 % under the optimal conditions of 14.130 cycles, current density of 53.07 A/m^2 and a flow rate of 0.234 L/s [36].

This paper therefore only considers the results related to ultrasound. Fig 5. shows that the use of sono-EC with iron electrodes (Fig. 5 left) increases mineral oil removal up to 50 % compared to electrocoagulation alone. When using aluminum electrodes, the efficiency of mineral oil removal is generally higher than when using iron electrodes, but the influence of ultrasound is not as significant. In

this case, the removal efficiency of sono-EC is about 15 % higher than electrocoagulation alone.

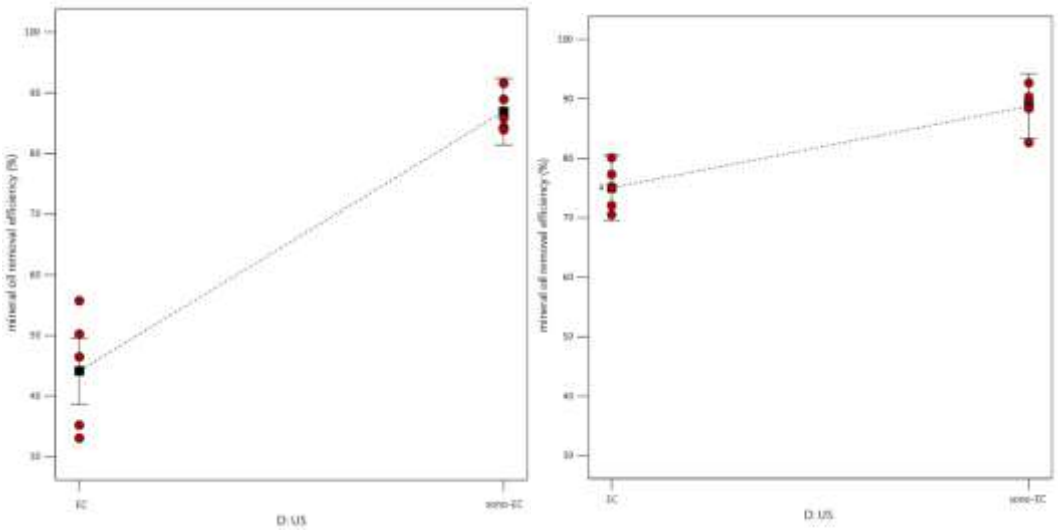

Figure 5. Effect of sono-electrocoagulation compared to electrocoagulation with iron (left) and aluminum (right) electrodes

This was also found in other papers that analyzed the treatment of oily wastewater for COD and turbidity, but not for mineral oil removal, as there is no work for this comparison. For example, Chu et al [46] found that COD removal efficiency was up to 30 % higher and turbidity up to 2 % higher when sono-EC with aluminum electrodes was used. The use of aluminum electrodes was more effective than iron due to the ionic charge. The aluminum charge is 3^+ (Al^{3+}), which is higher than the iron charge (Fe^{2+}). Fe^{2+} can oxidize into Fe^{3+}, but this takes longer. Therefore, the use of aluminum electrodes is more efficient because oxidation is faster [48].

In addition, two ultrasonic probes were used to compare the efficiency of the transducers. Each probe (Bandelin, Germany) had a power of 200 W and a frequency of 20 kHz. The probes were immersed in the oily wastewater from the top of the reactor. The efficiency of mineral oil removal was 20 % higher compared to the ultrasonic transducers. The reason for this is the increase in ultrasonic intensity of 4.2 kW/m^2. However, the use of ultrasonic probes is not recommended as it increases the cost of treatment by a factor of 500.

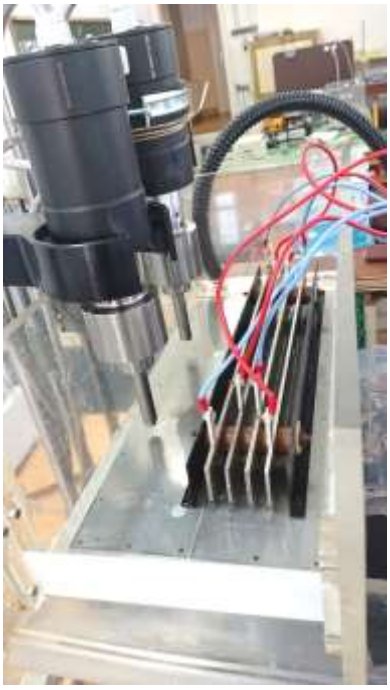

Figure 6. Ultrasonic probes [47]

6 Conclusion

Although ultrasonic technology can be used in various industries, its application for water and wastewater treatment has not yet been sufficiently researched. This research has confirmed the basic principle of ultrasonic technology that cavitation is the reason for the additional removal of mineral oil. The ultrasonic wave can be compared to what mixing or flow does in the electrocoagulation process. It causes the fusion of hydroxides and contaminants into flocs, but some additional removal effects (15 % to 50 %) prove that cavitation influences the entire removal process.

A comparison of different ultrasonic devices was also carried out. The efficiency of ultrasonic transducers and probes was compared. It was found that ultrasonic probes increase the efficiency of mineral oil removal by 20 %. However, the use of ultrasonic probes is not recommended as it significantly increases the cost of the treatment. The cost of sono-EC with ultrasonic transducers (for the optimal variant) was about 1,5 €/m^3 of treated wastewater, and the use of ultrasonic probes increased this cost by 500 times.

Acknowledgements
This work has been supported by Croatian Science Foundation under the project "IP-2019-04-1169 – Use of treated oily wastewater and sewage sludge in brick industry – production of innovative brick products in the scope of circular economy".

References:

[1] Naddeo, V., Cesaro, A., Mantzavinos, D., Fatta-Kassinos, D. and Belgiorno, V.: Water and wastewater disinfection by ultrasound irradiation-a critical review". Global Nest Journal 16(3), pp. 561–577, 2014.
[2] Mayyahi, A.A., and Al-asadi, H.A.A.: Advanced Oxidation Processes (AOPs) for Wastewater Treatment and Reuse: A Brief Review. 2(3), pp. 18–30, 2018.
[3] Son, Y.: Advanced Oxidation Processes Using Ultrasound Technology for Water and Wastewater Treatment, Handbook of Ultrasonics and Sonochemistry. Singapore: Springer Singapore. pp. 1–22.

2015
[4] Sutariya, S., Sunkesula, V. Kumar, R and Shah, K.: Emerging applications of ultrasonication and cavitation in dairy industry: a review. Cogent Food & Agriculture 4(1), pp. 1–21. 2018. doi: 10.1080/23311932.2018.1549187.
[5] Wang, J., Wang, Z., Vieira, C.L.Z., Wolfson, J.M., Pingtian, G. and Huang. S.: Review on the treatment of organic pollutants in water by ultrasonic technology. Ultrasonics Sonochemistry 55, pp. 273–278., 2019 doi: 10.1016/j.ultsonch.2019.01.017.
[6] Mason, T. and Lorimer, J.P.: Applied Sonochemistry: Uses of Power Ultrasound in Chemistry and Processing. Wiley-VCH Verlag GmbH. 2002.
[7] Doosti, M. R., Kargar, R., and Sayadi, M. H.: Water treatment using ultrasonic assistance: A review. Ecology, 2(2), pp. 96–110. 2012.
[8] Matei, N. and Scarpete, D.: Treatment of Wastewater by Ultrasound Intensity and Frequency Effect: A Review. ARPN Journal of Science and Technology, 5(11), pp. 591–597, 2015.
[9] Adewuyi, Y.G.: Sonochemistry: Environmental science and engineering applications. Industrial and Engineering Chemistry Research, 40(22), pp. 4681–4715. 2001. doi: 10.1021/ie010096l.
[10] King, W.G., Djun, L.M., Chioma Affam, A., Chung, W.C., Swee, I.W.C., and Adebayo, J.O.: Application of hybrid ultrasonic cavitation/adsorption and coagulation for treatment of palm oil mill effluent, 6th International Conference on Environment (ICENV2018). pp. 1-12, 2019
[11] Upadhyay, K., and Khandate, G.: Ultrasound Assisted Oxidation Process for the Removal of Aromatic Contamination from Effluents: A Review. Universal Journal of Environmental Reasearch and Technology 2(6), pp. 458–464. 2012
[12] Al-Juboori, R.A., and Bowtell, L.A.: Ultrasound Technology Integration into Drinking Water Treatment Train. Sonochemical Reactions, pp. 23, 2019
[13] Babu, S.G., Ashokkumar, M. and Neppolian, B.: The role of ultrasound on advanced oxidation processes“. Topics in Current Chemistry 374(5), pp. 1–32., 2016. doi: 10.1007/s41061-016-0072-9.
[14] Colmenares, J.C., Chatel, G., Ashokkumar, M., Ganesh Babu, S., Barge, A., Bhangu, S.K., Cravotto, G., Draye, M. and Rivas, D.A.: Topics in Current Chemistry Collections Sonochemistry. Springer. 2017.
[15] Gibson, J.H., Nien Yong, D.H., Farnood, R.R. and Seto, P.: A literature review of ultrasound technology and its application in wastewater disinfection“. Water Quality Research Journal of Canada 43(1), pp. 23–35, 2008.
[16] Mahvi, A. H.: Application of ultrasonic technology for water and wastewater treatment“. Iranian Journal of Public Health, 38(2), pp. 1–17. 2009.
[17] Posavcic, H, Halkijevic, I. and Vouk, D.: Oily wastewater treatment by hybrid ultrasound and electrocoagulation batch process. Desalination and Water Treatment 235, pp. 127–134. 2021 doi: 10.5004/dwt.2021.27665.
[18] Thangavadivel, K., Megharaj, M., Mudhoo, A. and Naidu, R.: Degradation of organic pollutants using ultrasound, Handbook on Applications of Ultrasound: Sonochemistry for Sustainability, pp. 47–74, 2011.
[19] Mahamuni, N. N., and Adewuyi. Y.G.: Advanced oxidation processes (AOPs) involving ultrasound for waste water treatment: A review with emphasis on cost estimation. Ultrasonics Sonochemistry 17(6), pp. 990–1003. 2010. doi: 10.1016/j.ultsonch.2009.09.005.
[20] Antes, F.G., Diehl, L.O., Pereira, J.S.F., Guimarães, R.C.L., Guarnieri, R.A., Ferreira, B.M.S., Dressler, V.L., Flores, E.M.M.: Feasibility of Low Frequency Ultrasound for Water Removal from Crude Oil Emulsions, Ultrasonics Sonochemistry, 2015. doi: http://dx.doi.org/10.1016/j.ultsonch.2015.01.003
[21] Ghanbari, F, Zirrahi, F., Lin, K.Y.A., Kakavandi, B. and Hassani. A.: Enhanced electro-peroxone using ultrasound irradiation for the degradation of organic compounds: A comparative study. Journal of Environmental Chemical Engineering 8(5):104167. 2020. doi: 10.1016/j.jece.2020.104167.
[22] Radi, M.A., Nasirizadeh, N. Rohani-Moghadam, M., and Dehghani. M.: The comparison of sonochemistry, electrochemistry and sonoelectrochemistry techniques on decolorization of C.I

Reactive Blue 49. Ultrasonics Sonochemistry 27, pp. 609–615. 2015. doi: 10.1016/j.ultsonch.2015.04.021.
[23] Osman, H.: Ultrasonic Disinfection using Large Area Compact Radial Mode Resonators. University of Glasgow, 2018.
[24] Bakhtiari, A., Berberashvili, T. & Kervalishvili, P.: Water Treatment Improvement by Ultrasonic Approach. American Journal of Condensed Matter Physics 7(4), pp. 81–86. 2017. doi: 10.5923/j.ajcmp.20170704.01.
[25] Chen, D., Sharma, S.K. & Mudhoo. A.: Handbook on Applications of Ultrasound Sonochemistry for Sustainability. Editors: D. Chen, S. K. Sharma, and A. Mudhoo. CRC Press LLC. 2012.
[26] Berlan, J. & Mason T.J.: Sonochemistry: from research laboratories to industrial plants". Ultrasonics 30(4), pp. 203–212, 1992. doi: 10.1016/0041-624X(92)90078-Z
[27] Fetyan, N. A. H. & Salem Attia, T. M.: Water purification using ultrasound waves: application and challenges". Arab Journal of Basic and Applied Sciences, 27(1), pp. 194-207, 2020, doi: 10.1080/25765299.2020.1762294
[28] Rocha, I.C.C., Marques, J.J., Silva, A.: Effects of ultrasound on the performance improvement of wastewater microfiltration through a porous ceramic filter, Brazilian Journal of Chemical Engineering, 26(4), pp. 641-648, 2009.
[29] Luhovskyi, O.F., Gryshko, I.A. and Bernyk, I.M.: Enhancing the Efficiency of Ultrasonic Wastewater Disinfection Technology. Journal of Water Chemistry and Technology. 40(2), pp. 95–101, 2018.
[30] Yang, W. Dong, L., Luo,Z., Cui, X., Liu, J., Liu, Z., Huo, M.: Application of ultrasound and quartz sand for the removal of disinfection byproducts from drinking water. Chemosphere, 101, pp. 34-40, 2014. doi: 10.1016/j.chemosphere.2013.11.018
[31] Hashim, K.S., Shaimaa Satae M.A., Jawad K.A., Kot, P., Shaw, A. Al Khaddar, R., Idowu, I. and Gkantou. M.: Escherichia coli inactivation using a hybrid ultrasonic–electrocoagulation reactor". Chemosphere, 247, 2020. doi: 10.1016/j.chemosphere.2020.125868
[32] Behnia, I., Prakash, A. and Williams, G.: Ultrasonic Based Device to Monitor Oil Separation from Oily Water Discharges. Canadian Journal of Chemical Engineering 97(1), pp. 115–22. 2019. doi: 10.1002/cjce.23243
[33] Li Y, Xiang D.: Stability of oil-in- water emulsions performed by ultrasound power or high-pressure homogenization". PLoS ONE 14(3): e0213189, 2019. doi: 10.1371/journal. pone.0213189
[34] Mohsin, M., and Meribout, M.: Oil-water de-emulsification using ultrasonic technology. Ultrasonics Sonochemistry 22, pp. 573–79. doi: 10.1016/j.ultsonch.2014.05.014, 2015.
[35] Posavcic, H., Halkijevic, I., Vouk, D., Druskovic, M.: Application of Box–Behnken design for circulating flow sono-electrocoagulation for oily wastewater treatment. Journal of Environmental Science and Health, Part A, 57(8): 645-655, 2022. doi:10.1080/10934529.2022.2099520
[36] Posavcic, H., Halkijevic, I., Vouk, D., Cvetnic, M.: Circulating flow hybrid ultrasonic and electrochemical process for the treatment of mineral oil wastewaters. Journal of Water Process Engineering, 49, 103024, 12, 2022. doi:10.1016/j.jwpe.2022.103024
[37] Fröhlich, A. C., Foletto, E. L., Dotto, G. L.: Ultrasonic Modification on Activated Carbon and Its Application for Ibuprofen Adsorption", 12 Encontro Brasileiro sobre Adsorcao, pp. 1-8, 2018
[38] Serna-Galvis, E.A., Silva-Agredo, J., Giraldo-Aguirre, A.L., Flórez-Acosta, O.A., Torres-Palma, R.A.: High frequency ultrasound as a selective advanced oxidation process to remove penicillinic antibiotics and eliminate its antimicrobial activity from water. Ultrasonics Sonochemistry, 2016. doi: http:// dx.doi.org/10.1016/j.ultsonch.2016.01.007
[39] Shemer, H., Narkis, N.: Sonolytic Destruction of Trihalomethanes by Ultrasonic Irradiation. Israel Journal of Chemistry. 46, pp. 27–32, 2006.
[40] Thokchom, B.: Degradation of trihalomethanes using ultrasound-based nanocatalyst, Disinfection By-products in Drinking Water, pp. 56-81, 2020.
[41] Ghernaout, D. Advanced oxidation phenomena in electrocoagulation process: a myth or a reality? Desalination and Water Treatment, 51(40–42), pp. 7536–7554, 2013 doi: 10.1080/19443994.2013.792520.
[42] Moradi, M., Vasseghian, Y., Arabzade, H. and Mousavi Khaneghah, A.: Various wastewaters

treatment by sono-electrocoagulation process: A comprehensive review of operational parameters and future outlook. Chemosphere, 263:128314. 2021, doi: 10.1016/j.chemosphere.2020.128314

[43] Maha Lakshmi, P., and Sivashanmugam, P.: Treatment of oil tanning effluent by electrocoagulation: Influence of ultrasound and hybrid electrode on COD removal. Separation and Purification Technology 116, pp. 378–384, 2013. doi: 10.1016/j.seppur.2013.05.026

[44] He, C.C., Hu, C.Y. and Lo, S.L.: Evaluation of sono-electrocoagulation for the removal of Reactive Blue 19 passive film removed by ultrasound. Separation and Purification Technology 165, pp. 107–113, 2016. doi: 10.1016/j.seppur.2016.03.047

[45] Al-Rubaiey, N.A., and Al-Barazanjy, M.G.: Ultrasonic Technique in Treating Wastewater by Electrocoagulation. Engineering and Technology Journal, 36(1), pp. 54–62. 2018. doi: 10.30684/etj.36.1C.9

[46] Chu, J., Li, Y., Li, N. and Huang, W.: Treatment of car-washing wastewater by electrocoagulation-ultrasound technique for reuse. Advanced Materials Research, 433–440, pp. 227–232, 2012. doi: 10.4028/www.scientific.net/AMR.433-440.227

[47] Posavčić, H.: The development of the continuous flow hybrid ultrasound and electrocoagulation process for the treatment of mineral oil wastewaters, doctoral thesis, 2022.

[48] Linares-Hernández, I., Barrera-Díaz, C., Roa-Morales, G., Bilyeu, B., Ureña-Núñez, F.: Influence of the anodic material on electrocoagulation performance, Chemical Engineering Journal, 148(1), pp. 97-105, 2009.

ELECTROCHEMICAL REMOVAL OF PESTICIDE ACERAMIPRID

KATARINA LICHT [1], ANTONIJA MATANČEVIĆ [1], DRAŽEN VOUK [1], IVAN HALKIJEVIĆ [1]

[1] *University of Zagreb Faculty of Civil Engineering, Croatia,* katarina.licht@grad.unizg.hr

[1] *University of Zagreb Faculty of Civil Engineering, Croatia,* amatancevic@student.grad.hr

[1] *University of Zagreb Faculty of Civil Engineering, Croatia,* drazen.vouk@grad.unizg.hr

[1] *University of Zagreb Faculty of Civil Engineering, Croatia,* ivan.halkijevic@grad.unizg.hr

1 Abstract

Acetamiprid, a neonicotinoid insecticide widely employed in agricultural practices, has garnered attention due to its persistence, toxicity, and potential adverse effects on non-target organisms. Traditional wastewater treatment processes often prove inadequate in efficiently removing pesticides necessitating the exploration of more adequate remediation technologies. Electrochemical methods offer a promising avenue for the degradation and removal of pesticide contaminants from aqueous environments.

In this study, the response surface methodology was used to investigate the possibility of electrochemical removal of acetamiprid from water. For statistical experimental design, central composite design was used, and three factors were studied – electrode material (Fe, Cu, Al), treatment time (15, 37.5, 60 min) and applied current (4, 9, 14 A). Electrochemical treatment proved to be a viable option with efficiencies over 50%.

Keywords: neonicotinoid, acetamiprid, electrochemical treatment, wastewater, oxidation

2 Introduction

In order to increase food production cost-effectively and with limited resources, the use of pesticides is essential.[1] Pesticides primarily protect crops from diseases and pests, but they also play a critical role in public health by safeguarding humans and animals from infectious diseases. These chemicals are persistent organic pollutants, predominantly synthetic, that are often resistant to photolytic, biological, and chemical degradation, leading to their bioaccumulation in the environment and integration into biogeochemical cycles and food chains.[2] Insecticides, a major category of pesticides, are designed to manage insect pests.

Neonicotinoids emerged in the 1990s as a more environmentally friendly alternative to traditional insecticides due to their high selectivity for insects and low toxicity to mammals, birds, and fish.[3] Their popularity stems from their selective targeting, low vertebrate toxicity, and high effectiveness against arthropods, sucking insects, and chewing insects. Additionally, their unique physicochemical properties allow them to be applied to a wide variety of crops. Beyond agriculture, neonicotinoids are used in homes, gardens, and lawns to control pests such as termites and cockroaches.[4]

Despite their effectiveness, concerns have arisen regarding the adverse effects of neonicotinoids. They pose significant risks to bees, leading to bans on neonicotinoid-treated seeds in some countries. They also threaten aquatic environments, particularly affecting invertebrates like mollusks. The excessive and uncontrolled use of neonicotinoids jeopardizes entire ecosystems due to their high polarity, solubility, and photostability.[5] Recent studies have confirmed the presence of neonicotinoids in aquatic ecosystems, highlighting the serious environmental risks posed by agricultural runoff and effluents.[4, 6–8] These waters often contain non-biodegradable compounds such as pesticides, which cannot be fully

removed through conventional biological treatment. Therefore, appropriate and comprehensive treatment methods are necessary to mitigate these environmental risks.[9]

Various methods, particularly advanced oxidation processes like photolysis, photocatalysis, photo-Fenton, ozonation, electrocatalytic oxidation, and electro-Fenton oxidation, have been successfully employed to remove neonicotinoids from water.[10–12] Furthermore, electrochemical processes have become prominent as effective methods for treating water containing various pollutants, including heavy metals, selenium, mineral oils, dyes, microorganisms, and pesticides.[10, 13–19]

Electrocoagulation (EC) is a widely utilized electrochemical wastewater treatment that combines the benefits of coagulation, flotation, and electrochemistry.[18, 20, 21] This process involves dissolving the metal anode under the influence of an applied current density, resulting in the in situ formation of the coagulant.[13, 15] These coagulant species can then react with organic compounds in the wastewater to form flocs, which can be easily removed by sedimentation or flotation. Simultaneously, oxygen evolves at the anode and hydrogen at the cathode, facilitating the removal of contaminants through flotation.[20]

In this study, the electrochemical degradation of acetamiprid was investigated in a batch reactor using the design of experiments methodology. The aim was to create a statistical model capable of forecasting pollutant conversion. This model would be useful for predicting the system's performance under various reaction conditions, ultimately aiming to optimize the efficiency of the wastewater treatment process.

3 Materials and methods

3.1 Statistical experimental design

A face-centered central composite design within the response surface methodology (RSM) was employed to create a statistical model and determine the optimal conditions for the electrochemical degradation of acetamiprid. RSM is a set of statistical and mathematical techniques designed for modeling and analyzing problems where the response of interest is affected by multiple variables, with the goal of optimizing this response.[19] The study examined the individual and interaction effects of applied electric current, treatment time, and electrode material on the efficiency of the process. The investigated factors and their corresponding leveles are listed in Table 1. The values of each factor were chosen based on the preliminary experimental results and literature.

Table 1. Factors used for the experimental design

Factor symbol	Factor name	Unit	Type	Minimum	Middle level	Maximum
A	**Current (I)**	A	Numeric	4	9	14
B	**Time (t)**	min	Numeric	15	37.5	60
C	**Electrode material**		Categoric	Aluminum (Al)	Iron (Fe)	Copper (Cu)

Two responses were studied – the efficiency of COD (chemical oxygen demand) and acetamiprid removal. The efficiencies were calculated following the Eq 1.

$$Removal\ efficiency\ (\%) = \frac{C_0 - C}{C_0} * 100 \quad (1)$$

C_0 represents the initial concentration of acetamiprid/COD measurment, while C is the COD/acetamiprid level after the EC treatment. Obtained results were analysed using the ANOVA (variance analysis) methodology. The experimental matrix with a total of 30 runs and corresponding responses are shown in Table 2. DesignExpert 13, a software by StatEase was used for this experimental design and analysis.

Table 2. Experimental matrix and corresponding COD and acetamiprid removal efficiencies

Run	I (A)	t (min)	material	ACM, %	COD, %
1	14	37.5	Al	4.30	10.87
2	14	60	Fe	38.95	37.78
3	9	37.5	Cu	48.45	54.55
4	14	15	Fe	9.47	13.33
5	9	37.5	Fe	9.09	15.91
6	4	15	Cu	12.36	27.27
7	9	15	Fe	10.64	18.18
8	9	37.5	Fe	12.77	20.45
9	4	15	Al	2.22	6.25
10	14	15	Cu	30.39	31.11
11	14	60	Cu	75.49	37.78
12	4	60	Cu	37.08	65.91
13	9	37.5	Al	14.95	7.50
14	9	60	Al	21.50	27.50
15	9	15	Al	14.02	2.50
16	9	60	Fe	21.28	29.55
17	4	37.5	Al	3.33	14.58
18	4	60	Al	4.44	16.67
19	14	15	Al	2.15	10.87
20	4	37.5	Cu	20.22	40.91
21	9	37.5	Cu	43.33	47.62
22	14	60	Al	16.13	13.04
23	9	60	Cu	71.11	50.00
24	4	15	Fe	8.42	5.45
25	9	15	Cu	14.44	30.95
26	14	37.5	Cu	56.86	35.56
27	4	60	Fe	13.68	27.27
28	9	37.5	Al	6.32	11.90
29	14	37.5	Fe	24.21	20.00
30	4	37.5	Fe	12.63	25.45

3.2 Experimental set-up

All of the experiments were carried out in a batch EC reactor, made from a modified ultrasonic bath (TI-H 10 MF2, Elma Ultrasonics) shown in Figure 1. The reactor was insulated by a thin plastic film, and diveded into two sections by a baffle. Each section housed 4 plate electrodes, which were arranged in a parallel bipolar mode with 1 cm interelectrode distance. A total of 8 electrodes (4 anodes and 4 cathodes) made from aluminum (Al), iron (Fe) or copper (Cu) were connected to the laboratory power supply (LBN-1990, MeanWell). All electrodes used for a certain experimental run were of the same material, according to Table 2. They were connected in a monopolar parallel mode (+-+-/+-+-). The voltage on the power supply was adjusted during each run to ensure the needed current strength, raging from 16 to 50 V. A pump (GC-TP 4622 from Einhell) was used for recirculation to ensure homogeneity before taking the samples. For each experiment, 5 litres of 10 ppm acetamiprid model solution was used. Average values of physical and chemical propetries of the treated water before and after the treatment are listed in Table 3. The inital COD value was measured at 55 mg O_2/L.

Experiments were conducted acording to the experimental matrix shown in Table 2, using 4, 9 and 14 A of applied current for 15, 37.5 and 60 minutes of treatment time. The samples were taken at the beginning and the end of each experiment and acetamiprid concentrations were determined by UV/Vis spectrophotometry at an absorption wavelength of 245 nm, using Agilent Cary 60 spectrophotometer. COD measurments were obtained using Nanocolor ready-made cuvette tests (potassium dichromate method) and photometer.

Figure 1. Modified ultrasonic bath used as an EC reactor in this study

Table 3. Physico-chemical properties of the treated water

	pH	Dissolved oxygen, ppm	Conductivity, µS/cm	Total dissolved solids, ppm	Turbidity, FNU	Temperature, °C
Before treatment	7.85	6.18	614	307	0.60	14.63
After Fe, 9 A, 60 min	7.99	5.90	423	113	6.70	25.55
After Al, 9 A, 60 min	8.31	3.02	319	91	4.50	30.69
After Cu, 9 A, 60 min	7.76	4.68	248	82	3.90	27.13

4 Results and discussion

In this study, an electrochemical process was used to treat wastewater containing acetamiprid. The influence and mutual interactions of three process parameters – applied current, treatment time and electrode material - were investigated. The highest acetamiprid (75.49%) and COD (65.91%) removal was achieved by using Cu electrodes for 60 minutes at 14 A and 4 A applied current, respectively. In general, treatment with Cu electrodes resulted in the highest efficiencies, while Al electrodes performed poorly. Also, the highest current density and the longest treatment time resulted in better COD and acetamiprid removal.

The 3 parameters investigated, are also the most important process parameters for any EC proccess, as they have a direct impact on the efficiency of the process, as well as its cost. The electrode material determines which ionic metal species will be present in the solution and metal hydroxides that will be formed. The applied current density determines the coagulant production rate and influences the production of gases, and thus the growth of the flocs.[16] According to Faraday's law, more metal ions are released into the solution at the same current density and consequently more flocs are formed with a longer treatment time.

The results of this study are consistent with other similar reports in the literature. [19] The sludge generated during the EC process was analysed and the results showed that the predominant mechanism of acetamiprid removal is chemical degradation rather than physical removal by the flocs formed. It is noteworthy that acetamiprid was found to be more resistant to EC degradation than the similar pesticide imidacloprid [10, 11] due to the differences in their chemical structure. The COD reduction does not

always correspond to the reduction of the acetamiprid, because, although electrochemical degradation of pesticides in water generally leads to a reduction in COD, the exact impact depends on the efficiency of the degradation process, the nature of the intermediate products formed, and the presence of any side reactions.

In the continuation of the text, the results of the variance analysis will be described. The significant factors and interactions were identified using a significance level of 0.05. A p-value below 0.05 signifies that the variable has a significant impact on the response, whereas a p-value above 0.1 suggests that the variable has minimal effect on the response.[17]

4.1 Acetamiprid degradation

The electrochemical degradation of acetamiprid is described by a reduced cubic model, described in Table 4. The F-value of the model of 41.44 implies that the model is significant. There is only a 0.01% chance that such a large F-value could occur due to noise. As mentioned before, p-values less than 0.05 indicate that the model terms are significant. In this case, all of the process parameters, as well as some of their interactions, appear to be significant with p-values of less than 0.0001. This means that the electrode material, the current density, and the treatment time have a similar relative impact.

The Cu electrodes performed better than the Al and Fe electrodes, regardless of the treatment time or current density. In the case of time and applied current the degradation was found to be greatest at high current densities and treatment times of more than 37.5 minutes. At the lowest current densities and a treatment time of less than 15 minutes, the decrease in acetamiprid concentration is only marginal. For long treatment times, the influence of current density is not very evident. With relatively short treatment times, however, the removal increases significantly with the current density.

Table 4. Results of ANOVA analysis for reduced cubic model

Source	Sum of Squares	df	Mean Square	F-value	p-value	
Model	11037,97	12	919,83	41,44	< 0.0001	significant
A-I	1145,13	1	1145,13	51,59	< 0.0001	
B-t	2124,43	1	2124,43	95,71	< 0.0001	
C-material	5652,88	2	2826,44	127,34	< 0.0001	
AB	264,70	1	264,70	11,93	0,0030	
AC	564,67	2	282,34	12,72	0,0004	
BC	978,87	2	489,43	22,05	< 0.0001	
A^2	78,73	1	78,73	3,55	0,0769	
A^2C	228,56	2	114,28	5,15	0,0179	
Residual	377,33	17	22,20			
Lack of Fit	320,21	14	22,87	1,20	0,5020	not significant
Pure Error	57,12	3	19,04			
Cor Total	11415,30	29				

A relatively good agreement between the calculated and experimental values (Figure 2) validate the obtained model. The graphical interpretation of the model through corresponding response surfaces can be seen in Figure 3. While Al and Fe electrodes show similar behavior, Cu electrodes stand out with clear area of optimal factor values. Equations 2, 3 and 4 represent the mathematical description of the model for Al, Fe and Cu electrodes, respectively. The equation in terms of actual factors can be used for making predictions about the response for given levels of each factor.

$$ACM\ removal\ (\%) = -10{,}48 + 5{,}17I - 0{,}20t + 0{,}04It - 0{,}35I^2 \quad (2)$$

$$ACM\ removal\ (\%) = 17{,}97 - 3{,}51I - 0{,}04t + 0{,}04It + 0{,}18I^2 \quad (3)$$

$$ACM\ removal\ (\%) = -22{,}78 + 5{,}57I + 0{,}56t + 0{,}04It - 0{,}22I^2 \quad (4)$$

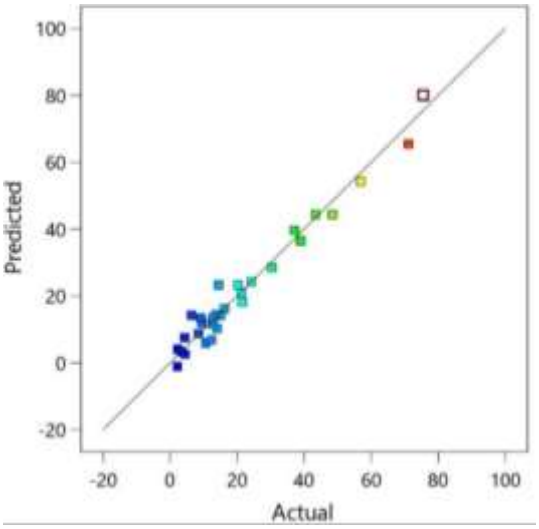

Figure 2. The comparison between predicted and actual acetamiprid efficiencies

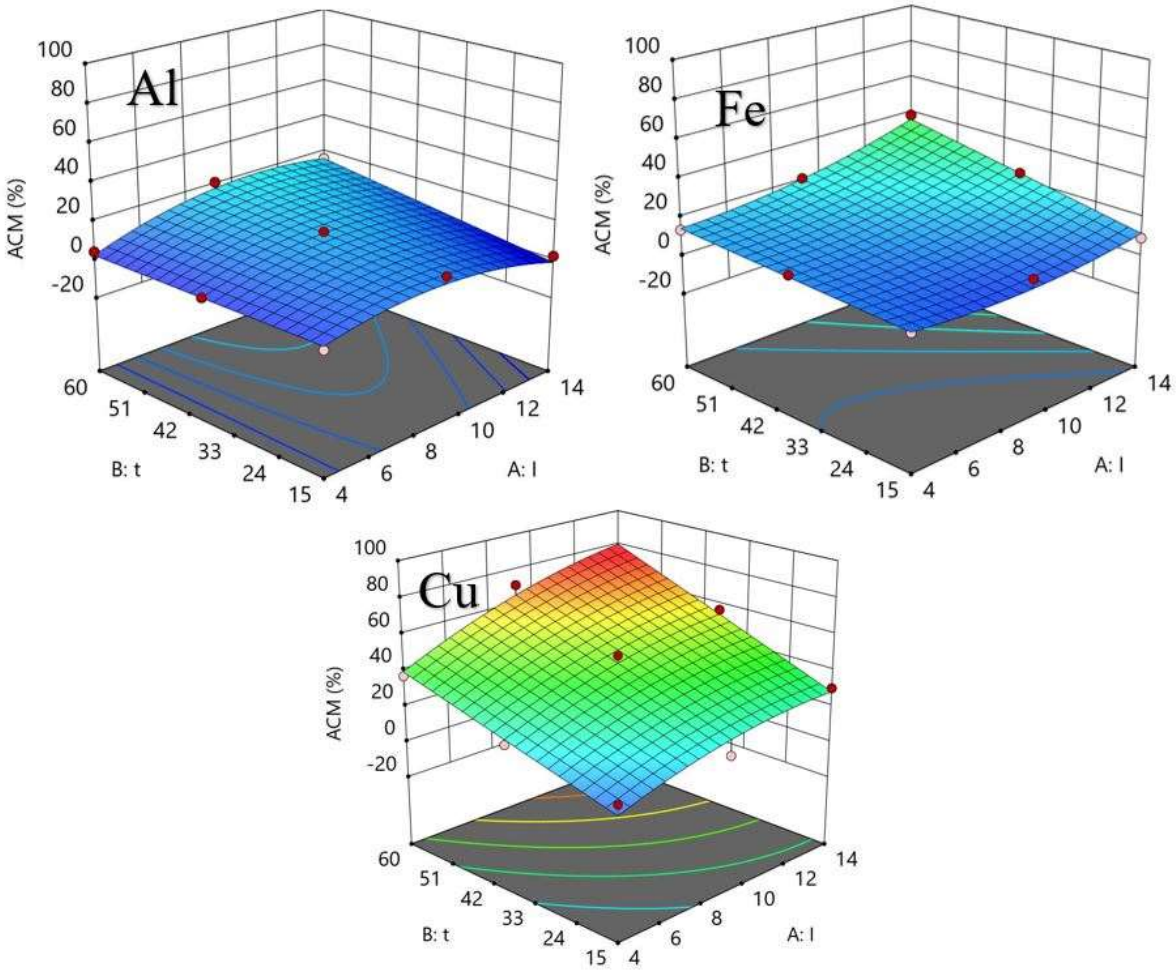

Figure 3. Response surfaces for acetamiprid removal using Al, Fe and Cu electrodes

4.2 COD removal

A reduced linear model is obtained for the description of the electrochemical removal of COD and the ANOVA results are listed in Table 5. As it can be seen, electrode material and treatment duration appear

to be the only significant factors with p-values of less than 0.0001.

Table 5. ANOVA results for reduced liner model

Source	Sum of Squares	df	Mean Square	F-value	p-value	
Model	6140,94	3	2046,98	48,75	< 0.0001	significant
B-t	1414,94	1	1414,94	33,70	< 0.0001	
C-material	4725,99	2	2363,00	56,27	< 0.0001	
Residual	1091,78	26	41,99			
Lack of Fit	1047,78	23	45,56	3,11	0,1906	not significant
Pure Error	44,00	3	14,67			
Cor Total	7232,72	29				

A graphical representation of the interaction of the two factors – time and electrode material - is given in Figure 4. It confirms that the treatment time has the greatest influence, meaning that the longer the treatment time, the higher the COD removal will be in the case of all 3 electrode materials. However, the Cu electrodes stand out with higher efficiencies for the same treatment time. The same can be concluded from the mathematical description of the model. The following equations describe reduced linear models of COD removal during the EC treatment with Al (Eq. 5), Fe (Eq. 6) and Cu (Eq. 7) electrodes.

$$COD\ removal\ (\%) = -2{,}61 + 0{,}39t \tag{5}$$

$$COD\ removal\ (\%) = 6{,}56 + 0{,}39t \tag{6}$$

$$COD\ removal\ (\%) = 27{,}39 + 0{,}39t \tag{7}$$

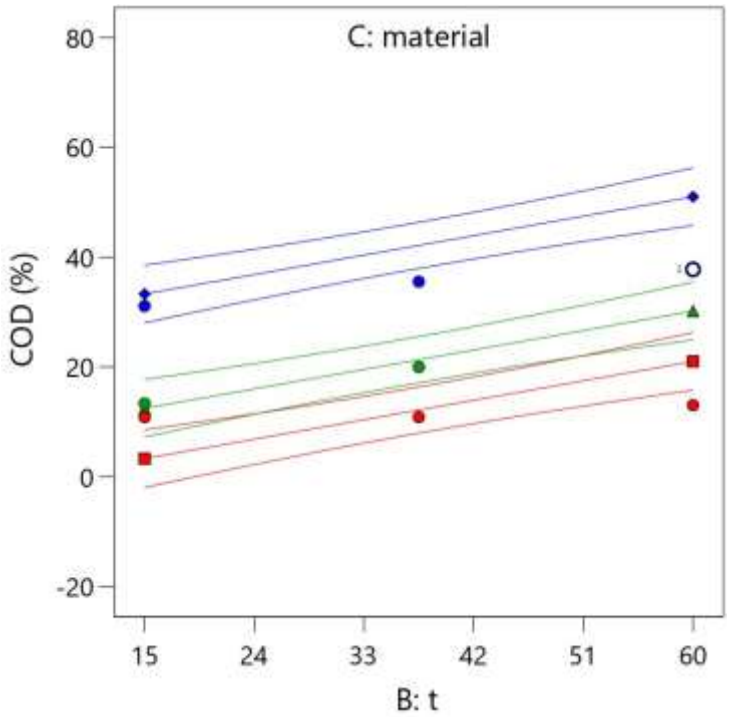

Figure 4. The effect of time and material on COD removal (Cu – blue, Fe – green, Al - red)

5 Conclusion

This paper investigates the application of statistical design of experiments and response surface analysis for the electrochemical degradation of the neonicotinoid insecticide acetamiprid. The experimental design allowed an evaluation of the influence of three process variables: applied current, treatment time

and electrode material. A reduced cubic model obtained showed a relatively good agreement with the experimental acetamiprid degradation efficiencies. The highest acetamiprid degradation of 71% was achieved by applying 14 A current to Cu electrodes for 60 minutes. In general, the longer the treatment time and the higher the current density, the higher the degradation rate.

Acknowledgements
This work was supported by the Croatian Science Foundation under the project PRIMEUS (UIP2020-02-1160).

References:
[1] Sraw, A.; Kaur, T.; Pandey, Y.; Sobti, A.; Wanchoo, R.K. and Toor, A.P.: Fixed bed recirculation type photocatalytic reactor with TiO2 immobilized clay beads for the degradation of pesticide polluted water, Journal of Environmental Chemical Engineering, 6, pp. 7035–7043, 2018.
[2] Mahmood, I.; Imadi, S.R.; Shazadi, K.; Gul, A. and Hakeem, K.R.: Effects of Pesticides on Environment, Plant, Soil and Microbes: Volume 1: Implications in Crop Science, Springer International Publishing, Cham, 2016, pp. 253–269.
[3] Serrano, E.; Munoz, M.; de Pedro, Z.M. and Casas, J.A.: Fast oxidation of the neonicotinoid pesticides listed in the EU Decision 2018/840 from aqueous solutions, Separation and Purification Technology, 235, p. 116168, 2020.
[4] Jeschke, P.; Nauen, R.; Schindler, M. and Elbert, A.: Overview of the status and global strategy for neonicotinoids, Journal of Agricultural and Food Chemistry, 59, pp. 2897–2908, 2011.
[5] Bonmatin, J.-M.; Giorio, C.; Girolami, V.; Goulson, D.; Kreutzweiser, D.P.; Krupke, C.; Liess, M.; Long, E.; Marzaro, M.; Mitchell, E.A.D.; Noome, D.A.; Simon-Delso, N. and Tapparo, A.: Environmental fate and exposure; neonicotinoids and fipronil, Environmental Science and Pollution Research, 22, pp. 35–67, 2015.
[6] Finnegan, M.C.; Emburey, S.; Hommen, U.; Baxter, L.R.; Hoekstra, P.F.; Hanson, M.L.; Thompson, H. and Hamer, M.: A freshwater mesocosm study into the effects of the neonicotinoid insecticide thiamethoxam at multiple trophic levels, Environmental Pollution, 242, pp. 1444–1457, 2018.
[7] Gonzalez-Rey, M.; Tapie, N.; Le Menach, K.; Dévier, M.-H.; Budzinski, H. and Bebianno, M.J.: Occurrence of pharmaceutical compounds and pesticides in aquatic systems, Marine Pollution Bulletin, 96, pp. 384–400, 2015.
[8] Hladik, M.L.; Kolpin, D.W. and Kuivila, K.M.: Widespread occurrence of neonicotinoid insecticides in streams in a high corn and soybean producing region, USA, Environmental Pollution (Barking, Essex: 1987), 193, pp. 189–196, 2014.
[9] Jiménez-Tototzintle, M.; Oller, I.; Hernández-Ramírez, A.; Malato, S. and Maldonado, M.I.: Remediation of agro-food industry effluents by biotreatment combined with supported TiO2/H2O2 solar photocatalysis, Chemical Engineering Journal, 273, pp. 205–213, 2015.
[10] Ghalwa, N. and Farhat, N.: Removal of Imidacloprid Pesticide by Electrocoagulation Process using Iron and aluminum Electrodes, Journal of Environmental Analytical Chemistry, 02, 2015.
[11] Halkijevic, I.; Licht, K.; Kosar, V. and Bogdan, L.: Degradation of the neonicotinoid pesticide imidacloprid by electrocoagulation and ultrasound, Scientific Reports, 14, p. 8836, 2024.
[12] Licht, K.; Kosar, V.; Tomašić, V. and Duplančić, M.: Removal of the neonicotinoid insecticide acetamiprid from wastewater using heterogeneous photocatalysis, Environmental Technology, 44, pp. 1125–1134, 2021.
[13] Biswas, B. and Goel, S.: Electrocoagulation and electrooxidation technologies for pesticide removal from water or wastewater: A review, Chemosphere, 302, p. 134709, 2022.
[14] Abdel-Gawad, S.A.; Baraka, A.M.; Omran, K.A. and Mokhtar, M.M.: Removal of Some Pesticides from the Simulated Waste Water by Electrocoagulation Method Using Iron Electrodes., Int. J. Electrochem. Sci., 7, 2012.
[15] Almukdad, A.; Hafiz, M.; Yasir, A.T.; Alfahel, R. and Hawari, A.H.: Unlocking the application potential of electrocoagulation process through hybrid processes, Journal of Water Process Engineering, 40, p. 101956, 2021.

[16] Ramya, T.; Premkumar, P.; Thanarasu, A.; Velayutham, K.; Dhanasekaran, A. and Sivanesan, S.: Degradation of pesticide-contaminated wastewater (coragen) using electrocoagulation process with iron electrodes, Desalination and Water Treatment, 165, pp. 103–110, 2019.
[17] Posavcic, H.; Halkijevic, I.; Vouk, D. and Cvetnic, M.: Circulating flow hybrid ultrasonic and electrochemical process for the treatment of mineral oil wastewaters, Journal of Water Process Engineering, 49, p. 103024, 2022.
[18] Simon, R.G.; Stöckl, M.; Becker, D.; Steinkamp, A.D.; Abt, C.; Jungfer, C.; Weidlich, C.; Track, T. and Mangold, K.M.: Current to Clean Water – Electrochemical Solutions for Groundwater, Water, and Wastewater Treatment, Chemie-Ingenieur-Technik, 90, pp. 1832–1854, 2018.
[19] John, S.; Soloman, P.A. and Fasnabi, P.A.: Study on Removal of Acetamiprid from Wastewater by Electrocoagulation, Procedia Technology, 24, pp. 619–630, 2016.
[20] Mao, Y.; Zhao, Y. and Cotterill, S.: Examining Current and Future Applications of Electrocoagulation in Wastewater Treatment, Water, 15, p. 1455, 2023.
[21] Moussa, D.T.; El-Naas, M.H.; Nasser, M. and Al-Marri, M.J.: A comprehensive review of electrocoagulation for water treatment: Potentials and challenges, Journal of Environmental Management, 186, pp. 24–41, 2017.

AMMUNITION FACTORY WASTEWATER TREATMENT BY ELECTROCOAGULATION

KATARINA LICHT [1], MARIJA GLAVAŠ [1], IVAN HALKIJEVIĆ [1], DRAŽEN VOUK [1], TOMISLAV BOLANČA [2], ANJA CRNOGAJ [3]

[1] University of Zagreb Faculty of Civil Engineering, Croatia, katarina.licht@grad.unizg.hr

[1] University of Zagreb Faculty of Civil Engineering, Croatia, glavasmari@gmail.com

[1] University of Zagreb Faculty of Civil Engineering, Croatia, ivan.halkijevic@grad.unizg.hr

[1] University of Zagreb Faculty of Civil Engineering, Croatia, drazen.vouk@grad.unizg.hr

[2] University of Zagreb Faculty of Chemical Engineering and Technology, Croatia, tbolanca@fkit.unizg.hr

[3] BO GROUP d.o.o., Croatia, acrnogaj.inzenjering@bp-group.hr

1 Abstract

The discharge from ammunition factories typically contains a cocktail of pollutants, including heavy metals, organic compounds, and suspended solids, posing potential ecological risks if left untreated. Electrocoagulation (EC) emerges as a promising alternative for the remediation of such challenging effluents. EC, a robust electrochemical process, involves the dissolution of sacrificial electrodes to induce coagulation and subsequent removal of contaminants through processes such as precipitation, flocculation, and electroflotation. This paper presents an investigation into the application of electrocoagulation for the treatment of ammunition factory wastewater. Using a simple set-up, two electrode materials, aluminum and iron, were tested, as well as their combinations. The influence of the initial pH value of the solution was, also, investigated. Treatment time varied from 5 to 30 minutes and electric current of 3 A was used in all of the experiments. 50% of COD and almost complete heavy metal removal was achieved in 30 minutes, indicating that electrocoagulation could be a promising technique for the remediation of heavily contaminated wastewaters.

Keywords: electrocoagulation, wastewater treatment, COD, heavy metals, ammunition factory wastewater

2 Introduction

Ammunition production wastewater typically contains a diverse array of pollutants, including heavy metals like lead, copper, zinc, sulphates, nitrates, organic compounds such as nitroaromatics and propellants, and other toxic substances originating from cleaning, plating, and degreasing operations within manufacturing facilities. These wastewaters are, also, characterized by a low pH and high chemical oxygen demand (COD) and could pose significant environmental and health risks if not properly treated.[1] Implementing efficient treatment methods is essential to comply with environmental regulations and ensure sustainable industrial practices. The treatment technologies employed must not only be capable of efficiently removing pollutants but also be economically viable and adaptable to the specific characteristics of ammunition production effluents. Conventional treatment methods, while effective for certain pollutants, often fall short in addressing the complex composition of this industrial effluent. Electrochemical processes offer a promising alternative for the remediation of ammunition production wastewater, leveraging the unique capabilities of electrochemistry to degrade organic compounds, neutralize heavy metals, and eliminate explosive residues.[2, 3]

Electrocoagulation (EC), a widely studied electrochemical process, involves the use of electric current to remove contaminants like organic pollutants, suspended solids, emulsified oils, and dissolved metals from water.[4–6] The most commonly reported electrocoagulation setup involves using iron, aluminum,

or steel electrodes connected to a direct current power supply.[7, 8] Various mechanisms of pollutant removal are recognized in electrocoagulation. The anode acts as a sacrificial electrode, generating dissolved metal ions and, through water electrolysis, producing protons and gaseous oxygen. At the cathode, hydroxide ions (OH^-) and gaseous hydrogen are formed, and the electrochemical reduction of metal ions, including heavy metals, occurs. The reaction of metal ions, specifically Fe^{3+} or $Al^{3+,}$ with OH^- results in the formation of different monomeric and polymeric hydroxy species, which serve as coagulating agents. [9, 10] Heavy metals can also undergo complexation or precipitate through reaction with OH^-, depending on the pH value of the solution.[11] The coagulating agent neutralizes the colloids' charge, leading to destabilization, agglomeration, and floc formation.[12, 13] Physical and chemical sorption between the flocs and contaminants can also occur.[13] The flocs can then be separated from the water through sedimentation or flotation with gas bubbles (electroflotation).[7, 14] Electrocoagulation offers many advantages compared to conventional methods, including relatively small reactors and simple equipment, the ability to treat various contaminants simultaneously, flexibility and the possibility of combining with other technologies, no need for additional chemicals, easy sludge separation and smaller sludge volume.[14–17] The main disadvantages of this method are related to energy costs and the electrode passivation.[15, 18]

In this study, the efficiency of electrocoagulation was investigated for the treatment of ammunition wastewater. Specifically, the influence of electrode material, the initial pH value of the water, and the treatment duration on the efficiency of heavy metals and COD removal, was studied.

3 Materials and methods

A simple EC setup (Figure 1) was used for the treatment of real wastewaters from an ammunition factory in Hungary. The initial values of the physicochemical properties of the treated wastewater are listed in Table 1. The experimental setup consisted of a 600 mL glass beaker placed on a magnetic stirrer (Hanna Instruments) set at 300 rpm. For each experiment, 500 mL of wastewater was used. Two pairs of plate electrodes (2 anodes and 2 cathodes) were placed in the beaker 1 cm apart in a monopolar mode and connected to the laboratory power supply MRGN-300s (MC Power).

The efficiencies of two electrode materials, aluminum (Al) and iron (Fe), as well as their combinations were investigated. Also, in order to investigate the effect of the initial pH value of the solution, two sets of experiments were conducted. In the first set, the initial pH value of about 2 was not adjusted, while in the other set NaOH was used to achieve a pH value of 8. Each set, consisted of 8 experiments (Table 2): 15 min of treatment using Fe or Al electrodes only, 5, 10 and 15 min of Al electrodes followed by 5, 10 and 15 min of Fe electrodes, 5, 10 and 15 min of Fe electrodes followed by 5, 10 and 15 min of Al electrodes. In all of the experiments, a direct current of 3 A was used.

The samples were taken every 5 minutes using a syringe and filtered through a 0.45 μm filter. Electrical conductivity, pH, total dissolved solids (TDS) and salinity were measured using a HI9829 multimeter (Hanna Instruments). The concentrations of the heavy metals, copper (Cu), lead (Pb) and zinc (Zn), were determined by ICP-OES analysis using the Agilent 5900 spectrometer (Agilent Technologies). COD measurements were conducted using Nanocolor CSB 1500 pre-made cuvette tests and Nanocolor 500D photometer (Macherey-Nagel).

The efficiencies for each pollutant removal were calculated using the following equation:

$$Removal\ efficiency\ (\%) = \frac{C_0 - C}{C_0} * 100 \quad (1)$$

C_0 represents the initial concentration of the pollutant, while C is the final pollutant concentration (after EC treatment).

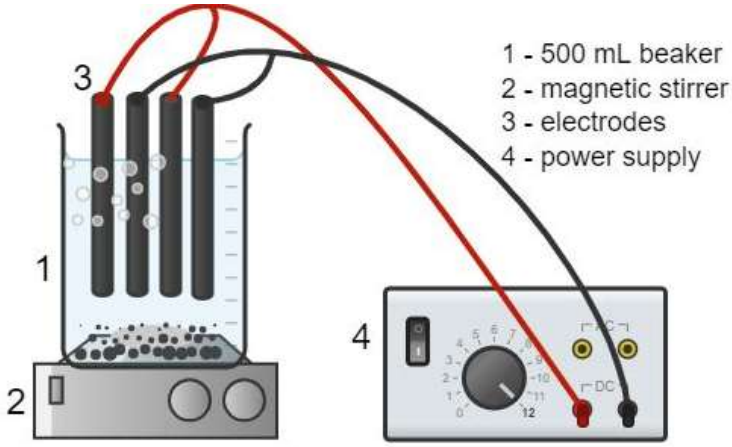

Figure 1. A schematic view of the experimental set-up

4 Results and discussion

In this study, a simple EC setup was used to investigate the efficiency of EC treatment for ammunition production wastewater. The initial physico-chemical properties of this wastewater include low pH value, high conductivity, high COD and TDS content. In addition, significant amounts of heavy metals including Cu, Pb and Zn are present. Various other pollutants, such as high concentrations of sulphates and organic compounds are also present, however, they were not analyzed in this study.
In general, the EC treatment proved to be quite an efficient treatment, as shown in Tables 1 and 2. TDS, salinity and COD were significantly reduced and heavy metals were completely or almost completely removed after 30 min (15 min Fe/ 15 min Al) of EC treatment.

Table 1. Physico-chemical properties of treated water

	pH	Conductivity (µS/cm)	TDS (mg/L)	Salinity (PSU)	COD (mg O_2/L)	Cu (mg/L)	Pb (mg/L)	Zn (mg/L)
Before EC	1.95	7 233	3 616	4.0	2 060	48.6	1.2	101
After 15 min Fe/15 min Al, pH=2	5.3	1 402	701	0.7	989	0.41	0.01	1.46
After 15 min Fe/15 min Al, pH=8	9.77	2 747	1 373	1.4	1169	0.62	0	0

4.1 The effect of pH, electrode material and treatment time

The most influential parameter in any EC process is the current density because, according to Faraday's law, it determines the amount of metal ions released from the anode and the amount of gasses produced. In general, a higher current density leads to a higher removal rate, at least up to a certain point in the optimal range.[7] Since the current strength was kept constant in this study according to Faraday's law, the treatment time proved to be the most important parameter. The longer the treatment time, the higher the efficiency. This is to be expected, because for the same current input, a longer time means that more metal ions are released into the solution and consequently more flocs are formed. A longer treatment also provides more time for the electrochemical degradation of the organic pollutants.

The electrode material is a parameter that affects both the performance and efficiency of the EC process as well as the cost. Key factors for EC efficiency include anodic dissolution, the percentage of contaminants removed and the amount of coagulant required, all of which depend on the ionic metal species released.[15] Metal ionic coagulants with higher charge valence improve the coagulation of the contaminants by better compressing the electrical double layer. Al and Fe electrodes are commonly used due to the coagulating properties of their multivalent ions, their availability, their low cost and their high electrical dissolution rates. In this study, both materials achieved similar results.

Table 2. An overview of experimental conditions and achieved efficiencies.

Initial pH	Electrode material	Time (min)	Cu (%)	Pb (%)	Zn (%)	COD (%)
2	Al	5	13.99	16.67	4.95	3.88
		10	21.19	16.67	6.83	11.65
		15	39.51	25.00	19.41	22.82
	Fe	5	9.88	16.67	2.67	10.68
		10	22.22	25.00	9.70	18.93
		15	41.15	66.67	20.99	33.01
	Al Fe	5 5	23.05	41.67	9.90	15.05
	Al Fe	10 10	95.47	100.00	49.31	43.20
	Al Fe	15 15	98.97	100.00	97.72	47.09
	Fe Al	5 5	43.99	60.00	45.78	9.22
	Fe Al	10 10	96.07	93.33	75.46	46.75
	Fe Al	15 15	99.16	99.17	98.55	51.99
8	Al	5	81.58	100.00	89.87	39.22
		10	98.01	100.00	99.95	40.59
		15	97.57	100.00	99.79	46.93
	Fe	5	96.79	91.67	96.69	36.39
		10	85.12	95.83	98.66	38.88
		15	98.95	100.00	99.43	46.15
	Al Fe	5 5	51.49	91.67	99.84	39.12
	Al Fe	10 10	88.33	100.00	86.25	43.32
	Al Fe	15 15	96.57	100.00	99.17	43.85
	Fe Al	5 5	99.12	87.50	100.00	36.98
	Fe Al	10 10	99.61	100.00	100.00	41.85
	Fe Al	15 15	96.57	100.00	100.00	42.98

As it can be seen from Table 2, the initial pH of the solution proved to be more influential than the electrode material, with heavy metal removal being higher in the alkaline environment. The pH can influence the solubility of metal hydroxides, the electrical conductivity and the size of the flocs formed. [15] In all experiments, an increase in pH was observed after EC treatment.

4.2 COD removal

COD measurements are used to quantify the amount of oxidizable pollutants, mostly organic substances, in wastewater. As can be seen in Figure 2, both electrode materials showed similar behaviour in the alkaline environment, achieving about 45% of COD removal in 15 minutes. In the acidic environment, the Fe electrodes performed slightly better than the Al electrodes. The lower removal efficiency under acidic conditions can be explained by the presence of the amphoteric $Al(OH)_3$, which leads to soluble Al^{3+} cations, and by the reduced oxidation of Fe^{2+} to Fe^{3+}.[19] Similar trends can be seen for Fe/Al and Al/Fe combinations (Figure 3). However, after an extended treatment time totaling 30 minutes, all experiments showed similar efficiencies ranging from 40 to 52%. For both electrode combinations, higher removal rates were observed in the first 10 minutes when the initial pH was set to 8. As mentioned above, the pH increased during the EC treatment, which could explain the sudden increase in COD removal after 15 minutes in experiments with acidic initial conditions.

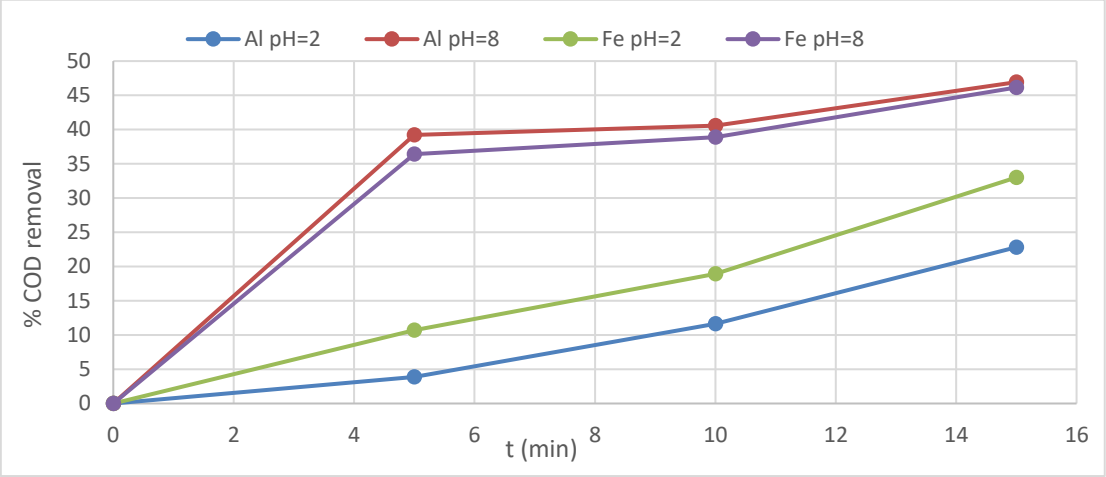

Figure 2. COD removal rate, depending on electrode material and pH value

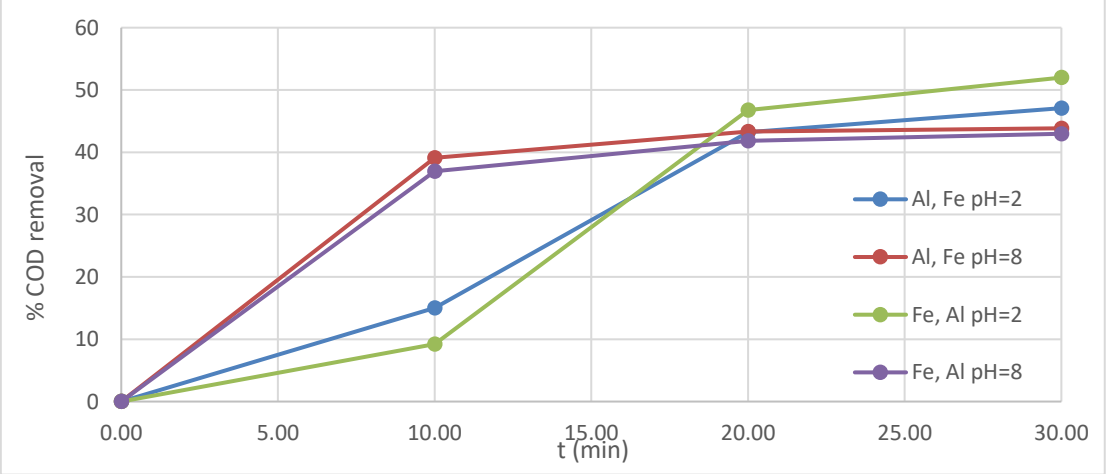

Figure 3. COD removal rate in the case of Fe/Al combination

4.3 Heavy metal removal

Copper, zinc and lead were successfully removed from the wastewater, with complete or nearly complete removal after 30 minutes of treatment. The electrode material had little effect on the efficiency of heavy metal removal, especially for Zn (Figure 4). However, the initial pH of the solution had more of the effect. Under alkaline conditions, the concentration of Cu was reduced by over 80%, that of Zn by 86% and that of Pb by 87% in all experiments. The higher rates of heavy metal removal in the alkaline environment indicate that solution pH is a crucial factor in the electrochemical coagulation process[13], which is consistent with literature reports and can be explained by the precipitation of metal hydroxides in alkaline environments.

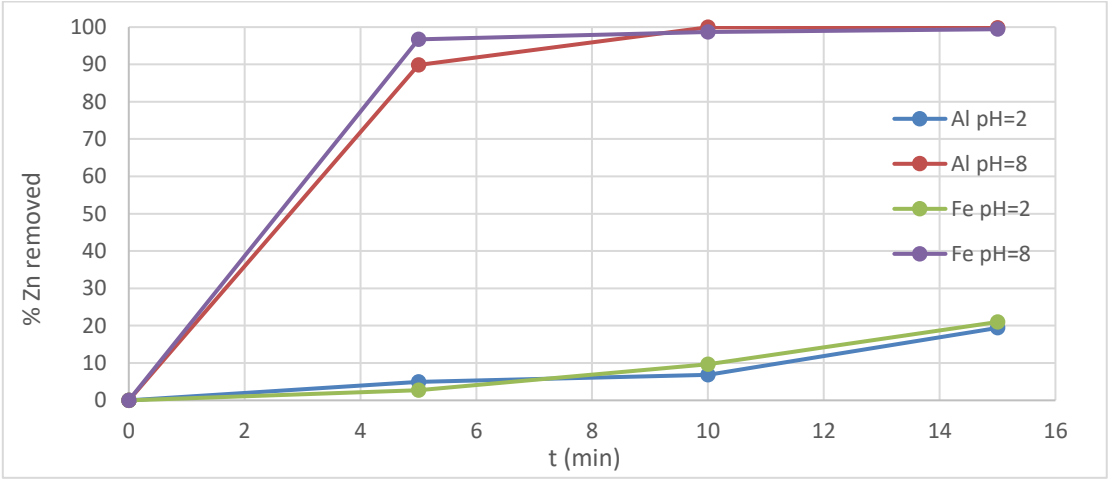

Figure 4. Removal rate of zinc ions, depending on electrode material and pH value

When Fe/Al and Al/Fe combinations were used, the Pb ions were completely removed in 20 and 30 minutes regardless of the pH value. In an alkaline environment, however, the removal rate is higher, as can be seen in Figure 5. The Fe/Al combination and alkaline conditions resulted in complete removal of zinc and 99% removal of copper in less than 10 minutes of treatment time.

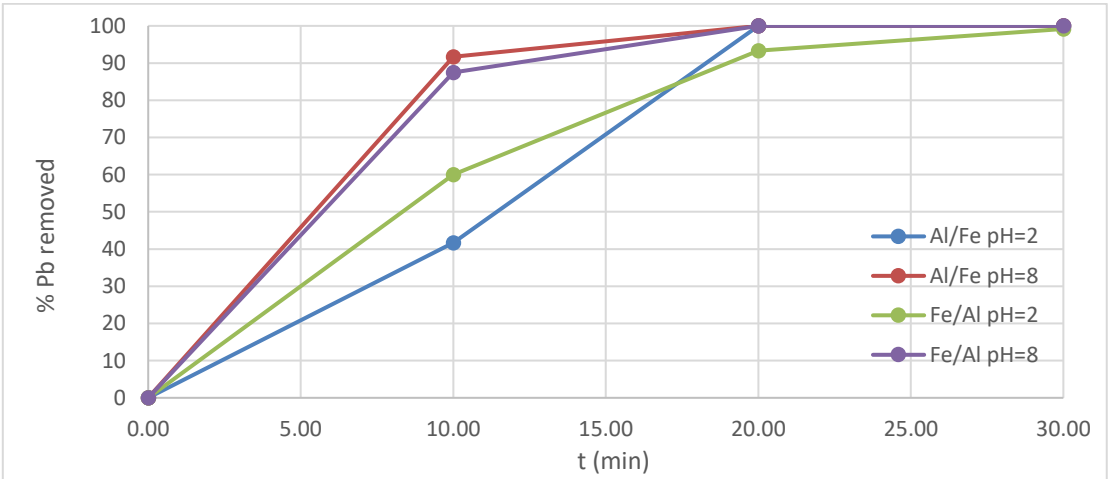

Figure 5. Removal rate of lead ions, depending on electrode material and pH value

5 Conclusion

The results of this study indicate that electrocoagulation is a viable alternative to conventional wastewater treatments for wastewater from munitions production. Both aluminum and iron electrodes showed similar behaviour. However, the highest efficiency in the removal of COD and heavy metals

was achieved with a treatment time of 15 minutes with Fe electrodes, followed by 15 minutes with Al electrodes. This combination also resulted in the fastest sludge precipitation and the lowest turbidity. A higher initial pH of the treated water resulted in slightly higher removal rates of heavy metals. In general, treatment time is a very important process parameter and longer treatment times led to better results. Although EC has proven to be an efficient option for wastewater treatment, further process optimization and scale-up is required.

Acknowledgements
This work was supported by the Croatian Science Foundation under the project PRIMEUS (UIP2020-02-1160).

References
[1] Bhanot, P.; Celin, S.M.; Sreekrishnan, T.R.; Kalsi, A.; Sahai, S.K. and Sharma, P.: Application of integrated treatment strategies for explosive industry wastewater—A critical review, Journal of Water Process Engineering, 35, p. 101232, 2020.
[2] Anotai, J.; Tanvanit, P.; Garcia-Segura, S. and Lu, M.-C.: Electro-assisted Fenton treatment of ammunition wastewater containing nitramine explosives, Process Safety and Environmental Protection, 109, pp. 429–436, 2017.
[3] Doppalapudi, R.B.; Sorial, G.A. and Maloney, S.W.: Electrochemical Reduction of Simulated Munitions Wastewater in a Bench-Scale Batch Reactor, Environmental Engineering Science, 19, pp. 115–130, 2002.
[4] Syam Babu, D.; Anantha Singh, T.S.; Nidheesh, P.V. and Suresh Kumar, M.: Industrial wastewater treatment by electrocoagulation process, Separation Science and Technology, 55, pp. 3195–3227, 2020.
[5] Abdulhadi, B.; Kot, P.; Hashim, K.; Shaw, A.; Muradov, M. and Al-Khaddar, R.: Continuous-flow electrocoagulation (EC) process for iron removal from water: Experimental, statistical and economic study, Science of the Total Environment, 760, p. 143417, 2021.
[6] Ahmad, A.; Das, S. and Ghangrekar, M.M.: Removal of xenobiotics from wastewater by electrocoagulation: A mini-reviewSpecial Issue J. Indian Chem. Soc2019.
[7] Simon, R.G.; Stöckl, M.; Becker, D.; Steinkamp, A.D.; Abt, C.; Jungfer, C.; Weidlich, C.; Track, T. and Mangold, K.M.: Current to Clean Water – Electrochemical Solutions for Groundwater, Water, and Wastewater Treatment, Chemie-Ingenieur-Technik, 90, pp. 1832–1854, 2018.
[8] Al-Shannag, M.; Al-Qodah, Z.; Bani-Melhem, K.; Qtaishat, M.R. and Alkasrawi, M.: Heavy metal ions removal from metal plating wastewater using electrocoagulation: Kinetic study and process performance, Chemical Engineering Journal, 260, pp. 749–756, 2015.
[9] Mollah, M.Y.A.; Schennach, R.; Parga, J.R. and Cocke, D.L.: Electrocoagulation (EC)- Science and applications, Journal of Hazardous Materials, 84, pp. 29–41, 2001.
[10] Alkhadra, M.A.; Su, X.; Suss, M.E.; Tian, H.; Guyes, E.N.; Shocron, A.N.; Conforti, K.M.; Souza, J.P.D.; Kim, N.; Tedesco, M.; Khoiruddin, K.; Wenten, I.G.; Santiago, J.G.; Hatton, T.A. and Bazant, M.Z.: Electrochemical Methods for Water Purification, Ion Separations, and Energy Conversion, Chemical Reviews, 122, pp. 13547–13635, 2022.
[11] Hakizimana, J.N.; Gourich, B.; Chafi, M.; Stiriba, Y.; Vial, C.; Drogui, P. and Naja, J.: Electrocoagulation process in water treatment: A review of electrocoagulation modeling approaches, Desalination, 404, pp. 1–21, 2017.
[12] Fu, F. and Wang, Q.: Removal of heavy metal ions from wastewaters: A review, Journal of Environmental Management, 92, pp. 407–418, 2011.
[13] Kabuk, H.A.; Avsar, Y.; Ilhan, F. and Ulucan, K.: Comparison of pH Adjustment and Electrocoagulation Processes on Treatability of Metal Plating Wastewater, Separation Science and Technology, 2014.
[14] Pulkka, S.; Martikainen, M.; Bhatnagar, A. and Sillanpää, M.: Electrochemical methods for the removal of anionic contaminants from water – A review, Separation and Purification Technology, 132, pp. 252–271, 2014.
[15] Garcia-Segura, S.; Nienhauser, A.B.; Fajardo, A.S.; Bansal, R.; Conrad, C.L.; Fortner, J.D.;

Marcos-Hernández, M.; Rogers, T.; Villagran, D.; Wong, M.S. and Westerhoff, P.: Disparities between experimental and environmental conditions: Research steps toward making electrochemical water treatment a reality, Current Opinion in Electrochemistry, 22, pp. 9–16, 2020.
[16] Aziz, A.R.A.; Asaithambi, P. and Daud, W.M.A.B.W.: Combination of electrocoagulation with advanced oxidation processes for the treatment of distillery industrial effluent, Process Safety and Environmental Protection, 99, pp. 227–235, 2016.
[17] Bajpai, M.; Katoch, S.S.; Kadier, A. and Singh, A.: A review on electrocoagulation process for the removal of emerging contaminants: theory, fundamentals, and applications, Environmental Science and Pollution Research 2022 29:11, 29, pp. 15252–15281, 2022.
[18] Ang, W.L.; McHugh, P.J. and Symes, M.D.: Sonoelectrochemical processes for the degradation of persistent organic pollutants, Chemical Engineering Journal, 444, p. 136573, 2022.
[19] Kobya, M.; Ciftci, C.; Bayramoglu, M. and Sensoy, M.T.: Study on the treatment of waste metal cutting fluids using electrocoagulation, Separation and Purification Technology, 60, pp. 285–291, 2008.

THE POTENTIAL OF USING RESIDUE FROM SEWAGE SLUDGE GASIFICATION IN AN EXPERIMENTAL PLANT

DOMAGOJ NAKIĆ [1*], HANA POSAVČIĆ [2], KATARINA LICHT [3], DRAŽEN VOUK [4], IVAN HALKIJEVIĆ [5]

[1*] *University of Zagreb, Faculty of Civil Engineering, Croatia,* domagoj.nakic@grad.unizg.hr

[2] *University of Zagreb, Faculty of Civil Engineering, Croatia,* hana.posavcic@grad.unizg.hr

[3] *University of Zagreb, Faculty of Civil Engineering, Croatia,* katarina.licht@grad.unizg.hr

[4] *University of Zagreb, Faculty of Civil Engineering, Croatia,* drazen.vouk@grad.unizg.hr

[5] *University of Zagreb, Faculty of Civil Engineering, Croatia,* ivan.halkijevic@grad.unizg.hr

[*] *Corresponding author*

1 Abstract

The derived gasification SS (sewage sludge) biochar product is porous and inexpensive, so it has a potential to be used as an adsorbent in wastewater treatment: in the removal of nutrients (phosphate and ammonium), heavy metals, or some pesticides. SS biochar has also shown the potential to replace part of the original raw materials in the construction industry. The final goal of the broader research is to examine the possibility of multiple use of SS biochar, firstly in wastewater treatment and subsequently in the production of innovative building materials and products.

Keywords: sewage sludge, gasification, hydrogen, biochar, adsorbent, construction materials

2 Introduction

Sewage sludge (SS) treatment and disposal have become one of the most important and most expensive issues within wastewater treatment cycle. Current requirements for disposal of SS mainly point to the possibility of "using it whenever appropriate", minimizing the adverse effects on the environment at the same time, as stated by Council Directive (91/271/EEC) [1]. The global production of SS is estimated to be around 45 million dry tons annually [2]. Improper management results in various environmental issues leading to air, water, and soil pollution. Consequently, growing concerns and strict regulations on traditional SS disposal methods have redirected attention towards its energy potential, with SS now being regarded as an energy resource. Thermal treatment methods such as incineration, pyrolysis, gasification, and hydrothermal carbonization are increasingly recognized as effective solutions for SS disposal. These methods are particularly favoured in the most developed countries of the EU, where legislation often supports their use. Thermal transformation processes like gasification, pyrolysis, and hydrothermal carbonization can convert sewage sludge from a waste material into a valuable resource [3]. This conversion produces new by-product biochar, which offers multiple benefits including climate change mitigation and environmentally safe disposal of SS [4].

Biochar is a porous, carbon-rich material created through the thermochemical decomposition of biomass feedstock in low or no oxygen conditions, and these can include organic waste materials such as crop and forest residues, wood chips, algae, sewage sludge, manure, and organic municipal solid waste [5]. Biochar's unique properties, such as its large surface area, microporosity, high adsorption capacity, and ion exchange abilities, make it valuable for addressing various environmental management issues [6]. It is used in applications including catalysis, energy production, soil amendment, composting, in agriculture fields to nourish soil, and as an adsorbent [7-10]. Low-temperature biochar is suitable for agricultural uses, while high-temperature biochar improves porosity and contaminant adsorption efficiency. The amount of heavy metals leached from sewage sludge biochar is minimal, ranging from

near zero to 17.96 mg/kg, making it safe for use without polluting treated wastewater and receiving water bodies [6].

Gasification process usually involves converting biomass into gas fuel using gasification agents at temperatures generally above 800°C [11]. Gasification of sewage sludge produces gas that can be used for energy production, with yield and composition (primarily CH_4, CO_2, and H_2, but also CO and other hydrocarbons in smaller quantities) varying with temperature and sludge composition. High amounts of H_2 are typically produced during the pyrolysis of sewage sludge due to the presence of mineral constituents like CaO that favour the production of H_2-rich syngas [12]. Generally, biochar contains high content of stable carbon, therefore, gasification and pyrolysis represent kind of methods for carbon capture and sequestration [13].

With the current widely used wastewater treatment technologies, it is challenging to remove all pollutants solely through biodegradation. Despite advancements in research on activated sludge, some non-biodegradable pollutants persist in the water. Consequently, research on sludge has increasingly focused on chemical and physical adsorption, which offers broader applications. The adsorption capacity of sewage sludge benefits from its loose and porous structure, as well as certain material ions that the sludge may inherently contain [14].

Croatian company working on the research and development of novel energy production systems has created an innovative gasification system that uses thermal energy to convert organic material into syngas (hydrogen) and carbon black. Almost any organic material can be used as feedstock and so does sewage sludge. Carbon black is the main by-product of the system, and it can be further used based on the principles of circular economy. The derived gasification biochar product is porous and inexpensive, so it has a potential to be used as an adsorbent supplementing traditional commercially activated carbon adsorbent in wastewater treatment. This paper investigates the possibilities of its use in this area, which is shown by concrete results of experimental research on synthetic solutions in the removal of nutrients (phosphate and ammonium), certain heavy metals, but also some pesticides. Previous research was focused on the examination of the possibility of using SS biochar in the production of building materials, where SS biochar has shown the potential to replace part of the original raw materials: cement in the production of concrete, or clay in the production of brick products.
The final goal of the broader research is to examine the possibility of multiple use of SS biochar in wastewater treatment and further use of the same material in the production of innovative building materials and products. This directly closes the cycle of the circular economy, where the by-product of one industry is used first in that same industry, and then finally disposed of in another industry, thereby reducing the need for natural raw materials.

3 Methods

3.1 Gasification – the process of obtaining SS biochar

The gasification pilot plant (LOOPER) converts solid organic material into clean syngas and an inert solid residue. The gasification process takes place in a reactor, where the syngas reaches temperatures up to 850°C. The syngas then enters a superheater, where any remaining hydrocarbons are broken down at temperatures above 1,000°C, resulting in syngas with a high hydrogen content. After superheating, the hot syngas passes through a hollow spindle inside the reactor, transferring its heat to the organic feedstock in the process. In subsequent processes, the generated syngas is purified of all particles and contaminants and then cooled. A small portion of the produced clean syngas rich in hydrogen (approximately 28-30% of the produced gas volume) is used to heat the superheater and reactor. The remaining syngas (the other 70% of the produced gas) can be used to generate energy or for other purposes such as producing pure hydrogen. The produced syngas contains about 45-60% pure, sustainable hydrogen. This hydrogen can be used to operate chemical plants, for transportation, and other applications. The syngas can also be used to produce thermal and electrical energy. By-products

of the process, such as ash and soot (biochar), can be used in the construction industry, for example. This syngas production technology from waste is a controlled process with minimal carbon dioxide emissions and the elimination of other harmful gas emissions due to the prevention of oxygen entering the process and maintaining high temperatures [15]. A schematic diagram of the pilot plant with the main technological units is shown in Figure 1. The most important innovative features of this plant are: superheating syngas for the purpose of cracking hydrocarbons, reduced thermal load on the reactor by separating the superheater and heating the feedstock in the reactor through a hollow spindle (internal heat recovery of the syngas). This technology for producing synthetic gas from waste is a controlled process that minimizes carbon dioxide emissions and eliminates other harmful gas emissions by preventing oxygen from entering the process and maintaining high temperatures. It can be applied to all types of organic waste. A remaining challenge, currently being addressed in broader research, is managing the residual byproduct—biochar. In this study, the produced biochar was further analyzed as described below and utilized as an absorbent for treating synthetic wastewater.

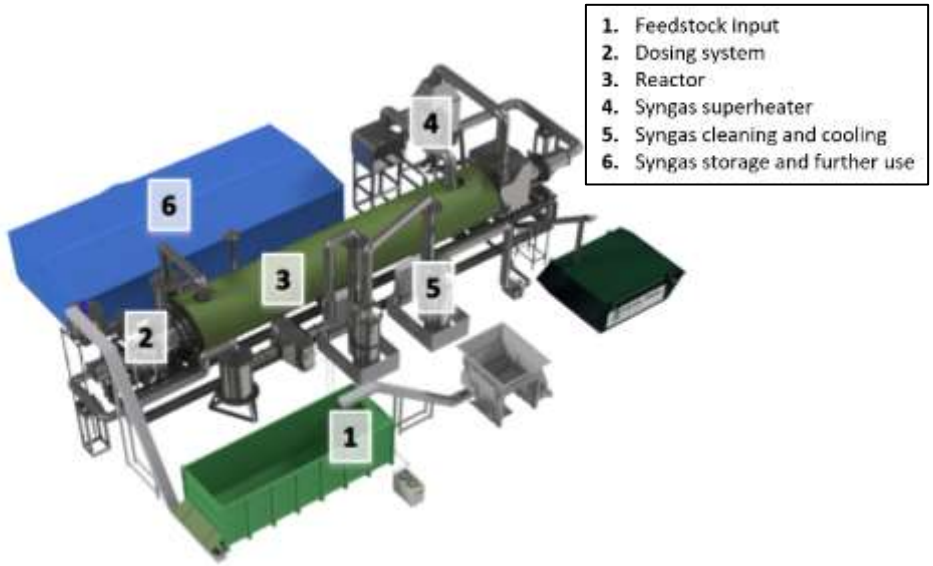

Figure 1. A schematic of gasification pilot plant (LOOPER) [15]

SS used in this study was gathered from the wastewater treatment plant (WWTP) in Zagreb, Croatia, where a second stage of treatment is implemented. These samples, which were stabilized and mechanically dewatered, were obtained in airtight plastic containers, kept at ambient temperature, and subsequently dried in a laboratory dryer at 105°C before undergoing LOOPER gasification.

3.2 Biochar characterization

Obtained SS biochar was further analyzed using following tests. The chemical composition was determined using atomic absorption spectroscopy (AAnalyst 200 instrument, PerkinElmer, Inc., Waltham, MA, USA). Additionally, the biochar sample underwent analysis by energy dispersive X-ray fluorescence (EDXRF) using a Siemens X-ray tube with a Mo anode and Mo secondary target in orthogonal geometry. Leaching tests were conducted following the guidelines of EN 12457-2. Approximately 90 g of biochar was placed in a 1 L glass vessel, and a specific amount of demineralized water was added to achieve a desired liquid-to-solid ratio (L/S=10). The glass vessel was then agitated at 2 rpm for 24 hours. After agitation, the sample was allowed to settle for 15 ± 5 minutes, and the eluate was filtered through a 0.45 μm pore size membrane filter under vacuum. The eluate was divided into the required number of samples for chemical analysis. Prior to analyzing for heavy metals by Atomic Absorption spectrometry (Perkin Elmer Analyst 800), the filtrate was acidified with 1 mL of 65% nitric acid per 100 mL of filtrate sample to prevent any unwanted precipitation during sample storage. Chloride and fluoride ion concentrations in the filtrates were determined by colorimetry using a Hach Lange DR 5000 spectrophotometer [16].

3.3 Adsorption experiments

Batch adsorption experiments were conducted to assess the adsorption capacity of biochar for ammonium, phosphate, cadmium, chromium, copper, and lead. Stock solutions of each ion were prepared by dissolving the appropriate amount of NH_4Cl, KH_2PO_4, $Cd(NO_3)_2$, $Cr(NO_3)_2$, $Cu(NO_3)_2$, and $Pb(NO_3)_2$ in 1000 mL of distilled water. A separate, preliminary, part of the research was performed with acetamiprid. Acetamiprid is an organic compound with the chemical formula $C_{10}H_{11}ClN_4$. It is an odorless neonicotinoid insecticide. It is systemic and intended to control sucking insects on crops such as leafy vegetables, citrus fruits, pome fruits, grapes, cotton, cole crops, and ornamental plants. It is also a key pesticide in commercial cherry farming due to its effectiveness against the larvae of the cherry fruit fly.
The initial pH of each solution was determined using the HI98194 multiparameter instrument (Hanna Instruments, Romania), and 1M HNO_3 and NaOH were used to adjust the pH value subsequnetly. All reagents utilized for the experiments and analyses were of analytical grade.
In 250 ml glass bottles, 100 ml of each stock solution was mixed with a specific quantity of biochar. The bottles were tightly sealed and placed on a rotary shaker set at 45 rpm for 24 hours. Samples of 1 ml were extracted from each bottle before the experiment, and after specified time intervals within 24 h. They were then filtered through a 45 μm PES syringe filter, diluted 10-fold, and analyzed. Cd, Cr, Cu, and Pb concentrations were determined by ICP-OES analysis (Agilent 5900, Agilent Technologies, USA), while PO_4^{3-} and NH_4^+ were measured using the Nanocolor 500 D photometer (Macherey-Nagel, Germany) and corresponding tube tests. All experiments were performed in triplicate, and the average value was used to calculate the amount of adsorbate adsorbed by biochar, which is presented in the results.

4 Results and discussion

4.1 Biochar characteristics

The biochar investigated in this study comprises various high-temperature aluminosilicates, with a crystalline composition primarily based on calcium-containing compounds. The sample is distinguished by the presence of quartz, cristobalite, along with a noticeable amount of illite and traces of calcite and calcium aluminum phosphate. No amorphous phase is observed.
Chemical composition analysis of the biochar using absorption spectrometry indicates that the highest proportions in the sample mass are attributed to Al_2O_3 (around 18%), CaO (around 16%), and Fe_2O_3 (somewhat below 10%). Additionally, nearly half (50%) of the sample mass remains undissolved, with this residual attributed to carbon (char).

Based on the examination of the primary element content in the obtained biochar, indices on a low presence of hazardous metals were drawn. Furthermore, it is expected that precipitation induced by alkaline substances, especially calcium compounds, and phosphate, will reduce leaching toxicity to levels below safety thresholds [17].

Additionally, leaching tests are utilized to assess the concentration of elements, primarily heavy metals, that migrate from the solid phase to the liquid phase within a specific timeframe, indicating their potential hazardous and bioavailable nature. The EN 12457-based leaching test, commonly employed for categorizing waste into hazardous, non-hazardous, or inert for landfill disposal, was employed to identify potential risks and constraints associated with the application of the resulting residue (biochar). Table 1 presents the outcomes of leaching tests conducted on the obtained biochar according to EN 12457 standards. The leachate concentrations are notably low, with some even falling below detection limits, consistent with previous findings [18], except for Mo, which exhibits significant leaching, but in terms of absolute values, these are still minimal quantities. This trend is also consistent with previous studies based on Croatian SS [16]. The most important conclusion regarding potential application of SS

biochar as an adsorbent is that heavy metals remain in a stable state within the SS derived biochar, thereby significantly mitigating the risk of heavy metal contamination during its application [19].

Table 1. EN 12457 leaching test results for obtained biochar [mg/kg]

PARAMETER	SS BIOCHAR SAMPLE
As	< DL
Ba	10.220
Cd	< DL
Co	0.006
Cr	0.362
Cu	< DL
Mo	0.805
Ni	< DL
Pb	0.072
Se	0.004
Zn	< DL

*DL – detection limit

4.2 Results of adsorption experiments

4.2.1 Results on nutrient removal

The efficiency of phosphate and ammonia removal was initially analyzed simultaneously by preparing a single solution containing both contaminants. During this process, a certain level of competition between the contaminants was observed, and the overall efficiency was relatively low. Therefore, the research continued using single stock solutions (containing only ammonia or phosphates). The parameters varied included: the initial concentration of contaminants, the mass of the adsorbent (biochar) used, the pH of the solution, and the adsorption duration. After repeated multiple tests, the optimal parameters for nutrient removal were determined based on the results of the initial experiments.

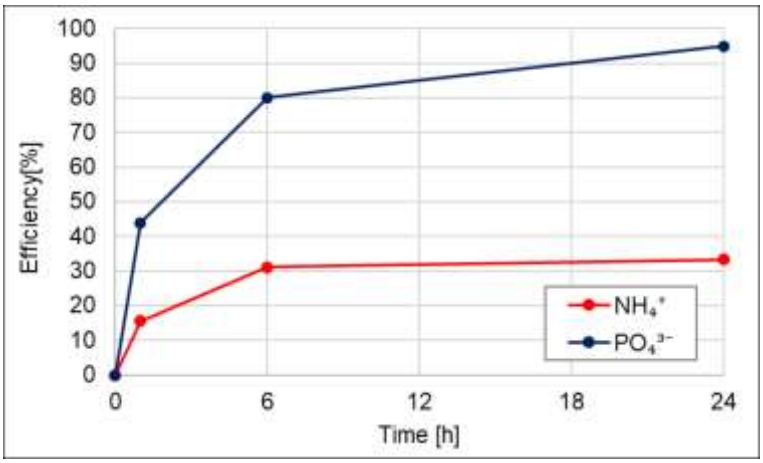

Figure 2. The efficiency of phosphate and ammonia removal depending on the duration of adsorption under optimal experimental settings

Tests were repeated with these settings, and samples were analyzed after 1, 6, and 24 hours. The optimal settings for nutrient removal were defined with the following values: initial contaminant concentration of 90 mg/L, mass of adsorbent (biochar) 0.5 g, and solution pH of 5. The results of the adsorption tests with these defined settings are shown in Figure 2. It is evident that the phosphate removal results are significantly better (removal efficiency around 95% over 24 hours) compared to the ammonia removal results (removal efficiency slightly below 35% over 24 hours). However, for both types of contaminants, it can be stated that significant removal percentages are achieved within the first few hours (6 h), after

which the further reduction in contaminant concentrations slows down considerably.

4.2.2 Results on heavy metals removal

When the efficiency of Cd, Cr, Cu, and Pb removal was initially analyzed simultaneously (using a multi-compound solution containing all these pollutants), the highest efficiencies were achieved in the removal of Cr (over 80% over 24 hours), followed by Pb (around 60% over 24 hours) and Cu (just below 50% over 24 hours), while the lowest efficiency was obtained for Cd removal (just below 30% over 24 hours). Similar trends have been noted by other researchers [14]. Ni et al. [20] reported the competitive removal of heavy metals (Pb^{2+} and Cd^{2+}) using biochar produced from the pyrolysis of anaerobically digested sludge, where Pb^{2+} showed higher affinity compared to Cd^{2+}. Tan et al. [21] found that increased Ca^{2+} concentration in the solution can drastically reduce Cd^{2+} adsorption.
Given that the main objective of this study is to initially test the feasibility of using a specific SS biochar from a gasification pilot plant, the tests were continued with single-compound solutions (containing only one of the selected heavy metals). Below (Figure 3) are the results of the adsorption tests from single-pollutant solutions and with adopted optimal process parameters (based on previous experiments): the initial contaminant concentration was defined as 85 mg/L, the mass of the adsorbent used (biochar) was 0.75 g, and the solution pH was 3.

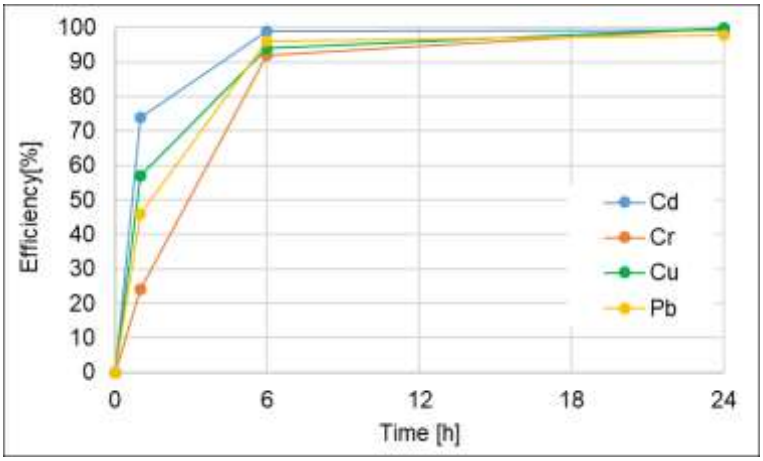

Figure 3. The efficiency of selected heavy metals removal depending on the duration of adsorption under optimal experimental settings

It should be emphasized that exceptionally high removal efficiencies were achieved for all four analyzed metals: over 99% over 24 hours for Cd, Cr, and Cu, and just below 98% for Pb. Additionally, it is noticeable that the majority of these metals are removed within the first 6 hours (over 90% for all 4 metals analyzed).

4.2.3 Results on acetamiprid removal

This separate part of the research was conducted without varying the process parameters (solution pH, initial contaminant concentration, mass of biochar used as an adsorbent) and served as an initial phase for investigating the additional potential application of the produced biochar for pesticides removal, specifically acetamiprid. The process parameters were defined approximately, based on previous experience with other types of contaminants. The following process parameters were applied: initial contaminant concentration of 22.3 mg/L, mass of biochar used as an adsorbent 0.5 g, and neutral solution (pH=7). The obtained results are shown in Figure 4, and it is evident that significant removal efficiencies of acetamiprid are achieved, with around 92% removal rate within the first 6 hours, and only a slight improvement to just under 94% over 24 hours.

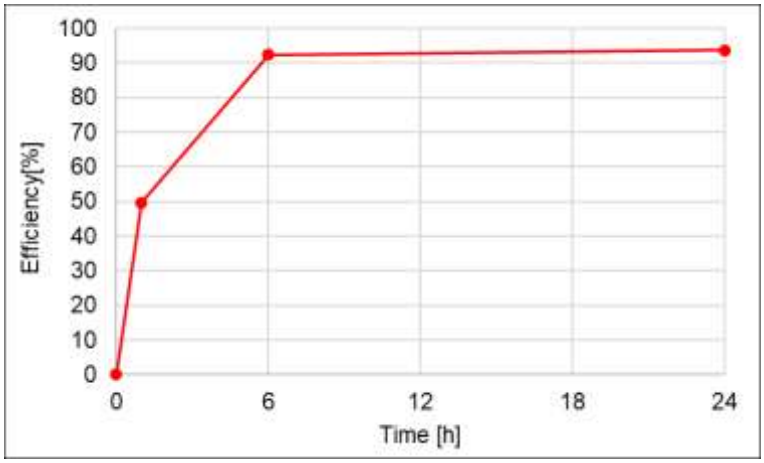

Figure 4. The efficiency of acetamiprid removal depending on the duration of adsorption

4.3 Discussion

Based on the results provided, it can be inferred that the SS biochar utilized in this study holds promise for eliminating certain types of contaminants from wastewater. Moreover, the results of removing phosphates, four heavy metals (Cd, Cr, Cu, and Pb), and acetamiprid pesticide from synthetic solutions with a single pollutant all demonstrate removal efficiencies exceeding 90% within 24 hours, with the majority of pollutants being removed within the first few hours. The results of ammonia removal, on the other hand, are significantly more modest, with just over 30% removal over 24 hours. While employing unmodified biochar, the results fell within the spectrum of prior research findings. Moreover, comparing the overall results with previous studies [14], it can be concluded that the obtained efficiencies are significantly better, especially considering that most published results with higher efficiencies are based on research using biochar that has been further enhanced through various chemical and physical treatments.

Optimizing the dosage of the adsorbent is crucial for attaining high removal efficiency of targeted pollutants while ensuring cost-effectiveness [22]. Evaluating the cost-effectiveness of an adsorbent, potential future applications, and the potential recovery of adsorbed pollutants necessitate the regeneration of the utilized biochar, a step to be undertaken in future research endeavors. The practical applications of SS derived biochar hinge on its regeneration and recycling capabilities alongside its adsorption capacity for various pollutants. Given that real wastewater comprises concurrent pollutants and diverse microorganisms simultaneously which could significantly influence the sorption capacity of SS derived biochar as these pollutants also adsorb onto biochar surfaces, further research is necessary for actual wastewater treatment operations.
SS based biochar has demonstrated considerable potential as an adsorbent for removing various pollutants from wastewater. Advances in technology are expected to facilitate the development of more efficient and cost-effective techniques for synthesizing biochar on a larger scale with better control over desired characteristics. With a greater emphasis on practical applications, future research in this realm could lead to more economical and sustainable wastewater treatment technologies [22]. Further investigation into the adsorption mechanisms of pollutants onto biochar surfaces is warranted to develop future adsorbents with tailored properties for specific applications. Similarly, emphasis should be placed on the removal of various pharmaceuticals, pesticides, and other emerging pollutants from wastewater and on assessing the potential environmental impacts of biochar. Similarly, forthcoming studies ought to concentrate on assessing the viability of utilizing SS derived biochar as a candidate material in crafting filters for wastewater treatment purposes.

To enhance the practical application of biochar as an adsorbent, it is crucial to consider its regeneration and reuse. Preliminary results indicate that the biochar retains a significant portion of its adsorptive capacity after undergoing a regeneration process. After biochar adsorbs contamination substances, it can

be desorbed by different methods, restoring its high adsorption capacity. This finding underscores the feasibility of using biochar in a sustainable cycle, thereby reducing the need for continuous production of new adsorbent material and enhancing its cost-effectiveness and environmental benefits [23].

Although there are concerns about secondary pollution from the desorption or release of heavy metals or organic materials from adsorbed biochar this has mostly been refuted already by the preliminary leaching tests of the biochar itself, but it is certainly something that requires further research. At the same time the release of nutrients (as nitrogen and phosphorus) from such biochar can be advantageous in agriculture as a fertilizer where it can improve soil fertility and promote plant growth by gradually releasing the adsorbed nutrients back into the soil. Nutrients-saturated biochar, post-adsorption, can serve as a slow-release fertilizer, enhancing nutrient utilization efficiency and minimizing nutrient loss due to runoff [24-26]. Additionally, Jiang et al. [27] found that phosphorus-loaded sludge biochar could be used as an agricultural fertilizer to improve soil fertility and remediate soils contaminated by heavy metals, presenting a new sustainable and eco-friendly method for waste utilization.

Considering the findings of previous studies [28-32], which have demonstrated the feasibility of utilizing SS biochar (or SS ash) from same source in construction materials, the concept of multiple utilization of this by-product, initially as an adsorbent and subsequently as a substitute for a portion of the original raw materials in construction material production, also appears feasible. This approach would also accomplish multiple objectives of the circular economy leading towards reduced consumption of multiple primary resources while simultaneously reducing the amount of waste deposited to landfills.

5 Conclusion

The utilization of SS biochar in this study demonstrates its potential as an effective and economical adsorbent for wastewater treatment regarding the removal of various types of pollutants (heavy metals Cd, Cr, Cu, and Pb), nutrients (particularly phosphates, to a lesser extent ammonia), and the pesticide acetamiprid. Biochar derived from gasification of SS aligns with the objective of long-term resource recovery and promotes the establishment of a circular economy centered around wastewater. The thermochemical conversion of SS into biochar addresses two key challenges: reducing disposal costs and providing a valuable material for the removal of various pollutants from water and wastewater. The results of Cd, Cr, Cu, and Pb removal under optimal experimental settings (24 h adsorption duration, initial contaminant concentration 85 mg/L, the mass of the adsorbent used (biochar) 0.75 g, and the pH=3) showed removal efficiencies at the level of 98-99%. When the removal of nutrients was analyzed, a significantly better result with an efficiency level of over 95% was achieved for phosphate removal, while the efficiency of ammonia removal was only slightly below 35% (with an adsorption time of 24 h, an initial pollutant concentration in the solution of 90 mg/L, an applied biochar mass as an adsorbent of 0.5 g, and a solution pH of 5). Significant removal efficiencies of acetamiprid were also achieved, with approximately 92% removal within the first 6 hours and a slight increase to just under 94% over 24 hours. This was accomplished using the following process parameters: an initial contaminant concentration of 22.3 mg/L, 0.5 g of biochar as the adsorbent, and a neutral solution (pH=7).

Further investigation is warranted to elucidate the mechanisms influencing the removal of different pollutants and to determine the maximum capacities of SS biochar for adsorption. Additionally, exploration of the possibilities and constraints of applying SS biochar in multiple cycles is essential. Plans include examining the potential leaching of other pollutants, primarily heavy metals, from biochar during wastewater contact, although significant quantities are not initially anticipated. Testing with actual raw wastewater is necessary to understand the mutual influence of various pollutants on the final outcome, particularly regarding potential competition among different pollutants. Finally, the suitability of repeatedly used SS biochar as an adsorbent for further use in the construction materials industry will be investigated, addressing both technical and health-environmental considerations.

Acknowledgements
This work was supported in part by the Croatian Science Foundation under the project PRIMEUS (UIP-2020-02-1160).

References:
[1] Council Directive 91/271/EEC of 21 May 1991 concerning urban wastewater treatment.
[2] Jellali, S., Khiari, B., Usman, M., Hamdi, H., Charabi, Y., Jeguirim, M.: Sludge derived biochars: a review on the influence of synthesis conditions on pollutants removal efficiency from wastewaters. Renew. Sustain. Energy Rev., 144, 111068, 2021.
[3] Fan, S., Li, H., Wang, Y., Wang, Z., Tang, Jie, Tang, Jun, Li, X.: Cadmium removal from aqueous solution by biochar obtained by co-pyrolysis of sewage sludge with tea waste. Res. Chem. Intermed., 44, pp. 135–154, 2018.
[4] Singh, S., Kumar, V., Singh Dhanjal, D., Datta, S., Bhatia, D., Dhiman, J., Samuel, J., Prasad, R., Singh, J.: A sustainable paradigm of sewage sludge biochar: Valorization, opportunities, challenges and future prospects. Journal of Cleaner Production, 269, pp. 1-16, 2020.
[5] Xiang, W., Zhang, X., Chen, J., Zou, W., He, F., Hu, X., Tsang, D.C.W., Ok, Y.S., Gao, B.: Biochar technology in wastewater treatment: A critical review. Chemosphere, 252, 126539, 2020.
[6] Agrafioti, E., Bouras, G., Kalderis, D., Diamadopoulos, E.: Biochar production by sewage sludge pyrolysis. Journal of Analytical and Applied Pyrolysis, 101, pp. 72-78, 2013.
[7] Rangabhashiyam, S., dos Santos Lins, P.V., de Magalhães Oliveira, L.M.T., Sepulveda, P., Ighalo, J.O., Rajapaksha, A.U., Meili, L.: Sewage sludge-derived biochar for the adsorptive removal of wastewater pollutants: A critical review. Environmental Pollution, 293, 118581, 2022.
[8] Paz-Ferreiro, J., Gasco, G., Gutierrez, B., Mendez, A.: Soil biochemical activities and the geometric mean of enzyme activities after application of sewage sludge and sewage sludge biochar to soil. Biol. Fertil. Soils 48, pp. 511-517, 2012. https://doi.org/10.1007/s00374-011-0644-3.
[9] Khanmohammadi, Z., Afyuni, M., Mosaddeghi, M.R.: Effect of sewage sludge and its biochar on chemical properties of two calcareous soils and maize shoot yield. Arch. Agron Soil Sci. 63, pp. 198-212, 2017. https://doi.org/10.1080/03650340.2016.1210787.
[10] Kahiluoto, H., Kuisma, M., Ketoja, E., Salo, T., Heikkinen, J.: Phosphorus in manure and sewage sludge more recyclable than in soluble inorganic fertilizer. Environ. Sci. Technol. 49, pp. 2115-2122, 2015. https://doi.org/10.1021/es503387y.
[11] You, S., Ok, Y.S., Chen, S.S., Tsang, D.C.W., Kwon, E.E., Lee, J., Wang, C.H.: A critical review on sustainable biochar system through gasification: energy and environmental applications. Bioresour. Technol., 246, 242-253, 2017.
[12] Gopinath, A. Divyapriya, G., Srivastava, V., Laiju, A. R., Nidheesh, P. V., Suresh Kumar, M.: Conversion of sewage sludge into biochar: A potential resource in water and wastewater treatment. Environmental Research, 194, 110656, 2021.
[13] Racek, J., Sevcik, J., Chorazy, T., Kucerik, J., Hlavinek, P.: Biochar – Recovery Material from Pyrolysis of Sewage Sludge: A Review. Waste and Biomass Valorization, 11, pp. 3677-3709, 2020.
[14] Wang, G., Xiang, J., Liang, G., Wang, J., Ma, S., He, C.: Application of common industrial solid waste in water treatment: a review. Environmental Science and Pollution Research, 30, pp. 111766–111801, 2023.
[15] INDELOOP d.o.o.: LOOPER – Technical description and technological specifications, Zagreb, Croatia, 2022.
[16] Nakić, D., Vouk, D., Donatello, S., Anić Vučinić, A.: Environmental impact of sewage sludge ash assessed through leaching. Engineering Review, 37 (2), pp. 222-234, 2017.
[17] Hu, H.Y., Liu, H., Shen, W.Q., Luo, G.Q., Li, A.J., Lu, Z.L., Yao, H.: Comparison of CaO's effect on the fate of heavy metals during thermal treatment of two typical types of MSWI fly ashes in China. Chemosphere, 93 (4), pp. 590-596, 2013.
[18] Chen, T., Zhang, Y., Wang, H., Lu, W., Zhou, Z., Zhang, Y., Ren, L.: Influence of pyrolysis temperature on characteristics and heavy metal adsorptive performance of biochar derived from municipal sewage sludge. Bioresource Technology, 164, pp. 47-54, 2014.
[19] Zielinska, A., Oleszczuk, P., Charmas, B., Skubiszewska-Zieba, J., Pasieczna-Patkowska, S.:

Effect of sewage sludge properties on the biochar characteristic. Journal of Analytical and Applied Pyrolysis, 112, pp. 201-213, 2015.
[20] Ni, B.J., Huang, Q.S., Wang, C., Ni, T.Y., Sun, J., Wei, W.: Competitive adsorption of heavy metals in aqueous solution onto biochar derived from anaerobically digested sludge. Chemosphere, 219, pp. 351–357, 2019.
[21] Tan, C., Zeyu, Z., Rong, H., Ruihong, M., Hongtao, W., Wenjing, L.: Adsorption of cadmium by biochar derived from municipal sewage sludge: Impact factors and adsorption mechanism. Chemosphere, 134, pp. 286-293, 2015.
[22] Ihsanullah, I., Khan, M. T., Zubair, M., Bilal, M., Sajid, M.: Removal of pharmaceuticals from water using sewage sludge-derived biochar: A review. Chemosphere, 289, 133196, 2022.
[23] Wu, X., Quan, W., Chen, Q., Gong, W., Wang, A.: Efficient Adsorption of Nitrogen and Phosphorus in Wastewater by Biochar, Molecules, 29, 1005, pp. 1-29, 2024. DOI: https://doi.org/10.3390/molecules29051005.
[24] López, R., Antelo, J., Fiol, S., Macías-García, F.: Phosphate adsorption on an industrial residue and subsequent use as an amendment for phosphorous deficient soils, Journal of Cleaner Production, 230, pp. 844-853, 2019. DOI: https://doi.org/10.1016/j.jclepro.2019.05.092.
[25] Nardis, B. O., Franca, J. R., da Silva Carneiro, J. S., Soares, J. R., Guimarães Guilherme, L. R., Silva, C. A., Azevedo Melo, L. C.: Production of engineered-biochar under different pyrolysis conditions for phosphorus removal from aqueous solution, Science of The Total Environment, 816, 151559, 2022. DOI: https://doi.org/10.1016/j.scitotenv.2021.151559.
[26] Yao, Y., Gao, B., Chen, J., Zhang, M., Inyang, M., Li, Y., Alva, A., Yang, L. Engineered carbon (biochar) prepared by direct pyrolysis of Mg-accumulated tomato tissues: Characterization and phosphate removal potential, Bioresource Technology, 138, pp. 8-13, 2013.
[27] Jiang, M., Yang, Y., Lei, T., Ye, Z., Huang, S., Fu, X., Liu, P., Li, H.: Removal of phosphate by a novel activated sewage sludge biochar: Equilibrium, kinetic and mechanism studies, Applications in Energy and Combustion Science, 9, 100056, 2022. DOI: https://doi.org/10.1016/j.jaecs.2022.100056.
[28] Bubalo, A., Vouk, D., Maljković, D., Bolanča, T.: Gasification of Sewage Sludge in a Rotary Kiln Reactor – A Case Study with Incorporation of Sewage Sludge Ash in Brick Production. Chem. Biochem. Eng. Q., 36 (1), pp. 77–87, 2022.
[29] Nakić, D., Vouk, D., Štirmer, N., Serdar, M.: Management of sewage sludge – new possibilities involving partial cement replacement. Civil Engineer, 70 (4), pp. 277–286, 2018.
[30] Bubalo, A., Vouk, D., Ćurković, L., Rogošić, M., Nakić, D., Cheeseman, C.: Influence of combustion temperature on the performance of sewage sludge ash as a supplementary material in manufacturing bricks, Construction and building materials, 404, 133126, 2023. https://doi.org/10.1016/j.conbuildmat.2023.133126.
[31] Nakić, D.: Environmental evaluation of concrete with sewage sludge ash based on LCA, Sustainable production and consumption, 16, pp. 193-201, 2018.
[32] Vouk, D., Nakić, D., Štirmer, N., Cheeseman, C.: Influence of combustion temperature on the performance of sewage sludge ash as a supplementary cementitious material, Journal of Material Cycles and Waste Management, 20, 3, pp. 1458-1467, 2018.

MATHEMATICAL MODELLING OF THE BATCH REACTOR FOR WATER PH CONTROL

IVAN HALKIJEVIĆ [1], KATARINA LICHT [2], HANA POSAVČIĆ [3], DOMAGOJ NAKIĆ [4],

[1] *University of Zagreb Faculty of Civil Engineering, Croatia,* ivan.halkijevic@grad.unizg.hr

[2] *University of Zagreb Faculty of Civil Engineering, Croatia,* katarina.licht@grad.unizg.hr

[3] *University of Zagreb Faculty of Civil Engineering, Croatia,* hana.posavcic@grad.unizg.hr

[4] *University of Zagreb Faculty of Civil Engineering, Croatia,* domagoj.nakic@grad.unizg.hr

1 Abstract

The pH value of water is one of the most important parameters when treating wastewater or conditioning drinking water. The desired pH can be achieved chemically by adding acid or alkali, but it can also be achieved by electrolysis of water using a semi-permeable membrane. A semi-permeable membrane allows anions or cations to pass through the membrane thus making areas where the pH value is higher or lower. This paper presents the procedure for developing a simple mathematical model for controlling the pH of water in a batch reactor using direct current and a cation exchange membrane. The influential parameters of the model are described, as well as the operating parameters and their values for designing a simple 3D model.

Keywords: pH value, mathematical modeling, water electrolysis

2 Introduction

The term pH stands for "potential of Hydrogen" and is a measure of the hydrogen ion concentration in a solution. The pH value of water is a measure of its acidity or alkalinity. It is a logarithmic scale ranging from 0 to 14, with 7 being neutral. A pH below 7 is acidic, and a pH above 7 is alkaline. The safe range for drinking water pH levels is generally considered to be between 6.5 and 8.5. This range is optimal for human consumption and usually ensures that the water is free from harmful contaminants, respectfully. Drinking water with extreme pH levels can have adverse health effects, including irritation of the skin and mucous membranes [1].

The pH value is essential for effective water and wastewater treatment. pH controls the proper functioning of various chemical reactions involved in water treatment. For example, coagulation, flocculation, and disinfection processes are all pH-dependent [2], [3], [4], [5]. Maintaining the optimal pH range ensures that these chemical reactions occur efficiently, resulting in the effective removal of contaminants and pollutants from the water.

pH levels also influence the growth and activity of microorganisms in biological treatment stages. Deviations from the optimal pH can inhibit microbial activity, leading to reduced treatment efficiency and longer processing times. Maintaining the pH near neutral is essential to protect microorganisms and favor efficient biological treatment [6]. pH is a key parameter in wastewater treatment that significantly influences treatment efficiency [7]. For example, in systems like sequencing batch reactors (SBR), wastewater pH is controlled to optimize the removal rates of contaminants such as total suspended solids (TSS), biological oxygen demand (BOD), and chemical oxygen demand (COD) [8], [9].

The effectiveness of disinfectants like chlorine and chloramine is also influenced by pH. Low pH enhances the disinfection power of chlorine by increasing the proportion of hypochlorous acid (HOCl), which is more effective than hypochlorite ions (OCl^-). Studies have shown that the pH of the water can

impact the formation of disinfection byproducts (DBPs) during chlorination and chloramination processes [10], [11], [12]. Factors such as the presence of organic matter, temperature, and nutrient composition of water can also affect the efficiency of disinfectants like chlorine and chloramine [13], [14]. Additionally, the pH level can influence the degradation of certain substances, such as nicosulfuron, under chlorine/chloramine conditions [15].

Mathematical modeling of the pH process can offer insights into the dynamics involved, facilitating precise control through model-based techniques [16]. Model Predictive Control (MPC) has been investigated as a strategy to tackle the nonlinearities and transient behavior linked with pH control processes [17]. Additionally, adaptive nonlinear control methods have been simulated for pH control, employing generic model control for feedback and static curve fitting for nonlinear adaptation [18]. These methods aim to improve the accuracy and efficiency of pH regulation systems.

In the realm of water treatment, proper pH control not only assists in eliminating impurities like turbidity and color but also aids in maintaining optimal levels of dissolved residual aluminum in treated water [19]. Mathematical models have been developed to forecast the pH of cooling water systems based on parameters such as alkalinity and operational conditions, underscoring the significance of pH in water quality management [20].

Moreover, the creation of mathematical models for pH control in various processes, such as fermentation and enzyme systems, has been highlighted [21], [22]. These models enable the fine-tuning of pH levels during different industrial processes, ensuring the desired outcomes are efficiently achieved.

Anion exchange membrane (AEM) has emerged as a promising technology for water electrolysis, offering advantages such as low footprint, large operational capacity, and rapid response to changing conditions [23], [24]. This method utilizes AEMs and catalyst layers for hydroxide ion conduction without the need for liquid electrolytes [23]. The use of inexpensive catalyst materials and components in AEM water electrolysis challenges traditional proton exchange membrane systems, making it a competitive option for green hydrogen production [25].

Research indicates that AEM water electrolysis can be a sustainable solution for achieving net-zero carbon emissions and meeting increasing energy demands through green hydrogen production [26]. The development of alkaline anion exchange membranes with enhanced ionic conductivity and stability has renewed interest in alkaline water electrolysis, which operates based on the anodic oxygen evolution reaction and concurrent cathodic hydrogen evolution reaction [26].

Moreover, AEM water electrolysis has been recognized for its ability to efficiently produce hydrogen at a low cost, making it an attractive option for water electrolysis technology [27]. The high pH environment associated with alkaline water electrolysis broadens the range of catalyst materials that can be used, enhancing stability and activity [26]. AEM research primarily focuses on developing suitable membranes for high-pH and high-temperature environments in various applications, including water electrolysis [28].

This paper presents the procedure for developing a simple mathematical model, which models the trend of pH value change of water in a laboratory batch electrochemical reactor using direct current and an anion exchange membrane. The influential parameters of the model are described, as well as the operating parameters and their values for designing a simple 3D model.

3 Methods

The laboratory electrochemical reactor (ECU) was constructed in the hydrotechnical laboratory of the Faculty of Civil Engineering, University of Zagreb. Its length is 0.26 m, width 0.12 m, and height 0.2 m

(upper edge of plexiglass walls). Water fills the device up to a height of 0.18 m. The electrode plates are made of carbon, have a width of 0.08 m, a height of 0.12 m, and a thickness of 0.003 m, and are raised from the bottom to a height of 0.06 m. The device is made with two sections (compartments), one section with cathode electrode and one section with anode electrode. The sections are separated with anion-exchange membrane (permeable to OH^-), Figure 1.

Figure 1. Laboratory electrochemical reactor with graphite electrodes for water pH control

Carbon electrodes were chosen since they are inert electrodes in the electrochemical processes of this type of reactor. Inert electrodes are essential components in various ECU, playing a crucial role in electroorganic synthesis, environmental applications, and electron transfer mechanisms [29]. Functionalizing inert electrodes can enhance properties such as capacitive behavior, catalytic activity, and sensing capabilities [30]. The utilization of three-dimensional electrodes, such as carbon felt, in electrochemical reactors has been demonstrated to enhance efficiency in applications like wastewater treatment and electrosynthesis [31].

An anion exchange membrane (AEM) is electrically conductive and commonly used in various applications, eg. fuel cells, desalinators, electrolysis. The membrane allows the passage of negatively charged hydroxide (OH^-) while hindering the movement of other ions or neutral molecules. The functionality of an anion exchange membrane is based on the presence of fixed cationic groups that are chemically bonded to the polymer backbone. These cationic groups, often quaternary ammonium or phosphonium groups, have a positive charge that attracts and facilitates the transport of negatively charged hydroxide ions, and they are responsible for the selective transport of anions across the membrane, while simultaneously repelling and blocking the passage of cations [28].

The impact of the cathode and anode's distance from the fixed membrane was analyzed (Figure 1). The cathode and anode were placed 0.02 meters apart from the membrane in the first test configuration. In the following configuration distance rose by 0.015 meters, reaching a maximum of 0.05 meters (electrode distances of 0.02 m and 0.05 m were analyzed). The electrodes in every ECU experiment are maintained at a voltage of 90 V. The electrodes were connected to a 3000 W laboratory power supply (CSP-3000-120, Mean Well, Taiwan) controlled via the output voltage by a function generator (JT-JDS6600, Joy It, Germany). The pH values were measured with a multiparameter probe HI-9829 (Hanna Instruments, USA). The laboratory ECU's pH value measurement findings made it possible to parameterize the developed numerical model for the modeling of the pH dynamics in the ECU sections (anode and cathode section).

Numerical simulations were performed with the 3D hydrodynamic model Flow-3D [32], [33], [34], [35]. Solving the system of mass, momentum and energy conservation equations is based on the finite volume method and Euler's approach. A structured spatial discretization (calculation) grid is used in the Cartesian coordinate system, and the boundary conditions are defined for 6 surfaces of each calculation block. The free area is calculated using the so-called "Volume of Fluid" technique.

The presence of OH^- ions in water is interpreted with model particles of charge $3.2 \cdot 10^{-13}$ C, diameter $d_p = 2 \cdot 10^{-5}$ m, and density $\rho_P = 1000$ kg/m^3 which are carried through the model domain shown by the coupling of the 3D hydrodynamic and electrostatic model, Figure 2. Initial conditions of homogeneous distribution of pH in EKU are modeled with homogeneous initial distribution of 1.2E+4 model particles. Furthermore, 5 model particles are generated on the cathode surfaces in every second (particle flux $Q_P = 5$ p/s) of the simulation. All numerical simulations were performed for a period of 600 s.

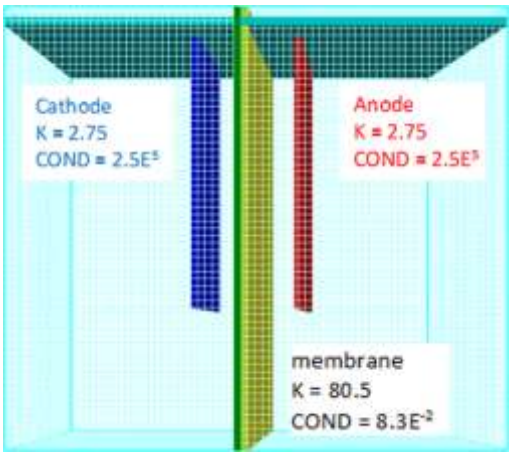

Figure 2. Spatial domain of the ECU model with calculation grid $\Delta x = \Delta y = \Delta z = 0.003$ m

The numerical model also yields the solution of the Laplace equation for the spatial distribution of electric potential (1) and electric field strength (2). The dynamic equation (3) is solved in order to define the transport of model particles OH^-.

$$\nabla \cdot (K \nabla \phi) = 0 \tag{9}$$

$$E = -\nabla \phi \tag{10}$$

$$\frac{d\boldsymbol{u}_P}{dt} = g - \frac{1}{\rho_P} \nabla p + \alpha(\boldsymbol{u} - \boldsymbol{u}_P) + \beta(\boldsymbol{u} - \boldsymbol{u}_P)|\boldsymbol{u} - \boldsymbol{u}_P| \frac{\rho}{\rho_P} + e_i E \tag{11}$$

where ϕ is the electric potential (adopted 0 V at the cathode and 90 V at the anode), E the strength of the electric field, K dielectric constant of the material (adopted for water = 80.5, carbon electrodes = 2.75, insulating polymer material on the reactor walls = 5), $\boldsymbol{u}_P$ particle velocity vector, ρ_P particle density (1000 kg/m^3), $\boldsymbol{u}$ liquid velocity vector (water), α and β shape resistance coefficients (adopted values $\alpha = 0$ and $\beta = 1$), d_p diameter of model particle (subject of calibration - adopted $d_p = 2 \cdot 10^{-5}$ m); e_i is the electric charge of the particle divided by the mass of the particle.

The calculation grid contains cells with equidistant lengths in the x, y, and z directions ($\Delta x = \Delta y = \Delta z$ 0.003 m). The entire computation domain is divided into two interconnected calculation blocks, which spatially coincide with the sections of the ECU (Figure 2). In the implementation of the simulations, the RNG k-ε turbulence model was used, and the influence of heat exchange was not taken into account. The pressure term was solved implicitly using the generalized minimal residual method, whereas the viscous stresses were explicitly computed. The boundary conditions in each of the two calculation

blocks (X_{min}, X_{maks}, Y_{min}, Y_{maks}, Z_{min}) are defined as "wall", while at the boundary Z_{max} is given atmospheric pressure, with only the gas (air) phase present. A fixed potential is given on the surfaces of the electrodes, while on the edges (reactor walls) the potential is dynamically calculated with the condition $\nabla\phi = 0$. A hydrostatic pressure distribution and a constant free water surface at 0.18 m are used as the initial conditions.

The model membrane was modeled in such a way that a vertical "porous" layer was placed on the left and right sides of the actual position of the membrane. The coefficient of restitution for the vertical porous layers in the ECU cathode sections is adopted with a value of -1, which means that the free transfer of particles is enabled towards anode. On the other hand, the coefficient of restitution for the vertical porous layers in the anode ECU section is adopted with a value of +1, which means that the transfer of particles from the anode to the cathode sections is prevented.

The basic calibration parameters in the numerical model is the diameter of the model particle d_p, which is varied in the value range from $d_p = 5 \cdot 10^{-6}$ m to $d_p = 3 \cdot 10^{-5}$ m ($d_p = 5 \cdot 10^{-6}$ m, $1 \cdot 10^{-5}$ m, $2 \cdot 10^{-5}$ m i $3 \cdot 10^{-5}$ m) and the zeta potential at the anode in the value range from 0 V to 70 V (0 V, 10 V, 40 V and 70 V). With a decrease in the diameter of the model particle, a decrease in the number of particles in the ECU section with the cathode (desirable trend) is achieved, but at the same time there is also a decrease in the number of particles in the anode section of the ECU (undesired trend).

In order to reduce the absorption of particles on the anodes, i.e. to achieve the desired trend of asymptotic increase in the number of particles in the anode section, the Zeta potential was used. Increasing the value of the Zeta potential also increases the number of particles in the anode section of the ECU.

The measured time required to reach the final value of pH in the section of the laboratory ECU served as a target value that needs to be achieved by numerical simulation along with the variation of d_p and zeta potential values. Adopting the values $d_p = 2 \cdot 10^{-5}$ m and Zeta = 20 V results in the required time for asymptotically reaching the maximum number of model OH^- particles in the anode section and the minimum number of model particles OH^- in the cathode section of 600 s, which is the same the measured time required to reach the final value of pH in the sections of the laboratory ECU.

4 Results and discussion

The measured series of pH values for the anode-containing section is displayed in Figure 3. The measurement findings are shown in comparison for the scenarios where the electrodes were positioned 0.02 and 0.05 meters apart from the membranes. pH readings show that the ECU portions have a roughly homogenous field in both the initial condition and the 600-second extension of the experiment (Figure 3). Additionally, Figure 3 shows that the distance between the electrodes affects the pH value increase, with a faster change in pH value corresponding to a smaller distance between the electrodes. The final pH value is not significantly influenced by the electrodes' position, but rather by the ECU operation time. The best option for electrode positioning, which reduces energy usage, is to place the electrodes 0.02 m from the membranes, according to the measurement data displayed in Figure 3.

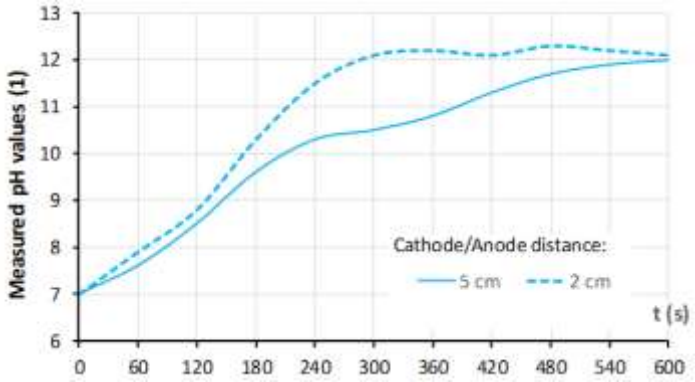

Figure 3. Measured pH values in the anode compartment of the ECU

A comparison of the time series for the quantity of model OH^- particles that flowed across the membrane over the 600 second simulation period is displayed in Figure 4. The strength of the electric field determines the difference in particle transport. The electric field is strongest in the upper part of the membrane, which is situated closest to the anode, and weakest in the lower part of the membrane, which is outside the shortest electric field lines.

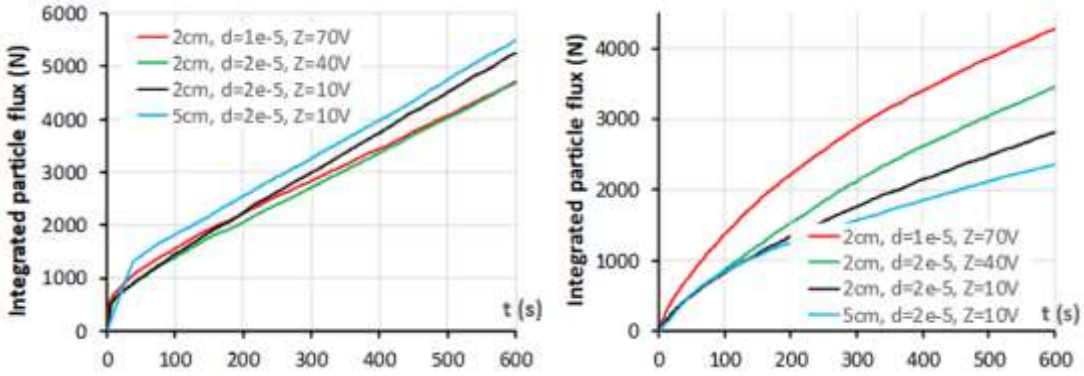

Figure 4. Time series of model particles that passed through the membrane during the 600 s of simulation period

An analysis of the time series pertaining to variations in the quantity of model OH^- particles in the anodic and cathodic sections is presented in Figure 5. The data from Figure 5 on the left demonstrate that while the asymptotic state of the number of particles is reached after 600 s, the reduction of the number of particles in the compartments with the cathode occurs faster when $d_p = 1 \cdot 10^{-5}$ m is adopted as opposed to $d_p = 2 \cdot 10^{-5}$ m. Conversely, Figure 5's results on the right demonstrate a higher rise of particles in the anodic region of the ECU occurs when $d_p = 2 \cdot 10^{-5}$ m is adopted.

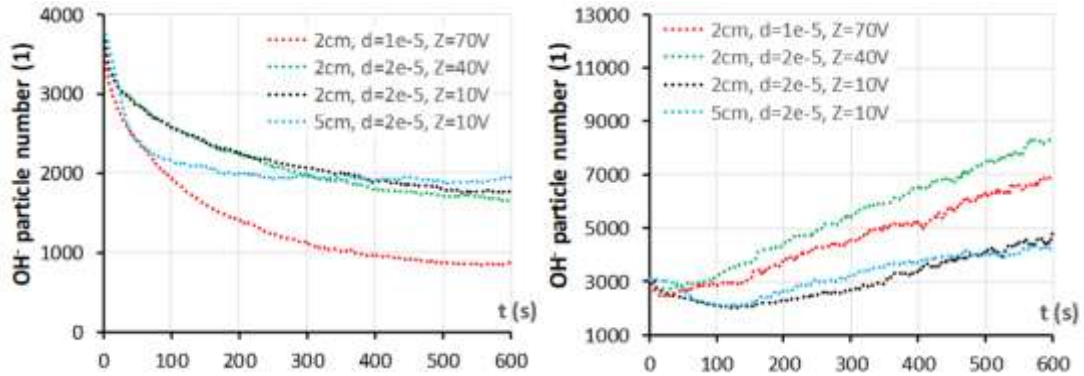

Figure 5. Time series of changes in model particles in the cathodic and anodic sections of ECU

Moreover, a comparison of the green and black lines illustrates how a rise in the Zeta potential causes a

more pronounced increase in the quantity of particles in the anode region. Additionally, it can be seen that, in accordance with the findings of the measurements at ECU, moving the electrodes away from the membranes (from 0.02 m to 0.05 m) causes a decrease in the number of particles in the cathode section and an increase in the number of particles in the anode section. As a result, it is determined that selecting a distance of 0.02 m, rather than 0.05 m between electrodes, is a more beneficial approach.

Figure 6 displays the iso lines of electric potential for the 60th and 600th seconds of the simulation period for the model's longitudinal vertical section ($X_{min} - X_{max}$) with, with $d_p = 2 \cdot 10^{-5}$ m and Zeta = 40 V.

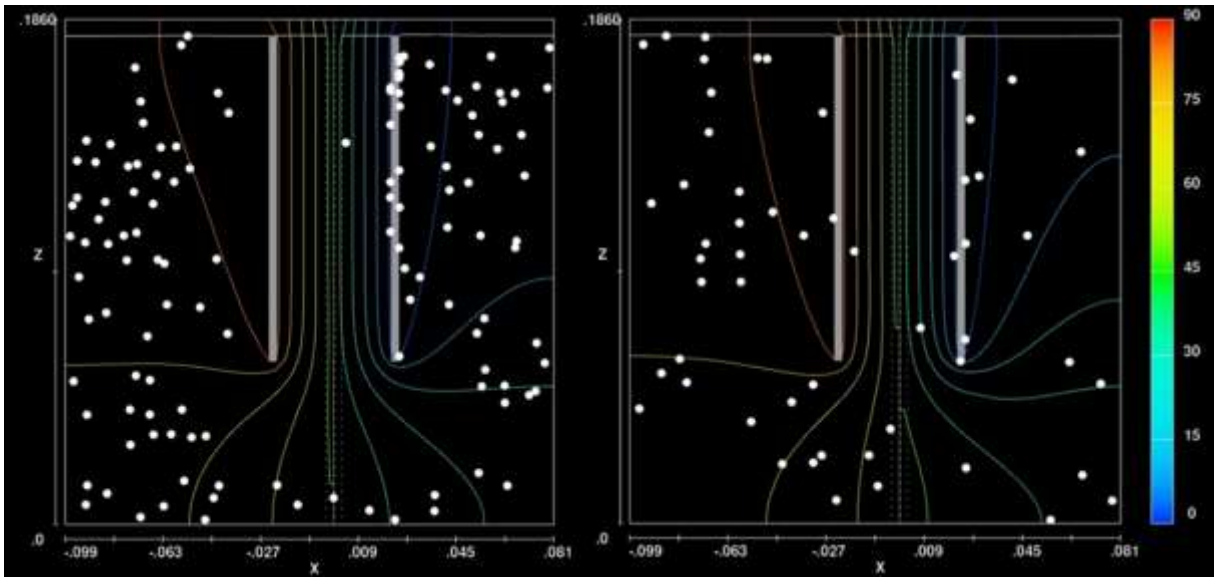

Figure 6. Iso line of electric potential in the longitudinal vertical section of the model for the 60th (left) and 600th second (right) of the simulation period with $d_p = 2 \cdot 10^{-5}$ m and Zeta = 40 V with electrodes at 2 cm from the membrane

Figure 7 provides a 3D representation of the spatial distribution of the model particles under the identical conditions for the 60th and 600th seconds of the simulation period. Figures 6 and 7 depict the scenario where the electrodes are positioned two centimeters away from the membranes.

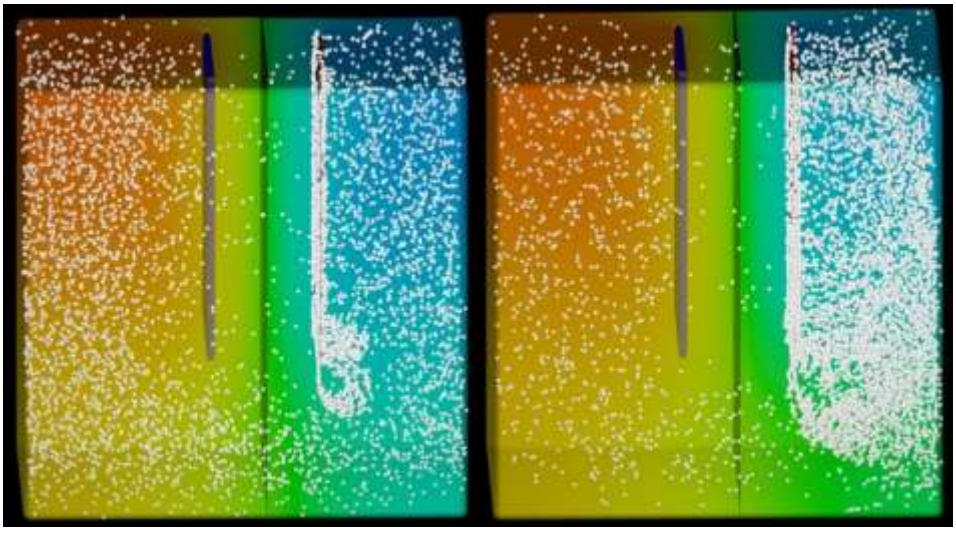

Figure 7. Spatial distribution of model particles for the 60th (left) and 600th (right) second of the simulation period under the conditions $d_p = 2 \cdot 10^{-5}$ m and Zeta = 40 V with electrodes at 2 cm from the membrane

5 Conclusion

Proper pH control leads to more efficient treatment processes, resulting in shorter treatment times, increased capacity, and better resource utilization. This enhances overall productivity and reduces energy consumption, contributing to sustainable water management practices. Electrochemical pH control helps minimize chemical usage and waste by ensuring that the optimal chemical reactions occur. This reduces the amount of chemicals required for treatment, minimizing chemical waste and reducing the environmental impact associated with their production, usage, and disposal.

The use of direct current and a semi-permeable membrane is certainly an energy-demanding way of controlling the pH value of water in the treatment process, but in some specific cases in which the use of acids or alkalis is not desirable due to the formation of additional by-products, this is an alternative way of changing the pH value, which has its price in terms of energy requirements and maintenance.
In this paper the influence of model particle size, electrode distance and zeta potential were analyzed as the most influential parameters of ECU for water pH control. It is important to emphasize that the created model represents the trend of the change in pH values, not the actual pH values. The reason for this is insufficient computing power required for modeling a large number of particles (1.2E+4 model particles instead of 1E+23 particles) that describes the actual pH values.

Using AEM in conjunction with a DC power supply and carbon electrodes in an electrodialysis setup offers a sophisticated and effective method for controlling the pH of water. By selectively removing or adding specific ions, the system can achieve precise pH adjustments, making it suitable for various water treatment applications. Regular monitoring and maintenance are essential to ensure optimal performance and longevity of the system.

Given that the change of pH value necessitates a certain duration of direct current application, for example 10 minutes as in this study, a very long and shallow reactors, membranes and inert electrodes would be needed to achieve the same detention time in the case of continuous flow reactor. Constructing such a reactor for pH control would be extremely complex and expensive.

Funding
This work was funded in part by the Croatian Science Foundation under the project PRIMEUS (UIP-2020-02-1160).

Acknowledgements
This work was supported in part by the Croatian Science Foundation under the project R3PEAT (UIP-2019-04-4046)

References:

[1] Khan, A. and Naz, B.: Fate of Urban Groundwater in Shallow Confined Aquifers. Case Study of Baldia Town, Karachi, Pakistan. Sustainable Development Research, (2019.), 1(1), pp. 1-10. https://doi.org/10.30560/sdr.v1n1p1
[2] Sheen, R.: Automatic pH control in water and industrial waste treatment. Industrial & Engineering Chemistry, (1947.), 39(11), pp. 1433-1439. https://doi.org/10.1021/ie50455a008
[3] Hu, C., Liu, H., Qu, J., Wang, D., & Jia, R.: Coagulation behavior of aluminum salts in eutrophic water: significance of Al_{13} species and pH control. Environmental Science &Amp; Technology, (2005.), 40(1), pp. 325-331. https://doi.org/10.1021/es051423+
[4] Pernitsky, D. and Edzwald, J. K.: Selection of alum and polyaluminum coagulants: principles and applications. Journal of Water Supply: Research and Technology - Aqua, (2006.), 55(2), pp. 121-141. https://doi.org/10.2166/aqua.2006.062
[5] Uhm, H. S., Lee, K. H., & Seong, B. L.: Inactivation of H1N1 viruses exposed to acidic ozone water. Applied Physics Letters, (2009.), 95(17), pp. 173704-1-173704-3. https://doi.org/10.1063/1.3242338

[6] Amin, M. S. A., Talukder, M. J., Raju, R. R., & Khan, M. R.: Conversion of food processing waste to bioenergy: bangladesh perspective. Trends in Renewable Energy, (2018.), 5(1), pp. 1-11. https://doi.org/10.17737/tre.2019.5.1.0080
[7] Placide, S. S., Mohamed, B., Hélène, L. E. M., Auguste, A. F. T., Quand-Même, G. C., Sanogo, I., … & Ouattara, L.: Assessment of the physicochemical and microbiological parameters of a teaching hospital's wastewaters in abidjan in côte d'ivoire. Journal of Water Resource and Protection, (2016.), 08(13), pp. 1251-1265. https://doi.org/10.4236/jwarp.2016.813096
[8] Mardarveran, P. and Mokhtar, N. M.: Analysis of artocarpus heterophyllus peel as a natural coagulant using response surface methodology (rsm). Jurnal Teknologi, (2020.), 82(4), pp. 99-107. https://doi.org/10.11113/jt.v82.14451
[9] Mulyani, H., Budianto, G. P. I., Margono, M., & Kaavessina, M.: Study of COD removal rate on a sequencing batch reactor (SBR) treating tapioca wastewater. agriTECH, (2019.), 38(3), pp. 243-250. https://doi.org/10.22146/agritech.29271
[10] Hua, G. and Reckhow, D. A.: DBP formation during chlorination and chloramination: effect of reaction time, ph, dosage, and temperature. Journal AWWA, (2008.), 100(8), pp. 82-95. https://doi.org/10.1002/j.1551-8833.2008.tb09702.x
[11] Sohrabifar, A., Asadollahi, A., & Fakhraei, H.: Impact of chlorination and chloramination on regulated trihalomethane formation: exploring doc reactions with disinfectants. PREPRINT, (2024.) https://doi.org/10.21203/rs.3.rs-4010653/v1
[12] Joo, S. H. and Mitch, W. A.: Nitrile, aldehyde, and halonitroalkane formation during chlorination/chloramination of primary amines. Environmental Science &Amp; Technology, (2007.), 41(4), pp. 1288-1296. https://doi.org/10.1021/es0612697
[13] Hwang, C., Ling, F., Andersen, G. L., LeChevallier, M. W., & Liu, W. T.: Microbial community dynamics of an urban drinking water distribution system subjected to phases of chloramination and chlorination treatments. Applied and Environmental Microbiology, (2012.), 78(22), pp. 7856-7865. https://doi.org/10.1128/aem.01892-12
[14] Donohue, M. J., Vesper, S., Mistry, J. H., & Donohue, J. M.: Impact of chlorine and chloramine on the detection and quantification of legionella pneumophila and mycobacterium species. Applied and Environmental Microbiology, (2019.), 85(24), pp 1-11. https://doi.org/10.1128/aem.01942-19
[15] Mari, A., Alonso-Prados, E., Villaverde, J. J., & Sandín-España, P.: Impact of drinking water treatment processes on the residues of plant protection products for consumer and aquatic risk assessment: theoretical and experimental studies. EFSA Journal, (2022.), 20., pp. 1-11. https://doi.org/10.2903/j.efsa.2022.e200906
[16] Shobana, S. and Panda, R. C.: Control of ph process using double-control scheme. Nonlinear Dynamics, (2011.), 67(3), pp. 2267-2277. https://doi.org/10.1007/s11071-011-0144-x
[17] Hermansson, A. W. and Syafiie, S.: Model predictive control of ph neutralization processes: a review. Control Engineering Practice, (2015.), 45, pp. 98-109. https://doi.org/10.1016/j.conengprac.2015.09.005
[18] Gustafsson, T. and Waller, K. V.: Nonlinear and adaptive control of ph. Industrial &Amp; Engineering Chemistry Research, (1992.), 31(12), pp. 2681-2693. https://doi.org/10.1021/ie00012a009
[19] Fosu, S., Yawson, D. J., & Owusu, C.:Computer simulation and control of a theoretical coagulation ph system in water treatment. Current Works in Mineral Processing, (2020.), 2(2)., pp. 11-21. https://doi.org/10.22606/cwimp.2020.22001
[20] Safari, I., Hsieh, M., Chien, S., Walker, M. E., Vidic, R. D., Dzombak, D. A., … & Abbasian, J.:Effect of CO_2 stripping on ph in open-recirculating cooling water systems. Environmental Progress &Amp; Sustainable Energy, (2013.), 33(1), pp. 275-282. https://doi.org/10.1002/ep.11769
[21] Balraj, B. and Senthilkumar, N.:Isolation, characterisation and enzymatic activity of streptomyces sp. and its ph control during fermentation process. IET Systems Biology, (2017.), 11(4), pp. 114-118. https://doi.org/10.1049/iet-syb.2016.0048
[22] Chen, G., Fournier, R. L., & Varanasi, S.:A mathematical model for the generation and control of a ph gradient in an immobilized enzyme system involving acid generation. Biotechnology and

Bioengineering, (1998.), 57(4), pp. 394-408. https://doi.org/10.1002/(sici)1097-0290(19980220)57:43.0.co;2-h
[23] Leng, Y., Chen, G., Mendoza, A. J., Tighe, T. B., Hickner, M. A., & Wang, C. Y.: Solid-state water electrolysis with an alkaline membrane. Journal of the American Chemical Society, (2012.), 134(22), pp. 9054-9057. https://doi.org/10.1021/ja302439z
[24] Henkensmeier, D., Najibah, M., Harms, C., Žitka, J., Hnát, J., & Bouzek, K.:Overview: state-of-the art commercial membranes for anion exchange membrane water electrolysis. Journal of Electrochemical Energy Conversion and Storage, (2020.), 18(2)., pp. 024001-1-024001-18 https://doi.org/10.1115/1.4047963
[25] Miller, H. A., Bouzek, K., Hnát, J., Loos, S., Bernäcker, C. I., Weißgärber, T., … & Meier-Haack, J.: Green hydrogen from anion exchange membrane water electrolysis: a review of recent developments in critical materials and operating conditions. Sustainable Energy &Amp; Fuels, (2020.), 4(5), pp. 2114-2133. https://doi.org/10.1039/c9se01240k
[26] Abbott, D. F., Meier, M., Meseck, G. R., Fabbri, E., Seeger, S., & Schmidt, T. J.:Silicone nanofilament-supported mixed nickel-metal oxides for alkaline water electrolysis. Journal of the Electrochemical Society, (2017.), 164(4), pp. F203-F208. https://doi.org/10.1149/2.0201704jes
[27] Cossar, E., Barnett, A. O., Seland, F., & Baranova, E. A.: The performance of nickel and nickel-iron catalysts evaluated as anodes in anion exchange membrane water electrolysis. Catalysts, (2019.), 9(10), pp. 814. https://doi.org/10.3390/catal9100814
[28] Hagesteijn, K. F. L. and Jiang, S.: A review of the synthesis and characterization of anion exchange membranes. Journal of Materials Science, (2018.), 53(16), pp. 11131-11150. https://doi.org/10.1007/s10853-018-2409-y
[29] Wang, A., Huang, Y., Sur, U. K., Wu, D., Ren, B., Rondinini, S., … & Zhang, T.: In situ identification of intermediates of benzyl chloride reduction at a silver electrode by sers coupled with dft calculations. Journal of the American Chemical Society, (2010.), 132(28), pp. 9534-9536. https://doi.org/10.1021/ja1024639
[30] Ambrosi, A., Moo, J. G. S., & Pumera, M.: Helical 3d-printed metal electrodes as custom-shaped 3d platform for electrochemical devices. Advanced Functional Materials, (2015.), 26(5), pp. 698-703. https://doi.org/10.1002/adfm.201503902
[31] González-García, J., Montiel, V., Aldaz, A., Conesa, J. A., Perez, J. R., & Codina, G.: Hydrodynamic behavior of a filter-press electrochemical reactor with carbon felt as a three-dimensional electrode. Industrial &Amp; Engineering Chemistry Research, (1998.), 37(11), pp. 4501-4511. https://doi.org/10.1021/ie980144a
[32] Hirt, C.W. and Nicholas, B.: Flow-3D User's Manual, Flow Science Inc.,1998,
[33] Prosperetti, A., Tryggvason, G.: Computational Methods for Multiphase Flow, Cambridge University Press, (2007.), pp. 488. https://doi.org/10.1017/CBO9780511607486
[34] Bombardelli, F.A., Meireles, I., Matos, J.: Laboratory measurements and multi-block numerical simulations of the mean flow and turbulence in the non-aerated skimming flow region of steep stepped spillways, Environ. Fluid Mech., (2011.), 11, pp. 263–288. https://doi.org/10.1007/s10652-010-9188-6
[35] Bombardelli, F.A.: Computational multi-phase fluid dynamics to address flows past hydraulic structures, Proceedings of the 4th IAHR International Symposium on Hydraulic Structures, Porto, pp. 9-11, 2012.

APPLICATION OF THE AHP METHOD TO THE SELECTION OF SEWAG SYSTEM TYPE

MARIJA ŠPERAC [1], TATJANA MIJUŠKOVIĆ SVETINOVIĆ [2], SILVIA IVA MILIČEVIĆ [3]

[1] *Josip Juraj Strossmayer University of Osijek Faculty of Civil Engineering and Architecture Osijek, Croatia, msperac@gfos.hr*

[2] *Josip Juraj Strossmayer University of Osijek Faculty of Civil Engineering and Architecture Osijek, Croatia, tatjanam@gfos.hr*

[3] *Josip Juraj Strossmayer University of Osijek Faculty of Civil Engineering and Architecture Osijek, Croatia, smilicevic3@gmail.com*

1 Abstract

In this paper, the AHP method is applied to the complex sewage system of the town of Županja (town in eastern Slavonia, Croatia), which consists of combined gravity sewage and vacuum sewage. It proved to be well applicable for selecting the type of sewage system. The selected method, which allows for a hierarchical structure of the problem, included analysis through social, economic and environmental criteria. In the process of choosing the appropriate type of sewerage system in the area of the city of Županja, vacuum sewerage proved to be adequate choice.

Keywords: multi-criteria decision-making, AHP method, combined gravity sewerage, vacuum sewerage, Županja (Croatia)

2 Introduction

Economic development and population growth are accompanied on the one hand by an increase in the need for water, and on the other hand by an increase in the pollution of water resources. Waste water is removed from urban areas through sewage systems. The sewage system is a very important urban infrastructure that collects, drains and treats wastewater. Considering the method of waste water removal, and the type of waste water that is removed by the sewage system, there are several types of sewage systems. The choice of the type of sewage system affects the efficiency of drainage and the standard of living of the urban environment.

The choice of drainage type depends on various factors, including the characteristics of the existing system, if any, the capacity and quality of the receiver, the nature of the water discharge into the system, the topography of the area and the need for preliminary treatment. The decision is mainly focused on local conditions and requirements of sanitary, ecological and economic aspects. Local conditions include the number of inhabitants, existing and planned industries, and the amount and composition of wastewater. The topography of the area and urban development plans are also considered. When expanding the sewage network, the key factor is the existing infrastructure and its characteristics. Sanitary requirements refer to maintaining health standards and preventing negative environmental impacts, while economic aspects refer to the costs of building and maintaining the system. Ultimately, the selection of the type of drainage should take into account all the above factors to ensure that the chosen system meets the specific needs and conditions of the area. [1]

Sewerage and sewage system management are invisible but key components of any urban environment, the efficiency of which directly affects the quality of life of residents and the preservation of natural resources. With the growth of urbanization and changes in the climate, the management of sewage is becoming more and more challenging, and it is necessary to invest in new technologies and approaches to ensure the sustainability of these systems.

The key element of good functioning lies in making quality and correct decisions, which requires careful

consideration. In this process, we are often faced with multiple criteria that can influence the final decision, often being in conflict with each other. In such situations, it is convenient to apply multi-criteria analysis, which will result in an optimal solution. The definition of multi-criteria decision-making is decision-making based on different criteria that are used to evaluate different variants of problem solutions. Multi-criteria decision-making methods are not only used to highlight one of the most suitable options, but can also be used to rank alternatives, then to select alternatives that are satisfactory, or to separate acceptable alternatives from unacceptable ones.
Problems related to multi-criteria decision-making are often extremely complex, not only because of the abundance of diverse criteria, but also because of variations in their importance. Therefore, it is crucial to carry out this process with a high degree of objectivity and structure in order to achieve decisions that are as good and high-quality as possible. Multi-criteria analysis represents a decision-making model that includes several key elements: a set of different solutions (variants that should be ordered or classified according to the decision-maker), a set of criteria (often multidimensional, enabling the assessment of different aspects using various measurement units), values (ratings) of each individual variant according to each of the criteria. [2]
Multi-criteria analysis methods can be applied in the decision-making process in order to adequately consider all relevant factors and aspects. [2] Choosing the appropriate method is a complex multi-criteria challenge. No specific technique can be universally best for all decision-making situations. Some of the applied multi-criteria methods are: Electra method, Promethee method, Victor method, ANP, AHP,...
Analyzes of the efficiency of sewerage systems in expert research were done from different aspects: from the implementation of a comprehensive assessment of the sewage system [3,4], to the safety assessment of the risks of sewage systems [5,6,7]. In this paper, the AHP method, which is often used in the management of the sewage system, was chosen. It is most often used for the choice of technology and location of the wastewater treatment plant. In works [5,6,7,8,9,10,11,12,13,14,15,16], the AHP method was applied to select the technology of the wastewater treatment plant. In the analyzed works[17,18,19], the AHP method was used to select the location of the waste water treatment plant, and in all works a hierarchical structure was formed, which includes two levels, criteria and sub-criteria.

3 Methods

To select the type of sewage system, the method of analytical hierarchical procedure was applied. (AHP method). This method was developed by Thomas L. Saaty in the 1970s. AHP is used to solve complex decision-making problems by decomposing those problems into a hierarchical structure that includes objectives, criteria (or sub-criteria), and alternatives. [20] A key component of the AHP method is a mathematical model that enables the calculation of priorities (weights) of elements at the same level of the hierarchy. This method is applied in multi-criteria decision-making, where the most acceptable solution is selected for each alternative based on defined criteria and attribute values, or the entire ranking of the importance of alternatives within the model is displayed. [21]

In order to more precisely rank the set criteria and alternatives with the aim of making optimal decisions about priorities in our area of interest, during the decision-making process it is necessary to break down the procedure into the following steps: [22]

1. Specify the problem and consider what needs to be decided.
2. Structure a decision hierarchy that has the goal at the top, with the decision criteria in the middle, while the alternatives are at the last level of the hierarchy. We will be tasked with choosing one of the alternatives, with the help of consultation with experts in the relevant field, literature review, deep thinking about the problem and similar approaches.
3. Compare elements pairwise, creating a set of comparison matrices as specified method. In this step, comparisons are made pairwise, respecting the hierarchy previously defined. For comparison, every two lower-level elements should be analyzed in relation to each higher-level element, using Saaty's scale. (Table 1)

Table 1. Saaty scale

INTENSITY OF IMPORTANCE	DEFINITION	EXPLANATION
1	Equal importance	Two activities contribute equally to the objective
3	Weak importance of one over another	Experience and judgment slightly favor one activity over another
5	Essential or strong importance	Experience and judgment strongly favor one activity over another
7	Demonstrated importance	An activity is strongly favored and its dominance demonstrated in practice
9	Absolute importance	The evidence favoring one activity over another is of the highest possible order of affirmation
2,4,6,8	Intermediate values between the two adjacent judgments	When compromise is needed

4. Calculate the priorities of the alternatives and the weights of the criteria based on the results of the comparisons

Mathematical model of the AHP method

In the AHP method, the key mathematical instruments are matrices. Therefore, we provide basic definitions and results related to matrices, starting from desirable properties of these mathematical structures.
In a situation where there are n priorities, whose weights w_i should be determined based on their ratios, the calculation procedure is carried out as follows: [23]

$$a_{ij} = \frac{w_i}{w_j} \tag{1}$$

From these ratios, we generate a matrix of relative importance, denoted as matrix A.

$$A = \begin{pmatrix} w_1/w_1 & w_1/w_2 & w_1/w_n \\ w_2/w_1 & w_2/w_2 & w_2/w_n \\ w_n/w_1 & w_n/w_2 & w_n/w_n \end{pmatrix} = \begin{matrix} a_{11} & a_{12} & a_{1n} \\ a_{12} & a_{22} & a_{2n} \\ a_{1n} & a_{2n} & a_{nn} \end{matrix} \tag{2}$$

For the case of consistent changes for which it is valid $a_{ij} = a_{ik} * a_{kj}$, the matrix A satisfies the equation $A * w = n * w$, where w represents the priority vector. Solving the weighting problem can be treated as solving an equation $A * w = \lambda * w$, where λ is different from zero.

$$\begin{bmatrix} w_1/w_1 & w_1/w_2 & \dots & w_1/w_n \\ w_2/w_1 & w_2/w_2 & \dots & w_2/w_n \\ w_n/w_1 & w_n/w_2 & \dots & w_n/w_n \end{bmatrix} * \begin{bmatrix} w_1 \\ w_2 \\ w_n \end{bmatrix} = \text{n} * \begin{bmatrix} w_1 \\ w_2 \\ w_n \end{bmatrix} \tag{3}$$

he matrix A has the property of positivity and reciprocity, because the elements contained in the matrix satisfy the equation $a_{ij} = \frac{1}{a_{ij}}$. Rank is $r(A) = 1$ and all its orders are proportional to the first, which is why only one of its eigenvalues is different from 0 and is equal to n. Given that the sum of the eigenvalues of a positive matrix corresponds to the trace of the matrix, i.e. the sum of the elements on the diagonal, the non-zero eigenvalue has the value n:

$$\lambda max = n \tag{4}$$

If the matrix A contains an inconsistency, the weight vector w can be calculated using the following system of equations:

$$(A - \lambda_{max} * I) * w = 0 \sum_i w_i = 1 \tag{5}$$

Considering the equation above, the following applies:

$$A * w = n * w \tag{6}$$
$$\sum_i w_i = n * w \tag{7}$$
$$w = \frac{1}{n} \sum a_{ij} * w_i \tag{8}$$
$$\sum_i a_{ij} = \frac{w_1 + w_2 + w_n}{w_j} \tag{9}$$
$$w_j = \frac{w_1 + w_2 + w_n}{\sum_i a_{ij}} \tag{10}$$

It follows that the weight of each alternative is:

$$w_i = \frac{1}{n} \sum \frac{a_{ij}}{\sum_i a_{ij}} \tag{11}$$

Researched area

In this paper, the AHP method for selecting the type of sewage system was applied to the city of Županje in the Eastern part of the Republic of Croatia (Figure 1).

Figure 1. Location of Županja on geographical maps (Europe and Croatia)

Županja is located on a flat terrain at an altitude of 83m along the Sava river, in the area of high groundwater levels. Two types of sewage system are used for waste water drainage: combined gravity sewage and vacuum sewage. Combined gravity sewage are networks of underground pipes that convey blackwater, greywater and, in many cases, stormwater from individual households to a (semi-) centralised treatment facility, using gravity and pumps where necessary. Vacuum sewage consist of a vacuum station, where the vacuum is generated, the vacuum pipeline system, collection chambers with collection tanks and interface valve units. In contrast to conventional gravity sewerage systems with intermediate pumping stations, the permanent pressure within the vacuum system is maintained below atmospheric pressure. Županja was chosen to apply the AHP method to compare these two sewage systems. The method evaluates criteria related to social, economic and environmental factors. Within the framework of the social criteria, the following sub-criteria were evaluated: impact during construction, accommodation in the space, complexity of the system for users and unpleasant smells. Under the economic criterion sub-criteria were evaluated: investment value, operating costs and construction complexity. Within the social criteria, the following were evaluated: environmental impact and energy consumption.

4 Results and discussion

4.1 Determining the most important criterion (element)

In this part, the determination of the most significant criterion will be defined. The analysis includes a social, economic and environmental element. They are assigned values according to the Saaty scale analyzed by pairs as shown in the matrix representation.

Table 2. Intensity of importance of criteria according to Saaty's scale

1	SOCIAL	ECONOMICAL	1	2	3	4	5	6	7	8	9
2	SOCIAL	ENVIRONMENTAL	1	2	3	4	5	6	7	8	9
3	ECONOMICAL	ENVIRONMENTAL	1	2	3	4	5	6	7	8	9

Table 2 shows that in the relationship between social and economic criteria, the social criterion is moderately more important; the relationship between social and environmental criteria is equally important; in the relationship between economic and environmental criteria, the environmental criterion is strictly more important.

First multiplication of decision matrices:

$$\begin{bmatrix} 1 & 3 & 1 \\ 0.33 & 1 & 0.33 \\ 1 & 5 & 1 \end{bmatrix} * \begin{bmatrix} 1 & 3 & 1 \\ 0.33 & 1 & 0.33 \\ 1 & 5 & 1 \end{bmatrix} = \begin{bmatrix} 3.00 & 11.00 & 2.60 \\ 0.86 & 3.00 & 0.73 \\ 3.65 & 13.00 & 3.00 \end{bmatrix}$$

Determination of the 1st vector priority:

- Summarizing the rows of the matrix:

$$\begin{bmatrix} 3.00 + 11.00 + 2.60 \\ 0.86 + 3.00 + 0.73 \\ 3.65 + 13.00 + 3.00 \end{bmatrix} = \begin{matrix} 16.60 \\ 4.59 \\ 19.65 \end{matrix} = 40.84$$

- Normalization of the sum of rows:

$$\begin{bmatrix} 0.41 \\ 0.11 \\ 0.48 \end{bmatrix}$$

Second multiplication of the decision matrix:

$$\begin{bmatrix} 3.00 & 11.00 & 2.60 \\ 0.86 & 3.00 & 0.73 \\ 3.65 & 13.00 & 3.00 \end{bmatrix} * \begin{bmatrix} 3.00 & 11.00 & 2.60 \\ 0.86 & 3.00 & 0.73 \\ 3.65 & 13.00 & 3.00 \end{bmatrix} = \begin{bmatrix} 27.95 & 99.80 & 93.63 \\ 7.83 & 27.95 & 6.17 \\ 33.08 & 118.15 & 27.95 \end{bmatrix}$$

Determination of the 2nd vector priority:

- Summarizing the rows of the matrix:

$$\begin{bmatrix} 27.95 + 99.80 + 93.63 \\ 7.83 + 27.95 + 6.17 \\ 33.08 + 118.15 + 27.95 \end{bmatrix} = \begin{matrix} 221.38 \\ 41.95 \\ 179.18 \end{matrix} = 442{,}51$$

- Normalization of the sum of rows:

$$\begin{bmatrix} 0.50 \\ 0.09 \\ 0.40 \end{bmatrix}$$

Calculation of the difference of vector priorities:

$$\begin{bmatrix} 0.41 \\ 0.11 \\ 0.48 \end{bmatrix} - \begin{bmatrix} 0.50 \\ 0.09 \\ 0.40 \end{bmatrix} = \begin{bmatrix} -0.09 \\ 0.02 \\ 0.08 \end{bmatrix}$$

Due to the small amounts of the difference vector, no further calculation of the priority vector is necessary.

Determining the most important criterion:

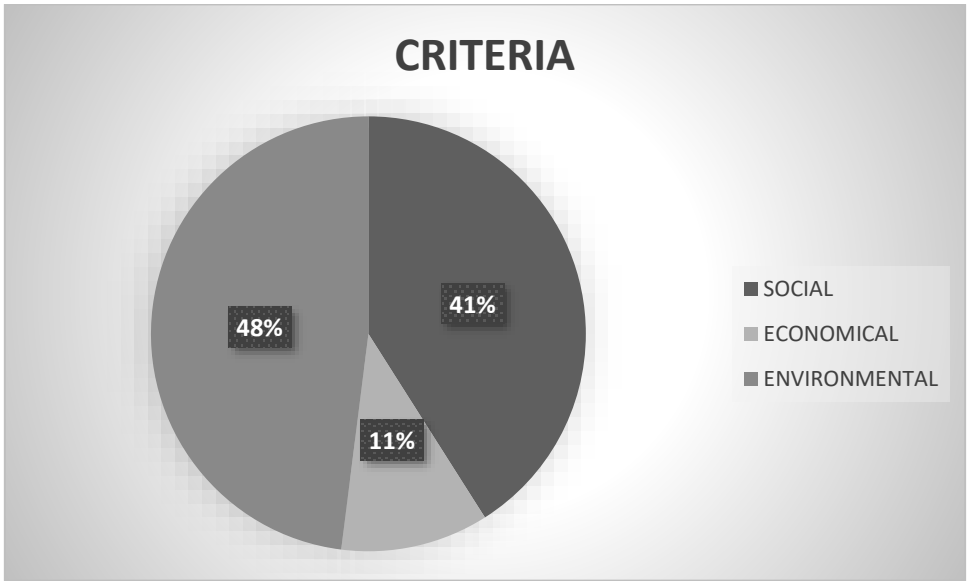

Figure 2. Representation of the analyzed criteria

The environmental criterion proved to be the most significant. They are important for the long-term sustainability of the project, so it is important to choose an option that has less negative impacts on the environment. Preservation of the environment also includes the reduction of air, water, and soil contamination, which certainly represents a challenge in the construction and management of construction infrastructures. Considering all the challenges faced by the modern population, such as the fight against climate change, it is clear how important this aspect is and how it indirectly affects certain social aspects and the quality of life.

According to the same methodology, the following results were obtained.

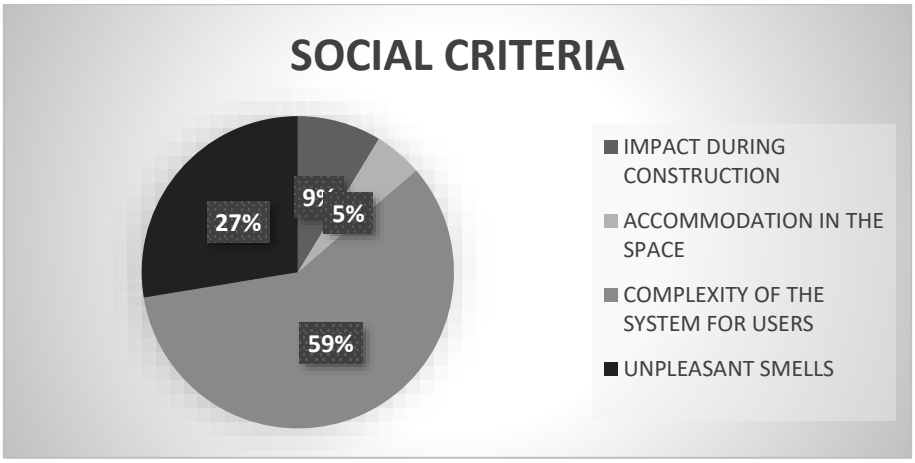

Figure 3. Representation of social sub-criteria

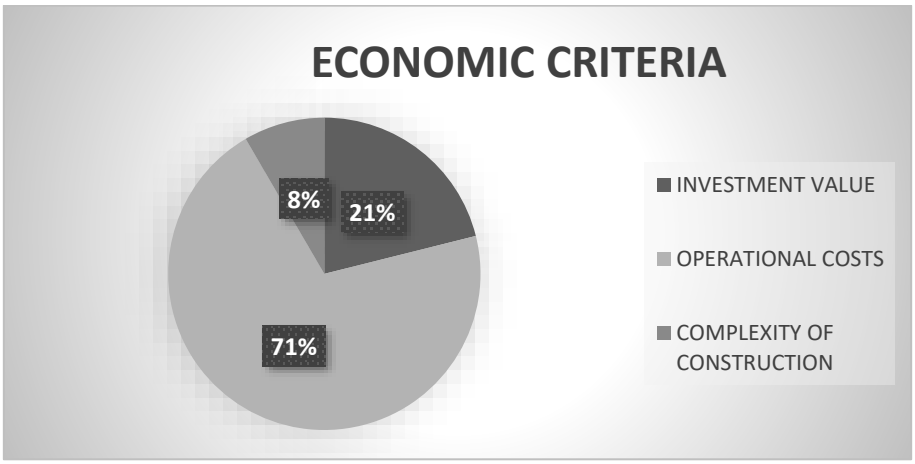

Figure 4. Representation of economic sub-criteria

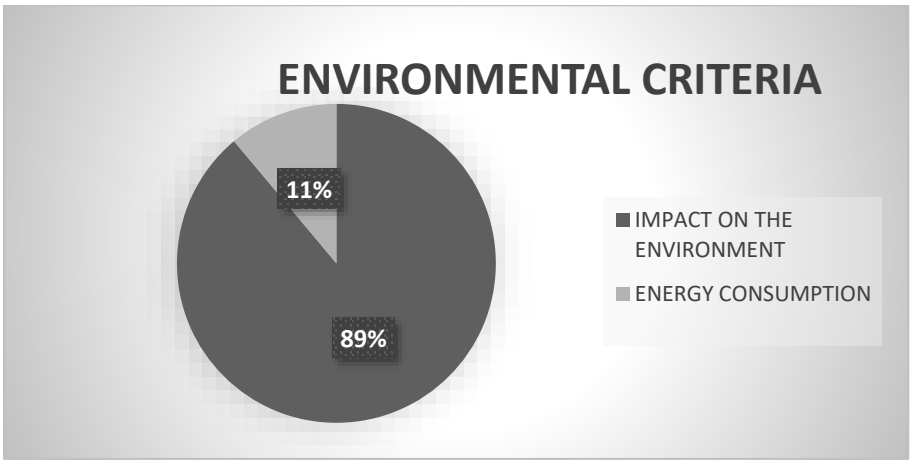

Figure 5. Representation of environmental sub-criteria

4.2 Determination of the final value of sub-elements

1. Social criteria:

	IMPACT DURING CONSTRUCTION	ACCOMMODATION IN SPACE	COMPLEXITY OF THE SYSTEM FOR USERS	UNPLEASANT SMELLS		
GRAVITY SEWERAGE	0.25	0.50	0.900	0.250	0.087	0.64
VACUUM SEWERAGE	0.75	0.50	0.100	0.750	0.050	0.36
					0.587	
					0.276	

2. Economic criteria:

	INVESTMENT VALUE	OPERATIONAL COSTS	COMPLEXITY OF CONSTRUCTION		
GRAVITY SEWERAGE	0.250	0.200	0.667	0.211	0.25
VACUUM SEWERAGE	0.750	0.800	0.333	0.705	0.75
				0.084	

3. Environmental criteria:

From an environmental point of view, certain criteria related to conservation and protection, as well as minimal negative impacts on natural resources, are included in order to ensure sustainable development and environmental protection. Today, and thus in the future, these criteria will play a key role in the choice of drainage type. The following sub-criteria were analyzed

a) Impact on the environment

Both systems have potential positive and negative impacts on the environment, therefore it is essential to carry out a detailed analysis in order to adopt the one where it is easier to avoid bad effects. Environmental impact factors should be taken into account when planning and implementing sewage systems to ensure that an optimal balance is achieved between technical requirements, economic feasibility and environmental protection.

b) Energy consumption

Energy consumption is an important environmental criterion that provides an insight into how much energy each sewage system requires for its operation. Gravity and vacuum sewers differ in the way they use energy and the amount of energy they require to function.

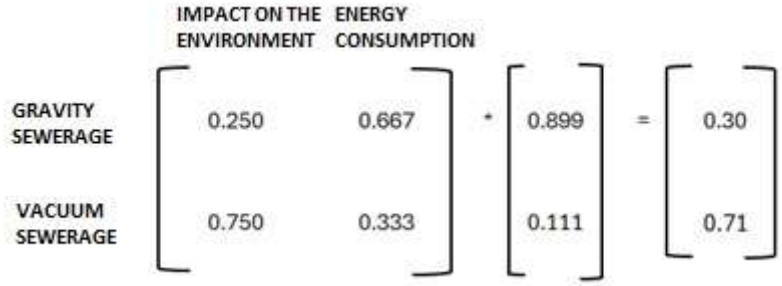

4. Final analysis:

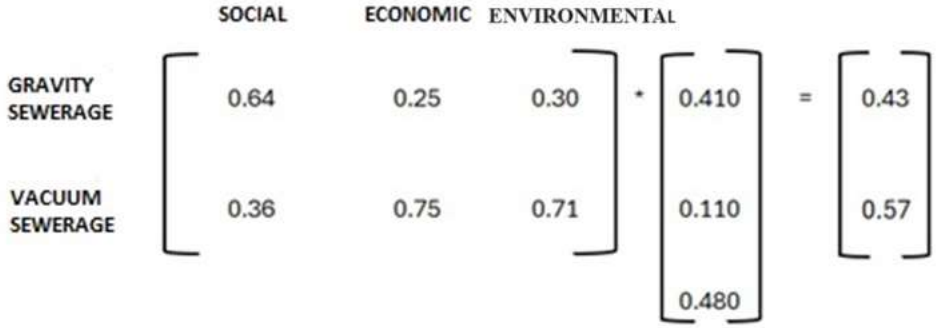

Through a detailed analysis using the AHP method for the agglomeration of Županja, based on all the processed criteria (social, economic, environmental), vacuum sewerage proved to be a little better choice. Vacuum sewerage is a modern and advanced technical solution for waste water management that brings a number of advantages. It is ideal for use on flat terrains and in cases of high groundwater levels, which is another benefit considering the observed area. This adaptability enables better use of urban space and reduces the need for intensive interventions in the environment during the construction phase. Thanks to the shallow burial depth, the possibility of groundwater infiltration is significantly reduced. Eliminating infiltration and draining only sanitary waste water results in lower channel contents and thus lower needs for purification at the purification devices. In terms of durability and maintenance, it can result in lower operating costs over the life of the system. Also, by performing vacuum sewerage, financial savings of approximately 30-40% are achieved. Smaller soil excavations, lower water consumption and reduced need for chemical wastewater treatment can reduce harmful effects on the environment and local ecology.

5 Conclusion

The advantages of multi-criteria decision-making both in the management of the sewage system and in the selection of the type of sewage system is in the integral approach to problem solving. Often, when designing sewage systems, only one criterion is analyzed - economic, and the cheapest technical solution is designed. The problems of multi-criteria decision-making are often extremely complex, not only because of the large number of different criteria, but also because of their different evaluation and ranking. Due to the large number of available multi-criteria decision-making methods, it is difficult to

choose the best one because each method has its own limitations, peculiarities, hypotheses, premises and perspectives and can lead to different results when applied to the same problem. .

The results of the presented AHP method for selecting the type of sewage system are the results for the current specific conditions of the selected location. For our location (the city of Županja), vacuum sewerage was given a slight preference for selection. It follows from this that for a given location, combined gravity sewerage and vacuum sewerage will work equally well for waste water drainage. In practice, this has proven to be true because both types of sewers work equally well in this area. Combined gravity sewerage has more elements and greater maintenance needs, while vacuum sewerage uses a substation to create a vacuum. For another location and other criteria, it is necessary to re-apply the steps of the AHP method and analyze the results. When choosing weighting factors for individual criteria and sub-criteria, in order to obtain the most objective results possible, the cooperation of a team of different experts dealing with the given issue is necessary..

References:

[1] Margeta, J.: Drainage settlement, authorized script, University of Split, Faculty of Civil Engineering, Architecture and Geodesy, University of Zagreb, Faculty of Geotechnics, Varaždin, Split/Varaždin, 2011.

[2] Deluka – Tibljaš, A., Karleuša B., Dragičević N.: Overview of the application of multi-criteria analysis methods when making decisions about transport infrastructure, Građevinar 7/2013, p. 619 – 631, 2013.

[3] Wang, H., Yan, M., Gao, J., Wang, Y., Dai, X. : En evaluation system for assesing the operationl efficiency of urban combined sewer system using AHP-Fuzzy comrehensive evaluation: A case study in Sanghai, China. Water 15 (19) 3434, 2023.

[4] Nam, S., Nguyen, T., Oh, J. : Performance Indicators Framework for Assessment of a Sanitary Sewer System Using the Analytic Hierarchy Process (AHP). Sustainability 11, 2746, 2019.

[5] Ghavami, S., Borzooei, Z., Maleki, J. : An effective approach for assessing risk of failure in urban sewer pipelines using a combination of GIS and AHP-DEA. Process Safety and Environment. Prot. *133*, pp 275–285, 2020.

[6] Liu, W., Dong, W. Risk assessment on the drainage pipe network based on the AHP-entropy weight method. Journal of safety and environment 21, pp 949–956, 2021.

[7] Xu, D., Zhang, Q. : Risk assessment of the integrated sewage pipeline conduction based on the AHP–GRA formula. Journal of safety and environment 19, pp 1149–1154, 2019.

[8] Ellis, K.V., Tang, S. L. : Wastewater Treatment Optimization Model for Developing World. I: Model Development. Journal of Environmental Engineering, 117, 501-518.,1991.

[9] Tang, S.L., Ellis, K.V.: Wastewater Treatment Optimization Model for Developing World. II: Model Testing. Journal of Environmental Engineering, 120, pp 610-624. ,1994.

[10] Tang, S.L., Wong, C., Ellis, K. V. : An Optimization Model for the Selection of Wastewater and Sludge Treatment Alternatives. Water and Environment Journal, 11.pp 14-20., 1997.

[11] Karimi, A.R., Mehrdadi, N., Hashemian, S.J., Bidhendi, G.R., Moghaddam, R. T.: Selection of wastewater treatment process based on the analytical hierarchy process and fuzzy analytical hierarchy process methods. International Journal of Environmental Science & Technology, 8, pp 267-280. 2011.

[12] Srdjevic, Z., Samardzic, M., Srdjevic, B. : Robustness of AHP in selecting wastewater treatment method for the coloured metal industry: Serbian case study. Civil Engineering and Environmental Systems, 29, pp147 - 161., 2012.

[13] Kalbar, P.P., Karmakar, S., Asolekar, S.R. : The influence of expert opinions on the selection of wastewater treatment alternatives: a group decision-making approach. Journal of environmental management, 128,pp 844-851., 2013.

[14] Aydiner, C., Sen, U., Koseoglu-Imer, D.Y., Dogan, E. : Hierarchical prioritization of innovative treatment systems for sustainable dairy wastewater management. Journal of Cleaner Production, 112, pp 4605-4617., 2016.

[15] Wei, C., Wei, J., Kong, Q., Fan, D., Qiu, G., Feng, C., Li, F., Preis, S., Wei, C. : Selection of optimum biological treatment for coking wastewater using analytic hierarchy process. The Science of the total environment, 742, 2020.

[16] Ćetković, J., Knežević, M., Vujadinović, R., Tombarević, E., Grujić, M. : Selection of Wastewater

Treatment Technology: AHP Method in Multi-Criteria Decision Making. Water 15(9), 2023.
[17] Deepa, K., Krishnaveni, M. : Suitable Site Selection of Decentralised Treatment Plants Using Multicriteria Approach in GIS. Journal of Geographic Information System, 2012, pp 254-260. 2012.
[18] Mansouri, Z., Moghaddas, N.H., Dahrazma, B. : Wastewater treatment plant site selection using AHP and GIS: a case study in Falavarjan, Esfahan., Geopersia 3 (2), pp 63-72., 2013.
[19] Kafil, M., Albaji, M. : Selecting wastewater sites using analytical hierarchy and geographic information system., ICE Proceedings Municipal Engineer 171(2), pp 1-7 .,2017.
[20] Saaty, T. L.: The Analytic Hierarchy Process, second edition, RWS Publications, Pittsburg, 1996.
[21] Šperac, M., Karleuša B., Bilić M., Application of the AHP method to the selection of waste water treatment devices, 8th Croatian Water Conference, Croatian Water in Food and Energy Production,pp 871-880 Poreč, 2023.
[22] Multiple Criteria Decision Analysis: State of the Art Surveys, International Series in Operations Research & Management Science, Vol. 78, Springer, New York, 2005.
[23] Miličević,S.I. : A multi-criteria analysis model for making decisions in sewage system management, J.J.Strossmayer University of Osijek, Faculty of Civil Engineering and Architecture Osijek, graduation thesis, 2024.

ANTHROPOLOGICAL IMPACT O SSMALL NATURAL WATER RESOURCES ON PAG ISLAND

IVANA SUŠANJ ČULE[1], DANIELA KALAFATOVIC[2], GORAN VOLF[1], PATRIZIA JANKOVIĆ[2], NATAŠA ATANASOVA[3], BARBARA KARLEUŠA[1], NEVENKA OŽANIĆ[1]

[1] *University of Rijeka, Faculty of Civil Engineering, Department of Hydrotehnics and Geotehnics, Croatia, isusanj@uniri.hr, goran.volf@uniri.hr, barbara.karleusa@uniri.hr, nozanic@uniri.hr*

[2] *University of Rijeka, Faculty of Biotechnology and Drug Development, Medicinal Chemistry Division, Croatia, daniela.kalafatovic@uniri.hr, patrizia.jankovic@uniri.hr*

[3] *University of Ljubljana, Faculty of Civil and Geodetic Engineering, Institute of Sanitary Engineering, Slovenia, natasa.atanasova@fgg.uni-lj.si*

1 Abstract

This investigation determined the anthropological impact on small naturally formed water resources, as well as the hydrological analysis and current water quality state. Moreover, this research provides an answer to the potential significance of locations, and the need for further observation, protection, and the possibility of revitalization. The obtained results can provide the foundation for the development of protection mechanisms and mitigation of human impact on yet unprotected and vulnerable natural water resources.

Keywords: anthropological impact, hydrological research, water quality parameters, synthetic polymer

2 Introduction

The quality, quantity, and availability of water resources, as well as their physicochemical and biological characteristics are constantly changing because of the impact of natural and human activities [1]. The anthropological impact on water resources is already well defined indicating that urbanisation, industrial, and agricultural activities introduce pollutants into water resources, and influence the water balance within water resource catchments [2]. Natural impact on water resource systems balance can be visible through weather extremes such as droughts and floods [2]. It is challenging to divide anthropological from natural activities' impact on water resource systems nevertheless their existence can be determined.

In this paper, the focus is placed on human impact on natural small water resources such as small lakes and ponds, in order to provide the foundation for the development of impact mitigation practices. Naturally formed small lakes or ponds that are located in or near urban areas are usually recognized by the local population and tourists because of their natural beauty and/or biodiversity. They are usually not used for human activities and have specific biotopes and biocenosis, and therefore can be significant for the overall ecosystem. Despite their recognition, the direct or indirect anthropological impact is visible on those small water resources and their catchments and therefore they become the focus of the present study.

Water bodies of mentioned resources are usually considered public water resources under the Croatian water that is a legal entity for water management and are not characterised as highly protected, vulnerable, or landscape significant areas according to any Croatian or European Union laws and directives. The catchment areas are usually under the jurisdiction of the local authorities and are not recognized in local authority urban plans. Since their importance has not been determined, there is no existing mechanism for their protection, and therefore natural small water resources such as small lakes and ponds are sometimes neglected and can face accelerated degradation. It should be noted that thousands of small lakes and ponds on the Croatian territory are not under protection from

anthropological actions, and we cannot expect that each of them should be highly protected, but there is a high importance in controlling and maintaining a stable ecosystem with mitigated human impact until they fall under some kind of regulatory protection in the future.

This paper aims to determine the existence of the anthropological impact on three naturally formed ponds located on the island of Pag, Croatia, namely Škuncini stani, Vrgnica (Dabovi stani), and Vidasovi stani. These ponds were chosen because of the defined fast-growing human impact of tourism, urbanisation, and agricultural activities on the catchment areas and water bodies. To provide insight into the anthropological impact, hydrological analysis and measurement of water quality properties were performed. The anthropological impact is also shown through the characterization of the synthetic polymer fragments collected near the water bodies or in the water itself.

3 Methods

The results of the research that will be presented in this work are a part of the project called "Development of the methodology for the condition evaluation, protection and revitalization on small urban water resources" (ZIP-UNIRI-1500-2-22). The goal of the aforementioned Project is to develop a methodology for quality assessment, protection from the anthropological impact, and revitalization of small water resources in urban areas, which will be the basis for the development of guidelines for better management of the urban catchment areas of the aforementioned water resources. The project itself, in its first phase, included hydrometric research, water quality assessment, and pollutant determination at selected localities. Criteria for the research localities selection were that the water resource is on the the Register of Water Resources list from Croatian Waters, does not dry out, has a functional ecosystem, and are placed in or near the urban area i.e. they are under the impact of human activities. Furthermore, as the anthropological impact of pollution by synthetic polymer fragments is determined on the locations near the water bodies or in the water itself, research is expanded on the synthetic polymer pollution analysis.

3.1 Hydrological analysis and measurements

The first preliminary hydrological analyses and measurements carried out before of this project were previously established at the location of Medulin pond (Istria County) by our team in 2022 [3].

The hydrological analysis encompasses a description of the selected water resources' topographic catchments, catchment basic physical characteristics, and analysis of the catchment landcover changes in the last fifty years in order to provide insight into the anthropological impact on the natural water balance. The topographic boundaries of the catchments are delineated on the topographic map, while the catchment landcover changes are determined by the visual analysis and delineation on the catchments' orthophotos that were taken through years from 1968 until 2021. Landcover changes provide insight into the human impact by urbanisation and land cultivation in general that can change the natural water balance [2].

The basic hydrological measurements are based on the bathymetry measurement that is carried out using instruments: probe CTD-diver (Van Essen Instruments B.V., Netherlands) for measuring depth, and Topcon positioning system HiPer V for geodetic measurements. The measurement process is performed by moving the geodetic instrument on the surface of the measuring site with the help of a vessel and placing the probe for depth measurements at that position. During this, the three-dimensional coordinates of the bottom, or bathymetry, are obtained.

3.2 Water quality evaluation

Water quality measurements are carried out by water sampling and water analyses in the Hydrotechnical Laboratory at the Faculty of Civil Engineering in Rijeka. The water quality parameters are measured by the Spectrophotometer - Hach DR 3900. In this paper physical and chemical properties are provided as

follows: pH, Total dissolved solids [ppm], Conductivity [μS/cm], Nitrates [mg/L; NO_3 -N], Ammonium [mg/L; NH_4^+ - N], Chloride [mg/L; Cl^-], Nitrites [mg/L; NO_2^- - N], Total nitrogen [mg/L; TNb], Orthophosphate [mg/L; $PO^3_4{}^-$ P], Total phosphorus TP [mg/L; $PO^3_4{}^-$ P], and Chemical oxygen demand CODcr [mg/L; O_2], in order to assess overall quality, ecological potential, and anthropological impact on the water.

Water quality evaluation was conducted according to the Regulation on the Water Quality Standard (NN 96/2019) [4] and Amendments to the Regulation on the Water Quality Standard (NN 20/2023) [5] issued by the Republic of Croatia government. It should be noted that there are no water quality standards for the ponds and they are not categorized in Regulations. Therefore, for the purpose of the water quality evaluation, the closest category is chosen, and that is small shallow lakes.

3.3 Synthetic polymers analysis

Synthetic polymers (widely known as plastics) consist of repeating units of organic monomers bound together. These monomers are made of carbon, hydrogen, and other atoms linked together by covalent bonds. The degradation of plastic can happen by abiotic and biotic degradation. Abiotic degradation makes the plastic weather through exposure to light, heat, chemicals or mechanical stress. The mentioned stresses make the polymer chain degrade through oxidation, dichlorination, chain scission, cross-linking, ablation, and fragmentation. Biotic degradation refers to the degradation of plastic by an organism [6].

The direct visible negative impact of human activities on water resources is provided through synthetic polymers that can be found in the water or in the vicinity of water resources. It is well known that synthetic polymers upon atmospheric action degrade, which means that both microplastics and smaller nano particles are released into the environment and enter natural water resources [6].

For the purpose of this research, macro plastics are collected, categorized, and analysed using Attenuated Total Reflectance-Fourier Transform Infrared (ATR-FTIR) spectroscopy performed on the Cary 630 FTIR spectrometer (Agilent) to determine the types of synthetic polymers. ATR-FTIR spectroscopy is based on the vibrations of molecules including stretching, bending, or twisting that result in transmittance or absorbance spectra upon exposition to infrared (IR) radiation and help to determine the chemical composition of a molecule of interest [7]. The unit of the *x-axis* is wavenumbers *w* measured in cm^{-1} where the $w = 1/\lambda$, and where λ is the wavelength of the photon measured in cm. The *y-axis* of an FTIR spectrum is typically transmittance or absorbance [8]. Transmittance is the fraction of incident IR radiation that passes through a sample without being absorbed, while absorbance is a measure of how much IR radiation is absorbed by a sample at a particular wavelength [7]. Transmittance and absorbance are mathematically dependent and can be calculated as shown in Equation 1, where *A* represents absorbance and *T* represents transmittance.

$$A = -log_{10}T \tag{1}$$

Samples' transmittance spectra were recorded with wavenumber resolution of the w =16 cm^{-1} and 100 sample scans. The recorded spectra for every sample were compared to a manually built library containing pre-recorded labelled synthetic polymer spectra. Samples were categorised into six common groups of synthetic polymers as follows: Polyethylene Terephthalate (PET), High-Density Polyethylene (HD-PE), Polyvinyl Chloride (PVC), Low-Density Polyethylene (LD-PE), Polypropylene (PP), Polystyrene (PS). There is also the seventh group that includes others types of synthetic polymers but in this research, the goal was to identify the most common types [9]. Also, samples that have not been identified by the ATR-FTIR library are placed in a group of the not recognised ones.

After the identification of the most common types of plastic, their possible degradation was assessed. The most detectable type of plastic degradation is photo-oxidation which can be recognised by the presence of carbonyl groups (C=O, a double covalent bond between a carbon atom and an oxygen atom)

in ATR-FTIR spectra of the sample. Carbonyl groups indicate that the plastic has been degraded and facilitates further degradation due to the photo lability (unstable near light) of carbonyl groups [7], which could also mean that the nano and micro particles are released into the environment.
In this paper, the degradation is determined by the calculation of the Carbonyl index (CI). Although there is currently no standard method to calculate the CI, in the last few years Specific Area Under Band (SAUB) method become widely used for the degradation assessment of the PE and PP samples [10]. SAUB method is also used in this paper and the calculation is represented with Equation 2.

$$CI = \frac{Area\ under\ band\ 1850{-}1650\ cm^{-1}}{Area\ under\ band\ 1500{-}1420\ cm^{-1}} \quad (2)$$

SAUB method is based on the area calculation by integration of the area under the absorbance curve at specific wavelength ranges of the IR spectra that are characteristic to the process of plastic degradation. In this paper, CI is calculated for the PE and PP samples found in or near water resources and then compared with the same new reference samples in order to determine the degradation.

4 Results and discussion

The results presented within this paper are focused on the analysis of three small naturally formed ponds that are recorded in the Register of Water Resources of Croatian Waters. The selection of a specific water resource was based on its registration in the Register of Water Bodies of the Croatian Waters, as a permanent resource, and a developed biocenosis within its biotope. In this paper, the selected small ponds, located in or near urban areas, are described in terms of their basic hydrological features, water quality analysis, and synthetic polymer presence in or around the ponds. The results of these analyses provide an insight into the ecological potential of the locations and their ecosystem stability and help in indicating the anthropological influence level.

4.1 Locations and hydrological characteristics

Three localities have been analysed, and they are: (i) Škunca stani pond (Novalja, Pag Island), (ii) Vrgnica pond (Dabovi stani, Novalja, island of Pag) and (iii) Vidasovi stani pond (Vidasovi stani, Novalja, island of Pag). Figure 1. show the location of ponds together with their specific topographic catchment.

a) b) c)

Figure 1. Location of processed ponds on the topographic map with the topographic boundaries of the catchment: a) Škunca stani, b) Vrgnica pond (Dabovi stani), and c) Vidasovi stani [11] notable

A developed ecosystem has been established on all three analysed ponds and they appear to be under the moderate influence of anthropogenic activity. A large number of various insects, amphibians, snakes, and aquatic plants were observed at all locations. The locations serve as watering places for wild animals and birds, as well as for the sheep of local shepherds, for whom these ponds are extremely important. Direct anthropogenic impact in the form of the arrangement of protective walls was carried out by the Croatian waters for the purpose of protection on the ponds of Škunca stani and Vidasovi stani. The first

hydrological measurements were carried out on the island of Pag in June 2023. Table 1 shows the basic results of the hydrological measurement and characteristics of the catchments.

Table 1. Results of the hydrological measurements and basic catchment characteristics

Name	Characteristics of the water resource			Characteristics of the catchment			
	Water surface area	Maximum water depth	Water volume	Altitude of the pond	Catchment area	Lowest altitude of the catchment	Highest altitude of the catchment
	Al [m²]	D [m]	V [m³]	Hmin [m a.s.l.]	As [km²]	Hmin [m a.s.l.]	Hmax [m a.s.l.]
Škunca stani	286,1	2	227,9	60	121035,2	60	131,4
Vrgnica (Dabovi stani)	465,37	1,81	412,31	30	31676,9	30	51
Vidasovi stani	1530,95	2,03	1205,2	48	230395,7	48	71,6

Water replenishment of the analysed ponds takes place with regard to the geological karstic formation by surface and subsurface flow, and according to the information available from the local population, the ponds are recording a gradual annual decrease in water levels, but without drying up.

The catchment landcover changes are determined by the visual analysis and delineation on the catchments' orthophotos that were taken through the years: 1968, 2011, 2014, 2017, 2019 and 2021 [11]. The area is divided into categories as urbanised, ground vegetation, bare, roads, and agricultural (garden) areas are. Landcover changes are providing insight into the anthropological impact by the urbanisation and land cultivation in general. The results of the analysis are shown in Figure 2., Figure 3. and Figure 4. The biggest change in landcover is recorded between 1968 and 2011. On the Škunca stani pond catchment area reforestation is noticed, as well as the biggest urbanisation rate in comparison to others. On the Vrgnica (Dabovi stani) pond catchment area, also the reforestation of one part of the area happened but with no significant growth of urbanisation. On the catchment area of the Vidasovi stani pond also the growth of the ground vegetation can be noticed.

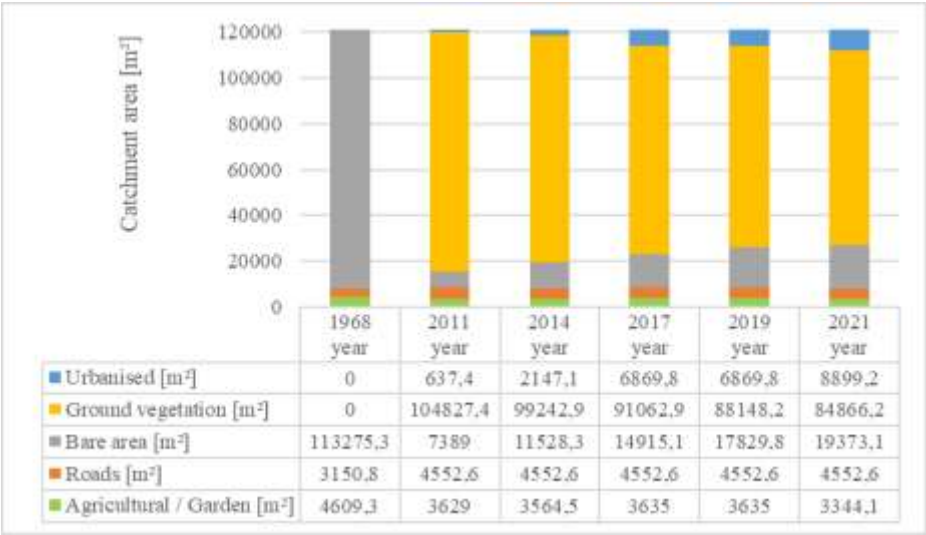

	1968 year	2011 year	2014 year	2017 year	2019 year	2021 year
Urbanised [m²]	0	637,4	2147,1	6869,8	6869,8	8899,2
Ground vegetation [m²]	0	104827,4	99242,9	91062,9	88148,2	84866,2
Bare area [m²]	113275,3	7389	11528,3	14915,1	17829,8	19373,1
Roads [m²]	3150,8	4552,6	4552,6	4552,6	4552,6	4552,6
Agricultural / Garden [m²]	4609,3	3629	3564,5	3635	3635	3344,1

Figure 2. Catchment landcover analysis on the pond Škunca stani

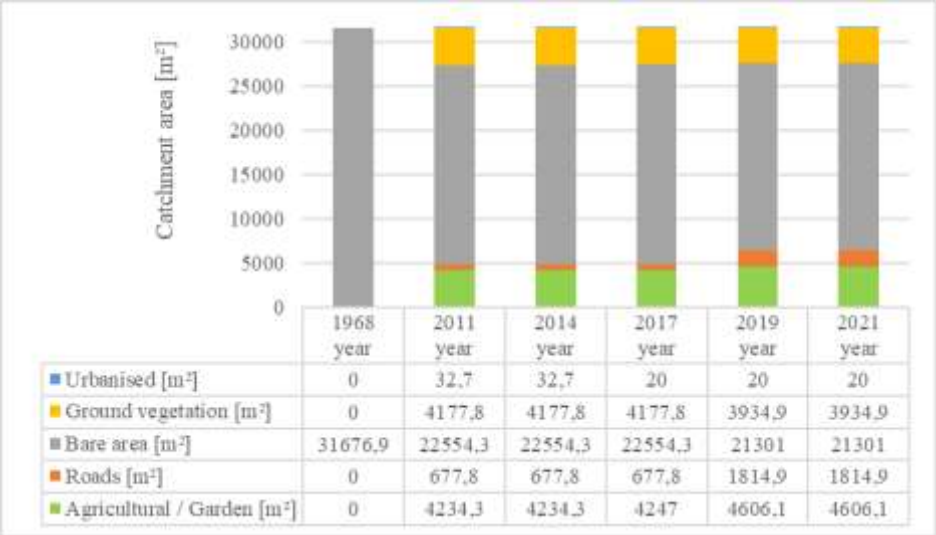

	1968 year	2011 year	2014 year	2017 year	2019 year	2021 year
Urbanised [m²]	0	32,7	32,7	20	20	20
Ground vegetation [m²]	0	4177,8	4177,8	4177,8	3934,9	3934,9
Bare area [m²]	31676,9	22554,3	22554,3	22554,3	21301	21301
Roads [m²]	0	677,8	677,8	677,8	1814,9	1814,9
Agricultural / Garden [m²]	0	4234,3	4234,3	4247	4606,1	4606,1

Figure 3. Catchment landcover analysis on the pond Vrgnica (Dabovi stani)

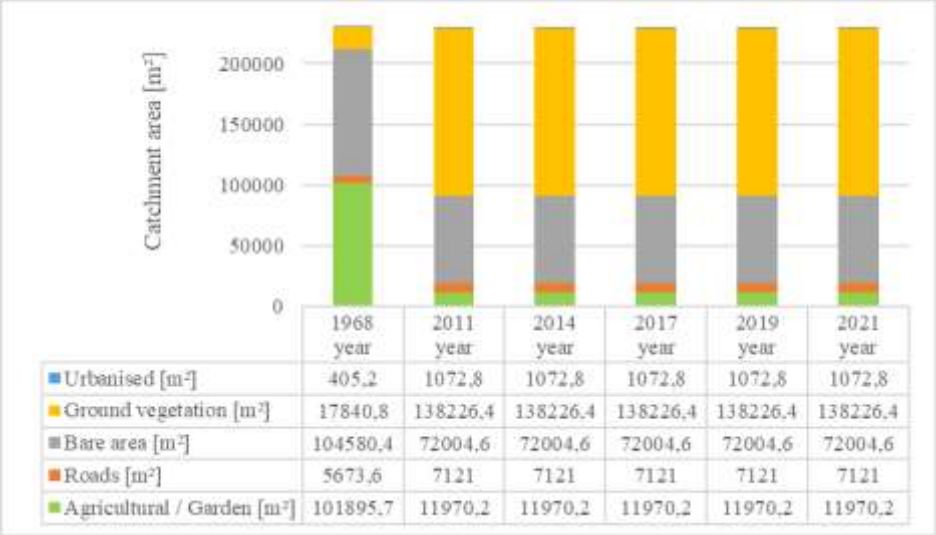

	1968 year	2011 year	2014 year	2017 year	2019 year	2021 year
Urbanised [m²]	405,2	1072,8	1072,8	1072,8	1072,8	1072,8
Ground vegetation [m²]	17840,8	138226,4	138226,4	138226,4	138226,4	138226,4
Bare area [m²]	104580,4	72004,6	72004,6	72004,6	72004,6	72004,6
Roads [m²]	5673,6	7121	7121	7121	7121	7121
Agricultural / Garden [m²]	101895,7	11970,2	11970,2	11970,2	11970,2	11970,2

Figure 4. Catchment landcover analysis on the pond Vidasovi stani

4.2 Water quality and evaluation of ecological potential

In the process of conducting basic hydrological measurements on ponds, water sampling was carried out at the positions shown in Figure 5.

a) b) c)

Figure 5. Display of water sampling locations on ponds: a) Škunca stani pond, b) Vrgnica pond (Dabovi stani), and c) Vidasovi stani pond [11]

The sampling of the water was performed by taking two samples per pond in three occasions, in summer and autumn in 2023 and in winter in 2024. To see changes in the water quality, it is necessary to perform water sampling in all four seasons of the year. The analyses of water samples are shown in Table 2. where every record represents the average result of two samples per pond measurement. Table 2., also shows the assessment of the ecological potential of water according to the regulations limits [4, 5, 12].

Table 2. Laboratory analysis of water samples from Škunca stani, Vrgnica (Dabovi stani) and Vidasovi stani ponds

Water quality parameter	Label/Unit	Škuncini stani			Vrgnica (Dabovi stani)			Vidasovi stani			*Evaluation of ecological potential*
		13.06.23.	09.10.23.	19.2.24.	13.06.23.	09.10.23.	19.2.24.	13.06.23.	09.10.23.	19.02.24.	
pH	*[ ]*	7,3	7,35	7,2	7,35	6,9	7,1	7,55	6,8	7,35	*Good: 7<pH<7,4*
Total dissolved solids (TDS)	*[ppm]*	282	349	192,5	299,5	420,5	246	162,5	240	220,5	*Marginally acceptable: 200 <TDS<300*
Conductivity (C)	*[µS/cm]*	520,5	677	431	553,5	783,5	523,5	301	429,5	453,5	*Fresh water*
Nitrates	*NO_3 -N / [mg/L]*	0,3335	0,4	0,3845	0,26	0,339	0,239	0,3145	0,363	0,2355	*0,15 - 0,35*
Ammonium	*NH_4^+ - N / [mg/L]*	0,4725	0,078	0,072	0,1545	0,4185	0,0165	0,0515	0,031	0,014	*Good: Cyprinid water <1)*
Chloride	*Cl^- / [mg/L]*	84,05	105	66,75	104,5	117	98,6	50,35	58,9	62,75	*Good: <0,005*
Nitrites	*NO_2^- - N / [mg/L]*	0	0,0285	0,0035	0	0,0035	0,0005	0	0,007	0,0095	*Good for water life: < 0,03*
Total nitrogen	*TNb / [mg/L]*	1,835	16,95	2,525	1,091	7,87	1,25	0,801	8,96	2,355	*Good: < 1,24*
Orthophosphate	*PO^3_4 - P / [mg/L]*	0,009	0,0915	0,008	0	0,179	0,0285	0,0065	0,007	0,323	*Good: <0,1*
Total phosphorus (TP)	*PO^3_4 - P / [mg/L]*	0,074	0,344	0,047	0,0035	0,227	0,1835	0,0235	0,1345	0,1475	*Good: <0,3*
Chemical oxygen demand (CODcr)	*O_2 / [mg/L]*	30,75	170	35,9	24,8	109,2	19,35	37,55	174,5	76,5	*Good: 20<CODcr<200*
Evaluation of the ecological potential:			*Within limits*			*Slight difference*			*Significant difference*		

The analysis of water samples showed that water is not contaminated with nitrates and nitrites, while at the location of the Vrgnica pond (Dabovi stani) and Vidasovi stani pond, a slightly increased level of orthophosphate was recorded, which usually can be correlated with the use of artificial fertilizers in nearby areas. The ammonium level is satisfactory and indicates that there are no significant microbiological activities. Chlorides in the water are increased at all analysed locations, and in this case, source of the chlorides needs to be jet determined as they can be introduced from the seawater and also as a result of the parent rock decomposition at the locations. Also, the impact of the chlorides on the ecological potential, in this case, can be estimated when its source is defined [13, 14]. Due to the above-mentioned increased concentration of chloride, the electrical conductivity and TDS level are expected to be higher. Since the nitrates, nitrites, and ammonium are rather low, the elevated total nitrogen refers to organic nitrogen. The origin of the organic nitrogen content cannot be determined with certainty since water microbiological analysis is not conducted. However, the increased total levels of organic nitrogen and phosphorus in the Škunca stani pond and occasionally in others indicate increased levels of nutrients that can lead to eutrophication, i.e. changes that can have a negative impact on existing ecosystems by overgrowth of algae for example. Considering that the CODcr is within acceptable limits indicates that the level of organic matter is still currently satisfactory [12].

4.3 Synthetic polymer analysis

More than 20 macroplastic fragment samples were manually collected in February 2024 directly from water and/or in vicinity of the water bodies and stored in the bags. Fragment samples are then processed in the laboratory by preparing size intended instrument pieces (usually 1 cm × 1 cm in size). Samples are next dried on room temperature, then categorised and analysed using ATR-FTIR spectroscopy. Transmittance spectra were recorded and typical polymer fingerprints were identified and subsequently compared with the self-built library that contained pre-labeled synthetic polymers including Polyethylene Terephthalate (PET), High-Density Polyethylene (HD-PE), Polyvinyl Chloride (PVC), Low-Density Polyethylene (LD-PE), Polypropylene (PP), and Polystyrene (PS). If the collected microplastic samples did not fall into one of the six main polymer categories found in the self-built library, they were marked as “Not recognized”. The results are shown in Table 3., and indicate that the most common types of plastic found in ponds of interest were PP, HDPE, and PET.

Table 3. Laboratory analysis of synthetic polymer samples from Škuna stani, Vrgnica (Dabovi stani) and Vidasovi stani ponds

Location	PET	HDPE	PVC	LDPE	PP	PS	Not recognized	**Number of samples**
Škunca stani	1	7	0	4	12	1	11	**36**
Vrgnica (Dabovi stani)	1	6	2	1	6	0	12	**28**
Vidasovi stani	6	3	0	1	13	0	1	**24**

In addition to the analysis of the main type of plastics in the environment, their degradation due to environmental conditions including mechanical, UV, thermal-induced stress was analysed. In order to determine the plastic degradation, recorded transmittance was converted to absorbance using Equation 1. According to the presented SAUB method, only identified PET and PP samples were assessed to determine degradation by calculating CI using Equation 2. Since the examined plastic fragments were visually recognised packaging of yogurt or crackers, water bottles, etc., new packaging from the supermarket was used to prepare referent samples to allow the comparison between new and environment exposed ones. It is expected that the absorbance and the CI of the degraded samples rises with time, when exposed to environmental conditions, especially the region of the IR spectra where the carbonyl groups appear, indicating photo oxidation of the plastic. Figure 6. shows the degradation analysis of PET sample found on the pond Vidasovi stani, while Figure 7. shows the degradation on the PP sample found on the pond Škunca stani. In both cases, CI increased indicating that plastic degradation occurred over time. Moreover, the change in absorbance is also visible in other wavelengths of the samples indicating on somekind of environmental condition process. The observed plastic degradation can indicate that the nano and micro particles are released into the environment, which needs to be further confirmed.

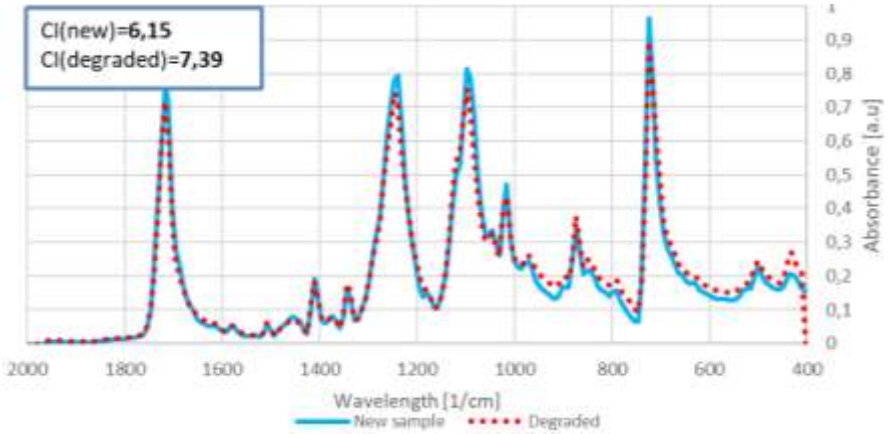

Figure 6. Absorbance spectra of the new and degraded PET sample (yogurt bottle)

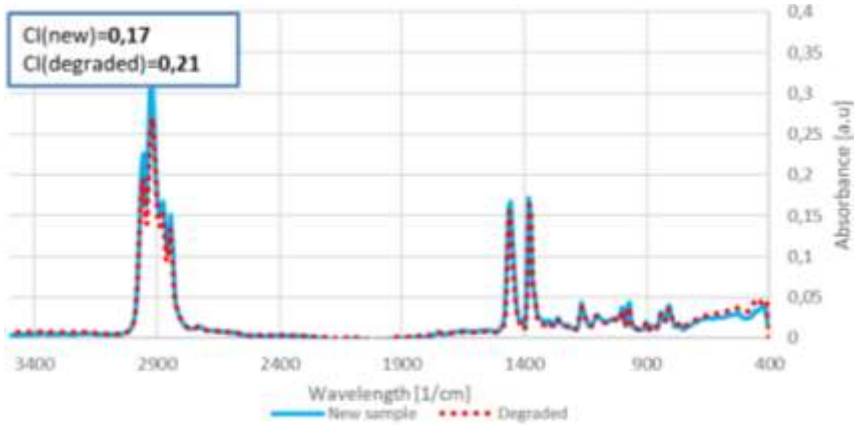

Figure 7. Absorbance spectra of the new and degraded PP sample (cracker packaging)

5 Conclusion

The paper presents the results of hydrological investigations, water quality evaluation of small natural water resources in or near urban areas, and analysis of the collected synthetic polymers found on sites to assess the anthropological impact on the ecological potential and natural water balance. The main goal of the overall research is to provide assessment methodology and guidelines for the protection and revitalisation of small natural water resources such as ponds that are currently not falling under specific national regulations. Small naturally formed water resources in the form of ponds and lakes located in or near urban areas have their significance at the local level for the population in terms of landscape, history, and ecology, and sometimes represent small natural oases with a developed specific biocenosis. The surface of water resources themselves is under the jurisdiction of Croatian waters, while the management of the catchment area is the responsibility of local self-government. As a rule, due to their size, so far they have not been recognised yet as valuable natural areas and are therefore not under the protection of the ecological network Nature 2000, nor are they recognised as landscape and nature value within urban development plans. The aforementioned water resources are mostly supplied by surface and underground water from the catchment area, which significantly affects their condition, and the water surface itself is often under the direct influence of human activities.

Within this paper, three localities have been analysed, and they are: (i) Škunca stani pond (Novalja, Pag Island), (ii) Vrgnica pond (Dabovi stani, Novalja, island of Pag) and (iii) Vidasovi stani pond (Vidasovi stani, Novalja, island of Pag). Hydrological research indicates that all ponds are very small and shallow with small karstic catchment areas. Despite their size, those ponds never dried up, and that is because of their specific way of water replenishment by the small local underground aquifer. Analysis of the landcover changes through the last fifty years indicates the catchment reforestation and the growth of urbanisation in smaller parts. The possible reason for the reforestation by ground vegetation on all analysed catchments, mainly between 1968 and 2011, can be found in the widespread electrification of the island of Pag and the change in human activities that took place around the 1970s. Namely, inhabitants were using vegetation as firewood before the 1970s, and with the arrival of electricity, they increasingly use other heating methods related to the use of electricity. The way of life for inhabitants also changed, and urbanization started with growth of tourism. Agricultural land is transforming into building areas, and further growth of urbanization can be expected in the future. All aforementioned indicates that humans have a potentially large impact on natural water balance. Reforestation has impact on the regeneration of the local underground aquifers by reducing of water infiltration, while urbanization affects the growth of surface runoff. Even though it is not straightforward to quantify the level of anthropological impact, its existence is evident.

Water quality evaluation has shown overall positive ecological potential, but also the anthropological impact through a slightly increased level of orthophosphate at two locations, which usually comes from the application of artificial fertilizers. The change in some of the water quality parameters through the annual season, such as nitrates, total nitrogen, and total phosphorus, refers to the fragility of the water system and potential eutrophication.

The anthropological negative impact concerning plastic pollution is unquestionable. The careless disposal of plastic packaging into our environment has undeniable consequences. The plastic samples based on synthetic polymers that were collected at the site of water ponds of interest do not only represent a visual contamination but they can have a negative impact on the local flora and fauna. Furthermore, the potential degradation of nano and micro plastics can enter into the water resources and in the ecological system. ATR-FTIR spectroscopy of the collected samples has shown the degradation of plastic in the ecological system. It is therefore important to define the importance and condition of the observed water resources in order to be able to establish basic guidelines for better management of the catchment area and the surface of the water resource itself to protect them and consequently our environment and us.

According to the presented research results, the need for further small water resources observation, and protection is visible. It is important to widen the research on additional locations to develop protection mechanisms and mitigation of human impact guidelines for small water resources that are placed in or near urban areas.

Acknowledgements
This work was supported by the University of Rijeka through projects „Development of the methodology for the condition evaluation, protection and revitalization on small urban water resources" (ZIP-UNIRI-1500-2-22); "Hydrology of water resources and risk identification of consequences of climate changes in karst areas" (uniri-iskusni-tehnic-23-74); "Implementing innovative methodologies, technologies and tools to ensure sustainable water management" (uniri-iskusni-tehnic-23-67); "Decision support system for improvement and management of treatment processes on drinking water treatment plant Butoniga" (ZIP-UNIRI-1500-3-22).

References:

[1] Khatri, N., & Tyagi, S.: Influences of natural and anthropogenic factors on surface and groundwater quality in rural and urban areas. Frontiers in life science, 8(1), 23-39, 2015.
[2] Akhtar, N., Syakir Ishak, M. I., Bhawani, S. A., & Umar, K.: Various natural and anthropogenic factors responsible for water quality degradation: A review. Water, 13(19), 2660, 2021.
[3] Sušanj Čule, I., Volf, G., Ožanić, N., & Ružić, I.: Hydrometric and Water Quality Properties of the Medulin Pond (Republic of Croatia). In *17th International Conference on Water Management and Hydraulic Engineering* (pp. 205-213). Gdańsk University of Technology Publishing House, 2022.
[4] Republic of Croatia Government: The Regulation on the water quality standard (NN 96/2019), https://narodne-novine.nn.hr/clanci/sluzbeni/2019_10_96_1879.html , 2019.
[5] Republic of Croatia Government: Amendments to the Regulation on the Water Quality Standard (NN 20/2023), https://narodne-novine.nn.hr/clanci/sluzbeni/2023_02_20_341.html , 2023.
[6] Zhang, K., Hamidian, A. H., Tubić, A., Zhang, Y., Fang, J. K., Wu, C., & Lam, P. K.: Understanding plastic degradation and microplastic formation in the environment: A review. Environmental Pollution, 274, 116554, 2021.
[7] Walfridson, M., & Kuttainen Thyni, E.: Automation of carbonyl index calculations for fast evaluation of microplastics degradation (Dissertation). Retrieved from https://urn.kb.se/resolve?urn=urn:nbn:se:kth:diva-315175 (accessed: 28.05.2024), 2022.
[8] Introduction to FTIR Spectroscopy. Thermo Fisher. url: https://www.thermofisher.com/hr/en/home/industrial/spectroscopy-elemental-isotope-analysis/molecular-spectroscopy/fourier-transform-infrared-spectroscopy/resources/ftir-spectroscopy-academy.html#ftir-basics (accessed: 28.05.2024).
[9] Schwarz, A. E., Ligthart, T. N., Boukris, E., & Van Harmelen, T.: Sources, transport, and accumulation of different types of plastic litter in aquatic environments: a review study. *Marine pollution bulletin*, *143*, 92-100, 2019.
[10] Almond, J., Sugumaar, P., Wenzel, M. N., Hill, G., & Wallis, C.: Determination of the carbonyl index of polyethylene and polypropylene using specified area under band methodology with ATR-FTIR spectroscopy. *e-Polymers*, *20*(1), 369-381, 2020.
[11] https://geoportal.dgu.hr (accessed: 28.05.2024).
[12] Chapman, D.: *Water quality assessment.* In D. Chapman (Ed.), (p. 585). London: Chapman & Hall (on behalf of UNESCO, WHO and UNEP), 1992.
[13] Terzic, J.: Hidrogeoloski odnosi na krskim otocima-primjer otoka Visa., Rudarsko-geolosko-naftni zbornik 16.1, 47., 2004.
[14] Müller, B., and René G. Increasing chloride concentrations in Lake Constance: characterization of sources and estimation of loads., Aquatic sciences 74, 101-112, 2012.

EVALUATING THE EFFECTIVENESS OF RAINWATER MANAGEMENT MEASURES IN URBAN SEWER NETWORKS: A COMPREHENSIVE REVIEW

RÉKA WITTMANOVÁ [1], JAROSLAV HRUDKA [2], ŠTEFAN STANKO[3], MARTIN MELIŠKA[4]

[1] *Slovak University of technology in Bratislava, Faculty of Civil Engineering, Department of Sanitary and Environmental Engineering, Slovakia, reka.wittmanova@stuba.sk*

[2] *Slovak University of technology in Bratislava, Faculty of Civil Engineering, Department of Sanitary and Environmental Engineering, Slovakia, jaroslav.hrudka@stuba.sk*

[3] *Slovak University of technology in Bratislava, Faculty of Civil Engineering, Department of Sanitary and Environmental Engineering, Slovakia, stefan.stanko@stuba.sk*

[4] *Slovak University of technology in Bratislava, Faculty of Civil Engineering, Department of Sanitary and Environmental Engineering, Slovakia, martin.meliska@stuba.sk*

1 Abstract

This article reviews the effectiveness of various rainwater management measures in reducing inflow into urban sewer networks and mitigating the risks of urban flooding. It emphasizes the role of numerical models in planning and designing green infrastructure solutions, including vegetative filter strips, bio-retention systems, and permeable pavements. The analysis draws on numerous studies to highlight the significant reduction in runoff volume and pollutant concentrations achieved through these measures. Factors influencing the efficiency of these measures, such as weather conditions, rainfall intensity, and material characteristics, are examined in detail. The paper also discusses the use of mathematical modeling tools like SWMM and MIKE URBAN for simulating and optimizing the performance of rainwater management measures. The integration of these measures into urban drainage systems is crucial for sustainable urban development, providing essential insights for future adaptation strategies and enhancing the resilience of cities to climate change impacts.

Keywords: wastewater, stormwater, runoff, infiltration, climate change, urban areas

2 Introduction

The impacts of climate change also affect the operation of sewer networks under the conditions of the Slovak Republic. Due to climate change, there are increasingly frequent periods of drought alternating with intense rainfall events, sometimes including heavy downpours. These events can lead to increased overflows of mixed wastewater into receiving waters or overload sewer networks, potentially resulting in urban flooding. The combination of negative aspects of climate change and urbanization is expected to globally increase flood risk in urban areas. During intense rainfall, the flow of stormwater can reach the capacity flow rate, fill the pipe cross-section, and create pressurized flow, or even backwater, subsequently causing urban flooding. The increased proportion of impermeable surfaces reduces evapotranspiration and water retention in the landscape, leading to increased surface runoff volume, concentration rates, and maximum flood volume. The intensification of these negative phenomena is caused by the combination of climate change and high levels of urbanization.

A new concept of urban drainage has been developed to mitigate the impact of climate change on urban environments. This concept is based on principles of sustainable stormwater management and the implementation of adaptation measures into urban systems. When designing effective measures to reduce stormwater inflow into sewer networks and regulate flow within the network, it is advantageous to involve mathematical models in the design process. These models can predict the behavior of wastewater flow under various scenarios. Using models, it is possible to identify problematic sections

of sewer networks and subsequently propose modifications to these network segments or implement flow accumulation devices. Additionally, nature-based solutions can be designed to mitigate the broader impacts of climate change.

The aim of adaptation measures and components of sustainable urban drainage systems is to create natural hydraulic and hydrological conditions for rainwater runoff from urban environments, aiming to mimic natural hydrological cycles. Directing surface runoff into sewer networks is considered a final resort in this context, applicable only after considering all other options [1]. In design, efficient rainwater drainage solutions from urbanized areas hold significant priority to positively impact the urban landscape [2]. However, the level of this impact depends on current local conditions and legislative regulations that set parameters for quantitative and qualitative runoff. Numerous studies emphasize the beneficial effects of integrated rainwater management on human health and the increase in property values within a given region [3]. Technologies for capturing rainwater fall under this category of devices, which can serve as a water source for flushing, washing, and irrigation [4]. The construction of rainwater management devices may utilize filtration materials capable of reducing organic pollutants (nutrients and heavy metals), sorption materials, or mechanical separators that remove floating debris. International research provides insights into the cleaning capabilities of these devices [5]. During the selection process of components for sustainable rainwater management systems, geological and hydrological characteristics of the site, ecological condition of the receiving body, urban layout, and architectural integration of devices are considered [6]. Integration of these elements into urban drainage systems aims to minimize surface runoff, reduce peak flow in sewer networks, and decrease the volume of discharged wastewater into receiving bodies. Objects supporting evaporation, infiltration, and delayed runoff are proposed to mitigate surface runoff.

Given the current trend and the support for sustainable urban development, numerical models are often used in hydrology of urban areas for simulating surface runoff, the transport of pollutants in catchment areas, the impact of stormwater runoff on sewer networks and surrounding areas, and for the design and assessment of rainwater management measures in urban areas [7].

Mathematical models of drainage systems are increasingly used in the planning and design of green solutions to reduce rainwater inflow into sewer networks and to decrease the likelihood of urban flooding. The optimal use and comparison of these models is addressed in a Swedish study by Broekhuizen et al. (2019), which analyzes various models (MOUSE, SWMM, and Mike SHE) and their differences in simulations of surface runoff from green areas. The analysis of the models was conducted using simulations involving 11 different soil types and 6 varying soil depths. Variations in the model results were attributed to differing mathematical formulations. The study concluded that these variations could have a significant impact on design and assessment processes. The simulation results indicate that the influence of green spaces is a crucial factor that must be considered when modeling urban drainage systems [8].

Kourtis and Tsihrintzis (2021), in their study on adaptation measures, compared 29 scientific papers that included case studies evaluating the impact of climate change on sewer networks. They found that 41% of the papers used the SWMM program and 25% used DHI programs. The remaining studies used various models [9].

Radinja et al. (2019) utilized a hydrological-hydraulic model of the sewer network to assess the functionality of SUDS (Sustainable Urban Drainage Systems) objects in the urban catchment area of the of Girona. This involved a comprehensive assessment of the sewer system's functionality with implemented devices to reduce the volume of overflow waters. The SWMM program was used to create the mathematical model, and based on the results of a multi-criteria analysis, the impact of SUDS objects on the network was assessed [10].

The topic of surface runoff reduction in relation to LID (Low Impact Development) measures is also

discussed by Kong et al. (2017) using simulations of various load scenarios, they monitored the efficiency of LID facilities [11]. This study focused on the hydrological responses of stormwater runoff characteristics to four different urban land use conversion scenarios using a GIS-based SWMM model. Procedures using similar principles to capacity assessment were also used in examining the reduction of the amount and volume of overflows and the risk of urban flooding.

Elliott & Trowsdale (2007) assess the suitability of 10 different models (MOUSE, MUSIC, P8, PURRS, RUNQUAL, SLAMM, StormTac, SWMM, UVQ, and WBM) for simulating LID objects in interaction with the sewer network. They compare the models in terms of potential use, temporal distribution, representation and spatial distribution of the catchment area, runoff formation, hydraulic progression, and modeled pollutants [12].

Hernes et al. (2020) assessed the impact of four design scenarios using SUDS measures on overflow discharges in the city of Oslo using the MIKE URBAN program. They evaluated the performance of two different SUDS measures, green roofs, and rain gardens, through simulations of a single rain event and continuous simulation. The study results showed that rain gardens have a greater impact on reducing overflow volumes, while green roofs are effective for smaller rain events [13].

Nguyen et al. (2020) explore and propose a new modeling framework for the future development and implementation of the "Sponge City" concept. The "Sponge City" concept is increasingly appearing as a new type of integrated urban water systems approach focusing on addressing stormwater management problems in cities. However, there are missing auxiliary tools for planning, assessment, and life cycle evaluation. The mentioned study addresses this issue by summarizing a proposal for a new "Sponge City" modeling framework capable of simulating environmental and socio-economic aspects of this integrated approach. The proposed model could be used in the future not only for assessing the efficiency of drainage capacity of sewer networks and "Sponge City" objects but also for multi-criteria analysis of the urban water system [14].

The sensitivity of urban flood simulations to stormwater drainage and infiltration infrastructure was investigated in a study at the University of Alabama by Anni et al. (2020). The case study examines the flood situation under the conditions of the university campus, where a measurement campaign was conducted to determine infiltration rates, soil moisture, and soil texture. Using the MIKE URBAN modeling tool, they compared different recurrence intervals of rainfall events to identify problem areas on the campus. The simulations further showed significant differences in water depth and flood extent. The study results demonstrate that urban flood simulations are sensitive to the inclusion of urban drainage infrastructure and to the values and spatial distribution of soil input data [15].

3 Adaptation measures to reduce rainwater inflow into the sewer network

The main goal of these devices is to minimize the intensity of surface runoff caused by rainwater, thereby ensuring a reduction in peak flow to the sewer network and wastewater treatment plant (WWTP) and preventing potential degradation of the quality of surface and groundwater. Measures for stormwater management (SWM) are essentially structures and devices that support evaporation, infiltration, and ensure slow runoff of rainwater, among others. A wide range of SWM measures are available for managing surface runoff from impervious areas, which can generally be divided into two basic categories: decentralized and centralized [16], [17].

Decentralized structures and devices for SWM are measures aimed at capturing rainwater runoff at its source, i.e., on the plot of the drained impervious area. In a broader sense, these are measures that contribute to the preservation of the natural water cycle, such as: grassed areas, permeable paved areas (vegetative pavers), ditches with grass cover, ditches with a filtration layer, drainage perforated pipes with gravel-sand backfill, and infiltration shafts. Based on their location, these measures can be divided

into surface and subsurface infiltration structures and devices, with a preference for surface measures as they support evaporation, provide aesthetic value, and thus create a pleasant environment for people [1], [17].

Centralized measures are proposed only when all suitable decentralized solutions have been exhausted. These are measures and devices intended for multiple buildings and are implemented following decentralized measures. Centralized measures include retention infiltration tanks and systems of depressions and infiltration ditches [1] [17].

Most adaptation measures are based on the infiltration of rainwater at its point of impact. These are among the most commonly used devices. However, the use of infiltration devices is limited by the geological substrate. The following table summarizes the suitability of various soil types.

Table 1. Suitability of Soils for Infiltration

SOIL TYPE	FILTRATION COEFICIENT (M/S)	SUITABILITY FOR INFILTRATION	NOTE
Gravelly soils	> 10^-3	Very suitable	Excellent permeability
Sandy soils	10^-3 až 10^-5	Suitable	Good permeability
Loamy soils	10^-5 až 10^-7	Moderately suitable	Limited permeability
Loess soils	10^-5 až 10^-6	Moderately suitable	Limited permeability
Clayey soils	< 10^-7	Unsuitable	Very low permeability

Loess soils have a filtration coefficient that places them in the category of loamy soils, making them moderately suitable for infiltration devices. In practice, this means that when using infiltration devices in loess soils, their limited permeability must be considered. Additional measures, such as optimizing the size and placement of infiltration devices, may be necessary to ensure their effectiveness.
In these areas, it is advisable to reconsider the use of devices and measures such as green roofs and accumulation tanks, which are not constrained by the filtration capacity of the geological substrate.

4 Computational Software and Modeling of Sewer Networks with Surface Runoff Reduction Measures

To model adaptation measures in a hydrological basins, dozens of software programs can be used, based on conventional methods of runoff creation and management. Some models include components for groundwater and infiltration from SWM devices. These models also use conventional methods to accumulate and treat, i.e., reduce, the content of contaminants by using specific types of SWM measures. The fundamental difference between these models lies in the hydrological and hydraulic criteria required for the simulation of various types of measures [18]. A list of software used for mathematical modeling of the rainfall-runoff process is provided in Table 2. Among the most commonly used softwares are the Storm Water Management Model (SWMM) and MIKE URBAN, due to their wide range of applications and ease of modeling.

Table 2. List of commonly used models and their applications [18].

MODELLING TOOL	DEVELOPER	APPLICATION
Green Infrastructure Flexible Model (GIF-Mod)	Massoudieh et al.	Modeling hydrological processes and water quality processes through green infrastructure
Green Values National Stormwater Management Calculator	U.S. EPA	Comparing the performance, costs, and benefits of green infrastructure
RECARGA	University of Wisconsin	Evaluating the effectiveness of bioretention measures, rain gardens, and infiltration tanks
Water Balance Model (WBM)	The British Columbia Inter-Governmental Partnership (BCIGP)	Supporting decision-making and scenario modeling through the implementation of green infrastructure

Long-Term Hydrologic Impact Assessment Model (L-THIA-LID)	Bernie Engel and Jon Harbor (Purdue University)	Simulating runoff and pollutant loadings using SWM measures
Hydrologic Engineering Centre – Hydrologic Modelling System (HEC-HMS)	U.S. Army Corps of Engineers	Simulating hydrological processes in a watershed
Win-Source Loading and Management Model (Win-SLAMM	Bob Pitt, University of Alabama	Evaluating runoff volume and pollutant loading
MIKE +/ Model for Urban Sewers (MOUSE)	DHI	Modeling system for analyzing urban drainage and sewer systems
Storm Water Management Model (PCSWMM) |	U.S. EPA	Dynamic hydrological and hydraulic modeling of watershed runoff, considering SWM as a component
HYDRUS	PC-Progress	Analyzing water flow, heat, and solute transport in porous media

5 Effectiveness of rainwater management measures

The effectiveness of measures applied to reduce rainwater inflow into a given catchment area, in terms of reducing the volume and speed of runoff, has been assessed by many authors in their research. For instance, Grey, V. et al. (2018) [19], Kolasa-Wiecek, A. et al. (2021) [20], Berndtsson, J.C. (2010) [21], Zhu, H. et al. (2019) [22], among others, in their studies, note that certain measures such as vegetated roofs, bio-retention systems, and permeable pavements significantly contribute to reducing runoff volume and are capable of capturing nearly the entire volume of surface rainwater runoff. By capturing nearly, the total volume of runoff (99%), these measures completely alleviate the burden on the sewer network. The high efficiency of these measures was particularly observed during rain events of lower intensity and shorter duration. At higher intensities, the efficiency of these measures was somewhat lower. Processes such as infiltration and evapotranspiration play an important role in reducing the volume of surface rainwater runoff, being able to reduce runoff by approximately half. Of course, the effectiveness of these measures is conditioned by several factors, primarily depending on the weather conditions of the catchment area (air temperature and humidity), the intensity and duration of the rain event, and the type and characteristics of the given measure (thickness of the filtration layers, used materials, infiltration capacity, etc.) [20], [21], [22].

Other studies have focused on the effectiveness of rainwater management measures in reducing pollutant concentrations, given that some measures involve processes such as filtration, sedimentation, adsorption, etc. The most frequently monitored parameters were total suspended solids (TSS), total nitrogen (TN), and total phosphorus (TP), heavy metals such as Pb, Cu, and Zn, considering the significant risk they pose to environmental degradation and human health [24], [25]. Berndtsson C.J. (2010) [21], Ahiablame, M.L., et al. (2012) [23], Griffin, D.R. (2018) [26] conducted review studies comparing dozens of research papers, technical reports, projects, government documents, and more. These authors, among others, evaluated the effectiveness of contaminant removal from surface runoff by comparing different measures. The authors of the review studies noted that the effectiveness of undesirable substance removal ranged from 0 to 99%, with the efficiency of removal and capture being conditioned by several important factors: the applied measure, characteristics of the filtration material (thickness, type of material), concentration of surface runoff pollution, physicochemical properties of pollutants, maintenance of devices, lifespan of the given device, geometric characteristics of the device, used vegetation, geological conditions of the catchment area, etc. [23], [22], [21], [26].

Table 3. The percentage expression of captured runoff volume and reduction in contaminants present in stormwater runoff) [27]

Measures	Runoff	TSS	TP	TN	Zn	Cu	Pb
	[%]						
Green roofs	23 - 99	-	26-80	-	> 96	> 96	> 93
Vegetative filter strips	35-95	>80	43-95	34-74	24-51	25-65	-
Trench	14 - 98	30- 97	24-99	14-61	68-93	-	<29
Bio-retention systems	23 - 97	47-99	29-99	32-99	62 - 97	43 - 99	31 - 97
Permeable pavements	50 - 94	58 -94	10-78	-	73 - 99	20 - 99	74 - 99

6 Conclusion

The effectiveness of various rainwater management measures, such as vegetative filter strips, bio-retention systems, and permeable pavements, in reducing rainwater inflow and mitigating urban flooding has been extensively studied. Numerical models of sewer networks play a crucial role in planning and designing these measures by providing detailed simulations of rainfall-runoff processes and enabling precise comparisons of different solutions. Studies have demonstrated that these measures can significantly reduce runoff volume, capture nearly the entire volume of surface rainwater runoff, and alleviate the burden on sewer networks, particularly during low-intensity rain events.

The efficiency of these measures is influenced by several factors, including weather conditions, rainfall intensity and duration, and the characteristics of the measures themselves. Processes such as infiltration and evapotranspiration contribute significantly to runoff reduction. Additionally, these measures are effective in reducing pollutant concentrations, with varying efficiencies depending on the type of pollutant and the specific characteristics of the filtration material and implemented devices.

Mathematical models, such as SWMM and MIKE URBAN, are essential tools for evaluating the impact of these measures on urban drainage systems. They enable the assessment of different scenarios and the optimization of design and operational strategies. Future developments, such as the "Sponge City" concept, aim to integrate environmental and socio-economic aspects into urban water management, further enhancing the capacity to address stormwater challenges.

In summary, the integration of rainwater management measures into sewer network models offers a comprehensive approach to sustainable urban development, providing a foundation for effective planning, design, and implementation of solutions to reduce rainwater inflow, improve water quality, and mitigate urban flooding. As urban areas continue to grow and climate change impacts intensify, these models and measures will be increasingly important in creating resilient and sustainable cities.

Acknowledgements
This work was developed within the project "Mathematical modelling of the sewer network as a decision-making tool in the selection of objects for stormwater inflow reduction", which was supported by a grant from the Faculty of Civil Engineering of the Slovak University of Technology in Bratislava and supported by the Scientific Grant Agency of the Ministry of Education, Youth and Sports of the Slovak Republic and the Slovak Academy of Sciences within the project VEGA 1/0682/23, co-funded by the Slovak Research and Development Agency under contract No. APVV-22- 0564.

References:

[1] Vítek, J., Stranský, D., Kabelková, I., Bareš, V., Vítek, R.: Hospodaření s dažďovou vodou v ČR. (Praha, ČR) ISBN: 978-80-260-7815-9. 2015

[2] Fathollahi, A., Coupe, S. J.: Life cycle assessment (LCA) and life cycle costing (LCC) of road drainage systems for sustainability evaluation: Quantifying the contribution of different life cycle phases, Science of the Total Environment, 776, 145937, 2021.

[3] Ahammed, F., Hewa, G. A., Argue, J. R.: Applying multi-criteria decision analysis to select WSUD and LID technologies, Water Science & Technology: Water Supply, Vol. 12(6), pp. 844–853, 2012.

[4] Stephens, D. B., Miller, M., Moore, S. J., Umstot, T., Salvato, D. J.: Decentralized groundwater recharge systems using roofwater and stormwater runoff, Journal of the American Water Resources Association, 48(1), pp. 134–135, 2012.

[5] Abhatt, A., Bradford, B., Abbassi, E.: Cradle-to-grave life cycle assessment (LCA) of low-impact-development (LID) technologies in southern Ontario, Journal of Environmental Management, 231, pp. 98–109,2019.

[6] Woods Ballard, B., Wilson, S., Udale – Clarke, H., Scot,t T., Ashley, R., Kellaghe, R.: The SuDS Manual. Version 5 [online]. London: CIRIA, 2015. © CIRIA 2015. 964 p. ISBN: 978-0-86017-760-9. [cit. 24. 02. 2021]. www.scotsnet.org.uk/documents/nrdg/ciria-report-c753-the-suds-manual-v6.pdf., 05.05.2024.

[7] Cao, Q., Yu, D.Y., Georgescu, M., Wu, J.G., Wang, W. Impacts of future urban expansion on summer climate and heat-related human health in eastern China. Environment International, 112, pp. 134-146, 2018.

[8] Broekhuizen, I., Muthanna, T. M., Leonhardt, G., Viklander, M.: Urban drainage models for green areas: Structural differences and their effects on simulated runoff. Journal of Hydrology X 5, 2019.

[9] Kourtis, I. M., Tsihrintzis, V. A.: Adaptation of urban drainage networks to climate change: A review. Science of The Total Environment 771, 2021.

[10] Radinja, M., Comas, J., Corominas, L., Atanasova, N.: Assessing stormwater control measures using modelling and a multi-criteria approach. Journal of Environmental Management 243, pp. 257-268, 2019.

[11] Kong, F., Ban, Y., Yin, H., James, P., Dronova, I.: Modeling stormwater management at the city district level in response to changes in land use and low impact development. Environmental Modelling & Software 95, pp.132-142, 2017.

[12] Elliott, A.H., Trowsdale, S.A.: A review of models for low impact urban stormwater drainage. Environmental Modelling & Software, 22 (3), pp. 394-405, 2007.

[13] Hernes, R.R., Gragne, A.S., Abdalla, E.M.H., Braskerud, B.C., Alfredsen, K., Muthanna, T.M.: Assessing the effects of four SUDS scenarios on combined sewer overflows in Oslo, Norway: evaluating the low impact development module of the Mike Urban model. Hydrology Research 51 (6), pp. 1437-1354. 2020.

[14] Nguyen, T. T., Ngo, H. H., Guo, W., Wang, X. C.: A new model framework for sponge city implementation: Emerging challenges and future developments. Journal of Environmental Management 253, Article No. 109689, 2020.

[15] Anni, A. H., Cohen, S., Praskievicz, S.: Sensitivity of urban flood simulations to stormwater infrastructure and soil infiltration. Journal of Hydrology 588, Article No. 125028, 2020.

[16] Urcikán, P., Rusnák, D. Stokovanie a čistenie odpadových vôd, Stokovanie II, Objekty na stokovej sieti. Slovenská technická univerzita v Bratislave vo Vydaveteľstve STU, Bratislava, 2011.

[17] Urcikán, P., Rusnák, D. Stokovanie a čistenie odpadových vôd, Stokovanie I, Návrhovanie stokových sietí. Slovenská technická univerzita v Bratislave vo Vydaveteľstve STU, Bratislava, 2004.

[18] Zhang, L., Ye, Z., Shibata, S.: Assessment of Rain Garden Effects for the Management of Urban Storm Runoff in Japan. Sustainability, 12, 23. Pp. 1-17, 2020.

[19] Grey, V., Livesley, J.S., Fletcher, D.T., Szota, Ch.: Tree pits to help mitigate runoff in dense urban areas. Journal of Hydrology, 565, pp. 400-410, 2018.

[20] Kolasa-Wiecek, A., Suszanowicz, D. The green roofs for reduction in the load on rainwater drainage in highly urbanised areas. Environmental Science and Pollution Research [online], [cit.

12. 03. 2021]. ISSN 0944-1344 Aviable: https://doi.org/10.1007/s11356-021-12616-3, 2021.
[21] Berndtsson, C. J.: Green roof performance towards management of runoff water quantity and quality: A review. Ecological Engineering, 36, 4, pp. 351-360. 2010
[22] Ahiablame, M.L., Engel, A.B., Chaubey, I.: Effectiveness of Low Impact Development Practices: Literature Review and Suggestions for Future Research. Water, Air, & Soil Pollution, 223, 7, pp. 4253-4273, 2012.
[23] Zhu, H., Yu, M., Zhu, J., Lu, H., Cao, R.: Simulation study on effect of permeable pavement on reducing flood risk of urban runoff, International Journal of Transportation Science and Technology, 8, 4, pp. 373-382, 2019.
[24] Charters, F.J., Cochrane, T.A., O´Sullivan D.A.: The influence of urban surface type and characteristics on runoff water quality. Science of The Total Environment, 755, 2021.
[25] Gikas, G.D., Tsihrintzis, A.V.: Assessment of water quality of first-flush roof runoff and harvested rainwater. Journal of Hydrology, 466–467, pp. 115-126, 2012.
[26] Griffin, D.R.: Principles of Stormwater Management. New York, USA. CRC Press, 2018.
[27] Marko, I.: Surface runoff variability and its impact on water quality in urbanized areas, Dissertation Thesis, Slovak University of Technology in Bratislava, 2021.

WATER TREATMENT PATHWAY FROM SLOW FILTRATION TO MEMBRANE PROCESSES

DANKA BARLOKOVÁ , JÁN ILAVSKÝ
Department of Sanitary and Environmental Engineering, SvF STU, Radlinského 11, 810 05 Bratislava, Slovakia
E-mail: danka.barlokova@stuba.sk, jan.ilavsky@stuba.sk

1 Abstract

Water treatment represents the necessary step in several cases related to obtain a quality and a safe drinking water. Treatment plants are among technically and technologically advanced constructions that anytime are to treat the ground or surface water to get drinking water complying with the requirements of the Decree of the Ministry of Health of the Slovak Republic no. 91/2023 Coll. which establishes details of drinking water quality, drinking water quality control, monitoring program and risk management in drinking water supply. A total of 138 water treatment plants were built in Slovakia, currently 80 of them are in operation.

Keywords: water treatment, groundwater, surface water, water treatment plant technology, drinking water quality

2 Introduction

82.2% of Slovakia's population is supplied with drinking water from underground sources; surface water is used in locations without a high-quality groundwater source. As regards the quality of the groundwater used for drinking water supplies, the decisive indicators are the contents of iron, manganese, ammonia ions, heavy metals (e.g. arsenic, antimony), etc., while the CO_2 content, hydrogen sulphide content and microbiological quality of the water are also not negligible. Approximately only 17.8% of the total amount of water supplied to public water supply systems is water obtained from surface sources.
The sources of surface water present surface flows in mountain and foothill areas and water reservoirs that were built for the purpose of intake of high-quality water for drinking purposes. For extraction of water from these sources water treatment plants with a projected capacity of 1 to 1,000 l/s have been built. Approximately only 17.8% of the total amount of water supplied to public water supply systems is water obtained from surface sources.
In the case of surface waters, substances that cause turbidity, colour and odour, humic substances, microbiological and biological recovery, etc. need to be removed from the water. The occurrence of micropollutants (pesticides, pharmaceuticals) and cyanobacteria, algae, which cause problems in some water sources, is now increasingly coming under the spotlight.
In this case, water treatment is necessary. Water treatment has evolved historically from slow sand filtration, dosing of chemicals, various separation stages, filtration in conjunction with sorption, to water disinfection. The choice of the appropriate water treatment technology depends on the quality of the water source, the quantity of the water to be treated and the legislative requirements, which are becoming increasingly stricter with regard to public health.

3 Overview of the History of Water Treatment

Man has striven to obtain and use relatively clean water over the course of the centuries of his existence. There are files in ancient Greek and Sanskrit dating back to about 4000 years BCE with the first references to water treatment; these contain recommendations on heating water in the sun or boiling it over fire, on filtering water through sand and gravel, percolating it so as to improve its properties. At that time, turbidity was the force driving people to use these methods, as they were then unaware of

microorganisms or chemical contaminants. In ancient Egypt, images were preserved on the walls of the tombs of Amenophis II in Thebes and later of Rameses II, which document for the first time the use of aluminium which was put in water receptacles to reduce the turbidity. This predecessor of the current coagulation process dates back to circa 1500 BCE. Hippocrates, regarded as the "father of medicine", discovered the healing effects of water and he also devised the so-called "Hippocratic sleeve" which was a filter made of fabric in the shape of a sleeve through which rainwater was filtered after boiling.

"A doctor who arrives in an unknown town should have a clear idea about the water used by its population." *Hippocrates (460-377 BC)*

In 1804, the first water treatment plant based on slow sand filtration was built in Scotland; it was designed by Robert Thom. In 1806, a large facility for water treatment was operated in Paris. The treated water was first retained in cisterns for 12 hours and then transported to filters consisting of sand and charcoal. In 1827, Englishman James Simpson designed for London the treatment of water from the Thames by slow sand filtration through a sand filter. In 1835, in his book "Public Health" Dr. Robley Dunlingsen recommended the addition of a small amount of chlorine to contaminated water to render it potable. The first rapid sand filters were put into operation in Sommerville (New Jersey, USA) in 1885 and in Europe in the water treatment plant in Zürich where, even today, slow sand filtration is still in operation. At the end of the 19th century, Dr. G. W. Fuller dealt with rapid filtration; in 1897 he found that bacteria are removed from water more efficiently when coagulation and sedimentation precede filtration [1].

4 History of Water Treatment in Slovakia

The history of water treatment within our territory started in the 1930s, given that in Slovakia groundwaters of excellent quality are the predominant source used for supplying the population with drinking water.

The development of water treatment plant construction in Slovakia was related to increased water consumption in the post-war period due to the development of industrial production. In the 1960s and 1970s, the largest increase in the population connected to the public water mains was achieved. The increase in the numbers of population served and the comfort of housing also disproportionately increased water consumption, which exceeded water consumption in developed countries elsewhere in the world. This trend continued until the early 1990s.

In the 1930s, the first water treatment plants were put into operation, all of them in Eastern Slovakia. The oldest one was built in 1930 – Smrdiace Mláky with an output of 8 l/s used slow sand filtration, while a further three treatment plants treating groundwater by filtration through crushed limestone were built in 1932–1934. None of these remains in operation today.

1930s: 4 treatment plants, slow sand filtration, contact filtration through crushed limestone.

In the war and post-war period (1940s), two groundwater treatment plants were put into operation – Vajs Springs and Modra – Harmónia where the water was de-acidified by way of contact filtration in crushed limestone filters. The Vajs Springs treatment plant near Krupina, built in 1942, was reconstructed in 2016; the limestone was replaced with semi-burnt dolomite; the water from this plant was supplied to Poltár.

1940s: 2 treatment plants.

Even in the following decade, water treatment plants using slow sand filtration were built; one of these plants – Kremnica treatment plant – with this technology, following its reconstruction in 1986, remains in operation with an output of 15 l/s. In this period, three surface water treatment plants were put into operation in which slow sand filtration was replaced with standard rapid filtration; however, this was ineffective in certain time periods. In 1958, the groundwater treatment plant Dedina Mládeže commenced operations; here, iron and manganese were removed from water for the first time in Slovakia. In this decade, 8 water treatment plants were built using slow, rapid and contact filtration and, for the first time, iron and manganese removal.

1950s: 8 treatment plants, contact filtration – HBD, rapid filtration, iron and manganese removal.

In the 1960s, the number of treatment plants increased considerably, in combination with the increase in the population linked to the public water supply and the development of industry. 42 treatment plants were built, 21 for the treatment of groundwater and 21 for the treatment of surface water, while in one of them both groundwater and surface water were treated. As regards groundwater, iron and manganese were removed and the water was de-acidified. In this period, coagulation first came into use in the treatment of surface waters. In 1963, the Štrbské Pleso water treatment plant was put into operation; it was reconstructed in 2019 and, membrane technology is currently employed here. In 1965, the construction of the Hriňová water treatment plant was completed; it was the first treatment plant treating water from a water reservoir and, at that time, with the largest design output – 260 l/s. In the southern part of Western Slovakia, several water treatment plants removing iron and manganese from groundwater were put into operation: Nitra I – Horné Lúky – 150 l/s, Nové Zámky – 111 l/s, Šaľa – 58 l/s. And the same issue was also resolved in Eastern Slovakia in the water treatment plants Borša – 75 l/s, Michalovce – 100 l/s and Hrádok – 200 l/s.

The Perlová Dolina water treatment plant treating surface water has been in operation since 1968; it was reconstructed several years ago and membrane technology and micro sieves are in use there as the first plant treating surface waters. In the same year, the Osuské water treatment plant for the treatment of groundwater was put into operation. It is the oldest plant for groundwater treatment; hydrogen sulphide and sulphuric bacteria are removed from the water there. The treatment plant has now been in operation for more than fifty years, following its reconstruction in 2015. It is located at the foot of the Small Carpathians and is an important part of the Senica group water supply system. Four sand filters were extensively modernised as part of the overall reconstruction of the water treatment plant (WTP). The original filter bottoms were replaced with the TRITON stainless steel drainage system; this was its first installation in Slovakia. The reconstructed water treatment plant was nominated in the 2015 Construction of the Year competition. In 1969, the Demänovská Dolina water treatment plant was put into operation; it is another of those which remain in operation, in this case after reconstruction in 2008. Of the water treatment plants built in this decade, 31 were decommissioned; this was due, in some cases, to utilisation of the large-capacity water resource on Žitný Ostrov.
1960s: 42 water treatment plants, coagulation.

Overview of the number of water treatment plants put into operation in individual decades is listed in Table 1.

Table 1. Overview of the number of water treatment plants put into operation in individual decades

YEARS	NUMBER OF WTPs	SOURCE: GROUND WATER	SOURCE: SURFACE WATER	WTP IN OPERATION	WTPs AFTER RECONSTRUCTION*
1930s	4	3	1	0	
1940s	2	2		1	1
1950s	8	4	4	4	1
1960s	43	20	21	11+1	6
1970s	37	12	27	27	3
1980s	26	4	21	23	1
1990s	9	2	7	7	
2000-2010	6	5	1	5	1
after 2010	3	2	1	2	1
TOTAL	**138**	**54**	**83**	**80**	**14**

* The reconstruction of the treatment plant, which was built in the mentioned years, does not mean the year of reconstruction
WTP – water treatment plant

Selected water treatment plants with used technology are listed in Table 2.

Table 2. Selected water treatment plants with used technology

Water Treatment Plant	Water Source	Capacity l/s projected/currant	Technology	Year of putting into operation	Note
Holíč Western Slovakia	Ground water	100/60	aeration, lime dosage, contact filtration, sedimentation	1975	removal of Fe a Mn, H_2S, NH_4, colour, odor, aggressive CO_2
Kúty Western Slovakia	Ground water	80/40	aeration, lime dosage, filtration	1999	removal of Fe a Mn, H_2S, colour, odor, aggressive CO_2
Osuské Western Slovakia	Springs, Ground water	35/70	aeration, filtration	1968-2015 reconstruction	removal of H_2S and sulphuric bacteria
Boťany Eastern Slovakia	Ground water - wells	180/ 80	contact filtration, sedimentation	1982	removal of Fe a Mn, aggressive CO_2
Lastomír	Ground water - wells	100/16	contact filtration	1980	removal of Fe a Mn, NH_4, aggressive CO_2
Demänová Central Slovakia	Surface-watercourse	90	coagulation, flocculation, filtration	1969	removal of turbidity, biological pollution
Nová Bystrica Northern Slovakia	Surface- Water supply reservoir	700/200	coagulation, flocculation, filtration, sedimentation	1983	removal of turbidity, biological pollution
Hriňová Central Slovakia	Surface- Water supply reservoir	280/140	coagulation, flocculation, filtration, sedimentation	1965	removal of turbidity, biological pollution-algae,cyanobacteria
Klenovec Central Slovakia	Surface- Water supply reservoir	460/120	flotation, filtration, **membrane** process	1974, 2019 reconstruction	removal of turbidity, biological pollution-algae,cyanobacteria
Málinec Central Slovakia	Surface- Water reservoir	230/120	coagulation, flocculation filtration, sedimentation	1995	removal of turbidity, biological pollution-algae, cyanobacteria
Turček Central Slovakia	Surface- Water supply reservoir	500/130	coagulation, flocculation, sedimentation (lamela settling tanks),filtration	1979,1999	removal of turbidity, biological pollution-algae,cyanobacteria
Bardejov Eastern Slovakia	Surface-watercourse	100/6,8	coagulation, flocculation filtration, sedimentation	1984	removal of turbidity, biological pollution
Bukovec Eastern Slovakia	Surface- Water supply reservoir	410/125	coagulation, flocculation, filtration, sedimentation	1979	removal of As, Sb, Mn, turbidity, biological pollution
Štrbské Pleso Eastern Slovakia	Surface-watercourse	10/13	Coagulation, **membrane** technology-ultrafiltration	1963. 2019 - reconstruction	removal of turbidity, biological pollution
Perlová Dolina Eastern Slovakia	Surface-watercourse	15/25	Microstrainer, **membran**e technology	1968. 2017 - reconstruction	removal of turbidity, biological pollution

In the 1970s, the trend of the construction of water treatment plants continued, 37 water treatment plants were built, 12 of them treating groundwater, for instance in Tatranská Štrba, Bardejov, Lekárovce, Holíč. Large water treatment plants for treating surface waters from water reservoirs were put into operation: Klenovec where the plant was reconstructed and ceramic microfiltration installed for the first time during the reconstruction, Bukovec WTP with an output of 700 l/s. The Turček WTP built in 1979, which treated water from surface sources, was reconstructed and extended in 2000; here water is extracted from a reservoir. In this treatment plant, the first separation stage is performed in lamella sedimentation tanks which represent an increase in sedimentation efficiency over the conventional settlement tanks; these are the only examples of this type in Slovakia. Currently, 27 out of 37 of these treatment plants are in operation.
1970s: 37 water treatment plants.

In the subsequent years up to the present, the number of water treatment plants increased by 18. The largest of them: Málinec in Central Slovakia with an output of 230 l/s: currently, it treats 120 l/s; Jakubany in Eastern Slovakia with a design output of 100 l/s: currently 29 l/s; Kúty in Western Slovakia where groundwater with an increased iron and manganese content is treated: currently 42 l/s are treated.
1980s: granular activated carbon: bromates removal.

5 Membrane technologies in Water Treatment in Slovakia

In 2005, as part of the reconstruction, ultrafiltration was first installed for supply to the public water supply network in the Čierny Balog water treatment plant. The Čierny Balog water treatment plant addresses turbidity and bacterial pollution in the surface water source. Ultrafiltration serves as a barrier to the iron and manganese present in the water source (0.07 to 0,40 mg/l Fe and 0.005 to 0.085 mg/l Mn) and in the coagulating agent – $Fe_2(SO_4)_3$. Ultrafiltration is not capable of capturing these metals in their dissolved form but it is effective in their oxidised form. The Čierny Balog WTP uses chlorine dioxide to disinfect water; this is a suitable oxidising agent not only for Fe but also for Mn.
After modernisation, the output of the Štrbské Pleso WTP increased from 10 l/s to 13 l/s. A new building was constructed on the site of the original water treatment plant without any option of spatial expansion as the building is sited in a level 5 nature protection zone. During reconstruction, the Štrbské Pleso treatment plant was supplied from the auxiliary source of Popradské Pleso. Ultrafiltration (UF) in hollow fibre membrane modules is the main water treatment stage. Coagulation and a tubular reactor are used for pre-treatment to achieve the necessary reaction time for flake formation. Figure 1 shows a view of the water treatment plants, Štrbské Pleso on the left with ultrafiltration modules and Štôla on the right with a hall filled with slow sand filters.

Figure 1 Štrbské Pleso WTP – view into the WTP with ultrafiltration modules (left), Štôla WTP – hall with slow sand filters (right)

After modernisation, the output of the Perlová Dolina WTP increased from the original 15 l/s to 25 l/s. A new building was constructed for the new technology within the premises of the old water treatment

plant. Membrane ultrafiltration is the main technological stage with a filtration degree of 0.1 – 0.2 μm. The membranes consist of hollow fibres set in the membrane modules.
The Jasná WTP was built in 1999. It treats drinking water from the Zadná Voda surface source in Demänovská Dolina. It was extensively reconstructed in 2017 when the water treatment technology was modernised. Two sieve filters are used for water treatment, one with an opening size of 500 μm and the other with an opening size of 200 μm, followed by 6 pressure sand filters; the final treatment stage consists of a cassette microfibre filter with an opening size of 20 μm. Subsequently, the water is disinfected with chlorine, accumulated in storage towers and provided to consumers. The design capacity of the water treatment plant is 30 l/s, the permissible extraction of water from the water source 15 l/s. At turbidities of over 50 NTU the water treatment plant is switched off, and the population and hotels are supplied from water accumulated in the storage towers which are located next to the water treatment plant. The accumulation is secured by two storage towers, one with a volume of 1,500 m^3 and the other 400 m^3.
The water treatment plant in Červený Kláštor is of special interest as history is combined with modern water treatment technology here: slow sand filtration with membrane technology. Slow sand filters are no longer in operation;, they have been replaced with ultrafiltration modules. The original capacity of the Červený Kláštor water treatment plant was 3.5 l/s; after reconstruction and installation of membrane technology, it has an output of 2 l/s.

In 2019, modernisation of the Klenovec WTP commenced; it treats surface water from the Klenovec water reservoir and, following reconstruction, flotation and membrane microfiltration are included in the water treatment process line. The treatment plant capacity is currently 140 l/s.
Membrane technologies are used to remove arsenic from water. The Jasenie WTP treats groundwater from the "Rástová" water source where the arsenic content has long achieved values of 40 to 90 μg As/l. The original technology of As^{3+} oxidation to As^{5+} by continuously dosing $KMnO_4$ solution was replaced in 2007 with ozonisation with subsequent As^{5+} sorption by hydrated iron oxides and filtration on the DynaSand® continuous sand filter; this was, in turn, replaced in 2021 with oxidation of As by chlorine dioxide followed by coagulation and flake separation by ultrafiltration. 200 μm mechanical filtration precedes ultrafiltration. The design output after reconstruction is 18 l/s.

The Selec water treatment plant removes arsenic from the water in a similar manner. The As concentration in raw water ranges from 14.3 to 26.7 μg/l, whereby As in treated water was measured from 2.5 to 7.79 μg/l. The water treatment plant is operated at a flow rate of 9.5 l/s. As(III) oxidation to As(V) by means of sodium hypochlorite is used for pre-treatment, thereby improving the affinity of arsenic for the coagulating agent. PAX18 is used as the coagulating agent, although other coagulating agents are also efficient in capturing As. A centrifugal pump is used for intensive mixing of chemical agents with water to provide the necessary pressure and flow, followed by a static mixer. A tubular reactor is used for the coagulation and formation of micro-flakes that are sufficiently large for effective filtration. Efficient water treatment is the outcome of this process which has been in use for years. The As concentration at the treatment plant exit can be readily adjusted and regulated by selecting the coagulating agent dose [2-6].

6 Discussion

In the course of obtaining drinking water, whether from underground or surface water sources, 138 water treatment plants were built in Slovakia; out of this number, 80 are currently in operation, of which 14 have been reconstructed. The number of reconstructed water treatment plants as a proportion of the total number of treatment plants and the year they were put into operation is inadequate.
The functioning water treatment plants have been in operation for several decades without any major intervention in the technological assembly or in the mechanical-technological equipment. It follows, therefore, that most of them are obsolete and no longer viable. Many of these treatment plants have become unreliable, especially in the event of a sudden deterioration in water quality caused by the impacts of climate change, such as torrential rain, sudden snow melt, water shortages due to drought, etc. Not only does the incidence of these unfavourable situations pose a problem but also their duration,

which requires operational interventions on the part of the operator. Many of them have to be shut down in these crisis situations as the existing water treatment technology is not able to ensure the production of high-quality drinking water. Most of the treatment plants situated at the foot of a mountain have just a single separation stage – filtration without coagulation, while in some of them even pressure filtration is used.

Due to the deterioration of the treated water and, in some cases, even due to inadequate technological equipment, the delivery of high-quality water in these water treatment plants is only practicable with major effort and increased funding. The rationale for this is as follows:

- ✓ obsolete and unreliable technological equipment with high energy consumption;
- ✓ inefficiency of technological equipment;
- ✓ deterioration in quality of water extracted from surface sources.

Deteriorations in water quality were recorded in the past years in the water reservoirs in Klenovec, Hriňová, Málinec, Rozgrund and also, recently, in Turček.

The water treatment plants can be rendered more efficient by enhancing:

- *the sedimentation process* by use of lamella sedimentation tanks, or replacing this process with *flotation;*
- *the filtration process* – by using a suitable filter design, especially by replacing the old bottom with nozzles with systems of the Leopold or Triton type which not only provide more effective filtration but also regeneration – washing of the filter cartridge and appropriate choice of material. Membrane technologies represent a very efficient separation process in water treatment.

More attention needs to be paid to the pre-treatment of water – removal of cyanobacteria and other living organisms, use of activated carbon to remove organic pollution, reduction in the aggressiveness of water and enriching the water with magnesium or calcium.

In recent years, there has been a considerable effort to modernise technological processes. This pertains also in Slovakia in the form of water treatment plant modernisations that are either in preparation, underway or have already been performed, e.g. the water treatment plants in Perlová Dolina, Štrbské Pleso, Demänovská Dolina, Osuské, Borinka, Holíč, Turček and currently, the water treatment plants in Klenovec and Málinec.

Directive (EU) 2020/2184 of the European Parliament and of the Council of 16 December 2020 on the quality of water intended for human consumption regulates the periodic control of the efficiency of solid form separation. The operator is also required to monitor the "turbidity" parameter of the treated water, for which a significantly stricter benchmark must be met – 0.3 NTU for 95% of samples whereof none of the samples may exceed 1 NTU (does not apply to groundwater sources in which turbidity is caused by iron and manganese) [7].

The Slovak Republic is obliged to implement this Directive within 10 years. However, the great majority of water treatment plants in Slovakia do not have a separation stage such as could meet the above requirement, hence they will need to be modernised. Given the relatively short implementation period and the high number of water treatment plants requiring modernisation of technology, it is necessary to commence their gradual reconstruction without delay.

There are two ways: to optimise the current water treatment technology or to use membrane technologies. For instance, ultrafiltration guarantees a turbidity of the treated water below 0.2 NTU.

7 Conclusion

Over the course of several decades, new technologies, materials, and equipment were developed, which led not only to the improvement of the efficiency of the water treatment process, but also to operational and energy savings. And in many cases, the deteriorating quality of the treated water is the cause of inadequate technology. The solution to this problem lies in the modernization and reconstruction of these objects, but the obstacle is often considerable financial resources related to these activities. In recent years, even in Slovakia, modern treatment methods have been put into operation (e.g. membrane

processes, adsorption on GAU, flotation, multi-material filtration, advanced oxidation processes, etc.). Water treatment processes are highly complex. Water quality is different in every location, due to the variability of incidence of various substances with various concentrations. Accordingly, the design of new technological processes in water treatment needs to be based on the results of semi-operational experiments.

The modernisation of the water treatment plants is now, and will surely be for years to come, the sole way to maintain their operational capacity and to improve the quality of operation by applying technical development. For all the parties involved, modernisation is far more demanding in terms of preparation and implementation than the construction of a new water treatment plant. The exchange of experience is the most effective way of overcoming the obstacles which are more or less inherent in every modernisation.

Acknowledgements

The article was prepared with financial support from projects VEGA 1/0666/23, APVV-22-0610, APVV-22-0564 and with the assistance of water company employees who provided us with the necessary information.

References:

[1] MWH's Water Treatment, Principles and Design, Third Edition, authors John C. Citenden, et al. John Wiley and Sons, Inc., 2012, ISBN 0470405392, pp. 1920

[2] Pelikán, P., Buchlovičová, J. 2016. Modernizácia úpravní vôd v Slovenskej republike. In: Sborník XX. mezinárodní konference Voda Zlín 2016, Zlín, ČR,17.-18.3.2016, ISBN 978-80-905716, pp. 47-52.

[3] Šimko V, 2007. Zásobovanie pitnou vodou v SR – zabezpečenie kvality a technológia úpravy vody. In: Sborník XI. mezinárodní konference Voda Zlín 2007, Zlín, ČR, ISBN 978-80-239-8740-9, pp. 23-26.

[4] Ilavský, J., Barloková, D., 2015. Modernizácia veľkých úpravní vôd v podmienkach Slovenska. In: Pitná voda 2015: zborník prednášok z XVI. Konferencie s medzinárodnou účasťou. Trenčianske Teplice, SR, 6. - 8. 10. 2015. 1. vyd. Bratislava: VodaTím, 2015, pp. 55--62. ISBN 978-80-971272-3-7.

[5] Barloková, D., Ilavský, J., Šimko, V., Kapusta, O, 2018. Úprava vody a jej budúcnosť v podmienkach Slovenska. In: Voda Zlín 2018. Olomouc: Moravská vodárenská, 2018, pp. 13--18. ISBN 978-80-905716-4-8.

[5] Drda, M., Červenka, J.: Použití keramických mikrofiltračných membrán pro úpravu pitné vody. In: Sborník XIII Mezinárodní konference Voda Zlín 2009, s. 143-148.

[7] Directive (EU) 2020/2184 of the European Parliament and of the Council of 16 December 2020 on the quality of water intended for human consumption. https://eur-lex.europa.eu/eli/dir/2020/2184/oj

CHANGES OF THERMOCLINE IN TWO DIFFERENT RESERVOIRS FOR DRINKING WATER SUPPLY IN SLOVAKIA

YVETTA VELÍSKOVÁ [1], VALENTÍN SOČUVKA [2], MAREK SOKÁČ [3], MÁRTA KOCZKA BARA [4], SAEID OKHRAVI [5]

[1] *Institute of Hydrology, Slovak Academy of Sciences, Slovakia, veliskova@uh.savba.sk*

[2] *Institute of Hydrology, Slovak Academy of Sciences, Slovakia, socuvka@uh.savba.sk*

[3] *Institute of Hydrology, Slovak Academy of Sciences, Slovakia, sokac@uh.savba.sk*

[4] *Institute of Hydrology, Slovak Academy of Sciences, Slovakia, bara@uh.savba.sk*

[5] *Institute of Hydrology, Slovak Academy of Sciences, Slovakia, okhravi@uh.savba.sk*

1 Abstract

This paper analyses the seasonal changes of the thermocline position in two water reservoirs in Slovakia: the Rozgrund and the Turček reservoir. As preliminary results show, stratification is formed in both cases. In the summer, its course is almost the same; the thermocline is at a depth of about 4-5 m below the water surface. In the spring and the autumn season, however, the thermal stratification in these reservoirs is different. The study presents measurements over the one year. In the next step, data from next measurement campaigns, as well as the results of numerical simulations, will be analysed to confirm the facts found.

Keywords: temperature, stratification, thermocline, seasonal changes, drinking water supply, the Turček reservoir, the Rozgrund Reservoir

2 Introduction

Water has a special position among the fluids. Its density in lakes, brooks, and rivers is not quite the same in different places and at different times. Although the differences that occur are generally small in themselves, they are nevertheless of great importance to the events in the water bodies [1]. In general, differences in density are mostly brought about through variations in temperature and salt content. In fresh water, it is primarily the temperature. It is known, that water occupies a special position in this respect. Its density does not increase continuously with decreasing temperature, as is the case with all other substances, but reaches its maximum at 4° C, after which it decreases. This anomalous behaviour of water is the cause of some very for life important natural phenomena [2].

Seasonal changes of thermal stratification are common phenomenon in deep lakes or reservoirs. Thermal stratification means that the water in such water bodies forms certain thermal layers due to solar heating. The heated atmosphere imposes a temperature signal on the water body surface. As a result, thermal stratification can be established during the warm season if a lake or reservoir is sufficiently deep. On the contrary, during the cold period, surface cooling forces vertical circulation of water masses and removal of gradients of water properties [3]. Additionally, the hydrological regime of many lakes and reservoirs has been modified to the extent that such water bodies have fundamentally changed their appearance, e.g., Aral Sea [4], or their stratification pattern has been altered by human impact, e.g., Dead Sea [5] or by climatic variability, e.g., Caspian Sea [6]. A considerable portion of the lakes or reservoirs on Earth is permanently stratified. Deep lakes or reservoirs especially show this feature. As a consequence, many of the largest water bodies (e.g., Caspian Sea, Baikal, Tanganyika, Malawi-Nyasa) and many middle size and small water bodies do not circulate completely in the vertical and do not show a homogenized, overturning water body at any time during the annual cycle. Anyway, stratification has

decisive impact on the redistribution of dissolved substances, such as nutrients or oxygen, and hence determines the biocenosis that can form in the water body [7, 8]. So, a good knowledge of the stratification of the water body thus helps to understand and predict the biota of the water body and thus the water quality in it.

When a water body stratifies, three different layers typically form (see Fig. 1):

- Epilimnion - the warm, upper layer that receives sunlight and contains the most dissolved oxygen
- Metalimnion - the middle layer where the temperature changes rapidly with depth
- Hypolimnion - the cold, dense bottom layer that rarely receives direct sunlight and has the least amount of dissolved oxygen.

Thermocline is a relatively thin part of the metalimnion layer in which temperature decreases rapidly with depth increase. The thermocline was defined as a layer of water in which the temperature decrease 1° or more along 1 meter of the depth.

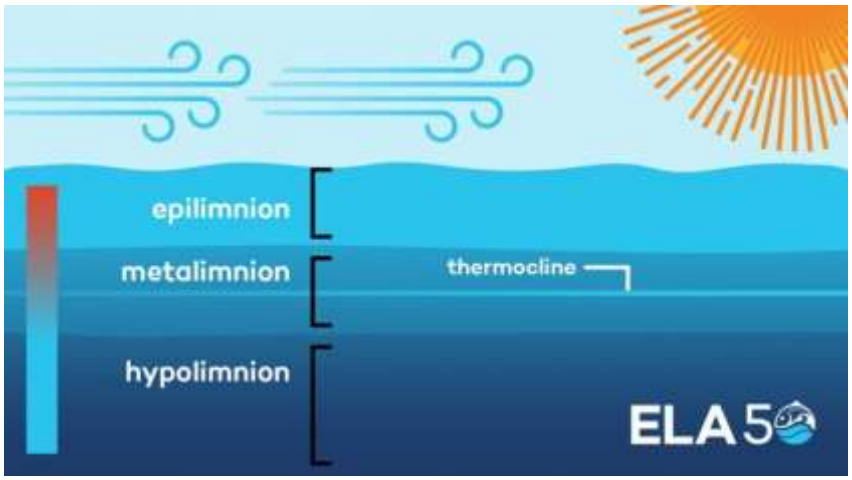

Figure 1. . Scheme of stratification in lakes and reservoirs (source:Fafard, 2018) (https://www.iisd.org/ela/blog/lakes-stratify-turn-explain-science-behind-phenomena/)

Seasonal changes in the intensity of solar radiation and air temperature cause continuous changes in thermal stratification. A change in water temperature causes a change in its density, which makes it move and thermal layers mixing. Such mixing in lakes or reservoirs is extremely important, as it is the event that, for example, causes replenishing dissolved oxygen levels in the deepest waters of such water bodies. This movement causes a change in the stratification of several water quality indicators (chemical stratification) and also the position of the thermocline.

The classification of lakes/reservoirs according to their circulation pattern is as follows [4]:
1. Holomictic lakes/reservoirs overturn and homogenize at least once a year.
2. Meromictic lakes/reservoirs are water bodies in which the deep recirculation does not include the entire water body.
4. Amictic lakes/reservoirs do not experience a deep recirculation. Usually, permanently ice-covered lakes are included in this class.
Holomictic lakes/reservoirs are subdivided into classes indicating the frequency and time of overturn. Lewis [9] subdivided the classes even further. ‘‘Polymictic’’ refers to lakes/reservoirs which are not deep enough to form a hypolimnion. The entire water body behaves like an epilimnion, which is mixed by sporadic strong wind events over the year or even on a daily basis in response to strong daily temperature cycle. ‘‘Dimictic’’ lakes/reservoirs are handled as prototypes of such water bodies in moderate to cold climates, with two circulation periods in general. ‘Monomictic’’ lakes/reservoirs

possess one circulation period in addition to the stratification period. Many lakes/reservoirs in the temperate climate belong into this class if they do not develop an ice cover during winter. Such water bodies are sometimes also referred to as warm monomictic to distinguish them from cold monomictic water bodies, which show an ice cover for most of the year and circulate during the short period without ice. ‘‘Oligomictic’’ lakes/reservoirs circulate less frequently than once a year, normally at irregular intervals, triggered by extreme weather conditions such as unusually cold winters for the respective location.

At the time of the ongoing climate change, questions related to the water balance, water availability and quality are starting to be discussed more and more. The availability of water resources is dwindling due to excessive use, persistent human impact, and the effects of climate change, potentially leading to severe impacts on water quality. This is a critical concern, as water is vital for human well-being, ecological balance, and economic activities [10]. The deterioration of water quality poses risks such as exposure to dangerous diseases and pollutants [11], a decline in ecosystem productivity and variety [12], and harm to sectors like aquaculture and agriculture that depend on water. Even though Slovakia is a country with a relatively good balance in this regard, it is still true that the distribution of water resources in time and space is not uniform.

Access to safe drinking water is a basic human right. In Slovakia, the majority of the population is supplied from ground water sources. However, there are locations with the problem to access the ground water [13], at which this is not possible. In such cases, it is solved through water reservoirs specifically designed to supply the population with drinking water. It is important to pay increased attention and care to this type of reservoir, because the threat to the quality of water in them can have immeasurable negative consequences. Such types of reservoirs are also the Turček and Rozgrund reservoirs. As mentioned above, lakes and reservoirs are subject to thermal stratification, which can affect the quality of the water in them. This study therefore addresses this issue and describes the initial results of the analyses confirming dimictic character of these reservoirs.

3 Methods

3.1 Description of localities

This paper analyses the seasonal changes of the thermocline position in two water reservoirs in Slovakia: the Rozgrund reservoir and the Turček reservoir. They are relatively close to each other, but have different parameters.

3.1.1 The Rozgrund reservoir

The Rozgrund water reservoir (Fig. 2) was built in the 18th century as part of a unique water management system in the vicinity of the Banská Štiavnica town (N48.458652, E18.893036). Samuel Mikovíni developed the project of this water structure in 1741. The dam was built in 1743-1744 and until the middle of the 19th century, it had the leading place in the height of the dam among mining reservoirs in Europe. It is a unique water structure that held the world championship in the angle of slope of the earth dam for 111 years (the slope on the water side is 1:1.5 and the slope on the air side is 1:1.25 to 1:1.75) [14]. The filling of the reservoir was solved in an ingenious way, mostly from a foreign catchment area (approx. 35 km^2). Water was also supplied from the own catchment with area of approximately 15 km^2. The original role of the Rozgrund reservoir was the accumulation of water to drive mining machines. From the beginning of the 20th century until the recent past, it was also used as a source of drinking water. Today it is operated as a potential reservoir for supplying the population with drinking water, but it also serves to flatten the flood wave and breed fish with the aim of increasing the water quality in the reservoir through the biological system of the reservoir. Its total volume is 0,515 mil. m^3, the elevation of the maximum operating level is 705 m above sea level, the current maximum depth is around 19 m.

Figure 2. The Rozgrund reservoir

3.1.2 The Turček reservoir

The Turček reservoir (Fig. 3) is younger and bigger, the construction of dam was finished in 1996. This water structure was built primarily for drinking water supply (this reservoir supplies 3 districts with drinking water: Žiar nad Hronom, Handlová and Prievidza), but also for flood protection of downstream part of the basin and for ensuring ecological discharges, as well. The Turček water reservoir also contributes to the production of electricity by three small hydroelectric plants with a total installed capacity of 300 kW. Total volume of the reservoir is 10,8 mil. m^3, the elevation of the maximum operating level is 775,3 m above sea level, the maximum depth is 60 m.

The Turček reservoir is located in central Slovakia near the Turček village (the Turčianske Teplice district) at the confluence of the Turiec and the Ružová streams. The total area of the catchment is 29.5 km^2.

Figure 3. The Turček reservoir

According to the available literature dealing with the topic of stratification [3, 4, 9, 15, 16, 17], the Rozgrund and Turček reservoirs were estimated to be dimictic, which means that the water in these bodies is mixed twice up to a year, in spring and autumn (spring and autumn circulation). With the onset of summer, after the surface has warmed and the climatic conditions have stabilized, the water is divided into temperature layers. This assumption was tried to be confirmed based on the measurements made at the Rozgrund and Turček water reservoirs, as well as those provided by the reservoir manager (Slovak Water Management Company - SVP, š.p.).

3.2 Field measurements

Monitoring of the spatial distribution of water quality indicators, including temperature, in larger water bodies can be complex and time-consuming, so it was necessary to find an optimal solution and design

a monitoring method in selected water reservoirs. The resulting solution is a combination of manual measurement of depth horizons in individual point locations of the water reservoir using the YSI Professional Plus multiparametric probe from a boat and the use of an autonomous AUV EcoMapper monitoring device capable of automatic data collection in the reservoir area.

A prerequisite for collecting correct data during experimental measurements with the AUV EcoMapper device is precise mapping of the site of interest, especially bathymetry, detailed route planning, planning of deep dives and calibration of the multiparametric probe. At both reservoirs, several variants of traversing and diving were tried, while the maximum depth achieved in the case of Rozgrund was 10 meters, and 20 meters in the case of Turček. Due to relatively little maneuvering space, in the case of Rozgrud, two monitoring lines for the EcoMapper device in the deepest part of the reservoir and four such lines for Turček were chosen in the final stage. In the shallower peripheral parts, and of course also at checkpoints identical to the trajectory of the AUV Eco Mapper, the spatial distribution of temperature, or other monitored indicators of water quality, is measured manually from a boat with a multiparametric probe. A sonar is used simultaneously to check the depths and a GPS device to check the exact location of the measured point. The manual measurement with a parametric probe was performed with a step of 1 m to a depth of 15 m in case of the Rozgrund reservoir and to the depth of 45 m in case of the Turček reservoir. The measurement with the EcoMapper device was carried out at depths of 1 m, 2 m, 4 m, 6 m, 8 m and 10 m. Further depths were measured with a step of 5 meters. A more detailed description of the EcoMapper device and the method of measurement with it is described in the paper [18]. Manually measured data were compared with data measured by EcoMapper and mutually calibrated. Continuous measurement with the AUV EcoMapper showed that the values of the measured water quality indicators did not change significantly in the area during one measurement campaign.

Figure 4. Photos from measurements of the site of the Rozgrund water reservoir (left) and the Turček water reservoir (right) (photo: Velísková)

Measurement campaigns took place at both locations in three different seasons - in spring (in the period after the melting of the ice cover of the reservoir and melting of the snow in its vicinity), in summer and

in autumn. In winter, it is not possible to take measurements on the reservoir due to the freezing of the surface up to a thickness of several tens of centimetres.

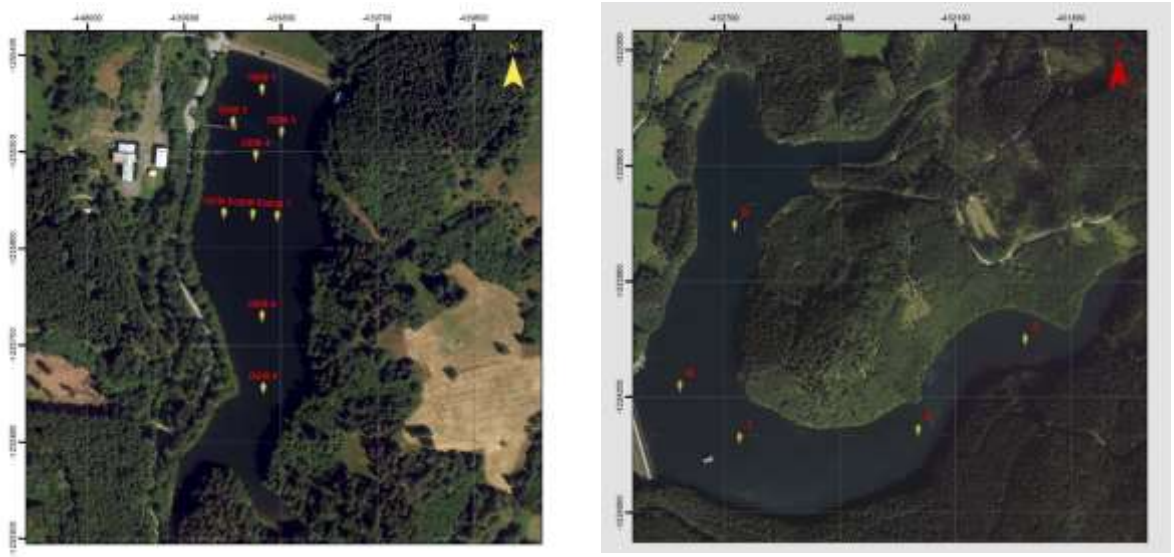

Figure 5. Manually measured points at the site of the Rozgrund water reservoir (left) and the Turček water reservoir (right)

4 Results and discussion

As the first of the measurements at the monitored locations, measurements of the current bathymetry of the reservoir were carried out. The results are presented in graphic form in Fig. 6 and 7.

This measurement served both to evaluate the current state of the bottom morphology and at the same time as a basis for planning the missions (measurement paths) of the EcoMapper device, as well as for the design of the distribution of manually measured points in the reservoir area.
Originally, manual measurements were done at 28 points in each reservoir. After the analysis of spatial changes within the framework of measurement in one period of the year, the number of measured points was reduced (Fig. 5). Besides, due to spatial reasons and due to the extensiveness of the data, only partial results in this study are presented, but even from these results (Fig. 8) it is possible to see that the most significant stratification occurs in the summer. Originally, it was assumed that in the spring and autumn the temperature distribution along the depth would be of approximately the same nature, since the reservoirs are not far from each other, the measurements were done within 2 weeks, and therefore it was not assumed that there would be very different meteorological conditions. However, the measurement results so far show that this is not the case. It depends not only on the depth, but probably also on the total mass of water that is mixed in the reservoir and also on the manipulation of levels and withdrawals [17]. According to [3], an important factor influencing the depth of the thermocline, which has the sharpest temperature gradient, is wind speed, with greater wind stress leading to a deeper thermocline and more mechanical energy used to stir the lake. Stronger surface winds can cause a longer duration of mixing, delaying ice formation [15]. On the other hand, the solar radiation absorbed by the water body can be reduced by the ice cover, what is leading to a later onset of stratification [19].

Anyway, as far as Rozgrund is concerned, there is a more pronounced degree of stratification in the spring than in the autumn. The most significant stratification is in the summer, when thermocline was created in the depth around 4-5 m.

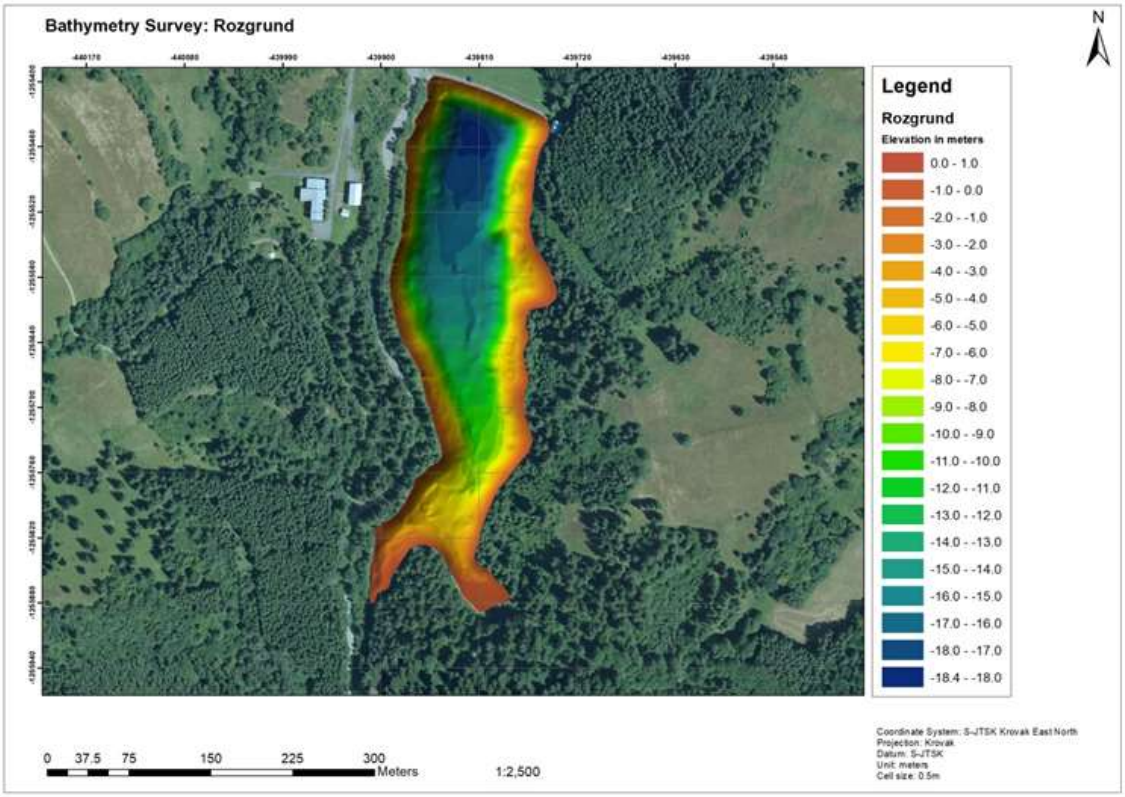

Figure 6. Current bathymetry of the Rozgrund water reservoir measured by the EcoMapper device

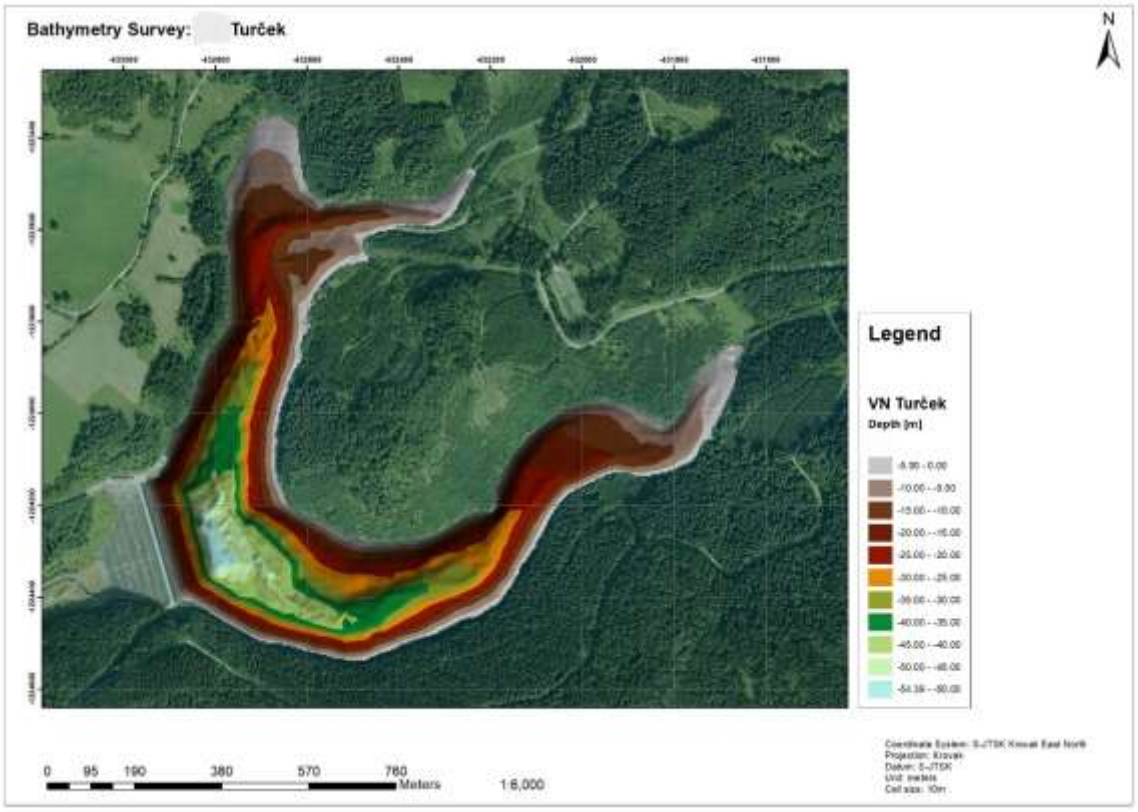

Figure 7. Current bathymetry of the Turček water reservoir measured by the EcoMapper device

In case of the Turček reservoir, the significant thermal stratification as well as the thermocline layer was created during the summer season, and in the same depth 4-5 m. However, as it can be noticed in Fig. 8, in the case of the deeper Turček reservoir, the transition to the temperature that occurs stably at the reservoir bottom is significantly longer than in the case of the Rozgrund reservoir.

The autumn circulation takes place in both reservoirs in a relatively similar manner and its extent is influenced by the deep of reservoir. The thermal stratification in the spring period has a slightly different character in these two mentioned reservoirs, even though the measurements on them took place within 2 weeks. On the curve of temperature distribution along the depth in the case of the Rozgrund reservoir, the initial stage of temperature increase in the upper layers of the reservoir is clearly visible, while this is not the case at the Turček reservoir, and a relatively constant distribution of temperature along the depth can still be observed. This is probably caused by the fact that the ice cover occurs longer to the spring months at the larger Turček reservoir and is thicker. Austin & Colman [19] confirmed this fact, as well.

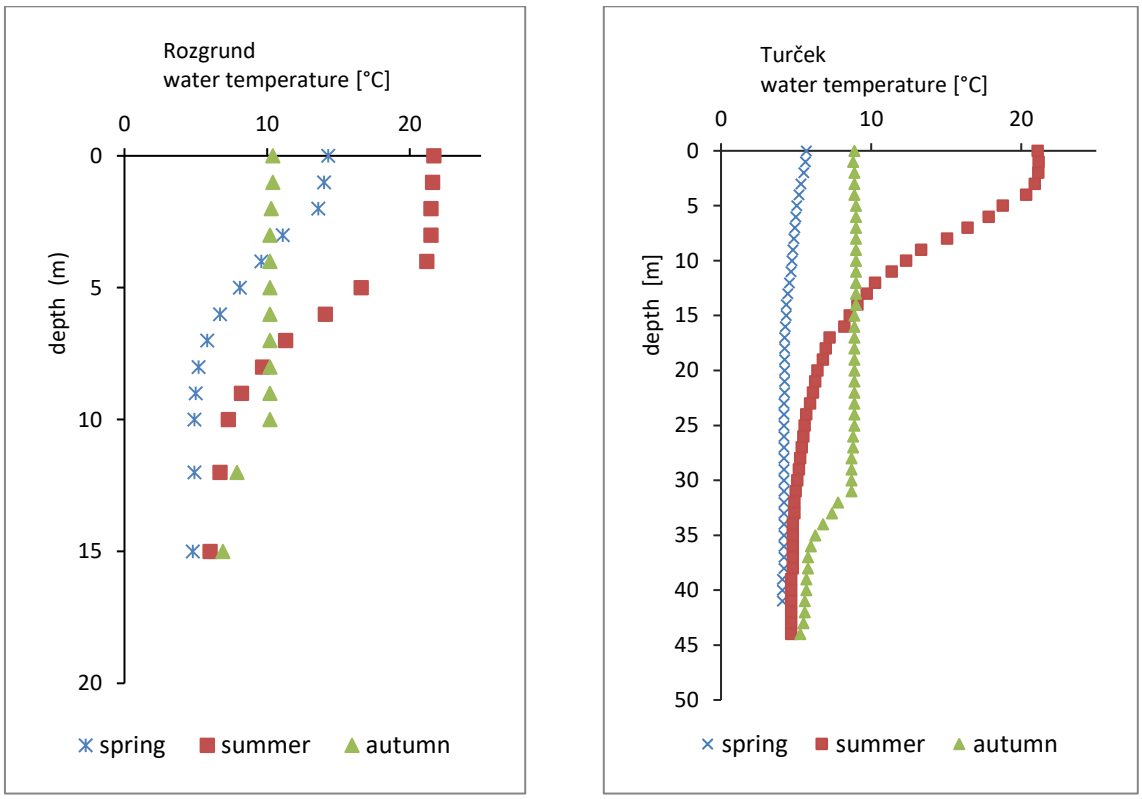

Figure 8. Thermal stratification at the site of the Rozgrund water reservoir (left) and the Turček water reservoir (right)

All findings represent preliminary results and they will need to be verified by further measurements in the following years.

Anyway, as it was mentioned above, the Rozgrund and Turček reservoirs were estimated to be dimictic, which means that the water in these bodies is mixed twice up to a year, in spring and autumn. So, based on the measurements performed at the Turček water reservoir, as well as those provided by the reservoir administrator, this assumption was confirmed.

5 Conclusion

The paper deals with the development of temperature stratification in two water reservoirs (Rozgrund and Turček), which are relatively close to each other, but have different parameters, and with the determination of changes in the position of the thermocline, which is characterized as a layer in which temperature decreases rapidly with depth increase.

As preliminary results show, thermal stratification is formed in both cases. In the summer, its course is almost the same in both reservoirs; the thermocline is formed at a depth of about 4-5 m below the water surface. In the spring and the autumn season, however, the thermal stratification in these reservoirs is different, and the existence and position of the thermocline in the same time period is different. It is probably caused by the different depth of the reservoirs, differences in the duration and thickness of the ice cover on the reservoirs and their area size (which is related to the effect of the wind on mixing mainly in the surface layer). Level manipulation is also an assumed possible influence, but this aspect was not analyzed in this study. All of these facts affect the dynamics of the water in the reservoirs and thus also the mixing of temperature layers.

The result of the study is the confirmation of the assumption that both reservoirs are dimictic, that is, the water in the body of the reservoir is mixed twice a year. Thanks to the EcoMapper device use, the current bathymetry was mapped, as well as a detailed distribution of the measured basic indicators of water quality in selected lines. A complex continuous measurement of the distribution of these water quality indicators was not possible due to the limited spatial possibilities of maneuvering this device.

Finally, it should be mentioned and emphasized that the study presents measurements over the one year. In the next step, data from next measurement campaigns, as well as the results of numerical simulations, will be analyzed to confirm the facts found.

Acknowledgements
This work was supported by the Scientific Grant Agency VEGA - grant number VEGA 2/0140/24, and by the project APVV – 18-0205 and APVV – 22-0610.

References:

[1] Ruttner, F.: Fundamentals of limnology, University of Toronto press, Toronto and Buffalo, ISBN 0-8020-2028-3, 1972.
[2] Water Quality Assessments - A Guide to Use of Biota, Sediments and Water in Environmental Monitoring - Second Edition, edited by D. Chapman, 1996, https://iris.who.int/bitstream/handle/10665/41850/0419216006_eng.pdf?sequence=1, 28.05.2024.
[3] Boehrer, B., Schultze, M.: Stratification of lakes. Reviews of Geophysics, 46, RG2005, 27 p., 2008. https://doi.org/10.1029/2006RG000210, 14.05.2024
[4] Cre´taux, J.-F., A. V. Kouraev, F. Papa, B. Berge´-Nguyen, A. Cazenave, N. Aladin, and I. S. Plotnikov: Evolution of sea level in the big Aral Sea from satellite altimetry and its implications for water balance, J. Great Lakes Res., 31(4), pp.520–534, 2005.
[5] Gat, J. R.: Stable isotopes of fresh and saline lakes, in Physics and Chemistry of Lakes, edited by A.|Lerman et al.,pp. 139 – 165, Springer, Berlin, Germany, 1995.
[6] Peeters, F., R. Kipfer, D. Achermann, M. Hofer, W. Aeschbach-Hertig, U. Beyerle, D. M. Imboden, K. Rozanski, K. Frohlich: Analysis of deep-water exchange in the Caspian Sea based on environmental tracers, Deep Sea Res., Part I, 47(4), pp. 621 – 654, doi:10.1016/S0967-0637(99)00066-7, 2000.
[7] George, D. G., Hewitt, D. P.: The impact of year-to-year changes in the weather on the dynamics of Daphnia in a thermally stratified lake, Aquat. Ecol., 40(1), pp. 33 – 47, doi:10.1007/s10452-005-9013-3, 2006.
[8] Thackeray, S. J., D. G. George, R. I. Jones, and I. J. Winfield: Statistical quantification of the effect

of thermal stratification on patterns of dispersion in a freshwater zooplankton community, Aquat. Ecol., 40(1), pp. 23 – 32, doi:10.1007/s10452-005-9021-3, 2006.
[9] Lewis, W. M., Jr.: A revised classification of lakes based on mixing, Can. J. Fish. Aquat. Sci., 40, pp. 1779 – 1787, 1983.
[10] Čubanová, L., Rumann, J., Vidová, A., Almikaeel, W., Rebenda, F.: Verification of hydraulic parameters of nature-like fish pass. In Water. Vol. 15, iss. 13 (2023), online, [17] s., art. no. 2478. ISSN 2073-4441, doi: 10.3390/w15132478
[11] Hu, Y.N., Cheng, H.F.: Water pollution during China's industrial transition. Environmental Development, 8, pp. 57–73. doi:10.1016/j.envdev.2013.06.001, 2013.
[12] Kaiblinger, C., Anneville, O., Tadonleke, R., Rimet, F., Druart, J.C., Guillard, J., Dokulil, M.T.: Central European water quality indices applied to long-term data from peri-alpine lakes: Test and possible improvements. Hydrobiologia, 633, pp. 67–74. doi:10.1007/s10750-009-9877-7, 2009.
[13] Baroková, D., Šoltész, A., Červeňanská, M., Čubanová, L. : Innovative groundwater management in industrial park: optimization and modelling of extraction system. In World Multidisciplinary Civil Engineering - Architecture - Urban Planning Symposium (WMCAUS 2023) Les Ulis : EDP Sciences, 2024, [online], 8 s., art. no. 04003. ISSN 2261-236X. doi: 10.1051/matecconf/202439604003.
[14] Lichner, M., Kašiarová, E., Novák, J., Podkonický, L.: Banskoštiavnické tajchy (Water reservoirs system around Banská Štiavnica town), Banská Bystrica – štúdio Harmony, 127 pages, ISBN 80-89151-08-6, 2005. (in Slovak)
[15] Kirillin, G., Leppäranta, M., Terzhevik, A., Granin, N., Bernhardt, J., Engelhardt, C., Zdorovennova, G.: Physics of seasonally ice-covered lakes: A review. Aquatic Sciences, 74(4), pp. 659–682. https://doi.org/10.1007/s00027-012-0279-y, 2012.
[16] Weitzel, D.: Stratification and Oxygen Loss. Fish's Point of View, 2002 [Online] Available: http://www.scientificfisherman.com/fishpoint/fishptjuly.asp, 22.07.2021
[17] Wetzal, R.G.: Limnology, Lake and River Ecosystem (3rd Ed) Chapter 6: Fate of Heat, pp. 71-92, Academic Press, New York, 2001.
[18] Sočuvka, V., Velísková, Y.: Determination of reservoir capacity changes by autonomous underwater vehicles (AUVs), Acta Hydrologica Slovaca, 16 (2), 2015, p. 102 – 108.
[19] Austin, J. A., Colman, S. M.: Lake Superior summer water temperatures are increasing more rapidly than regional air tempera-tures: A positive ice-albedo feedback. Geophysical Research Letters, 34, L06604, 2007. https://doi.org/10.1029/2006GL029021, 24.05. 2022

URBAN SURFACE RUNOFF AS A POTENTIAL SOURCE OF ENVIRONMENTAL POLLUTION

JAROSLAV HRUDKA [1], ŠTEFAN STANKO[2], IVONA ŠKULTÉTYOVÁ [3], RÉKA WITTMANOVÁ [4], ADAM KOLLÁR [5],

[1] *Slovak University of Technology in Bratislava, Faculty of Civil Engineering, Department of Sanitary and Environmental Engineering, Radlinského 11, 810 05 Bratislava, Slovakia, E-mail: jaroslav.hrudka@stuba.sk*

[2] *Slovak University of Technology in Bratislava, Faculty of Civil Engineering, Department of Sanitary and Environmental Engineering, Radlinského 11, 810 05 Bratislava, Slovakia, E-mail: stefan.stanko@stuba.sk*

[3] *Slovak University of Technology in Bratislava, Faculty of Civil Engineering, Department of Sanitary and Environmental Engineering, Radlinského 11, 810 05 Bratislava, Slovakia, E-mail: ivona.skultetyova@stuba.sk*

[4] *Slovak University of Technology in Bratislava, Faculty of Civil Engineering, Department of Sanitary and Environmental Engineering, Radlinského 11, 810 05 Bratislava, Slovakia, E-mail: reka.wittmanova@stuba.sk*

[5] *Slovak University of Technology in Bratislava, Faculty of Civil Engineering, Department of Sanitary and Environmental Engineering, Radlinského 11, 810 05 Bratislava, Slovakia, E-mail: adam.kollar@stuba.sk*

1 Abstract

Changing climatic conditions in urbanized areas have a tremendous impact on the quality of life in urbanized areas. Persistent prolonged dry periods, extreme downpours with high runoff or prolonged rainfall are extreme problems for efficient urban water management. Extreme weather changes also result in environmental risks for the seepage or discharge of highly contaminated water from the first flush. These effluents are a potential source of groundwater and surface water pollution in which various types of pollutants are concentrated. Our research focuses on evaluating the water quality of surface runoff with an emphasis on micropollutant concentrations. The analyses are aimed at evaluating the concentrations of heavy metals, microplastics, and other pollutants in surface runoff with respect to receiving water quality and groundwater quality.

Keywords: storm water, micropollutants, urban pollution, first flush

2 Introduction

Rainwater captured from rooftops is considered an alternative source of water for supplying the population, especially in arid areas where water resources are scarce. In the past, rainwater was considered a water source with minimal pollution that could be used after simple treatment [1]. Nowadays, the quality of rainwater is greatly influenced by the lifestyle of the population.

The nature of pollutants in stormwater runoff from paved areas can be divided into primary and secondary pollution. Primary pollution is caused by the stormwater itself, which absorbs airborne emissions. Secondary pollution occurs after the rain has come into contact with paved surfaces. In stormwater management (capture and reuse) in urbanised catchments, secondary pollution is an important factor that can significantly affect stormwater quality.

The chemical composition of the stormwater itself is influenced by natural factors such as the chemical composition of the air (content of gases such as nitrogen and oxygen), the spatial distribution of the area and the conditions. The quality of atmospheric precipitation is greatly influenced by the sudden development of urbanized areas, transport infrastructure and industry [2] [3]. The intensification of the formation of paved areas and the suppression of permeable vegetation areas have caused the presence of undesirable and environmentally hazardous substances in stormwater runoff, which are considered to be the main source of pollution of water bodies (rivers, lakes) [4].

Unwanted substances in surface runoff can be organic or inorganic and originate from paved areas such as roads, car parks and building roofs. These substances may exist in soluble or insoluble form. Inorganic

substances present in surface runoff include dust particles, sand, heavy metals (Cd, Cu, Ni, Pb, Zn), sulphates, chlorides, nitrogen and phosphorus compounds. Organic pollutants are mainly petroleum products, chlorinated hydrocarbons, polycyclic aromatic hydrocarbons (PAHs), polychlorinated biphenyls (PBCs), pesticides, and various microbial pollutants such as coliforms and mesophilic bacteria [3].

The variability of pollutants in surface runoff depends on several parameters, mainly land use, materials used, pollutant and soil characteristics, and rainfall intensity and duration. Studies show various relationships between rainfall characteristics and pollutant concentrations. For example, Lee et al. (2011) argue that this dependence can be influenced by the intensity and duration of rainfall and the length of the rain-free period [5]. On the contrary, Soller et al. (2005) state that pollutant concentrations are not dependent on land use and duration of rain, but rather on the intensity of the rain itself [6]. Other studies suggest that the greatest amount of pollutants in surface runoff occurs after a long rain-free period [7]. The findings of these studies indicate that the highest pollutant concentrations accumulate at the beginning of the surface runoff period, and this is influenced by the intensity of the rain and the length of the rain-free period. If a rainfall event occurs, these pollutants are set in motion and can be transported into the storm drain system and subsequently discharged to the nearest watercourse.

In the last ten years, many studies have been carried out to analyse the quality parameters of stormwater. The reason? The manifestation of climate change and the associated risk of a crisis due to water scarcity and rising air temperatures. The current over-exploitation of good quality water and the diversion of heavily polluted water are causing significant damage to the aquatic ecosystem. As an alternative solution to this problem, rainwater harvesting from paved areas and its reuse - for example for washing, flushing toilets or irrigating green areas in homes - is being offered as an alternative solution. However, it should be stressed that this solution may have the disadvantage of the possible presence of microbiological and chemical substances in the captured rainwater, which can cause serious health problems for humans and also environmental degradation

3 Methods

Surface runoff sampling methodology is highly variable and must be carefully tailored to the specific characteristics of the runoff source. Understanding the source of contaminated water is crucial because the type of surface from which the runoff originates significantly influences its quality indicators. For example, runoff from rooftops primarily carries contaminants such as dust, particulate matter, and residues from roofing materials. In contrast, runoff from roadways is likely to contain a higher concentration of pollutants like oil, heavy metals, and tire residues due to vehicular traffic. Green spaces, on the other hand, might contribute organic matter, pesticides, and nutrients like nitrogen and phosphorus from fertilizers. The methodology for sampling surface runoff involves selecting appropriate sampling points and times to capture representative samples of the runoff. This often requires considering the frequency and intensity of rainfall events, as these factors can affect the concentration and composition of contaminants. For instance, initial runoff during the first flush of a storm event typically has higher pollutant concentrations than later runoff. Therefore, capturing samples at different stages of a rainfall event can provide a more comprehensive understanding of the runoff quality. Furthermore, the tools and techniques used for sampling can vary. For rooftop runoff, collectors positioned at downspouts might be used, while roadway runoff sampling might involve the use of automated samplers placed in storm drains or along the edges of roads. Sampling from green spaces might require placing collection devices at strategic low points where water naturally accumulates. Accurate and consistent sampling is essential for assessing the environmental impact of surface runoff and for informing mitigation strategies. By understanding the variability in sampling methodologies and the influence of different sources, better management practices can be developed to address the specific pollutants associated with each type of surface runoff.

3.1 Pollution of surface runoff from roads

The chemical composition and concentration of pollutants in surface runoff discharged from different types of roads e.g. roadways, parking lots and pedestrian walkways depends on the type of material used, traffic volume, road gradient [8], amount of emissions from vehicles themselves, winter maintenance, abrasion and corrosion as results of vehicle movement and crashes, etc. As a result of these pollution sources, various oil and grease, lubricants, gritting salt substances, dust particles, heavy metals (lead, cadmium, zinc, copper, iron), polyaromatic hydrocarbons (PAHs) and other organic and inorganic substances are thus released into the surface runoff. In the foreign literature these substances are termed "road-deposited sediments" (RDS) or road sediments, which accumulate on the road surface in the dry season and are at best discharged to the sewer network in the event of a rainfall event. Information on the pollutants found in stormwater runoff from roads and their sources of generation is presented in Table 1.

Table 1. Sources of stormwater surface runoff pollution from roads [9]

	Source of pollution	Pollutants
From vehicles	Brakes	Ba, Cu, Fe, Mo, Na, Ni, Pb, Sb
	Tyres	Al, Zn, Ca, Cd, Co, Cu, Mn, Pb, hydrocarbons, PAHs (pyrene, benzo(a)pyrene, fluoranthene)
	Catalyst	Pt, Pd, Rh
	Vehicle bodywork	Cr, Fe, Zn
	Exhaust gases	Ag, Ba, Cd, Cr, Co, Mo, Ni, V, +Sb, Zn, PAU (for naphthalene), MTBE, BETX
	Motor oil leaks	PAHs, Pb, Ni, Zn, organics, oils, fats, hydrocarbons, Cu, Cr
Others	Road surface (asphalt, bitumen)	Al, Ca, Fe, K, Mg, Na, Pb, Si, Sr, Ti, PAU
	Dust substances	Ca, Mg, Na, Cl, ferrocyanide
	Road equipment (e.g. road signs)	Ca (galvanized steel)
	Detergents used for tunnel washing	tensides
	Spraying on vegetation	herbicides

The concentration of road sediments has been the subject of research for many years due to the potential impact on the environment and human health. Among all these substances, considerable attention has been paid to the occurrence of heavy metals due to their high toxicity and non-biodegradability in the environment, due to the characteristics of the pollutants, the complexity of identifying the source of pollution and risk assessment. Comparing many studies, the most frequently occurring metals in surface runoff from roads are lead and zinc, due to their high applicability in the automotive industry (batteries, tires, oils and lubricants, etc.) [10]. Examples of concentrations of road sediments occurring in urban surface runoff are shown in Table 2. (Mean concentrations from an urban road located in China are shown) [11].

Table 2. Concentrations of pollutants in urban surface runoff [11]

Indicator	Concentration [mg.l^{-1}]	Indicator	Concentration [mg.l^{-1}]
TSS	631 ± 608	Zn	0,69 ± 0,43
CHSK	418 ± 311	Cu	0,13 ± 0,07
N $_{total}$	8,1 ± 5,0	Pb	0,58 ± 0,08
P $_{total}$	1,2 ± 1,4	Cd	0,051 ±0,009
N-NH$_3$	4,3 ± 2,3	Fe	11,8 ± 5,6

In addition to heavy metals, in recent years some scientists have begun to look at the presence of polyaromatic hydrocarbons (benzene, naphthalene, pyrene) in surface runoff due to their high concentrations in soil (in some cases higher than in air). The presence of these pollutants in stormwater runoff is conditioned by emissions from cars, which are due to incomplete combustion of biomass and fossil fuels are considered one of the main sources of PAHs. [12].

3.2 Pollution of surface runoff from roofs

The quality of surface runoff from building roofs depends on a number of factors, just as it does from roads. It is determined by the type of roofing material (wood shingle, concrete tile, clay tile, etc.), the geometry of the roof (slope, length, width), and the environmental conditions of the area (climatic conditions, air pollution, etc.). Pollutants in surface runoff may originate from:
- from roofing - material used for roofing, flashing, etc,
- from dry deposition on the roof surface - flying substances, insects, leaves, bird droppings
- from atmospheric contaminants washed off by rainwater.

Various studies have demonstrated the presence of inert roof sediments (e.g., dust and animal fecal sediments), heavy metals (nickel, chromium, zinc, iron, copper, aluminum), nitrogen pollution, suspended solids, and bacteria (Escherichia colli, Enterococci) in roof runoff. The concentration of these substances also depends on the characteristics of the rain event: length of the rain-free period, intensity of rainfall, duration of rainfall, wind direction, etc. The presence of high concentrations of pollutants in roof runoff can be particularly problematic in areas with elevated levels of air emissions, i.e. in urban agglomerations due to intensive traffic and local sources of pollution.

The influence of roofing type on the quality of surface runoff from roofs was confirmed by Lee in his study. Lee et al. (2010) [4] compared four types of roofing materials in their study and found that wood shingle, among all the types of roofing materials considered, had the greatest effect on the increase in pH, electrical conductivity and zinc, with galvanized steel roofing proving to be the most suitable material. Zang et al (2014) compared the quality of surface runoff from conventional roofing and green roofing, finding that green roofing, despite all its positive environmental impacts, is not the most suitable solution when it comes to collecting rainwater from paved areas, but ceramic tile is. An example of the average concentrations of pollutants in roof runoff depending on the type of roofing material used is described in Table 3.

Table 3. Average pollutant concentrations in roof runoff depending on the type of roofing material used [4]

Parameters	**Unit**	**Wooden shingle**	**Concrete tile**	**Ceramic covering**	**Metal roof tile**
pH	[-]	6,0 – 9,0			
TSS	[mg.l^{-1}]	213,9	309	219,3	285,8
TOC		49,7	32,9	35,6	31,8
SO_{42}-		5,57	3,64	3,1	2,87
Al	[µg.l^{-1}]	227	535	243	622
Cu		34	58	37	59
Fe		154	160	155	302
Pb		10	14	11	12
Zn		135	196	131	428

At the same time, rainwater runoff from the roofs of buildings is increasingly being captured and used as an alternative source of water - domestic water or for irrigating vegetation, etc. The presence of nutrients, microbial pathogens, heavy metals and other pollutants in roof runoff is undesirable and can have a negative impact on the environment and human health.

"First flush" or the first flush (runoff) of stormwater from a paved area is an important aspect in urbanized areas that is related to the occurrence or assumption that the first portion of stormwater runoff is the most contaminated. This view is shared by most scientists, while some question whether the actual mass of the first runoff represents a significant portion of the runoff. In general, the first flush of surface runoff represents an important aspect of surface runoff that is characterized by high pollutant concentrations in the initial runoff phase at the onset of a storm event. A first flush can only be said to occur when the first runoff has a higher pollutant concentration compared to later runoff. The mass (pollutant concentration) of the first runoff event depends on the intensity of the rainfall event and the

catchment's storage capacity, and will only occur if the pollutant concentration in the initial runoff is higher compared to the pollutant concentration in the later runoff.
Understanding the quality of surface runoff and its proper definition has been the subject of many studies (Deletic A. (1998), Huang (2012) , Seget at al., (1995). The first definition was attempted by Bertrand-Krajewski in 1998. In his study, he stated that the first stormwater runoff from surface runoff can be considered as that surface runoff in which at the beginning of the rainfall event (in the first 30% of the runoff), 80% of the pollutants reach the runoff. The authors of the other studies are identical to the Bertrand-Krajewski view, except that theytra assume the greatest concentration of emissions in the early phase of runoff, approximately in the first 20% to 40% of the total runoff volume. In any case, it can be argued that surface runoff generated during a rain event represents the primary pollutant transport medium.

4 Results and discussion

Infiltration of rainwater from surface runoff into the soil horizon has a positive effect on the hydrological regime of the area. First of all, it ensures the replenishment of groundwater reserves and the partial interception of flood waves, and also has a positive effect on the microclimate of the city. Significantly high concentrations of nutrients, heavy metals and organic compounds that infiltrate the soil horizon can be a problem. The presence of pollutants in surface runoff varies widely and depends on the season, location, traffic density and the volume and intensity of rainfall. Infiltration of contaminated water into the soil aquifer causes localised changes in groundwater hydrology, influences groundwater level rise (flood level), causes groundwater pollution, and may even cause surface water pollution as a result of sediment transport. In recent decades, infiltration of stormwater from paved areas has been addressed by many authors (Datry et al. (2004), Tedoldi et al. (2016) and many others), who have pointed out that the topsoil and unsaturated zone act, as a filtering layer and most of the pollutants do not penetrate deep into the groundwater, but remain in the shallow groundwater levels. An example of the most commonly occurring contaminants in groundwater due to infiltration (seepage) is given in Table 4.

Table 4. Example of the most frequently occurring substances in groundwater due to infiltration of surface runoff, the source of occurrence and the possibility of risk reduction

Pollutant	Risk of impairment	Source of occurrence	Risk reduction options
Nitrate	low to medium	fertilisers, atmospheric deposition, animal waste, etc.	slow infiltration using a finer textured material,
Chloride	high	road salt	zníženie aplikovania cestnej soli
Phosphorus	Low	plant and leaf waste, soil particles, animal waste, fertilisers, road salt and atmospheric deposition particles	the concentration of phosphorus in the soil should not exceed 30mg-p/kg-soil
Toxic metals	Low	substances caused by the transport and surface treatment of paved surfaces	replacing a few centimetres of soil
Pathogens	low to medium	areas where there are ducks, geese, pets and other animals	use infiltration processes with higher concentrations of organic matter: avoid infiltration into very coarse soils if bacterial concentrations are high
Organic compounds	low to medium	transport, industry, pest control, manufacturing and more	addition of organic matter to the soil or medium

Qualitative indicators of groundwater piramo follow qualitative indicators of surface water in this article we are only dealing with the first part and that is surface water. Their impact on groundwater will be evaluated in a separate article.
On the territory of the Slovak Republic, stormwater management in urbanised areas is not yet comprehensively addressed by legislation and technical standards. This issue is partially tackled in the

Slovak Water Plan in accordance with Article 4.7(d) of the Water Framework Directive (2000/60/EC). This directive unreservedly supports measures for the construction of water retention facilities in urbanised areas. Additionally, Slovak Government Regulation No. 269/2010 Coll. of Laws (Z. z.) lays down requirements for achieving good water status, which includes some provisions related to stormwater management. The Slovak Government Decree No. 269/2010, specifically in § 9, points 1-3, sets out the requirements for the discharge of water from surface runoff into surface and groundwater. It specifies that when hazardous substances are presumed to be present in the surface runoff, necessary measures must be taken before any indirect discharge. According to Slovak regulations, surface runoff from paved areas refers to runoff from staging and assembly areas, industrial sites, and other locations where there is a risk of pollutant accumulation. The discharge requirements for surface runoff to surface waters are also outlined in the Water Act No. 364/2004 Coll. The Water Act No. 364/2004 Coll., in Section 2(i), defines storm (rain) water as "water from surface runoff" that does not soak into the ground and is discharged from the ground or external parts of buildings to surface and groundwater. Section 36(17) of the same act describes the management of stormwater from surface runoff, specifying the conditions under which it is permissible to discharge stormwater runoff to surface waters and the circumstances that necessitate the formulation of specific measures. Despite these provisions, there are significant shortcomings in Slovak regulations regarding stormwater management. One major deficiency is the lack of precise definitions for limit indicators of pollution when discharging stormwater from surface runoff (such as from roads, car parks, and roofs of buildings) into groundwater and surface water. This gap makes it challenging to effectively monitor and control the quality of discharged stormwater, potentially leading to environmental degradation and non-compliance with broader EU water management objectives. Effective stormwater management in urban areas is crucial for several reasons. Firstly, it helps to mitigate the risk of flooding, which can cause extensive damage to infrastructure, property, and natural ecosystems. Secondly, it plays a critical role in reducing the pollution load entering water bodies, thus protecting water quality and the health of aquatic ecosystems. Urban runoff often contains a variety of pollutants, including oils, heavy metals, nutrients, and sediments, which can have detrimental effects on water quality if not properly managed. Moreover, implementing comprehensive stormwater management practices contributes to the resilience of urban areas against climate change.

5 Conclusion

As climate change increases the frequency and intensity of extreme weather events, such as heavy rainfall, effective stormwater management becomes even more important. Green infrastructure solutions, such as green roofs, permeable pavements, and rain gardens, can enhance urban resilience by increasing water retention, reducing runoff volumes, and promoting groundwater recharge. In light of these challenges and opportunities, there is a growing recognition of the need for more detailed and robust legislative and technical standards for stormwater management in Slovakia. This includes setting clear pollution limits, adopting best practices for runoff management, and integrating green infrastructure solutions into urban planning. The legislative framework dealing with the quality of water from surface runoff on the territory of the Slovak Republic is described in detail in the chapter results and disscusion. By doing so, Slovakia can ensure that its urban areas are better equipped to handle stormwater, protect water quality, and enhance overall environmental sustainability. In conclusion, while current Slovak regulations provide a foundational framework for stormwater management, there is a critical need for more comprehensive and precise guidelines. Addressing these gaps will not only help to meet EU directives but also ensure that urban areas in Slovakia are resilient, sustainable, and capable of effectively managing the challenges posed by stormwater runoff.

Acknowledgements
This paper was supported by the Agency for Research and Development Support under contract No. APVV-22-0564" and by the Scientific Grant Agency of the Ministry of Education and Science of the Slovak Republic and the Slovak Academy of Sciences with the designation VEGA 1/0682/23.

References:

[1] YANNOPOULOS, S., ANTONIOU, G., KAIAFA-SAROPOULOU, M., ANGELAKIS, N.A. Historical development of rainwater harvesting and use in Hellas: A preliminary review. Water Science & Technology: Water Supply, 2017. Volume 17. Issue 4. 1022–1034. © IWA Publishing 2017. ISSN 1606-9749.

[2] LI, CH., LIU, M., HU, Y., SHI, T., QU, X., TODD WALTER, M. Effects of urbanization on direct runoff characteristics in urban functional zones. Science of the Total Environment. 2018, Volume 643. Pages 301-311. ISSN 0048-9697.

[3] PITTER, P. Hydrochémie, 4. aktualizované vydání. VŠCHT Praha. 2009. 580 s. ISBN 978-80-7080-701-9.

[4] LEE, J.Y., BAK, G., HAN, M. Quality of roof-harvested rainwater - Comparison of different roofing materials. Environmental Pollution, 2012. Volume 162. Pages 422-429. ISSN 0269-7491.

[5] LEE, J.Y., KIM, H., KIM, Y., HAN, M.Y. Characteristics of the eventmean concentration (EMC) from rainfall runoff on an urban highway. Environmental Pollution, 2011. Volume 159. Issue 4 Pages 884-888. ISSN 0269-7491.

[6] SOLLER, J., STEPHENSON, J., OLIVIERI, K., DOWNING, J., OLIVIERI, A.W. Evaluation of sesonal scale first flush pollutant loading and implications for urban runoff management. Journal of Environmental Management, 2005. Volume 76. Issue 4. Pages 309-318. ISSN 0301-4797.

[7] QIAN, W., QIONGAHUA, Z., XIAOCHANG, C.W., JIEGUANG, H., YUAN, G. Impact of key factors on heavy metal accumulation in urban road-deposited sediments (rds): Implications for RDS management. Chemosphere, 2020. Volume 261. Article No. 127786. ISSN 0045-6535.

[8] WANG, Q., ZHANG, Q., WANG, X.C., HUANG, J., GE, Y. Impact of key factors on heavy metal accumulation in urban road-deposited sediments (rds): Implications for RDS management. Chemosphere, 2020. Volume 261. Article No. 127786. ISSN 0045-6535.

[9] MELAND, S. Management of contaminated runoff water: current practice and future research needs . Brussels, Belgium. 2016. 84 p. ISBN 979-10-93321-18-9.

[10] HAYNES, M.H., TAYLOR, G.K., ROTHWELL, J., BYRNE, P. Characterisation of road-dust sediment in urban systems: a review of a global challenge. Journal of Soils and Sediments, 2020. Volume 20. Issue 12. Pages 4194–4217.

[11] WANG, S., HE, Q., AI, H., WANG, Z., ZHANG, Q. Pollutant concentrations and pollution loads in stormwater runoff from different land uses in Chongqing. Journal of Environmental Sciences, 2013. Volume 25. Issue 3. Pages 502-510. ISSN 1001-0742.

[12] SUMAN, S., SINHA, A., TARAFDAR, A. Polycyclic aromatic hydrocarbons (PAHs) concentration levels, pattern, source identification and soil toxicity assessment in urban traffic soil of Dhanbad, India. Science of The Total Environment, 2016. Volumes 545–546. Pages 353-360. ISSN 0048-9697.

GEOTECHNICAL ENGINEERING

STABILITY OF STRUCTURES DURING FLOOD

JOZEF HULLA[1], MARTIN BRČEK[2], ELIŠKA KUČOVÁ[3]

[1] Civil Engineering Faculty STU, Department of Geotechnics, Slovak Republic, Bratislava, jozef.hulla@stuba.sk

[2] Civil Engineering Faculty STU, Department of Geotechnics, Slovak Republic, Bratislava, martin.brcek@stuba.sk

[3] Civil Engineering Faculty STU, Department of Geotechnics, Slovak Republic, Bratislava, eliska.kucova@stuba.sk

1 Abstract

Between 2023 and 2024, devastating floods occurred worldwide, affecting every country. The primary cause was the exceptionally heavy rainfall, which resulted in widespread damage and the failure of various structures such as dams and flood defences (dikes), leading to numerous landslides. China and Libya were the most severely affected. The intense rainfall caused water levels to rise several meters above the ground, compromising building constructions due to uplift, flow pressure, and erosion. The knowledge gained from these events is crucial for us, as scientists and engineers, as it provides valuable insights and places a significant responsibility on our shoulders for minimizing structural failures during future flood events.

Keywords: floods, water levels, constructions, dams, dikes, protection.

2 Introduction

Intense rainfall can cause rising water levels in rivers, lakes, reservoirs, and land surfaces. Dam incidents and failures mainly occur during flood events [1]. Dams, reservoirs, and flood dikes are the most significant protective measures. These measures can prevent or significantly reduce water rises in protected areas near human settlements. Between 2023-2024, extreme flood events caused water levels to increase up to 5 meters above ground level, resulting in damage and numerous environmental accidents such as slope instability, damage to transportation routes and other infrastructures, and intense uplift, induced loads, and hydraulic flow effects.

The currently advanced construction techniques and technologies for building new structures and reconstructing older ones promise to ensure structure stability and resistance in flood conditions. While this may be costly in some cases, technical means are available, encompassing a wide range of tools, machinery, software, knowledge, and skills to mitigate the damage. This paper mainly focuses on geotechnical methods, which hold the potential to reduce the impact of floods significantly, instilling a sense of hope and optimism in the face of such challenges. It is assumed that the building structure is made of suitable materials and is stable under all loading conditions.

In the Department of Geotechnics at the Faculty of Civil Engineering of the Slovak University of Technology in Bratislava, there was a significant focus on studying inundated environments from 1999 to 2001. This was part of the project 'Geotechnical Problems of Flooded Areas', funded by the Scientific Grant Agency of the Ministry of Education, Science, Research and Sport of the Slovak Republic. The most important findings and recommendations are summarised in the book [2]. Following this, several publications and presentations were published at scientific and professional conferences both domestically and abroad.

3 Methods

The causes and consequences of flood situations are very broad. In this paper, we have decided to include only some selected information about the developments of flood-water levels, characteristic

failures of structures, conditions of their stability, and protective measures. Dams, water reservoirs and flood dikes protect buildings over large areas. However, dams and dikes need to be stable; then, there is no need to worry about the stability of individual structures. Even in such cases, however, it cannot be ruled out that some objects will require their own protective measures. Suitable stabilization measures need to be created in critical sections of watercourses where protective effects of dams, polders and flood dikes are not provided.

4 Results and discussion

4.1 Development of flood-water levels

The temporal development of water levels depending on discharge and some flood patterns in Bratislava are shown in Figure 1. In 1954, several flood protection dikes broke in Hungary. In 1965, dikes broke in our country near Čičov and Patince. In 1991, the Gabčíkovo waterworks were practically completed but not yet put into operation. In 2002, the maximum water level was the same as the maximum level in 1954. The mentioned figure also includes information about the surface ground level near the Slovak National Gallery in Bratislava (SNG; 138 meters above sea level) and the record of the millennial flood level (140 meters above mean sea level). Flood conditions on the Danube with various patterns usually occur during the summer months.

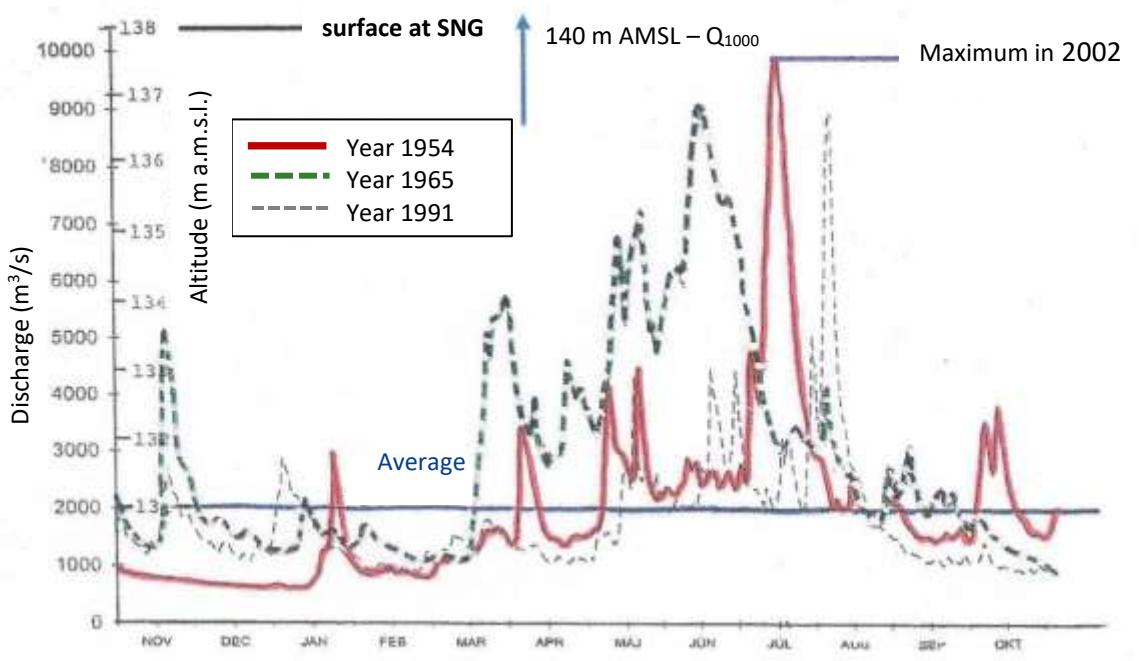

Fig. 1 Development of characteristic flood flows of the Danube in Bratislava according to SHMU data.

In Bratislava, on the wall of the Old Town Hall, the water level was marked when a millennial flood occurred on the Danube in February 1850. At that time, there were no flood protection measures in Bratislava, so water covered a significant part of the old town. Currently, Bratislava has permanent flood protection structures in the lowest areas and mobile flood barriers available to protect the city even from a millennial flood. Major cities worldwide have massive underground drainage systems, which allow significant amounts of water (pressure flow) to be managed during intense rainfall.

4.2 Examples of dams and dikes failure

Dam failures and dikes primarily occur due to structure errors during the planning and building phases. Failures and accidents of dams and dikes during their operation most often happen due to water overtopping the dam crest, leading to destructive effects (external erosion) on the downstream slopes.

Another common cause is suffusion, which occurs due to intense seepage flow in the foundation of dams and dikes.

The failure of the dam at Edenville Reservoir, Michigan, USA, following intense rainfall in 2020 is depicted in Figure 2. It is one of 10 documented dam failures worldwide captured on camera [3]. According to the final report [4], the cause of the failure was soil liquefaction in a section of the dam, which led to a loss of stability and subsequent failure of the downstream slope, resulting in the dam's collapse. During the rainfall, the water level in the reservoir rose approximately 1 meter above the maximum level reached in 1929. The water released from the reservoir caused overtopping and subsequent failure of the downstream Sanford Dam. Similarly, protective dikes can also breach during floods.

Fig. 2 The failure of the Edenville Dam, USA [3].

The breaching of dams during intense rainfall was the main cause of extensive damage of structures in Libya and Russia. The damages are among the largest caused by intense rainfall and floods worldwide between 2023 and 2024.

A different failure mechanism occurred with the Danube dikes during the flood in 1965 near Čičov and Patince. The hydrological regime indicated by the water level development, shown in Figure 1, points to a prolonged flood. The foundation layer of the dikes contains thick layers of gravelly soil. According to Figure 3, during the first stage, water emerged from the foundation layer to the surface at the downstream toe of the dikes; more than 2000 such springs were identified in Slovakia then. Due to increased hydraulic gradients, water flow velocities increased, and during the second stage of failure, a tunnel formed under the dike, concentrating the intense water flow from the Danube. Subsequently, during the third stage, the dike collapsed and was washed away. A trench was several meters deep below the original contact level of the dike with the foundation remained at the site. Approximately 10,000 houses made of unfired bricks were destroyed in the flooded area.

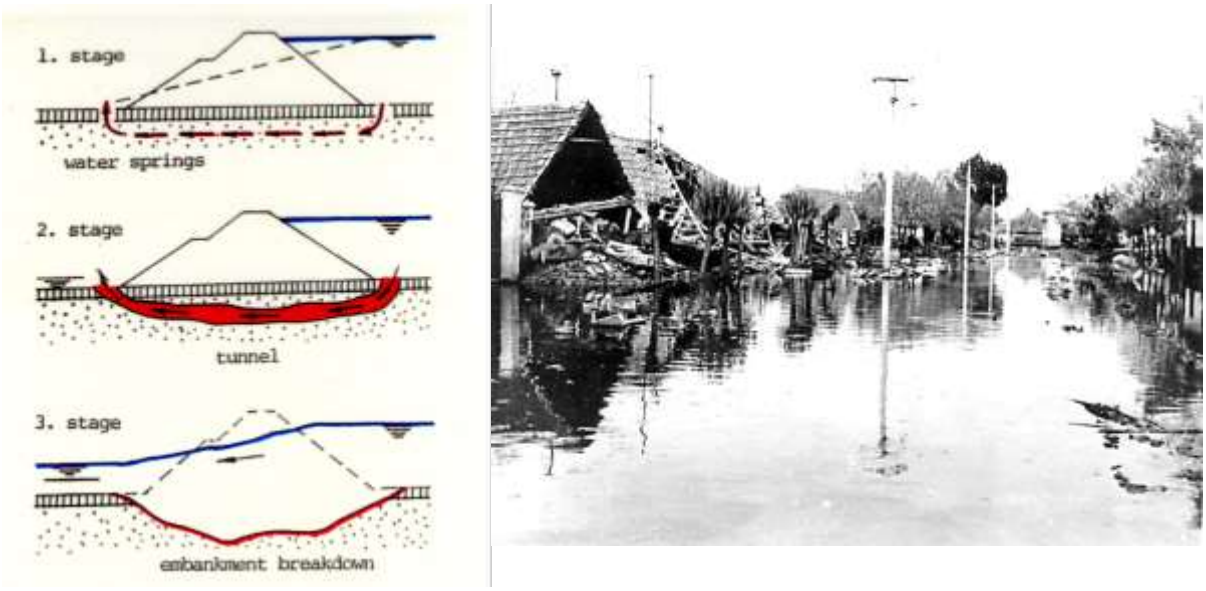

Fig. 3: Development of the breach of Danube dikes in 1965 and the damaged structures [8].

4.3 Characteristic failures of structures and buildings

The higher flood levels result in buoyant forces acting on structures, increasing vertical and horizontal hydrostatic and hydrodynamic loads. These forces can potentially lead to failures, damage, or even collapses. During floods, buoyant forces can lift and sweep away almost all securely sealed automobiles. Similarly, light and sealed structures can also be set in motion. This can destroy buildings or bridges at the nearest bridge when a building hits the bridge. Structures with several vertically segmented underground parts typically suffer from cracks.

When underground parts of buildings is flooded during a flood event, vertical loads on the foundation soil can significantly increase. For example, tall buildings approximately 100 meters high have a contact loading of around 300 kPa. When four underground floors and one above-ground floor are flooded with surface water, the contact stress increases by about 150 kPa. This is a significant addition for stability calculations, significantly when fine-grained soils above the foundation base hinder the buoyant forces.

The flood in Prague in 2002 caused incredible problems. According to reports [5], 18 metro stations and 19.6 km of tracks were flooded, and the damage to public transportation was estimated at 7 billion CZK. Such a metro disaster was reportedly unprecedented in the world.

Intense horizontal loads occur mainly in the initial stages of floods caused by heavy rainfall as water flows from surface areas. Their effects on structures gradually decrease in line with the reduction of hydraulic gradients of flowing surface water and the filling of internal spaces of structures with water. Extremely high river water levels increase flow forces, which cause bank erosion, disruptions to transportation networks, and the removal of soils around the foundations of bridge piers. Similarly, the increased levels of groundwater cause an increase in flow effects, which affects the stability of landslide areas. Landslides are often triggered by heavy rainfall, which can worsen the destabilising effects of flowing groundwater. The reduced shear strength of fine-grained soils at the shear plane represent also significant impact [6]. As shown in Figure 4 [7], structures near unstable slopes are at risk.

Fig. 4: Landslide threatening a family house [7].

4.4 Notes on building stability

The stability of buildings during destructive floods depends on their location, geology, loads, suitable materials, structural systems, and reliable foundations. Unsuitable locations for buildings are those near watercourses. All stability conditions must be met from the perspective of foundation of the structures. It has been noted that current construction and geotechnical technologies allow for stable structures even during extreme flood conditions. Figure 5 illustrates the spread of taller buildings and deep foundations, along with geological conditions and load states, which form the basis for stability calculations. It is assumed that the buildings will be constructed from suitable materials and that their structural systems will be safe for all load conditions.

The highest water level during a flood is an important basis for the calculations; it should correspond to flows close to a millennial flood. Verifying these data with the Slovak Hydrometeorological Institute is recommended. The structure's foundation, shown in the left part of Fig. 5, is spread, which assumes the presence of coarse-grained soil and that the groundwater level usually does not reach the surface of the area. It is further assumed that the structure has adequate waterproofing, at least to the proposed flood level, preventing surface water from entering its interior spaces.

The entire structure will be quickly uplifted as the water level rises to the design flood level. Under the water level, horizontal hydrostatic and hydrodynamic loads will act on the structure's walls. The hydrodynamic load component will be the highest immediately upon the arrival of the flood wave at the structure when the water level on its upstream side is near the surface of the area. The hydrodynamic component will very quickly decrease as the hydraulic gradient reduces due to the rising water level on the upstream side of the structure.

The vertical component of the load on the structure will mainly consist of its weight. If the structure was not waterproofed, the load from water would be added to the structure's weight.

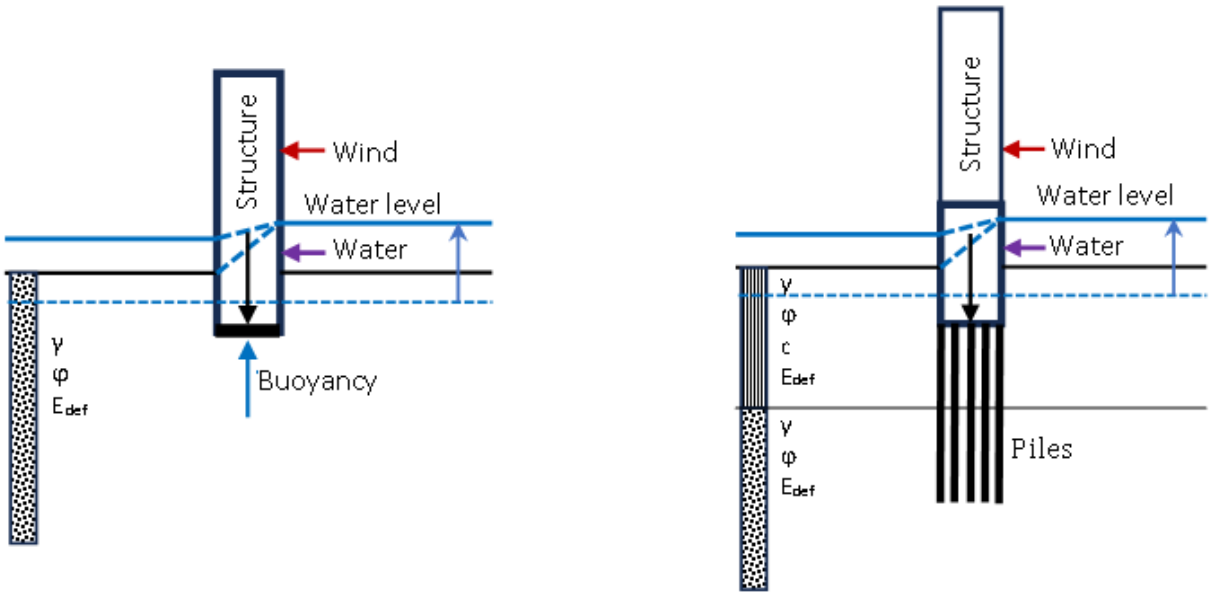

Fig. 5 Loads for designing stable foundation structures during extreme flood conditions.

If the waterproofing and sealing elements are extensively damaged during extreme rainfall, the water level inside the structure will quickly reach the level on the upstream side of the structure. Additionally, intense rain and extreme flood conditions may involve strong wind gusts (wind loads).
Uplift is crucial for the stability of lighter structures in flooded areas, which typically have foundations at shallower depths below the ground surface. These are usually older structures that were unprepared for the effects of extreme flood loads. Such objects are the most damaged or completely destroyed.

In Figure 5, a taller building is indicated on the right side, with a thicker layer of fine-grained soil at its base. Therefore, it would require deep foundations. Large-diameter drilled piles are commonly used, and for greater depths, sections of diaphragma walls created using hydro-cutter are dapplied. The same considerations as those stated for spread foundations apply to load-bearing conditions. The only debatable aspect is the effect of buoyancy. If the contact between the underground part of the structure and the surrounding fine-grained (practically impermeable) soil is reliably proofed, surface floodwater couldn't enter below the foundation slab above the heads of the piles, and buoyancy wouldn't apply. In the case of uncertain assumptions about tight contact between the structure and the soil, it is safer to consider buoyancy.

4.5 Protective measures and their effectiveness

Almost all dams in Slovakia have their bodies secured against seepage by internal or external sealing elements, beneath which sealing grouting curtains are installed. Flood protection dikes along the Danube have outer downstream sealing elements created in critical sections connected to sealing walls made of self-hardening suspensions reaching depths around 30 meters.

The sealing efficiency of dam and dike elements in Slovakia are regularly monitored by observing the behavior of water levels and flow velocities in observation boreholes installed in their bodies and foundations. In homogeneous environments, water level behavior data are usually sufficient. The most intense water flows occur at places with maximum water levels or maximum increases within the compared time intervals. Privileged seepage flow occurs in heterogeneous environments, concentrating into more permeable positions of degraded gravelly or fractured rock environments, from which sandy and dusty particles are flushed out. In such cases, more intense flow may also occur at positions with decreasing tendencies in groundwater flow levels. This reduces the filtration stability of soil and rock massifs on the slopes and foundations of dams and dikes, which may also cause the loss of structural

stability.
To monitor the flow velocities of groundwater and seepage water in the bodies and foundations of dams and dikes (as well as in construction pits, landslide areas, and water sources), indicator methods based on dilution and vertical flows of indicators in the permeable sections of observation boreholes are used. These methods were developed and successfully implemented at the Department of Geotechnics, primarily based on significant scientific studies by an international team of authors [8].
Based on the dilution of the indicator solution (NaCl, ^{131}I, and other substances), the filtration velocity of groundwater flow (v_f) is calculated using the following equation:

$$v_f = \frac{\pi\, d}{4\,\alpha\, t} \ln \frac{c_o - c_p}{c - c_p} \tag{1}$$

where d is the inner diameter of the observation tube in the permeable part of the borehole,
α – coefficient of the drainage effect of the borehole during horizontal flow,
c_o – artificial initial concentration (or volumetric activity) of the indicator,
c_p – natural concentration of the indicator,
c – concentration of the indicator at time t.

Equation (1) can only be used for horizontal water flow through the observation borehole.

Based on the vertical water flow in the borehole, the filtration velocity of water flow in the surrounding soil or fractured rock mass is calculated using the following equation.

$$v_f = \frac{\Delta q_v}{\overline{\alpha}\, d\, \Delta h} \tag{2}$$

where Δq_v is the increase or decrease in vertical flow in the section of the borehole with height Δh,
α – coefficient of the drainage effect of the borehole during vertical flow,
d – inner diameter of the observation borehole tube.
Vertical flow is also used to determine the conditions for the applicability of the dilution method; in this case, $\Delta qv = 0$.

The results of measurements using the mentioned methods are evaluated in the form of depth dependencies of filtration velocities, from which the maximum values can be easily determined. Internal suffusion involves the migration of fine-grained soil particles by the seepage forces. For practical purposes, these effects are assessed using limit states and critical velocities. Figure 6 graphically illustrates the results of filtration stability problems research, described in more detail in [10].

Soil fine-grained particles or small-sized fragments in rock fissures will remain stable and will not migrate if filtration velocities do not exceed the limit state velocity values. Fine-grained particles may or may not move when filtration velocity values are between the limit state and critical velocities. Beyond critical filtration velocity values, the migration of fine-grained particles becomes a lawful natural phenomenon. The limit state velocity value for gravelly soils is 7.10^{-4} m/s, and the critical value is 2.10^{-2} m/s. The limit state velocity for rocks is $1.2.10^{-3}$ m/s [11].

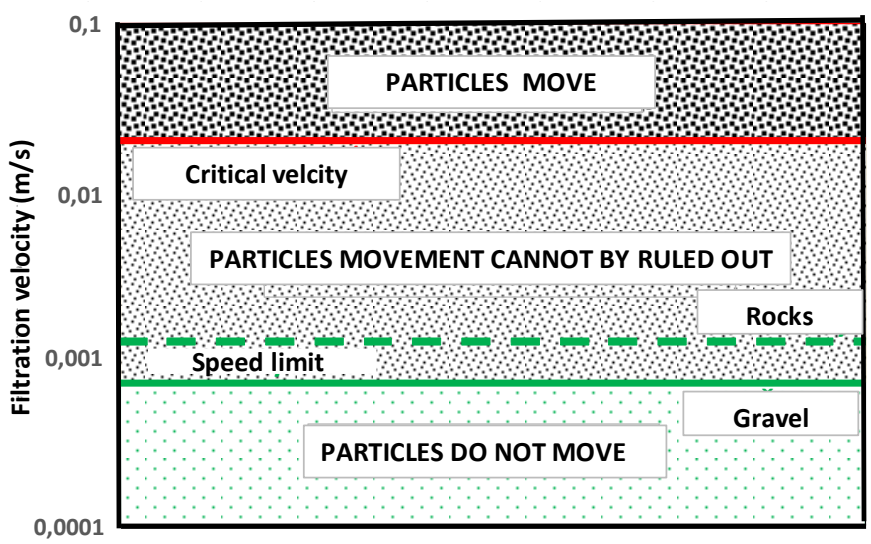

Fig. 6 Limit state and critical velocities for gravelly soils and fractured rocks [10].

The absolute maximum value for the monitored locality can be easily determined from the maximum filtration velocities for individual boreholes. The monitored dam or section of the dike will be reliably stable in terms of internal suffusion if the following conditions hold:

$$max\ v_f \leq v_{f\,medz} \tag{3}$$

(max v_f is the absolute maximum measured value of the filtration velocity, $v_{f\,medz}$ - limit state velocity)

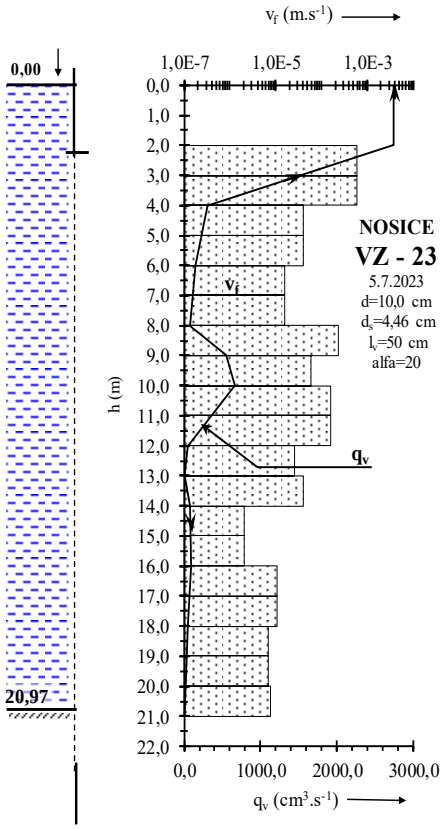

Main Data:

Measured on 05/07/2023
Water level at a depth of 0.00 m.
Start of perforation at a depth of 2.40 m.
End of perforation at a depth of 22.6 m.
Internal diameter of the observation tube 100 mm.
External diameter of the measure probe 44.6 mm.
Monitored section 50 cm.
Coefficient of borehole drainage influence 20.
Geology in the permeable part of the borehole - claystone.

Fig. 7 Results of vertical water flow measurements in borehole VZ 23 [12]

An example of measured values and evaluation of results in the bottom layers of the Nosice Dam is shown in Fig. 7 [12]. The Slovak Nosice Dam is problematic because there is a mineral water spring in

the subsoil of the gravity structure, which is aggressive to concrete. Therefore, special protective measures were taken during construction of the dam. The most intense water flow in the entire locality was found in borehole VZ-23. The sublayer of the borehole contains claystone, a fractured zone with fissure permeability, for which the limit state velocity value $v_{f\,medz}$ = 1.2*10^{-3} m/s applies. The absolute maximum measured filtration velocity was *max* v_f = 6*10^{-4} m/s at a depth of 2 to 4 m below the floor of the injection gallery. Based on this fact, it can be concluded that there are no unstable positions in the sublayer and around the Nosice Dam regarding internal suffusion. The filtration stability was not threatened by other factors such as the breach of the impermeable cover, contact and chemical suffusion, hydraulic and seismic liquefaction, and surface erosion of slopes.

Indicator methods for monitoring the stability of dams and dikes have been used in Slovakia for long time. The conditions of stability are determined by equation (3). The results from Nosice dam characterize one of the most intense flows of groundwater and seepage under Slovak dams and protective dikes so far.

5 Conclusion

Information about water level behavior during floods in recent years indicates that in Bratislava stretch of the Danube, their maximum levels were approximately 9 meters higher than before the floods reaching approximately the level of the terrain. In 1850, the maximum level was about 2 meters higher and reached the level of a thousand-year flood. Recently, maximum levels of flood water worldwide have been 5 meters above ground level, and even higher below breached dams. Maximum water levels are important for designing and evaluating the effectiveness of protective measures.

The knowledge gained from studying failures and collapses has enabled the creation of characteristic scenarios. Dams have breached due to excessively elevated water levels, which caused liquefaction and loss of soil shear strength, as well as overtopping the dam crest. Flood protection dikes have been breached due to the flushing out of sand from gravelly soils in the sublayer. In the conditions of Slovak Republic, accidents involving high dams have not occurred. Their safety is continuously monitored by technical safety supervision – Vodohospodárska výstavba š.p. Systematic monitoring of water levels and velocity flow regimes by indicator methods plays an important role in monitoring the safety of dams.

Structures were mainly damaged due to uplift, pressure from water flow, and deteriorated soil properties; these factors also contributed to the activation of landslide processes threatening buildings and transportation infrastructure. Intense water flow during high river levels causes erosion of riverbanks, failures of nearby transportation routes, scouring and undermining of bridge foundations, and building collapses after the flushing out of the soil from foundation subsoil. Flooding of underground spaces of transportation routes, basements or garages of buildings is also hazardous.

When solving stability problems, special attention must be paid to the effect of uplift, which manifests fully in the subsoil composed of permeable gravelly or sandy soils and fractured rocks under spread-founded buildings. Suppose the underground parts of the structures, reinforced concrete underground walls, or piles pass through relatively impermeable subsoil formed by silt and clay soils. In that case, the uplift on the structures is practically not manifested during relatively short periods of extreme flood conditions. During extreme flood conditions with high water levels above the terrain's surface, it is important to create conditions for the reliable transfer of intense water flow pressure in the early stages of flooding.

Protective measures can have a regional character when the intense effects of floods are contained in reservoirs, polders, and reliable dikes alongside the river. Structures in such protected regions do not require special stabilisation measures. If regional measures do not exist or are unreliable, the stability of each structure must be ensured individually. For these purposes, piles, anchors, sealing underground

walls, and improvement of subsoil properties (compaction, grouting, or other means) can be used. The basic requirement is designing a stable structure below the maximum flood level. Particularly, considered maximum flood level during the design phase is also problematic. Failures of dams, dikes, and other hydraulic structures during extreme floods in recent years have shown that maximum flood levels were not correctly considered in many cases or were not considered at all.

Acknowledgements
The authors of the article gratefully remember the deceased heads of the current Department of Geotechnics, Prof. Ing. Pavol Peter, DrSc., for his significant work in the field of filtration stability and radioindicator methods, as well as Doc. RNDr. Arnold Nemčok, CSc., for his pioneering work in the field of landslide processes. These issues remain relevant in the department's current scientific and professional activities and construction practice. The project presented in this article is supported by grant project VEGA-1/0745/21.

References:

[1] Kotaška, S., Říha, J.: Dam incidents and failures – Cases in the Czech Republic, Slovak Journal of Civil Engineering, Vol. 31, 2023, No. 1, 22 – 33.
[2] Turček, P., Hulla, J.: Zakladanie stavieb (Foundation engineering), 1st edition, Jaga, Bratislava, 2005.
[3] 10 Massive Dam Failures Caught on Camera, https://www.youtube.com/watch?v=lYbFLBqJXVc, 30.05.2024.
[4] France, J. W., Alvi I. A., Miller, A. C., Williams, J. L., Higinbothan, S.: Investigation of Failures of Edenville and Sanford Dams, Independent Forensic Team, Final Report, 2022.
[5] Floods 2002: Největší katastrofa svého druhu na světě …, (in Czech) https://zoom.iprima.cz/zajimavosti/povodne-2022-praha-170193, 30.05.2024.
[6] Nemčok, A.: Zosuvy v slovenských Karpatoch (Landslides in Slovak Carpathians), 1st edition, Veda, Bratislava,1982.
[7] Jánová, V., Házyová, K., Danková, B., Paluchov, K.: Svahové deformácie (Slope deformations), 1st edition, SAŽP, Banská Bystrica, 2021.
[8] Peter, P.: Kanálové a ochranné hrádze (Chanel and protection embankments), 1st edition, SAV, Bratislava, 1975.
[9] Halevy, E., Moser, H., Zellhofer, O., Zuber, A.: Borehole dilution techniques: a critical review, Isotopes in Hydrology, IAEA, Vienna, pp. 531 – 564, 1967.
[10] Hulla, J., Cábel, J.: Analýza kritérií pre filtračnú stabilitu (Analysis of criteria of filtration stability), Inžinierske stavby, vol. 45, iss. 4-5, pp.145-149, 1997.
[11] Ronžin, I. S.: Nekotorye kriterii ocenki fiľtracionnoj pročnosti osnovanij gidrotechničeskich sooruženij (Some criteria for evaluating the filtration strength of the foundations of hydrotechnical structures), Gidrotechničeskoe stroiteľstvo, vol. 24, iss. 7, 1974, 24-27.
[12] Bednárová, E., Hulla, J., Grambličková, D., Brček, M., Škvarka, J., Václavik, P., Veleba, H.: Water Structure Nosice. Seepage analysis in the dam foundation WS Nosice. Expertise. SvF STU, 2023

MEASURING FILTRATION VELOCITIES IN THE OBSERVATION WELLS OF DAM AND THEIR TIME DEVELOPMENT

JURAJ ŠKVARKA[1], JURAJ CHALMOVSKÝ[2]

[1] *Faculty of Civil Engineering STU in Bratislava, Slovakia, juraj.skvarka@stuba.sk*

[2] *Faculty of Civil Engineering, Brno University of Technology, Czech Republic, chalmovsky.j@fce.vutbr.cz*

1 Abstract

Special methods for measuring filtration velocities can be used to monitor groundwater flow and seepage flow in dams' bodies and subsoil. In Slovakia, single-well indicator methods are most commonly used to measure water flow velocities. For monitoring vertical water flow in wells, a submerged device is used, which incorporates a dosing unit with pneumatic-hydraulic control of the injection of the indicator and two conductometric sensors positioned below and above the injection point. The indicator is often sodium chloride in powder form or an aqueous solution. The submerged device is connected to a computer converter via a multi-core cable, and then to a portable computer. On the computer screen, concentration curves can be directly monitored, and the time at which maximum concentration occurs (peak time) can be determined.

Keywords: groundwater, seepage, vertical water flow, concentration curve, observation well, filtration stability

2 Introduction

This paper focuses on measuring filtration velocities by monitoring the vertical flow of water in a well. The correct interpretation of these measurements has a significant impact on the results of these measurements, which are used to assess the safety of the water structure, mainly from the point of view of filtration stability. The output of the measurement are concentration curves, from which the filtration velocities are then calculated. The paper analyses and compares concentration curves at Veľká Domaša dam at different times under the same loading state, from which the filtration velocities are then derived. The Veľká Domaša Dam was built between 1962 and 1967. The maximum height of the dam above the terrain is 25.4 m, and above the foundation joint is 35.0 m. The reservoir was created by damming the Ondava River valley with a heterogeneous earth dam with internal sealing (Figure 1). The stabilization prisms of a heterogeneous earth-fill dam were constructed of alluvial gravel. Internal inclined sealing consists of sandy loams, which, in contact with stabilizing prisms, are protected by a single-layer filter. The dam is connected with bedrock by a wide sealing tooth and a concrete grouting tunnel. The reservoir is located in the geological environment, which consists of Paleogene rocks (Magura flysch) and quaternary sediments [1].

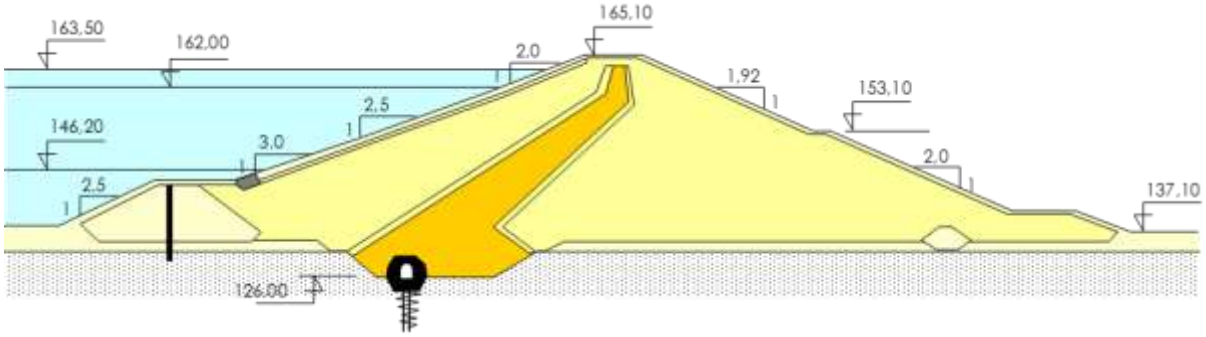

Figure 1. The cross-section profile of the dam Veľká Domaša

3 Methods

Special methods for monitoring groundwater flow can be broadly divided into indirect (non-invasive) and direct (invasive) methods. Indirect methods include geophysical measurements, aimed at obtaining preliminary information on geological and physical properties of the rock environment by studying physical fields. Specifically, geo-electrical measurements are used for groundwater flow measurements. Accurate interpretation of results is essential in geophysical measurements, as anomalies might lead to false interpretations, requiring verification by direct measurements. Direct measurements are appropriate for verifying the filtration stability of dams and their subsoil [2]. In Slovakia, single-well tracer methods are commonly used to measure groundwater flow velocities, with sodium chloride in powder or aqueous solution serving as the tracer.

3.1 Method for Monitoring Vertical Water Flow in Wells

A submersible device with a built-in tracer dispenser and two conductivity sensors, placed above and below the injection point at a distance of l_v = 0.5 m, is used for vertical water flow monitoring. The tracer is a sodium chloride solution.

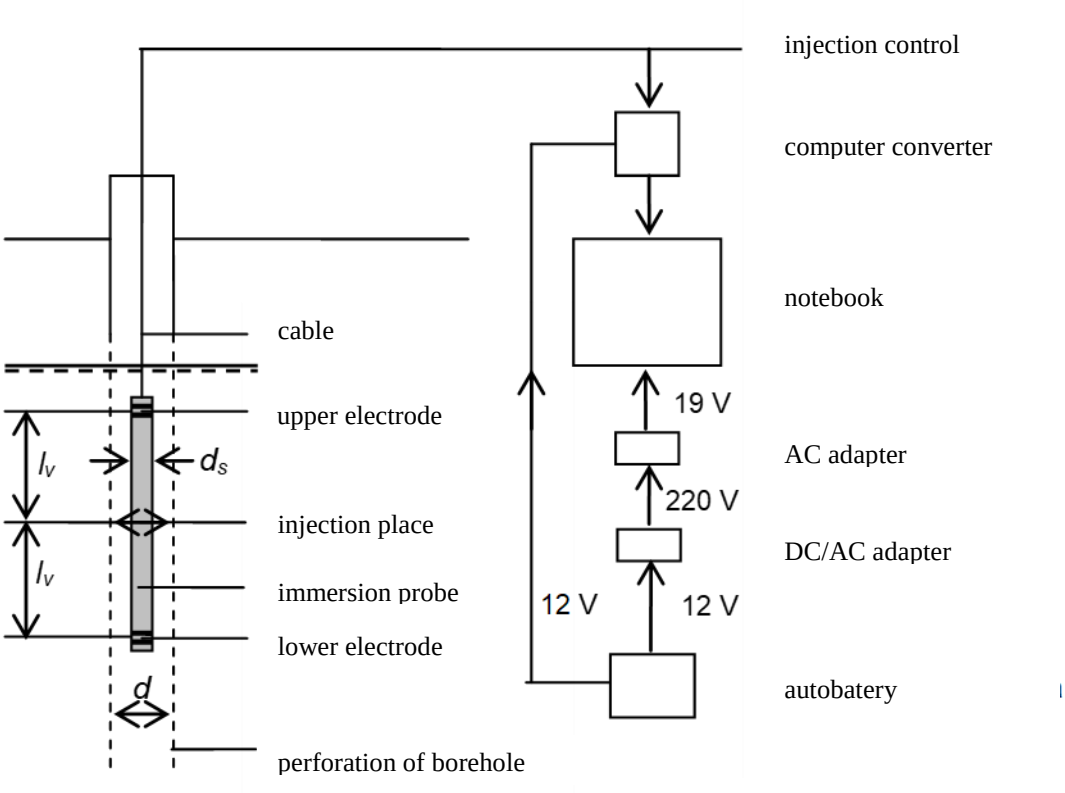

Figure 2. Setup of devices for measuring vertical water flow in boreholes

The submersible device is connected to a computer converter and then to a portable computer, where concentration curves are directly monitored, and the peak concentration time t_{vr} is determined. From the results of calibration laboratory tests performed for our measuring devices [2], the calculation time equation was determined t_v, which should be used to calculate the average value of the vertical velocity v_v [2].

$$t_v = 0.266\, t_{vr}^{1,474} \tag{1}$$

$$v_v = \frac{l_v}{t_v} \tag{2}$$

where: t_{vr} is the peak concentration time (s),
l_v is the distance between the tracer injection and the corresponding electrode (cm).

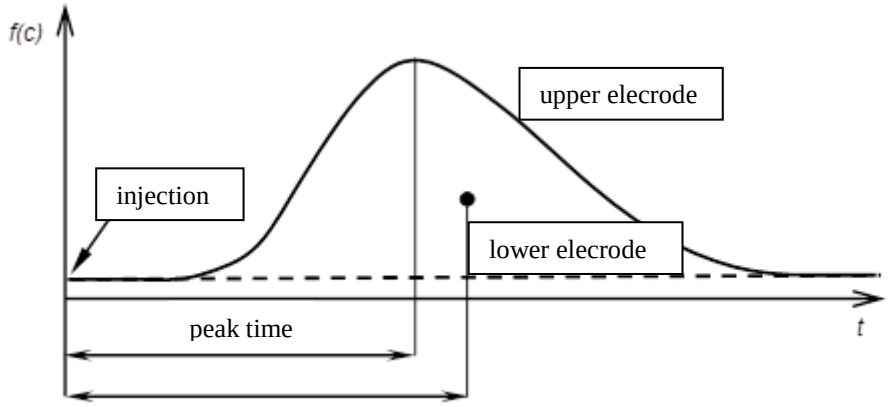

Figure 3. Concentration curve for evaluating measurements of downward vertical flow, where c - concentration, t - time

Vertical flow is determined from the continuity equation:

$$q_v = v_v\, A = v_v \frac{\pi(d^2 - d_s^2)}{4} \tag{3}$$

where: A is the cross-sectional flow area of the observation well (cm²),
d the inner diameter of the observation well (cm),
d_s the outer diameter of the observation well (cm).

Measurements are repeated at appropriate intervals to evenly cover the entire saturated permeable part of the borehole, allowing graphical representation of the depth dependency of vertical flows:

$$q_v = f\,(h) \tag{4}$$

The relationships of dependency of vertical flows can be interpreted as follows:

- increasing vertical flow in the direction of flow indicates water entering the borehole,
- decreasing vertical flow indicates water exiting the borehole,
- constant vertical flow around the borehole indicates a relatively impermeable environment.

From the results of vertical water movement measurements in the well, which is due to the connection of different pressure horizons, the filtration velocity of water flow in the surrounding environment, approximately in the horizontal direction, is determined using [3]:

$$v_f = \frac{\Delta q_v}{\bar{\alpha} d \Delta h} \tag{5}$$

where: v_f is the filtration velocity (cm·s⁻¹),
Δq_v is the increase or decrease of vertical flow in the segment of the borehole of height Δh (cm³·s⁻¹),
$\bar{\alpha}$ is the well drainage influence coefficient for vertical flow ($\bar{\alpha}$ = 2 to 20),
d is the inner diameter of the observation tube (cm).

In homogenous gravel aquifers usually can be assumed α = 2 [4]. In more heterogeneous karst or fractured aquifers, α can differ at a small scale, depending on the permeabilities of the surrounding rock.
Calculations of filtration velocities according to previous equations are graphically represented in depth dependencies. The average filtration velocity for the respective well is determined from the following relationship and is usually a vector, which are determined from hydroisohypses, constructed on the basis of measured water levels in boreholes.

4 Results and discussion

Special measurements of the filtration velocities in all observation points are regularly carried out at the Veľká Domaša dam. These measurements are part of assessing the reliability of the anti-seepage measures in the dam body and its subsoil, and also to evaluate the filtration stability of the dam body and its subsoil over time. Currently, there are 63 observation points at the dam where water levels and filtration velocities can be measured (Figure 4). In this paper, we present only the results from borehole S3 and SJ, with analysed data from the year 2005 [5], 2008 [6], 2018 [7], and 2022 [8]. Measurements were also carried out before 2005, but the results of the concentration curve measurements are no longer available.

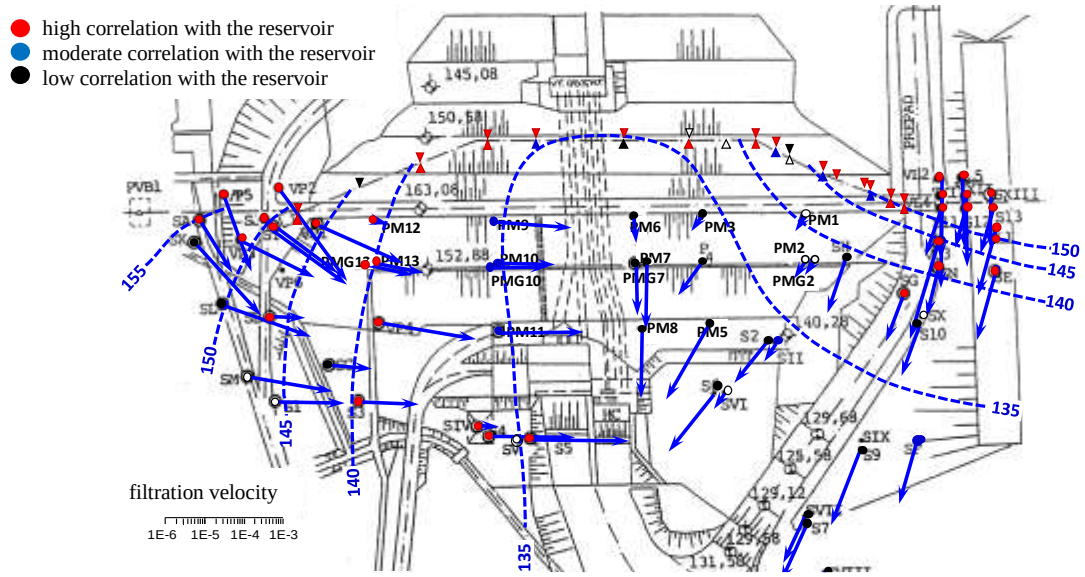

Figure 4. The scheme of the dam Veľká Domaša layout with monitoring boreholes

To be able to compare the measurements, it was necessary to select measurements with approximately the same boundary conditions – at least the water level in the reservoir and the water level in the downstream channel. Besides the reservoir and downstream channel water levels, several other factors influence the measurements, which cannot be controlled, such as daily precipitation accumulation, reservoir water level fluctuations, etc. The boreholes S3 and SJ are located on the right slope of the dam in the flow direction. These boreholes were selected due to the calculated high correlation of water level in boreholes with the water level in the reservoir (Figure 4) for selected time periods. The diameter of borehole S3 is 8 cm, and for SJ, it is 9 cm. The start of perforation for borehole S3 begins at 10.60 m and for SJ at 8.00 m, both extending to the bottom. Hence, the water level is within the perforated section.
Table 1 presents the water level during measurements and the water levels in boreholes S3 and SJ, selected for analysis due to their high correlation with the reservoir water level over the recent period. However, it should be noted that the correlation is indicative and applies only to a specific observed period.

Table 1. Water levels during measurements of filtration velocities

Date of measurements	19.-20.6.2022	21.-22.6.2018	1.-2.5.2008	1.-2.5.2005
Reservoir water level (m a.s.l.)	157.5	160.0	159.7	161.2
Water level in the downstream channel (m a.s.l.)	133.1	133.0	133.1	132.7
Water level in borehole S3 (m) below borehole cap	12.95	10.60	10.90	7.90
Water level in borehole SJ (m) below borehole cap	18.68	15.54	15.75	13.53

Measurements are typically carried out at 2 m intervals, depending on the water column and the water level in the borehole. The duration of each measurement depends on the operator when determining the peak time, usually the time is not longer than 5 minutes at one depth level.
The following figures illustrate the measurement results from borehole S3 at a depth of 13.0 m and from borehole SJ at a depth of 21.5 m. From the measurements, it can be observed that the concentration curves have a similar trend of development, but the read peak times may slightly differ for individual measurements. Different peak times read from the concentration curves are influenced by various factors mentioned earlier, as well as the amount of injected tracer, which may vary. This could be due to the manual injection of the tracer and also depends on the pressure in the pressure bottle and the depth of the borehole and the water column above the probe.

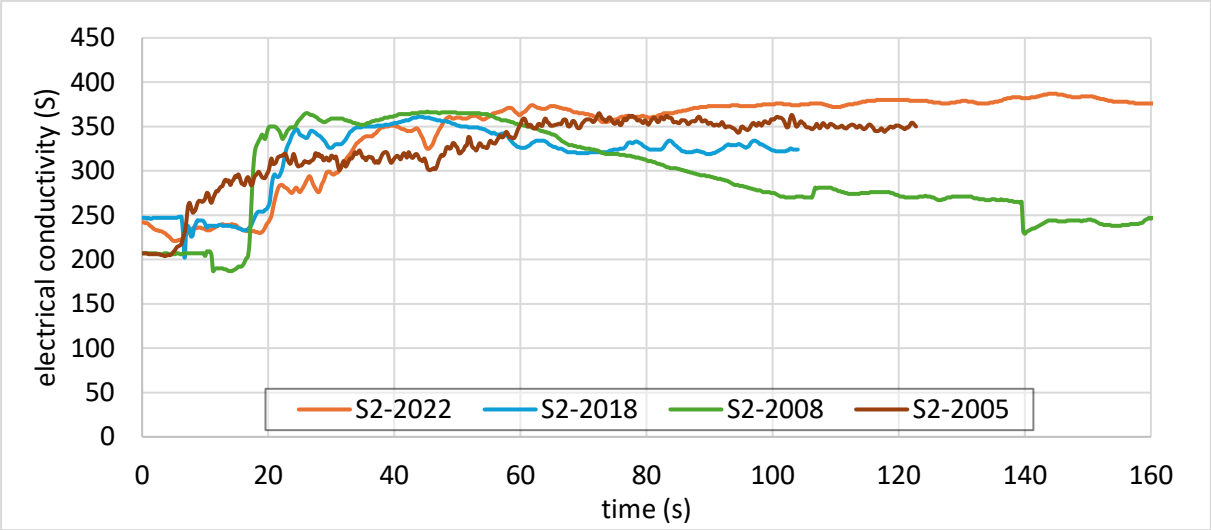

Figure 5. Results of concentration curve measurements in borehole S3 at a 13 m depth

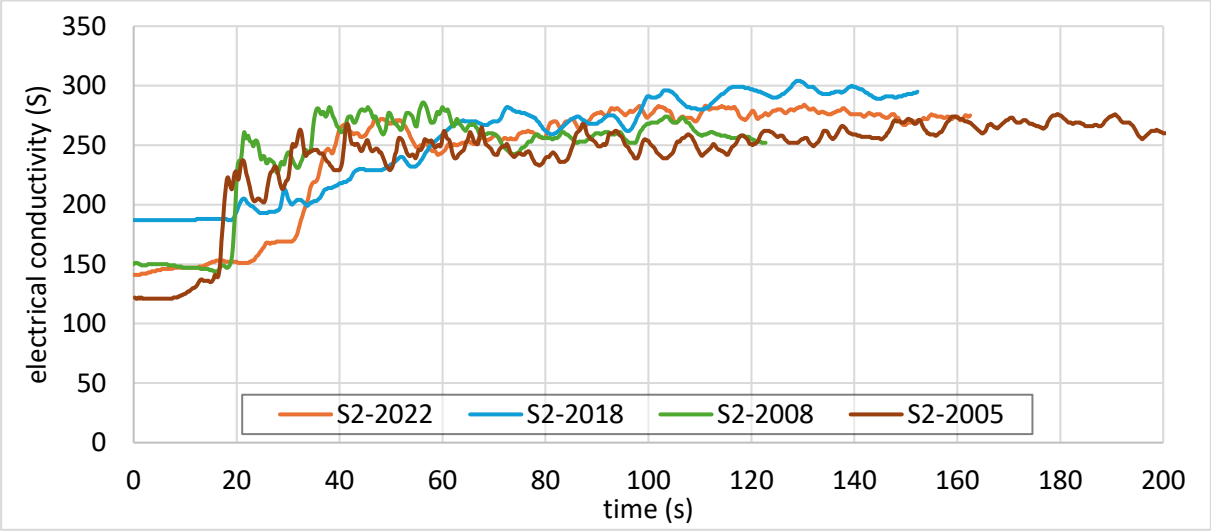

Figure 6. Results of concentration curve measurements in borehole SJ at a 21.5 m depth

The results of vertical flow and filtration velocity calculations are presented in the following figures. From the measurement evaluation, it can be observed that the magnitude of vertical flow may vary within individual measurements. Comparing individual measurements, it can be inferred for concentration curves that the important aspect is the shape or trend of the curves' development, based on which the peak time can be reliably determined. The actual values of measured concentrations are not as crucial because they are influenced by the mineralization of groundwater and infiltrating waters, which can change over time. The calculated filtration velocities at different depths show very good agreement between individual measurements. For this type of geophysical measurement, a dispersion of values within the same order can be considered as very good agreement.

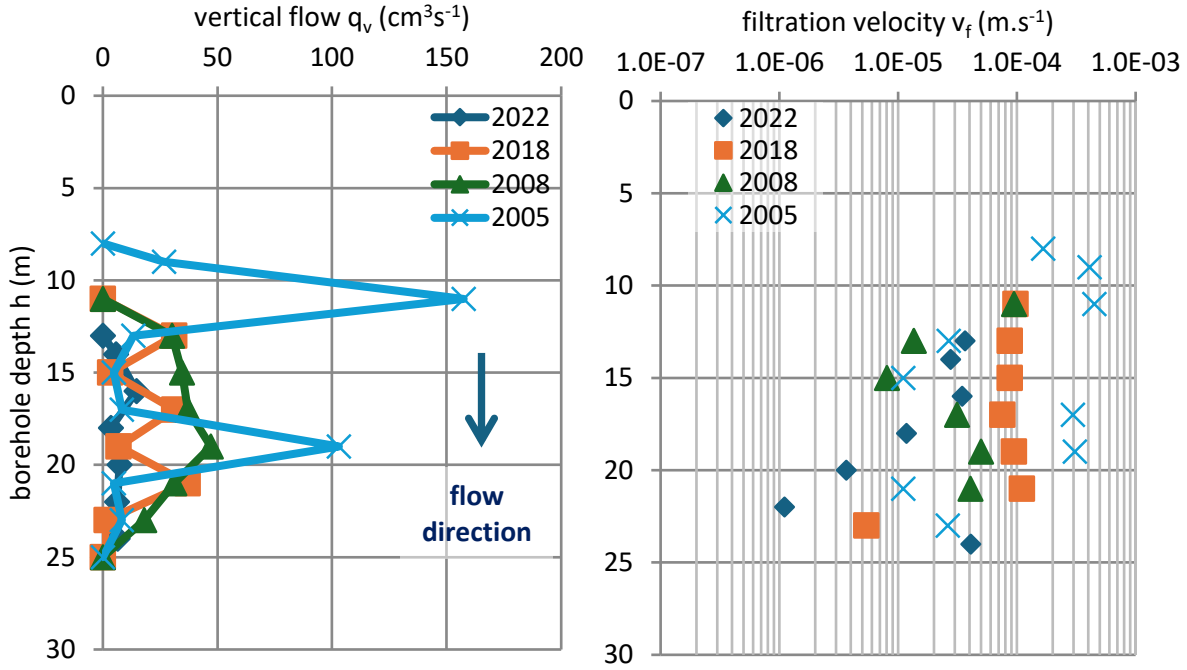

Figure 7. Vertical flow and calculated filtration velocities in borehole S3

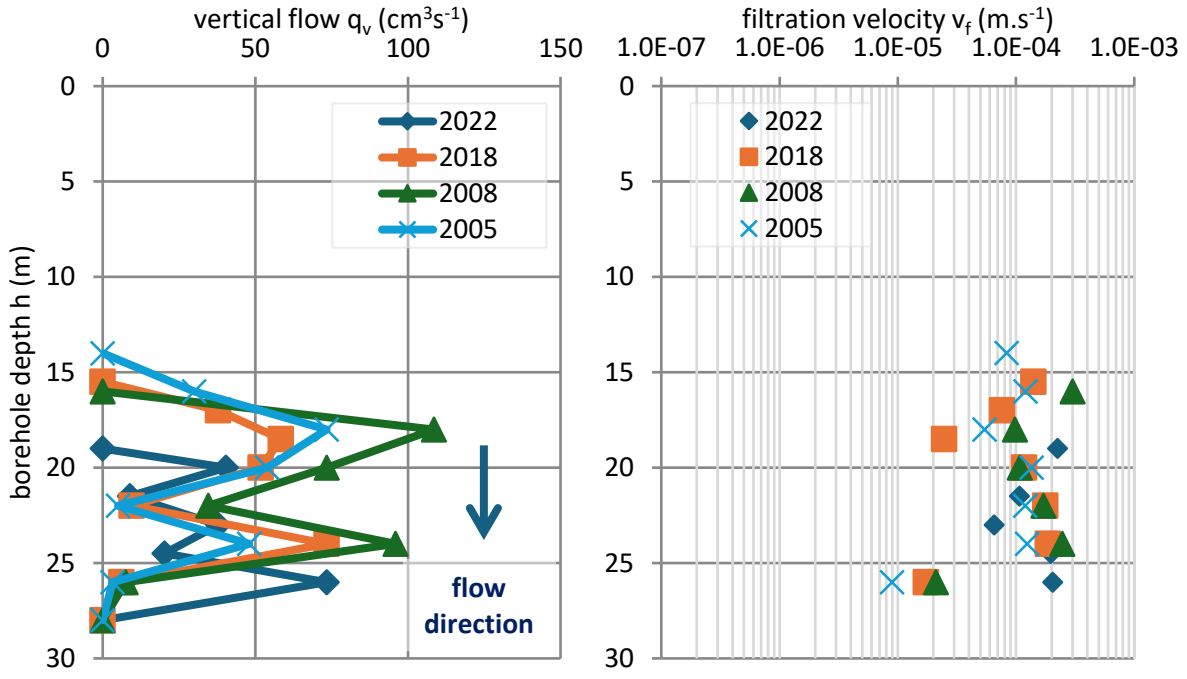

Figure 8. Vertical flow and calculated filtration velocities in borehole SJ

The individual results of the measurement evaluation in borehole S3 (Figure 7) show good agreement, despite varying vertical velocities, except for the measurements in 2005 at higher elevations and in 2022, mainly at lower elevations. In 2005, measurements were also performed at higher elevations because the water level in the borehole was approximately 3 m higher than in the measurements in 2008 and 2018 and 5 m higher than in 2022. The measurements in this borehole may also be influenced by precipitation and slope waters, which are not closely addressed in this paper. Furthermore, we note more significant differences at lower depths in 2022. These differences may also be caused by boundary conditions, as during the measurements, the water level in the borehole was approximately 2 m lower than in 2018 and 2008. Additionally, differences may arise because measurements in 2022 were carried out at different depths (even depths in 2022 - 14, 16, 18, 20, and 22 m) compared to previous years (odd depths - 13, 15, 17, 19, 21, and 23 m).
In borehole SJ (Figure 8), very good agreement was achieved between individual measurements, except for the last depth in 2022. However, from the development of the concentration curves, it was not possible to determine the peak time. In this paper, concentration curves from these depths are not presented due to paper limitations. When the peak of the concentration curve is not entirely clear, it is advisable to select the most unfavourable peak time value so that the filtration velocity is as high as possible. Because if the highest possible calculated filtration velocity does not reach the limit values of filtration velocities, the filtration stability of the rock environment is ensured [9, 10].

5 Conclusion

The essence of assessing filtration stability lies in the maximum filtration velocities measured in the observation objects of the investigated environment. The calculated filtration velocities from special geophysical measurements should then be compared with the acceptable (limit) velocities. If the limit velocities are exceeded, conditions for the development of internal suffusion may be created. In the geological conditions of the Veľká Domaša dam, long-term attention has been paid to the potential risk of internal suffusion within the dam body and its subsoil, as well as the filling of cracks in the bedrock. When assessing the risk level of its occurrence, hydraulic criteria, represented by permissible (limit) filtration velocities, are taken into account [11]. These threshold values were determined based on the results of geological and geotechnical investigation, mainly from water pressure tests performed during the construction of Veľká Domaša dam. These values are as follows [8]:

- cover layers and stabilization prisms (Quaternary deposits) $v_{fp,kvart.} = 6.10^{-4}$ to 9.10^{-3} m.s^{-1},
- Paleogene with a predominance of sandstones (valley slopes) $v_{fp,pal,p} = 1.2.10^{-3}$ to 4.10^{-3} m.s^{-1},
- less permeable Paleogene with a predominance of claystones $v_{fp,pal,p.il} = 1.2.10^{-4}$ to 4.10^{-4} m.s^{-1}.

This paper presrents only selected measurements along with their overall evaluation for chosen boreholes. It is clear that measurements could vary over time due the influence of several factors. Therefore, it is advisable to carry out such measurements continuously and monitor the trend of calculated filtration velocities. An increasing trend in filtration velocities and exceeding the established limit values may indicate a threat to the filtration stability of the rock environment. The presented boreholes are located on slopes where the limit velocities ranges from $1.2.10^{-3}$ to 4.10^{-3} m.s^{-1}. From the evaluation, it is evident that these velocities were neither reached nor exceeded, and the calculated filtration velocities over time have a relatively stable character. Therefore, it can be concluded that filtration stability is not threatened in the given boreholes. The same applies to other boreholes not presented in this paper, thus for entire water structure based on the latest measurements from 2022. This report concludes that, based on the current development of maximum filtration velocities and their comparison with permissible values for the Quaternary and Paleogene formations, there is currently no risk of internal suffusion within the dam body, its foundation, and the adjacent valley slopes.

Acknowledgments
The project presented in this article is supported by grant project APVV DS-FR-22-0032.

References:
[1] BEDNÁROVÁ, E., et. al.: Influence of climate change on the water management of Veľká Domaša reservoir. In Proceedings of the second SLOCOLD-MACOLD Symposium on topic Water reservoirs, 2020, Skopje - Ljubljana., 2020, ISBN 978-608-65373-9-5.
[2] Drost W, Klotz D, Koch A, Moser H, Neumaier F, Rauert W (1968) Point dilution methods of investigating ground water flow by means of radioisotopes. Water Resour Res 4:125–146. https://doi.org/10. 1029/WR004i001p00125
[3] Fahrmeier, N., Goeppert, N. & Goldscheider, N. Comparative application and optimization of different single-borehole dilution test techniques. Hydrogeol J 29, 199–211 (2021). https://doi.org/10.1007/s10040-020-02271-2
[4] Hall SH (1993) Single well tracer tests in aquifer characterization. Groundw Monit Remediat 13:118–124. https://doi.org/10.1111/j. 1745-6592.1993.tb00443.x
[5] BEDNÁROVÁ E. a kol.: VS Veľká Domaša. Posúdenie filtračného režimu v telese a v podloží priehrady v roku 2005. Správa pre SVP, š.p., PBaH Košice, SvF STU Bratislava 2005.
[6] BEDNÁROVÁ E. a kol.: VS Veľká Domaša. Analýza vývoja filtračného režimu v telese a v podloží priehrady v roku 2008. Správa pre SVP, š.p., PBaH Košice, SvF STU Bratislava 2008.
[7] BEDNÁROVÁ E. a kol.: VS Veľká Domaša. Analýza vývoja filtračného režimu po zabudovaní nových pozorovacích objektov. Správa pre SVP, š.p., PBaH Košice, SvF STU Bratislava 2018.
[8] BEDNÁROVÁ E. a kol.: VS Veľká Domaša. Posúdenie bezpečnosti priehrady z hľadiska filtračnej stability. Správa pre SVP, š.p., PBaH Košice, SvF STU Bratislava 2022.
[9] C. F. Wan a R. Fell, Experimental investigation of internal instability of soils in embankment dams and their foundations. New South Wales, 2004.
[10] J. Hulla a J. Cábel, "Analýza kritérií pre filtračnú stabilitu", Inžinierske stavby, vol. 45, issue 4–5, pp. 145–149, 1997.
[11] J. Hulla a E. Bednárová, "Zdokonalené indikátorové metódy na sledovanie rýchlostných zložiek priesakových režimov v podložiach priehrad", XXXI. Přehradní dny, vol. 2, 182 pp., 2008.

CLIMATE CHANGE AND FLOOD RISK MANAGEMENT

ANALYSIS OF TWO NORMAL PERIODS IN TERMS OF BASIC HYDROMETEOROLOGICAL ELEMENTS

DANA PAVELKOVÁ[1*], BRANISLAV KANDRA[1], ANDREJ TALL[1],
HELENA HLAVATÁ[2], MILAN GOMBOŠ[1]

[1] *Institute of Hydrology, Slovak Academy of Sciences, Slovak Republic, E-mail: pavelkova@uh.savba.sk*

[2] *Slovak Hydrometeorological Institute, Regional Office Košice, Slovak Republic*

1 Abstract

Air temperature, precipitation and potential evapotranspiration are analyzed in two consecutive normal periods (1961–1990) and (1991–2020) to quantify climate change and its trends. Descriptive statistics methods were applied for the analysis of climatic elements. The analysis was implemented in the meteorological station Milhostov on the East Slovak Lowland. The above analysis shows that in the normal period (1991–2020) there is a significant trend of increasing temperature and potential evaporation. Precipitation increased slightly, statistically insignificant. From this, it is possible to conclude about the increased drying of the natural environment in the mentioned period.

Keywords: air temperature, precipitation, potential evapotranspiration, normal periods

2 Introduction

In recent decades, climatic changes have been observed in the atmosphere [1], [2], [3]. These are manifested by an increase in the frequency of occurrence of extreme hydrological events. In order to quantify climate change, it is necessary to identify the development of basic meteorological elements in different normal periods. The minimum representative length of the normal period is a 30-year series of measurements. The World Meteorological Organization (WMO) [4] stipulated that the periods 1901–1930, 1931–1960 and 1961–1990 will be used for global comparison of normals, [5]. The World Meteorological Organization has recommended that the 30-year standard reference periods be updated every decade to better reflect the changing climate. The WMO meeting [6] recommended that a new 30-year baseline be adopted globally, for the reference period 1991–2020.

Basic meteorological elements affected by climate change include air temperature, precipitation, and evaporation. At the same time, they are decisive elements that influence hydrological processes in the system atmosphere – plant cover – unsaturated zone – groundwater, [7], [8], [9], [10], [11]. In recent decades, an increase in the average air temperature has been recorded almost all over the Earth. Atmospheric precipitation is an inseparable factor influencing the weather, the climate of the territory, the water regime of the unsaturated zone of the soil and the availability of water in this environment. Water from precipitation enters the soil through the process of infiltration. In the opposite direction, i.e. water gets from the soil to the atmosphere by evaporation. Evaporation of water is a natural thermodynamic process in which a solid or liquid turns into a gas. In the hydrological cycle, it is one of the decisive elements regulating energy flows. Evaporation of water from plants, water surface and soil is called evapotranspiration. The maximum value of evaporation from the soil with vegetation that is possible under the given meteorological conditions is the potential evapotranspiration (ET_{pot}). Evaporation is characterized in this paper through potential evapotranspiration [12], [13], [14].

The aim of the contribution is to compare air temperatures, precipitation and evaporation in the selected meteorological station Milhostov, on the East Slovak Lowland (ESL) in the normal periods 1961–1990 and 1991–2020.

3 Methods

The analysis is based on the hypothesis that the mentioned climatic elements will increase in the normal period (1991–2020). Two normal periods NP1 (1961–1990) and NP2 (1991–2020) are selected for comparison. Annual and monthly totals of precipitation (*P*), annual and monthly totals of potential evapotranspiration (ET_{pot}) and average annual and monthly air temperatures (*T*) were compared in the mentioned normal periods. The mentioned climatic elements are compared in the meteorological station Milhostov (48°40′11″; 21°44′18″). The station is located in the central part of the East Slovak Lowland. The station is characterized by rapid change of air masses in each season and developed cyclonic activity [15], [16]. Complete, uninterrupted measurements of selected climatic elements are available for NP1 and NP2 in the mentioned station. Potential evapotranspiration was calculated according to [12]:

$$ET_{pot} = \frac{0.408\,\Delta\,(R_n - G) + \gamma \frac{900}{T+273} u_2\,(e_s - e_a)}{\Delta + \gamma\,(1 + 0.34\,u_2)} \quad (1)$$

where:
ET_{pot} – reference evapotranspiration [mm day^{-1}],
R_n – radiation balance of the crop surface [MJ m^{-2} day^{-1}],
G – heat flow in the soil [MJ.m^{-2} day^{-1}],
T – average daily air temperature at a height of 2 m [°C],
u_2 – average daily wind speed at a height of 2 m [m s^{-1}],
e_s – saturated water vapor pressure [kPa],
e_a – current water vapor pressure [kPa],
Δ – derivative of saturated water vapor pressure [kPa C^{-1}],
γ – psychrometric constant [kPa °C^{-1}].

Mathematical statistics methods were applied for the analysis of climatic elements. The results are processed graphically and in tabular form.

4 Results and discussion

Table 1 shows the descriptive statistics parameters of the series of average annual air temperatures, annual precipitation totals and potential evapotranspiration in NP1 and NP2.

Table 1. Descriptive statistics for the average annual air temperatures, annual precipitation totals and annual ET_{pot} totals at Milhostov meteorological station in the normal periods 1961–1990 and 1991–2020

	average annual air temperature		annual precipitation total		annual ET_{pot} total	
	NP1 1961–1990	NP2 1991–2020	NP1 1961–1990	NP2 1991–2020	NP1 1961–1990	NP2 1991–2020
Mean	9.0	10.0	546.9	578.4	678.0	758.6
Standard Error	0.1	0.1	16.7	17.6	8.4	9.2
Median	9.0	10.0	546.3	562.5	675.2	750.9
Standard Deviation	0.6	0.7	91.6	96.4	45.8	50.6
Sample Variance	0.4	0.6	8389.8	9284.4	2096.5	2560.4
Kurtosis	-0.5	-0.8	-0.3	2.6	-0.8	-0.7
Skewness	-0.2	0.2	-0.1	1.2	0.1	0.2
Range	2.2	2.6	364.7	453.7	166.5	192.4
Minimum	7.8	8.7	351.9	438.1	596.2	667.0
Maximum	10.0	11.4	716.6	891.8	762.7	859.4
Sum	268.9	300.7	16405.9	17351.0	20339.6	22759.5
Count	30	30	30	30	30	30
Confidence Level (95.0%)	0.2	0.3	34.2	36.0	17.1	18.9

It follows from Table 1 that the period NP2 (1991–2020) is on average 1.0°C warmer than NP1 (1961–

1990) with higher variability in absolute value and relative to the average. The skewness and kurtosis values show that the air temperature distribution in NP2 is significantly flat with a positive skew to the right. The distribution of mean annual air temperatures in NP1 is less flat and skewed to the left. The test of average annual air temperatures showed that the *P*-value for the *t*-test is less than 0.05 and there is a statistically significant difference between the means at the 5% significance level. The *F*-test showed that the null hypothesis of equality of variances could not be rejected.

Figure 1 shows the average annual air temperatures in the normal periods NP1 (1961–1990) and NP2 (1991–2020) and their linear trends in the climate station Milhostov. Their trends show a significant increase in air temperatures in NP2 and an increasing trend in average annual air temperatures. Figure 2 analyzes the long-term average monthly temperature values and their differences between NP1 and NP2. The analysis shows that the biggest increase in air temperature was recorded in July (1.9°C) and in January (1.7°C). In the summer half-year NP2 (April–September), the average air temperature rose by (1.2°C) in the cold half-year by (0.9°C). Figure 3 shows histograms and box plots of average annual air temperatures in both normal periods. The figure graphically displays the results from Table 1 and illustrates the analysis of air temperatures so far. Histograms and boxplots show the shift and change in the shape of the temperature distribution between the studied periods.

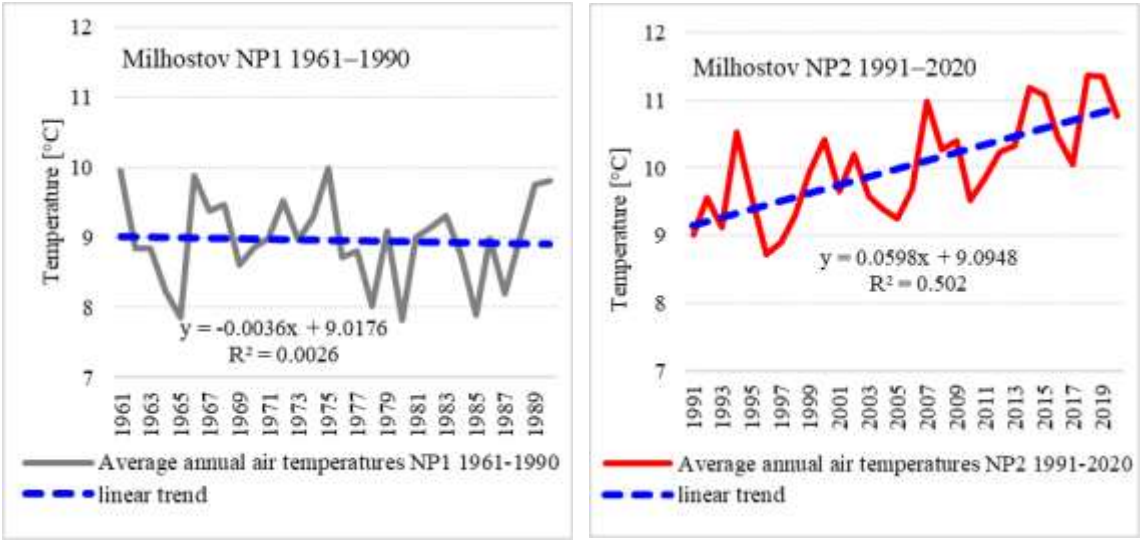

Figure 1. Average annual air temperatures and their trends at Milhostov meteorological station in the normal periods of NP1 1961–1990 and NP2 1991–2020.

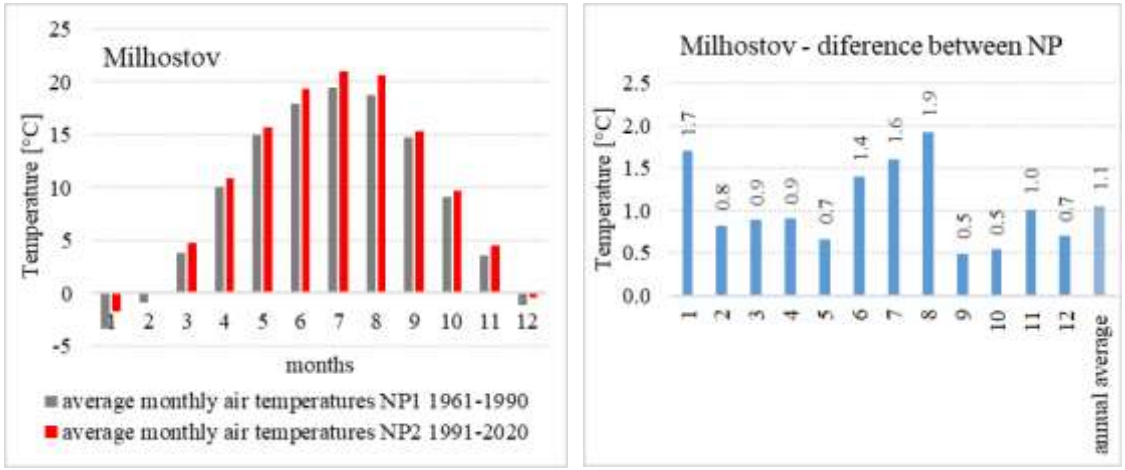

Figure 2. Comparison of long-term average monthly air temperatures at Milhostov meteorological station between the two normal periods NP1 1961–1990 and NP2 1991–2020 (in left).
Air temperature difference between the normal period 1961–1990 and 1991–2020 (in right).

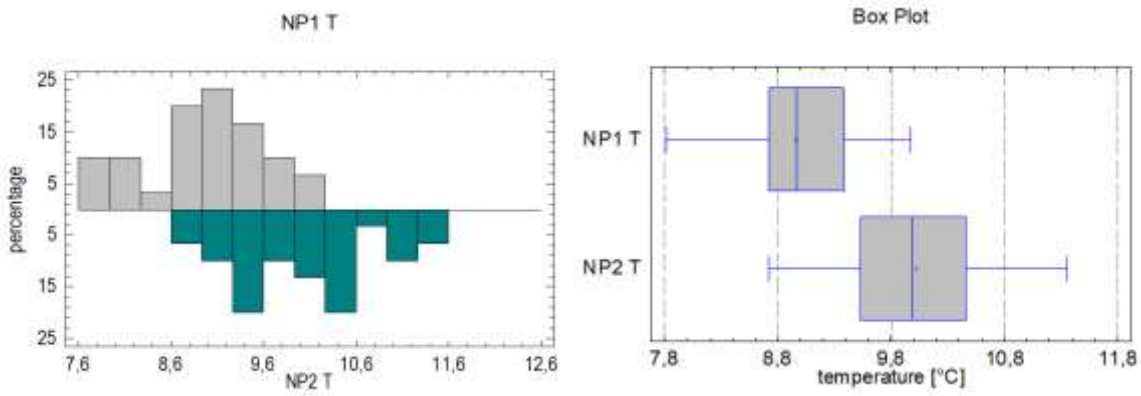

Figure 3. Comparison of average annual air temperatures of normal periods NP1 (1961–1990) and NP2 (1991–2020) using histograms and box plots.

Average annual precipitation totals (Table 1.) are 5.8% greater in NP2 than in NP1. Precipitation variability is slightly greater in NP2. NP1 is left-skewed and flat, while the NP2 set is right-skewed and more pointed. The *F*-test and *t*-test for the comparison of the variances and means of the average annual rainfall totals did not show statistically significant differences between NP1 and NP2 at the 5% level of significance.

Figure 4 shows the annual rainfall totals in the examined normal periods. In NP1, precipitation totals are balanced without a significant trend. In NP2, it is possible to identify a slight increase in the linear trend and an increased variability of precipitation totals.

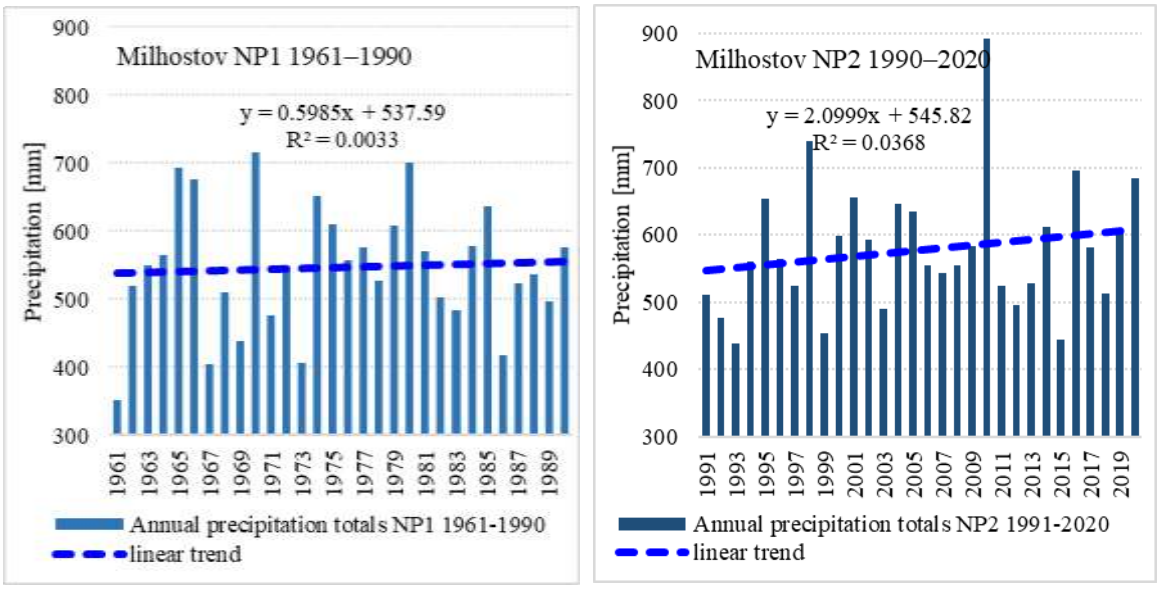

Figure 4. Annual precipitation totals and their trends at Milhostov meteorological station in the normal period of NP1 1961–1990 and NP2 1991–2020.

Figure 5 shows the long-term average monthly atmospheric precipitation totals in NP1 (1961–1990) and NP2 (1991–2020) in the meteorological station Milhostov. The slight increase in precipitation in NP2 compared to NP1 is caused by an increase in precipitation totals, especially in the months of May, July, September and October.

Figure 6 shows a comparison of the average annual precipitation totals of the normal periods NP1 (1961–1990) and NP2 (1991–2020) using histograms and box plots. The figures show a significant negative skew to the left in the NP1 data set. In the boxplot for the NP2 period, one outlier was identified that lies more than 3 times the interquartile range to the right of the box. The identified value belongs to the precipitation total from 2010. The mentioned year was very wet and the annual precipitation total

was 158.5% of the average value in NP2. At the same time, it was the wettest year in terms of precipitation for the entire period 1961–2020. The absolutely driest year for the mentioned period was 1961. The annual precipitation total was 64.2% of the average value in NP1.

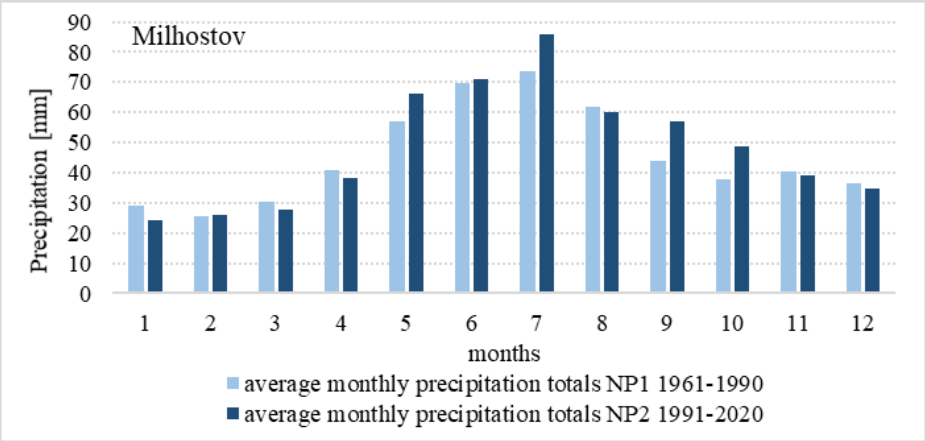

Figure 5. Long-term average monthly precipitation totals and long-term average precipitation totals at Milhostov meteorological station in the normal periods of NP1 1961–1990 and NP2 1991–2020.

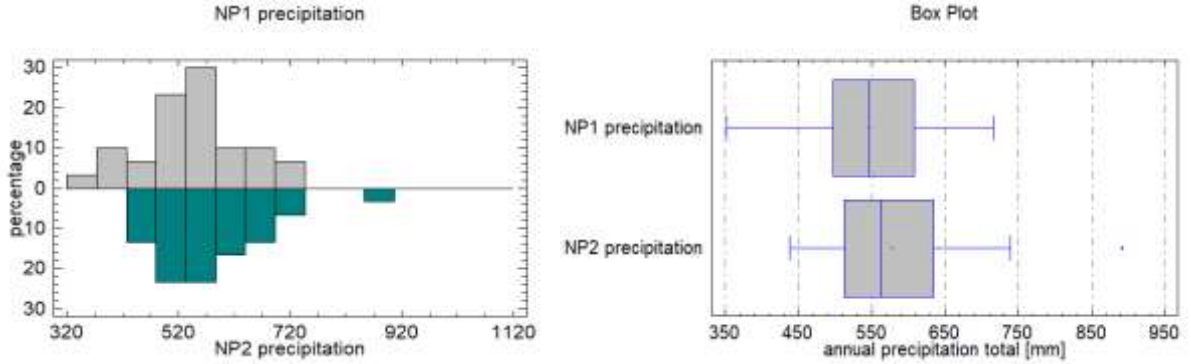

Figure 6. Comparison of mean annual precipitation totals of normal periods NP1 (1961–1990) and NP2 (1991–2020) using histograms and boxplots

The average annual totals of ET_{pot} are 11.9% greater in NP2 than in NP1. The skewness and kurtosis values show that ET_{pot} distributions in both normal periods have similar characteristics. The ET_{pot} distribution is flat in NP2 with a positive skew to the right. The distribution of mean annual ET_{pot} totals in NP1 is more flat with a positive skew to the right. A test of mean annual totals of ET_{pot} showed that the *P*-value for the t-test is less than 0.05 and there is a statistically significant difference between ET_{pot} at the 5% level of significance. The *F*-test showed that the null hypothesis of equality of variances could not be rejected. It is worth noting that the average annual ET_{pot} increased by 80.6 mm and precipitation by 31.5 mm in NP2. From this, it is possible to conclude about increased drying of the natural environment at ESL in NP2.

Figure 7 shows the average annual totals of ET_{pot} in the normal periods NP1 (1961–1990) and NP2 (1991–2020) and their linear trends in the climate station Milhostov. Their trends show a significant increase in ET_{pot} in NP2 and a growing trend of average annual ET_{pot} totals.

Figure 8 analyzes the long-term average monthly ET_{pot} totals and their differences between NP1 and NP2. The analysis shows that the greatest increase in long-term average ET_{pot} totals in NP2 compared to NP1 was recorded in August by 19.6 mm (19.7%) and in July by 13.5 mm (11.4%). In the summer half-year of NP2 (April–September), the average total ET_{pot} increased by 70.7 mm (12.6%) compared to NP1, in the cold half-year by 9.7 mm (8.2%).

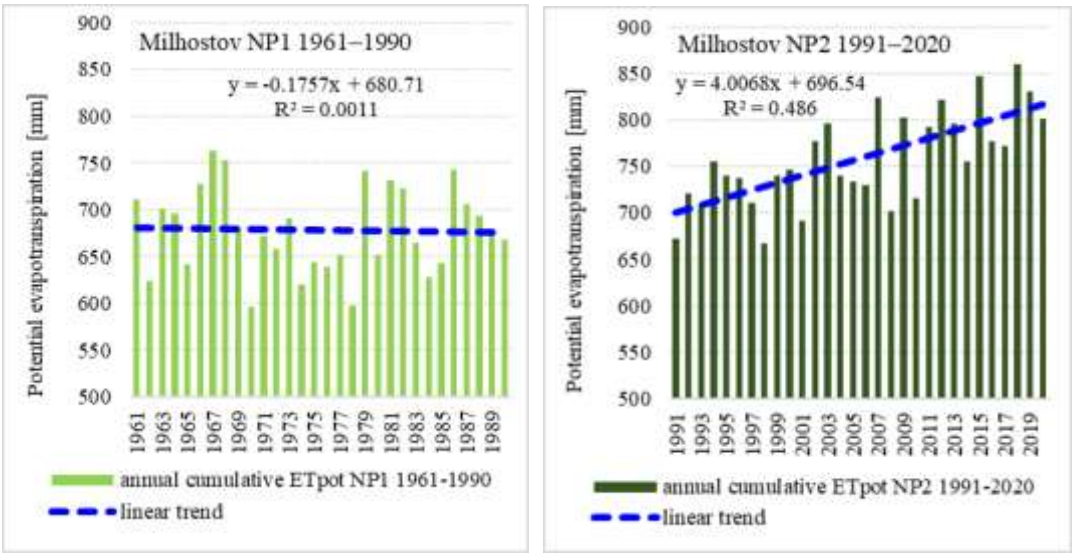

Figure 7. Trend analysis of the annual cumulated values of potential evapotranspiration (ET_{pot}) at Milhostov meteorological station in the normal periods of NP1 1961–1990 and NP2 1991–2020.

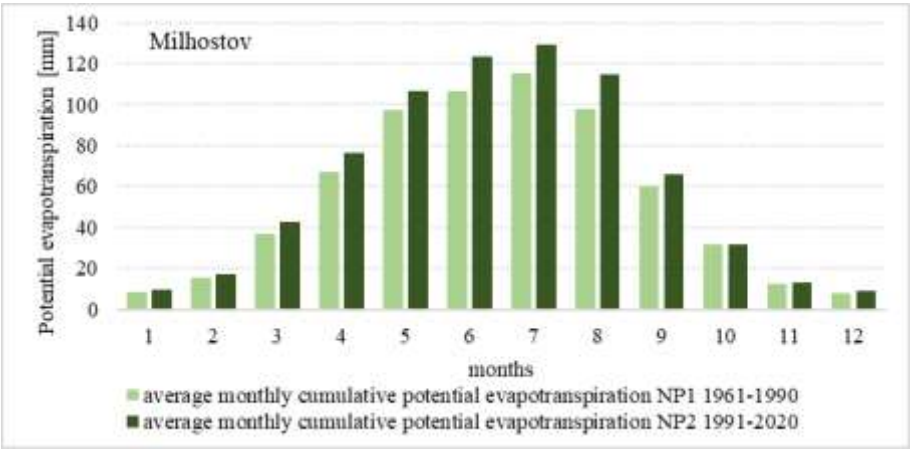

Figure 8. Long-term average monthly cumulated potential evapotranspiration (ET_{pot}) at Milhostov meteorological station in the normal periods of NP1 1961–1990 and NP2 1991–2020.

Figure 9 shows the histograms and boxplots of annual totals of ET_{pot} in both normal periods. The figure graphically displays the results of descriptive statistics from Table 1 and illustrates the ET_{pot} analysis so far.

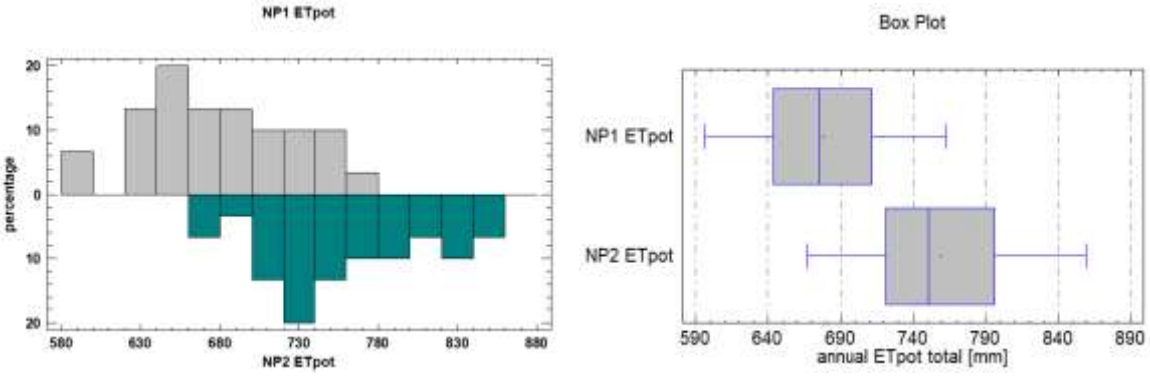

Figure 9. Comparison of annual totals of ET_{pot} of normal periods NP1 (1961–1990) and NP2 (1991–2020) using histograms and box plots

5 Conclusion

In recent years, the frequency of occurrence of extreme hydrological events has been increasing in the natural environment of Slovakia and within it also the East Slovak Lowland. In order to quantify these changes and their development trends, basic hydrometeorological elements are analyzed in two consecutive normal periods NP1 (1961–1990) and NP2 (1991–2020). They were air temperatures, precipitation and ET_{pot}. The analysis was based on the hypothesis that the mentioned hydrometeorological elements will increase in NP2 compared to NP1.
In the case of average annual temperatures, a significant increasing trend was identified in NP2. The differences in average annual temperatures between NP1 and NP2 are statistically significant. As for the variance, it is not possible to reject the hypothesis of equality of variances.
In the case of annual rainfall totals, the hypothesis was not confirmed. No significant statistical differences were identified between the size and variance of precipitation totals in the investigated periods NP1 and NP2 at the 5% level of significance. Nevertheless, precipitation in NP2 was 5.8% greater than in NP1.
Annual totals of ET_{pot}, similar to temperatures, had a significant increasing trend in NP2 compared to NP1. The differences in average annual temperatures between NP1 and NP2 are statistically significant at the 5% significance level. As for the variance, it is not possible to reject the hypothesis of equality of variances. It is worth noting that the average annual ET_{pot} increased by 80.6 mm and precipitation by 31.5 mm in NP2.
The above analysis shows that in NP2 (1991–2020) compared to NP1 (1961–1990), there is a trend of increasing temperature and potential evaporation. Precipitation increased slightly, statistically insignificant. From this, it is possible to conclude about increased drying of the natural environment at ESL in NP2.

Acknowledgements
Authors are grateful to Scientific Grant Agency of the Ministry of Education, Science, Research and Sport of the Slovak Republic: (project VEGA 2/0025/24).

References:
[1] Klimatický atlas Slovenska: Climate atlas of Slovakia. Banská Bystrica: Slovenský hydrometeorologický ústav, 228 p., 2015. (in Slovak)
[2] Rodný, M., Šurda, P.: Stanovenie indexov meteorologického sucha a ich spojitosť s vodným režimom pôdy lokality Báč na Žitnom ostrove. Hydrologické dny 2010, 2010 Hradec Králové, ISBN 978-80-86690-84-1, Praha: Nakladatelství Český hydrometeorologický ústav, pp. 109-116, 2010. (in Slovak)
[3] Soľáková, T., Zeleňáková, M., Mikita, V., Hlavatá, H., Simonová, D., Abd-Elhamid, H.: Assessment of meteorological and hydrological drought using drought indices: SPI and SSI in eastern Slovakia. Acta Hydrologica Slovaca, vol. 23, issue 2, 267-272, 2022.
[4] WMO, World Meteorological Organization (wmo.int), 1935.
[5] Lapin, M., Faško, P.: Klimatické normály. Metodický predpis 3-09-1/1. SHMÚ Bratislava, 1987. (in Slovak)
[6] WMO, Updated 30-year reference period reflects changing climate https://public.wmo.int/en/media/news/updated-30-year-reference-period-reflects-changing-climate, 2021.
[7] Faško, P., Lapin, M., Šťastný, P.: Maximum Daily Precipitation Totals in Slovakia in 1951–2000 Period. National climate Program of the Slovak Republic, ročník 9, s. 107-119, 2000.
[8] Hlavatá, H., Tomková, M.: Analýza vývoja teploty vzduchu na stanici Michalovce v zimnom období počas rokov 1961–2014. Acta Hydrologica Slovaca, ÚH SAV Bratislava, č.2, s.153-159, 2015. (in Slovak)
[9] Mikulová, K., Faško, P., Bochníček, O., Ondruška, P., Čepčeková, E., Šťastný, P., Pecho, J.: Klimatické normály 1961–1990 meteorologických prvkov teploty vzduchu a atmosférických zrážok. Záverečná správa výskumnej úlohy. 2008. (in Slovak)
[10] Šoltész, A., Baroková, D., Možiešiková, K., Čubanová, L.: Detailed analysis of the possible impact

of surface stream training on the groundwater level regime. International Multidisciplinary Scientific GeoConference Surveying Geology and Mining Ecology Management, SGEM. ISSN 13142704, 2018-01-01, 18, 1.2, pp. 199-206, 2018. Registrované v: SCOPUS

[11] Vitková, J., Toková, L., Botková, N.: Modeling of soil water retention curves based on two programs. Acta Hydrologica Slovaca, vol. 23, no.2, 157-162, 2022. 2644-4690. DOI: https://doi.org/10.31577/ahs-2022-0023.02.0017

[12] Allen, R. G., Pereira, L. S., Raes, D., Smith, M.: Crop evapotranspiration - Guidelines for computing crop water requirements: FAO Irrigation and drainage paper 56. Rome: FAO, 301 p. 1998.

[13] Novák, V.: Výpočet potenciálnej evapotranspirácie homogénnych povrchov. In: Vyparovanie vody v prírode a metódy jeho určovania, s. 211-214, 1995. (in Slovak)

[14] Šoltész, A., Baroková, D.: Impact of landscape and water management in Slovak part of the Medzibodrožie region on groundwater level regime. Journal of Landscape Management. 2011, vol. 2, no. 2, pp. 41-45, 2011.

[15] Kveták, Š.: Príspevok ku kontinentalite podnebia na Slovensku. Bratislava, ALFA 1983. 220 p., 1983a. (in Slovak)

[16] Kveták, Š.: Niektoré vzťahy medzi klimatickými prvkami vo vybraných lokalitách na Slovensku. Bratislava, ALFA 1983. 264 p., 1983b. (in Slovak)

HYDROLOGICAL PROCESSES IN THE WATER UNSATURATED SOIL ENVIRONMENTS ON THE EAST SLOVAK LOWLAND IN THE EXTREMELY DRY GROWING SEASON OF 2022

MILAN GOMBOŠ[1], BRANISLAV KANDRA[1], DANA PAVELKOVÁ[1*], ANDREJ TALL[1]

[1] *Institute of Hydrology, Slovak Academy of Sciences, Slovakia, E-mail: pavelkova@uh.savba.sk*

1 Abstract

Hydrological processes in the unsaturated zone are the results of the interaction processes of the unsaturated zone with the surrounding subsystems. In the growing season of 2022 in the East Slovak Lowland a soil drought occurred. In this paper, the components of the water regime are quantified and analyzed. The data base for the analysis was obtained by monitoring and numerical simulation on the HYDRUS mathematical model. Extremely low actual evapotranspiration and a significant influence of the water table on the water storage in the root zone of the soil profile were identified.

Keywords: soil water regime, unsaturated zone, monitoring, numerical simulation

2 Introduction

Hydrological processes in the unsaturated zone are part of the hydrological cycle. The hydrological cycle is studied as a physical system, which is divided into atmosphere – vegetation cover – unsaturated zone – groundwater. The water storage (WS) in the unsaturated zone is the result of the interaction processes of the unsaturated zone with the surrounding subsystems. Anthropogenic activity in the country also has a direct impact on the quality, quantity and dynamics of water in the unsaturated zone. In the region of the East Slovak Lowland (ESL), it is mainly agriculture, the chemical industry, and complex water management measures implemented since the 1960s [1], [2], [3], [4], [5].

Water in the unsaturated zone is a source of water for the biosphere. This source supplies water to the vegetation cover during the growing season. In order to assess available water storage in the soil for vegetation cover, the characteristic points of the moisture retention curve are selected based on the convention [6]: field water capacity (FC), threshold point (TP) and wilting point (WP). FC is the moisture state of the soil, which occurs after gravity water drains from the pores. With TP, plants are put under stress and their biological activities are oriented towards survival. If the water reserves in the soil fall below the value corresponding to the WP, the soil becomes dry and the plants die. It follows from the above that the available source of soil water for the biosphere is the volume of water in the soil aeration zone, which corresponds to the interval of the energy binding of water with the solid phase of the soil between FC and WP. It is the existence interval of the water content for the plant cover in the given location of the territory. This volume of water does not have the properties of free water. In order for plants to be able to use it, they must have a developed root system and a suction pressure that is able to overcome the binding of water with the soil. Information on the temporal and spatial distribution and dynamics of moisture in the unsaturated zone of the soil environment is crucial for agricultural production, water management in the country and the design of adaptation measures. The mentioned information can be obtained by monitoring and calculation.

In the past growing season of 2022, it was possible to see the manifestations and feel the consequences of the lack of water in the unsaturated zone of soils on the territory of Slovakia. In ESL conditions, the lack of water manifested itself in the form of soil drought. The aim of the work was to quantify and analyze the components of the water regime of the soil in the site Milhostov on the ESL during the growing season of 2022. The data base for the analysis was obtained by monitoring and numerical simulation on the HYDRUS mathematical model.

2.1 Description of the locality

The investigated site of Milhostov is located on the East Slovak Lowland. The ESL represents the northernmost part of the extensive Inner Carpathian tectonic depression. It covers an area of 2 638 km^2. It was created by uneven tectonic subsidence of the earth's crust inside the Carpathian mountain in the Neogene and Quaternary periods. Soil conditions correspond to geological conditions. ESL is characterized by a high proportion of heavy and very heavy soils (Table 1).

Table 1. Soil types in the East Slovak Lowland

soil types				
light soils	**medium heavy soils**		**heavy soils**	**very heavy soils**
sand loamy sand	sandy loam	loam	clay loam	clayey clay
[%]	[%]	[%]	[%]	[%]
2.64	50.70	4.92	21.88	19.86

From a climatic point of view, the territory of ESL lies in the transition zone between oceanic and continental climate. The territory belongs to a warm, slightly humid region with a cold winter. One of the basic features of the local climate is the great temporal variability of the weather and thus of all meteorological elements. The rapid change of air masses in each season and developed cyclonic activity are characteristic here [7]. From the temperature point of view, the territory of ESL forms a relatively homogeneous temperature area. The long-term average temperature in this region is around 9.6°C. The coldest month of the year in the mentioned period is January (-2.8°C) and the warmest is July (20.5°C). Circulation factors are decisive for precipitation formation. At ESL, the most precipitation falls during the flow of moist warm air from the south. Precipitation from the west, north and east is reduced by the precipitation that falls on the Carpathian massif. The area with annual precipitation below 600 mm lies in the central to south-western part of the plain. The investigated site of Milhostov also falls into this area. In the direction to the northeast, precipitation increases and reaches 800 to 900 mm in the territory of the East Slovak hillock.

3 Methods

The methodological procedure was divided into two stages. The goal of the first stage was the creation of a database for further analysis. In the second stage, its analysis and interpretation of the results was carried out. The data base was formed by the results of monitoring and numerical simulation on the HYDRUS mathematical model.

As part of the monitoring, the texture of the soil profile was analyzed in layers of 0.1 m to a depth of 1 m, the bulk moisture of the soil samples and the basic hydrophysical characteristics were measured. Volumetric humidity was measured gravimetrically to a depth of 1 m in layers of 0.1 m. The results of volumetric moisture measurements were displayed using isolines (isolines, isopleths). From a physical point of view, an isoline is defined as a line along which the selected scalar physical quantity has the same value. The name of the isoline depends on what quantity it shows. Isolines along which there is the same humidity in the soil profile at different times are called chronoisopleths. In the form of a chronoisopleths, a picture of the time development of moisture in the soil profile is obtained.

To obtain difficult-to-measure characteristics, the method of numerical simulation on the HYDRUS-1D model was used. The mathematical model HYDRUS-1D in version 4 was used to calculate the analyzed members of the balance equation in the evaluated time period. HYDRUS-1D is a one-dimensional model for the simulation of water flow, heat transfer and movement of soluble substances involved in subsequent first-order reactions in variably saturated soils [8]. It is based on the solution of the Richards equation [9] for variably saturated flow and on the advection-dispersion type of equations for the transfer of heat and soluble substances. The flow equation allows for a drop to account for water uptake by plant roots. The chosen hydraulic model of van Genuchten [10] and Mualem [11] was single-pore without hysteresis. For each layer, the basic hydrophysical characteristics of soils were measured in

the laboratory and the parameters of the analytical expression of moisture retention curves according to van Genuchten were defined. The input data on groundwater were provided by the regional office of SHMI Košice as part of the cooperation. The time calculation step of the simulation was set to 1 day. This corresponds to the time scale of all inputs and outputs from the model. The submitted paper presents information from them on evapotranspiration, evapotranspiration deficit and water reserves up to a depth of 1 m. Descriptive statistics and correlation analysis methods were used to describe the investigated parameters and quantify their interrelationships.

4 Results and discussion

The investigated site of Milhostov is situated in the central area of ESL (48°40'11'; 21°44'18"). The site is covered with silty clay loams, which change to sandy loams in the lower soil horizons (80 cm) (Figure 1). The average retention characteristics of the investigated soil profile to a depth of 1 m expressed in the form of hydrolimits, field water capacity (FC), point of reduced availability (TP) and wilting point (WP) are shown in Table 2.

Table 2. Average values of hydrolimits in the investigated profile up to a depth of 1 m

Locality	Hydrolimits [%]		
	WP	TP	FC
Milhostov	23	31	42

During 2022, 463.6 mm of precipitation fell in the investigated location. It is 61.1% of the long-term normal period 1991–2020.
In the growing season (April–September) 2022, the precipitation total in Milhostov was 295.4 mm (63.7% of the annual total), which represents a 13% probability of occurrence in the 53 annual series of measurements. In this context, it should be noted that 47.5% (140.2 mm) of the total vegetation precipitation fell at the end of the growing season in the month of September (Figure 2). If the precipitation from July (63.3 mm) is added to this, it is 68.9% of the entire growing season. In addition to small amounts of precipitation, the examined growing season is characterized by high air temperatures. Their average monthly temperatures and maximum and minimum monthly temperatures are shown in Figure 2. This fact had an impact on water reserves in the soil, and thus the growing season of 2022 ranks among the absolute driest since 1970.

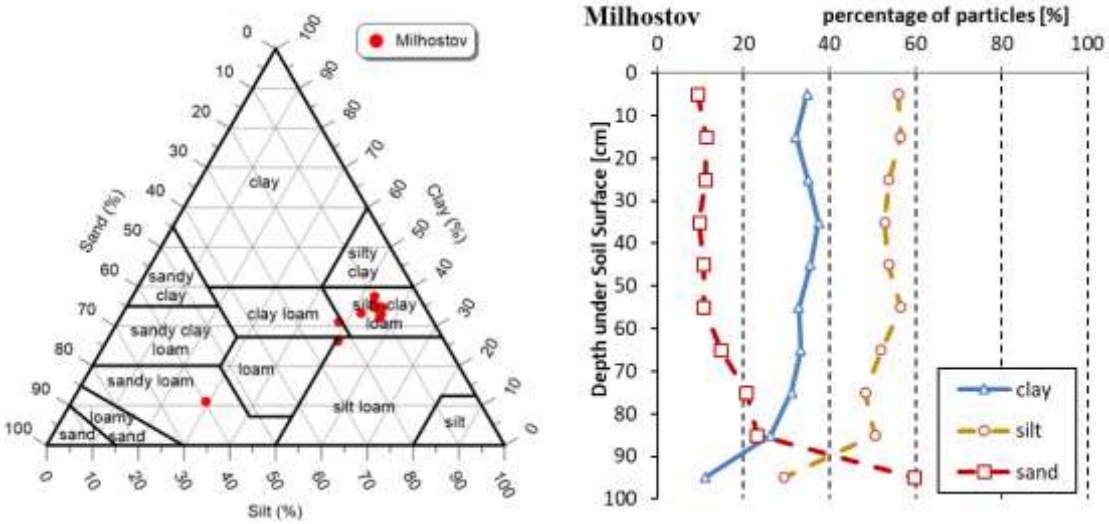

Figure 1. Identification of soil types and texture along the vertical of the investigated soil profile

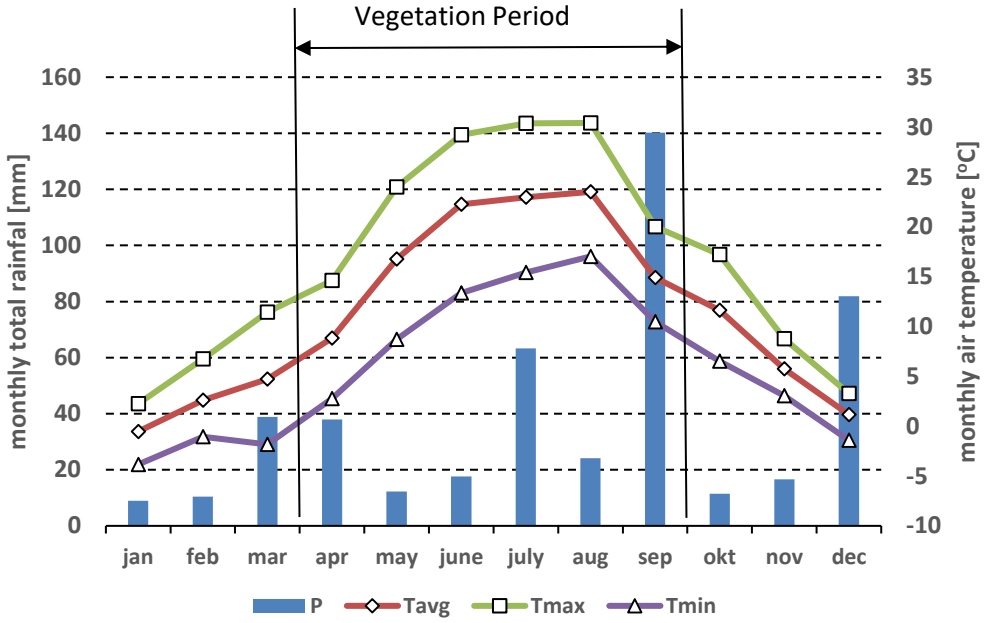

Figure 2. Temperature and precipitation conditions in the investigated location in the growing season of 2022

Figure 3 shows in the form of isolines the course of bulk moisture in the studied profile during the growing season of 2022. The bulk moisture was measured gravimetrically, by taking soil samples in layers of 0.1 m to a depth of 1.0 m. In the picture, the individual humidity levels are also distinguished by colour. It is clear from the given display that the entire profile to a depth of 1 m was dried. Drying in the surface layer up to 0.1 m already occurred at the beginning of May. The moisture content of the soil profile was continuously below the stress point until mid-September. Parts of the soil profile dropped below the wilting point. The condition of the grass, which was dry, also corresponded to this. The September precipitation gradually saturated the upper soil horizons to an optimal state.
The mentioned results are more prominently presented in Fig. 4. In this display, the intervals of moisture isolines are defined by hydrolimits FC, TP and WP.
The monitoring results shown in Figures 3 and 4 also confirm the results shown in Figure 5. Numerically simulated daily totals of potential (ET_0) and actual (ET_a) evapotranspiration, evapotranspiration deficit $ET_D = ET_0 - ET_a$ and calculated WS_c and measured WS_o water reserves are shown there, in the soil profile to depth 1 m. The water supply to a depth of 1 m on 21/05/2022 falls below the wilting point and remains continuously below it until 12/9/2022, when the water supply rises above the wilting point due to September precipitation. This corresponds to the totals of the current evapotranspiration, which, due to the lack of water in the soil profile, oscillates above zero. For that reason, the evapotranspiration deficit is almost identical to the total potential evapotranspiration. Temperatures (T), precipitation (P) and groundwater level (GWL) shown in Figure 5 supplement the information field on evaporation processes and changes in water reserves in the soil profile.

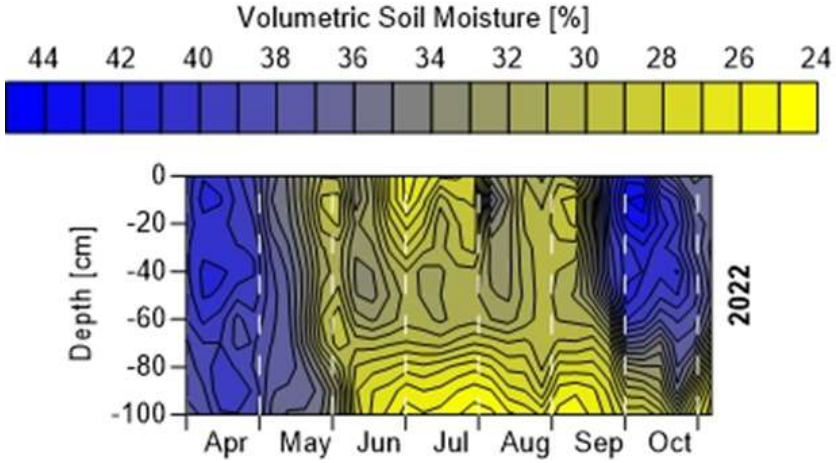

Figure 3. Volumetric soil moisture isolines to a depth of 1 m during the growing season of 2022

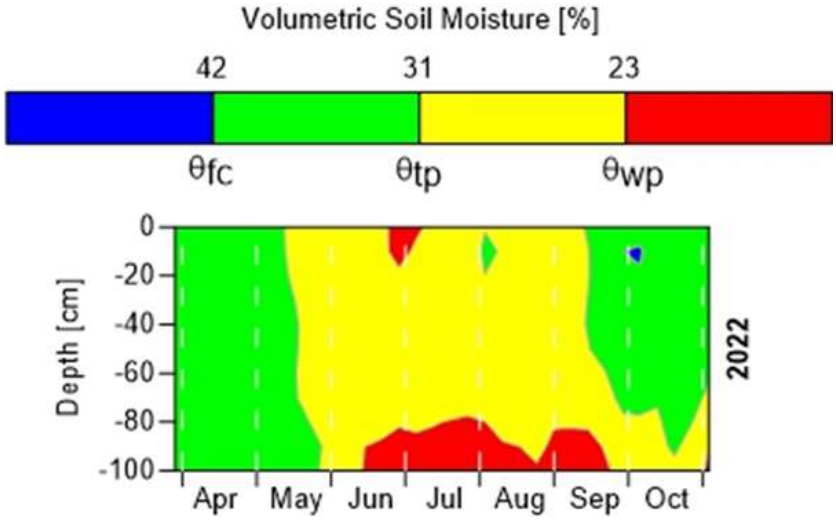

Figure 4. Volumetric soil moisture isolines to a depth of 1 m during the 2022 growing season defined by hydrolimits FC, TP and WP

The statistical characteristics of the descriptive statistics of the course of the investigated parameters are shown in Table 3. These, in numerical form, summarize the course of the examined parameters shown in Figure 5.

In Table 4, correlation coefficients are given to assess the closeness of the relationships between the investigated parameters. The closest relationship was identified between ET_0 and ET_D. The strength of this bond is due to the low ET_a (3.2% of ET_0). Then, if $ET_D = ET_0 - ET_a \Rightarrow \lim_{ET_a \to 0} ET_D = ET_0$ which causes the correlation coefficient to close to the functional value. This is confirmed by the descriptive statistics values shown in Table 3 and the graphical illustration using histograms and boxplots shown in Figure 6.

A highly significant relationship was identified between groundwater level GWL and water storage WS_c (0.82), indicating interaction processes between groundwater and water storage in the root layer of the soil profile. The expected significant correlations were confirmed between temperature T and ET_0, ET_D and thus GWL.

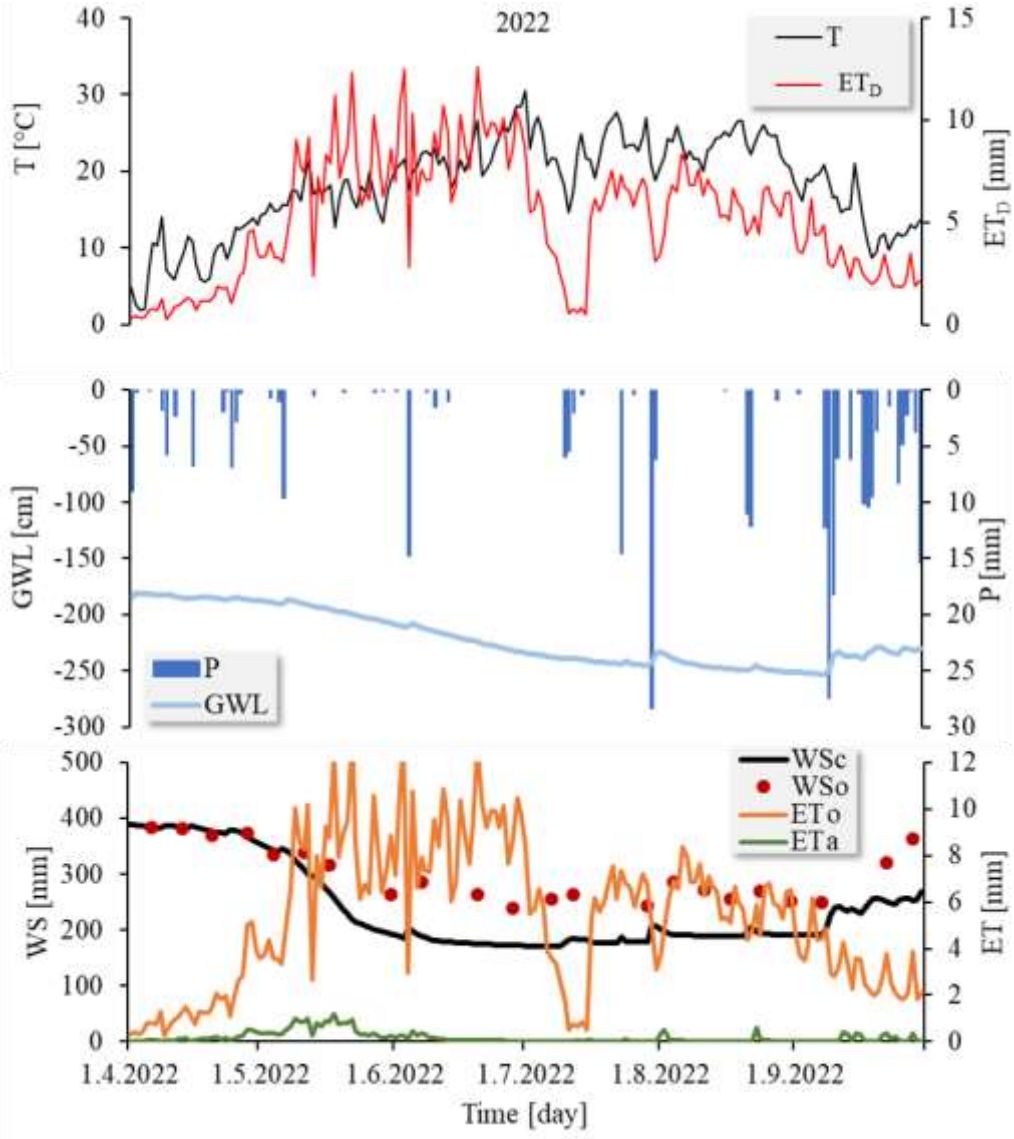

Figure 5. Course of daily totals of potential and actual evapotranspiration ET_0, ET_a, evapotranspiration deficit ET_D, precipitation P, water reserves WS in the soil profile to a depth of 1 m (WS_c – calculated, WS_o – observed), groundwater level GWL and average daily temperatures T

Table 3. Characteristics of descriptive statistics

Parameter	***GWL*** [cm]	***ET₀*** [mm]	***ETₐ*** [mm]	***ET_D*** [mm]	***WS_c*** [mm]	***T*** [°C]
Mean	-220.90	5.34	0.17	5.17	238.86	18.24
Standard Error	1.79	0.23	0.02	0.22	5.60	0.45
Median	-229.82	5.58	0.05	5.48	194.97	19.15
Standard Deviation	24.24	3.10	0.24	3.02	75.70	6.04
Sample Variance	587.43	9.62	0.06	9.13	5730.18	36.53
Kurtosis	-1.40	-0.70	3.78	-0.76	-0.57	-0.30
Skewness	0.39	0.21	2.02	0.19	1.01	-0.55
Range	73.26	13.27	1.21	12.64	217.27	28.65
Minimum	-253.60	0.00	0.00	0.00	171.46	1.88
Maximum	-180.35	13.27	1.21	12.64	388.73	30.53
Sum	40424.38	976.76	31.37	945.39	43711.78	3338.60
Count	183	183	183	183	183	183
Confidence Level (95.0%)	3.54	0.45	0.04	0.44	11.04	0.88

Table 4. Correlation table of dependencies between the investigated parameters

	P	GWL	ET_0	ET_a	ET_D	WS_c	T
P	**1**						
GWL	-0.13	**1**					
ET_0	-0.27	-0.17	**1**				
ET_a	-0.22	0.49	0.36	**1**			
ET_D	-0.26	-0.21	0.997	0.29	**1**		
WS_c	0.04	0.82	-0.56	0.26	-0.59	**1**	
T	-0.12	-0.67	0.63	-0.13	0.65	-0.82	**1**

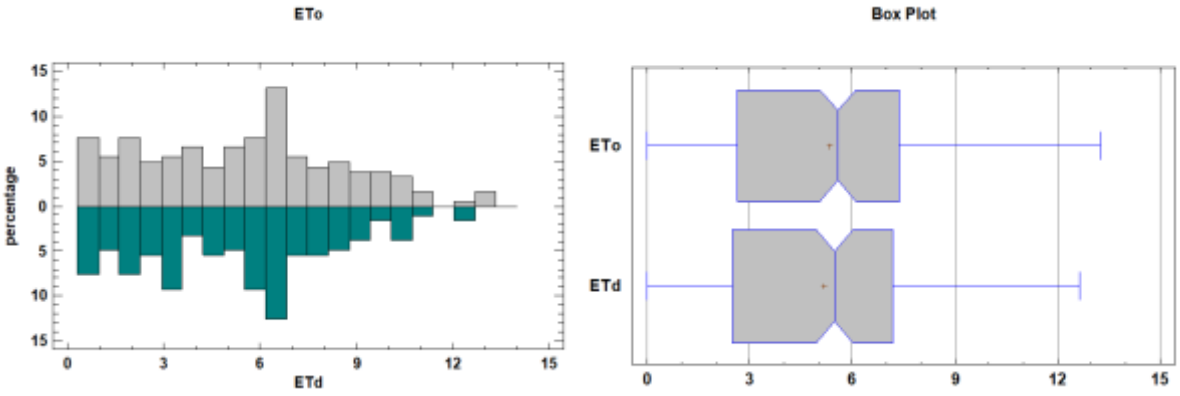

Figure 6. Comparison of potential evapotranspiration ET_0 evapotranspiration deficit ET_D

5 Conclusion

The work analyzed the basic components of the water regime of the soil profile to a depth of 1 m in the Milhostov area on the ESL. The analysis was carried out in the extremely dry growing season of 2022. The analysis was based on the results of monitoring and numerical simulation of the components of the water regime on the HYDRUS-1D mathematical model. Correlation analysis confirmed the significant level of interaction processes between groundwater and water supply in the soil profile. This is due to the fact that groundwater replenishes the water reserves in the root zone of the soil profile up to a certain critical depth.

A very low level of actual evapotranspiration ET_a was identified, the total of which for the entire growing season was only 3.2% of ET_0. This was reflected in a high evapotranspiration deficit that almost duplicated ET_0. In addition, the expected significant correlations between temperature T and ET_0, ET_D and subsequently GWL were confirmed.

Acknowledgements

Authors are grateful to Scientific Grant Agency of the Ministry of Education, Science, Research and Sport of the Slovak Republic: (project VEGA 2/0025/24).

References:

[1] Baroková, D., Červeňanská, M., Šoltész, A.: Assessment of the impact of proposed cut-off walls on ground-water level regime during extreme hydrological conditions. In *Acta Hydrologica Slovaca*, vol. 21, no.1, pp. 113-122, 2020. 2644-4690. DOI: https://doi.org/10.31577/ahs-2020-0021.01.0014

[2] Čubanová, L., Šoltész, A., Mydla, J.: Analysis of droughts due to the operation of water structures: Gidra river case study. Pollack Periodica, 17, 1, pp. 111-116, 2022. DOI: 10.1556/606.2021.00463.

[3] Almikaeel, W., Čubanová, L., Šoltész, A.: Hydrological drought forecasting using machine learning – Gidra river case study. Water. 14, 3, no. 387, 2022. DOI: 10.3390/w14030387

[4] Vitková, J., Šurda, P., Rončák, P., Botková, N., Zvala, A.: Statistical analysis of soil water content differences after biochar application andits repeated application during 2020 growing season. Acta

Hydrologica Slovaca, vol. 22, no.2, pp. 320-325, 2021. 2644-4690. DOI: https://doi.org/10.31577/ahs-2021-0022.02.0036

[5] Vitková, J., Toková, L., Botková, N.: Modeling of soil water retention curves based on two programs. In *Acta Hydrologica Slovaca*, vol. 23, no.2, pp. 157-162, 2022. 2644-4690. DOI: https://doi.org/10.31577/ahs-2022-0023.02.0017

[6] Kutilek, M.: Vodohospodářská pedologie. Praha (SNTL a ALFA), 1978. (in Slovak)

[7] Kveták, Š.: Niektoré vzťahy medzi klimatickými prvkami vo vybraných lokalitách na Slovensku. Bratislava, ALFA 1983. 264 p., (1983). (in Slovak)

[8] Šimůnek, J., Šejna, M., Saito, H., Sakai, M., Van Genuchten M.Th.: The HYDRUS-1D software package for simulating the one-dimensional movement of water, heat, and multiple solutes in variably-saturated media, Version 4.0x, Hydrus Series 3, Department of Environmental Sciences, University of California Riverside, Riverside, CA, USA, 2008.

[9] Richards, L. A.: Capillary conduction of liquids through porous mediums. Physics 1, 1931, pp. 318-333, 1931.

[10] Van Genuchten, M. Th.: A closed-form equation for predicting the hydraulic conductivity of unsaturated soils. Soil Science Society of America Journal. 1980, 44, pp. 892-898, 1980. https://doi.org/10.2136/sssaj1980.03615995004400050002x

[11] Mualem, Y. A.: A new model for predicting the hydraulic conductivity of unsaturated porous media. Water Resources Research. 1976, 12, 3, pp. 513-522, 1976. https://doi.org/10.1029/WR012i003p00513

EFFECT EVALUATION OF DIFFERENT ADAPTATION MEASURES APPLIED ON URBAN CATCHMENT

MAREK SOKÁČ [1], YVETTA VELÍSKOVÁ [2], MARTA KOCZKA BARA [3]

[1] *Institute of Hydrology, Slovak Academy of Sciences, Slovakia, sokac@uh.savba.sk*

[2] *Institute of Hydrology, Slovak Academy of Sciences, Slovakia, veliskova@uh.savba.sk*

[3] *Institute of Hydrology, Slovak Academy of Sciences, Slovakia, bara@uh.savba.sk*

1 Abstract

Paper analyses design of various adaptation measures for a part of urban catchment with focus to the legislation, hydraulic and environmental aspects of the urban stormwater management. There were estimated required range and composition of adaptation measures and their effects on the overall urban stormwater management are described with regard to the achievement of the required goals. The results show that that green measures (green infrastructure) alone cannot eliminate all the negative impacts of climate change.

Keywords: urban drainage, stormwater runoff, green infrastructure, climate change, adaptation measures

2 Introduction

The climatic change implies implementation of adaptation measures in the field of urban drainage. Higher rainfall intensities typically requires larger hydraulic / storage capacity of the urban drainage systems in aim to better manage the increased stormwater flows and volume.

Without amendments to the prevailing concept of urban drainage in the Slovak Republic, the likelihood of flooding in urban areas due to increased rainfall intensities will remain high, as the current sewerage network is unable to cope with the increased demand. Furthermore, climate change will result in an increased amount of pollution transported from sewerage networks to surface waters (receiving waters) due to the more frequent hydraulic overflow of wastewater through combined sewer overflow (CSO) structures. Additionally, the larger volumes of such water will reach the receiving waters directly without any treatment.

Two approaches can be taken to address this issue: increasing the hydraulic capacity of the sewer network or reducing the inflow to the sewer network. Increasing the capacity of the sewerage network typically involves structural modifications to the network, such as increasing the diameter of pipes, create or increase of central retention volumes. These modifications are often accompanied by extensive civil works, traffic constraints and high financial requirements. It is therefore advisable to utilise the second option as frequently as possible, namely to reduce the inflow to the sewerage network in order to ensure that its current capacity is sufficient to convey stormwater.

The second method, reduction of inflow to the sewer network, assumes local area retention or disposal / use of stormwater at the place of its generation. In this case, retention means interception of stormwater and its slow, regulated discharge into the sewerage network so as not to exceed the maximum flow limits set by the relevant authority (e.g. local authority, Water Company). The disposal of the water is understood to be the evaporation or discharge to local surface waters, thus preventing its entry into the sewerage system.

For the retention of rainwater, but also for its local disposal, it is advantageous to use natural solutions, often based on different types of vegetation, whose action resembles the hydrological characteristics of the natural basin. These solutions are collectively known as 'green infrastructure'.

This development resulted also in the update of the existing EU legislation in the field of urban drainage, which requires elaboration of the integrated urban wastewater management plans. These plans shall comprise methodology and procedures for achieving the objectives in the field of urban stormwater management, such as a surcharge or flooding as well as minimising the pollution load of untreated water to the local recipients. Such measures could include the adaptation of the existing or the creation of new urban wastewater collection infrastructure including creation of additional stormwater storage (detention measures). New infrastructure implementation plans should prioritize the implementation of green infrastructure (e.g. and storage ponds, wetlands, semipermeable surfaces, green roofs etc.) designed in order to support biodiversity and water reuse.

a) b)

c) d) e)

Figure 1. Examples of adaptation measures in urban stormwater management: a) micro pond at the Faculty of Forestry, TU Zvolen, b) wetland park in Portland **[1]**, c) family house infiltration system **[2]**, d) grassed semipermeable paving **[3]**, e) green roof **[4]**

The impact of discharge from CSO's on the biological regime is a complex and non-trivial issue, highly individual and local in nature. Simple calculation methods can typically provide an approximate balance load to the receiving water, which does not take into account the effect of individual rain events, nor the duration or frequency of CSO's events. Similarly, calculations using complex rainfall-runoff models may not provide sufficiently reliable results due to uncertainties and variability of parameters during rainfall events (e.g. in larger catchments due to spatial variability of rainfall, quantitative and temporal variation of pollutants in rainwater and wastewater depending on several local and temporally variable factors, etc.).

At present, we can formulate the characteristic effects of the annual pollutant load to the receiving waters in the CSO waters, the CSO volume as well as the number of CSO events and their duration during the non-freeze period of the year (or whole year).

However, the scientific question we ask in this paper is the extent to which green infrastructure can reduce or eliminate the negative effects of CSO events on receiving water. Impact of CSO events can be quantified in a variety of ways, but the most common expression is its impact on reducing the risk of flooding and its impact on reducing the amount of pollution transported through the CSO structures to the receiving water.

This paper focuses on the impact of green infrastructure on the balance parameters of pollution transport through CSO's to receiving waters. This issue is one of the key indicators mentioned in the aforementioned EU Directive, namely Directive 91/271/EC, which sets a (non-binding) indicator for the

pollution of receiving waters by discharged water of 2% of the total annual pollution transported to waste water treatment plants. This is an emission based balance parameter and the details and methodology for calculating this indicator have not yet been defined.

3 Methods

For the calculations and assessments that we have carried out in this paper, several calculation methods have been considered. Firstly, the method of prof. Urcikán, presented in his publication [5] was considered. This method allows, based on statistically processed rain gauge data according to [6], [5] to determine approximately the number of cases of CSO events, the duration and the volume of CSO sewage water. However, this method does not allow taking into account some aspects that occur in real sewer networks, such as the inclusion of rainwater basins, etc.
Therefore, we decided to use a simple balance method presented at the NATO Advanced Science Institute (ASI) series in Harrachov in 1996 [7]. This method also has its shortcomings, but it allows a simple and understandable consideration of practically all aspects occurring in the drainage networks (e.g. stormwater basins, dynamic effect of WWTPs, etc.) and also allows fast and simple recalculation of several alternatives for the application of water retention features (green infrastructure) in an urbanised catchment.
The principle of this method is a simple comparison of the rainfall depth (volume) occurring in the catchment with the available retention depth (volume) in the catchment (hydrological losses, but also the retention capacity of the drainage system elements). Each rainfall event is defined by its duration and total rainfall. The rainfall defined in this way produces the scatter plot shown in Figure 2.

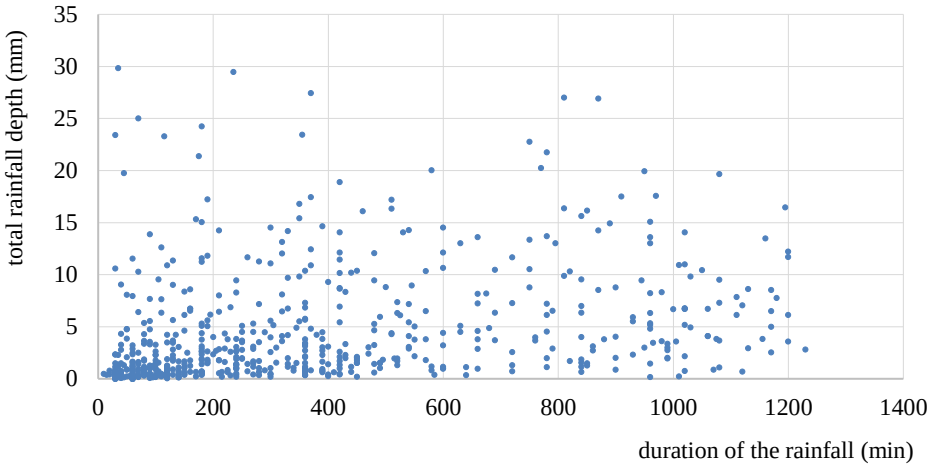

Figure 2. Rainfalls in Bratislava city (10-year rain gauge records)

From the precipitation, defined in terms of total amount and duration, we successively subtract the hydrological losses - surface wetting / retention, infiltration, interception, etc. We have subtracted these losses from a value that includes the sum of these losses (see Table 1).

Table 1. Used values of hydrologic losses

PERCENTAGE OF THE GREEN INFRASTRUCTURE IMPLEMENTATION	CATCHMENT HYDROLOGIC LOSSES h_{HL}
(%)	**(mm)**
0%	1
25%	1,5
50%	2
75%	2,5
100%	3

Next, we subtracted the retention capacity of the sewer network and the rainwater storage tank (ST) from the total rainfall, but both were converted to the total rainfall according to the relationship

$$h = \frac{V}{A_{red}} \tag{1}$$

Where *h* is the corresponding volume retention (sewer system, storage tank), expressed as rainfall depth (m),
V is the retention volume (m^3) and
A_{red} is the reduced catchment area (m^2), i.e. total catchment area multiplied by runoff coefficient (A_{red} = A.φ)

The dynamic part of the system volume balance, i.e. the volume taken from the urban drainage system by the Waste Water Treatment Plant (WWTP) or simply flowing out of the system towards the WWTP can be expressed as

$$h_{WWTP} = \frac{Q_{WWTP}.t}{A_{red}} \tag{2}$$

Where
h is the corresponding outflow volume for time *t*, expressed as depth (m/min),
Q_{WWTP} is the flow rate of the wastewater flowing out of the urban drainage system (towards the WWTP)
t is the rainfall duration time (min).

The CSO volume can then be determined graphically or by calculation (e.g. using a simple spreadsheet SW) according to the following relationship (Eq 3):

$$h_{CSO} = h_{HL} - h_S - \sum h - h_{WWTP}.t \tag{3}$$

Where
h_{CSO} is the CSO outflow volume, expressed as depth (m),
h_{HL} are the total hydrologic losses (surface losses) on the urban catchment (m),
Σh is the sum of the total retention (accumulation) capacity of the drainage system, see Eq. 1 (m).

If the value of the h_{CSO} is zero or negative, CSO event does not occur, i.e. the retention / storage capacity is bigger than the rainfall.
To express the CSO overflow volume in volumetric units, we can use following equation (Eq. 4):

$$V_{CSO} = h_{CSO} . A_{red} \tag{4}$$

For practical calculations, we have created a hypothetical catchment area in the city of Bratislava with the following parameters (Table 2):

Table2. Parameters of the hypothetical case study catchment area

PARAMETER	VALUE	UNITS
CATCHMENT AREA	100	ha
NUMBER OF INHABITANTS	4000	Nr. of inhabitants
POPULATION DENSITY	40	$Inh.ha^{-1}$
POPULATION EQUIVALENT (PE) INDUSTRY	20 %	Small industry pollution production (surcharge to the inhabitant production)
SPECIFIC WASTEWATER PRODUCTION	100	$l.inh^{-1}day^{-1}$
SMALL INDUSTRY WASTEWATER PRODUCTION	20 %	Additional charge to dry weather flow
INFILTRATED WATER	50 %	Ratio of infiltrated water to sewage water
SPECIFIC BOD_5 PRODUCTION	60	g BOD_5 inh^{-1} day^{-1}

BOD_5 CONCENTRATION IN DRY WEATHER FLOW	327	mg BOD_5 . l^{-1}
BOD_5 CONCENTRATION IN CSO	175	mg BOD_5 . l^{-1}
SPECIFIC LENGTH OF THE SEWER NETWORK	3	$m.inh^{-1}$
SHARE OF ROOFS	15 %	Percentage share of the total catchment area
SHARE OF ROADS	25 %	Percentage share of the total catchment area
SHARE OF PAVEMENTS, PEDESTRIAN ZONES	5 %	Percentage share of the total catchment area
SHARE OF CAR PARK LOTS	15 %	Percentage share of the total catchment area
SHARE OF GREEN AREAS	40 %	Percentage share of the total catchment area
MIXING RATIO	1:4	Proportion of flow to WWTP

The area shares (buildings, streets…) were obtained by analysing a map of the sample catchment area in the Bratislava-Petržalka district based on the ZBGIS digital map [8].
We considered the implementation of green infrastructure only on roofs (green roofs), sidewalks (soakaways, swales, rain gardens) and parking lots (semi-permeable surfaces with infiltration).
The calculation was carried out in alternatives for the status quo, 25%, 50%, 75% and 100% implementation of green infrastructure on the potential areas, as well as alternatives with the construction of a rainwater retention basin with a volume of 720 m^3 (12 x 2.5 x 24 m) and 1350 m^3 (15 x 3 x 30 m).
As the updated Directive 91/271/EC [9] requires as a guideline to achieve a maximum of 2% of the yearly pollution load in the CSO effluent (of the total yearly WWTP pollution load in the dry period), we also calculated this indicator to the value of BOD_5, taking into account the pollution values (concentration) according [10].

4 Results and discussion

The results of the calculations are shown in Table 3.

Table 3. Calculation Results

ALTERNATIVE	NR. OF CSO EVENTS PER YEAR	CSO YEARLY VOLUME	% ACCORDING THE DIRECTIVE 91/271/EC	SHARE COMPARED TO STATUS QUO
	(-)	(m^3 $year^{-1}$)	%	%
STATUS QUO	16.4	45 044	9.99	100.00
25% GI	14.0	34 661	7.69	76.95
50% GI	11.5	25 913	5.75	57.53
75% GI	9.7	18 610	4.13	41.31
100% GI	8.1	12 496	2.77	27.74
STATUS QUO + ST 720 M^3	12.5	34 667	7.69	76.96
25% GI + ST 720 M^3	10.4	25 910	5.75	57.52
50% GI + ST 720 M^3	9.1	18 547	4.11	41.18
75% GI + ST 720 M^3	7.1	12 505	2.77	27.76
100% GI + ST 720 M^3	5.4	7 902	1.75	17.54
STATUS QUO + ST 1350 M^3	10.3	27 466	6.09	60.98
25% GI + ST 1350 M^3	8.9	19 809	4.39	43.98
50% GI + ST 1350 M^3	7.0	13 563	3.01	30.11
75% GI + ST 1350 M^3	4.9	8 752	1.94	19.43
100% GI + ST 350 M^3	3.3	5 395	1.20	11.98

Note: ST – storage tank

We present the results in graphical form in the following graphs (Figure 3, Figure 4):

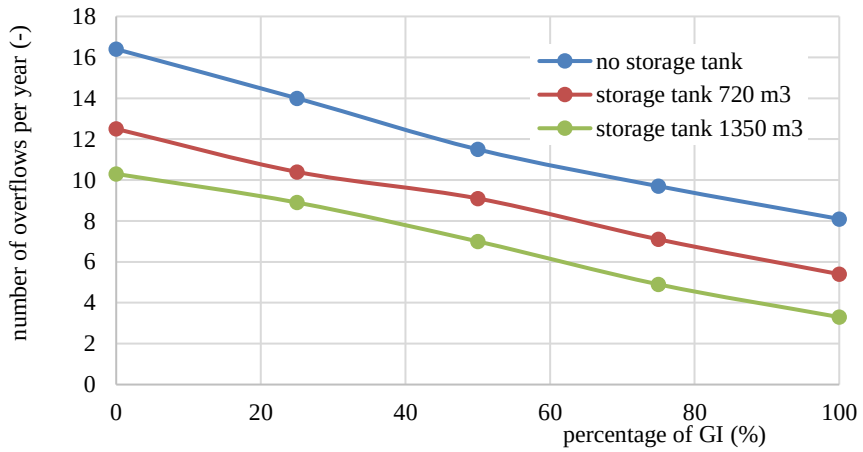

Figure 3. Number of CSO events in year

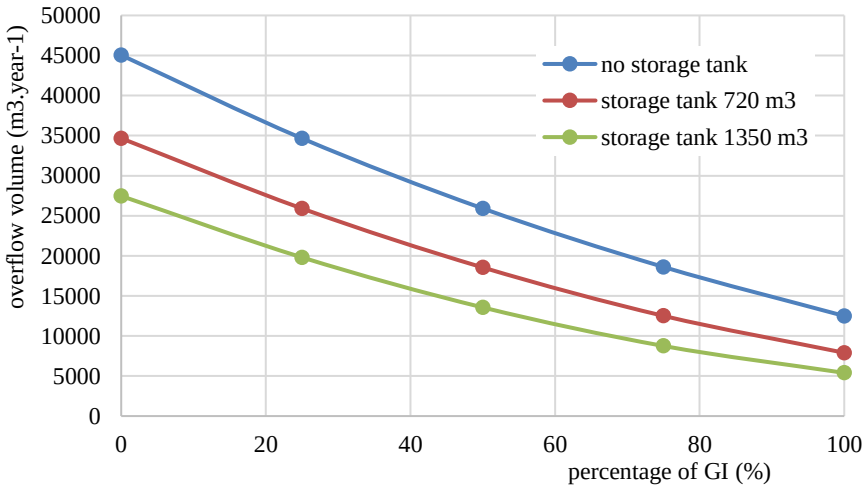

Figure 4. Discharged CSO volume

As can be seen from the model results, the implementation of GI reduces the number of CSO events as well as the CSO volume as the proportion of its implementation increases (decreasing trend of the curves in Figure 3 and Figure 4). The inclusion of a stormwater detention basin also reduces these parameters (lower position of the curves with inclusion of a stormwater detention basin in Figure 3 and Figure 4). For both trends, however, we can see some non-linearity in the results, e.g. when comparing the curves with both rainwater stormwater tanks. In the case of the larger tank, the tank volume is approximately twice (1350 vs. 720 m^3), but the decrease of the curve with the larger reservoir is not proportional to this ratio of reservoir volumes. This could lead to the hypothesis that for both green and grey infrastructure there are some technical (physical) limits to the minimum runoff from the urban catchment, which cannot be exceeded by common available technologies, or only at disproportionately high cost.

In this section, it is also necessary to mention the uncertainties and simplifications of the model used, which can significantly affect the results of this study.

The first simplification is the neglect of the spatial rainfall distribution, which plays an important role in runoff of large urbanised catchments. In addition, the typical catchment areas assigned to the Bratislava CSO's chambers are much larger than the catchment area we have chosen, which may lead to a bias in the results. Niemczynowicz [11] recommended in case of large catchments one rain gauge per every square kilometre. Schilling [12] find out in his study, that in case of studies based on statistical processed data causes the spatial rainfall distribution only a minor errors, whereas in cases of studies, based on single rain events, the spatial rainfall unevenness has fundamental importance.

The uneven spatial rainfall distribution causes only a small error in our study, because on the area of chosen virtual catchment 100 hectares (= 1km^2) can be spatially even rainfall distribution assumed; this

corresponds fully with the assumptions in our study.
It should be emphasized that the problem of spatial rainfall unevenness is independent of the type of model used. Current technologies of radar rainfall measurements and their combination with ground-based rain gauge data eliminate this problem, but the problem is the availability - this data are charged in Slovakia. This causes a problem in obtaining and using this data in research, as well as in engineering and design practice.
Another aspect is the neglect of the dynamics of the rainfall-runoff process. Our method assumes a constant runoff coefficient as well as a constant rainfall intensity during its duration (essentially a block rain assumption). The method assumes constant storage volumes (which is acceptable in the case of stormwater basins), but neglects the dynamics of flows in the sewer network and its dynamic, non-uniformity, non-stationarity and time-varying filling with wastewater. Neglecting of the rainfall-runoff process dynamic is often used in engineering practice (e.g. assumption of flow stationarity). To incorporate the dynamics of the rainfall –runoff processes dynamics into the model will lead to a complete change of the model used, which will require also time-dependant input data (e.g. rainfall time series).
Removing the above-mentioned simplifications of the model would enormously increase the requirements for input data into the model; the calculation would also be more difficult, without possibility of using simple means (MS Excel). If detailed modelling approach is required, the complex hydrodynamic model (approach) shall be used (e.g. SWMM [13], MIKE [14])
The technical feasibility of implementing green infrastructure is also uncertain, e.g. will it be possible to implement adaptation measures on 100% of the selected areas? Probably not, e.g. green roofs are cannot be often easily (and cost-effectively) implemented due to the static load-bearing capacity of older buildings or inadequate building structures (e.g. insulation, pitched roofs), semi-permeable surfaces of car parks cannot be used in heavily frequented car parks (e.g. industry, shopping centres, etc.). Insufficient space for their location, land ownership, hygiene and operational problems are also frequent problems (especially in densely built-up areas in city centres).
The described method is based on rainfall data from previous periods, which could be also a source of errors. In the context of climate change short-term rainfall intensities are expected to increase in the order of units to tens of percent [15], and work published so far confirms this trend [16, 17].
Other options for surface runoff retention, such as surface retention ponds (microponds), infiltration or direct discharge to receiving waters, are not included in the methodology used. Such measures can substantially improve the local microclimate [18]. The urban catchment in Bratislava suffers from a lack of local stream, so the restoration of the river network in urbanised areas is also of great importance [19].
In addition, in real catchments there are likely to be other catchment parameters that we have only estimated in our hypothetical example (local and time-varying parameters). These are in particular the length of the sewerage network or the utilisable volume of the sewerage network, the wastewater flows (amount of industrial wastewater, infiltrated water) as well as the concentrations of pollutants in the wastewater or in the discharged water.

5 Conclusion

The overall approach and design of urban stormwater adaptation measures is very specific and individual depending on local conditions, like the availability of a suitable recipient and its hydraulic capacity, hydrogeological properties of the soil (stormwater infiltration) or the hydraulic capacity of the urban sewerage system. It is also necessary to emphasize that green measures (green infrastructure) alone cannot eliminate all the negative impacts of climate change and a comprehensive restructuring of the existing urban drainage system is often necessary.
As the results show, the implementation of the GI (also in maximum possible extent) is not guarantee for the achieving the goals, proposed in the Directive 91/271/EC [9] (see Table 3). As it can be seen in in this table, only extensive combined approach (GI and grey infrastructure - stormwater tanks) can secure the required 2% of the yearly pollution load, transported through the CSO directly to the surface

water.
However, this study is a virtual study; in the real engineering practice can be such extensive implementation of adaptation and retention measures even more difficult due to various technical problems.
Another important question is the technical vs. financial effectivity of implemented measures, i.e. to find the optimal solution to achieve the required parameters. This will be most probably a "mix" of green and grey infrastructure, whereas the share and extent of each infrastructure type will determine the total costs (investment and maintenance costs). However, we assume that such optimal solution will be very case specific and has to be determined for each particular case.
Another set of issues that we want to address in the future is the comparison of the results of the method described in this paper with the results of the numerical rainfall-runoff model. It is also necessary to address the fact that the calculation method used is based on historical data, thus does not include the effects of climate change.

Acknowledgements
This study was supported by a grant from the Slovak Academy of Sciences (project VEGA No. 2/0140/24 entitled "Optimisation of adaptation measures for extreme torrential rainfall in urbanized catchments").

References:
[1] Greenworks: Tanner Springs Park, GreenWorks | People + Nature by Design, https://greenworkspc.com/ourwork/tanner-springs-park, 14.06.2024
[2] MANADA Trading s.r.o.: Zber a využitie dažďovej vody, http://www.dazdovavoda.sk/, 14.06.2024
[3] Prodlažba: Zatrávňovacia dlažba, https://www.prodlazba.sk/produkt/zatravnovacia-dlazba/, 14.06.2024
[4] Sky Gardens: Extensive green roof, https://www.zelena-strecha.sk/wp-content/uploads/2023/04/extenzivna_zelena_strecha.jpg, 14.06.2024
[5] Urcikán, P. and Imriška, L.: Stokovanie a čistenie odpadových vôd. Tabuľky na výpočet stôk. (in Slovak. Sewerage and waste water treatment. Tables for sewer design.), SNTL Alfa, Bratislava, 1986.
[6] Šamaj, F. and Valovič, Š.: Intenzity krátkodobých dažďov na Slovensku (in Slovak, Short-term rainfall intensities in Slovakia), SPN - Slovenské pedagogické nakladateľstvo, Bratislava, 1973.
[7] Marsalek, J.; Maksimovic, C.; Zeman, E. and Price, R. eds.: Hydroinformatics Tools for Planning, Design, Operation and Rehabilitation of Sewer Systems, Springer Netherlands, Dordrecht, 1998.
[8] GKU Bratislava: ZBGIS Client, https://zbgis.skgeodesy.sk/mkzbgis/sk/zakladna-mapa.
[9] Council of the European Union: Council Directive 91/271/EEC of 21 May 1991 concerning urban waste-water treatment, https://eur-lex.europa.eu/legal-content/EN/TXT/?uri=celex%3A31991L0271, 25.04.2023.
[10] Sztruhár, D.; Sokáč, M.; Holienčin, A. and Markovič, A.: Comprehensive assessment of combined sewer overflows in Slovakia, Urban Water, 4 (2002), no. 3, pp. 237–243.
[11] Niemczynowicz, J. Necessary level of accuracy in rainfall input for runoff modelling. In Proceedings of the Fifth Inter. Conf. On Urban Storm Drainage, Osaka, Japan , (1990), pp. 593-602.
[12] Schilling, W.: Rainfall data for urban hydrology: what do we need?, Atmospheric Research, 27 (1991), no. 1, pp. 5–21.
[13] US EPA: Storm Water Management Model (SWMM), https://www.epa.gov/water-research/storm-water-management-model-swmm, 15.04 2024
[14] DHI: MIKE+ Collection Systems | Urban Drainage Modelling Software, DHI, https://www.dhigroup.com/technologies/mikepoweredbydhi/mikeplus-collection-systems, 16.07.2024
[15] Presentation on the BVS Workshop 'Water retention measures', 27.3.2024, Waterworks museum, Bratislava, Slovakia.2024.
[16] Onderka, M.; Sokáč, M.; Pecho, J. and Mikulová, K.: Digital atlas of rainfall design intensities

in Slovakia, Meteorologický časopis, 26 (2023), pp. 27–38.
[17] Onderka, M. and Pecho, J.: Návrhové hodnoty intenzít krátkodobých dažďov na Slovensku. (Design values of short-term rainfall intensities in Slovakia.), Národný klimatický program Slovenskej republiky (National climate program of the Slovak Republic), Vol. 17/22 (2023).
[18] Pokrývková, J.; Jurík, L.; Lackóová, L.; Halászová, K.; Hanzlík, R. and Banihabib, M.E.: The Urban Environment Impact of Climate Change Study and Proposal of the City Micro-Environment Improvement, Sustainability 2021, Vol. 13, Page 4096, 13 (2021), no. 8, p. 4096.
[19] Halajova, D.; Halaj, P.; Macura, V. and Skrinar, A.: Urban River Design: A River Restoration Case Study, IOP Conference Series: Materials Science and Engineering, 471 (2019), no. 9, p. 092090.

IMPROVING COASTAL FLOOD ASSESSMENT THROUGH THE USE OF LIDAR DATA - A CASE STUDY OF ROVINJ CITY

NINO KRVAVICA [1], DAMJAN BUJAK [2], GORAN LONČAR [3], MARTA MARIJA BILIĆ [4]

[1] University of Rijeka, Faculty of Civil Engineering, Croatia, nino.krvavica@uniri.hr

[2] University of Zagreb, Faculty of Civil Engineering, Croatia, damjan.bujak@grad.unizg.hr

[3] University of Zagreb, Faculty of Civil Engineering, Croatia, goran.loncar@grad.unizg.hr

[4] University of Rijeka, Faculty of Civil Engineering, Croatia, marta.marija.bilic@uniri.hr

1 Abstract

The paper outlines the findings from numerical simulations of flooding in the city of Rovinj, Croatia. The simulations using a numerical spectral model were carried out under conditions of moderate (RP = 100 years) and high (PP = 5 years) probabilities of elevated sea levels and intense wave action. The integration of elevation data into these wave models involved incorporating two different resolutions: 5 m and 1 m. The research findings indicate that when using LiDAR data at a resolution of 1 m, the estimated flooded areas are, on average, 2% larger for a 100-year return period and 8% smaller for a 5-year return period compared to results obtained with elevation data at a 5 m resolution.

Keywords: coastal flood, mareographic measurements, digital elevation model, phase averaged wave numerical model

2 Introduction

By 2050, 2 billion people in flood-prone areas will be affected by population growth, climate change, deforestation, loss of wetlands, and rising sea levels [1]. Coastal areas are prone to flooding due to oceanographic and hydrological factors. Approximately 86 million EU residents live within 10 km of the coast [2]. Migration and urbanization may increase this number in the future, heightening vulnerability to flooding [3]. The UN's 2030 Agenda for Sustainable Development and the Sendai Framework for Disaster Risk Reduction are important global documents that focus on flood occurrences [4].

The Croatian Adriatic coast is prone to marine flooding [5]. Winter months primarily cause floods due to synoptic atmospheric actions [5], with a few events identified as meteorological tsunamis [6]. Storm surges cover larger areas and last longer, typically predicted with combined models [7]. Besides synoptic processes, additional factors contribute to high sea levels. Additional processes include long-period sea level oscillations and tidal oscillations [8]. Sea levels can rise by over 30 cm during cyclone passages due to slow-propagating atmospheric planetary waves lasting longer than 10 days, leading to flooding. Tidal oscillations in the Mediterranean are mainly caused by those in the Atlantic Ocean through Gibraltar [9]. Mediterranean tidal oscillations are typically weak (20-30 cm). Exceptions include the Tunisian Gulf, where tidal oscillations can exceed 2 m [10], and the Adriatic, where tidal oscillations in its northern part can reach 1.2 m. In Croatia and the EU, marine flooding risks are evaluated for low (1000-year return period, 0.1% annual exceedance probability), medium (100-year return period, 1.0% annual exceedance probability), and high (25-year return period, 4% annual exceedance probability) occurrences.

This study aims to analyse the impact of terrain elevation data resolution on flood area and wave height calculations. The following chapter provides an overview of available sea level measurement data at the Rovinj tide gauge station, explanations of the applied methodology for estimating the probability of high sea levels, and the established wave deformation model. Numerical analyses results are in the third

chapter. The fourth chapter concludes with a review of the research results.

3 Methods

3.1 Analysis of Sea Level Dynamics

Hourly sea level data are available, measured at the Rovinj tide gauge station (λ = 13.6291, φ = 45.0837) from 1991 to 2020 (Figure 1).

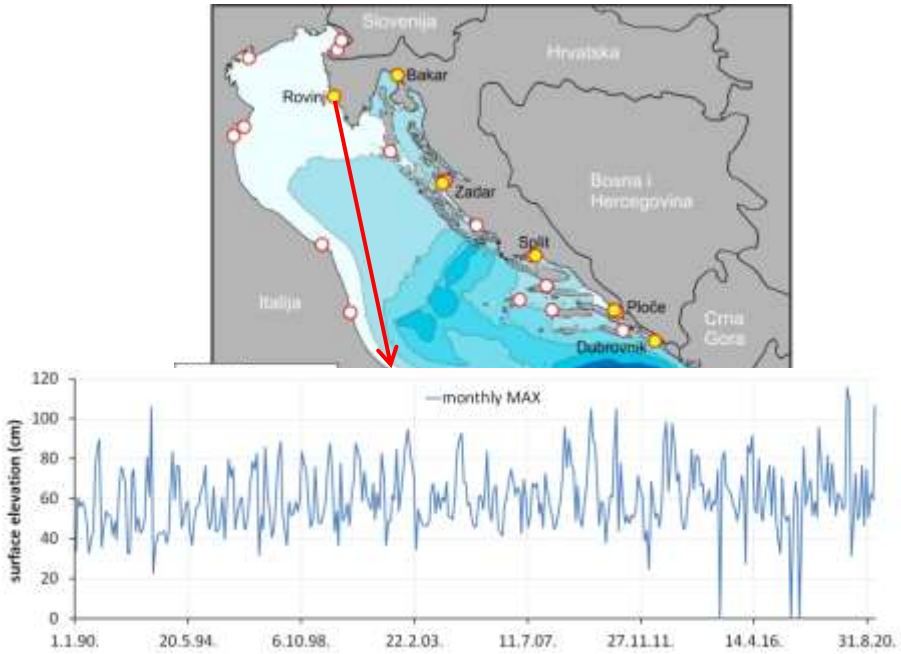

Figure 1. The position of the Rovinj tide gauge station is (λ = 13.6291, φ = 45.0837), and a time series of monthly maximums measured during the period from 1990 to 2020 is presented.

The estimation of extreme sea level values at the selected location was carried out using the measured data series following the methodology proposed by [11]. The basic steps in the extreme value analysis consist of the following procedures (after trend removal and peak grouping):

3. Selection of Extreme Values: Two standard approaches were used to select appropriate extremes:

a) Block Maxima (BM) series, corresponding to the Generalized Extreme Value (GEV) distribution, using yearly segments and analyzing the top r = 1 to 10 highest values in each segment.

b) Peak Over Threshold (POT) series, corresponding to the Generalized Pareto Distribution (GPD), with extremes defined as all values exceeding a specified threshold. The threshold was chosen to match the average number of annual extremes as in the BM method (on average r = 1 to 10 extremes per year).

4. Parameter Selection: Parameters of the GEV distribution (for BM) and GPD distribution (for POT) were estimated using the Maximum Likelihood Estimation (MLE) method. GEV distribution reduces to Weibull, Frechet, and Gumbel distributions, while GPD reduces to Pareto and exponential distributions, depending on shape parameters.

5. Distribution Fitting: GEV and GPD distributions were fitted to the extremes to define the corresponding high sea levels for annual exceedance probabilities (AEP) of 1.0% and 20.0%. The goodness of fit was assessed using two statistical measures: Root Mean Square Error (RMSE) and Akaike Information Criterion (AIC).

The original time series of sea levels was corrected by removing long-term trends and ensuring a stationary data series. The data series must be stationary, meaning the mean and standard deviation do not change over time [12]. Linear regression is commonly used to remove trends (min. 30 years). However, sea level changes can be highly nonlinear due to acceleration and deceleration of MSL changes and long-term oscillations. Therefore, moving annual average is considered a more reliable

trend removal method for sea level data and is commonly used in extreme value analyses [11]. The second step involved reducing the hourly sea level data to daily maximum sea levels. Independent events in this case are defined with a 3-day (72-hour) interval between two events, estimated in previous research as the average duration of storm surge impacts on sea levels in coastal areas. The third step involves selecting representative extremes from the overall sample. In the case of the BM approach corresponding to the GEV distribution, the r highest values within each year are selected. While some extreme analyses focus solely on annual maxima (e.g., [13]), better outcomes can be achieved by considering a sample of multiple values, if available [12]. It is important to mention that in a given year, the second or third highest value may surpass the maximum value recorded in another year within the observed series. Therefore, the analysis was conducted for r = 1 to 10 highest values each year. When the number of peak values per year increases, it is anticipated that the variance will decrease, which will enhance the selection of parameters for the corresponding theoretical distribution. However, selecting too many non-extreme events could increase model bias. Thus, selecting an appropriate r value is a compromise between bias and variance [12]. For the Mediterranean region, [14] suggest choosing r = 5. Since return periods associated with extreme sea level estimates generally exceed the sea level monitoring periods by several times, threshold selection can cause significant differences in the extrapolation range. To compare POT results with BM, an analysis was conducted for various thresholds defined by durations resulting in the same number of extremes as in the BM method (on average 1 to 10 extremes per year). Figure 2 shows the selection of extremes using BM and POT approaches for the Rovinj station for r = 5 (BM approach) and a 2.2% duration with a threshold of 69 cm above MSL (POT approach).

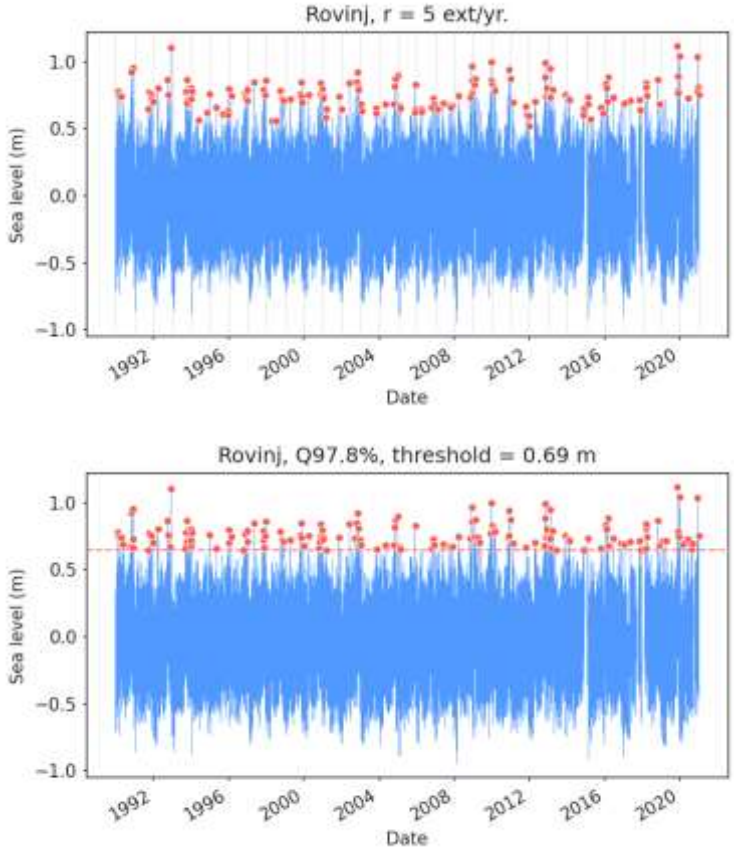

Figure 2. Selection of Extremes at the Rovinj Location According to the BM Approach (r = 5 Extremes per Year) and the POT Approach (Threshold 69 cm, $Ht_{2.2\%}$)

The three most commonly used methods for estimating distribution parameters are the Method of Moments (MOM), the Method of L-moments (LMOM), and the Maximum Likelihood Estimation

(MLE). Given that the sensitivity of extreme value analysis to the parameter estimation method is very weak compared to other elements, such as the choice of trend removal method and the selection of the number of extremes or the threshold for exceedance selection, the MLE method was chosen for parameter estimation in line with recent research on this topic [11].
In the block maxima method, the Generalized Extreme Value (GEV) distribution is used. The sample size is usually relatively small, so the estimated values in the area of low probabilities also show a high degree of uncertainty. Recognizing this property served as motivation for finding more sophisticated methods that rely on a larger data set over the same time period, such as the Peaks-over-Threshold (POT) method. The POT method involves consistently fitting the Generalized Pareto Distribution (GPD) or another distribution to the set of peak values that exceed a defined threshold (Davidson and Smith, 1990). Exceedances above the set threshold are assumed to follow a Poisson process with a parameter representing the average number of threshold exceedances per year with a corresponding independent distribution. The goodness of fit for these distributions to the data series is assessed using statistical measures of Root Mean Square Error (RMSE) and the Akaike Information Criterion (AIC). Lower RMSE/AIC values indicate a better model and fit. Figure 3 shows the results of the extreme value analysis for Rovinj using the POT approach for r = 5.

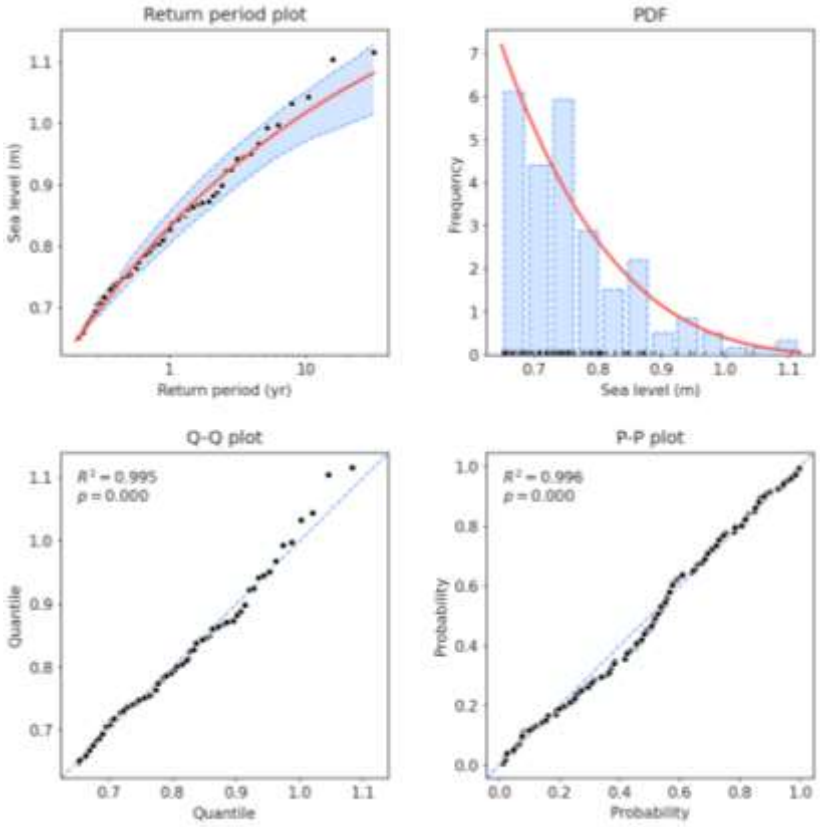

Figure 3. Return Period Diagram, Probability Density Function, and Q-Q and P-P Diagrams for Rovinj Location, POT Approach (GPD Distribution) with a Threshold of 72 cm ($Ht_{2.5\%}$) and an Average of 5 Extremes per Year

3.2 Estimation of Extreme Sea Levels and the Impact of Climate Change

We calculated the probabilities and expected maximum sea levels for annual exceedance probabilities ranging from 50% to 0.1% (return periods from 2 to 1000 years). For Rovinj, the representative distributions are the Gumbel distribution (BM approach) and the exponential distribution (POT approach), which have approximately linear forms on a logarithmic scale, while the POT approach yields higher extreme values for the same exceedance probability.

To estimate the impact of climate change on extreme high sea levels along the Adriatic coast, results from numerical climatological oceanographic models for the Adriatic Sea area can be used. The average modeled sea level rise is taken, and the mean value of sea level rise over the observed period is added to the previously calculated extreme sea level distributions. The dominant cause of sea level rise currently is the melting of glaciers and ice sheets (Greenland and Antarctic ice sheets), and to a lesser extent, the thermal expansion of the ocean. The expected future sea level rise will largely depend on greenhouse gas emissions and their future concentration in the atmosphere. In the Adriatic region, a mean sea level rise of 50 to 80 cm is expected by the end of the 21st century [15]. In this study, an estimated increase in extreme sea levels due to climate change of 60 cm for an annual exceedance probability of 1% (return period of 100 years) is used.

3.3 Digital Elevation Model (DEM)

The Digital Terrain Model (DTM) of the State Geodetic Administration (SGA) is created through photogrammetric stereo measurements based on aerial images with a spatial resolution of about 30 cm (Ground Sampling Distance – GSD). This terrain model is produced in the HTRS96/TM cartographic projection on the GRS80 ellipsoid, with the latest update made in 2019. By interpolating the vector data of the DTM, it is possible to create a regular grid of elevation points, which in raster form represents the Earth's surface and is called a Digital Elevation Model (DEM). For the purposes of this study, a Digital Elevation Model with a spatial resolution of 5 m was created, using the formal name DGU-5. The State Geodetic Administration created another detailed DEM from a Lidar survey project with a resolution of 1 meter, which will also be used here as DGU-1 [16].

3.4 Numerical Wave Model

The maritime area covered by the spatial domain of the spectral wave deformation model Mike 21/SW is shown in Figure 4. Figure 4 also depicts the applied model's spatial discretization with triangular cells (unstructured computational grid). The computational grid has a variable spatial step, ranging from 22 m in deeper waters to 2 m in the coastal area and on land (Figure 4). The computational grid consists of approximately 185,000 numerical cells. Depth data were obtained from detailed bathymetric surveys conducted in 2004, with a spatial data step ranging from 2 m to 10 m in the analyzed area (Figure 4). Data on significant wave heights (H_S) and peak wave periods (T_P) at the open boundary position of the wave deformation model (Figure 4) were taken from [17] for return periods of 5 and 100 years (Figure 4).

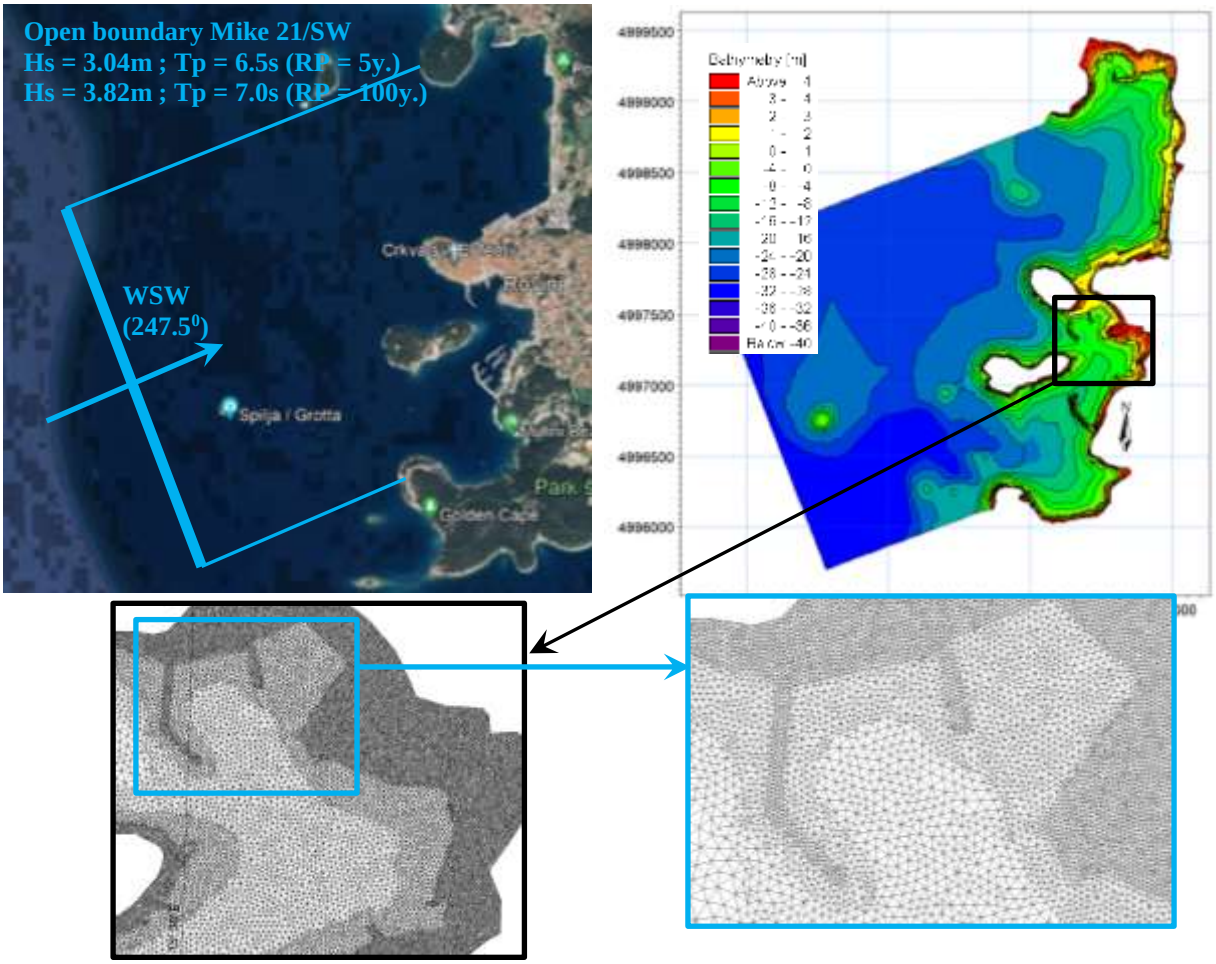

Figure 4. The Maritime Area Covered by the Spatial Domain of the Numerical Wave Deformation Model Mike 21/SW with a Display of the Computational Grid (Triangular Finite Volumes)

In the numerical spectral model Mike 21/SW, the full spectral formulation [18] was used, and for the spectral discretization of the frequency domain, a logarithmic scale from a minimum frequency of 0.05 Hz (wave period 20 s) to a maximum frequency of 0.95 Hz (wave period 1.05 s) was used, through 32 discrete steps. The model encompasses processes of nonlinear wave-wave interactions (triads), refraction and shallow water effects [19], diffraction, and wave breaking [20], while the dissipation process due to surface wave breaking (white capping) was not considered. The implementation of the desired degree of reflection from the shoreline and breakwater structures within the spatial domain of the numerical model was defined using appropriate reflection coefficients. Reflection coefficients were applied along the modeled shoreline, while the model domain boundary at locations with elevations > 5 m was treated with a reflection coefficient $K_r = 0$.

4 Results and discussion

Figure 5 shows the results of numerical simulations using the spectral model Mike 21/SW in the form of significant wave height (HS) fields with wave propagation vectors for the scenario with a 5-year return period without climate change (still water level at +1.01 m above mean sea level) and for the scenario with a 100-year return period with climate change (still water level at +1.82 m above mean sea level). The comparison is given for models with terrain height data from DGU-5 and DGU-1. Figure 6 shows the spatial distribution of depths in the flooded area for the simulation with a 100-year return period with the impact of climate change (as shown in Figure 5).

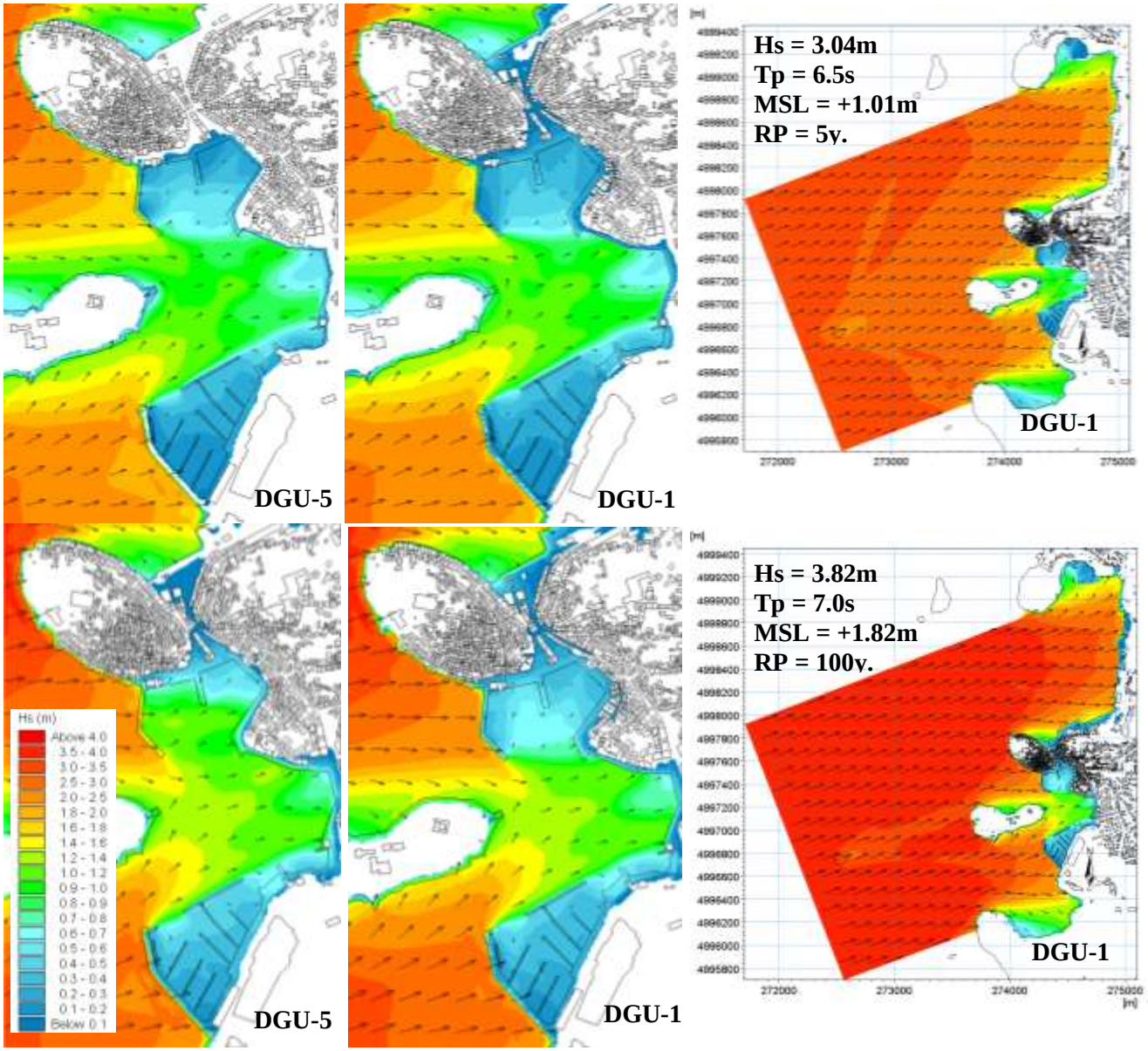

Figure 5. Fields of Significant Wave Heights (Hs) with Wave Propagation Vectors for the Scenario with a 5-Year Return Period without Climate Change (top) and for the Scenario with a 100-Year Return Period with Climate Change (bottom), with Implemented Terrain Height Data from DGU-5 (left) and DGU-1 (middle and right)

Based on the results of the numerical wave deformation simulations, flooding areas of the coastal zone (heights > 0 m above mean sea level according to HVRS71) were obtained for 4 analyzed scenarios (a total of 8 simulations: 4 for DGU-5 and 4 for DGU-1). In addition to the total flooding area (A_{Flood}), Tables 1 and 2 also show the partial flooding areas by elevation classes of flooding height, z. Furthermore, for each elevation class of flooding height z, the average significant wave heights ($H_{S\text{-}mean}$) on the corresponding flooding area were calculated.

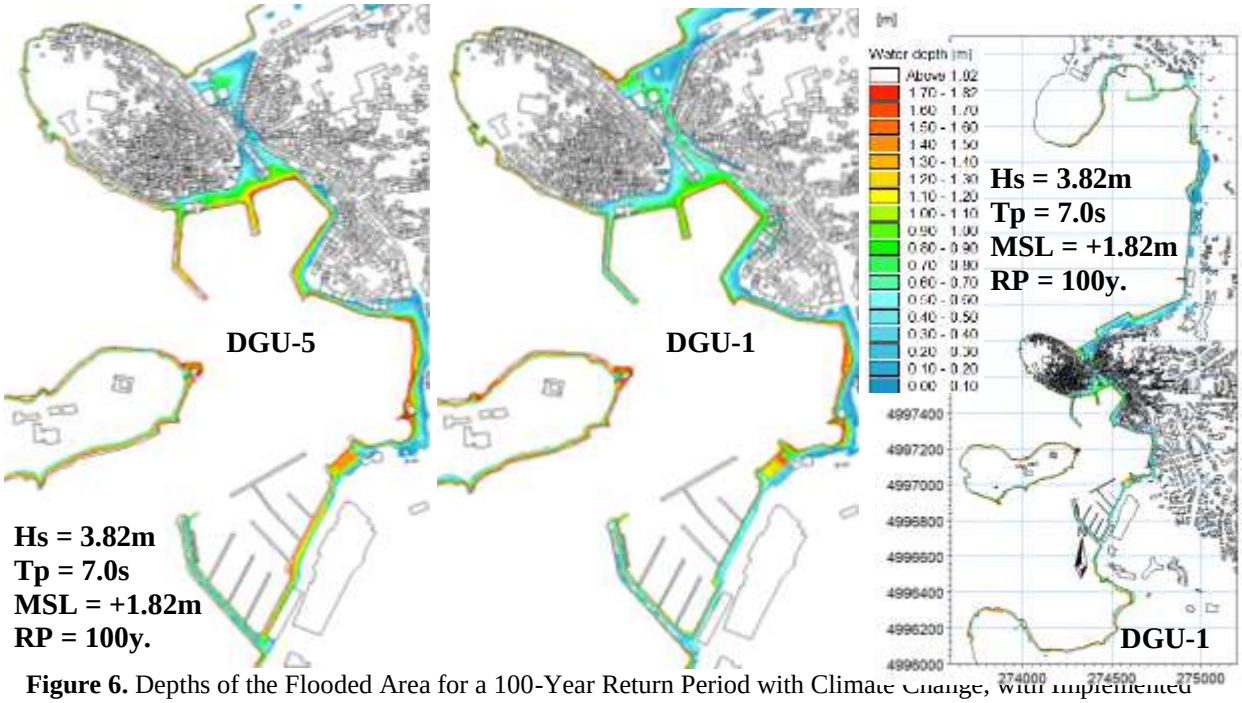

Figure 6. Depths of the Flooded Area for a 100-Year Return Period with Climate Change, with Implemented Terrain Height Data from DGU-5 (left) and DGU-1 (middle and right)

Table 1. Total Flooding Areas and Partial Flooding Areas by Elevation Classes of Flooding Height z, and Average Significant Wave Heights (**Hs_{-mean}**) for the Corresponding Flooding Areas According to the Results of the Mike 21/SW Model (Using Data from DGU-5)

	RP (year.)	Climate change included	A_{flood} (m^2)	A_{flood} for 0m<z<0.5 m (m^2)	A_{flood} for 0.5m<z<1.0m (m^2)	A_{flood} for 1.0m<z<1.5m (m^2)	A_{flood} for 1.5<z<2m (m^2)
1	5	No	9.52E+04	4.37E+04	5.15E+04		
2	100	No	1.20E+05	4.52E+04	4.38E+04	3.12E+04	
3	5	Yes	1.86E+05	8.22E+04	4.37E+04	4.49E+04	1.54E+04
4	100	Yes	2.34E+05	1.02E+05	4.77E+04	4.40E+04	3.96E+04
	RP (year.)	Climate change included		Hs_{-mean} in A_{flood} for 0m<z<0.5 m (m)	Hs_{-mean} in A_{flood} for 0.5m<z<1.0m (m)	Hs_{-mean} in A_{flood} for 1.0m<z<1.5m (m)	Hs_{-mean} in A_{flood} for 1.5m<z<2m (m)
1	5	No		0.25	0.58		
2	100	No		0.26	0.61	0.83	
3	5	Yes		0.16	0.56	0.77	0.91
4	100	Yes		0.16	0.57	0.85	1.07

Table 2. Total Flooding Areas and Partial Flooding Areas by Elevation Classes of Flooding Height z, and Average Significant Wave Heights (**Hs_{-mean}**) for the Corresponding Flooding Areas According to the Results of the Mike 21/SW Model (Using Data from DGU-1)

	RP (year.)	Climate change included	A_{flood} (m^2)	A_{flood} for 0m<z<0.5 m (m^2)	A_{flood} for 0.5m<z<1.0m (m^2)	A_{flood} for 1.0m<z<1.5m (m^2)	A_{flood} for 1.5<z<2.0m (m^2)
5	5	No	8.19E+04	3.23E+04	4.96E+04		
6	100	No	1.14E+05	4.83E+04	3.18E+04	3.37E+04	
7	5	Yes	1.84E+05	9.34E+04	3.56E+04	3.62E+04	1.93E+04

8	100	Yes	2.53E+05	1.17E+05	6.44E+04	3.12E+04	4.04E+04
	RP (year.)	Climate change included		Hs_{-mean} in A_{flood} for 0m<z<0.5 m (m)	Hs_{-mean} in A_{flood} for 0.5m<z<1m (m)	Hs_{-mean} in A_{flood} for 1.0m<z<1.5m (m)	Hs_{-mean} in A_{flood} for 1.5m<z<2.0m (m)
5	5	No		0.26	0.62		
6	100	No		0.22	0.68	0.86	
7	5	Yes		0.17	0.57	0.85	0.88
8	100	Yes		0.17	0.51	0.93	1.10

5 Conclusion

Calculated fields of significant wave heights and flooding areas for the city of Rovinj under conditions of medium (annual exceedance probability of 1%, return period of 100 years) and high (annual exceedance probability of 20%, return period of 5 years) probabilities of coastal flooding. In estimating flooded areas, two sources of terrain height data were used: one with a spatial resolution of 5 m (DGU-5) and the other with a spatial resolution of 1 m (DGU-1), while the same database was used for depths. For the estimation of extreme still water levels, data on measured sea levels at the Rovinj tide gauge station during the period 1990-2020 (hourly data resolution) were used, and extreme value analysis was conducted using block maxima series (BM) (with the adaptation of the generalized extreme value distribution) and peak-over-threshold series (POT) (with the adaptation of the generalized Pareto distribution). The POT approach yields higher extreme values for the same exceedance probability, and these values were adopted for defining still water levels in the numerical simulations of wave deformation.

The obtained results of the estimated flooding areas show that the application of terrain height data from DGU-1 (1 m resolution) results in smaller areas by an average of 8% under conditions of a 5-year return period (high probability) and larger flooding areas by an average of 2% under conditions of a 100-year return period (medium probability). The maximum percentage difference in the estimation of the flooding area occurs under conditions of a 5-year return period without the impact of climate change, where the flooding area using heights from DGU-1 is 14% smaller than the flooding area using heights from DGU-5.

Regarding wave heights in the flooded area, it was found that the application of DGU-5 or DGU-1 does not significantly affect the average values of significant wave heights, and that in zones with flooding depths from 0 m to 0.5 m, the average significant wave heights are $H_{s\text{-}mean}$(h = 0m - 0.5m) = 0.2 m, in flooding zones from 0.5 m to 1 m, $H_{s\text{-}mean}$(h = 0.5m - 1.0m) = 0.6 m, in flooding zones from 1.0 m to 1.5 m, $H_{s\text{-}mean}$(h = 1.0m - 1.5m) = 0.9 m, and in flooding zones from 1.5 m to 2.0 m, $H_{s\text{-}mean}$(h = 1.5m - 2.0m) = 1.0 m.

Given the results of the conducted research, it can be concluded that the height data from DGU-5 provide a good basis for estimating coastal flooding areas and the spatial distribution of wave heights in those areas. This allows for significant financial savings compared to using the much more expensive data from DGU-1.

References:

[1] The United Nations world water development report 2019: leaving no one behind - UNESCO Digital Library, https://unesdoc.unesco.org/ark:/48223/pf0000367306, 14.06.2024.

[2] EEA Annual report 2010 and Environmental statement 2011, https://www.eea.europa.eu/publications/annual-report-2010, 14.06.2024.

[3] Neumann, B., Vafeidis, A. T., Zimmermann, J., Nicholls, R. J.: Future Coastal Population Growth and Exposure to Sea-Level Rise and Coastal Flooding - A Global Assessment, *PLOS ONE*, 2015

[4] Colglazier, W.: SUSTAINABILITY. Sustainable development agenda: 2030, Science, 2015

[5] Međugorac, I., Orlić, M., Janeković, I., Pasarić, Z., Pasarić, M.: Adriatic storm surges and related cross-basin sea-level slope. J. Mar. Syst., 181:79–90, 2018.
[6] Denamiel, C., Šepić, J., Ivanković, D., Vilibić, I.: The Adriatic Sea and Coast modelling suite: Evaluation of the meteotsunami forecast component. Ocean Model., 135:71–93., 2019
[7] Cavaleri, L., Barbariol, F., Benetazzo, A.: Wind–Wave Modeling: Where We Are, Where to Go. J. Mar. Sci. Eng., 8, 2020.
[8] Vilibić, I., Šepić, J., Pasarić, M., Orlić, M.: The Adriatic Sea: A Long-Standing Laboratory for Sea Level Studies, Pure Appl. Geophys, 174:3765–3811., 2017.
[9] Arabelos, D. N., Papazachariou, D. Z., Contadakis, M. E., Spatalas, S. D.: A new tide model for the Mediterranean Sea based on altimetry and tide gauge assimilation, Ocean Sci., 7:429–444. 2011.
[10] Sammari, C., Koutitonsky, V., Moussa, M. Sea level variability and tidal resonance in the Gulf of Gabes, Tunisia, Cont. Shelf Res, 26:338–350, 2006.
[11] Arns, A., Wahl, T., Haigh, I. D., Jensen, J., Pattiaratchi, C.: Estimating extreme water level probabilities: A comparison of the direct methods and recommendations for best practice, Coast. Eng., 81:51–66. 2013.
[12] Coles, S.: An Introduction to Statistical Modeling of Extreme Values. Springer, London. doi:10.1007/978-1-4471-3675-0., 2001.
[13] Acero, F. J., García, J. A., Gallego, M. C.: Peaks-over-Threshold Study of Trends in Extreme Rainfall over the Iberian Peninsula, J. Clim, 24:1089–1105, 2011.
[14] Šepić, J., Pasarić, M., Međugorac, I., Vilibić, I., Karlović, M., Mlinar, M.: Climatology and process-oriented analysis of the Adriatic sea level extremes, Prog. Oceanogr, 209:102908, 2022
[15] Intergovernmental Panel on Climate Change (IPCC). Summary for Policymakers. In *Climate Change 2021 – The Physical Science Basis: Working Group I Contribution to the Sixth Assessment Report of the Intergovernmental Panel on Climate Change*., https://www.cambridge.org/core/books/climate-change-2021-the-physical-science-basis/summary-for-policymakers/CBBF8E93AC3A66A16D29C14D0815A45A, 14.06.2024.
[16] Multisenzorsko zračno snimanje Republike Hrvatske, https://dgu.gov.hr/multisenzorsko-zracno-snimanje-republike-hrvatske/5700, 14.06.2024
[17] Berbić, J., Ocvirk, E., Carević, D., Lončar, G.: Application of neural networks and support vector machine for significant wave height prediction, Oceanologia, 59:331–349, 2017.
[18] Komen, G. J., Cavaleri, L., Donelan, M., Hasselmann, K., Hasselmann, S., Janssen, P.: Dynamics and modelling of ocean waves. Cambridge University Press. 1994.
[19] Johnson, H. K., Kofoed-Hansen, H.: Influence of Bottom Friction on Sea Surface Roughness and Its Impact on Shallow Water Wind Wave Modeling. J. Phys. Oceanogr, 30:1743–1756, 2000.
[20] Ruessink, G.: Calibration and verification of a parametric wave model on barred beaches, Coast. Eng., 2003.

UNEVEN SHIFTS: HOW CLIMATE CHANGE ALTERS SEASONAL DISCHARGE PATTERNS IN SLOVAK RIVERS

WAEL ALMIKAEEL [1]

[1] *Slovak University of Technology in Bratislava, Department of Hydraulic Engineering, 810 05 Radlinského 11, Bratislava, Slovakia, wael.almikaeel@stuba.sk*

1 Abstract

This study examines the impact of climate change on the seasonality of discharge patterns in Slovak rivers, focusing on lowland and mountain types. Using STL decomposition the changes in seasonal discharge before and after 2000 were analyzed. The results show significant alterations, with the lowland Topľa River experiencing increased variability, intense peaks in maximum flows, and reduced minimum flows post-2000, highlighting its vulnerability. In contrast, the mountain Gidra River displayed more stable discharge patterns with minor changes in variability and peak flows. These findings underscore the differential responses of river types to climate change, with important implications for water resource management.

Keywords: climate change, seasonality, STL decomposition, lowland river, mountain river

2 Introduction

Climate change is a complex and urgent global challenge that significantly impacts various environmental processes, including the hydrological system [1]. Changes in temperature and precipitation patterns resulting from climate change disrupt the natural balance of water distribution, leading to shifts in surface runoff dynamics [2]. The hydrological system, encompassing rivers, lakes, and groundwater, is particularly vulnerable to these alterations [3]. Therefore, understanding the effects of climate change on the hydrological system and surface runoff is essential for assessing future water availability and managing water resources effectively.

Slovakia's diverse topography, characterized by highlands and lowlands, plays a crucial role in shaping its hydrological landscape [4]. Mountainous rivers, in particular, are significant components of the hydrological cycle, influencing surface runoff characteristics in various ways [5]. These characteristics vary across different regions due to factors such as elevation, land cover, and precipitation patterns [6]. Additionally, the presence of highland-lowland gradients further complicates runoff dynamics as water flows from mountainous areas to lowland plains, impacting water quality and quantity [7]. Studying surface runoff in Slovakia provides valuable insights into the intricate interactions between climate, geography, and hydrology.

Time series data analysis is a fundamental tool for understanding long-term trends and variability in surface runoff [8]. By analyzing time series data, researchers can identify seasonal patterns, trends, and anomalies, which are crucial for informed water resource management [9]. Dissecting the components of surface runoff, such as baseflow and stormflow, enables a deeper understanding of the underlying processes driving hydrological changes [10]. This knowledge is pivotal for developing adaptive strategies to mitigate the impacts of climate change on water resources effectively.

Statistical methods play a pivotal role in quantifying and monitoring changes in surface runoff over time [11]. Techniques such as trend analysis, regression modeling, and frequency analysis allow researchers to detect shifts in runoff patterns and assess their significance [12]. Statistical approaches also help identify potential drivers of change, such as land use changes or climate variability, thereby informing decision-making processes in water management [13]. Applying rigorous statistical methods enables

stakeholders to track evolving surface runoff dynamics and develop evidence-based strategies to address emerging challenges.

Case studies conducted in neighboring countries, such as Austria and the Czech Republic, have highlighted the increasing frequency and intensity of extreme rainfall events due to climate change [14]. These events lead to significant runoff volumes and flood risks, emphasizing the need for proactive measures to mitigate risks and enhance resilience [15]. Coping with climate change and runoff changes is crucial for sustainable water management in Slovakia and beyond [16]. Adapting to shifting hydrological conditions requires a multifaceted approach integrating scientific knowledge, policy interventions, and community engagement [17]. Investing in climate-resilient infrastructure, implementing water conservation measures, and promoting ecosystem-based adaptation strategies are essential steps toward building resilience to future challenges.

The primary aim of this study is to investigate how climate change influences the seasonal discharge patterns of Slovak rivers, with a particular focus on the differences between lowland and mountain river systems. This research examines the changes in seasonal discharge patterns in Slovak rivers before and after the year 2000, identifying specific differences in discharge pattern changes between lowland and mountain rivers. Additionally, the study explores the implications of these changes for water resource management and ecosystem health.

3 Study area

3.1 Topľa River

This study delves into the hydrological features of the Topľa River, a significant tributary in eastern Slovakia. With a length of 129.8 km and a catchment area of 1,544 km², it courses through diverse landscapes of agriculture and forests. The river's flow follows a distinct seasonal pattern influenced by precipitation variations, ranging from 600 to 1000 mm annually across its basin. The southern areas experience warmer climates with frequent hot summer days, while the north is cooler, with increased precipitation in July, driving summer discharge peaks [18].

Monitoring discharge at key gauging stations like Hanušovce nad Topľou provides crucial data on mean daily discharge (8.1 m³/s) and seasonal fluctuations. Additional insights from the Bardejov station, covering a 325.8 km² catchment area, reveal a mean annual discharge of 2.978 m³/s, enriching our understanding of the river's hydrology. This investigation isn't just academic; it has practical implications. By comprehending the Topľa's discharge patterns and their responses to climate shifts, we can proactively manage risks like floods and droughts. Such understanding is vital for preserving the health of the river ecosystem and the well-being of local communities reliant on it [18].

3.2 Gidra River

This study examines the hydrology of the Gidra River, situated in Slovakia's Carpathian Mountains. Unlike the Topľa River, it's smaller but still significant. Originating from the Little Carpathians, the Gidra is notable for its forest cover exceeding 95%, especially in its upper reaches. Several factors shape the Gidra's hydrological behavior. Its mountainous terrain likely leads to faster flow rates, while the extensive forest cover acts as a natural regulator, absorbing and slowly releasing water. Additionally, western Slovakia's lower precipitation levels may contribute to comparatively lower discharge volumes.

The Gidra's catchment area presents unique challenges for water management. Numerous water intakes, both private and public, dot its course, posing risks of water loss if not carefully monitored. A notable event in 2018 saw parts of the lower Gidra River dry up, emphasizing the need for improved monitoring and management practices. Despite limited available data, daily discharge records from gauging stations provide valuable insights spanning over five decades. These records are crucial for understanding the river's hydrological dynamics and informing future management strategies [18, 19].

4 Methods

4.1 Seasonal and Trend Decomposition using Loess (STL)

Seasonal variations in river discharge play a vital role in hydrological applications like flood prediction and water resource management. This study utilizes Seasonal and Trend decomposition using Loess (STL), a non-parametric technique, to analyze annual river discharge data [1].

STL breaks down time series data into three components: trend, seasonal, and remainder. The trend component captures long-term changes in the data, while the seasonal component reveals recurring patterns within fixed periods. The remainder component represents the residuals after the trend and seasonal components have been removed, indicating irregular fluctuations.

The core function of STL, Loess (Locally Estimated Scatterplot Smoothing), employs localized weighted regressions to capture non-linear trends and seasonality [1]. The STL method can be mathematically expressed as in Eq. (1):

$$X(t) = T(t) + S(t) + R(t) \tag{1}$$

Where:
- X(t): is the observed time series at time (t).
- T(t): is the trend component at time (t).
- S(t): is the seasonal component at time (t).
- R(t): is the remainder component at time (t).

The Loess smoothing technique used in STL is defined by as in Eq. (2):

$$\widehat{y_i} = \sum_{j=1}^{n} w(x_j) y_j \tag{2}$$

Where:
- $(\widehat{y_i})$ is the fitted value at point (i).
- $(w(x_j))$ is the weight assigned to the (j)-th data point, determined by the distance between (x_i) and (x_j).
- (y_j) is the observed value at point (j).

By applying STL, this study isolates the seasonal component of annual river discharge data, facilitating further analysis of recurring patterns and their hydrological impacts. The analysis focuses on annual variations, using STL to effectively isolate periodic patterns and underlying trends. This enables the identification of trends, anomalies, and recurring patterns over time.
The seasonal component is crucial for understanding recurring discharge patterns, while the trend component provides insights into long-term changes influenced by climate dynamics. The remainder component helps in identifying anomalies and short-term variations not explained by the seasonal or trend components.

In summary, utilizing STL for seasonal discharge analysis provides a robust framework for understanding the interplay of seasonal variations and long-term trends in hydrological data. By isolating the seasonal component, this study enhances insights into annual discharge patterns and informs effective water resource management strategies [20,21].

4.2 Statistical analysis

4.2.1 Coefficient of Variation (CV)

Coefficient of Variation (CV) serves as a crucial metric in hydrological studies, providing a unitless

measure of discharge variability around the mean annual discharge. Unlike standard deviation, which varies with measurement units, CV expresses variability as a percentage, allowing direct comparisons across rivers with different flow rates. While assuming a normal distribution of discharge values, CV remains valuable despite deviations in real-world data. It aids in comparing discharge variability between rivers and assessing environmental impacts on discharge patterns, such as those induced by climate change or human water management practices.

Calculating CV for distinct periods enables the investigation of discharge variability changes over time. A rising CV may indicate an increasing influence of climate change, leading to more extreme weather events affecting river flow. Conversely, a stable or decreasing CV suggests minimal changes in flow patterns. Integrating CV into analysis alongside STL decomposition provides a comprehensive understanding of both seasonal rhythm and discharge variability, crucial for effective water resource management and assessing environmental impacts on rivers [22].

4.2.2 Annual Maximum and Minimum Flow

This study extends beyond seasonal discharge rhythm and variability (as examined by STL and CV) to explore annual maximum and minimum flows, crucial for flood risk assessment and drought planning. Annual Maximum Flow (AMAX) represents peak discharge during heavy precipitation or snowmelt, informing flood control measures. Conversely, Annual Minimum Flow (AMN) indicates drought severity, guiding sustainable water withdrawal practices.

Applications of Annual Flow Extremes encompass flood risk assessment, drought monitoring, and water resource management. Analyzing trends in AMAX aids in flood risk assessment, informing adaptive measures amidst climate change and land-use alterations. Monitoring AMN is vital for drought preparedness, prompting conservation efforts and water use restrictions. Understanding both AMAX and AMN is pivotal for sustainable water management across sectors.

Statistical techniques like frequency and trend analysis facilitate the examination of annual flow extremes. Frequency analysis estimates the likelihood of surpassing specific flow values annually, while trend analysis detects changes in AMAX or AMN over time. By integrating annual flow extremes analysis with STL decomposition and CV calculations, this study offers a comprehensive view of river discharge patterns, critical for effective water resource management and ecosystem sustainability [12, 23].

5 Results and discussion

5.1 Topľa River Analysis

Comparing the seasonality of the Topľa River discharge between the periods of 1988-2000 and 2000-2020 reveals notable shifts in hydrological patterns, particularly in response to changing climatic conditions. Utilizing the Seasonal and Trend decomposition using Loess (STL) method and the additive method allows for a nuanced examination of these changes.

In the months of January and February, the seasonal discharge appears relatively consistent between the two periods, with slight variations. However, before 2000, there is a discernible small peak at the end of February, indicating the onset of intense precipitation. This peak suggests a distinct precipitation pattern characteristic of this period, potentially signaling the beginning of the rainy season. March marks the beginning of more pronounced differences in seasonal discharge patterns. After 2000, there is evidence of two local peaks emerging, contrasting with the single peak observed before the turn of the century. This shift could be attributed to changes in precipitation intensity or distribution, leading to altered runoff dynamics during the spring months.

Before 2000, the seasonal discharge continues to increase steadily until reaching a peak in early May,

followed by a gradual decrease with intermittent local peaks. These peaks may be associated with factors such as snowmelt or increased rainfall, contributing to elevated discharge levels during this period. From June to August, the seasonal discharge exhibits a decreasing trend, punctuated by occasional peaks attributed to summer rainstorms and accelerated ice melting. This decline reflects the typical progression of hydrological conditions during the summer months, with the influence of precipitation events and melting snow contributing to fluctuations in discharge.

After 2000, the increase in seasonal discharge from January to March becomes more gradual, with the emergence of two moderate peaks in March. April experiences a significant drop in discharge compared to February, possibly indicating a shift in precipitation patterns or hydrological dynamics during this period. May stands out with two significant peaks in seasonal discharge, accompanied by a substantial increase in discharge levels. These peaks may be linked to intensified rainfall or other meteorological phenomena, leading to heightened runoff during this time. The discharge then returns to lower levels until July, when a moderate peak occurs, likely driven by summer precipitation events or increased glacial melt. August sees a small peak before reaching a stable low level of seasonal discharge for the remainder of the year. Overall, the comparison highlights the complex interplay between climate change, precipitation patterns, and hydrological dynamics, underscoring the importance of continued monitoring and analysis to inform effective water resource management strategies.

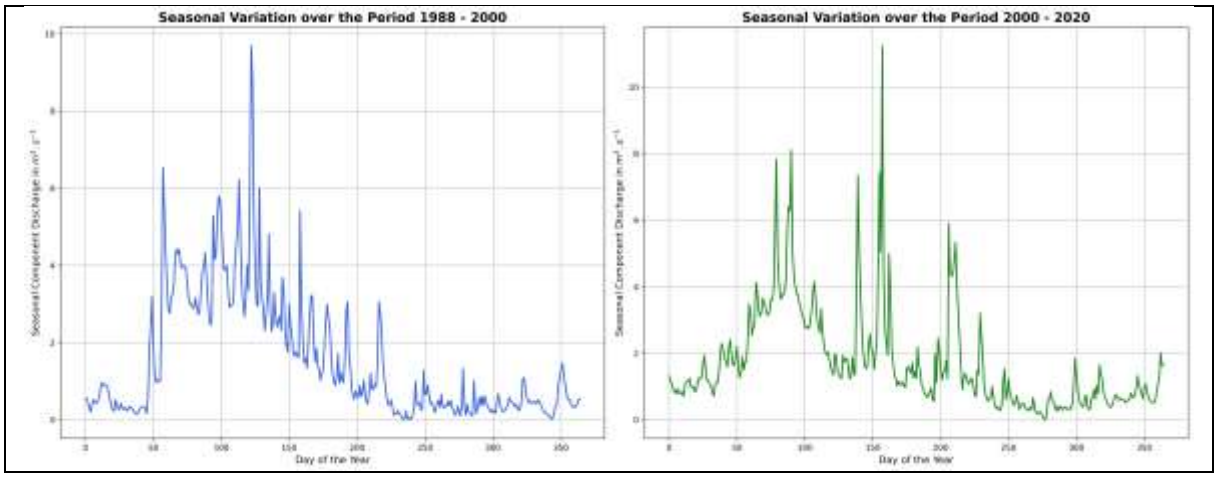

Figure 1. Comparison of the seasonal discharge component (1988-2000 vs. 2000-2020) - Topľa River

The analysis of the coefficient of variation (CV) for the seasonal component of discharge reveals a significant increase exceeding 20% after the year 2000 [1]. This rise in CV, alongside a comparison of CV values using quantiles, indicates a clear increase in the relative variability of seasonal discharge patterns in the later period, even after removing outliers.

Examining the annual extremes of discharge further strengthens the evidence for a changing hydrological regime. The post-2000 period exhibits a trend towards more frequent and intense peak flows, with the year 2010 witnessing a discharge tripling the pre-2000 maximum [2]. Furthermore, the Topľa River experienced four additional high-flow events exceeding the previous maximum within the post-2000 timeframe. This statistically significant increase in both the frequency and magnitude of peak flows suggests a growing tendency towards extreme high-flow events.

On the other hand, annual minimum flows (AMN) also paint a concerning picture. The post-2000 period has seen a new record low, with a discharge decrease of 90% compared to the historical minimum [2]. This dramatic decline in low-flow conditions highlights the potential for increased water scarcity during dry periods. These observed trends in both seasonal variability and annual extremes point towards a potentially changing hydrological regime in the Topľa River. The statistical findings underscore the importance of continuous monitoring and data collection for informing future research. Further

investigations should identify the potential drivers of these changes using advanced statistical modeling techniques and develop effective water resource management strategies to address these emerging challenges [3].

This analysis indicates a shift towards more extreme variability in both high and low-flow conditions in the Topľa River [1]. This has significant implications for flood risk management, ecological sustainability, and water resource planning. It necessitates the development of robust water management strategies that can adapt to the increasing unpredictability and extremity of river discharge patterns.

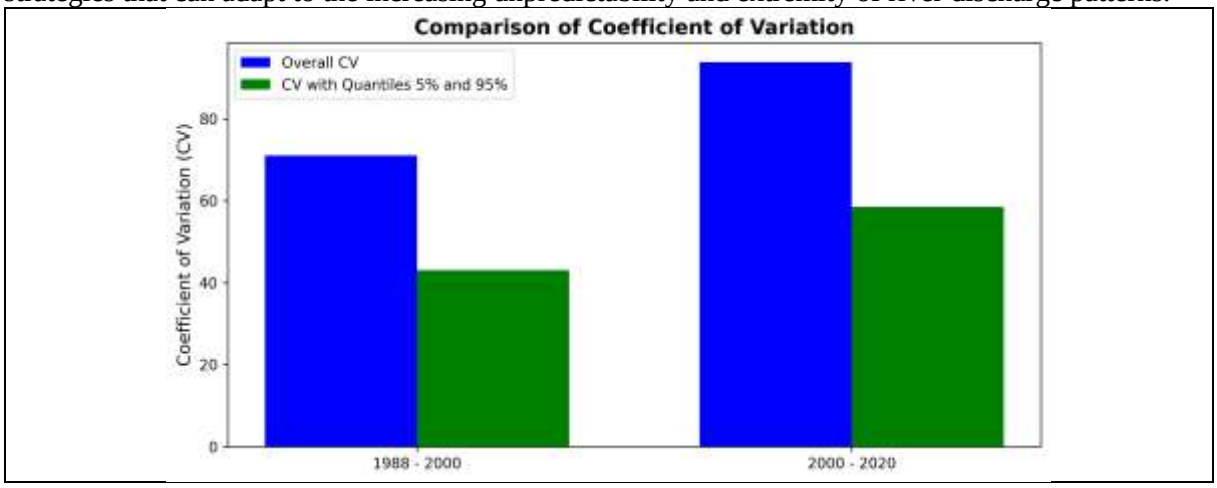

Figure 2. Comparison of Variation Coefficient (1988-2000 vs. 2000-2020) - Topľa River

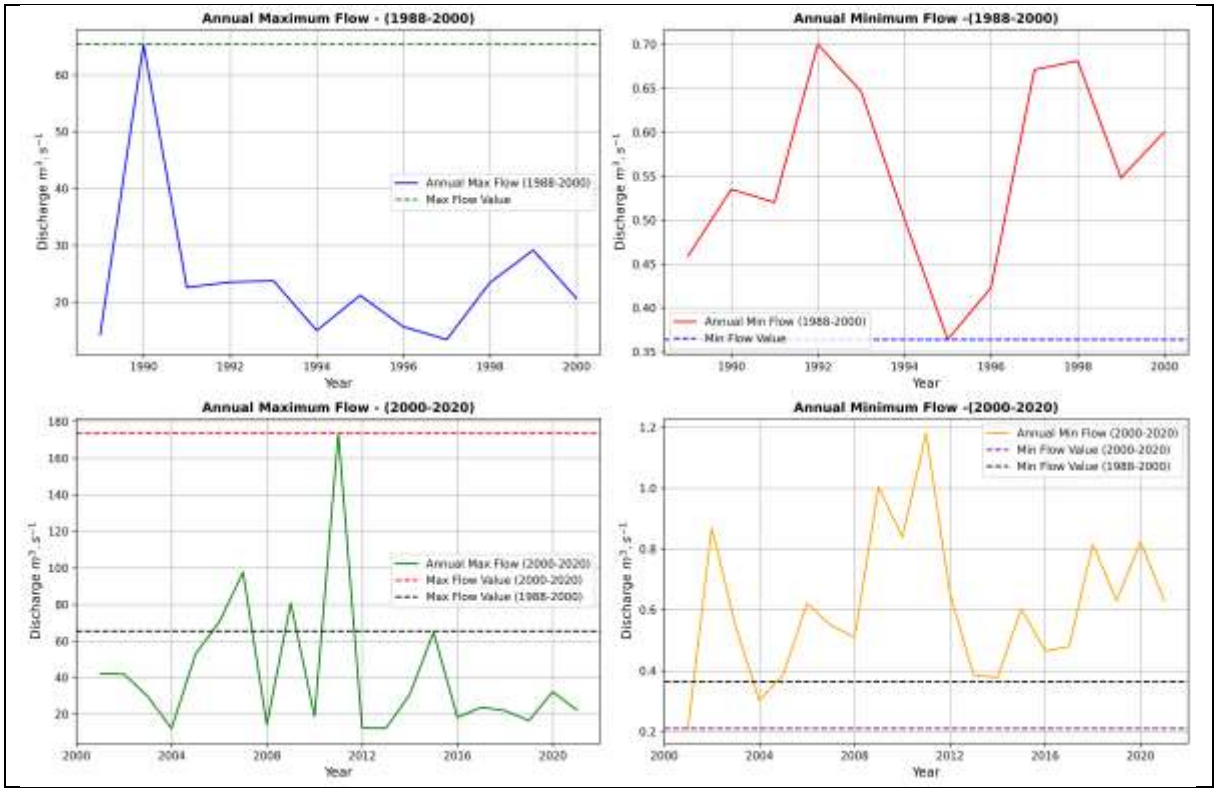

Figure 3. Comparison of Annual Maximum and Minimum Flow Rates (1988-2000 vs. 2000-2020) - Topľa River

5.2 Gidra River Analysis

Comparing the seasonality of the Gidra River discharge between the periods of 1961-2000 and 2000-2020 reveals some notable similarities and differences. Before 2000, the seasonality exhibited a

characteristic pattern, with a small peak in January followed by a drop until mid-February. Then, a rapid, gradual increase led to a moderate peak in February, indicating a period of sustained high seasonal discharge. March saw a gradual rise culminating in the highest peak in late March or early April, followed by a decline until June, reaching its minimum in July.
After 2000, the overall pattern remained largely similar, although with noticeable differences in discharge volume and timing. The peak in early February shifted slightly later towards the end of February and the beginning of March. March experienced the highest peak, notably larger in magnitude compared to the preceding period. However, in April, there was a steep decrease in discharge until mid-May, followed by a slow increase towards the end of the year. One significant observation is the decrease in the volume of seasonal discharge after 2000, particularly pronounced from March to May, indicating potential impacts of changing environmental factors on the river's flow patterns.

Overall, while the general seasonality remained similar between the two periods, the noticeable decrease in discharge volume and alterations in peak timing and magnitude after 2000 underscore the influence of changing environmental factors on the river's hydrological regime. Understanding the specific causes behind these observed changes requires further investigation. Analyzing precipitation data alongside a longer time series for discharge analysis could shed light on potential factors such as variations in winter snowfall and spring rain patterns, the influence of upstream water management practices, and the potential effects of climate change on regional hydrology.

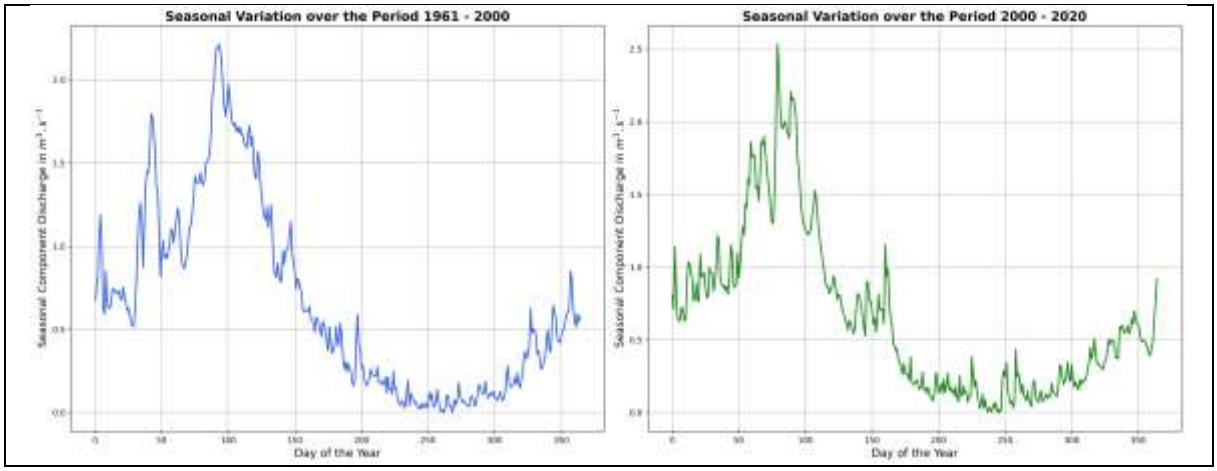

Figure 1. Comparison of the seasonal discharge component (1961-2000 vs. 2000-2020) - Gidra River

The Coefficient of Variation (CV) of the seasonal component, Annual Minimum, and Maximum Flow analysis are also conducted on the data of Gidra River. The analysis indicates that the CV percentage has slightly decreased after 2000, suggesting a stabilization or homogenization in the variability of seasonal discharge. The stability in CV persists even when considering the data filtered by various quantile ranges to mitigate the impact of outliers. These results underline a modest but consistent decrease in variability, pointing to changes in the watershed, such as improved regulatory mechanisms controlling river flow or alterations in land use that stabilize runoff patterns.

The AMAX from 2000 onwards shows a nuanced picture. While the peak discharge has increased slightly in specific years like 2007 compared to the maximum peak before 2000, the general trend does not reach the peak levels observed in the earlier period. This pattern might suggest that while the river retains the potential for significant discharge events due to extreme rainfall or snowmelt, such events have become less frequent. The AMN shows minimal change in the post-2000 period, with a negligible increase compared to earlier records. This stability in the minimum flow suggests that the river maintains a consistent base flow level across the years.

The analysis reveals contrasting trends between the Gidra and Topľa Rivers in Slovakia. Unlike the

Topľa River, the Gidra River shows a decrease in the variability of seasonal discharge and a reduction in extreme maximum flows. While this may aid in flood risk management and water planning, it poses challenges for ecosystems reliant on periodic flooding for regeneration. Further investigation into climate patterns, land management, and hydrological modifications is essential to understand these changes fully. In the Gidra River, a minor decrease in the coefficient of variation (CV) after 2000 suggests a potential stabilization in seasonal discharge variability. This differs from the Topľa River's trend, warranting further exploration into underlying causes. Despite the decrease in the extreme high flows in the Gidra, future extreme events remain possible. The complexity of climate change impacts on hydrological systems is evident in these contrasting patterns, emphasizing the need for comprehensive analysis to understand regional hydrological cycles better. Integrating these insights can enhance strategies for managing water resources and environmental protection efforts effectively.

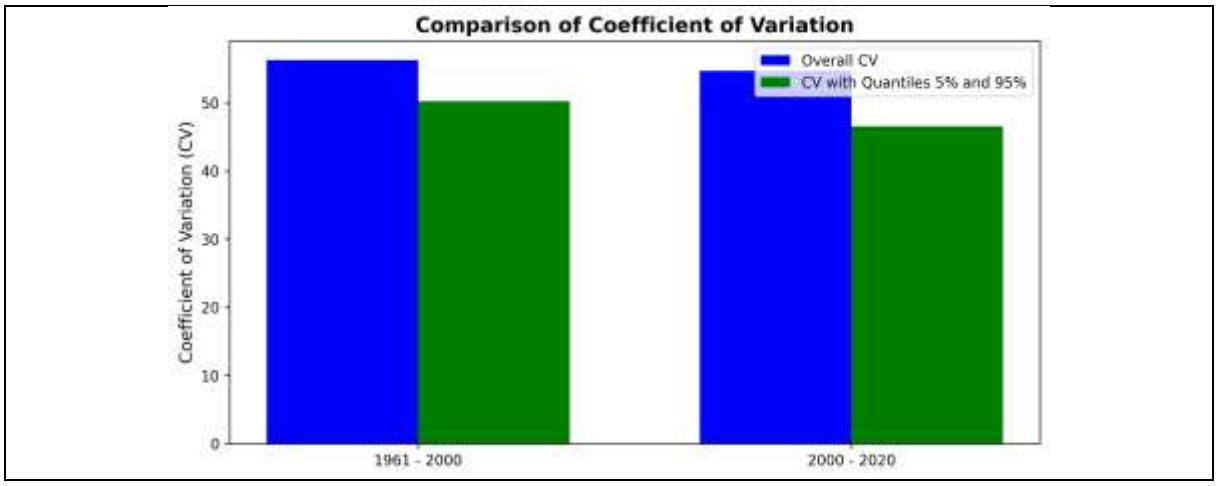

Figure 5. Comparison of Variation Coefficient (1961-2000 vs. 2000-2020) - Gidra River

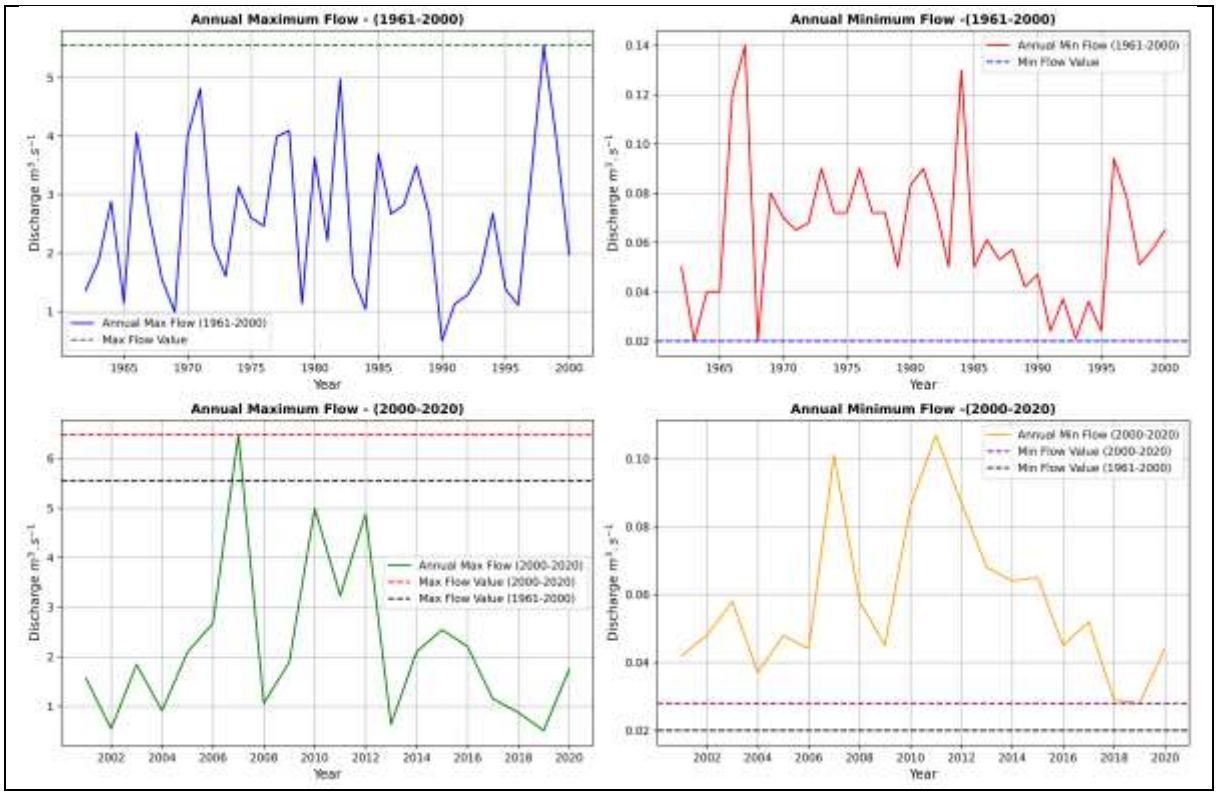

Figure 6. Comparison of Annual Maximum and Minimum Flow Rates (1961-2000 vs. 2000-2020) - Gidra River

6 Conclusion

In conclusion, this study systematically compared the seasonal discharge patterns of the Topľa and Gidra Rivers in Slovakia over two periods: 1988-2000 or 1961-2000 and 2000-2020. The analysis revealed significant variations in how these rivers respond to climatic and environmental changes, emphasizing the intricate relationship between geographical characteristics and hydrological responses. The Topľa River displayed substantial changes in seasonal discharge patterns, especially post-2000, marked by increased variability, intense peaks in annual maximum flows, and notable reductions in annual minimum flows. Conversely, the Gidra River exhibited a more stable discharge pattern, with comparatively minor changes in variability and less extreme peak flows.

These observed changes reflect the broader impacts of climate change on river systems. For the Topľa River, intensified peak flows and diminished minimum flows indicate heightened extremes in the hydrological cycle, possibly influenced by factors such as precipitation intensity and land use changes. Understanding these changes is essential for effective water resource management, particularly in developing adaptive strategies to address flood and drought risks. While the Topľa River requires comprehensive management approaches, focusing on conservation and sustainable usage might suffice for the Gidra, given its less extreme changes.

Adapting to these shifts necessitates a multifaceted approach, integrating advanced hydrological modeling, enhanced monitoring systems, and flexible policy frameworks. Investments in green infrastructure can mitigate flood risks, while strategies to enhance water storage and conservation during high-flow periods can counteract challenges posed by reduced flows in dry periods. In summary, the divergent responses of the Topľa and Gidra Rivers underscore the need for tailored, river-specific management strategies, informed by a thorough understanding of hydrological dynamics and climate change impacts. This ensures sustainable water management that meets both human and ecological needs in Slovakia.

Acknowledgments
This work was supported by The Slovak Research and Development Agency under the contract No. APVV-19-0383, together with APVV-20-0023.

References:

[1] Intergovernmental Panel on Climate Change (IPCC): Climate Change 2014: Impacts, Adaptation, and Vulnerability. Part A: Global and Sectoral Aspects, Cambridge University Press, 2014.
[2] Trenberth, K. E., Fasullo, J. T., Shepherd, T. G.: Attribution of climate extreme events, Nature Climate Change, 5(8), pp. 725-730, 2015.
[3] Kundzewicz, Z. W., Mata, L. J., Arnell, N. W., Döll, P., Kabat, P., Jimenez, B., Miller, K.: The implications of projected climate change for freshwater resources and their management, Hydrological Sciences Journal, 53(1), pp. 3-10, 2008.
[4] Fendeková, M., Blaškovičová, L.: Prognosis of hydrological drought development in Slovakia, Comenius University in Bratislava, Bratislava, 2018.
[5] Viviroli, D., Weingartner, R., Messerli, B.: Assessing the hydrological significance of the world's mountains, Mountain Research and Development, 23(1), pp. 32-40, 2003.
[6] Allan, R. P., Soden, B. J.: Atmospheric warming and the amplification of precipitation extremes, Science, 321(5895), pp. 1481-1484, 2008.
[7] Li, L., Zhang, L., Wang, X.: Effects of land cover change on hydrological processes in a large plain region: A case study of the Yellow River Delta, Journal of Hydrology, 456-457, pp. 247-258, 2012.
[8] Wilks, D. S.: Statistical Methods in the Atmospheric Sciences, Vol. 100, Academic Press, 2011.
[9] Hipel, K. W., McLeod, A. I.: Time Series Modelling of Water Resources and Environmental Systems, Elsevier, 1994.
[10] Smakhtin, V. U.: Low flow hydrology: A review, Journal of Hydrology, 240(3-4), pp. 147-186, 2001.

[11] Helsel, D. R., Hirsch, R. M.: Statistical Methods in Water Resources, Vol. 323, U.S. Geological Survey, 2002.
[12] Helsel, D. R., Hirsch, R. M.: Statistical methods in water resources, U.S. Geological Survey, 1997.
[13] Hirsch, R. M., Slack, J. R.: A nonparametric trend test for seasonal data with serial dependence, Water Resources Research, 20(6), pp. 727-732, 1984.
[14] Schär, C., Vidale, P. L., Lüthi, D., Frei, C., Häberli, C., Liniger, M. A., Appenzeller, C.: The role of increasing temperature variability in European summer heatwaves, Nature, 427(6972), pp. 332-336, 2004.
[15] Blöschl, G., Montanari, A.: Climate change impacts—throwing the dice?, Hydrological Processes, 24(3), pp. 374-381, 2010.
[16] Kundzewicz, Z. W., Schellnhuber, H. J.: Floods in the IPCC TAR perspective, Natural Hazards, 31(1), pp. 111-128, 2004.
[17] Adger, W. N., Arnell, N. W., Tompkins, E. L.: Successful adaptation to climate change across scales, Global Environmental Change, 15(2), pp. 77-86, 2005.
[18] Mitkova, V. B., Pekarova, P.: Analysis of maximum runoff volumes with different time durations of flood waves: A case study on Topl'a river in Slovakia, IOP Conference Series: Earth and Environmental Science, 362(1), p. 012013, 2019.
[19] Čubanová, L., Šoltész, A., Mydla, J.: Analysis of droughts due to the operation of water structures: Gidra River Case Study, Pollack Periodica, 17(1), pp. 111–116, 2022.
[20] Liu, Z., Zhu, Z., Gao, J., Xu, C.: Forecast Methods for Time Series Data: A Survey, IEEE Access, 9, pp. 91896–91912, 2021.
[21] Dokumentov, A., Hyndman, R. J.: STR: A seasonal-trend decomposition procedure based on regression, Department of Econometrics and Business Statistics, Monash University, Australia, 32 p., 2015.
[22] Viglione, A.: Confidence intervals for the coefficient of L-variation in hydrological applications, Hydrology and Earth System Sciences, 14(11), pp. 2229–2242, 2010.
[23] Medina, Y., Muñoz, E.: Estimation of annual maximum and minimum flow trends in a data-scarce basin. Case study of the Allipén River watershed, Chile, Water, 12(1), p. 162, 2020.

RESEARCH OF THE INFLUENCE OF FLOOD FLOWS ON THE AREA BETWEEN THE ANTOŠOV IRRIGATION CHANNEL AND THE LAMAČSKÝ STREAM

MARTIN ORFÁNUS [1], LEA ČUBANOVÁ [2], JÁN RUMANN [3], PETER ŠULEK [4]

[1] *Faculty of Civil Engineering STU Bratislava, Slovakia, martin.orfanus@stuba.sk*

[2] *Faculty of Civil Engineering STU Bratislava, Slovakia, lea.cubanova@stuba.sk*

[3] *Faculty of Civil Engineering STU Bratislava, Slovakia, jan.rumann@stuba.sk*

[4] *Faculty of Civil Engineering STU Bratislava, Slovakia, peter.sulek@stuba.sk*

1 Abstract

The aim of the work was to assess the current situation in the area of interest (between the Antošov channel and the Lamačský stream) in terms of flood flows using a 2D mathematical model. As part of the work, 2D flow simulations were made at Q_{100} discharge in the area of interest for the current state, topography measurements and objects. The area of interest falls within the basin of the Morava River. The system creates a characteristic fan-shaped drainage framework of the Western part of the Bratislava territory.

Keywords: discharge, measurements, floods, hydrodynamic model, Q_{100}

2 Introduction

The aim of the work is to assess the current situation in the area of interest (between the Antoš channel and the Lamačský stream) in terms of flood flows using a 2D mathematical model. As part of the work, 2D flow simulations were made at discharge of Q_{100} in the area of interest for the current state. The work is divided into the analysis, study and processing of delivered and obtained documents, measuring the topography, or objects in the location of interest for building a model of the current state, processing of documents into the necessary format for a 2D model of the current state, development of a mathematical 2D model of the area of interest (the land between the Antoš channel and the Lamačský stream) – current state on the Figure 1.

The area of interest falls within the basin of the Morava River. The main stream is the Morava River, which flows into the Danube near Devín Castle. The type of runoff regime of the treated area is rain-snow. The maximum flows occur in the winter and spring months (March, April) in connection with the melting of snow and in the summer months, when they are conditioned by heavy rains. The minimum flows are mainly in September and October. Currently, the river network no longer has a natural character. As a result of frequent flooding and waterlogging of the territory, most of the streams were modified for water management (relocation and regulation of streams, establishment of irrigation and drainage canals), which, together with other melioration modifications, have a significant impact on the groundwater level. As a result of the regulation of flows, at maximum water levels, they emerge from the riverbeds only occasionally, floods mainly occur in the Morava floodplain [1].

Lamačský stream - originates in the Small Carpathians. The upper stream has a rapid nature. In the lowland part, its bed is adjusted and straightened. The stream is watery all year round and empties into the Vápenické stream. The length of the stream is 6.2 km. It causes flooding of adjacent lands under the forest area, especially during torrential rains and increased flows. Due to culverts and bridges with insufficient capacity, it is also embanked on the adjacent road, so the water flows outside the channel and floods the adjacent apartment buildings [2]. Erosion can potentially occur not only due to a lack of culvert capacity, but also due to the clogging of culverts and narrowed areas of the streambed by alluvium brought by the flow during increased flows from higher-lying forest areas.

Figure 1. Area of interest. Area between the Antoš channel and the Lamačský stream)

Antoš's canal - is an artificial watercourse and its bed begins at the state road Lamač - Devínska Nová Ves. It runs for 2.5 km through agricultural land, has a well-maintained, straight riverbed. Several objects have been built on the stream within the treated territory - concrete stabilization thresholds, small steps to reduce the slope of the level and economic crossings, built as pipe culverts, with concrete faces and using reinforced concrete pipes DN1000.

The channel also serves as a recipient for the outlet of systematic pipe drainage, and drainage outlet objects are installed in its bank. The bottom of the channel is in some places clogged with deposits of mud, the bank vegetation and the surroundings of the channel are largely marked by succession and a large presence of moisture-loving plants. After studying the background and available materials, it was necessary to enlarge the model beyond the scope of the site of interest in order to determine the influence of adjacent roads, which (according to the currently valid flood risk maps, they look like they overflowed at flood flow Q_{100}, because of the culverts that lead under the communications.

3 Methods

The two-dimensional mathematical model HEC-RAS 2D v.6.3 (U.S. Army Corps of Engineers, Hydrologic Engineering Center's River Analysis System) was used to determine the water level regime and overall hydraulic conditions in the area. The software can work with both steady and unsteady 1D

and 2D flows, which HEC-RAS solves using a diffuse or dynamic wave, using a finite difference numerical method.

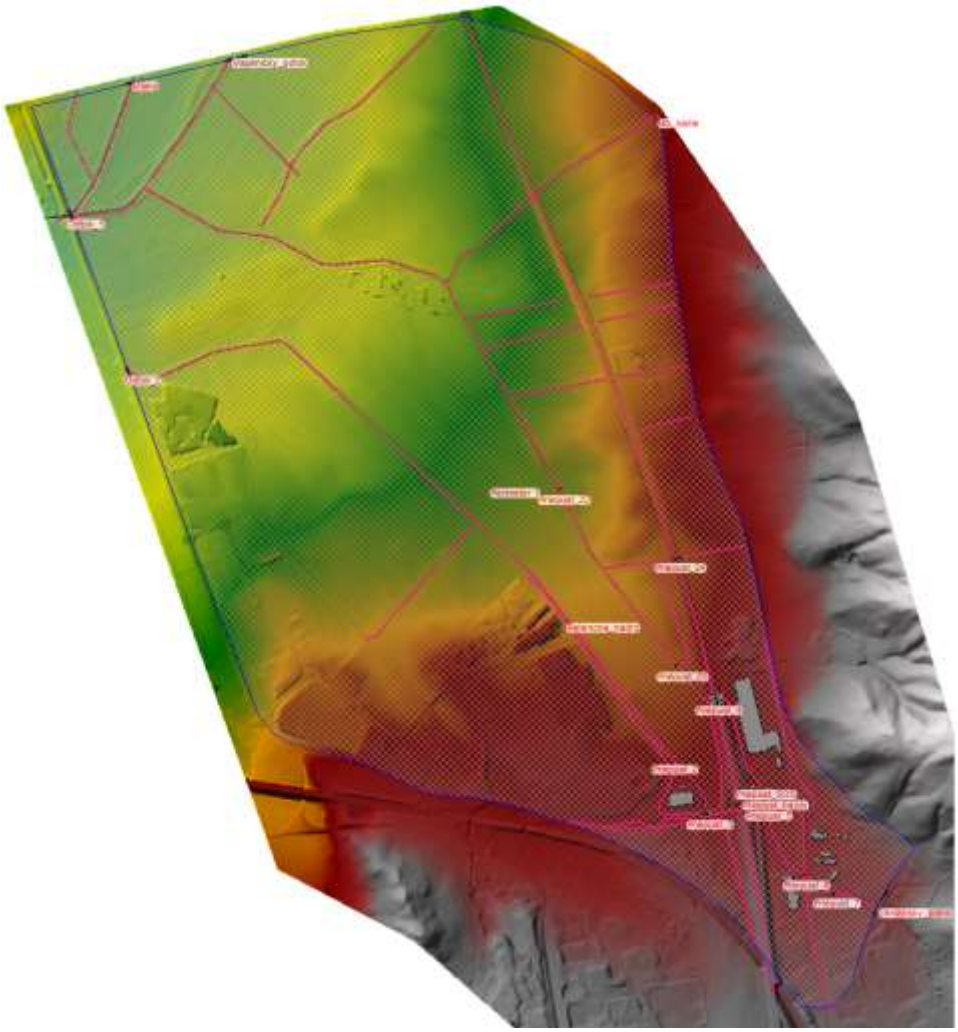

Figure 2. Two-dimensional mathematical model HEC-RAS of the area

The equation of motion, the so-called the diffusion wave is used for larger models that do not require a detailed solution for the flow around certain obstacles. It finds its application in e.g. in models of open channels, in the design of anti-flood measures. The diffusion wave is practically a simplified dynamic wave, where the approximation consists in neglecting the non-linear term of the inertial force, since it assumes a small change in the flow with increasing time.
The dynamic wave is also known as the de Saint-Venant equation, which is used to describe unsteady flow in open channels. The basis for the derivation of the Saint-Venant equations was the system of Navier-Stokes equations. The HEC-RAS 2D model uses it in an approximate form, as the so-called Shallow Water Equations (SWE) because in 2D flow negligible vertical velocity components are assumed and also that the flowing liquid is incompressible and has a constant density [3].
Solving these equations requires higher demands on computing technology and longer simulation times. The advantage is the possibility of solving a large number of scenarios, including dynamic flood waves, sudden widening or narrowing of the current, mixed flow regime, wave propagation, etc. If the fluid is incompressible, then the continuity equation in the form of a differential equation for an unsteady state has the form

$$\frac{\partial h}{\partial t} + \frac{\partial (hu)}{\partial x} + \frac{\partial (hv)}{\partial y} = q \quad (1)$$

where t is time, u and v are the components of velocity in the x and y directions, q is the discharge.

3.1 Current state

From the point of view of solving the site of interest at Q_{100}, a 2D mathematical model of the current state was compiled with basic schmee based on Eq (1), This model serves to create an idea where the embankment from the Lamačské stream and the Antoš channel to the area of interest occurs.
A digital relief model (DMR) of the area of interest was downloaded from the Basic Database for Geographic Information System (ZBGIS). At the locations of the identified objects on the streams, culverts according to the focus were defined in the model. The bed of the Lamačské stream and the Antoš channel was deepened in the model of the current state according to the geodetic focus shown in the Figure 2. The calculation network of the area of interest was entered with a dimension from 1 m depending on the need for detailed calculation, with a roughness factor according to Manning n = 0.090, while the value 0.090 corresponds to an unmaintained channel with dense weeds, the height of which is equal to the depth of the flow and with unremoved rustling.

3.2 Simulation model

Simulation calculations for steady flow were made for the area defined in this way. Calibration of the model was not possible because there were not enough data available to carry it out [4]. The boundary conditions were specified as:

- flows: QN annual flows (Q Q_{100} = 7.4 m3.s-1 on the Lamačský stream rkm 3.5 Q_{100}= 8.4 m3.s-1 on the Lamačské stream rkm 2.8 and Q100 = 2.1m3.s-1 on Antošov channels rkm 2.2
- lower boundary condition: free runoff from the modeled area at the confluence of Mláka-Muriansky stream-Lamačský stream The result of the simulations is a depth map in the solved area of interest for Q_{100}.

3.3 Uncertainty of the model

The 2D mathematical model was developed with certain uncertainties resulting from the data provided for the solution, in particular:
• the geodetic measurement was carried out in the growing season and many sections were inaccessible due to overgrown vegetation (measurement in the autumn-winter period would be more appropriate),
• the model was not calibrated, there would have to be a reconciliation of the measurement of the level and the flow, which in summer reaches unmeasurable values,
• some culverts were partially blocked, there were transverse obstacles in the flow from fallen trees, which was transferred to the model in the form of an increased level of roughness.

4 Results and discussion

From the simulations for the current state model, flood locations were confirmed according to the currently valid flood hazard map [5], which are easily identifiable even with the naked eye in the field (places with a high growth of sedge, terrain depressions, with otherwise very sloping terrain in the direction of the flow of both streams). Since the simulation was created with higher detail (Figure 3), it can be seen that the water depths in the area of interest at flood flow $Q_{100}$are in the range of 0-25 cm (Figure 4).

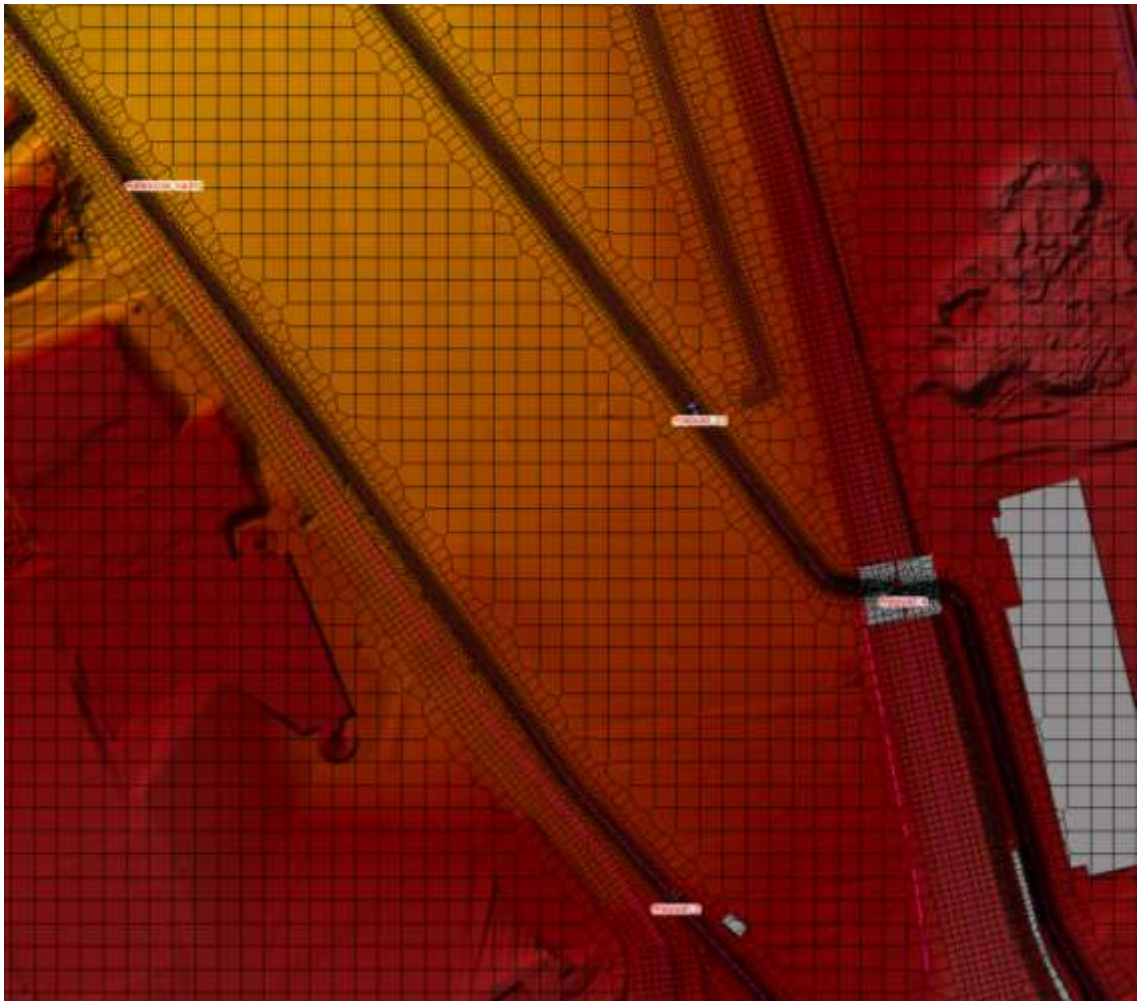

Figure 3. The simulation model - higher detail.

The critical places in relation to the area in question are the culverts on the Lamačské and Antošov canals, which do not have the necessary capacity to implement Q100. The maintainability of the riverbed plays a big role in the transfer of flows [6]. Due to the high degree of overgrowth of the Lamačské stream and the Antoš channel, the capacity of the bed is significantly limited. High longitudinal slope defines the high velocities shown in figure Figure 5 with potencial to higher capacity but under the conditions of clear riverbed with proper vegetation modifications.

Figure 4. The map of depths.

Figure 5. The map of velocity

5 Summary and conclusions

The aim of the work was to assess the impact of flood flow Q_{100} on the Lamačský stream and Antošov canal on the area of interest by creating a depth map at Q_{100}. As part of the work, measurements were carried out and a 2D mathematical model was compiled based on current topographical and hydrological data for the current state. The current state model has not been calibrated. For possible calibration of the model in the future, it would be advisable to supplement the measurement of the level regime at a higher water level (harmonize the level measurement at a relatively stable and at the same time known water

level) so that the entire model can be calibrated. The result of this work is a recommendation for the purification of both streams (Lamačské stream and Antoš channel) to the originally designed profile, as well as the maintenance of culverts, respectively. For their conversion to frame structures, or ground level bridges which are less prone to clogging/maintenance and have higher capacity than pipe bridges. Of course, this only applies to culverts on the Antošov canal and Lamačský stream. Along most of the watercourse beds in the wider area of interest, mature greenery is planted, but of varying quality. They are also accompanied by accompanying low greenery (shrubs).
Watercourse beds are important biocorridors. From the point of view of the flow rate and capacity of the riverbeds, some overgrown and clogged sections of the riverbeds are a problem. In the spring, during the melting of the snow or during torrential rains, waters from upper basin at Lamačský stream are washed out.
However, the solved issue must be viewed in a broader context, as the Lamačský stream has a torrential nature in its upper part, which is characterized by fast drainage due to the large slope of the territory, which is propagated further along its course into the residential zone of the Lamač district.
As for the possible close-to-nature modifications of the treated stream beds, they are not in accordance with the territorial system of ecological stability (ÚSES), because currently the already stabilized corridors of the Antoš channel and Lamačské brook with riparian vegetation and other elements of the ÚSES in the wider area are part of the provincial biocorridor leading in the Little Carpathian Mountains and feeding into the Devínsk Kobyla provincial biocenter. They thus represent the last possibility of connecting the entire Lesser Carpathians with Devínská Kobyla in an area that has not yet been built on. Although it is also necessary to state that the functionality of the given biocorridor is limited by the existence of current linear barriers, such as highways, roads, railways, partial development and also large-scale agricultural.

Acknowledgements
This paper was supported by the Grant agency under contract VEGA 1/0161/24.

References:
[1] HYDROCOOP, spol. s.r.o.: Update of the territorial general of water courses and flood protection of the city of Bratislava. Bratislava, 2022, listed at: https://cdn-api.bratislava.sk/strapi-homepage/upload/textova_cast_a73c1b7990.pdf (available 20.06.2023)
[2] Bugár, J.: General principles of functional organization of the territory - part "A" - surveys and analyzes of the territory (VZFU part "A" - Surveys, analyzes and analysis of the current state - documentation of the Project of simple land adjustments in the section of the Lamač , Štamperky location). Bratislava, 2014, listed at: https://docplayer.net/43422528-Vseobecne-zasady-funkcneho-usporiadania-uzemia-cast-a-prieskumy-a-rozbory-uzemia.html (available 20.06.2023)
[3] HEC-RAS Documentation (2023) HEC-RAS Hydraulic Reference Manual, found at: https://www.hec.usace.army.mil/confluence/rasdocs/ras1dtechref/latest/theoretical-basis-for-one-dimensional-and-two-dimensional-hydrodynamic-calculations/2d-unsteady-flow-hydrodynamics/hydraulic-equations (accessible 20.06.2023).
[4] Report on the progress and consequences of floods in the territory of the Slovak Republic from January 1 to August 31, 2011, listed at: https://lrv.rokovania.sk/data/att/107817_subor.doc (available on June 20, 2023)
[5] Slovenský vodohospodársky podnik, š. p.: Flood hazard maps and flood risk maps of Slovak waterways (according to Directive 2007/60/EC of the European Parliament and Council of October 23, 2007 on flood risk assessment and management). Selection of the class - Bratislava IV district (2), listed at: https://mpompr.svp.sk/okres.php?id=4 (available 20.06.2023)
[6] Raplík, M., Výbora, P., Mareš, K.: Uprava tokov. Alfa, Bratislava, 1989. ISBN 80-08-00128-2.

Ing. Michaela Červeňanská, PhD., prof. Ing. Andrej Šoltész, PhD., doc. Ing. Dana Baroková, PhD., Ing. Lea Čubanová, PhD.

18th International Symposium
WATER MANAGEMENT & HYDRAULIC ENGINEERING WHME 2024
10th – 14th September 2024, Štrbské Pleso, Slovakia
SYMPOSIUM PROCEEDINGS

Published by the Slovak University of Technology in Bratislava in SPEKTRUM STU Publishing, Bratislava, Vazovova 5, in 2024.

Extent 491 pages, 324 figures, 105 tables, 34.305 author sheets, 34.307 publisher sheets, 1st edition.

ISBN 978-80-227-5433-0
ISSN 3027-5032

PARTNERS AND SPONSORS

ISBN 978-80-227-5433-0